Der Naturwissenschaftlichen Fakultät der Friedrich-Alexander-Universität Erlangen-Nürnberg

zur

Erlangung des Doktorgrades Dr. rer. nat.

Synthesis and Characterization of Amphiphilic Porphyrin–Perylene Dyads: Towards Optoelectronic Membranes in Water

Synthese und Charakterisierung von amphiphilen Porphyrin–Perylen Dyaden: Die Grundlagen für optoelektronische Membranen in Wasser

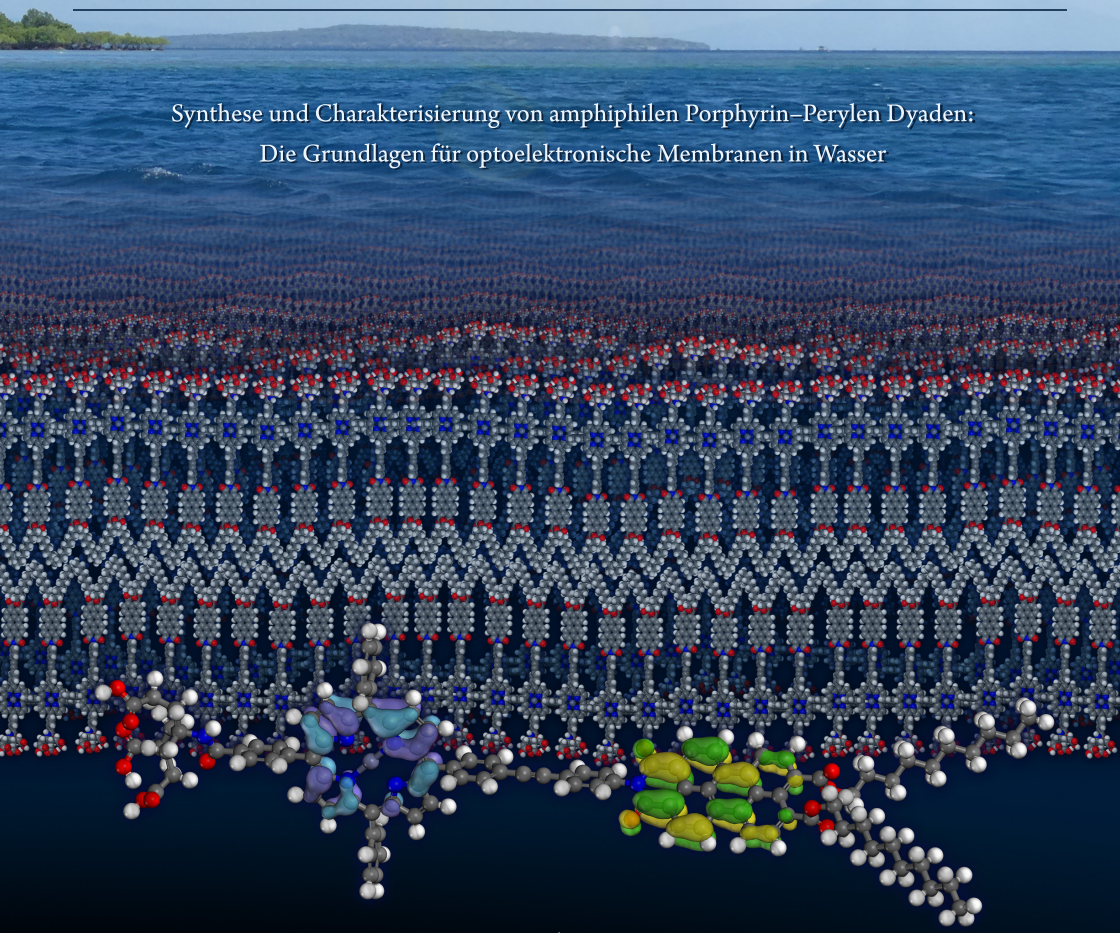

vorgelegt von

Christian D. Methfessel

aus Hamm

Christian D. Methfessel

Synthesis and Characterization of Amphiphilic Porphyrin–Perylene Dyads: Towards Optoelectronic Membranes in Water

Der Naturwissenschaftlichen Fakultät der Friedrich-Alexander-Universität Erlangen-Nürnberg

zur

Erlangung des Doktorgrades Dr. rer. nat.

Synthesis and Characterization of Amphiphilic Porphyrin–Perylene Dyads: Towards Optoelectronic Membranes in Water

Synthese und Charakterisierung von amphiphilen Porphyrin–Perylen Dyaden: Die Grundlagen für optoelektronische Membranen in Wasser

vorgelegt von

Christian D. Methfessel

aus Hamm

FRIEDRICH-ALEXANDER
UNIVERSITÄT
ERLANGEN-NÜRNBERG

Als Dissertation genehmigt von der Naturwissenschaftlichen Fakultät
der Friedrich-Alexander-Universität Erlangen-Nürnberg

Tag der mündlichen Prüfung: 17. Januar 2020

Vorsitzender des Promotionsorgans:	Prof. Dr. Georg Kreimer
Gutachter:	Prof. Dr. Andreas Hirsch
	Prof. Dr. Jürgen Schatz

"The significance and joy in my science
comes in those occasional moments of discovering something new
and saying to myself, 'So that's how God did it.'

My goal is to understand a little corner of God's plan."

— Henry F. Schaefer[1]

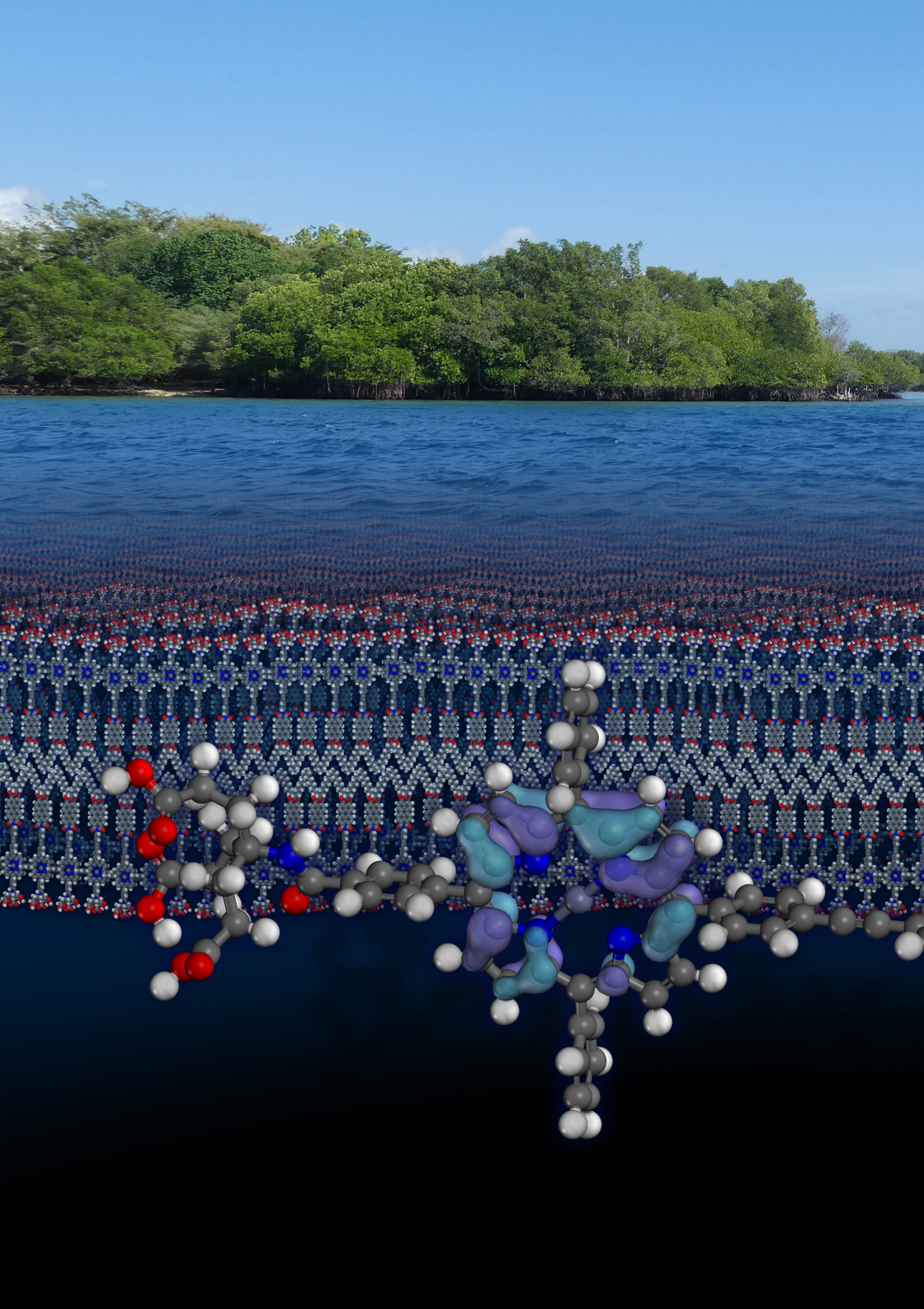

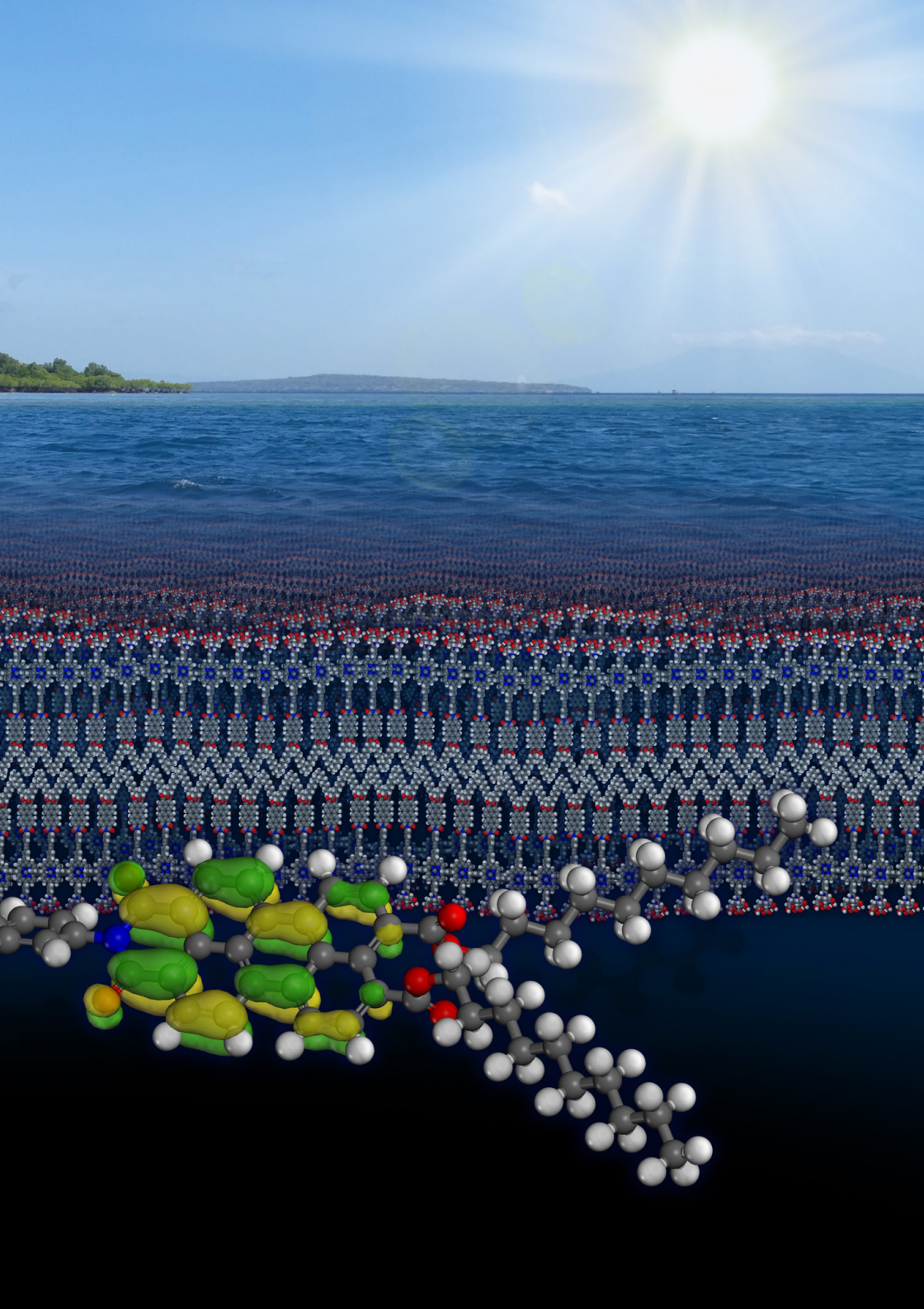

List of abbreviations

APPI	Atmospheric pressure photo ionization, a MS method
aq.	aqueous
a.u.	arbitrary units
br	broad (peak form, NMR)
Boc	*tert*-Butyloxycarbonyl (protective group)
Boc_2O	Di-*tert*-butyl decarbonate
ca.	*circa* [lat.], around, approximately
calcd.	calculated
CBz	Carboxybenzyl (protective group)
cf.	*confer/conferatur* [lat.], compare, see
consec.	consecutive, step-by-step
COSY	Correlated Spectroscopy, a 2D-NMR method
CV	Cyclic voltammetry
d	doublet (peak multiplicity, NMR)
d	deuterated (NMR solvents)
DBU	1,8-Diazabicyclo[5.4.0]undec-7-ene
DCC	*N,N'*-Dicyclohexylcarbodiimide
DCU	Dicyclohexylurea
DDQ	2,3-Dichloro-5,6-dicyano-1,4-benzoquinone
decomp.	Decomposition
DEPT	Distortionless Enhancement by Polarization Transfer, a ^{13}C NMR method
DLS	Dynamic Light Scattering, a method to determine the size of particles
DMAP	4-Dimethylaminopyridine
DMF	*N,N*-Dimethylformamide
DMSO	Dimethylsulfoxide
DNMR	Dynamic NMR, to measure reaction rates of reversible molecular processes
DOSY	Diffusion-Ordered Spectroscopy, a 2D-NMR method
DPM	Dipyrromethane
DSSC	Dye sensitized solar cells
EA	Electron affinity
e.g.	*exempli gratia* [lat.], for example
E_g	(HOMO – LUMO) energy gap
eq	Equivalent(s)
ESI	Electrospray ionization, a MS method
et al.	*et alius/alii* [lat.], and other(s)
etc.	*et cetera* [lat.], and so on

ex. M.	exact Mass (of most abundant molecular isotope)
FGI	Functional group interconversion, a chemical operation in retrosynthesis
FT-IR	Fourier-transform infrared spectroscopy
G^1	1st generation NEWKOME dendron
G^2	2nd generation NEWKOME dendron
GPC	Gel permeation chromatography. Also: Size exclusion chromatography
HMBC	Heteronuclear Multiple Bond Correlation, a special 2D-NMR method
HOBt	1-Hydroxybenzotriazole
HOMO	Highest occupied molecular orbital
HPLC	High-performance liquid chromatography
HSQC	Heteronuclear Single Quantum Coherence, a special 2D-NMR method
i.e.	*id est* [lat.], that is
int.	Intensity
IP	Ionization potential
IR	Infrared spectroscopy
LUMO	Lowest unoccupied molecular orbital
m	Minute(s); multiplet; medium/middle (intensity, IR); milli (10^{-3})
M	Molar (mol/L)
M	(target) molecule [in mass spectrometry]
MALDI	Matrix assisted laser desorption/ionization, a MS method
MP	Melting point
MS	Mass spectrometry
MW	Molecular weight, molecular mass
m/z	Mass-to-charge ratio (MS)
n	nano (10^{-9})
NMR	Nuclear magnetic resonance, a spectroscopic method
NOESY	Nuclear Overhauser Enhancement Spectroscopy, a NMR method
p	pentet = quintet (peak multiplicity, NMR)
p.	page
$PABE_{10}$	Perylene monoanhydride bisdecylester
PAH	Polycyclic aromatic hydrocarbons, a class of organic molecules
PDA	Perylene dianhydride
PDI	Perylene diimide: perylene with two (nonspecific) imide functionalizations
PDI_S	Perylene (swallowtail)diimide: perylene imide with a hexyl(1-pentyl) chain
PDT	Photodynamic therapy
PEG-400	short-chained polyethylene glycol with average MW of 400 g/mol
PEP	Phenyl-ethynyl-phenyl: a rigid, linear spacer
PIA	Perylene imide monoanhydride

PI_SA	Perylene-(swallowtail)imide monoanhydride
$PIBE_{10}$	Perylene imide bisdecylester
$POCl_3$	Phosphoryl chloride, a reagent used for the Vilsmeier reaction
ppm	Parts per million (unit for NMR)
PTCDA	Perylene-3,4:9,10-tetracarboxylic acid bisanhydride, also called PDA
PTE_{10}	Perylene tetradecylester
p-Tos	*para*-Toluenesulfonic acid (monohydrate)
PVC	Polyvinyl chloride, a polymer used for plastic
q	quartet (peak multiplicity, NMR)
R_f	Ratio of fronts / redardation factor (TLC)
rt	Room temperature
s	Second(s); singlet (peak multiplicity, NMR); strong (intensity, IR)
satd.	saturated
SOMO	Single occupied molecular orbital
t	triplet (peak multiplicity, NMR); tertiary
TBAB	Tetrabutyl ammonium bromide, a phase transfer catalyst
TBAF	Tetrabutyl ammonium fluoride
TFA	Trifluoroacetic acid
THF	Tetrahydrofuran
TLC	Thin layer chromatography
TM	Target molecule
TMS	Trimethylsilyl (acetylene protecting group)
TOAB	Tetraoctyl ammonium bromide, a phase transfer catalyst
TPP	Tetraphenylporphyrin
UV-Vis	Ultraviolett and visible light (often referred to as UV-Vis spectroscopy)
w	weak (intensity, IR)

δ	Greek letter delta: chemical shift (ppm)
ε	Greek letter epsilon: extinction coefficient ($L \cdot mol^{-1} cm^{-1}$)
λ	Greek letter lambda: wavelength (nm)
μ	Greek letter my: micro (10^{-6})
$\tilde{\nu}$	Greek letter ny with tilde: wave number (cm^{-1})
π	Greek letter pi: used for double bonds and delocalized electrons
ϕ	Greek letter phi: quantum yield

Table of contents

1 Abstract

In this dissertation, two unsymmetrically substituted chromophores (porphyrin and perylene) were synthesized and coupled *via* a linear and rigid phenyl-ethynyl-phenyl linker to a dyad. By introduction of a NEWKOME dendron with three or nine negative charges, four novel and water-soluble porphyrin–perylene assemblies were produced for the first time.

The 18 – 21 step synthesis procedure was planned, realized and constantly optimized. Using an improved perylene synthesis cascade with novel purification methods, complex perylene imides were obtained in 80 – 90% yield. A multistep porphyrin synthesis provided unsymmetrical AB_2C porphyrins without scrambling in up to 30% yield.

The four synthesized dyads were systematically analyzed *via* NMR, IR, MS, UV-Vis and emission spectroscopy. The absorption and emission behavior in THF and water indicated a photoinduced excited-state interaction between both chromophores and the formation of a porphyrin$^+$–linker–perylene$^-$ charge-separated state. Energy and electron transfer between porphyrin and perylene were calculated, simulated and measured by spectroscopic experiments. The aggregation behavior could be adjusted by addition of base or by amine/nitrogen compounds (such as pyridine) which were found to coordinate axially to the zinc porphyrin in the dyad.

Kurzfassung

Im Rahmen dieser Dissertation wurden zwei unsymmetrisch substituierte Chromophore (Porphyrin und Perylen) synthetisiert und mittels einer linearen und starren Phenyl-ethinyl-phenyl-Brücke zu einer Dyade verknüpft. Durch Anfügen eines NEWKOME-Dendrons mit drei bzw. neun negativen Ladungen wurden erstmalig vier neuartige und wasserlösliche Porphyrin–Perylen-Systeme hergestellt.

Der 18–21-stufige Syntheseprozess wurde geplant, durchgeführt und durchgehend optimiert. Durch eine verbesserte Perylen-Synthese-Kaskade mit neuentwickelten Aufreinigungsmethoden wurden komplexe Perylenimide in 80 – 90% Ausbeute erhalten. Eine mehrstufige Porphyrinsynthese ermöglichte es, unsymmetrische AB_2C-Porphyrine ohne Scrambling in bis zu 30% Ausbeute zu erhalten.

Die vier synthetisierten Dyaden wurden intensiv mittels NMR, IR, MS, UV-Vis und Emissionsspektroskopie untersucht. Das Absorptions- und Emissionsverhalten in THF und Wasser wies auf eine photoinduzierte Interaktion zwischen beiden Chromophoren und auf die Entstehung eines ladungsgetrennten Porphyrin$^+$–Linker–Perylene$^-$ Zustandes hin. Der Energie- und Elektronentransfer zwischen Porphyrin und Perylen wurde berechnet, simuliert und in spektroskopischen Experimenten nachgewiesen. Das Aggregationsverhalten konnte reguliert werden durch Zugabe von Base oder durch Amin- bzw. Stickstoffverbindungen (z.B. Pyridin), welche axial an das Zink-Porphyrin der Dyade koordinierten.

2 Introduction

2.1 Porphyrins

2.1.1 Porphyrins in Nature

Porphyrins are often counted among the most influencing molecules in nature and certainly belong to the most important organometallic aromatic macrocycles in chemistry. Their occurrence in nature is vast and their role is versatile, ranging from the active metal center in hemoglobin over the well-investigated enzyme Cytochrome P450 up to the green pigments of Chlorophyll, just to name a few (Figure 2.1).[2-5]

All these molecules share a similar active center (often referred to as "heme", originating from Greek αἷμα (*haima*) meaning blood) which mainly consists of a porphyrin (or related structures such as chlorins). The metal in the center can reversibly bind molecules such as oxygen or carbon dioxide and is thus essential for transport, storage, and conversion of oxygen to carbon dioxide and *vice-versa*.[6] This, and the fact that porphyrins are intensely colored, earn them the by-name "the pigments of life".[7]

Figure 2.1. Typical examples of porphyrins in nature: chlorophyll (left) in plants, hemoglobin (right) in blood cells (picture licensed under CreativeCommons, cc by 4.0).[3]

While the periphery can vary strongly, the aromatic center is a fundamental commonality of porphyrins (Figure 2.2). 18 of the 22 π electrons in the ring contribute to the aromatic system, which hence complies with the (4n+2) HÜCKEL rule (Figure 2.2 right, blue). This aromaticity is responsible for the strong color of porphyrins, which ranges from purple and red to green. The four nitrogen atoms in the center are ideal to form chelating complexes with many different metal ions, *e.g.*, Fe, Zn, Mg, Cu, Co, Pd, and many more.[4,8-9] This ability of porphyrins to coordinate metal atoms at the center is the reason why porphyrins belong to the most important and catalytically active molecules in nature. They can be found responsible for the photosynthesis of green plants as well as for the oxygen and carbon dioxide transport in red blood cells of nearly every vertebrate.[4] Myoglobin stores oxygen in the muscles.[10] Cytochromes are essential for electron

transport and catalytic processes.[5] Coenzyme B_{12} (Cobalamin) possesses a large variety of axial ligands coordinating to the cobalt ion in the center and is involved in the metabolism of the cell (mainly DNA synthesis and regulation).[4] Without porphyrins, life on earth would be unimaginable.

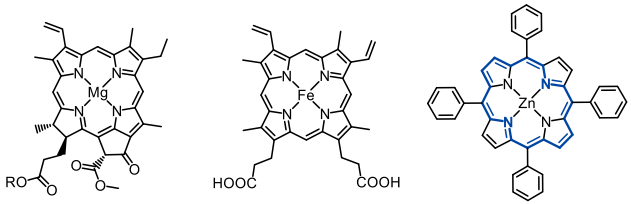

Chlorophyll a | Heme b | Tetraphenylporphyrin

Figure 2.2. Selected porphyrin derivates: Chlorophyll a (left) for CO_2 conversion in green plants, Heme b (center) for oxygen transport in red blood cells, and Tetraphenylporphyrin (right) as basic model compound for all porphyrin systems.[3,10]

Today, many applications have been found which use the intense color, lightfastness, and catalytic activity of porphyrins. Simple porphyrins can be used in biological model systems,[11] in order to understand and adopt the biosynthesis of porphyrins.[7] In photodynamic therapy (PDT), the high absorptivity and photosensitivity of porphyrins is utilized to specifically induce cell death/apoptosis of cancer cells.[12] Additionally, the photoelectronical properties allow the application of porphyrins as sensors,[13] as well as in catalysis,[3] molecular electronics and photonic devices,[14-15] molecular wires,[16] light-harvesting antennae,[17-18] and in dye sensitized solar cells (DSSC).[19-20]

2.1.2 History of Porphyrin Synthesis

The biosynthesis of porphyrins (*e.g.*, heme) is very complex and proceeds over many different reactions in the cytoplasm (formation of porphyrinogen precursors) and in the mitochondria (porphyrin oxidation and insertion of iron by ferrochelatase).[2,7,21]

In the 1920s, HANS FISCHER was the first person to carry the porphyrin into the laboratory. His investigations of blood and leaf pigments as well as the synthetic preparation of haemin were rewarded with the Nobel Prize in 1930.[22] ROTHEMUND discovered in 1935 the formation of porphyrins after reaction of pyrrole and acetaldehyde or formaldehyde in a sealed tube at 220 °C for 48 hours.[23] ADLER and LONGO found an improved synthesis under still rather harsh reaction conditions, using refluxing propionic acid as solvent at 141 °C.[24] From 1986 on, LINDSEY developed new and milder reaction conditions with catalytic amounts of acid (often BF_3 etherate or trifluoroacetic acid) in CH_2Cl_2 at room temperature, and stayed a global player in porphyrin chemistry ever since.[25-33]

A great improvement in porphyrin synthesis was accomplished in 1960 by MACDONALD, who introduced a [2+2] condensation strategy for the formation of porphyrins. Using dipyrromethane building blocks, he paved the way for the synthesis of unsymmetrical porphyrins.[34-37]

2.1.3 Statistical Porphyrin Synthesis via Dipyrromethanes

Dipyrromethanes (DPM) consist of two pyrrole units which are condensed in a nucleophilic addition/elimination reaction with an aldehyde *via* acid catalysis. To improve the yield and suppress polymerization reactions, pyrrole is often used as solvent, causing a 40-200 fold excess compared to the aldehyde.[38-40] To obtain complex and unsymmetric porphyrins, different dipyrromethanes can be employed (Figure 2.3).

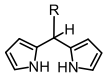

Figure 2.3. A typical dipyrromethane.

Like many pyrrole compounds, DPMs are very prone to polymerization reactions.[41-42] Elevated temperatures as well as the presence of oxygen and light induce the formation of oligomers and polymers which tend to be unwanted reactions. In fact, for a long time DPMs were thought to be too unstable to play a role in porphyrin synthesis.[34] Nowadays, the dipyrromethane condensation reaction is well investigated and belongs to the most significant synthetic pathways for unsymmetric porphyrins.[38,40-42]

The pyrrole ring possesses two different electron-rich carbon positions (α, β) which can undergo nucleophilic reactions (Scheme 2.1). An arbitrary – but acid-stable – aldehyde can be used as reaction partner. The presence of a (LEWIS) acid increases the electrophilicity of the aldehyde carbon and facilitates the nucleophilic addition/elimination reaction.[38] In the course of the reaction, the aromaticity of the pyrrole is temporarily disrupted, forming a transition state with three or two mesomeric structures (Scheme 2.1, blue/red pathway). Thus, the nucleophilic attack from the pyrrole α-position (blue pathway) is kinetically favored over the reaction at β-position (red pathway).[42-43] Elimination of a proton leads to re-aromatization of the pyrrole and a highly unstable intermediate.

The progress of this reaction is time-dependent: in the first 10 minutes, mainly the kinetically favored dipyrromethane is built *via* reaction at the α-position (blue pathway). In contrast, longer reaction times and higher temperatures favor the formation of thermodynamically more stable so-called N-confused dipyrromethanes. These are formed in an equilibrium by nucleophilic attack from the β-position of the pyrrole (red pathway).

Since the formation of N-confused dipyrromethanes would only result in "ill-formed" N-confused porphyrins,[44] it is sought to suppress this thermodynamically favored pathway by using short reaction times, low temperatures and suitable catalysts/solvents.[42]

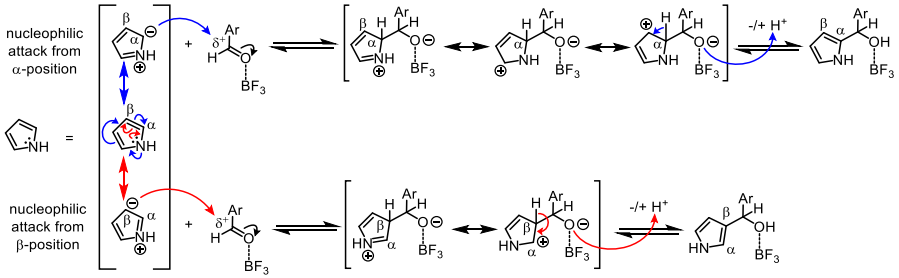

Scheme 2.1. Mechanism of DPM condensation I: Nucleophilic attack from α position of pyrrole (blue) leads to the kinetically favoured transition state.[42]

After the addition of the first pyrrole to the aldehyde (Scheme 2.1), the condensation continues by addition reaction of a second pyrrole unit (Scheme 2.2). Under elimination of another proton and formation of H_2O, the target dipyrromethane is formed. As the reaction perpetuates, tri- and polypyrranes develop.[42,45] This displaces the equilibrium and leads to drastical decrease of the yield. For this reason, an excess of pyrrole has to be used and the reaction has to be stopped by addition of a base (*e.g.*, NaOH) as soon as the starting compound had been consumed completely. The right timing as well as a quick and skilled purification under exclusion of light and air ensures an satisfactory yield (often: 20 – 80%, in this thesis: > 80%).[40,42] The obtained and purified DPMs have to be stored at -10 °C and in absence of oxygen and light.

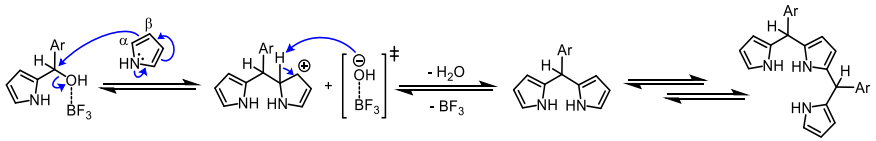

Scheme 2.2. Mechanism of DPM condensation II: A second pyrrole attacks and the DPM is formed under cleavage of H_2O. Longer reaction times lead to tri- and polypyrranes.

Two of these DPMs can be reacted with an aldehyde at identical reaction conditions to form a porphyrinogen ring. This porphyrin precursor is rather unstable and readily forms aromatic porphyrin upon oxidation, usually by air or DDQ.[35,46-48]

2.1.4 Disadvantages of Statistical Porphyrin Reactions

Statistical considerations. Elementary pyrrole/aldehyde condensation reactions are convenient for simple, symmetric A_4 or A_3B porphyrins. The dipyrromethane pathway can easily afford A_2B_2 porphyrins. However, these reaction methods are often not suitable for the formation of more complex porphyrins.[35,49]

Using the mixed-aldehyde approach (Scheme 2.3 left) with pyrrole and two different aldehydes A and B, a total number of $4^2 = 16$ porphyrins can be expected, of which six products are chemically different.[50-51] Three aldehydes A, B and C would lead to $4^3 = 64$ combinations. With PÓLYA's theorem as a combinatorial approach, a distribution of 21 condensed formulas (*e.g.*, AB_2C) can be found.[52-53] Six "combinatorial" isomers are identified, which can be chemically interpreted as constitutional/structural isomers. It has to be emphasized that these combinatorial isomers do not necessarily have to be chemical isomers, as the substitution pattern of the porphyrin may differ. This can be shown for the case AB_2C, which stands for chemically different "cis"-ACBB and "trans"-ABCB porphyrins (*cf.* substitution pattern in Scheme 2.3 center). Hence, the condensation of three different aldehydes with pyrrole indeed leads to 21 chemically different porphyrins.[52]

To increase the yield of the desired ABCB porphyrin (further addressed as trans-AB_2C), the number of (undesired) statistical by-products has to be reduced. The MACDONALD type [2+2] condensation of two different dipyrromethanes (A, C) with two identical aldehydes B leads to four statistical products (ABAB, ABCB = CBAB, CBCB; Scheme 2.3 right).[36-37,54] The desired AB_2C porphyrin could – statistically – be obtained in up to 50% yield.

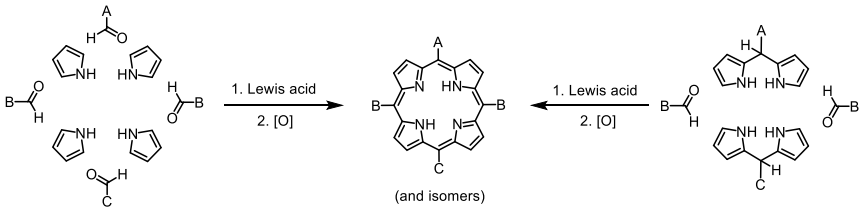

Scheme 2.3. Statistical porphyrin syntheses: Lindsey's method of condensation of pyrrole and aldehyde (left) or a MacDonald [2+2] condensation of two dipyrromethane with aldehyde (right) both lead to porphyrins. A statistical distribution of products is found.

Formation of oligomers. However, the tetramers which are built during the reaction process do not necessarily undergo a ring-closure to cyclic porphyrinogen. Instead, the formation of larger macrocycles or longer oligomers can occur, which drastically decreases the yield.[25] In many cases, the competing formation of these undesired by-products limits the porphyrin yield to 50% or less.[55] In reality, yields in the range of 1 – 15% are regularly obtained.

Scrambling processes. The porphyrin formation reaction is a reversible process up to the point where the porphyrinogen is finally oxidized.[33] Under acid catalyzed conditions, a back-reaction can occur, which also disassembles the individual DPMs. This enables the aldehydes (B) in solution to displace the initially incorporated substituents (A, C). Re-arrangement and subsequent ring-closure leads again to a broad statistical distribution of porphyrin products. This process is called "scrambling" and strongly impedes formation of complex porphyrins by the classical synthetic routes.[40,47,56]

2.1.5 Methods to Suppress Scrambling in Porphyrin Reactions

To suppress scrambling, two different methodologies can be used. First, solvents or reaction conditions can be found which inhibit scrambling reactions while at the same time allow the reaction to proceed towards the porphyrinogen. The use of DPMs with sterically demanding groups (such as mesityl) can suppress the reversibility of the reaction.[37,56] The presence of a few drops ethanol may act as a stabilizer and benefit the formation of porphyrinogen.[10,31] In very special cases, the porphyrin reaction could be performed in alkaline conditions or even without solvent, which also prevents scrambling.[57] The concentration and equivalents of the precursors can be adjusted in order to maximize the yield.[27] Different acids/catalysts, solvents, and additives (such as molecular sieves and other inorganic drying agents to bind water) as well as reaction temperatures were thoroughly investigated.[26-28] The use of microwave irradiation was found to reduce the reaction time and sometimes also decreases the degree of scrambling.[43,58]

As a second method, both scrambling and the formation of statistical by-products can be inhibited by drawing inspiration from naturally occuring porphyrin syntheses:[21] By a sequential approach using highly selective step-by-step reactions (bilanes)[59] or by unsymmetric precursors, more complex porphyrins may be built. Dicarbinols, which can basically be interpreted as intermediates towards porphyrinogen formation (*cf.* Scheme 2.5), are highly reactive and unstable. Hence, different groups are sought as a replacement in order to start the condensation reactions with more stable precursors.

Imines,[60] amines,[46,61] and carboxyl groups,[11] all have in common that the methyl group attached to the α-position of the pyrrol/dipyrromethane is strongly electrophilic and possesses a potential leaving group which can be detached readily (Scheme 2.4). Often, the selective acylation of one of the dipyrromethanes using GRIGNARD reactions,[40,42,62-63] or FRIEDEL-CRAFTS acylations,[41,46,64] is applied to obtain a mono- or dicarbonyldipyrromethane.[8,46,57]

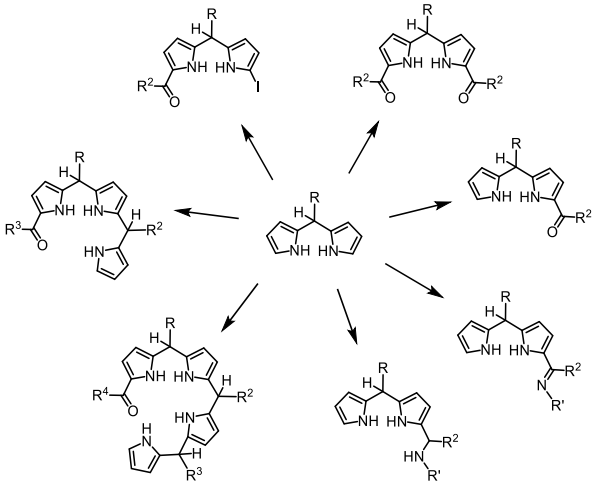

Scheme 2.4. Survey on different methods for porphyrin synthesis: Starting from dipyrromethane, various reactions can be performed to promote the synthesis of unsymmetrically substituted porphyrins.

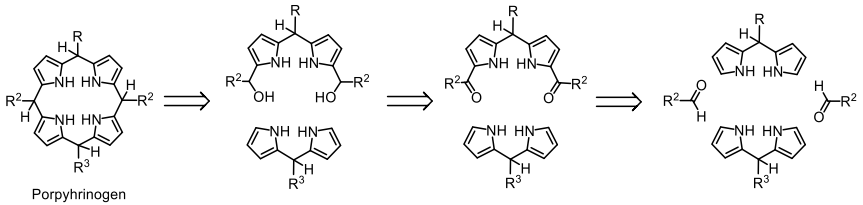

Scheme 2.5. Retrosynthetic approach for a sequential porphyrin synthesis: The porphyrinogen – which can be further oxidized to porphyrin – is formed by condensation of a dicarbinol with a dipyrromethane. The dicarbinol was synthesized from a dicarbonyldipyrromethane which can be derived from a dipyrromethane.

In recent cases, the use of a VILSMEIER acylation variant did also lead to the formation of diphenyldicarbonyldipyrromethanes.[65] The classic VILSMEIER reagent is based upon N,N-dimethylformamide (DMF) which reacts with phosphoryl chloride ($POCl_3$) to give a chloroiminium ion.[66] This VILSMEIER reagent is subjected to an electrophilic aromatic substitution, leading to an arylformate after aqueous workup.

Instead of DMF which leads to formate, REINHARD applied a phenyl amide, namely 1-benzoylmorpholine. When used in a VILSMEIER reaction with pyrrole, the resulting product was a phenylketopyrrole. After reduction, the resulting dicarbinol leads to direct condensation with

other dipyrromethanes under mild conditions. The reverse reactions are suppressed and no by-products are formed (Scheme 2.5).

Overall, a great number of different and highly specialized optimizations were found, including a multitude of acidic catalysts,[26] the addition of salts,[28] gas phase[67] or microwave assisted reactions,[43,58,68] as well as templated syntheses.[29] However, only few alkaline catalyzed, template assisted cyclic condensations with specially prepared dipyrromethanes (*e.g.*, 1-acyldipyrromethane,[57,63] 1-formyldipyrromethane)[62] are known, which limits the scope of porphyrin formation reactions to acid stable groups.[46,60]

2.2 Perylenes

Perylenes are another class of deeply colored dyes. The name "peri-lene" is an amalgamation of the Greek word περί (peri) and naphthalene, meaning: two naphthalene units linked in both *peri* position (Figure 2.4).[69-70] Perylenes were first synthesized by SCHOLL in 1910.[70] The SCHOLL reaction is a coupling reaction between two arene molecules, catalyzed by a LEWIS acid (often $AlCl_3$) under oxidative conditions.[71] In contrast to porphyrins, perylenes rarely occur in nature. To date, perylene quinones were only found in certain liches.[72] However, perylenes and other polycyclic aromatic hydrocarbons (PAHs) can frequently be detected in coal tar and atmospheric particulate matter.[73-76]

Perylenes are highly symmetrical molecules with a D_{2h} point group.[77] They possess a high photostability and thermal stability up to 550 °C as well as an outstanding chemical stability.[78] For example, perylenes are stable against both concentrated sulfuric acid, and molten KOH at 220° C.[79-80] Due to their planarity and large delocalized aromatic systems, perylenes are deeply colored (Figure 2.4).[81] The colors typically range from red to yellow, depending on the molecular structure and the chromophore concentration in solution.[82] Upon excitation, perylenes are highly effective fluorescence emitters with a quantum yield close to unity ($\phi \approx 1$).[78,80,83-85] Additionally, the considerable intermolecular π–π stacking forces lead to a strong aggregation and the formation of varnishes (Figure 2.4).

Perylenes can be functionalized to adjust their properties. Modification of the bay region increases the solubility by weakening the intermolecular π interactions.[81,86-88] Furthermore, the color of the dye can be influenced by various substituents (especially when building push-pull systems with electron rich phenoxy groups in the bay region)[89-90] or by expansion of the delocalized aromatic system.[80,82]

Accordingly, perylenes can be elongated at the *peri* position to obtain higher rylenes, such as terrylenes and quaterrylenes.[81-82,91] Introduction of substituents such as dicarboxylic acid anhydrides or imides leads to a new sub-class of perylenes, the perylene imides. Starting from perylene tetracarboxylic acid dianhydride (PTCDA), simple functionalization reactions allow for a merely inexhaustible scope of new, colorful and highly soluble molecules (Figure 2.4).

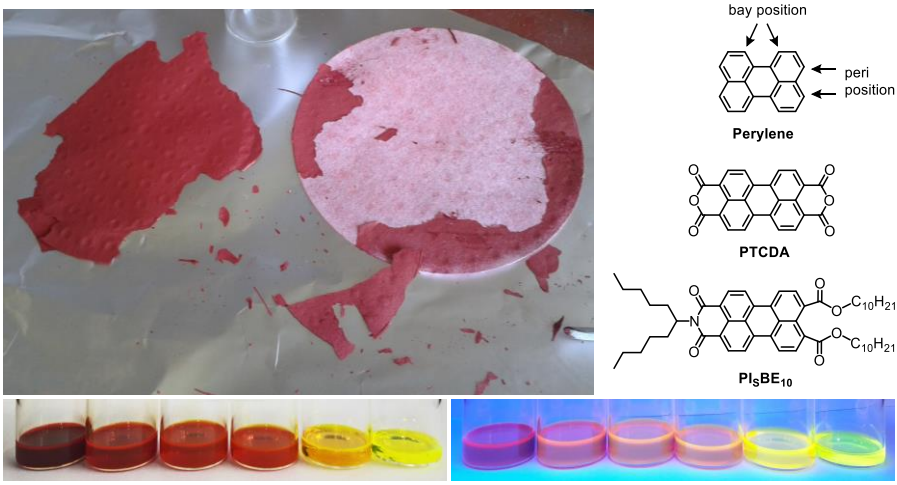

Figure 2.4. Perylenes are a class of pigments which form strongly colored and lightfast varnishes (top left). Selected examples of perylenes are: perylene, perylene tetracarboxylic acid anhydride (PTCDA), and perylene swallowtailimide bisdecylester (PI_5BE_{10}) (top right). The colors of perylenes strongly depend on their concentration (bottom left). Perylenes also possess high fluorescence with a quantum yield close to unity (bottom right).

2.2.1 Reactions of Perylene Dicarboxylic Acid Dianhydride

To adjust the solubility and the properties of perylenes, perylene tetracarboxylic acid dianhydride (PTCDA) is reacted with amines in a condensation reaction to perylene diimide (PDI). The introduction of aliphatic chains drastically increases the solubility with chain lengths of up to 19 carbon atoms. At even higher chain lengths, the solubility decreases again.[80]

The nearly insoluble PTCDA can be successfully solubilized in molten imidazole at 160 °C (Scheme 2.6).[79] Zinc acetate can be used as reaction promoter.[81,84] Depending on the amine compound, the solubility of the resulting PDI is magnitudes higher compared to PTCDA. The increased solubility of the monoimides drives the reaction to completion. This is the reason why only in rare cases unilateral functionalization can be obtained by this reaction.[92]

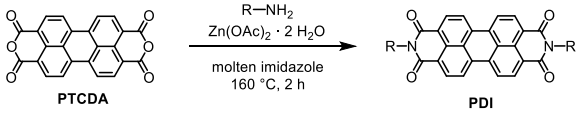

Scheme 2.6. Imide condensation reaction from PTCDA to a perylene diimide (PDI) in molten imidazole.[79]

To obtain unsymmetrically substituted perylene diimides, PTCDA can be reacted with KOH to give the monopotassium salt (Scheme 2.7).[93-94] TRÖSTER first synthesized the dipotassium salt in a warm KOH solution. He then utilized the low solubility of the perylene monopotassium salt:[95] Adjusting the pH to 5.5 with acetic acid precipitates the monopotassium salt in 95 – 98% yield while maintaining the dipotassium salt in solution.[93] Due to the low solubility, this perylene salt can only be characterized by infrared spectroscopy (IR) and mass spectrometry (MS). Subsequently, the perylene monopotassium salt is stirred with the amine at 90 °C for 2 h. The formed peryleneimide monopotassium salt is then converted to the peryleneimide monoanhydride (PIA) and precipitated by addition of HCl. PIA can be obtained typically in 30 – 70% yield.[94,96] Even with exact adjustment of the pH, the formation of PDI and PTCDA cannot be suppressed, leading to a mixture of hardly soluble perylenes which has to be separated by chromatography or selective precipitation. Additionally, solely water-soluble and sterically unhindered amines can be used, which limits the scope of this reaction.[95]

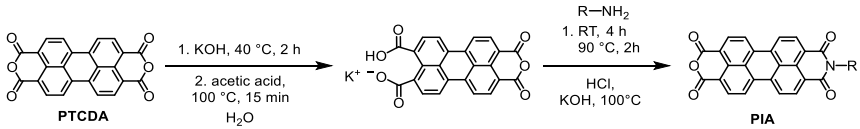

Scheme 2.7. Formation of a perylene monopotassium salt and condensation to a perylene monoimide anhydride (PIA).[93-94]

Another pathway towards PIA would be the unilateral saponification of a symmetrical PDI. NAGAO reacted perylene diimide under strongly alkaline conditions with KOH at 100 °C (Scheme 2.8).[81,94,97] The reaction time is a crucial parameter as the overreaction to PTCDA is fast compared to the first saponification step. The reaction should be stopped after few minutes by adding diluted aqueous HCl solution. Even so, low yields (15 – 40%) are obtained following this pathway and the chromatographic workup of this procedure is very tedious.[81,94]

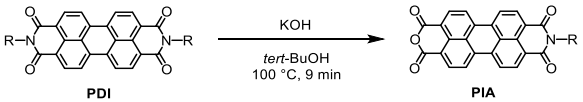

Scheme 2.8. Unlilateral saponification reaction from perylene diimide to a perylene monoimide anhydride.[97]

To counteract these disadvantages, the synthesis can proceed *via* a perylene tetraester (PTE) intermediate. The ester bond is less stable compared to the imide bond and can be cleaved more easily. For example, the ester can be cleaved using sulfuric acid in refluxing acetic acid while leaving the imide unaffected.[98] Additionally, the solubility in organic solvents is improved and the chromatographic separation of different perylenes can be facilitated. PTE can be synthesized using alkaline aqueous conditions and a phase transfer catalyst (Aliquat 336 or tetraoctyl ammonium bromide, TOAB).[81,99] The tetrapotassium salt of PTCDA is converted to PTE either by adding a bromoalkane or an alcohol in the presence of potassium iodide (Scheme 2.9).[100-101]

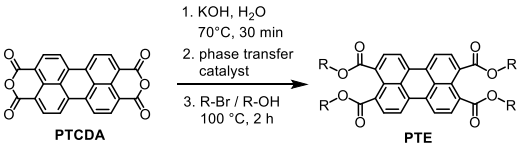

Scheme 2.9. Synthesis of perylene tetraester (PTE) *via* the perylene tetrapotassium salt utilizing a phase transfer catalyst (*e.g.,* Aliquat 336 or TOAB).[81,99]

For the next step, Xue and co-workers developed a selective unilateral cleavage reaction of PTE utilizing the solubility differences between PTE and perylene monoanhydride bisester (PABE) in a well-adjusted precipitation method (Scheme 2.10).[100] PTE is only moderately soluble in a mixture of n-dodecane and toluene (5:1) at 95 °C. Addition of *p*-toluenesulfonic acid monohydrate (*p*-Tos) leads to a hydrolysis equilibrium and the formed PABE is precipitated from the reaction.[100] Using this smart synthesis, yields of 80 – 90% can be achieved.[81] However, the mixture of PTCDA, PTE and PABE has to be purified by tedious column chromatography.

Condensation of an amine with PABE can again be performed by reaction in molten imidazole (*cf.* Scheme 2.6). If needed, the resulting perylene monoimide bisester (PIBE) can now be subjected to a second de-esterification/imidification reaction cascade to form a perylene diimide (PDI) with two different imide substituents.

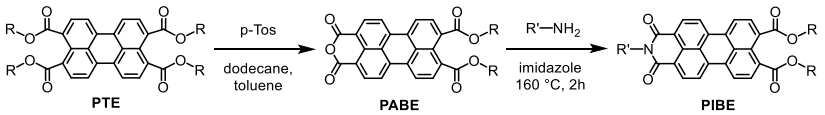

Scheme 2.10. Unlilateral de-esterification of perylene tetraester (PTE) and subsequent imide condensation reaction to obtain perylene monoimide bisester (PIBE). This reaction cascade can be repeated a second time to yield unsymmetrically substituted perylene diimides (PDI).[100]

In 2011, LANGHALS developed a mild and high-yielding one-pot three-step reaction towards unsymmetrically substituted perylene imides (Scheme 2.11).[98,102] At room temperature, insertion of an aliphatic alcohol to PTCDA at reasonably alkaline conditions (1,8-diazabicyclo[5.4.0]undec-7-ene, DBU) leads to a perylene diester diacid intermediate. Two isomers are formed, which however does not influence the further progress of the reaction. Next, an alkylamine (≤ 1 eq) is added and displaces the alcohol at one side. Finally, the residual perylene carboxylic acid functionality is condensed to an ester by adding an alkyl halide. Following this strategy, a perylene monoimide bisester (PIBE) can be obtained with up to three different aliphatic groups (Scheme 2.11).

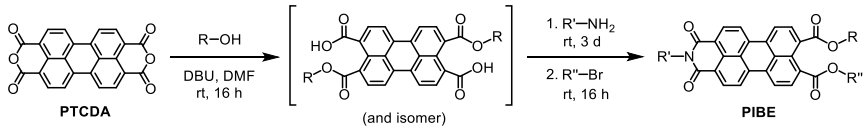

Scheme 2.11. Synthesis of perylene imide bisester (PIBE) starting from PTCDA using the Langhals one-pot three-step reaction: Sequential addition of alcohol, alkylamine and alkyl halide leads to unsymmetrically substituted PIBE in high yield.[98,102]

This reaction has several advantages against conventional perylene reactions:

1. Very mild reaction conditions at room temperature and reasonably alkaline pH.
2. PIBE can be obtained in more than 50% yield (with respect to the amine) in a convenient one-pot reaction.
3. The three products (PIBE, PDI, PTE) are well-soluble and can be separated according to their polarity differences.
4. The aliphatic alcohol and alkyl halide are usually readily available. The often more complex aliphatic amine is converted in high yield.[79]

However, this is only true for aliphatic alcohols, amines and halides. Incorporating arylamines leads to a mixture of PDI and PTE with only traces of PIBE. Additionally, the separation of the perylene products is more difficult, as the polarity differences decrease while the insolubility and aggregation tendency of the perylenes increase. Generally, the LANGHALS reaction leads to optimal results using polar, short-chained alcohols (*e.g.*, ethanol and ethyl bromide) and aliphatic, branched amines.[98] Again, the separation and purification of the perylenes has to be performed *via* column chromatography, and a suitable eluent mixture has to be found.

2.2.2 Industrial Applications of Perylenes

The pronounced low solubility of most perylenes renders them ideal for the application as pigments, where solid particles are dispersed and used to color plastic, ink, paint, fabric and to manufacture blends and varnishes, *e.g.,* for the automotive industry (Figure 2.5).[103-104] In contrast, dyes have to be well-soluble in order to bind evenly and well-distributed to the target which should be colorized (such as paper, leather, wood, textiles).[80,89] Due to their light- and weatherfastness as well as their intense colors, perylenes are counted to the most important class of industrial pigments and are available in many different shades.[104-106] Selected examples are Pigment Red 224 (PTCDA), which is used for industrial paints and particularly for metallic automotive finishes, and Pigment Red 179 (perylene di(methyl)imide), which is used in high-grade coatings and provides both clean shades of red and different maroon/bordeaux shades.[103] Pigment Red 149 (perylene di(3,5-dimethylphenyl)imide) is a bluish red pigment with a melting point above 450 °C and is used primarily in the coloration of plastics (*e.g.,* polystyrene or PVC).[103]

Figure 2.5. Due to their intense red color, perylenes belong to the most important class of paints (left), pigments (center) and coatings (right) for industrial applications.[107]

However, the intrinsically low solubility of perylenes markedly delayed the discovery of other interesting properties.[78] In 1959, GEISSLER and REMY discovered that most perylenes exhibit an intense yellow fluorescence with quantum yields close to unity.[78,84-85,108-109] This high quantum efficiency enables the application of perylenes as molecular detectors,[110-111] fluorescence markers,[83,112] and for the labeling of biomolecules.[87,113] Moreover, perylenes can be electrochemically reduced and oxidized. It was shown that they are ideal electron acceptors and can be charged with up to six electrons.[78,100] Thus, perylene molecules can participate in charge-transfer and redox reactions.[114-115] Perylenes are incorporated in solar cells and donor-acceptor systems as well as in optoelectronics (such as photoelectrical gates/switches and molecular wires).[82,114-123] With their extended aromatic system and high aggregation force, perylenes can furthermore be used for diameter-dependent solubilization and enrichment of carbon nanotubes,[124-128] and the exfoliation of graphene.[129-130]

2.3 Dendrimers and Dendritic Structures

In chemistry, large, tree-like structures consisting of regular, repetitively branched subunits are referred to as "dendrimers".[50] These highly ordered macromolecular systems mimic a tree with branches, which is reflected in the word "dendron" from Greek "δένδρον", which can be translated to "tree". The repetitive and tree-like scaffold of dendrimers is also described by synonymous terms, such as arborols or "cascade molecules".[131]

In the strict definition, a dendrimer is a symmetric macromolecule with a core from which several dendrons (branches) arise. These dendrons can split further in subbranches by an iteratively repeating cascade (called generations), usually forming a more or less well-defined spherical three-dimensional morphology (Figure 2.6). According to VÖGTLE, a pioneer in the field of dendrimers, three different main motifs exist:

(i) a dendron, *i.e.,* a fractal branch with a given functional group at the focal point

(ii) a dendron-substituted or dendronized core unit which is obtained by coupling the dendron to a specific core moiety

(iii) a dendrimer whose structure incorporates multiple dendritic wedges.[131-132]

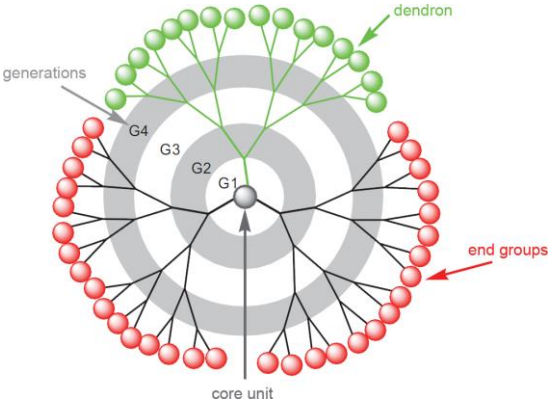

Figure 2.6. Dendrimer with three dendrons (idealized).[133]

There exists a large variety of dendritic molecules. Elongation and branching is usually achieved by means of simple and controllable chemistry, such as the formation of amide bonds,[134] ether formation,[135] MICHAEL addition of amines with acryl nitriles,[132,135] DIELS-ALDER reactions,[136] click chemistry (*e.g.*, azide-alkyne reactions,[137-139] or thiol-yne reactions),[140] or a combination of these methods.[132,141-143]

To prevent formation of oligomers and in order to have full control over the reaction and the products, the dendrimer synthesis often consists of two alternating reaction steps.[132] First, the binding sites have to be activated selectively. Suitable reactions are for example deprotection of ester moieties,[134] or the reduction of nitril or nitro groups to amines.[132,135] Second, the connection of the branching units to the dendron can be the accomplished by means of the methods stated above, then followed by another activation of the new binding sites. Following this cascadic synthesis, large molecules can be built in a very controlled manner. The dendritic generation G is linearly increased with each iterative step, whereas the number of end groups multiplicates as B·G (for B branches at each branching point).[131] To obtain large dendritic structures, the build-up can be divergently (*i.e.,* from the core to the outside), or convergently (*i.e.,* from the periphery to the core).

2.3.1 Divergent Synthesis

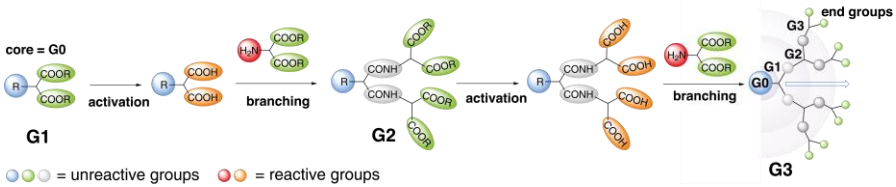

Figure 2.7. Schematic illustration of a divergent, iterative dendron synthesis.[50]

The divergent synthesis starts from a core unit (also called generation 0, G^0), which can be either a single moiety or even a very complex system (such as a porphyrin–perylene dyad in this work). At this G^0 core, a branching unit is added (or already present). After the activation (deprotection/reduction) of these attached end groups, another branching unit can be connected in a subsequent step (Figure 2.7). The dendritic growth proceeds from the core to the exterior.

This controllable and scalable pathway was established by NEWKOME and VÖGTLE,[134-135] and became a standard synthesis method for dendrimers and dendrons. As the growth proceeds, the sterical hindrance between the branching units and end groups increases. This leads to structural errors and vacancies, as not every branching unit can be connected. The purification of these mixtures of structure-perfect and structure-defect dendrimer molecules is virtually impossible as they usually exhibit very similar chemical and physical properties.[140] In cases where the divergent growth strategy can dramatically amplify imperfections and structural defects in dendritic macromolecules, other procedures have to be found.[131]

2.3.2 Convergent Synthesis

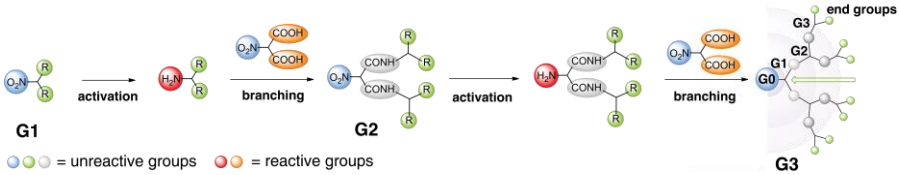

Figure 2.8. Schematic illustration of a convergent, iterative dendron synthesis.[50]

The convergent synthesis, first described by FRÉCHET,[144] begins at the exterior, where independent dendritic branches are grown iteratively (Figure 2.8). As the mass of the branches multiplies at each branching step, the separation of these molecules is often very straightforward. When the completed dendrimer is finally attached to the core, it might occur that this last condensation step fails completely due to sterical hindrance. If that happens, it is often possible to recover the starting compounds, as no reaction took place. In contrast to the divergent synthesis, no semi-defective products are obtained. Another advantage of the convergent synthesis is that fewer reactions per molecule are needed and thus a higher overall yield can be expected, especially regarding the core molecule.[50]

2.3.3 Double Exponential Synthesis

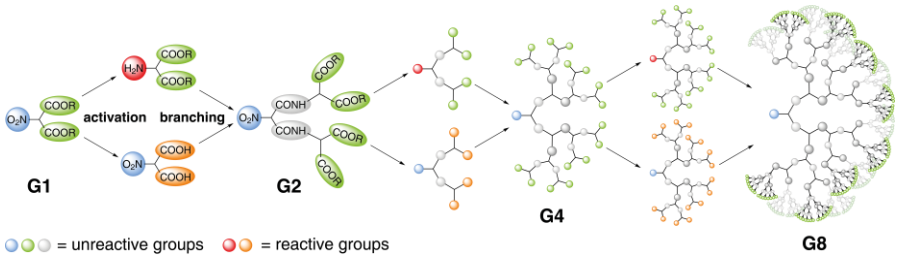

Figure 2.9. Schematic illustration of the double exponential dendron synthesis.[50]

The double exponential dendron synthesis is a way to obtain high-generation dendrimers in few steps, following a bidirectional synthesis both to the periphery and the focal point.[50,131,145] A branching unit with independently accessible protected end groups (*e.g.*, esters) and core functionalities (*e.g.*, nitro group) is required. In two separate reactions, the protected branching unit is activated either at the end groups (*e.g.*, hydrolysis to acid moieties) or at the core (*e.g.*,

reduction to an amino group). The thus obtained molecules can be condensed in a controlled manner. Iteration of the separate and independent deprotection followed by condensation leads to doubling of the generation with an exponential increase in mass (Figure 2.9). With the double exponential synthesis, large dendrimers can be obtained in a very efficient and convenient manner.[131]

2.3.4 Newkome Dendrimers

Many chemists in the HIRSCH group rely on NEWKOME-type dendrons which are attached to a large variety of (usually hydrophobic) core molecules.[50,77,124-127,129,146-152] The increasing number of acid groups (3, 9, 27, *etc.*) leads to a good and scalable water-solubility at high pH values (when acids are deprotonated) while retaining a certain degree of hydrophobicity at low pH values (Figure 2.10). Strong adsorption onto nanoparticles and formation of lipid layers can also be realized since the acid groups are closely located. Moreover, the stability of amide bonds and the broad scope of amine-acid-coupling reactions keep presenting the prospect of NEWKOME dendrimers as versatile and easily accessible branching moieties.

The IUPAC nomenclature of dendritic systems can be very complicated and unintuitive. Usually, it is not essential for dendrimers to find the longest chain, rather than finding a structure of repeating and self-similar units and the segmenting in different generations.[132] Therefore, proposals have been made by NEWKOME in 1993,[153] revised and extended by the VÖGTLE group in 2006,[132,154] to simplify the naming of dendrimers and dendritic structures. In this thesis, the NEWKOME Cascade-nomenclature was used for labeling the G^2 dendrons.

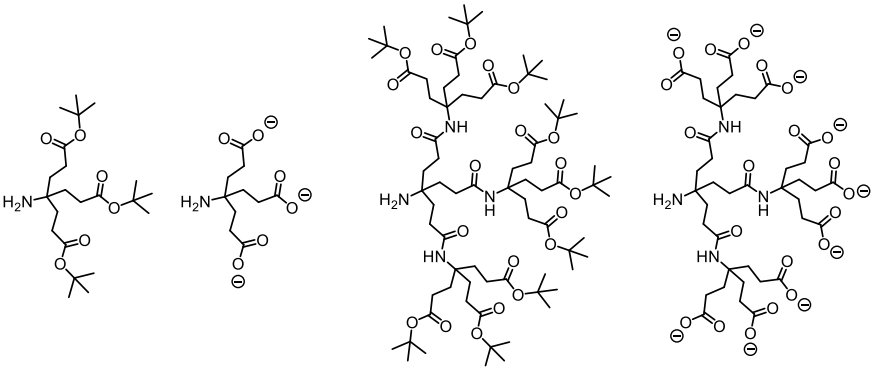

Figure 2.10. Protected and deproctected water-soluble Newkome dendrons of first (left) and second (right) generation.

2.4 Porphyrin–Perylene Donor–Acceptor Systems

The research both on porphyrin and perylene chemistry is vast and well-established. However, although porphyrins and perylenes are such interesting molecules, the field of porphyrin–perylene assemblies still is relatively new and emerging.[155] Incorporating porphyrins and perylenes into one molecule provides interesting assemblies and photonic systems. Porphyrins with a high-lying HOMO can be used as electron donors, while perylenes are ideal compounds for electron acceptors (Figure 2.11). Indeed, the number of publications for porphyrin–perylene donor–acceptor systems increased strongly over the last twenty years. As new synthetic methods were developed, unsymmetric and more complex porphyrin–perylene assemblies became accessible and moved into focus.

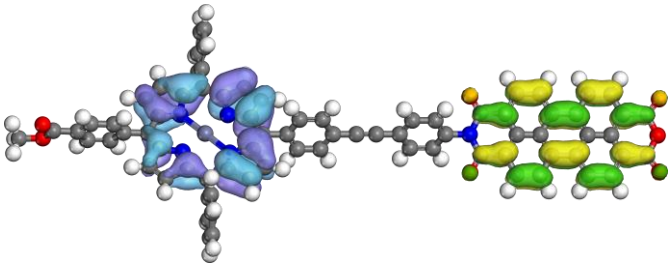

Figure 2.11. A model compound of a porphyrin–perylene dyad. It is calculated that the HOMO lies at the porphyrin (blue) while the LUMO is located at the perylene (green).[156]

2.4.1 Porphyrin–Perylene Assemblies in the Literature

A porphyrin-PDI-porphyrin triad (Figure 2.12a) and a porphyrin-PDI-trypticene dyad were synthesized by WASIELEWSKI and co-workers in 1992 using a simple perylene condensation reaction in molten imidazole.[157] It was found that from the excited porphyrins (3.8 eV *vs.* a satd. calomel electrode in pyridine) a charge-transfer to the perylene monoanion (3.3 eV) and the perylene dianion (3.0 eV) occured on a picosecond time scale. Further complex porphyrin–perylene assemblies were synthesized in the WASIELEWSKI group in the following decade.[158-159] In 2004, the WÜRTHNER group devised several zinc porphyrin–perylene imide dyads and triads (Figure 2.12b).[160-161] The self-assembly behavior in $CHCl_3$ was investigated utilizing amine ligands (bipyridine and perylene diimide) which coordinated axially to the metal center.[162] A linear perylene-bis(porphyrin)-phthalocyanine array was developed by the LINDSEY group in 2000, building a highly complex donor–mediator–acceptor light-harvesting system with long-distance ultrafast energy-transfer dynamics (Figure 2.12c).[163] The LINDSEY group also devised a series of perylene–porphyrin dyads which were coupled – amongst others – *via* a phenyl-ethynyl-phenyl linker. They observed fluorescence quenching upon formation of charge-transfer states with lifetimes of several nanoseconds (Figure 2.12d).[15,164-167]

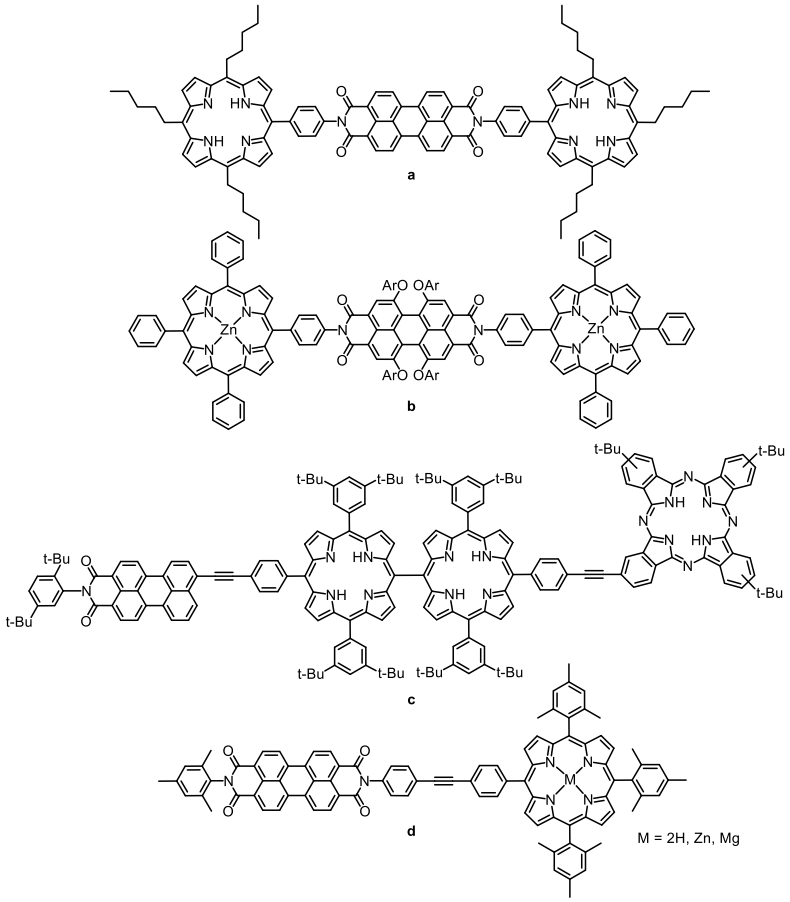

Figure 2.12. Different porphyrin–perylene charge–transfer systems found in the literature: a porphyrin-perylene-porphyrin triad (a),[157] a triad with two zinc porphyrins (b),[160-161] a perylene-bis(porphyrin)-phthalocyanine array (c),[163] and a series of phenyl-ethynyl-phenyl bridged perylene–porphyrin dyads (d).[15,164-167]

2.4.2 Light–Harvesting of Porphyrin–Perylene Assemblies

Porphyrin–perylene dyads possess an enhanced light-harvesting ability: they absorb visible light in a wide spectral range.[168-169] The great potential of these assemblies for organic photovoltaics has been proven by calculations,[170-172] as well as in experiments yielding power conversion efficiencies of up to 7.4%.[173-175] In the last years, especially the LINDSEY group concentrated on the electronic interactions between porphyrins and perylenes and their application in dye sensitized solar cells (DSSC).[176-180]

2.4.3 Self-Assembly of Water-Soluble Porphyrin-Perylene Systems

Despite these interesting and promising progresses, to date no effort has been made to synthesize water-soluble porphyrin–perylene systems. PARQUETTE developed a water-soluble naphthalene-porphyrin-naphthalene bolaamphiphile which assembled to hollow, nanotubular structures in MeOH/H_2O with diameters of 13.6 nm and wall thicknesses of 4.6 nm (Figure 2.13).[181-182] In general, amphiphiles can self-arrange to lipid membranes, micelles, vesicles,[182-183] but also to more complex nanorods,[184-185] or nanotubular structures.[181,186-190] In membranes and self-assembled molecular structures, energy transport from one molecule to another is possible.[185,191] This was shown by WANG, who investigated the intermolecular electronical interactions between the non-covalent self-assembly of a negatively charged porphyrin with a bis(β-cyclodextrin) PDI in aqueous phosphate buffer (Figure 2.14).[192]

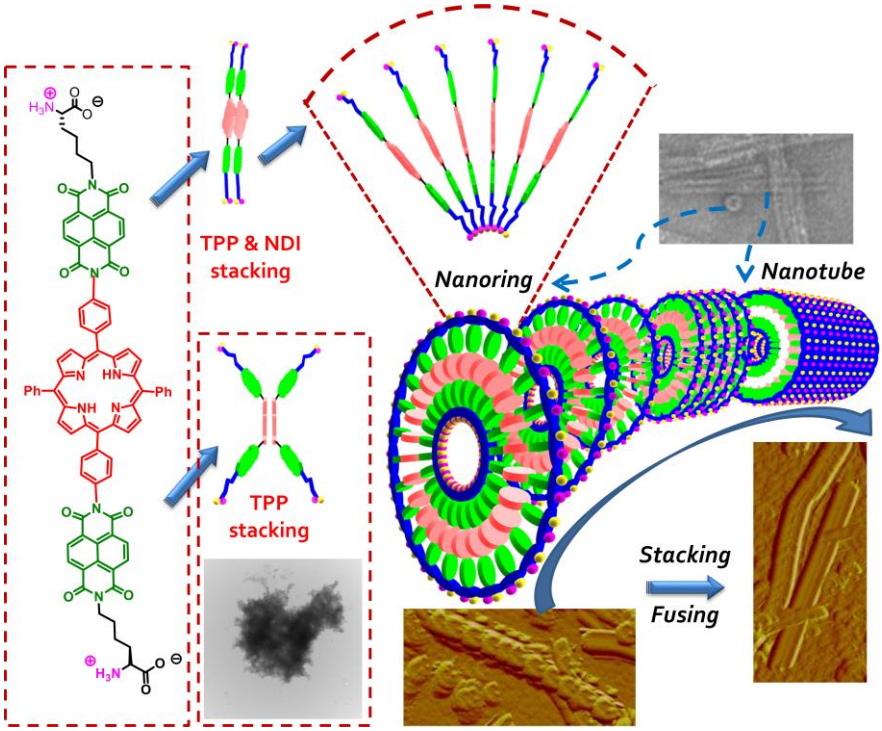

Figure 2.13. A symmetric, water-soluble naphthalene-porphyrin-naphthalene bolaamphiphile was synthesized by the Parquette group.[181] Self-assembly to stacked aggregates and nanotubular structures was observed.[193]

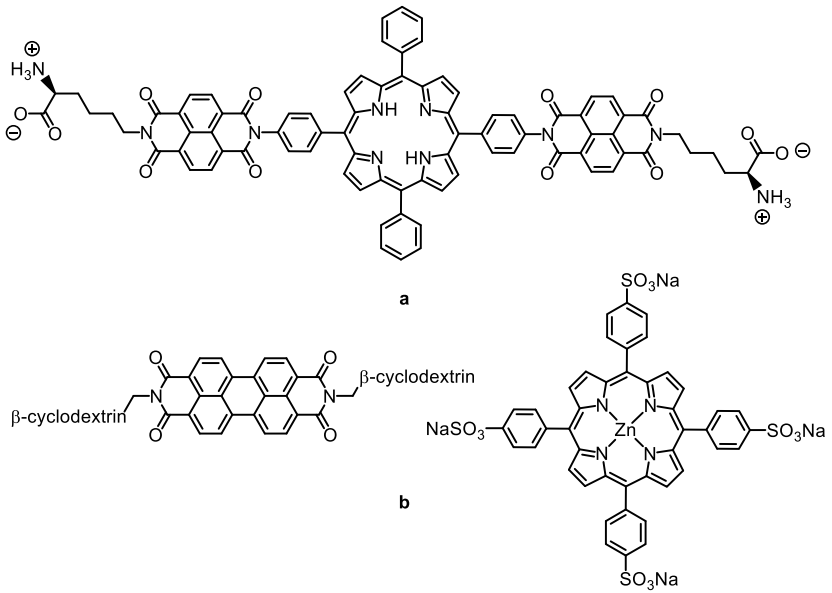

Figure 2.14. No water-soluble porphyrin–perylene dyad has been published to date. Parquette developed a naphthalene-porphyrin-naphthalene triad (a, see Figure 2.13).[181] A non-covalently linked, self-aggregated system of a water-soluble bis(β-cyclodextrin)-PDI and a simple water-soluble zinc porphyrin was investigated by Wang and co-workers (b).[192]

A survey on possible aggregation patterns of amphiphilic porphyrin–perylene dyads is depicted in Figure 2.15. For clarity, the complex chemical structure of the dyad is simplified as a schematic representation. The proportions and spacings do not correspond to reality. The sub-structures of the dyad are colored (porphyrin: purple, perylene: red, linker: grey, aliphatic chain: green, hydrophilic head: blue). It is energetically favored that the large hydrophobic part of the dyad aggregates in polar media to minimize the exposition/interaction of these parts to the solvent. For one part, this can be accomplished by self-assembly to lipid bilayers similar to membranes in human cells (Figure 2.15 top). When taking into account that the steric demand of the polar dendron and the porphyrin (with its phenyl groups twisted at around 90°) is greater than the steric demand of the flat perylene and the linear hydrocarbon chains, it is reasonable to expect that the membrane is not completely flat. Instead, the bilayer may be bent to spherical shape (vesicle) or even self-assemble to nanotubular structures (*cf.* Figure 2.13). The bending of a monolayer would lead to micelles or single-walled nanotube aggregates, where the hydrophilic head would lie at the outside and the lipophilic tail would arrange at the inside. The radius of these spheres or columns strongly depends on the steric demand ratio of the sub-parts. It is probable that the radius could be adjusted by adding axially double-coordinating spacers (*e.g.*, pyrazine or 4,4'-bipyridine) which could further increase the distance between two zinc porphyrin units.[162]

Additionally, the strong π–π stacking tendency of the perylenes could lead to a columnar assembly with stacked perylenes in the center. The sterically more demanding porphyrin and dendron would arrange at the exterior of this column in a helical order (Figure 2.15 bottom right).

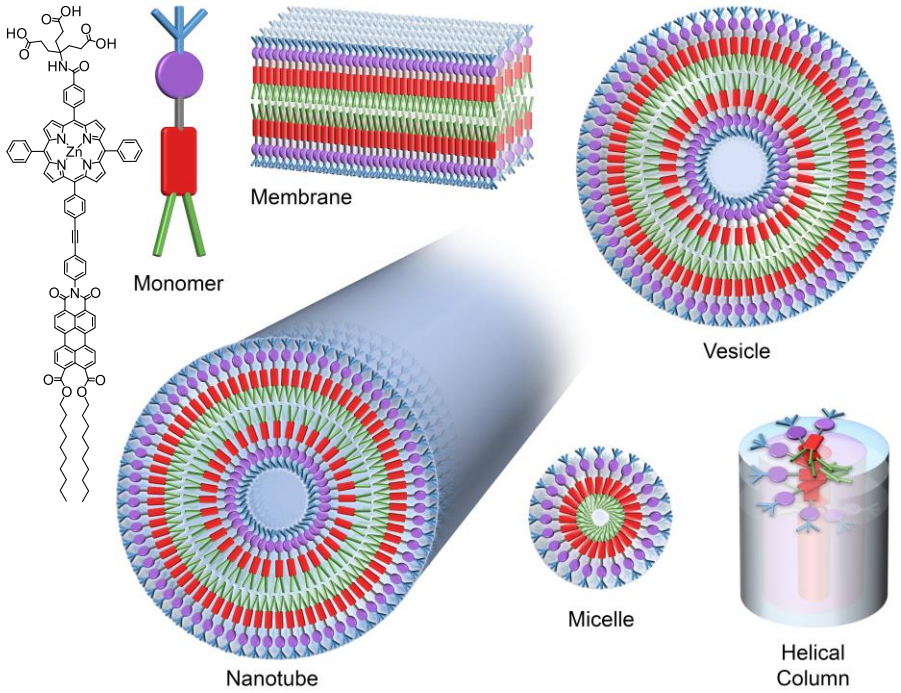

Figure 2.15. Theoretical survey on possible aggregation patterns of an amphiphilic porphyrin–perylene dyad in polar media: Structural and schematic representation of a dyad monomer (left). Possible aggregation to lipid bilayers/membranes (top) or vesicles (right). Nanorings (monolayer or bilayer) could assemble to nanotubular structures (bottom left, *cf.* Figure 2.13). Other aggregation patterns could be spherical micelles with a hydrophobic core (bottom center) or π stacked columnar structures (bottom right). In this case, a helical columnar aggregate would be most probable owing to the π stacking affinity of perylenes as well as the distinct steric demands of the dyad sub-structures (*i.e.*, porphrin, perylene, aliphatic chain, hydrophilic dendron).

In conclusion, porphyrin–perylene dyads show promising properties as models of photosynthesis and photocatalysis. Many different molecules combining both porphyrins and perylenes have been synthesized and characterized.[15,164-167] But until today, no water-soluble and linearly linked porphyrin–perylene dyad is found in the literature. Both the aggregation behavior and the optoelectronics of these dyads in water are promising fields of research which are yet unexplored: In water, these dyads could self-assemble to micellar, lamellar, or more complex nanotubular structures. The optoelectrical behavior and charge-transfer capabilities of these structures in polar media would be a valuable contribution to current research.

3 Proposal

In this thesis, a total synthesis should be developed to create a comprehensive set of linearly-linked porphyrin–perylene dyads **1a-d** carrying hydrophobic alkyl chains and an unilateral functionalization with a NEWKOME dendron (Figure 3.1). To investigate the characteristics of the molecules, several structural features should be varied and compared: Attaching a NEWKOME G^1 (**1a,c,d**) or G^2 (**1b**) dendron should influence the water-solubility and the aggregation behavior of the dyad by inducing additional sterical hindrance. The hydrophobic tail should be constructed of either two decyl ester chains (**1a,b,d**) or a branched aliphatic swallowtail imide (**1c**) to investigate if the solubility in organic solvents and the self-assembly of the amphiphile in polar media can be controlled. Additionally, the zinc ion at the porphyrin center should be removed (**1d**).

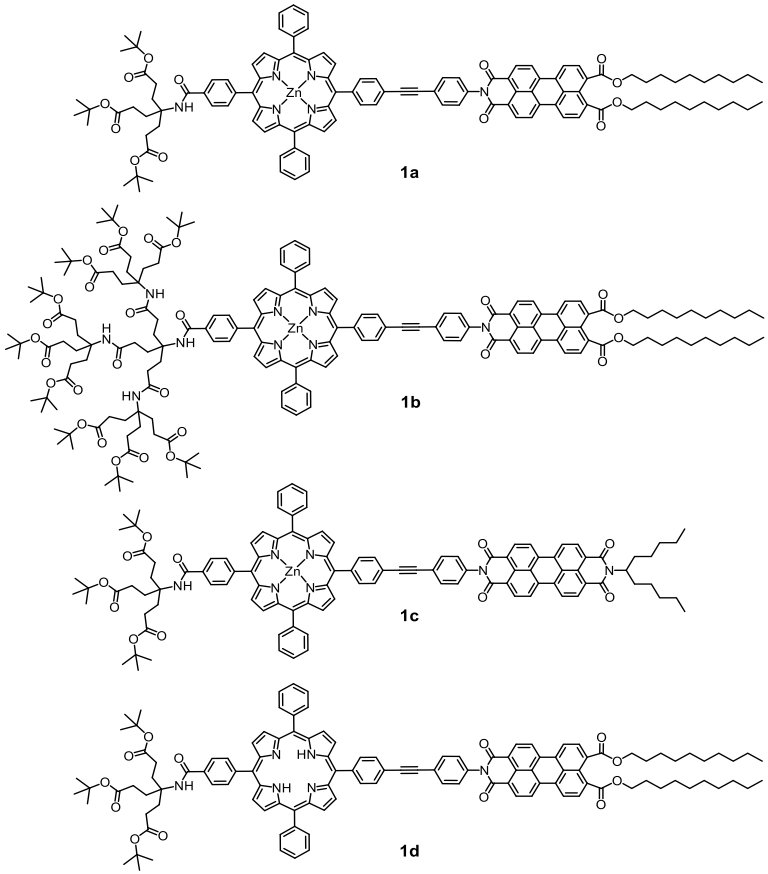

Figure 3.1. Porphyrin–perylene dyads with appended Newkome dendrons of G^1 (**1a,c,d**) and G^2 (**1b**) containing *tert*-butyl protected ester terminal groups. The hydrophobic decyl chain is modified to a branched swallowtail group (**1c**) and the zinc at the porphyrin is removed (**1d**) to create a comprehensive set of porphyrin–perylene dyad target molecules.

The four porphyrin–perylene dyads are expected to possess distinct optoelectrical features by modification of the electronic HOMO–LUMO structure. Finally, the selective deprotection of the NEWKOME dendrons should lead to the corresponding water-soluble target molecules **2a-d** (Figure 3.2). These dyads are expected to exhibit water-solubility at pH > 7 as well as characteristic features of both porphyrins and perylenes.

To complete this dissertation, an in-depth characterization should be performed to verify the successful synthesis and the structure of the dyads. The amphiphilic character should be investigated by solubility studies. Additionally, preliminary spectrophotometric analyses and semiempirical HOMO–LUMO calculations should be performed to outline the spectroscopic and optoelectronic properties and to investigate the possibility of charge-transfer states for these dyads.

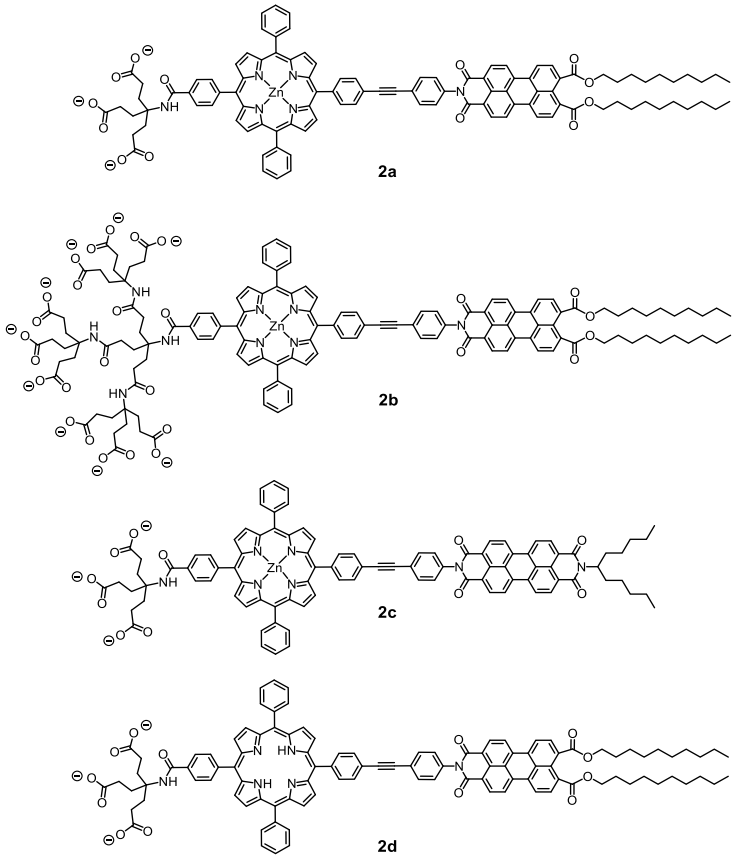

Figure 3.2. Porphyrin–perylene dyads with appended Newkome dendrons of G^1 (**2a,c,d**) or G^2 (**2b**) containing three or nine carboxylic acid groups, respectively. At pH > 7, increased water-solubility is expected by deprotonation of the carboxylic acids to carboxylate groups. The branched swallowtail alkyl chain (**2c**) and the free-base porphyrin (**2d**) complement the comprehensive set of water-soluble, amphiphilic porphyrin–perylene dyad target molecules.

4 Synthesis Strategy

4.1 Retrosynthetic Analysis

To find the best synthesis strategy and optimal starting materials, the target molecule **1b** was retrosynthetically analyzed (Scheme 4.1).[194] Different approaches have been drafted, tested and discarded (red).[195] To maintain clarity, only the successful retrosynthesis to the final target compounds is discussed in detail (green).

Disconnecting at the acetylene linker (a or b) would be ideal since the combination of different porphyrin and perylene components would lead to a large variety of different products by a simple C-C connection (*e.g.*, SONOGASHIRA reaction) as a last reaction step. Moreover, a modification of the linker (*e.g.*, using double acetylene bridges) could be easily accessible. In contrast, disconnection at the perylene imide position (c) would require the synthesis of a complex porphyrin with the linker already attached. This would limit both the scope of easily available porphyrin compounds and the diversity of the linker. On the other hand, variations of the perylene compounds could then be accomplished with less synthetic effort.

The NEWKOME G^2 dendron would be cleaved at the tailored amide bond (d) and deconstructed *via* functional group interconversion (FGI) of the amine to a nitro function (e). The G^2 dendron would then be disassembled to the NEWKOME G^1 dendrons in a convergent approach (f, see chapter 2.3.2, p. 17). Further deconstruction according to the literature would lead to the commercially available precursors *tert*-butyl acrylate and nitromethane (g).[134,196]

To obtain the porphyrin component, several retrosynthetic disconnections would be feasible (h). The condensation to the porphyrin should be successfully accomplished using either a combinatorial approach, different dipyrromethane-based synthesis strategies, or a well-defined stepwise synthesis (i, see chapter 2.1, p. 4ff). In theory, the acetylene linker (j) could be attached subsequent to the porphyrin formation. As stated above, the linker should generally be introduced as late as possible in the synthesis pathway to provide easy access to a potential variation of target molecules. The dipyrromethanes could be further deconstructed to aldehydes (k, l). The linker at the aniline-acetylene DPM could be cleaved either at the DPM or the aniline site (m). Both pathways would finally lead to a halogen aldehyde and a halogen aniline (n) as precursors.

Disconnection of the perylene at imide position (c) would lead to a mono-substituted perylene diester anhydride (o, see chapter 2.2.1, p.10ff). From there, cleavage of the esters would result in PTCDA as starting compound (p). The retrosynthetic cleavage both at the imide or ester positions of the perylene is promising, as it enables the straightforward formation of several perylene compounds bearing different imides and esters. For example, instead of targeting a perylene monoimide diester, a perylene diimide could be designed. Furthermore, the length or structure of the aliphatic chains (q) could easily be modified, and other functional groups (*e.g.*, hydrophilic NEWKOME dendrons) could be attached.

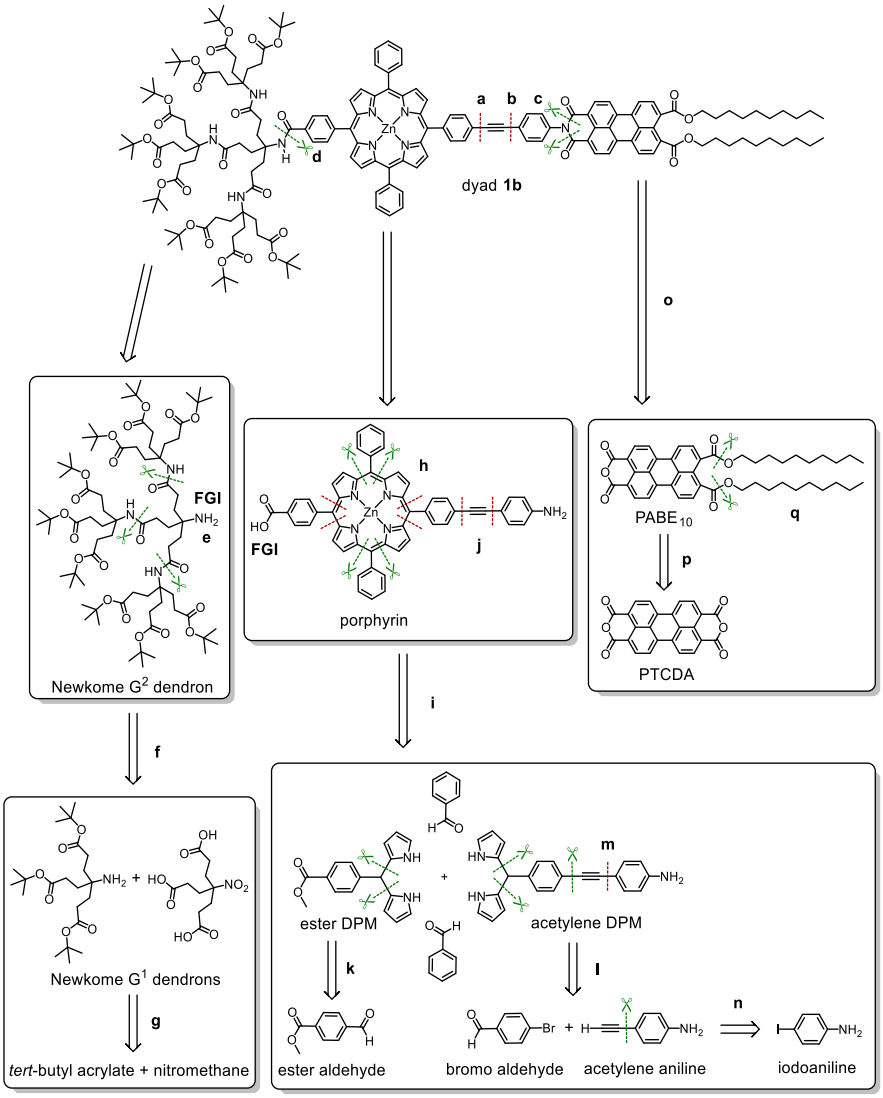

Scheme 4.1. Retrosynthetic strategy: target molecule **1b** is disassembled to commercially available precursors. Different retrosynthetic approaches were evaluated (a-q). Disassembly at the red marks was tested and discarded, as the synthesis did not lead to the target molecule. The Newkome G^2 dendron is deconstructed to Newkome G^1 dendrons (f) and further disassembled to *tert*-butyl acrylate and nitromethane (g). The porphyrin (h) is deconstructed to two DPMs and benzaldehyde (i). Further cleavage of the DPMs leads to commercially available aldehydes (k, l) and iodoaniline (n). The perylene can be cleaved *via* a perylene anhydride bisdecylester (o) to PTCDA (p). See text for further in-depth discussion.

4.2 Orthogonal Protecting Group Strategy

Already at an early stage of the synthetic concept it became apparent that the use of an elaborate orthogonal protecting group strategy would be essential. Acidic, alkaline, reductive and other sensitive reactions would be performed during the whole synthesis sequence (Scheme 4.2). It was of greatest importance that sensitive moieties such as acetylenes, amines, acids and anhydrides could be protected and deprotected independently, according to the requirements of the synthesis pathway. This required a diligent fine-tuning of the reaction conditions and the discovery of new protection/deprotection methods.

Aldehydes – which are reactive towards acid catalyzed nucleophilic substitutions – are the basic elements in porphyrin synthesis (Scheme 4.2 a).[197] Together with pyrrole as a counterpart – which usually undergoes acid catalyzed electrophilic substitutions (b, c) – dipyrromethanes and porphyrins can be formed.[25,198] Hence, when working with aldehydes and pyrroles, the application of (LEWIS) acid has to be limited and acid-stable carboxyl protecting groups have to be used (d).[199]

Applying the stepwise porphyrin synthesis procedure *via* dicarbinols established by Anja Reinhard,[65] the ester DPM would first be condensed to a diphenyl diketone DPM (e) and subsequently reduced to a dicarbinol (f). Therefore, a mild reducing agent has to be found to reduce the aromatic ketones while maintaining the aromatic methyl ester during the stepwise porphyrin synthesis. As the dicarbinol is very reactive towards polymerization and nucleophilic attack, it cannot be stored for longer times.

For the acetylene DPM, the base labile trimethylsilyl (TMS) protective group would be applied to prevent the acetylene unit from polymerization reactions (g).[200] Additionally, the amino function has to be protected by a *tert*-butoxycarbonyl (Boc) group in order to perform the following SONOGASHIRA reaction in high yields and turnover numbers without poisoning the catalyst (h).[201] The amino protecting group has to be stable both in alkaline and slightly acidic conditions to allow the base-driven deprotection of the TMS acetylene (i), as well as the (LEWIS) acid catalyzed stepwise synthesis to the DPM (j) and porphyrin. Carboxybenzyl (CBz) protective groups or the hydration of a nitro group proved to be unsuitable alternatives, since the acetylenic triple bond (k) would be affected by the deprotection under reductive conditions.[201]

Condensation of the dicarbinol and the acetylene DPM under LEWIS acidic conditions with subsequent oxidation leads to the porphyrin (l), bearing a reduction labile acetylene bond, a base labile methyl ester, an acid labile Boc protective group, and inner pyrrolic N-H groups which could coordinate to metal ions.

Next, the Boc group has to be cleaved while leaving these different reactive groups unaffected (m). For this purpose, a novel entropy driven deprotection mechanism was found and optimized,[202-203] which allows the separation of the Boc group at elevated temperatures under vacuum conditions (*cf.* p. 49).

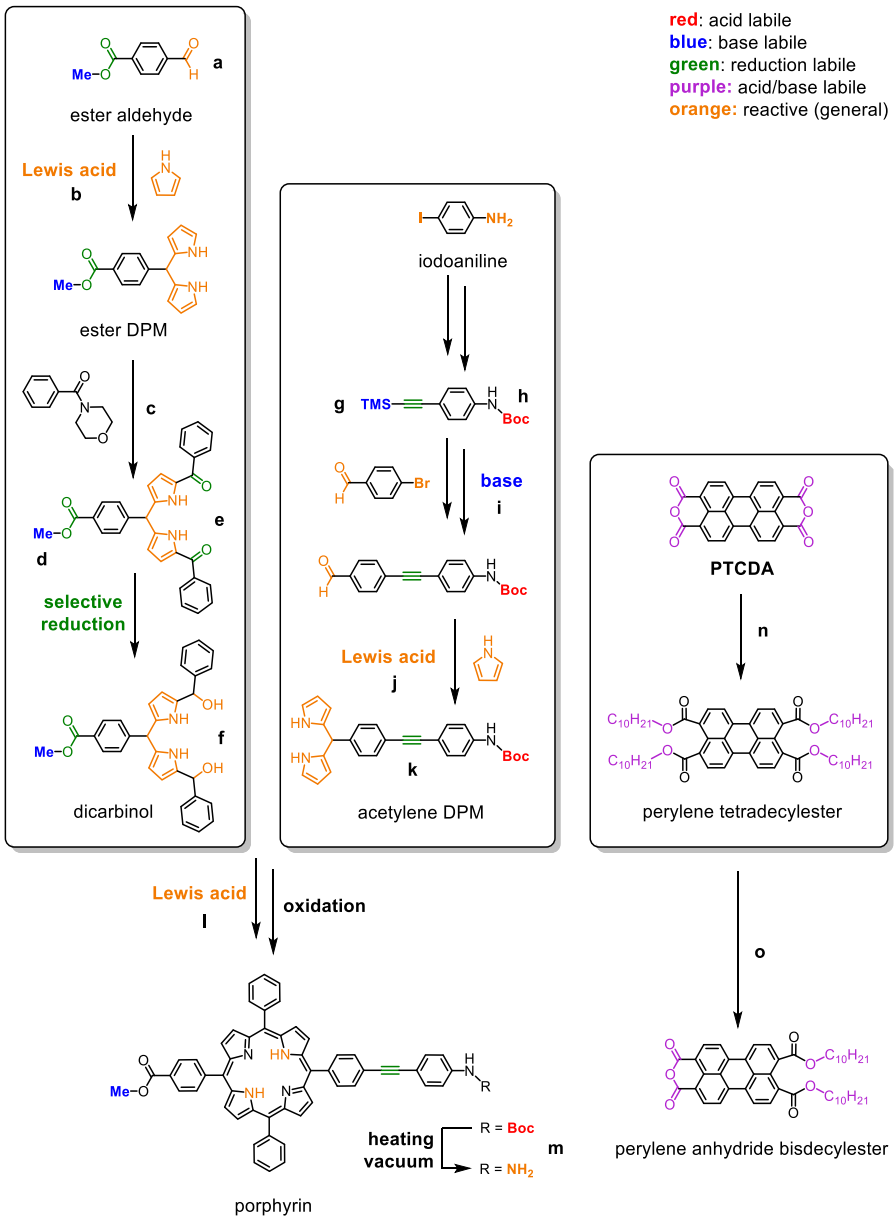

Scheme 4.2. Orthogonal protecting group strategy I: Stepwise synthesis of acetylene DPM and ester DPM, followed by subsequent conversion to porphyrin (left) as well as reaction of PTCDA to perylene anhydride bisdecylester (right). The distinct reactive groups are differentiated, highlighted and protected when necessary. See text for further in-depth discussion.

Perylene monoanhydride bisdecylester ($PABE_{10}$) was planned to be synthesized starting from perylene tetracarboxylic acid dianhydride (PTCDA; Scheme 4.2 n). The reactive anhydrides can be converted to esters or imides using acid or base catalysis (*cf.* chapter 2.2.1, p. 10ff). If the LANGHALS one-pot three-step reaction would not lead to the desired unsymmetrically substituted perylenes,[98] it was envisaged to unilaterally cleave the perylene tetraester using XUE's acid catalyzed hydrolysis-precipitation method (o) to yield perylene monoanhydride bisdecylester ($PABE_{10}$).[100] Here, the diverging aggregation behaviors and the reactivity differences between anhydride, esters and imides are applied to obtain the desired compounds.

The porphyrin and perylene components should then be linked and the porphyrin should be metallated using standard perylene condensation methods in molten imidazole (Scheme 4.3 p).[79] This specific reaction should only induce imide formation without affecting the other reactive groups. To attach the NEWKOME dendrons, the base labile methyl ester on the porphyrin has to be cleaved (q). It can be expected that under controlled alkaline conditions the longer decyl ester groups at the perylene would be more stable than the methyl ester.[199] However, exact chemicals and conditions have to be identified and tested.

The NEWKOME dendrons of first and second generation can be synthesized according to the literature-known protecting group synthesis procedure.[134,196] If both the carboxylic acids and the amine compounds of the NEWKOME dendron were unprotected, the DCC amide coupling reaction would lead to uncontrollable polymerization. Instead, two different dendrons have to be applied: First, a dendron with acid labile *tert*-butyl ester protective groups and an unprotected reactive amine. And second, a dendron with unprotected carboxylic acids and a nitro protective group, which could be converted to an amine by reduction. Coupling of the two different first generation dendrons leads to the second generation NEWKOME dendron in a controlled manner (Scheme 4.3 r, *cf.* chapter 2.3, p. 15ff).

In another specific DCC amide coupling reaction, the thus prepared NEWKOME dendron (G^1 or G^2) should then be attached to the dyad (r). As a final step, the porphyrin–perylene dyad has to be rendered water-soluble by hydrolysis of the NEWKOME *tert*-butyl esters (s). Both the *tert*-butyl/decyl esters and the coordinated Zn ion are sensitive to acidic conditions. However, it can be expected that stirring in formic acid would be sufficiently mild to cleave only the *tert*-butyl esters of the NEWKOME dendrons.[134,196] The total synthesis of the dyads **1a-d** and **2a-d** (*cf.* p. 24f) using this drafted synthesis pathway will be presented and discussed on the following pages.

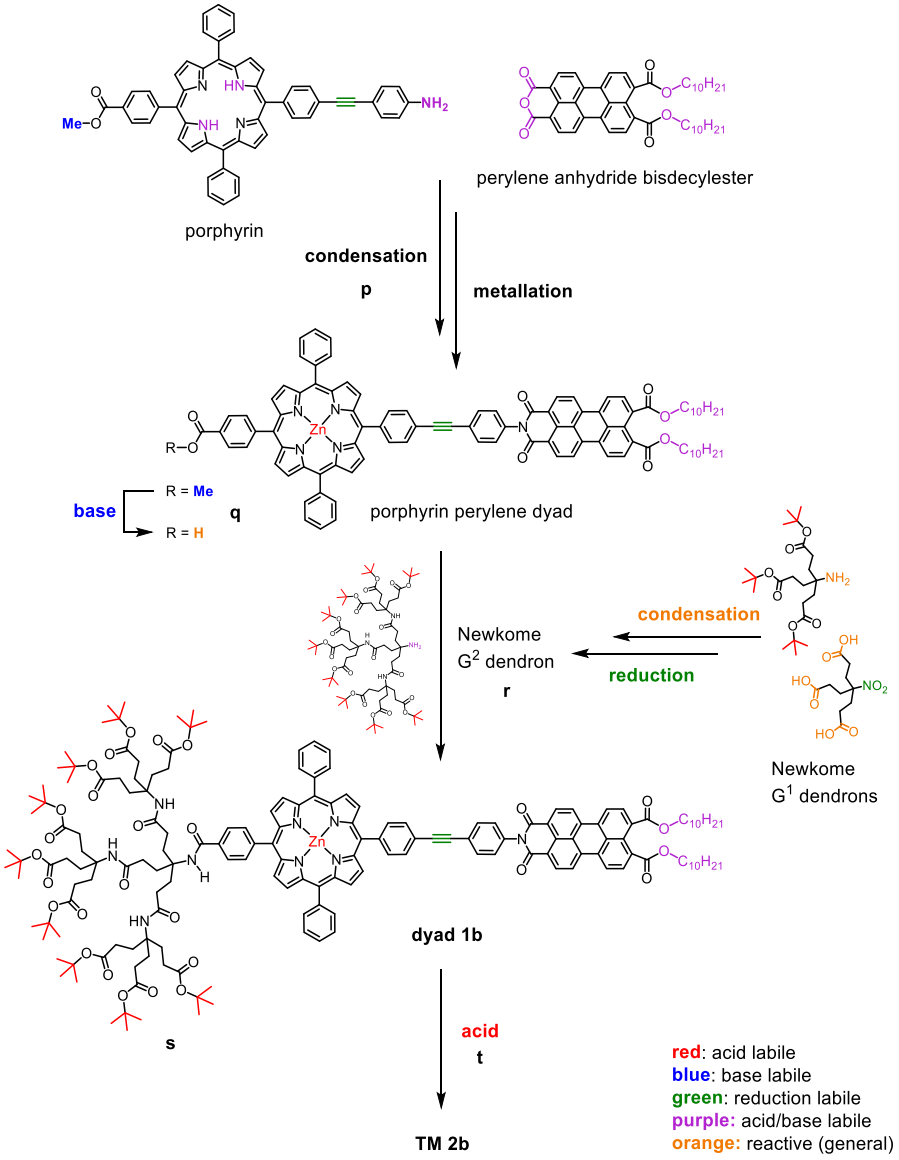

Scheme 4.3. Orthogonal protecting group strategy II (continued): Condensation of porphyrin and perylene with subsequent attachment of a Newkome G^2 dendron leads to dyad **1b**. This dyad can be selectively deprotected to obtain the water-soluble target molecule **2b**. The distinct reactive groups are differentiated, highlighted and protected when necessary. See text for further in-depth discussion.

5 Results and Discussion

5.1 Porphyrin Synthesis

To obtain the unsymmetrically substituted trans-AB_2C porphyrin, several different approaches were tested and evaluated:

1. classical statistical approach
2. combined statistical approach under alkaline reaction conditions
3. stepwise porphyrin synthesis

The best method regarding yield, isomer separation and feasibility was the straightforward multistep porphyrin synthesis (3), which will be discussed in chapter 5.1.3 (p. 37). All of these approaches rely on the use of DPMs as sub-parts which allow a certain degree of control during the reaction. Thus, these DPMs had to be synthesized prior to the evaluation of the different porphyrin syntheses.

5.1.1 Stepwise Synthesis of Acetylene Dipyrromethane

As discussed in chapter 4, the rigid linear spacer connecting porphyrin and perylene is of great importance. The linker was designed as a phenyl-ethynyl-phenyl group (PEP), allowing electron and exciton transfer between the porphyrin and the perylene. The acetylene group promises a wide accessibility and flexible chemistry using high-yielding carbon cross coupling reactions (*e.g.*, SONOGASHIRA reactions) while being sufficiently stable against acidic and alkaline conditions. Further promising arguments for this linker are the perfect linearity and the π system for electron transport along the molecular axis without the chance of back-folding. Additionally, it can be imagined that the final self-assembled lipid structures could be reacted to a covalently bonded supramolecular assembly by polymerization reactions of the adjoined triple bonds, which rendered the PEP group even more preferable.

To obtain a dipyrromethane bearing an acetylenic PEP group, the commercially available *p*-iodoaniline was subjected to a SONOGASHIRA reaction with TMS acetylene (Scheme 5.1).[204] It proved best to use freshly prepared $Pd(PPh_3)_2Cl_2$ catalyst and copper iodide in catalytic amounts of 0.77 mol-% and 1.42 mol-%, respectively. The 1:2 ratio of Pd catalyst to copper iodide was important; a higher percentage of copper iodide led to drastic reduction of the yield. Using these conditions, less than 1 mol-% Pd catalyst already led to a fast and complete conversion within 21 h. The reaction was performed in dry THF with NEt_3 as base and under argon atmosphere. The solvents were degassed to prevent oxygen-induced homo coupling. Purification *via* Kugelrohr distillation proved convenient to obtain aniline **3** in good yields (79.0%).

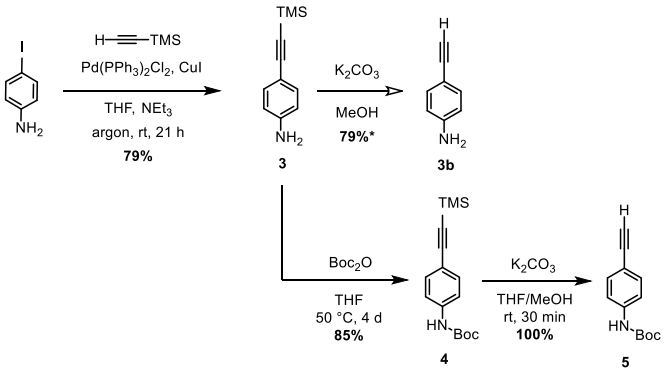

Scheme 5.1. Sonogashira reaction with subsequent protection/deprotection cascade to Boc protected 4-ethynyl-aniline **5**. * The deprotection of **3** to **3b** using K_2CO_3 in MeOH succeeded only once and could not be reproduced.

In the next step, the amino group had to be protected until the synthesis of the porphyrin had been completed. It turned out that the free amino groups tend to inhibit the second SONOGASHIRA reaction which led to drastically decreased yields (*cf.* p. 34).[205] Moreover, the protection of the amino groups prevented side reactions in later steps. The previously discussed orthogonal protection strategy (p. 28) was applied to protect the amino group while keeping the TMS acetylene unaffected. The exact order of this protection-deprotection sequence proved to be crucial as otherwise the yields dropped drastically. The deprotection of the TMS acetylene **3** succeeded once (79.2%, 245 mg) using K_2CO_3 in MeOH, but could not be reproduced satisfactorily.[206] Every other reaction yielded product **3b** only in traces. This observation was also confirmed by Bhasem Gharib, a former laboratory colleague at the HIRSCH group,[207] who investigated the deprotection of the TMS acetylene **3** with many different conditions (*e.g.*, K_2CO_3, $AgNO_3$, $CsCO_3$, TBAF) and solvents with little success.

The Boc protection of the aniline **3** and the deprotection of the acetylenic TMS group of compound **4** were performed in two single steps in very high yields (85.3%, 99.8%). The use of any base (K_2CO_3, NEt_3, DMAP)[208] or TBAF would readily lead to partial deprotection of the TMS group. In combination with methanol as (co-)solvent, this would give rise to other by-products, mainly methyl carbamates. Thus, the Boc protection reaction of aniline **3** to **4** with Boc anhydride was stirred for four days at elevated temperatures without addition of any base.[201] In contrast, the subsequent TMS deprotection reaction to **5** with K_2CO_3 in THF/methanol with additional water was finished after 30 min.[200]

Alternatively, a two-step one-pot reaction of **3** to **5** could be performed in 2.5 h by using a mixture of PEG-400, THF, methanol and water as solvents, K_2CO_3 as base and TBAB as phase transfer catalyst.[209] This reaction combined both the Boc protection and the TMS deprotection while suppressing the formation of methyl carbamates and other side products. Since the yield of

Boc protected 4-ethynyl aniline **5** was comparably low (69.7%) and the removal of PEG-400 proved tedious, the previously discussed reaction cascade in two separate steps is recommended.

MS investigations revealed that the expected product mass (*i.e.*, 289.1498 m/z in case of Boc protected 4-(TMS-ethynyl)aniline **4**) was only found in traces. Instead, mainly fragments without the Boc protective group (*i.e.*, 189.0974 m/z which matches the Boc-deprotected molecule **3**) and intermediate fragments such as [M – *t*-butyl] (218.0636 m/z) were found. This can be explained by the – of course well-intended – facilitated cleavage of the *tert*-butyloxycarbonyl group. Under moderate to harsh thermal or chemical conditions, the Boc group readily degrades to gaseous isobutene and carbon dioxide.

SONOGASHIRA optimization test reactions revealed ideal catalyst amounts (2 mol-% freshly prepared Pd catalyst, 4 mol-% CuI) and solvents (THF, NEt_3 as base).[210] Prior to use, the solvents were degassed by an argon stream and the reaction was conducted under argon atmosphere. It was found that SONOGASHIRA reactions with an unprotected amine–acetylene such as **3b** led to drastically decreased yields. In contrast, the SONOGASHIRA reaction of the Boc-amino-protected acetylene **5** and commercially available *p*-bromobenzaldehyde was completed with high yields (89.8%) under standard conditions (Scheme 5.2). The obtained and recrystallized phenyl-ethynyl-phenyl (PEP) building block **6** could then be further reacted to a dipyrromethane and finally to the porphyrin.

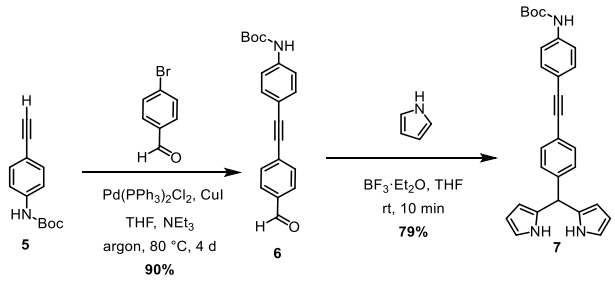

Scheme 5.2. Second Sonogashira reaction with 4-bromobenzaldehyde followed by DPM condensation reaction.

The dipyrromethane **7** was synthesized in 78.9% yield from aldehyde **6** using LINDSEY-conditions with freshly distilled and degassed pyrrole and dry THF.[38,42,46,211] To prevent N-confused dipyrromethanes as well as tri- and polypyrranes and other side products, the reaction was performed under nitrogen atmosphere and light exclusion at room temperature. The progress was monitored by Thin-layer chromatography (TLC) analysis, where dipyrromethane could be easily detected: The DPM could be stained pink with bromine vapor.

When the starting compound **6** had been consumed completely (usually after 10 to 15 minutes) the reaction was quenched by addition of NaOH. Workup and purification had to be done preferably under light exclusion and nitrogen atmosphere. Immoderate exposure to air, sunlight and high temperatures gradually leads to a darkening of the product. This is a known phenomenon for pyrrole and pyrrolic compounds which readily undergo polymerization reactions.[25,212] Notwithstanding the foregoing, DPMs are reasonably stable against aqueous workup, column chromatography and even Kugelrohr distillation (< 150 °C) when working fast and carefully. As it turned out, pure solid DPMs can be stored at -10 °C under exclusion of oxygen and light for several years.[38]

After some optimization, high individual yields in the range from 80 – 100% were obtained. Following this synthesis pathway, a maximum yield of 47.8% over 5 consecutive steps was achieved (Table 5.1). As the starting compounds were relatively cheap and the reactions could be performed in multigram scale, sufficient material could be synthesized in this early stage of the reaction cascade.

Table 5.1. Overall yield for the synthesis cascade to acetylene DPM **7**.

	applied		obtained		yield	
	m	n	m	n	reaction	consec.
3	40.00 g	182.6 mmol	27.33 g	144.4 mmol	79.2%	79.2%
4	10.0 g	52.8 mmol	13.03 g	45.06 mmol	85.3%	67.6%
5	1.00 g	3.46 mmol	750 mg	3.45 mmol	99.8%	67.4%
6	3.80 g	17.5 mmol	5.05 g	15.70 mmol	89.8%	60.5%
7	7.95 g	24.7 mmol	8.540 g	19.52 mmol	78.9%	47.8%

As the porphyrin–perylene target compounds are complex structures and thus provide sophisticated NMR spectra, it was important to investigate and assign the NMR protons of the sub-groups already at an early stage. Using NOESY NMR spectroscopy and comparative values from the precursors (see experimental part), the protons of DPM **7** could be clearly assigned (Figure 5.1). Both pyrrolic NH-protons are found as a broad singlet at 7.96 ppm (a). The four phenylic protons next to the acetylene bridge are overlapping at 7.52 – 7.41 ppm (g, h). The other phenylic protons next to the Boc amide and the DPM can be found at 7.35 ppm (i) and 7.18 ppm (f), respectively. The coupling pattern (pair of doublets) is characteristic for *para*-disubstituted phenyl rings.[213] The nuclear Overhauser effect observed at 5.47 ppm (single DPM proton at the methylene bridge, e) helps to elucidate the spatial vicinity of the phenylic protons (7.18 ppm, f) and the directly neighboring pyrrolic NH protons (a) as well as the β' pyrrolic protons at 5.92 ppm (d).[214] The multiplet at 6.70 ppm can be attributed to the α pyrrolic protons (b). The β pyrrolic protons (c) can be found at 6.17 ppm (see also the spectroscopic evaluation of DPM **10**, p. 40). In

accordance with the NMR spectra of precursor **6** (see experimental part), the Boc amide NH is found at 6.57 ppm (j). The nine *tert*-butyl protons of the Boc protective group at 1.54 ppm (k) are not displayed in Figure 5.1 (see spectroscopic supplement).

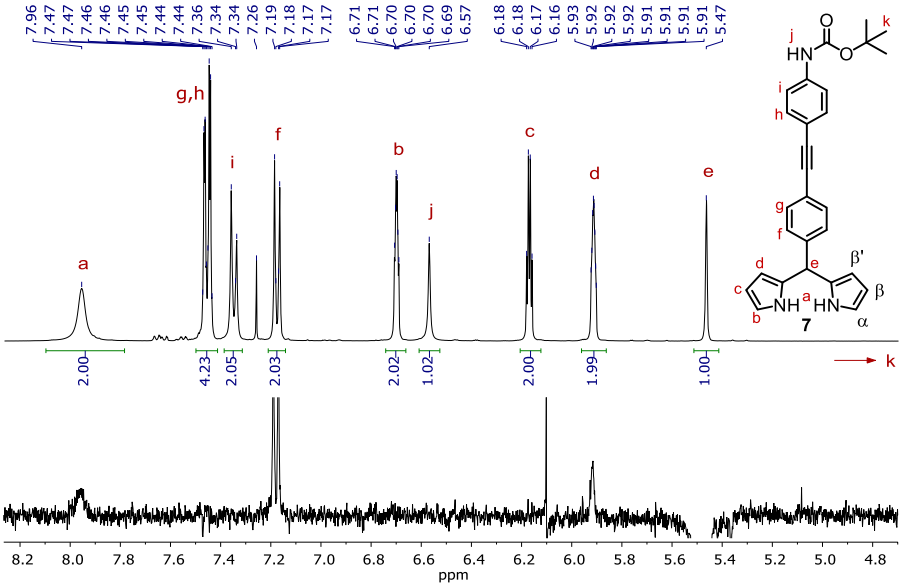

Figure 5.1. NOESY NMR spectrum of **7** in $CDCl_3$ at 5.5 ppm. The *t*-butyl protons at 1.54 ppm are not displayed (see spectroscopic supplement). The measuring artefact at 6.1 ppm is not discussed.

5.1.2 Synthesis of Ester Dipyrromethane

The second DPM carrying a methylester moiety was synthesized according to the literature in 88.3% yield starting from 4-formylbenzoate (Scheme 5.3).[39] Freshly distilled pyrrole was used and it was taken care to degas all solvents by a nitrogen stream prior to use. Furthermore, it was worked under nitrogen atmosphere and light exclusion whenever possible. After addition of 0.2 eq $BF_3{\cdot}Et_2O$ as LEWIS acid catalyst, the reaction was stirred for 10 minutes until judged complete by TLC analysis. The reaction was quenched by addition of NaOH to prevent further side reactions. A fast column chromatography yielded pure DPM **8**. A few drops of NEt_3 were added to the mobile phase to deactivate the stationary phase. Otherwise, the acidic silanol groups of the silica gel would promote polymerization reactions.

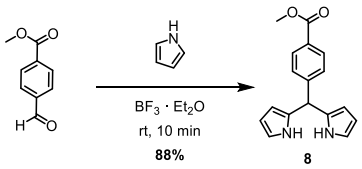

Scheme 5.3. Synthesis of methyl ester DPM **8** using a standard condensation reaction with pyrrole.

5.1.3 Preparation of a Diphenyl Diketone Dipyrromethane

With these two dipyrromethanes **7** and **8** at hand, a statistical AB_2C porphyrin synthesis was attempted. It was found that the yields were as low as 0.2% due to statistical product distribution and – more importantly – massive scrambling. Hence, an alternative, scrambling-free porphyrin synthesis was utilized. This reaction is based upon an organized, stepwise build-up of the porphyrin *via* a VILSMEIER analogous reaction and a dicarbinol synthesis which was reacted *in situ* to the final, highly structured AB_2C porphyrin.[65] Employing the ester DPM **8** as "A" part of the porphyrin, the "B" part was designed to be a phenyl group, followed by addition of the N-Boc protected PEP DPM **7** as part "C".

4-Benzoylmorpholine **9** was synthesized according to a standard amide synthesis found in the literature using benzoyl chloride and morpholine (Scheme 5.4).[65] The reaction was completed in 98.7% yield and high purity. Excess morpholine could be easily removed by aqueous workup. The resulting yellowish oil could be turned into a fine white powder by lyophilization.

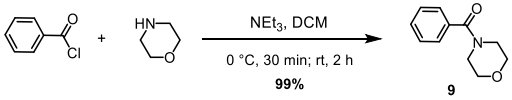

Scheme 5.4. Synthesis of benzoylmorpholine from benzoyl chloride and morpholine.

Excursus: NMR spectroscopy of benzoylmorpholine. The NMR spectra of benzoylmorpholine showed an interesting peculiarity: In ^{1}H NMR, the axial and equatorial protons in the heterocyclic six-membered morpholine ring were extremely broad and poorly resolved at 3.90 – 3.33 ppm (Figure 5.2 top, a/b). In $^{13}C\{^1H\}$ NMR, the measured chemical shifts suited perfectly to the predicted spectrum, except for the α-N carbons of the morpholine (*cf.* Scheme 5.4), which did not appear at all (Figure 5.2 bottom). This anomaly was investigated and the conclusions shall be shortly outlined:

In piperidinyl amides exist three types of conformational isomers: Amide rotation (1), ring inversion (2) and nitrogen inversion (3).[215] The pyramidal shift of the nitrogen electron pair (3) is a fast process below the range detectable by temperature dependent dynamic NMR (DNMR) measurements.[215-216] The ring inversion (2) of a six-membered ring (*cf.* cyclohexane) is known to occur at 10 – 13 kcal/mol for morpholines,[216] whereas the amide rotation barrier (1) can be measured to be in the range of 14 – 15 kcal/mol for benzoylmorpholine in $CDCl_3$.[216-217] The rotation barrier is greatly influenced by temperature, solvent and method of data analysis, whereas the substituents at β and γ positions of the piperidinyl ring had little or no effect at all.[216] In low-temperature ^{13}C-DNMR studies at 248 K, distinct peaks were found at 47.9 and 42.2 ppm which can be assigned to the two – now clearly distinguishable – α-N carbons of the morpholine ring.[216-217] At room temperature (295 K), only a very broad and indistinct signal between 40.2 and 52.0 ppm was found,[217] the signals of the α-N carbons finally coalesced at 305 K.[216]

In conclusion, the disappearance of the α-N carbons in the $^{13}C\{^1H\}$-NMR experiment at 295 K in this thesis can be attributed to amide rotation (1) which greatly influences the chemical vicinity of the α-N carbons (especially relating to the carbonyl group). This leads to a broad distribution of chemical shifts by which the signals of the α-N carbons disappear in the spectroscopic background noise (Figure 5.2).

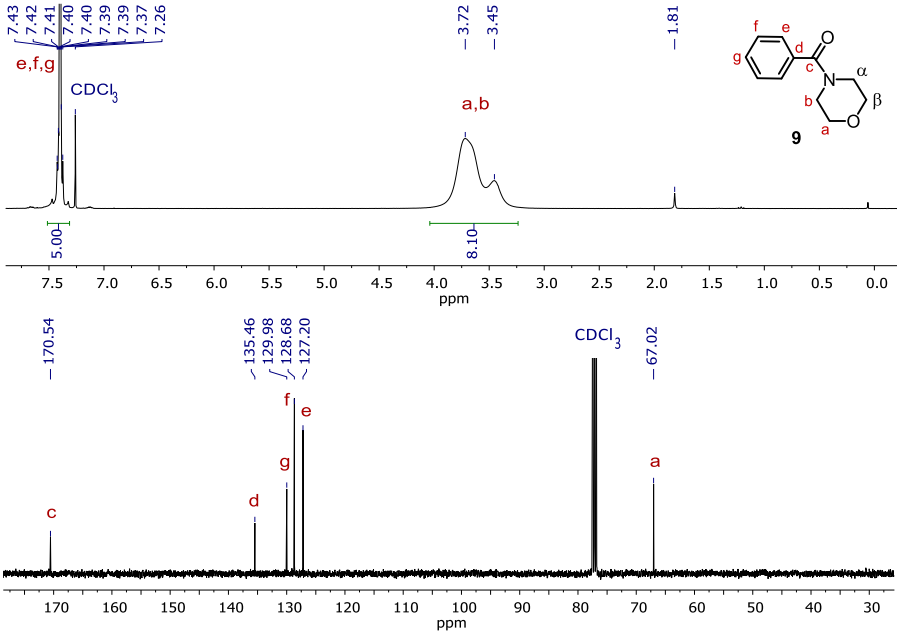

Figure 5.2. ^1H NMR spectrum (top) and ^{13}C NMR spectrum (bottom) of benzoylmorpholine **9**. The α-N carbons of morpholine do not appear in the ^{13}C spectrum.

Vilsmeyer reaction of benzoylmorpholine: VILSMEIER reactions are widely used for selective attachment of formyl groups to electron-rich aromatic systems.[66] These reactions allow milder conditions and greater regioselective control compared to other FRIEDEL-CRAFTS acylation methods.[41,218] In this case, instead of formylating, a phenylketone was introduced in pyrrolic α position.

In this VILSMEIER analog reaction using benzoylmorpholine **9** instead of DMF, the VILSMEIER reagent was produced by reaction with $POCl_3$ for 3 h at 65 °C (Scheme 5.5). This chloroiminium intermediate was then subjected to an electrophilic aromatic substitution with ester DPM **8**. Reaction in electron-rich pyrrolic α position led to an iminium ion intermediate, which then was hydrolyzed by addition of aq. satd. NaOAc. The released morpholine was removed by aqueous workup. Column chromatographies and recrystallization yielded 78.4% of diphenyl diketone ester dipyrromethane **10** as a light brown powder. The product proved to be less prone to polymerization than the DPM due to the higher substitution degree of the pyrrolic units. The improved stability allowed the storage at room temperature and without any need for light and air exclusion, which is uncommon for dipyrromethanes.

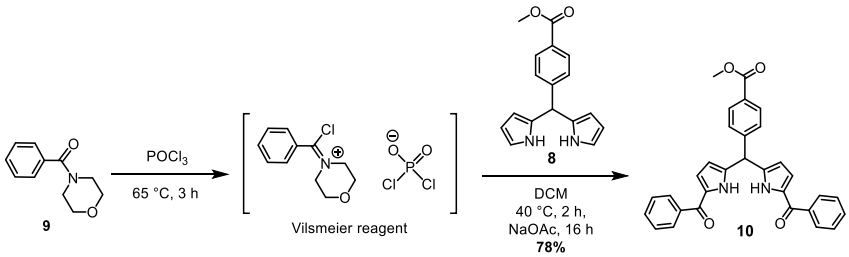

Scheme 5.5. Vilsmeier analog acylation of ester dipyrromethane **8** to diphenyl diketone ester dipyrromethane **10**.

The reaction towards the diphenyl diketone DPM **10** proceeded in 3 steps with an overall two-step consecutive yield of 69.2% (Table 5.2). The syntheses were optimized to give a high yield and the reaction to the DPM **10** could be performed in a very straightforward manner, rendering the diphenyl diketone **10** an ideal starting compound for the following porphyrin synthesis.

Table 5.2. Overall yield for the synthesis cascade to diphenyl diketone DPM **10**.

	applied		obtained		yield	
	m	n	m	n	reaction	consec.
8	3.50 g	21.3 mmol	5.27 g	18.8 mmol	88.3%	88.3%
9	10.0 g	71.1 mmol	13.425 g	70.203 mmol	98.7%	-
10	2.29 g	8.17 mmol	2.72 g	5.57 mmol	78.4%	69.2%

To allow the assignment of ^{1}H and ^{13}C NMR spectra of DPM **10**, HSQC and HMBC spectra were recorded (Figure 5.3). Using heteronuclear single quantum coherence (HSQC, red), a direct correlation for protons attached to specific carbon atoms can be observed.[213] Further assignments were possible when performing a heteronuclear multiple bond correlation experiment (HMBC, blue), which measures the interaction between carbons and protons separated by several (two up to four) bonds.[213]

In the carbonyl region, the ketone and ester carbons at 184.7 ppm (m) and 167.0 ppm (b), respectively, can be identified. HMBC permits the attribution of the neighboring groups: the methyl ester at 52.3 ppm / 3.93 ppm (a) and the aromatic carbons (130.3 ppm) and protons (8.05 ppm) *ortho* to the ester group (d). In this HMBC experiment, no aromatic ^{2}J coupling between *ortho* protons (d) and *meta* carbons (e) and *vice versa* can be observed. Instead, a ^{3}J coupling of the *ortho* protons (d) to the opposing *ortho* carbon (d', irrelevant) and to the *para* carbon at 145.7 ppm (f) can be found. The *ipso* carbon at 129.4 ppm (c) exhibits a weak ^{4}J coupling to the methyl ester protons (a) and a distinct ^{3}J coupling to the *meta* protons (7.67 ppm, e). According to HSQC, the *meta* carbons can be found in the ^{13}C spectrum at 129.1 ppm (e). This attribution is substantiated by the correlation of these atoms to the methylene bridge (45.1 ppm / 5.81 ppm, g).

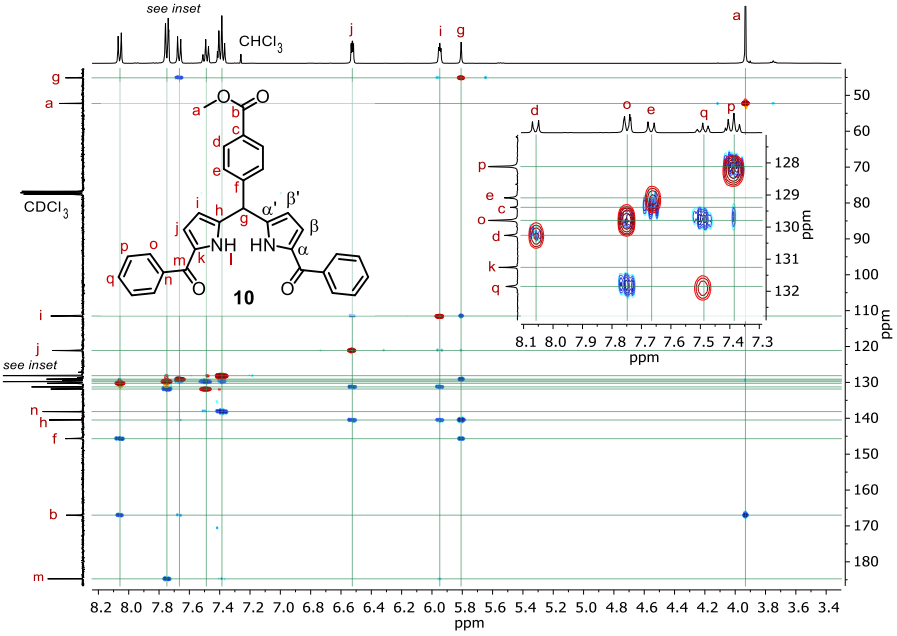

Figure 5.3. Combined HSQC (red) / HMBC (blue) NMR spectrum of **10** in $CDCl_3$. See text for detailed attribution of the peaks. The signal at 12.04 ppm (NH protons) is not displayed in this spectrum.

Next, the α' pyrrole carbons at 140.5 ppm (h) and the β' pyrrole carbons/protons (111.5 ppm / 5.95 ppm, i) can be attributed. The chemical shift of the pyrrole group is completed by assigning the β pyrrole carbons/protons (121.1 ppm / 6.53 ppm, j) and the α pyrrole carbons at 131.3 ppm (k). The shifts of the mono substituted phenyl group (neighboring the ketone) can be derived accordingly: the *ipso* carbons (138.1 ppm, n), the four *ortho* carbons/protons (129.8 ppm / 7.75 ppm, o), as well as the four *meta* carbons/protons (128.1 ppm / 7.39 ppm, p) and the two *para* carbons/protons (131.9 ppm / 7.48 ppm, q) illustrate a typical coupling pattern. Again, no ^2J coupling between *ortho* and *meta* carbons/protons is observed .The two NH protons at 12.04 ppm (broad singlet, l) are not displayed in Figure 5.3.

5.1.4 Stepwise AB_2C Porphyrin Synthesis via a Dicarbinol

To obtain an AB_2C porphyrin in a controlled fashion, the "AB_2" precursor **10** had to be reduced to a reactive dicarbinol. A carbinol is an outdated term for a (substituted) methanol unit and is mostly used for secondary or tertiary alcohols. However, in porphyrin and corrole synthesis, the terminus dicarbinol is still frequently used.[35,40,219] The diketone **10** was reduced by addition of 2.2 eq $NaBH_4$ in a mixture of THF/methanol under nitrogen atmosphere (Scheme 5.6). It was important to find a mild reducing agent which would reduce the ketones while leaving the ester group unharmed. $NaBH_4$ turned out to be the ideal choice as it was selective and easy to handle. The intermediate diphenyl dipyrromethane dicarbinol **11** was unstable and could not be purified without complete degradation.[220] Hence, only a short workup was performed with quenching by aq. satd. NH_4Cl, addition of CH_2Cl_2, phase separation and drying. The solvent was then quickly removed *in vacuo* at low temperatures to obtain a brown, quickly darkening solid. The theoretical yield exceeded 100% which was a hint that residual solvent and potentially minor impurities were present. As this should not hinder the following porphyrin reaction, it was decided to apply the crude dicarbinol **11** instantly without further purification and characterization.

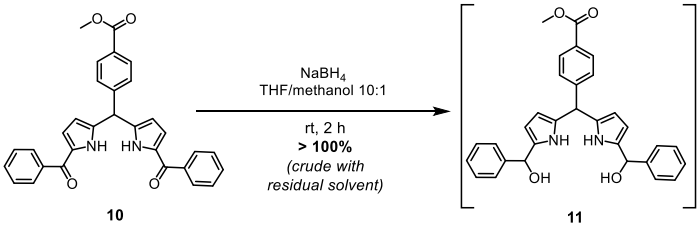

Scheme 5.6. Synthesis of diphenyldipyrromethane dicarbinol intermediate **11** by selective reduction of diphenyl diketone dipyrromethane **10**.

The dicarbinol **11** (part "AB_2") and N-Boc protected PEP DPM **7** (part "C") were dissolved in acetonitrile and slowly added to a 1 L flask with acetonitrile, DMF and TFA at 0 °C under nitrogen atmosphere (Scheme 5.7). Already at the first drops the solution turned strongly purple, which intensified even further upon continuing addition (Figure 5.4). After complete addition (15 min), the solution was stirred for another 15 min and the reaction was stopped by addition of DDQ to oxidize the porphyrinogen to the final porphyrin product **12** (Scheme 5.7). The crude mixture was passed through a short plug of silica gel (eluent: ethyl acetate) to remove excess DDQ and other unwanted by-products. Green-colored protonated porphyrin would not pass through the plug. Hence, 5% NEt_3 was added to neutralize the acidic environment and to deprotonate the free-base porphyrin. The crude product was thoroughly washed and purified by several column chromatographies. No isomers due to scrambling or statistical synthesis were found. Yields between 23.6% and 30.3% (related to the DPMs as starting materials) have been achieved, which is among the best yields known for such complex unsymmetric AB_2C porphyrins.[10,40,65,220-221]

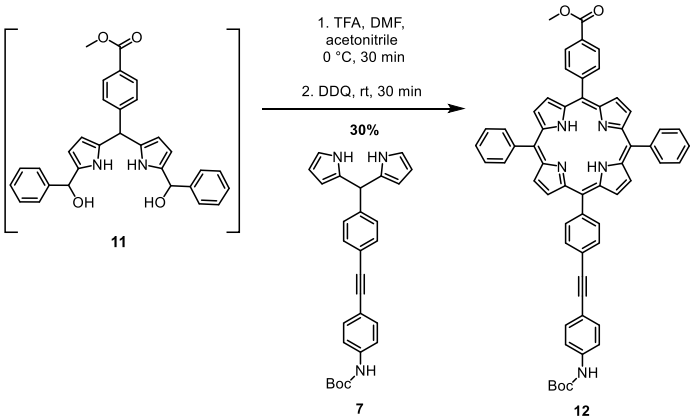

Scheme 5.7. Condensation of dicarbinol intermediate **11** with dipyrromethane **7** and oxidation to porphyrin **12**.

Figure 5.4. Porphyrin synthesis: color change upon dropwise addition of dicarbinol **11** and dipyrromethane **7**.

Literature shows that porphyrin syntheses under acid catalyzed conditions give best yields when working at low temperatures, low concentrations (usually less than 10^{-3} M), low catalyst amounts, and rigorous stirring to favor the formation of porphyrinogen over penta- and higher oligophyrines as well as oligomeric chains.[26-27,33,46] Applying this sequential synthesis in acetonitrile as solvent, the formation of side products is minimized and scrambling effects are avoided completely, even when working in concentrations as "high" as $0.9 \cdot 10^{-2}$ M.[40] Compared to other porphyrin synthetic pathways, this method was by far the most suitable and convenient in order to obtain a complex AB_2C porphyrin in high yield (*cf.* chapter 5.1, p. 32).

Porphyrin **12** was fully characterized *via* ^{1}H-NMR, ^{13}C-NMR, IR, UV-Vis and MS spectrometry. The NMR signals were assigned by comparison of calculated spectra, precursor spectra (*e.g.*, Boc-protected amino-PEP-acetylene **6**, p. 133), and the spectra of subsequent molecules featuring additional HMBC/HSQC measurements (*cf.* molecule **13b**, p. 46). As expected, the porphyrin signals are crowded in the aromatic region of the NMR spectra, but can nevertheless be clearly assigned both in ^{1}H-NMR and ^{13}C-NMR (Figure 5.5): The β-pyrrolic protons are found between 8.94 and 8.77 ppm, identifying an AB_2C porphyrin with overlapping signals.[9] The β-pyrrolic carbons are found as a broad peak at around 131.4 ppm while the α-pyrrolic carbons are attributed to the broad peak at around 144.3 ppm. The quaternary *meso*-porphyrin carbons can be assigned to the peaks at 120.7 ppm (m_P), 119.9 ppm (m_A), and 118.9 ppm (m_E). According to tetraphenylporphyrin (TPP), the phenyl groups attached to the *meso* positions can be identified as follows:[9] *ipso*-carbon atoms at 142.2 ppm (P_i), *ortho*-carbon atoms at 134.69 ppm (P_o), *ortho*-protons in the cluster at 8.28 – 8.15 ppm (P_o, superimposed by A_o at the downfield edge of the cluster), *meta*-carbon atoms at 126.8 ppm (P_m), and *para*-carbon atoms at 128.0 ppm (P_p). The *meta*- and *para*-protons are found overlapping in the region between 7.85 – 7.70 ppm (P_m, P_p).

The phenylic ester signals can be fully assigned, the designations (*ipso*, *ortho*, *meta*, *para*) again referring to the position of the phenyl carbons/protons related to the porphyrin substituent. At 129.8 ppm, the *para*-carbon can be identified (E_p). The signal of the *ipso*-carbon (E_p) is strongly shifted upfield to 147.2 ppm according to calculation and comparison with the precursor **10**. The *ortho* and *meta* signals can be found at 134.72 / 8.37 – 8.29 ppm (E_o) and 128.1 / 8.50 – 8.42 ppm (E_m), respectively. Overlapping with the $o_{porphyrin}$-m_{ester}-carbon signal at 134.72 ppm (E_o) and in direct vicinity to the $o_{porphyrin}$-phenyl signal at 134.69 ppm (P_o) lies the $o_{porphyrin}$-$m_{ethynyl}$-carbon signal at 134.72 ppm (A_o). This exact attribution in the ^{13}C NMR as well as in the ^{1}H NMR at 8.20 ppm (A_o) can only be achieved by accurate evaluation and comparison with the HMBC/HSQC spectra of **13b** (p. 46, *vide infra*). Hence, the signals of the phenyl group (A) between the porphyrin and the triple bond can be assigned as follows: *ipso*-carbon atom at 140.9 ppm (A_i), *ortho* signals at 134.72 / 8.28 – 8.15 ppm (A_o), *meta* signals at 130.0 / 7.97 – 7.88 ppm (A_m), and the *para*-carbon atom at 123.3 ppm (A_p, next to the ethynyl bridge).

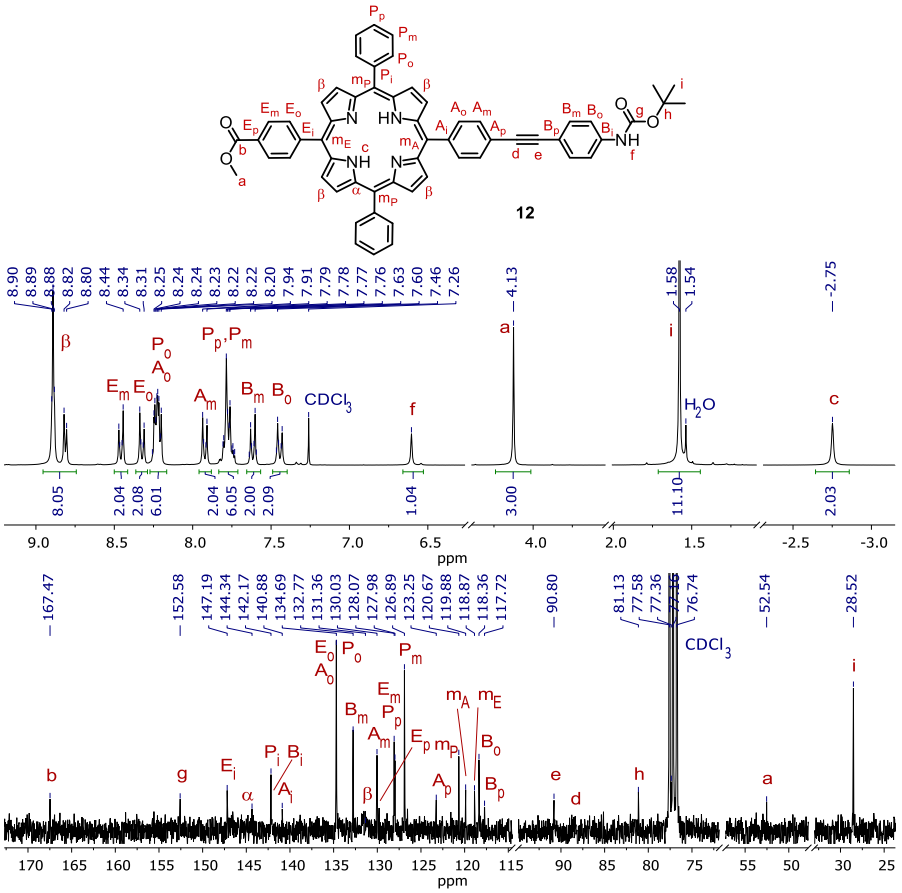

Figure 5.5. ^{1}H NMR spectrum (top) and ^{13}C NMR spectrum (bottom) of porphyrin **12**. One ethynyl carbon atom (e) is superimposed or missing in the spectrum. See text for a detailed description of the assignments.

Of the two carbon atoms of the ethynyl group, one signal is found at 90.8 ppm (e). The other signal is missing or superimposed. The resolution of the spectra does not allow for a clear identification of this signal which is expected to be at around 88 ppm (d). The residual signals can be attributed to the Boc phenyl group (B): The *ipso*$_{Boc}$-carbon is detected at 142.1 ppm (B_i), the *ortho*$_{Boc}$-atoms are found at 118.4 / 7.49 – 7.39 ppm (B_o), the *meta*$_{Boc}$-atoms are assigned to the signals at 132.8 / 7.66 – 7.57 ppm (B_m), and the *para*$_{Boc}$-signal is found at 117.7 ppm. It should be noted that the ^{13}C signals of the phenyl carbons *ortho* to the Boc amide group at 118.4 ppm (B_o) are broadened and the signal intensity is reduced in comparison to the *meta*-phenyl carbons at 132.8 ppm (B_m). This observation can be also made in every precursor molecule (**4-7**) carrying a

Boc protective group. As discussed before, this can most likely be attributed to the energetic amide rotation barrier which is overcome partially at room temperature (295 K), thus influencing the chemical vicinity of the *ortho*$_{Boc}$-phenyl carbons (*cf.* benzoylmorpholine **9**, p. 38). The Boc-carbonyl group is detected downfield at 152.6 ppm (g), the amide proton appears at 6.60 ppm (f) in the ^{1}H NMR spectrum, the quaternary *tert*-butyl carbon atom is found at 81.1 ppm (h), and the *tert*-butyl group can be assigned to the signals at 28.5 / 1.58 ppm (i). The ester CH_3 group is found at 52.5 / 4.13 ppm (a), and the ester carbonyl atom can be identified as the most downfield shifted signal at 167.5 ppm (b). The porphyrinic NH signals are found upfield at -2,75 ppm (c) as a broad singlet, which is characteristic for the strong shielding effect which occurs inside of aromatic ring systems.

5.1.5 Solvent-Free Deprotection of *N*-Boc Porphyrin

The N-Boc protected PEP porphyrin **12** had to be deprotected before coupling to the perylene unit. Usually, Boc protective groups are cleaved under acidic conditions, often methanolic or etheric HCl,[222-223] or TFA in CH_2Cl_2.[222,224] Apart from this, various deprotection reactions in TBAF,[225-226] TMS chloride,[227] Na_2CO_3,[228] t-$BuNH_2$,[229] and others are known. According to the orthogonal protecting group synthesis strategy (chapter 4.2, p. 28), an acidic deprotection using HCl or TFA should not affect the methyl ester or the triple bond. In experiments, however, the deprotection reaction with methanolic HCl and TFA did not lead to the desired results: Side products **13b** (using methanolic HCl) and **13c** (using TFA) were isolated and characterized by Mass Spectrometry and NMR spectroscopy. Polarity differences in TLC analysis and measured masses of the three products **13** (7.9%), **13b** (2.9%), and **13c** (21.1%) indicated that two different additions to the triple bond had occurred as severe side reactions (Table 5.3, see also experimental part, p. 140).

Table 5.3. Mass differences of the three products with corresponding additional atoms.

measured mass		formula	+ atoms
13	787.294	$C_{54}H_{37}N_5O_2$	–
13b	823.271	$C_{54}H_{38}ClN_5O_2$	H, Cl
13c	805.337	$C_{54}H_{39}N_5O_3$	2H, O

In-depth 2D-NMR investigations (HSQC/HMBC) revealed the structure of **13b** and **13c**: The triple bond was turned into a chloroethene or a ketone, respectively (Scheme 5.8). The Boc group had been cleaved successfully while leaving the methyl ester unharmed. The exact addition pattern of H-Cl in **13b** could not be substantiated definitely. However, the evaluation of HSQC/HMBC spectra indicates that the depicted isomer is most likely correct (Figure 5.6):

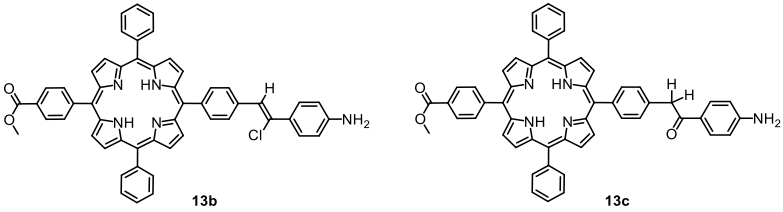

Scheme 5.8. Structure of side products **13b** (H-Cl adduct) and **13c** (2H-O adduct) as determined by HSQC/HMBC NMR.

A definite attribution is difficult since the C-H alkene carbon (d) at 127.18 ppm is superimposed by the $m_{\text{porphyrin}}$-o_{alkene}-carbon atoms (A_m) and the phenyl protons in *ortho* position of the alkene are overlapping in the region between 7.50 – 7.41 ppm (A_m, N_m). However, according to selective 1D NOESY experiments in CD_2Cl_2, the A_m protons appear slightly more downfield (doublet at 7.47 ppm) and exhibit a spatial proximity to the alkene proton (d) at 7.15 ppm (*cf.* spectroscopic supplement, p. 236). Further HMBC correlations substantiate the aforementioned substitution pattern: The alkene proton (d) at 7.15 ppm shows ^3J couplings to A_m carbons at 127.18 ppm and N_p at 127.7 ppm, as well as an olefinic ^2J coupling to the C-Cl carbon at 134.9 ppm (e). From the C-Cl carbon (e), a HMBC ^3J coupling to the N_m protons (7.50 – 7.41 ppm) can be found. The signals *ipso* (147.4 ppm, N_i) and *ortho* (114.9 / 6.70 ppm, N_o) to the amine can be assigned accordingly.

As already seen before, the carbon atoms *ortho* to the porphyrin (E_o, A_o, P_o) are clustered at 134.7 ppm and the *ortho* protons are likewise aggregated at 8.32 ppm (E_o), 8.26 – 8.18 ppm (P_o), and 8.03 ppm (A_o). The quaternary *meso*-porphyrin carbons at 120.5 ppm (m_P), 120.3 ppm (m_A), and 118.7 ppm (m_E) resemble closely the peaks found in the ^{13}C spectrum of precursor **12**. The remaining signals of the phenyl ester group (E) can again be found at 147.0 ppm (E_i), 128.1 / 8.46 ppm (E_m), 129.7 ppm (E_p), 167.5 ppm (b), and 52.6 / 4.12 ppm (a). Compared to precursor porphyrin **12**, the shifts of the phenyl group (A) between the porphyrin and the alkene group differ notably: The *ipso*-carbon atom is assigned to the peak at 140.9 ppm (A_i), the *ortho* signals are found at 134.7 / 8.03 ppm (A_o), the *meta* signals at 130.8 / 7.50 – 7.41 ppm (A_m), and the *para*-carbon atom (A_p, next to the alkene group) at 135.6 ppm. The residual phenyl carbon atoms are assigned to the signals at 142.2 ppm (P_i), 126.9 ppm (P_m), and 128.0 ppm (P_p), while the protons again coalesce at 7.83 – 7.71 ppm (P_p, P_m).

To complete the spectroscopic investigation, the β-pyrrolic protons in the ^{1}H NMR region between 8.96 – 8.74 ppm exhibit a distinct HSQC coupling to the broad peak at 131.6 ppm in the ^{13}C spectrum. Owing to the low resolution, the α-pyrrolic carbon atoms (expected at around 145 ppm) are not visible. The amine protons can be assigned to the broad signal at 3.83 ppm (f) and the inner porphyrin NH-protons are again found at -2.75 ppm (c).

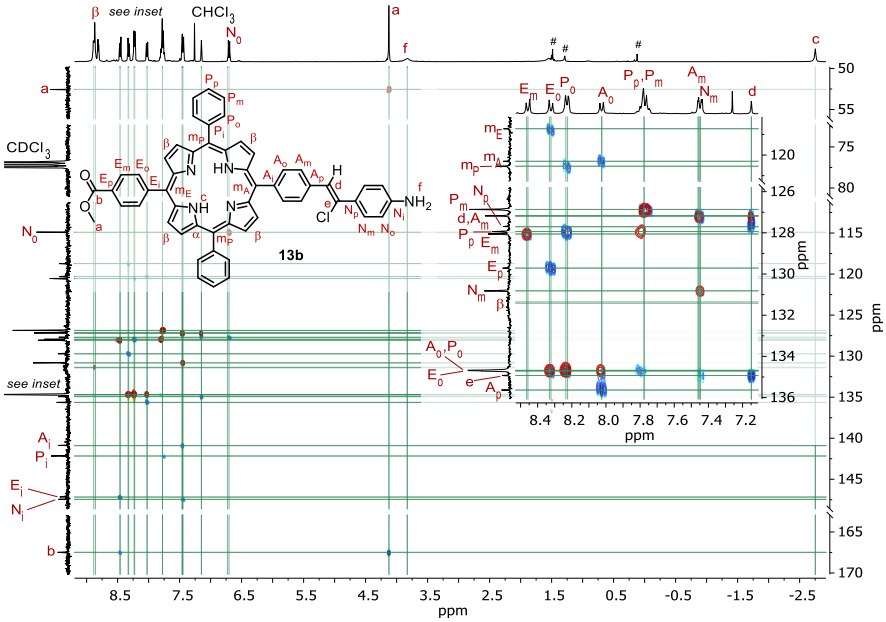

Figure 5.6. Combined HSQC (red) / HMBC (blue) NMR spectrum of **13b** in $CDCl_3$. See text for detailed attribution of the peaks.

The molecular formula $C_{54}H_{39}N_5O_3$ of **13c** was determined by MS (Table 5.3). Compared to the desired product **13**, a surplus of H_2O was found. Again, an electrophilic addition reaction to the triple bond was assumed to be the cause. TFA as a strong Brønsted acid is known to add to double and trible bonds (Scheme 5.9).[230] Addition reactions are regioselective, as the formation of a stable carbocation intermediate is favored (Markovnikov's rule). In this case, the resonance of the aniline stabilizes the intermediate, leading to an allene species. The TFA anion coordinates to the carbocation and is replaced by water upon aqueous workup following an S_N1 mechanism (dissociation of TFA^-, nucleophilic attack of H_2O, cleavage of H^+). The resulting enol rapidly tautomerizes to the more stable ketone product **13c**.

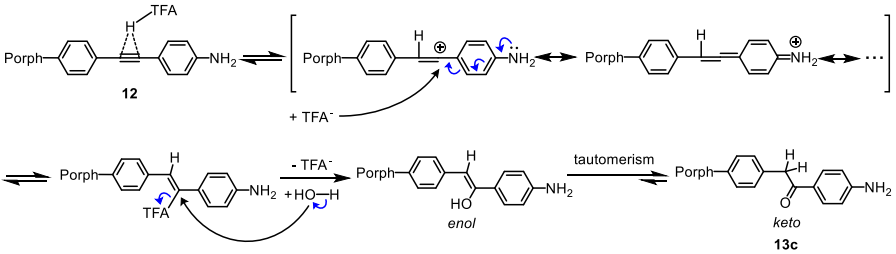

Scheme 5.9. Electrophilic addition of H-TFA to the triple bond. The cation intermediate in vicinity to the aniline is favored due to resonance stability (Markovnikov's rule). Aqueous workup (hydrolysis) leads to S_N1 substitution of TFA by H_2O (enol form) and tautomerization to the more stable ketone **13c**.

MONTES *et al.* asserted in 2006 that indeed an addition of TFA to a triple bond is possible.[230] They tried to cleave a Boc protective group with TFA in the presence of a triple bond and found – apart from the expected Boc cleavage – an addition of TFA to the triple bond which was then replaced by H_2O on aqueous workup (Scheme 5.10). Again, keto-enol tautomerism finally led to a ketone.

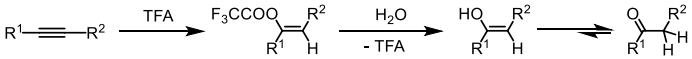

Scheme 5.10. Addition of TFA to a triple bond, followed by OH substitution and keto-enol tautomerism.[230]

The above mentioned deprotection pathways for the Boc group cleavage were tried in low-scale test reactions but did not lead to a successful, clean result. Reaction of TBAF in DMF at varying temperatures (rt to 100 °C) and time scales (5 min to 24 h) occasionally led to formation of product **13** but with extremely low yields and large amounts of side products. Luckily, there were a few alternative routes to deprotect the Boc group employing microwave irradiation,[231-232] heating in a continuous flow reactor,[233-234] or even solvent-free by thermolytic and entropy driven silica-gel mediated deprotection under vacuum.[202-203] For the latter, the Boc protected nitrogen should be in conjugation or part of an aromatic system.[202] The silanol groups of the silica gel are expected to mediate the reaction. Tests showed that the reaction with activated silica did indeed lead to a complete conversion of the starting compound, though with a notable amount of side products. Higher temperatures (180 °C) and longer reaction times (24 h) also favored the formation of decomposition products. Using deactivated silica gel, a clean reaction could be observed, albeit with traces of starting compound remaining.

Hence, compound **12** was dissolved in dichloromethane with 1% NEt_3 to deactivate the silica gel (Scheme 5.11). After application on silica gel, the solid brownish powder was stirred and heated at 120 °C under vacuum ($2 \cdot 10^{-3}$ mbar). Under these conditions, the Boc group decomposed to isobutene and carbon dioxide. These gases were removed under reduced pressure from the vessel, which was probably the driving force of this reaction.[202] Although after 4 h still starting compound **12** was detected by TLC, it was decided to stop the reaction. The product **13** (45.8%) was separated by short flash column chromatography and recovered **12** (53.5%) was reacted a second time. Following this procedure, only pure porphyrin-PEP-amine **13** (overall yield: 585.3 mg, 91.0%) and starting compound **12** (38 mg, 5.2%) were obtained; no side products were formed. In low-scale test reactions, conversions of up to 98.9% could be achieved after two steps. Product **13** was fully characterized by $^{1}H/^{13}C$ NMR, MS, IR and UV-Vis.

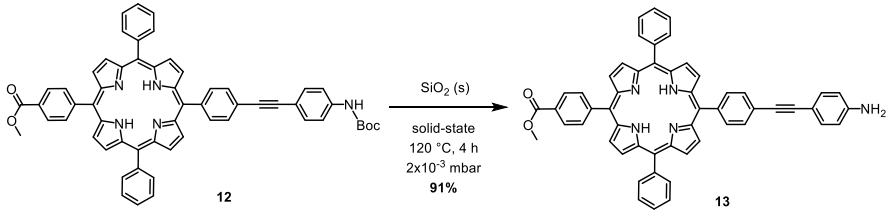

Scheme 5.11. Solid-state deprotection reaction of Boc-amine-PEP-porphyrin **12** to amine-PEP-porphyrin **13**.

Considering the whole reaction cascade from the commercially available starting compounds to porphyrin **13**, an overall yield of 13.2% could be obtained (Table 5.4). This was calculated using the maximum yields of the longest consecutive reaction pathway (7 consecutive steps, 11 total steps) starting from compound **3** over dipyrromethane **7** to the porphyrin **13**. Except for the porphyrin reaction **12** with only 30.3% yield, it was possible to optimize each single reaction to reach yields of approx. 80% and higher.

It has to be emphasized again that a yield of 30% is an excellent result for a complex and unsymmetric AB_2C porphyrin. In the literature, usually yields of 5 – 25% for AB_2C porphyrins are reached.[10,40,65,220-221]

Table 5.4. Overall yield for the synthesis cascade to porphyrin **13**.

	applied		obtained		yield	
	m	n	m	n	reaction	consec.
7	7.95 g	24.7 mmol	8.540 g	19.52 mmol	78.9%	47.8%
12	1.409 g	2.860 mmol	770.6 mg	867.8 µmol	30.3%	14.5%
13	725 mg	816 µmol	585.3 mg	742.8 µmol	91.0%	13.2%

5.2 Perylene Synthesis using an Optimized Reaction Cascade

The perylene part of the dyad was synthesized starting from perylene-3,4:9,10-tetracarboxylic acid bisanhydride (PTCDA). Many reactions for the N-functionalization of PTCDA derivatives are known (*cf.* chapter 2.2.1, p. 10ff), but no satisfactory reaction and purification conditions for the desired reaction cascade have been reported yet. Several synthesis pathways yielding unsymmetrically substituted perylene imide compounds were tried, *e.g.*, using KAISER's perylene monopotassium salts,[93-94] one-pot imidification-esterification LANGHALS reactions,[98] and statistical syntheses.

The LANGHALS reaction first seemed to be very promising, as it allows the synthesis of a perylene imide diester directly in a one-pot multistep reaction. Starting from PTCDA, first an excess of aliphatic long-chained alcohols and 1 eq of an amine were applied, followed by an excess of long-chained alkyl bromides. The alcohol first opens the anhydride on both sides of PTCDA to two esters and two carboxylates (Scheme 5.12). The amine then displaces one of the alcohols and a subsequent ring closure reaction leads to an imide. Here, it is important that the imide and ester provide approximately comparable solubilities. The remaining carboxylate group undergoes a S_N2 reaction with the later added alkyl bromide to yield a second ester. Hence, in theory, a perylene imide diester could be directly formed in a one-pot multistep reaction (Scheme 5.12).

However, this reaction did not work when using aromatic amines, as nearly exclusively the perylene tetraester (PTE) was formed. Moreover, the main problem turned out to be the separation of the products, since the extended π system leads to strong intermolecular aggregation and the formation of varnishes. Purification by column chromatography typically resulted in extreme smearing/overlapping. Separation only worked with high dilution and very strong polarity differences. Recrystallization or precipitation always gave a mixture of products. The purification methods used in the literature could not be reproduced satisfactorily.[81,94,98] Hence, in this dissertation it was aimed to develop and describe a purification method in such a way that it could be performed in a straightforward and easy-to-understand manner with constantly good results.

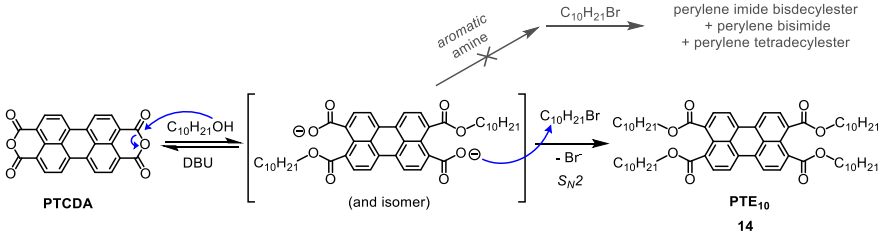

Scheme 5.12. The anhydride was opened by nucleophilic addition-elimination of the decanol. A dark red dicarboxylate was formed. The subsequent S_N2 reaction with decyl bromide led to the perylene tetraester **14** as an orange precipitate. Using aromatic amines, no addition reaction and formation of perylene imide bisester occured (Langhals reaction).

The variation and optimization of a known multistep reaction led to a high yielding and reliable synthesis cascade towards unsymmetrical substituted perylene compounds. Special attention was paid to find a straightforward, simple and reproducible way to purify the interstage products. Usually, large amounts of solvent have to be used for purification due to the low solubility and the strong π interactions of the perylenes. It is possible and recommended to recycle and reuse the solvents to minimize the waste.

First, the perylene tetradecylester PTE_{10} **14** was synthesized starting from PTCDA. It was chosen to perform the LANGHALS reaction described above without addition of amine (Scheme 5.12).[98] This led to by-product-free PTE_{10} in high yields and at very mild conditions. This reaction allows to fine-tune the target products, *e.g.,* by using a different set of alcohols and alkyl bromides. Hence, this reaction would also be suitable for the esterification of more complex perylene tetraester compounds.

In a small flask, PTCDA was suspended in little amounts of DMF and n-decanol (4 eq). 1,8-Diazabicyclo[5.4.0]undec-7-en (DBU, 4 eq) was added as a base (Scheme 5.13). After 16 h of stirring at rt, the red suspension had turned into a homogeneous dark red solution, indicating the formation of perylene bisdecylester biscarboxylate (*cf.* Scheme 5.12). Addition of decyl bromide (3 eq) led to decylester formation at the carboxylates. While stirring for further 16 h, a precipitate was formed and the color changed to bright orange. The reaction progress was monitored by TLC analysis. It proved useful to use $CHCl_3$ as eluent and to add 1% of acetone for best separation of the products on the TLC plate (*cf.* p. 83). Furthermore, only tiny amounts should be applied to prevent smearing of the perylenes. The reaction mixture was then poured on acidified ice water and the resulting orange precipitate was filtered, washed with water and dried *in vacuo*. Under these reaction conditions, only negligible amounts of perylene anhydride bisdecylester ($PABE_{10}$) and no other side products were formed.

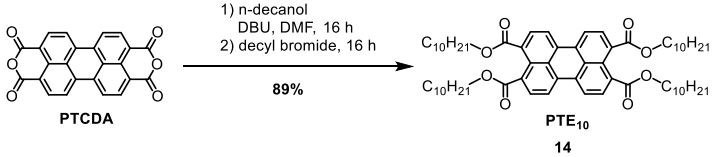

Scheme 5.13. Synthesis of perylene tetraester **14** starting from PTCDA using a modified two-step one-pot Langhals reaction.

The crude mixture was applied onto a short plug with silica gel and washed with acetonitrile to elute traces of residual decyl bromide and decanol. Both reagents could be detected by TLC analysis (using either vanillin–sulfuric acid staining solution or iodine applied onto silica gel).[235] Switching to $CHCl_3$ + 1% acetone (4 L, recycled) led to elution of pure product PTE_{10}

while insoluble PTCDA remained on the plug. Using ether or ethyl acetate should be avoided as perylenes tend to form hardly soluble varnishes which clog the column/plug. The product was lyophilized (*cf.* p. 54) to yield PTE_{10} **14** (88.9%) as an orange, voluminous powder. The reaction could be reliably performed in multigram scale (1–15 g) without problems and in consistently good yields (83 – 89%).[236] PTE_{10} **14** was fully characterized by $^{1}H/^{13}C$ NMR, IR, UV-Vis and melting point analysis. MS analysis and fluorescence emission spectra can be found elsewhere.[81]

The perylene tetraester **14** is a central molecule in perylene reactions, allowing further modifications with different functional groups by selective unilateral hydrolysis to form the perylene anhydride bisdecylester ($PABE_{10}$, **15**). This was achieved by following a literature-known procedure (Scheme 5.14).[100] Here, an exact amount and ratio of solvents (dodecane/toluene 5:1; 10 mL for 10 g PTE_{10} **14**) had to be used. At room temperature, absolutely no solubility could be observed (Figure 5.7a). But upon heating to approx. 75 °C, the slurry mass melted and rapidly became a homogeneous red liquid (Figure 5.7b).

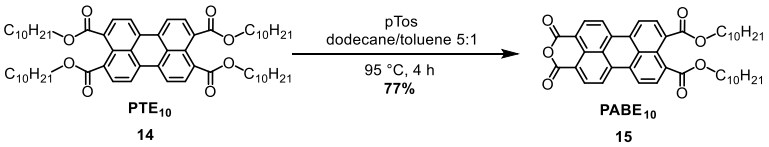

Scheme 5.14. Acid catalyzed unilateral ester cleavage of PTE_{10} **14** and anhydride formation to $PABE_{10}$ **15**.

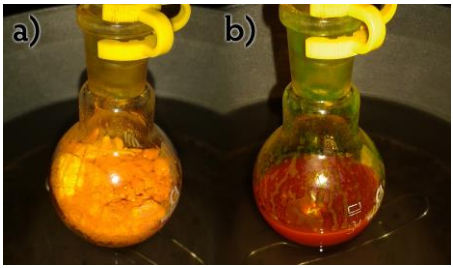

Figure 5.7. Solubility of PTE_{10} **14** in dodecane/toluene at rt **(a)** and at 95 °C **(b)**.

To obtain the mono anhydride, *p*-toluenesulfonic acid (*p*-Tos) was added and the reaction was stirred at 95 °C for 4 h. The product **15** proved to be insoluble under these conditions and precipitated, forming a viscous red mass which had to be stirred manually using a spatula. When PTE_{10} **14** was (almost) consumed completely, the reaction was stopped and cooled down. The crude product was dissolved in chloroform (+ 1% acetone), and mixed with silica gel (at least 250 g

per 10 g of PTE_{10} **14**). Perylenes generally tend to clog the column/plug when eluting with ethyl acetate or ethers, especially at high perylene concentrations. For this reason, it was essential to apply the perylenes on silica gel prior to washing/eluting. Evaporation of the solvent led to a red $PABE_{10}$/silica gel powder which was put onto a short plug and washed with acetonitrile (1.2 L) to remove decanol and *p*-Tos (Figure 5.8a-b). Again, the solvents were constantly recycled to limit the waste. Washing with ethyl acetate (1.4 L) eluted residual PTE_{10} **14** and minor amounts of $PABE_{10}$ **15** (Figure 5.8c).

When all PTE_{10} was eluted, it was switched to chloroform (+ 1% acetone, 6 L) to obtain pure $PABE_{10}$ **15** (Figure 5.8d-h), which was fully characterized by $^{1}H/^{13}C$ NMR, MS, IR and UV-Vis. The prior isolated crude fractions (as mixture of PTE_{10} **14** and $PABE_{10}$ **15**) were purified accordingly. This optimized workup procedure could be performed in multigram (~ 10 g) scale. If the silica gel was too alkaline, it could happen that the perylene anhydride was opened and retained on the plug. If this occurred, slight acidification using acetic acid helped.

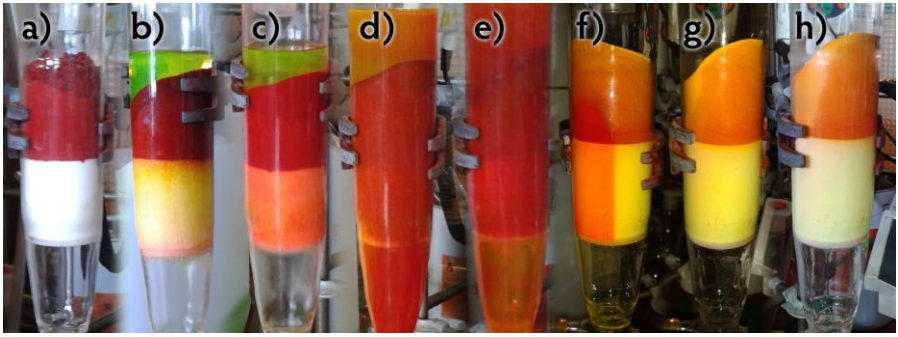

Figure 5.8. Purification of $PABE_{10}$ **15** *via* a plug of silica gel: **(a)** The perylene was applied on silica gel and put on top of the plug. **(b)** Washing with acetonitrile eluted decanol. **(c)** Washing with ethyl acetate eluted PTE_{10} **14** and traces of $PABE_{10}$ **15**. **(d-e)** As soon as no PTE_{10} was eluted anymore, it was switched to chloroform + 1% acetone to rapidly elute pure $PABE_{10}$. **(f)** The plug may elute irregulary, this has no effect on separation quality. **(g-h)** The elution of $PABE_{10}$ is complete.

Drying led to a sticky red varnish (Figure 5.9a) which could hardly be removed from the flask. To provide better handling of the perylenes, lyophilization (*i.e.*, freeze-drying) is recommended. Thus, the varnish was dissolved in little amounts of hot THF. An excess of water (20:1 or higher) was added and the mixture was quickly frozen in liquid nitrogen. Evaporation of the solvents using a lyophilizer yielded $PABE_{10}$ **15** (77.3%) as a voluminous red powder (Figure 5.9). This reaction was as well performed by several bachelor students, generally leading to high yields (72.3 – 77.3%).[237] One exception was a reaction with too long heating time (21 h) yielding only 43.2% $PABE_{10}$. Further reactions which led to mixtures of PTE_{10} and $PABE_{10}$ were combined and purified accordingly following this optimized workup procedure.

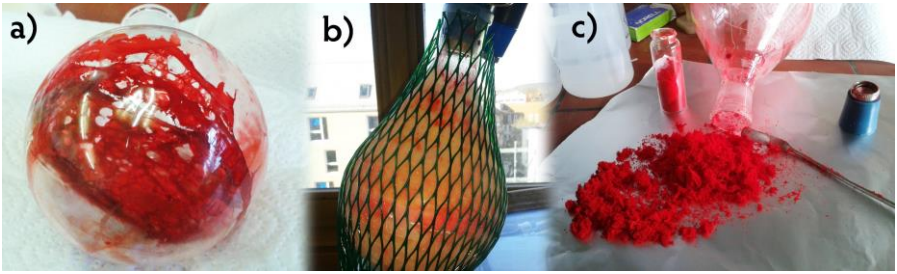

Figure 5.9. (a) Perylenes tend to form varnishes which stick to the walls of the glassware. **(b)** The freeze-drying process of $PABE_{10}$ **15** using a lyophilizer. **(c)** $PABE_{10}$ **15** became a voluminous red powder after freeze-drying.

In theory, the ester cleavage reaction of PTE_{10} **14** could either proceed *via* base or acid catalysis.[100] The alkaline saponification is an irreversible reaction and should proceed clean and complete. However, it proved difficult to control the reaction in order to obtain only the monoanhydride. The reversibility of the acid hydrolysis, in contrast, can be used to our advantage: Even if the initial ester bond cleavage does not occur at the "correct" positions to allow for the formation of an anhydride (Scheme 5.15 bottom), the conversion to the desired product can be directed by the equilibrium and reversibility of the reaction (Scheme 5.15).[100] Hence, PTE_{10} **14** can be unilaterally hydrolyzed to $PABE_{10}$ **15** in good yields.

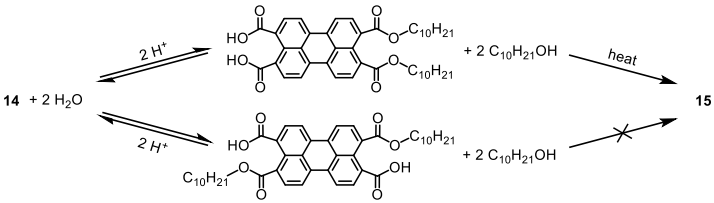

Scheme 5.15. Mechanism of acid catalyzed ester cleavage of PTE_{10} **14**: Reversibility is an advantage as the reaction can be directed to form only the desired product **15**. The trans-disester (bottom) is consumed while **15** is removed from the equilibrium due to low solubility.[100]

At high temperatures (> 90 °C), a ring closure reaction forming the anhydride occurs rapidly, leading to the desired product $PABE_{10}$ **15**. As the second hydrolysis of $PABE_{10}$ to PTCDA had to be avoided, the solubility of PTE_{10} and $PABE_{10}$ in the dodecane/toluene 5:1 solvent mixture at 90 °C was accurately adjusted. Under these conditions, the former was dissolved well while the latter was hardly dissolved. This allowed to precipitate the product $PABE_{10}$ **15**, removing it from equilibrium and driving the reaction to completeness.[100] Using *p*-Tos as acid comprised several advantages:

1. The solubility of the organic acid concurred well with the solvents and perylene compounds.
2. The acid strength suited well to the hydrolysis reaction
3. The *p*-Tos monohydrate served as water source, supplying the exact amount of water necessary for the reaction.[100]

Having the perylene monoanhydride $PABE_{10}$ **15** at hand, a coupling with the porphyrin amine **13** (see page 49) could be performed. Additionally, further derivatization reactions on the perylene core could be made. The synthesis of the perylene(swallowtail)imide bisdecylester (PI_SBE_{10}) **16** was performed by Corinna Weiß, a colleague in the HIRSCH group, during the course of her MSc thesis (Scheme 5.16).[238] "Swallowtail" is a common term for long aliphatic molecules which originate at a single point and divide into usually two chains of same (or – less commonly – different) length.[77,111,118,121,150,238-239] In this work, 6-undecylamine was reacted with the perylene anhydride to give a symmetrical (hexyl-1-pentylimide)swallowtail perylene.[238] Swallowtail groups usually induce a higher solubility in peryleneic structures. This is accomplished by the increased steric demand of the swallowtails, which inhibits the intermolecular π-π interactions and leads to the formation of less ordered molecular stackings. Indeed, the solubility of PI_SBE_{10} **16** in organic solvents is higher compared to PTE_{10} **14**.

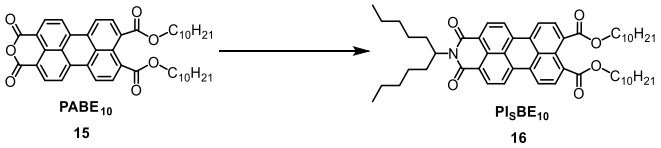

Scheme 5.16. Imidization of $PABE_{10}$ **15** to the swallowtail imide PI_SBE_{10} **16**, performed by Corinna Weiß.[238]

Thankfully, Corinna Weiß provided 250 mg of PI_SBE_{10} **16** for further syntheses in this thesis.[238] This swallowtail perylene was reacted to perylene(swallowtail)imide anhydride (PI_SA **17**) using the same hydrolysis reaction with *p*-Tos which was already presented above (p. 52). As amides and imines are considerably more stable than esters, the reaction time could be extended to 27 h and higher amounts of *p*-Tos (1.5 eq) could be used to ensure complete conversion without risking the retrieval of PTCDA (Scheme 5.17). Furthermore, it was not necessary to adjust the exact solubility: No other side products were expected and the equilibrium could instead be shifted towards the product PI_SA **17** by increasing the amount of *p*-Tos.

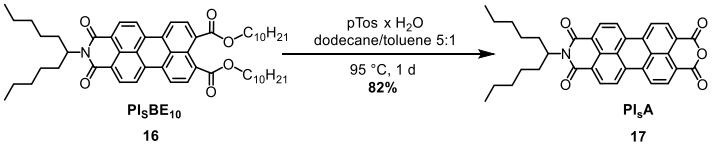

Scheme 5.17. Acid catalyzed unilateral ester cleavage of PI_SBE_{10} **16** and anhydride formation to PI_SA **17**.

After the reaction, the mixture was allowed to cool down. The raw product was dissolved in THF and applied on silica gel. Here it proved reasonable to add a few drops of acetic acid, as otherwise some of the PI_SA would be retained on the column due to anhydride opening induced by the silanol groups of the silica gel. The silica gel plug was washed with hexanes and diethyl ether. Switching to chloroform (+1% acetone) yielded traces of starting compound PI_SBE_{10} **16** in the first fraction and pure PI_SA **17** (82.1%) in the following fractions. PI_SA **17** was fully characterized by $^1H/^{13}C$/DEPT-135 NMR, IR, UV-Vis and melting point analysis. MS analysis and fluorescence emission spectra can be found elsewhere.[238]

After elaborate optimization of the perylene reactions – especially regarding the purification – high yields of approx. 80 – 90% could be achieved (Table 5.5). An overall consecutive yield of 56.4% in three steps was calculated. The yield of Corinna Weiß' PI_SBE_{10} **16** was not included in this calculation, as this synthesis was not part of this thesis.[238]

Table 5.5. Overall yield for the perylene synthesis cascade.

	applied		obtained		yield	
	m	n	m	n	reaction	consec.
14	5.00 g	12.7 mmol	11.29 g	11.33 mmol	88.9%	88.9%
15	10.24 g	10.35 mmol	5.53 g	8.00 mmol	77.3%	68.7%
17	211.3 mg	250.3 µmol	112.1 mg	205.4 µmol	82.1%	56.4%

5.3 Condensation of Porphyrin and Perylene

Both $PABE_{10}$ **15** and PI_SA **17** could be connected to the porphyrin core by standard LANGHALS perylene imidification reactions in molten imidazole.[84,108] The addition of $Zn(OAc)_2$ led to higher yields and better conversions, but with a concurrent metallation of the porphyrin center.

The amine porphyrin **13** and a slight excess of $PABE_{10}$ **15** (1.2 eq) were mixed with $Zn(OAc)_2$, NEt_3 and imidazole. The mixture was melted (MP of imidazole: 90 °C) and stirred at 100 °C for 1 h until the reaction was completed (Scheme 5.18). Imidazole could be removed by dissolving the crude mixture in $CHCl_3$ and washing with water multiple times. As the porphyrin was converted quantitatively, a purification *via* a plug of silica gel (eluent: chloroform + 1% NEt_3) yielded pure zinc porphyrin–PEP–$PIBE_{10}$ dyad **18** (92.6%). $PABE_{10}$ was completely retained on the plug. Switching to chloroform (+ 1% acetone) eluted residual $PABE_{10}$ **15**. Additional crude $PABE_{10}$ could be recovered after acidifying and washing with THF + 1% acetic acid. Dyad **18** was fully characterized by ^1H/DEPT-135/COSY NMR, IR, UV-Vis and melting point analysis. Owing to the size and complexity of the molecule, no sufficiently well-resolved ^{13}C NMR spectrum could be recorded and the molecule was not detected in MS measurements.

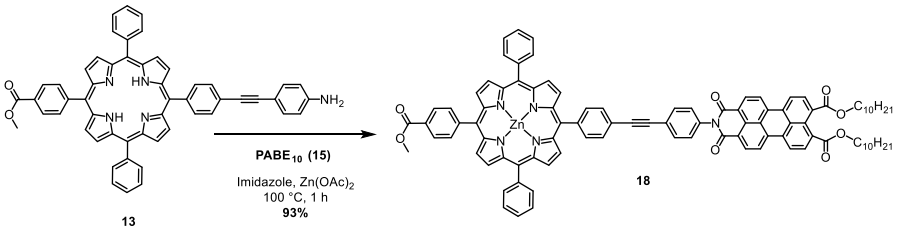

Scheme 5.18. Condensation of amine porphyrin **13** with $PABE_{10}$ **15** to the metallated porphyrin–perylene dyad **18**. See Figure 5.10 for NMR assignment of the aromatic protons.

For correct attribution of the NMR spectra – especially in the crowded aromatic region – a two-dimensionally correlated ^1H NMR spectrum (COSY) was recorded (Figure 5.10). Using COSY NMR, the scalar spin-spin couplings between protons can be detected to identify and assign vicinal groups.[213] This spectrum was measured in DMSO-d_6. To increase the resolution and to prevent overlapping of the peaks, a drop of $CDCl_3$ was added which led to an additional strong singlet at 7.97 ppm. The porphyrinic β-pyrrole protons are observed at 8.85 – 8.72 ppm (a/b) and exhibit a coupling pattern which is characteristic for polarized porphyrin systems.[9] The perylene imide bisester is likewise polarized and the coupling pattern can be compared to PI_SBE_{10} **16** (see spectroscopic supplement, p. 248). The perylene protons *ortho* to the imide are slightly shifted from 8.62 ppm to 8.58 ppm (e). COSY allows an exact assignment of the inner perylene protons:

meta$_{imide}$ and *meta*$_{ester}$ protons are found overlapping at 8.70 (c) and 8.66 ppm (d), respectively. As expected, the *ortho*$_{ester}$ perylene protons are strongly shifted upfield to 8.14 ppm (j). The correlated signals at 8.35 (f) and 8.25 ppm (g) can be attributed to the aromatic methyl benzoate protons. The doublets at 8.20 (h) and 7.94 ppm (k) are assigned to the aromatic protons at the PEP bridge *ortho* and *meta* to the porphyrin. The residual four protons of the PEP bridge are found at 7.82 (l) and 7.48 ppm (n). The coupling pattern of the unsubstituted phenyl groups at the porphyrin correlate with the spectrum of tetraphenylporphyrin (TPP):[9] the *ortho* protons exhibit an multiplet at 8.14 ppm (i) while the *meta* and *para* protons overlap in the region between 7.77 – 7.68 ppm (m).

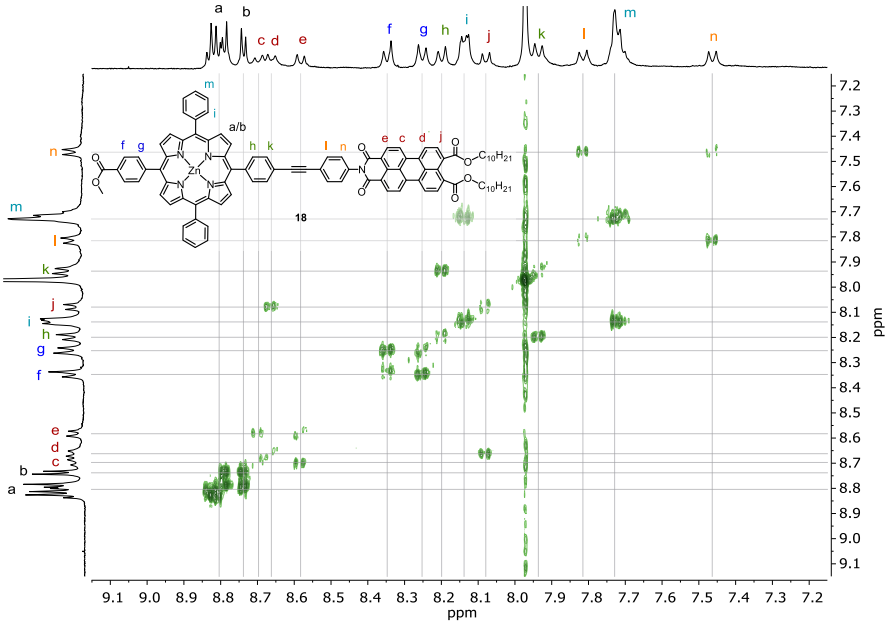

Figure 5.10. Combined COSY NMR spectrum of **18** in DMSO-d_6 (with traces of $CDCl_3$ at 7.97 ppm). Only the aromatic region is displayed.

Accordingly, porphyrin **13** was reacted with PI$_S$A **17** to the metallated zinc porphyrin–PEP–PDI$_S$ dyad **18b** (PDI$_S$ = perylene diimide(swallowtail), Scheme 5.19). Here, porphyrin **13** was applied in excess as only small amounts of **17** were available. Unfortunately, after 3 h of reaction time, perylene **17** was still present, lowering the expected yield. The purification could not proceed as smooth as in the case of **18**, since chloroform as a solvent would elute both starting compounds **13** and **17** as well as product **18b** owing to the increased solubility of the swallowtail group. To circumvent this, the crude product was adsorbed on a short plug of silica gel and first

washed with hexanes/ethyl acetate (3:2 + 1% acetone + 5% NEt_3) to obtain pure porphyrin **13**. Switching to chloroform + 1% NEt_3 and chloroform + 1% acetone, a mixture of product **18b** and PI_5A **17** were eluted. In a second purification step, zinc porphyrin–PEP–PDI_5 dyad **18b** was purified *via* column chromatography and isolated in 41.2% yield.

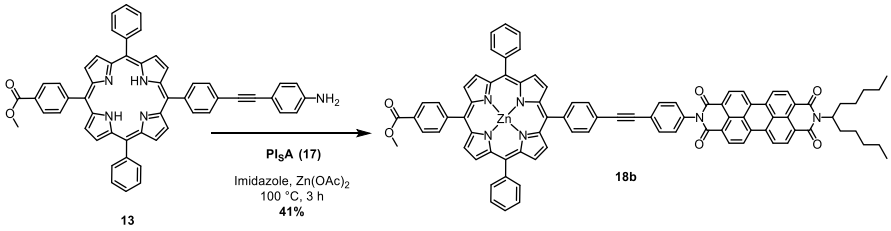

Scheme 5.19. Condensation of amine porphyrin **13** with PI_5A **17** to the metallated porphyrin–perylene dyad **18b**.

The condensation reaction of porphyrin **13** and $PABE_{10}$ **15** (see Scheme 5.18, p. 57) could also be performed without $Zn(OAc)_2$ in good yield (87.6%). Complete conversion took reasonably longer (16 h at 120 °C) but could finally be reached by addition of traces of THF (Scheme 5.20). Although LANGHALS found that the presence of $Zn(OAc)_2$ in this reaction is crucial,[84] in this case the reaction worked, albeit at the expense of longer reaction times. The crude product was suspended in water and filtered through celite (eluent: water) to elute imidazole. Subsequent extraction with THF and multiple gel permeation chromatographies (GPC) yielded the free-base porphyrin–PEP–$PIBE_{10}$ dyad **18c**.

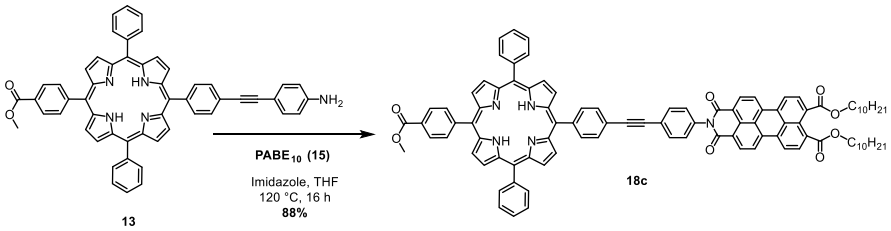

Scheme 5.20. Condensation of amine porphyrin **13** with $PABE_{10}$ **15** in the absence of $Zn(OAc)_2$ to the free-base porphyrin–perylene dyad **18c**.

Dyads **18b** and **18c** were fully characterized by ^1H/DEPT-135 NMR, IR and UV-Vis. The ^{13}C NMR spectrum of **18c** was reasonably well-resolved, although not every peak (*e.g.*, the triple bond carbon atoms) could be detected over the background noise. The free-base porphyrin **18c** could be successfully detected by MS spectrometry, which was not the case for the metallated Zn porphyrin dyads **18** and **18b**.

In the next step, the methyl ester group at the porphyrin should be hydrolyzed to give the free acid porphyrin–PEP–perylene dyad **19**. A sufficiently selective strategy had to be developed which would spare the decyl esters, the metallated porphyrin and the quite susceptible triple bond. As the methyl ester is reasonably acid stable and the acetylene bond previously showed instability towards acids (p. 45), it was planned to hydrolyze the methyl ester using well-adjusted alkaline conditions (see chapter "Orthogonal Protecting Group Strategy", p. 28).

To find optimal reaction conditions, different reagents, solvents and temperatures were tested (Table 5.6). Upon reaction with NaOH, the solution was strongly green-colored (a). Test reaction (b) showed that this color change can be assigned to – not further investigated – reactions at the perylene core. The starting compound was consumed completely, but the hardly soluble green products were not the desired product and could not be assigned by NMR. The use of weaker bases such as K_2CO_3 or LiCl did not lead to any conversion (c-f). Acid catalyzed reactions with *p*-Tos did not lead to a hydrolysis of the methyl ester (g-k). Here, the green color change was caused by protonation of the free-base porphyrin (compare i and k). Additionally, a ester cleavage reaction at the perylene was expected (*cf.* Scheme 5.15). Using toluene as a solvent, indeed a conversion of the starting compound could be observed upon longer reaction times or higher temperatures (i-k). However, NMR spectroscopic evaluations showed that neither the methyl ester nor the decyl ester had been cleaved. The respective approaches were abandoned therefore.

Finally, LiOH turned out to be an appropriate reagent for selective base catalyzed methyl ester hydrolysis (l-s). It was found that the decyl esters stayed completely untouched and neither the – metallated or free-base – porphyrin nor the triple bond were affected. At room temperature, the reaction did not proceed in THF (reagent grade) with or without addition of water (l, m, q). Upon heating to 80 °C in THF, the first hints of a reaction could be observed after 1 d (r). The addition of water to support the hydrolysis was important, but still did not lead to complete conversion (n). Interestingly, by using more than just a few drops of water, the solution again turned green (compare to reaction a, b).

In the small-scale test reactions, the addition of MeOH turned out to be crucial to ensure a fast and complete reaction, which only occurred when heating to 80 °C in a closed vessel (o, s). The ratio of solvents had to be adjusted carefully. The use of THF/MeOH/H_2O (50/10/1 mL) and 15 eq of LiOH led only to 43.3% conversion of the free-base Por-PEP-$PIBE_{10}$ **18c** to dyad **19c** after 3 d of reaction (p, Scheme 5.23). In contrast, the reaction of ZnPor-PEP-$PIBE_{10}$ **18** using a larger excess of LiOH (63 eq) in THF/MeOH/H_2O (50/5/0.5 mL) could be successfully completed to dyad **19** in 93.5% yield after only 2 h at 80 °C (t, Scheme 5.21). Finally, the reaction of ZnPor-PEP-PDI_S **18b** with 60 eq of LiOH and the solvent mixture THF/MeOH/H_2O (10/1/0.1 mL) proceeded successfully to dyad **19b** with 61.7% yield after 2 h (u, Scheme 5.22). Astonishingly, traces of free perylene (mainly PI_SA **17**) and the corresponding counterpart (acid-ZnPor-PEP-NH_2, according to mass spectrometry) could be isolated. This was the first indication of instability of the aromatic peryleneic imide bond under certain conditions (*cf.* p. 67f).

Table 5.6. Test reactions towards the selective methyl ester hydrolysis of the porphyrin–perylene dyads **18/b/c**. It was found that NaOH, K_2CO_3, *p*-Tos and LiCl did not lead to successful conversion. The amount of LiOH as well as the exact ratio of solvents was investigated at different temperatures and the reaction was optimized to yield up to 94% (entry t).

	reagents	conditions	yield & results
a)	**Por-PEP-PIBE$_{10}$** (5 mg), **NaOH** (10 mg), THF/MeOH (2/1 mL)	rt, 4 h	strong green color, insoluble, not the product
b)	**G^1-PIBE$_{10}$** (5 mg), **NaOH** (10 mg), THF (3 mL)	80 °C, 3 d	strong green color, soluble in H_2O, NMR: no product, not assignable.
c)	**Por-PEP-PIBE$_{10}$** (5 mg), **K_2CO_3** (10 mg), THF/MeOH (2/1 mL)	rt, 3 d	no reaction
d)	**Por-PEP-PIBE$_{10}$** (5 mg), **K_2CO_3** (10 mg), THF/MeOH (2/1 mL) + drop H_2O	100 °C, 22 h	no reaction
e)	**Por-PEP-PIBE$_{10}$** (5 mg), **LiCl** (10 mg), DMF (3 mL) + drop H_2O	rt, 3 d	no reaction
f)	**Por-PEP-PIBE$_{10}$** (5 mg), **LiCl** (10 mg), DMF (3 mL) + drop H_2O	100 °C, 22 h	no reaction
g)	**Por-PEP-PIBE$_{10}$** (5 mg), ***p*-Tos** (10 mg), DMF (3 mL)	rt, 4 h	green due to protonation of porphyrin, no reaction
h)	**Por-PEP-PIBE$_{10}$** (5 mg), ***p*-Tos** (200 mg), DMF (3 mL)	rt, 3 d	green due to protonation of porphyrin, no reaction
i)	**Por-PEP-PIBE$_{10}$** (5 mg), ***p*-Tos** (10 mg), toluene (3 mL)	100 °C, 22 h	green, complete reaction, NMR: no product; C_{10} still present.
j)	**G^1-PIBE$_{10}$** (5 mg), ***p*-Tos** (10 mg), toluene (3 mL)	rt, 3 d	complete reaction, NMR: no product; C_{10} still present.
k)	**G^1-PIBE$_{10}$** (5 mg), ***p*-Tos** (10 mg), toluene (3 mL)	80 °C, 2 d	complete reaction, NMR: no product; C_{10} still present.
l)	**Por-PEP-PIBE$_{10}$** (5 mg), **LiOH** (10 mg), THF (3 mL)	rt, 1 d	no reaction
m)	**Por-PEP-PIBE$_{10}$** (5 mg), **LiOH** (10 mg), THF (3 mL) + drop H_2O	rt, 1 d	no reaction
n)	**Por-PEP-PIBE$_{10}$** (5 mg), **LiOH** (10 mg), THF (3 mL) + H_2O (2 mL)	80 °C, 1 d	green, reaction not complete
o)	**Por-PEP-PIBE$_{10}$** (5 mg), **LiOH** (10 mg), THF/MeOH (1/1 mL) + drop H_2O	rt –> 80 °C, 3 d	reaction complete
p)	**Por-PEP-PIBE$_{10}$** (210 mg), **LiOH** (50 mg), THF/MeOH/H_2O (50/10/1 mL)	80 °C, 3 d	43%, can be further optimized, **19c**
q)	**ZnPor-PEP-PIBE$_{10}$** (28 mg), **LiOH** (50 mg), THF (20 mL)	rt, 1 d	no reaction
r)	**ZnPor-PEP-PIBE$_{10}$** (28 mg), **LiOH** (50 mg), THF (20 mL)	80 °C, 1 d	reaction, but not complete
s)	**ZnPor-PEP-PIBE$_{10}$** (28 mg), **LiOH** (50 mg), THF/MeOH/H2O (10/5/2 mL)	80 °C, 16 h	complete
t)	**ZnPor-PEP-PIBE$_{10}$** (648 mg), **LiOH** (685 mg), THF/MeOH/H_2O (50/5/0.5 mL)	80 °C, 2 h	94%, complete reaction, **19**
u)	**ZnPor-PEP-PDI$_S$** (67 mg), **LiOH** (70 mg), THF/MeOH/H_2O (10/1/0.1 mL)	80 °C, 2 h	62%, perylene (PI_SA) was partially cleaved, **19b**

The thus obtained free-acid porphyrin–perylene dyads **19**, **19b**, and **19c** were characterized by ^{1}H NMR, IR and UV-Vis. The solubility in organic solvents ($CHCl_3$, THF) is decreased by the presence of the acid group and the resolution of FT-IR and ^{1}H NMR spectra is poor. However, it was possible to record a DEPT-135 NMR spectrum for dyad **19** and MALDI MS for dyads **19** and **19c**. In the case of **19b**, only the cleaved by-product (acid-Zn-porphyrin-PEP-amine) could be detected by mass spectrometry.

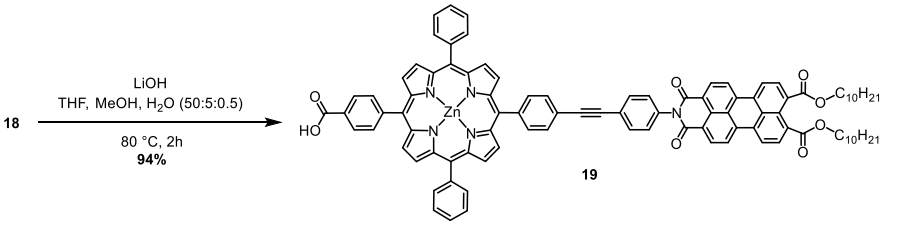

Scheme 5.21. Selective hydrolysis of methyl ester porphyrin-PEP-perylene dyad **18**.

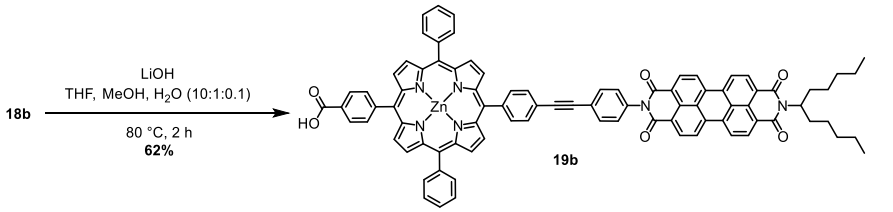

Scheme 5.22. Selective hydrolysis of methyl ester porphyrin-PEP-perylene dyad **18b**.

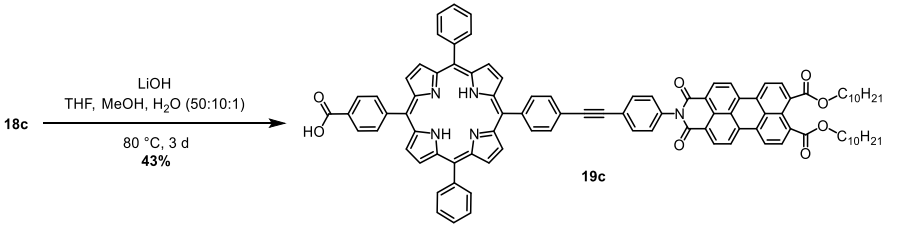

Scheme 5.23. Selective hydrolysis of methyl ester porphyrin-PEP-perylene dyad **18c**.

5.4 Newkome Dendrimer Synthesis

NEWKOME dendrimers are well-known and widely applied in the HIRSCH group. The convergent reaction cascade towards G^1 and G^2 NEWKOME dendrons is straightforward– these reactions are explained in greater detail in the literature.[50,134,196] As the dendron compounds are colorless and do not exhibit any fluorescence, iodine adsorbed on silica gel was found to be an ideal and reversible stain for TLC analysis.[235]

Nitro G^1 triester **20** is usually prepared as a standard compound in Bachelor laboratory courses and is available in kilogram amounts. The nitro G^1 triester was reduced with Raney nickel in cyclohexane (Scheme 5.24). Purification by column chromatography yielded 30 g of amino G^1 triester **21** (92.2%). A second batch of **20** was deprotected by stirring in formic acid for 20 h (Scheme 5.25). The *tert*-butyl ester groups were cleaved and excess formic acid was removed *via* azeotropic distillation with toluene under reduced pressure. Pure nitro G^1 triacid **22** (98.4%) was obtained. Characterization *via* ^{1}H NMR was sufficient to ensure the successful conversion.

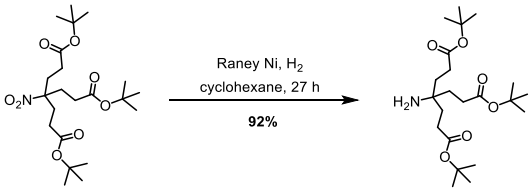

Scheme 5.24. Reduction of the nitro group of **20** to amino G^1 triester **21**.

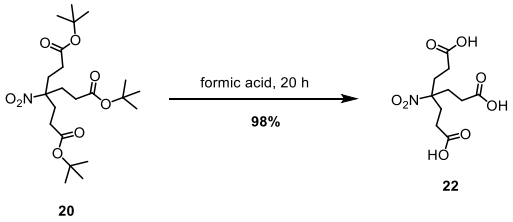

Scheme 5.25. Hydrolysis of the *tert*-butyl ester groups of **20** to nitro G^1 triacid **22**.

Compounds **21** and **22** were combined using a DCC peptide coupling reaction with HOBt hydrate in DMF.[196,240] After 6 days, the reaction mixture was filtered and purified by column chromatography to obtain nitro G^2 nonaester **23** in 85.4% yield (Scheme 5.26).

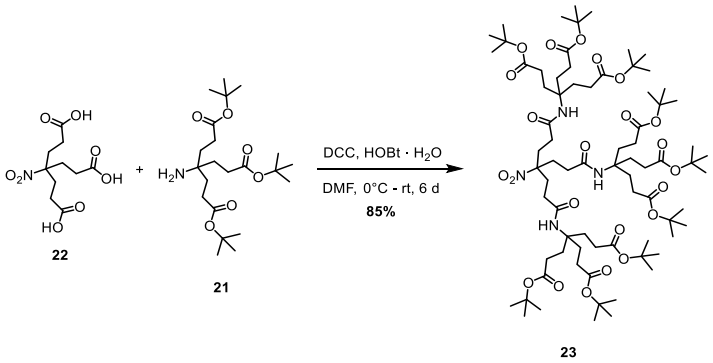

Scheme 5.26. Synthesis of nitro G^2 nonaester **23** out of 1 eq nitro G^1 triacid **22** and 3 eq amino G^1 triester **21**.

Finally, nitro G^2 nonaester **23** was reduced to amino G^2 nonaester **24** by hydrogenation with Raney nickel (Scheme 5.27). The amino G^2 nonaester was obtained pure after filtration through celite (eluent: EtOH) and lyophilization in high yield (99.6%). ^{1}H NMR and MP analysis sufficiently identified the literature-known compounds.[50,134,196]

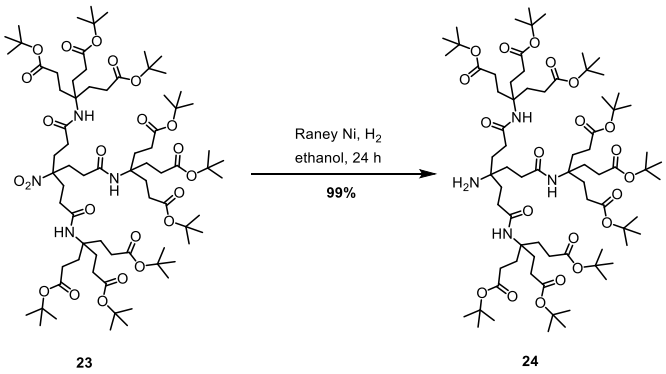

Scheme 5.27. Reduction of the nitro group of **23** to amino G^2 nonaester **24**.

The well-elaborated synthesis cascade to NEWKOME dendrimer **24** could be performed with a maximum consecutive yield of 77.2% over 4 steps (Table 5.7). The first reaction step of nitromethane and *tert*-butyl acrylate to nitro G^1 triester **20** was omitted in this table as the synthesis was not part of this thesis.[50,134]

Table 5.7. Overall yield for the Newkome dendrimer synthesis cascade.

	applied		obtained		yield	
	m	n	m	n	reaction	consec.
21	35.00 g	78.55 mmol	30.11 g	72.46 mmol	92.2%	92.2%
22	10.00 g	22.44 mmol	6.12 g	22.11 mmol	98.4%	90.7%
23	1.00 g	3.61 mmol	4.53 g	3.08 mmol	85.4%	77.5%
24	4.10 g	2.79 mmol	4.00 g	2.78 mmol	99.6%	77.2%

5.5 Attachment of Dendrimers to the Porphyrin–Perylene Dyads

The free amino groups of **21** (amino G^1 triester) and **24** (amino G^2 nonaester) could be attached to the acid group of the acid porphyrin-PEP-perylene dyad. For this purpose, again a DCC coupling was applied.[240-242]

Condensation of acid zinc porphyrin–perylene dyad **19** with amino G^1 triester **21** led to G^1 zinc porphyrin-PEP-perylene dyad **1a** in 11.5% yield after a reaction time of 11 days in DMF and several tedious column chromatographies (Scheme 5.28). As stated before (p. 60), again cleavage of $PABE_{10}$ could be detected. Interestingly, this degradation did not only occur during reaction, but more importantly also on the silica gel or Bio-beads columns upon purification, being a reason for the low yield. Moreover, it proved difficult to drive the reaction to completeness, resulting in considerable amounts of the starting compounds.

Accordingly, dyad **19** was reacted with amine G^2 nonaester **24** to the dyad **1b** equipped with the second generation dendron in 14.5% yield after a reaction time of 7 days (Scheme 5.29). To separate excess amine G^2 nonaester from the product, gel permeation chromatography was applied, which unfortunately again led to partial cleavage of the perylene. Products **1a** and **1b** were fully characterized by ^{1}H/DEPT-135 NMR, IR, UV-Vis and emission spectroscopy. Both molecules could not be detected by mass spectrometry. G^1 dyad **1a** was reasonably soluble in THF and ethyl acetate, and less soluble in $CHCl_3$. In contrast, G^2 dyad **1b** showed only minor solubility in $CHCl_3$. Nevertheless, it still was possible to record the ^{1}H/DEPT-135 NMR spectra in $CDCl_3$.

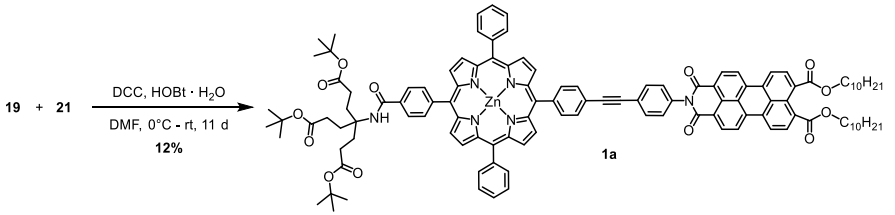

Scheme 5.28. DCC coupling of Zn porphyrin-perylene dyad **19** with amine G^1 triester **21** to **1a**.

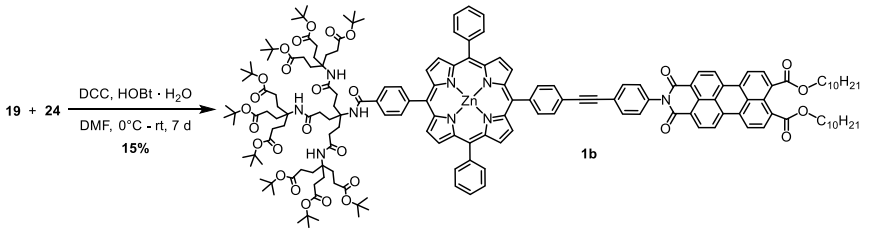

Scheme 5.29. DCC coupling of Zn porphyrin-perylene dyad **19** with amine G^2 nonaester **24** to **1b**.

To broaden the variety and scope of the products, two more reactions were performed: The zinc porphyrin-PEP-perylene dyad **19b** carrying a swallowtail aliphatic chain was condensed with amine G^1 triester **21** to the dyad **1c** in 37.9% yield after 7 days (Scheme 5.30). Here, the higher solubility induced by the swallowtail moiety allowed the use of hexanes/ethyl acetate instead of THF as solvents. Furthermore, a short flash column chromatography (instead of gel permeation chromatography) sufficed to purify the product **1c**. These might be the reasons that in this case no cleavage of perylene was observed.

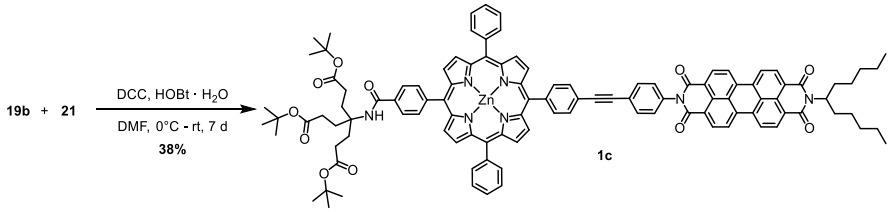

Scheme 5.30. DCC coupling of Zn porphyrin-perylene swallowtail dyad **19b** with amine G^1 triester **21** to **1c**.

Lastly, free-base porphyrin-PEP-perylene dyad **19c** was reacted with amine G^1 triester **21** to yield the non-metallated dendritic porphyrin–perylene dyad **1d** (Scheme 5.31). Here, the reaction temperature was raised to 80 °C for 4 days to provide a complete reaction. THF previously prove crucial to cleavage side reactions, indicating a destabilizing effect on the imide system. Nevertheless, THF had to be applied again for purification and after short column chromatography (hexanes/THF) and gel permeation chromatography (THF), two main fractions were isolated. Fraction 1 was rather pure **1d** (36.5%) and could be used for the upcoming hydrolysis reaction. NMR spectra of fraction 2 (29.7%) confirmed a reduced ratio of the perylene signals, which was a further sign of the perylene cleavage.

Mass spectrometry investigations indicated mainly the presence of $PABE_{10}$ **17** with other unidentified by-products. Further investigations into the stability issues of the aromatic phenyl-ethynyl-phenyl perylene imide bond as well as the exact structure of the obtained decomposition products were beyond the scope of this thesis and were omitted.

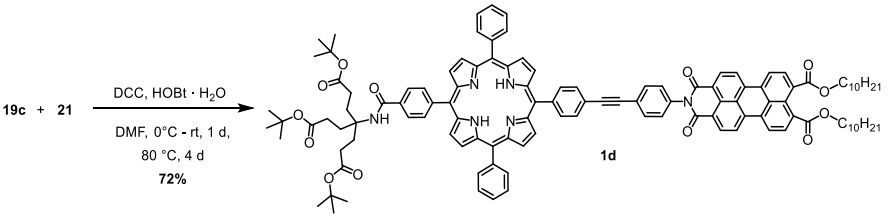

Scheme 5.31. DCC coupling of free-base porphyrin–perylene dyad **19c** with amine G^1 triester **21** to **1d**. During the reaction and chromatography steps, partial cleavage of product **1d** occurred.

Dyad **1c** was fully characterized by $^{1}H/^{13}C$/DEPT-135 NMR, IR, UV-Vis and emission spectroscopy. It was possible to detect a weak molecular signal in APPI-MS. No ^{13}C/DEPT-135 spectra could be recorded in a reasonable time period for unmetallated free-base porphyrin–perylene dyad **1d**. However, it was possible to characterize product **1d** by ^{1}H NMR, IR, UV-Vis, emission spectroscopy and mass spectrometry. Both products were obtained as a brownish powder. The dyads were well soluble in THF and ethyl acetate while showing only limited solubility in $CHCl_3$.

Carboxylic imide systems possess a high resonance stabilization, which is further increased in conjugation with additional aromatic ring structures.[78] Usually, perylene imides are said to exhibit outstanding chemical, photochemical and environmental stability,[116,243] and the imide bond is known to be unaffected by a large variety of solvents.[116] For example, the acidic hydrolysis of a perylene imide is usually performed in conc. sulfuric acid at 180–200 °C because of the persistency of this kind of molecules.[80,92] The alkaline hydrolysis of aromatic imides is performed under considerably milder – but nevertheless strongly alkalic – conditions with KOH in *tert*-BuOH.[80,93] The general hydrolytic stability of imides was investigated by DONSKIKH *et al*. in 1987 using N-(*o*-carboxyphenyl)naphthalimide and N-phenyl-phthalimide as model compounds.[244] It was shown that the hydrolysis proceeds irreversibly in the pH range between 11.6–12.6. At pH range 9.9–11.0, the ring-opening reaction is reversible but still occurs readily. At pH < 8, the imide hydrolysis rate is pH independent and only proceeds slowly, rather shifting the equilibrium towards imide cycle formation.

Furthermore, it was found by DONSKIKH *et al*. that phthalimides are more prone to hydrolysis than naphthalimides, and phenylimides are less stable than *o*-carboxylphenylimides. The former was attributed to the stronger electron donor properties of the naphthalene ring which renders the imide carbonyl groups less electrophilic. The latter was explained by the repulsive negative charge of a carboxyl group at high pH, preventing the formation of the "*active ionized form of imide*" – that is, one of the imide carboxyl groups being hydrolyzed, leading to an acetal.[244] LANGHALS found that the hydrolysis reaction using KOH in *tert*-BuOH proceeds faster with aromatic perylene imides (*i.e.*, with an aromatic group attached to the nitrogen) compared to perylene imides with aliphatic chains.[93]

Bearing this in mind, it is still questionable why the imide bond is so weak in the presented molecules **1a-d** using DMF or THF as solvents – both at ambient conditions and in silica gel or Bio-Beads columns. This behavior possibly limits the scope of application for the synthesized molecules. However, as soon as the deprotection of the dendritic *tert*-butyl esters – which proceeds under acidic conditions – is completed, it can be expected that the hydrolytic stability at higher pH should be greatly enhanced: The molecules should be less prone to hydrolysis under formation of carboxylate anions when they are already carrying three or nine negative charges.

5.6 Hydrolysis to a Water-Soluble Porphyrin–Perylene Dyad

The cleavage of the dendritic *tert*-butyl protective groups is usually performed by stirring the reagent in formic acid at rt for 24 h.[134] Under these mild acidic conditions, the *tert*-butyl ester is cleaved completely while retaining other acid labile groups, such as other aliphatic esters or the metallated porphyrin (*cf.* chapter 4.2, p. 31). After the reaction was complete, the formic acid was removed *via* azeotropic distillation with toluene under reduced pressure. By washing the product with CH_2Cl_2, ethyl acetate, ethanol and finally with slightly acidified water, all organic and inorganic impurities – such as salts or decomposition products – could be successfully removed. The amphiphilic products **2a-d** showed only slight solubility in THF and reasonable solubility in DMF and water at alkaline pH. As expected, the products were insoluble in ethyl acetate, ethanol, $CHCl_3$, and CH_2Cl_2.

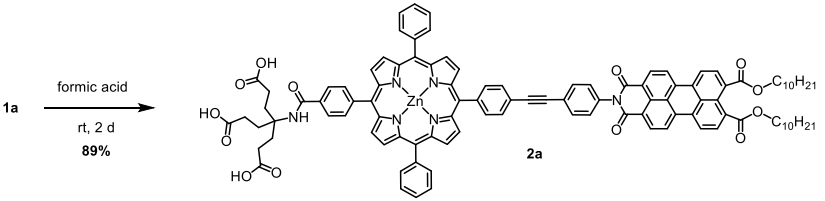

Scheme 5.32. Synthesis of target product **2a** by hydrolysis of the dendritic dyad **1a** in formic acid.

The G^1-dendritic triester zinc porphyrin–PEP–$PIBE_{10}$ dyad **1a** was stirred in formic acid for 2 days and filtered through a plug of celite after the removal of formic acid (Scheme 5.32). Different slightly purple fractions were obtained by washing with water (500 mL, slightly acidified by addition of 3 drops of 1 M HCl), ethanol, and CH_2Cl_2. Both TLC analysis and solubility experiments confirmed that these fractions did not contain the desired product, as no water solubility at elevated pH was observed. Further washing with THF (slightly acidified by 1% acetic acid) eluted the pure dyad **2a** in 89% yield. As only minor amounts (13.2 mg) of **1a** could be applied for this reaction, the final product **2a** was obtained merely in 10.7 mg (Table 5.8). Luckily, this was enough to perform multiple measurements to characterize this product. Dyad **2a** was fully characterized by $^1H/^{13}C$/DEPT-135 NMR (in THF-d_8 acidified with TFA-*d*), IR, UV-Vis and emission spectroscopy. The molecule could not be detected in mass spectrometry.

Over the whole reaction cascade, 18 separate reactions were performed in total. The longest consecutive reaction sequence consisted of 11 successive steps, originating from compound **3** to product **2a**. The maximum consecutive yield of these 11 steps was as low as 1.2%, mainly owing to two bottlenecks of the cascade:

1. the formation of unsymmetric AB_2C porphyrin **12** with 30.3% yield (p. 41ff),
2. the final DCC-mediated coupling reaction of amine G^1 triester **21** with the zinc porphyrin-PEP-perylene dyad **19** to product **1a** with 11.5% yield (p. 66).

Especially the latter reaction reduced the overall consecutive yield drastically. DCC couplings can usually be performed in high yields (compare for example reaction **23** with 85.4%, p. 64). However, the reaction conditions of DCC or EDC couplings often have to be fine-tuned to work well with larger and diverse molecules. In this special case of dyad **1a**, additional investigations and optimizations should be performed to reduce side reactions and degradation. If the yield of this penultimate reaction could be further improved, the total outcome of this reaction cascade and the availability of dyad **2a** can be increased considerably.

Table 5.8. Overall yield for the 18 step synthesis cascade to product **2a**.

	applied		obtained		yield	
	m	n	m	n	reaction	consec.
13	725 mg	816 µmol	585.3 mg	742.8 µmol	91.0%	13.2%
18	400 mg	508 µmol	716.7 mg	407.2 µmol	92.6%	12.2%
19	648.2 mg	452.3 µmol	638.4 mg	422.7 µmol	93.5%	11.4%
1a	209.5 mg	109.8 µmol	30.51 mg	15.99 µmol	11.5%	1.3%
2a	13.2 mg	6.92 µmol	10.7 mg	6.1 µmol	88.9%	1.2%

The reaction to G^2-dendritic zinc porphyrin–PEP–PIBE$_{10}$ dyad nonaacid **2b** was performed likewise. The cleavage of the nine *tert*-butyl groups led to a large, water soluble linear dyad with a molar mass of 2427 g/mol (Scheme 5.33). The pure product was again washed with acidified water, ethanol, CH_2Cl_2, and finally extracted with acidified THF. At the first glance, no substantial differences could be found for the solubilities of dyads **2a** and **2b** with three and nine acid groups, respectively: The amphiphilic dyad **2b** was insoluble in ethyl acetate, ethanol, $CHCl_3$, CH_2Cl_2, and other organic solvents while showing low solubility in THF and DMF. At pH > 9, **2b** was soluble in water. Product **2b** could be characterized by ^{1}H NMR in THF-d_8 (acidified with one drop of TFA-d). However, both amount and time were missing to record reasonably well-resolved ^{13}C/DEPT-135 NMR spectra. The molecule could not be detected in mass spectrometry. Further characterization (UV-Vis, fluorescence emission spectroscopy) and aggregation studies are discussed in chapter 5.7 (p. 102ff).

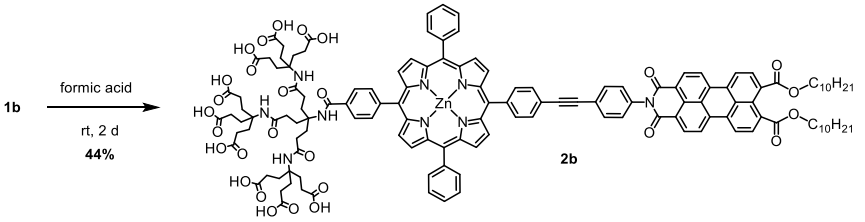

Scheme 5.33. Synthesis of target product **2b** by hydrolysis of the dendritic dyad **1b** in formic acid.

The consecutive yield of the reaction cascade (11 consecutive steps, 21 overall steps) sums up to 0.7% (Table 5.9). Just like product **2a**, the bottleneck turned out to be the last DCC coupling with 14.5% yield (p. 66). Additionally, the final hydrolysis reaction (43.7% yield) performed inferior than expected, leading to a reduced overall yield.

Table 5.9. Overall yield for the 21 step synthesis cascade to product **2b**.

	applied		obtained		yield	
	m	n	m	n	reaction	consec.
13	725 mg	816 µmol	585.3 mg	742.8 µmol	91.0%	13.2%
18	400 mg	508 µmol	716.7 mg	407.2 µmol	92.6%	12.2%
19	648.2 mg	452.3 µmol	638.4 mg	422.7 µmol	93.5%	11.4%
1b	182.3 mg	120.7 µmol	51.3 mg	17.5 µmol	14.5%	1.7%
2b	33.2 mg	4.94 µmol	12.0 mg	4.94 µmol	43.7%	0.7%

Dyad **1c** initially showed a slightly better solubility in organic solvents (*e.g.*, $CHCl_3$) due to the swallowtail branch attached to the perylene. After hydrolysis of the dendritic *tert*-butyl ester groups in formic acid, again no solubility of product **2c** in most organic solvents (*e.g.*, ethanol, ethyl acetate, CH_2Cl_2, $CHCl_3$) and only minor solubility in non-acidified THF was observed (Scheme 5.34). The water-solubility at slightly alkaline pH was comparable to the other target compounds **2a/b**. Dyad **2c** was characterized by ^1H /DEPT-135 NMR, IR, UV-Vis and emission spectroscopy. As it is common for dyads equipped with a metallated porphyrin, the molecule could not be detected in mass spectrometry.

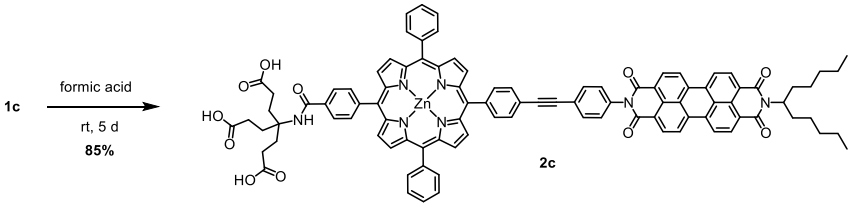

Scheme 5.34. Synthesis of target product **2c** by hydrolysis of the dendritic dyad **1c** in formic acid.

The behavior of the hydrophobic swallowtail group compared to the two decyl chains is a very interesting field, especially when building lipid bilayers from these amphiphilic molecules. Unfortunately, the obtained 11.5 mg of dyad **2c** did only suffice for some basic characterizations and investigations. Now, as a functional synthesis pathway for water soluble porphyrin–perylene dyads has been explored, it would be interesting to synthesize larger amounts of the final dyads. Again, the total consecutive yield is very low with only 1.1% (Table 5.10). The porphyrin building

reaction **12** (p. 41ff) and the low-yielding DCC coupling **1c** (p. 67) have already been discussed. Additionally, the interjacent reactions of dyads **18b** and **19b** with 41.2% and 61.7% yield could not be optimized. This was mainly owing to the limited availability of PI_SBE_{10} **16** and PI_SA **17** during the preparation of this thesis. This reaction cascade featured an overall number of 20 synthetic steps. The consecutive yield of 1.1% in the course of this reaction pathway was determined using the longest succession of reactions (11 steps) starting from **3** to **2c**.

Table 5.10. Overall yield for the 20 step synthesis cascade to product **2c**.

	applied		obtained		yield	
	m	n	m	n	reaction	consec.
13	725 mg	816 µmol	585.3 mg	742.8 µmol	91.0%	13.2%
18b	164.8 mg	209.2 µmol	106.3 mg	77.09 µmol	41.2%	5.4%
19b	67.3 mg	48.8 µmol	41.1 mg	30.1 µmol	61.7%	3.3%
1c	34.9 mg	25.6 µmol	17.1 mg	9.70 µmol	37.9%	1.3%
2c	14.9mg	8.45 µmol	11.5 mg	7.21 µmol	85.3%	1.1%

One last and very interesting member in the group of water-soluble linear amphiphiles was the non-metallated dendritic porphyrin-PEP-$PIBE_{10}$ dyad **2d**. After stirring in formic acid for 3 days, the trisester **1d** had been completely hydrolyzed (Scheme 5.35). Analog to the previously discussed reactions, the formic acid was removed *via* azeotropic distillation with toluene under reduced pressure. Washing with acidified water, ethanol and CH_2Cl_2 did not elute any product. Again, the product **2d** could be dissolved in (slightly acidified) THF or aqueous alkaline solutions while being insoluble in most organic solvents (*e.g.*, ethanol, ethyl acetate, CH_2Cl_2, $CHCl_3$). Pure dyad **2d** could be easily obtained by eluting with acidified THF and subsequent precipitation by addition of hexanes. Compound **2d** was characterized by ^{1}H NMR, IR, UV-Vis, emission spectroscopy and mass spectrometry. Owing to the low amount and solubility in THF-d_8, no reasonably well-resolved ^{13}C/DEPT-135 NMR spectra could be recorded.

The product **2d** is basically the same molecule as **2a**, but without a Zn^{2+} ion in the porphyrin center. Due to this resemblance, it will be exciting to compare these two molecules in regard to spectroscopic properties, solubility and the tendency to build lipid bilayers or self-assembled structures in aqueous media. The possibility to influence these aggregates by addition of nucleophilic ligands (such as pyridine, 4,4'-bipyridine, and others) will be of special interest. It was already observed in the literature that these ligands could coordinate axially to metalloporphyrins.[162] To complement these investigations, product **2d** – without any zinc center in the porphyrin core – will allow an indispensable cross check in future research.

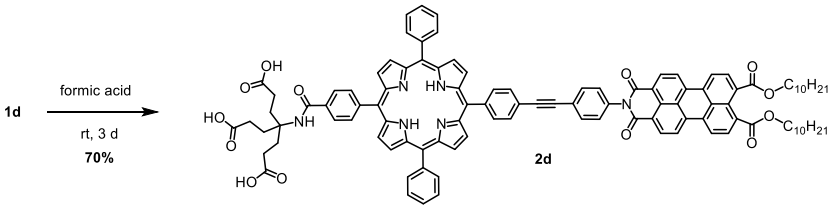

Scheme 5.35. Synthesis of non-metallated product **2d** by hydrolysis of the dendritic dyad **1d** in formic acid.

Unfortunately, at this point of this thesis, only 18 mg (2.5%) of **2d** could be synthesized in an 18 step synthesis with a largest chain of 11 consecutive steps (Table 5.11). This is sufficient for basic characterizations, but is too little amount for further in-detail investigations. Apart from the methyl ester deprotection reaction **19c** with 42.1% (p. 61), the yields of the single reactions are predominantly satisfactory.

Table 5.11. Overall yield for the 18 step synthesis cascade to product **2d**.

	applied		obtained		yield	
	m	n	m	n	reaction	consec.
13	725 mg	816 µmol	585.3 mg	742.8 µmol	91.0%	13.2%
18c	150 mg	190 µmol	243.5 mg	167 µmol	87.6%	11.5%
19c	210 mg	144 µmol	87.5 mg	60.5 µmol	42.1%	4.9%
1d	64.9 mg	44.9 µmol	59.9 mg	32.5 µmol	72.4%	3.5%
2d	28.3 mg	15.3 µmol	18.0 mg	10.7 µmol	70.0%	2.5%

5.7 Characterization of the Dyads

5.7.1 NMR Spectroscopy

The NMR spectrum of **1d** in $CDCl_3$ was chosen to present the characteristic features of the dyad. Despite the complexity and large mass of this molecule, the signals of all protons can be found and attributed. Most striking is the signal of the inner NH protons of the porphyrin, which is strongly shifted upfield to -2.8 ppm as a result of the anisotropic effect of the aromatic ring current (Figure 5.11).[9,245] As the molecule **1d** is achiral and the rate of interconversion of the N-H tautomerism is very fast,[246] a single, broad singlet is visible. The line broadening effect is mainly attributed to the heterocoupling to the quadrupolar ^{14}N nucleus.[247]

The solvent signal of $CDCl_3$ is calibrated to 7.26 ppm, water is observed at 1.57 ppm.[248] At around 0 ppm, only impurities such as grease and unpolar contaminations are found. The decyl chain attached to the perylene is situated at 0.8 (terminal CH_3 group), 1.3, 1.8, and 4.4 ppm (directly coupled to the perylene ester). The signals of the NEWKOME dendron are clearly visible as an intense singlet at 1.5 ppm (27 *tert*-butyl protons), and the two CH_2 groups appear at 2.3 and 2.5 ppm.

The aromatic region at 7 – 9 ppm gets more crowded and interesting: The amide proton at 7.3 ppm is very distinct. The *para*-substituted phenyl rings of the pheny–ethynyl–phenyl group can be attributed to the signals at 7.4, 7.9 and 8.0 ppm. Comparison with the precursor molecules leads to the conclusion that the missing doublet can be found in the crowded region at 8.2 – 8.3 ppm at around 8.2 ppm (*cf.* spectra of **12**, **13**, **18**, **18c** , see also p. 58).

As confirmed both in comparison to the spectrum of pristine tetraphenylporphyrin and own HMBC/HSQC and COSY studies (especially of compounds **13b** and **18**, see p. 58), the four *ortho* and six *meta*/*para* signals of the unsubstituted porphyrinic phenyl groups are situated at 8.22 – 8.25 ppm and 7.80 ppm.[9] The two doublets of the *para*-substituted phenyl group next to the amide appear in the cluster at around 8.3 ppm. In the precursor molecules (with a neighboring ester or acid instead of an amide, *e.g.,* dyads **18c** and **19c**), these protons could be definitely assigned to peaks at 8.45 and 8.33 ppm. In case of dyad **18** in DMSO, these signals appear at 8.35 and 8.25 ppm (see p. 58). It is reasonable to argue that the protons in *ortho* position to the amide bond will be shifted 0.1 – 0.2 ppm upfield. This is substantiated by simulation (ChemDraw 16, model compounds: methyl benzoate *vs.* N-methylbenzamide), comparison (SDBS Online database),[249] and the increment model.[213] The four doublets of the perylene protons are attributed to the peaks at 8.70, 8.55, and 8.45 ppm, as well as in the cluster at around 8.2 ppm. The β-pyrrolic protons of the porphyrin can be found furthest downfield at 8.8 – 8.9 ppm.

In contrast to this well-resolved ^1H NMR spectrum in $CDCl_3$, no ^{13}C NMR spectrum of **1d** could be recorded and evaluated in a reasonable time period. The obtainable ^{13}C/DEPT-135 NMR spectra of compounds **1a-d** and **2a-d** are too complex and crowded to be discussed here in detail.

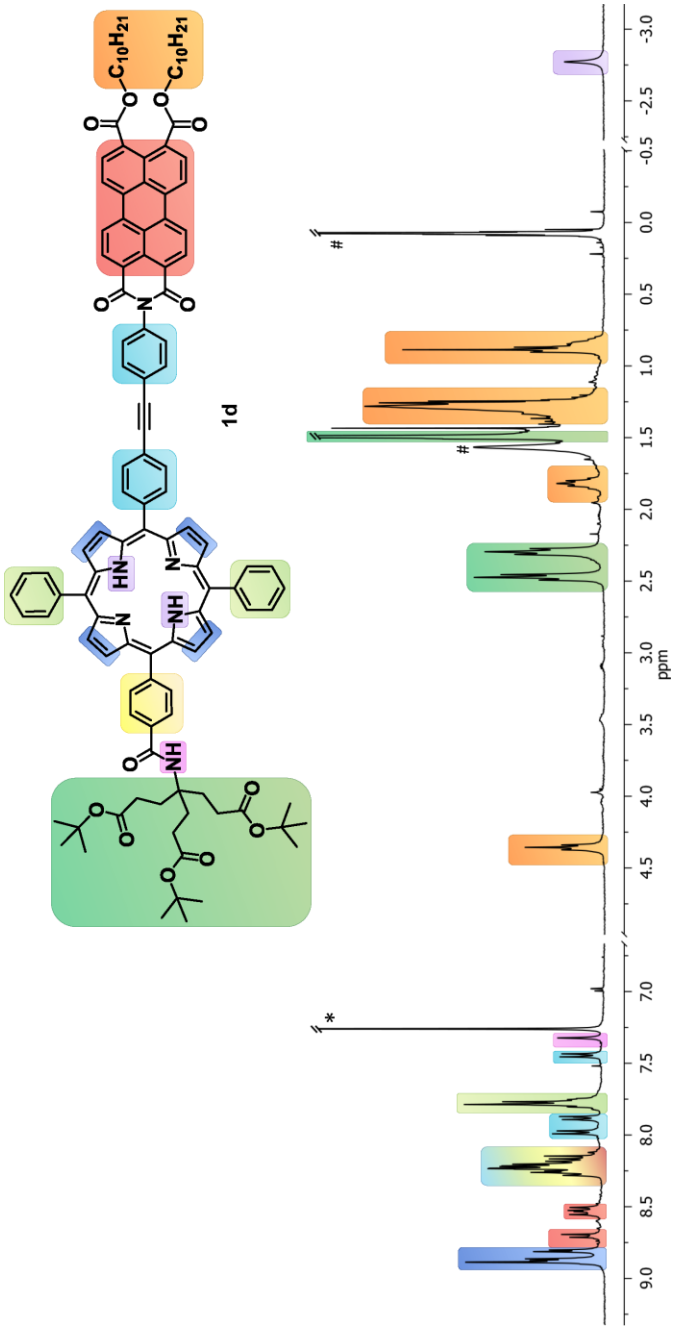

Figure 5.11. ^{1}H NMR spectrum of **1d** in $CDCl_3$ with designation of the peaks to the molecular groups. Solvent (* = $CDCl_3$) and impurities (# = water, grease) are marked.

NMR spectra of water-soluble products. Owing to the limited amount of products, the low solubility in THF-d_8, and the high complexity of **2a-d**, it proved difficult to obtain a well-resolved NMR spectrum of these final products. The addition of a few drops of TFA-*d* (fully protonating the dendritic acids and thus lowering the polarity) induced higher solubility and was essential in order to measure a reasonably resolved spectrum in THF. However, this solubility was achieved at the cost of overlapping the aromatic area with an intense, broad TFA signal (Figure 5.12 bottom). The products were insoluble in pure D_2O. Addition of pyridine-d_5 led to such a strong pyridine signal that the product was virtually invisible. With the aid of Harald Maid, it was possible to measure a long-term ^{1}H NMR spectrum of **2a** in D_2O after addition of 1 drop NaOD using water suppression techniques (Figure 5.12 top). In general, a strong aggregation behavior of dyads **2a-d** in water is expected, which certainly influences the observed chemical shifts.

It can be found that the peak positions of the aromatic region vary strongly and it is no longer possible to clearly assign the peaks. The signals in the aliphatic region at 0.5 – 3 ppm stay rather constant and are only weakly shifted. Typical features of the dyad can be identified in both spectra: the aliphatic decyl chain at 0.8, 1.3 and 2.2 ppm, the NEWKOME dendron at 2.5 and 2.3 ppm, as well as the porphyrin core at 8.9 and 7.7 ppm. The perylene and PEP signals are not clearly assignable. Astonishingly, the CH_2 group closest to the perylene ester – which usually appears at 4.4 ppm in $CDCl_3$ and THF – is either not visible or strongly shifted in the spectrum measured in D_2O/NaOD. Other unattributable signals were found. This could be a hint at the cleavage of the peryleneic decyl esters induced by NaOD, which also could explain the turbidity and low resolution of the D_2O/NaOD samples.

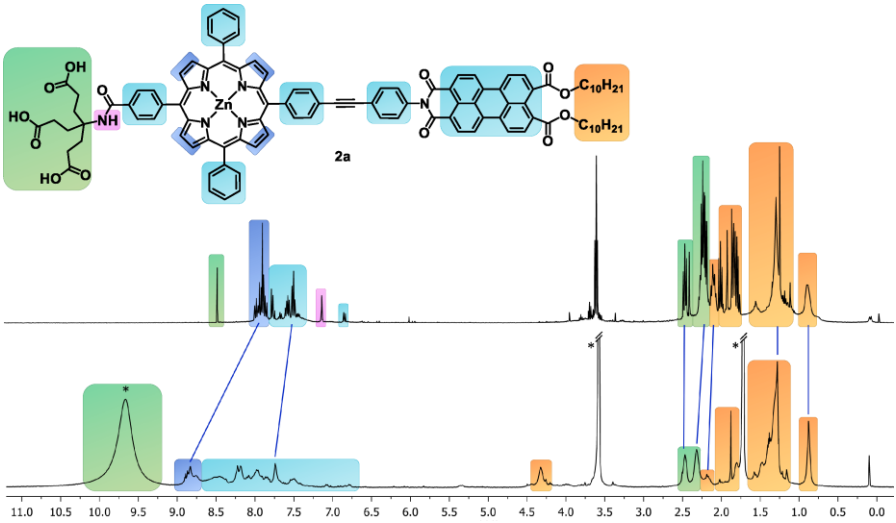

Figure 5.12. ^{1}H NMR spectrum of **2a** in in D_2O/NaOD with water-suppression (top) and in THF-d_8/TFA-*d* (bottom). Solvents (* = THF-d_8/TFA-*d*) are marked and the peaks are assigned. Prominent peak shifts between the two spectra are highlighted.

5.7.2 Mass Spectrometry

Recording mass spectra of the final products turned out to be difficult. The more complex the molecules became, the more complicated it was to obtain a suitable mass spectrum. This was true in particular for most of the porphyrin–perylene dyads carrying a Zn^{2+} ion. In spite of intense efforts made by Wolfgang Donaubauer and Margarete Dzialach from the MS department, it was often not possible to analyze compounds by mass spectrometry. Usually, various matrices, ionization methods (MALDI, ESI, APPI), and ionization energies had to be tested to be able to detect even traces of the product. Referring to the spectroscopic supplement on p. 180ff, no spectra could be measured for compounds **1a/b**, **2a/b/c**, **18b**, **19b** and only low resolution spectra were recorded for **1c**, **18**, and **19**. All of these products are equipped with a Zn^{2+} ion in the porphyrin. In contrast, dyads carrying no Zn^{2+} in the center could be ionized more easily. Hence it was much less problematic to obtain mass spectra for **1d**, **2d**, **18c**, and **19c**.

This observation was substantiated by Jakob Hitzensberger, who approached the difficulties of low solubility, usually low fragmentation, and difficult ion formation processes based on acid-base chemistry for metalloporphyrins.[250] He discovered in his PhD thesis, that a good method to counteract these problems in ESI MS was the coordination–ionization using formate, which would axially bind to the metal center of the porphyrin.[251]

The series of successfully recorded mass spectra – together with other characterization techniques – assure that the proposed synthesis pathway leads to the stated target molecules. The mass spectrum of the final water-soluble free-base porphyrin–perylene dyad **2d** (Figure 5.13, top) and the perfectly fitting simulation (bottom, error: 1.6 ppm) proves that the product is present.

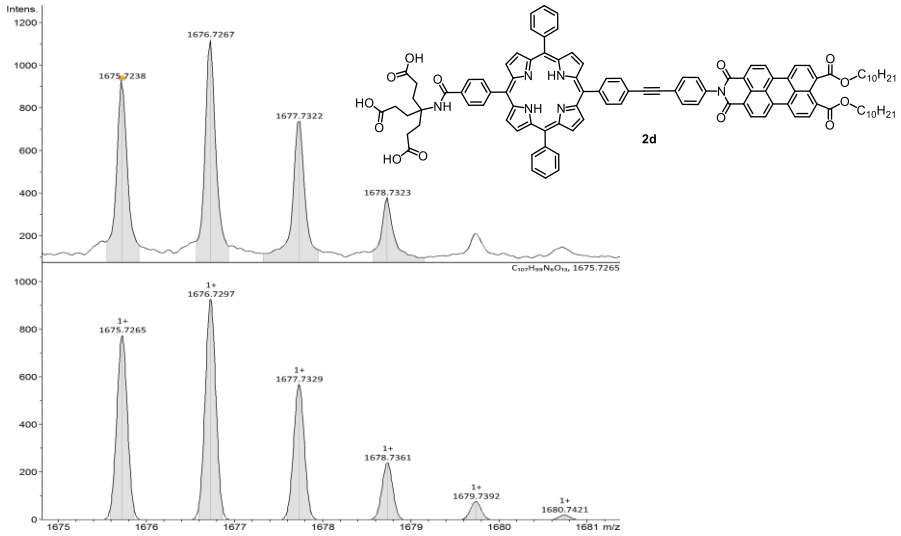

Figure 5.13. Recorded (top) and simulated (bottom) ESI Mass spectrum (positive ionization) of non-metallated dyad **2d**. For an overview spectrum, see spectroscopic supplement at p. 206.

5.7.3 IR Spectroscopy

In IR spectroscopy, the energies of atomic vibrations are visualized, thus providing evidence for the presence of certain groups. Using the IR spectra of **1c** and **2d** as an example, the observations shall be explained. In order to correctly attribute the molecular characteristics to certain peaks of vibrational energies, the fundamentals of literature, vibrational simulation, and comparison with previous spectra have been included in this discussion.[213] However, one has to bear in mind that due to the overlapping of the different vibrational energies, no exact and accurate attribution can be made and thus the following attribution should be considered with care.

For the *tert*-butyl protected and hydrophobic dyad **1c**, an amide N-H valence vibration at 3370 cm^{-1} can be found (Figure 5.14). The aromatic C-H valence vibrations at > 3000 cm^{-1} are usually weak compared to the aliphatic C-H valence vibrations at < 3000 cm^{-1}. A very weak signal at 2217 cm^{-1} is visible which might be a hint of the vibration of the C≡C triple bond. This speculation is substantiated by comparing Figure 5.14 to the IR spectra of the precursor molecules, especially compounds **13** (with triple bond) *vs.* **13b** (without triple bond).

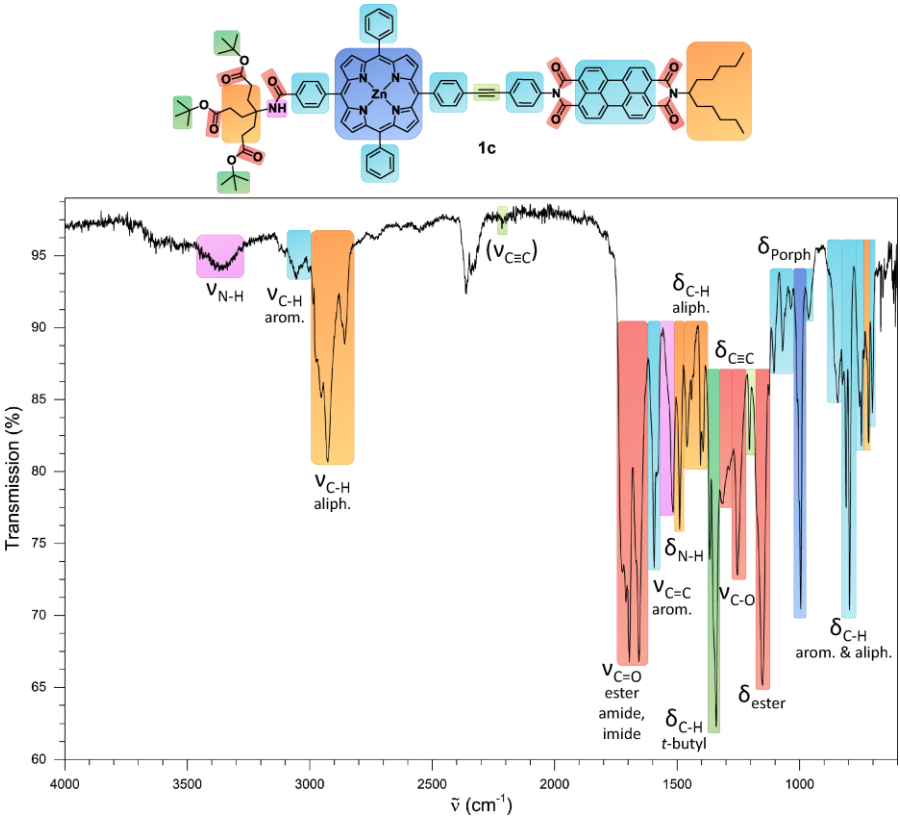

Figure 5.14. IR vibrational spectrum and careful assignment to molecular characteristics of dyad **1c**.

The prominent C=O valence vibrations at 1750–1650 cm^{-1} are characteristic and can be easily identified. The absorption bands for the perylene imide at 1660 and 1709 cm^{-1} are also present in this region.[78] In the region between 1600 and 1000 cm^{-1}, a large variety of different vibrations can be found, including N-H (1516 cm^{-1}) and C-H (1500–1370 cm^{-1}) deformation vibrations, aromatic C=C (1600, 1580 cm^{-1}) valence vibrations and CO-O-C vibrations of the ester groups (1330–1050 cm^{-1}, compare PI_SBE_{10} **16** *vs.* PI_SA **17** at 1166 cm^{-1}).[213] The peaks at 1516 and 1593 cm^{-1} are also a typical perylene skeleton pattern.[78] Again, the presence of a C≡C deformation vibration at around 1200–1150 cm^{-1} is supposed by simulation (1170 cm^{-1}) and comparison (*cf.* compound **3** at 1177 cm^{-1}). In the fingerprint region between 850 and 700 cm^{-1} appear various aromatic and aliphatic C-H deformational vibrations.

Characteristic porphyrin vibration. Another strong peak at 990–1000 cm^{-1} can be found in a multitude of spectra (except **2a–c**, **3–10**, and **21–24**). This peak can be assigned either as an anhydride vibration (compare **15**/**17** *vs.* **14**/**16** at 1009 cm^{-1}) or most probably as a characteristic porphyrin vibration at 995 cm^{-1} for zinc porphyrins and at 966 cm^{-1} for free-base porphyrins. This theory can be substantiated by comparing spectra from the SDBS Database (968 cm^{-1} for TPP),[249] and by vibrational calculation (955 cm^{-1}) of a free-base porphyrin model compound (Figure 5.15). Indeed, ALBEN *et al.* wrote in 1973 that *"a band in the 960– 990 cm^{-1} region appears to be reasonable for the in-plane NH-bending vibration"*,[252] and GARIBOV *et al.* confirmed in 1991 that *"the in-plane CH vibrations δ(CH) of the pyrroles [as subunits of the porphyrin] are active in the 980–995 and 1000–1008 cm^{-1} regions"*.[253] This in-plane NH-bending vibration observed at 995 cm^{-1} is shifted only slightly compared to the dipyrromethane precursors **7**, **8**, and **10** with 970–975 cm^{-1}. In the IR spectra of compounds **2a–c**, the peak in question is probably superimposed by the broadening of the carboxylic acid vibrations.

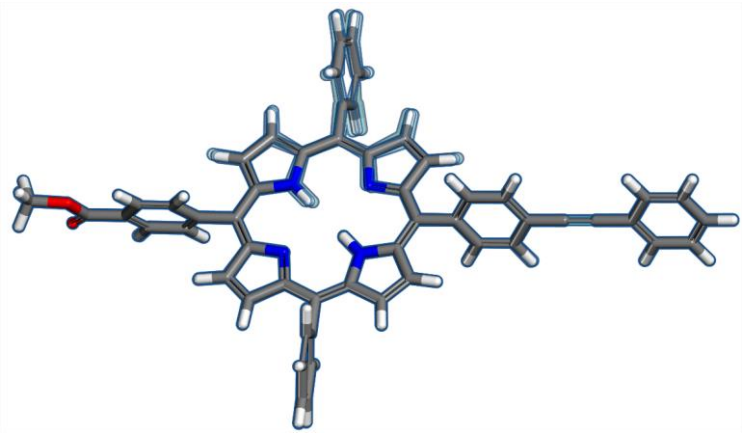

Figure 5.15. Calculation and simulation of the molecular vibration at 955 cm^{-1} for a simplified model compound. The in-plane NH-bending vibration concentrates on the porphyrin ring (semi-emp. GeomOpt NDDO PM6/UHF).[156]

IR spectrum of water-soluble dyad 2d. In the IR spectrum of dyad **2d**, the most salient feature is the presence of a broad peak from 3700–3200 cm^{-1} which can be attributed to the now deprotected three acid groups (Figure 5.16). Owed to this, the other vibrational features are superimposed and do not come out as clear as in the previous spectrum. The aromatic C-H valence vibration nearly vanishes and the C≡C valence vibration is not detectable. The assignments in the lower range of the spectrum (< 1700 cm^{-1}) can be made according to the spectrum above, albeit the peaks are less distinct. The pyrrolic in-plane bending vibration can be found at 966 cm^{-1}.

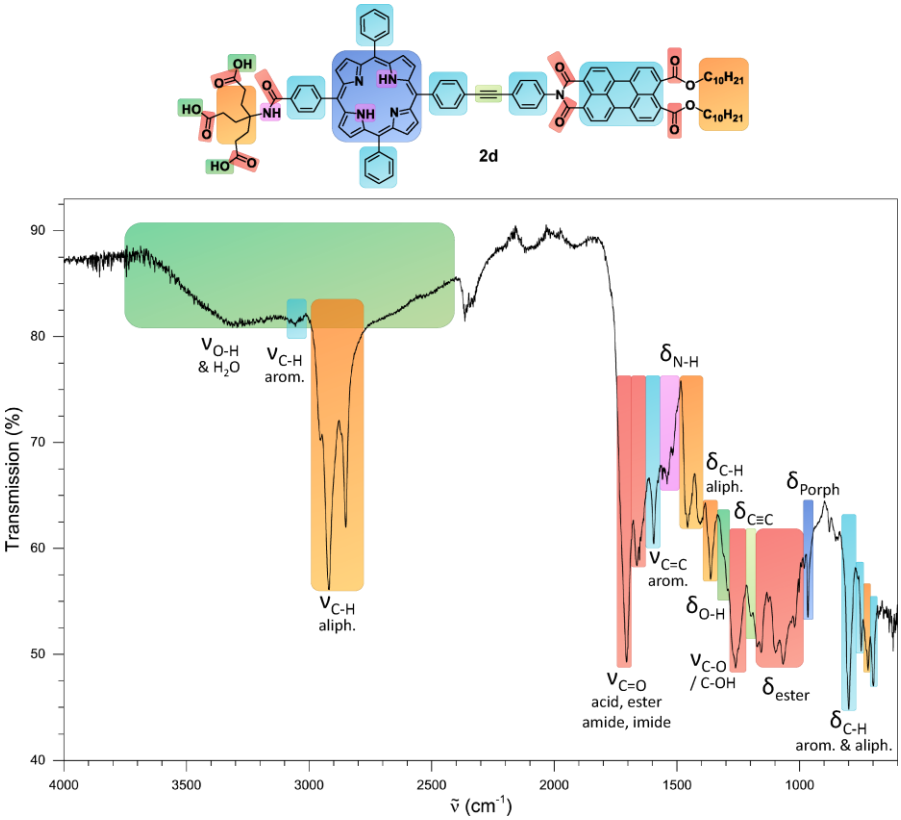

Figure 5.16. IR vibrational spectrum and careful assignment to molecular characteristics of dyad **2d**.

5.7.4 UV-Vis and Fluorescence Spectroscopy

In UV-Vis spectroscopy, the typical optical features of porphyrins and perylenes can be investigated. Comparing the perylene and porphyrin precursors to the final dyad, some interesting properties can be found.

The free-base porphyrin exhibits its characteristic bands on exact the same wavelengths, regardless of the substitution pattern at the periphery. The three non-metallated porphyrin precursors **12**, **13**, and **13b** are depicted in Figure 5.17. The strongest band at 419 nm with a very high extinction coefficient in the range of 3–5·10^5 M^{-1}cm^{-1} is called Soret band (or B band). Additionally, several weaker Q bands at 514, 550, 592 and 648 nm are found in all spectra.

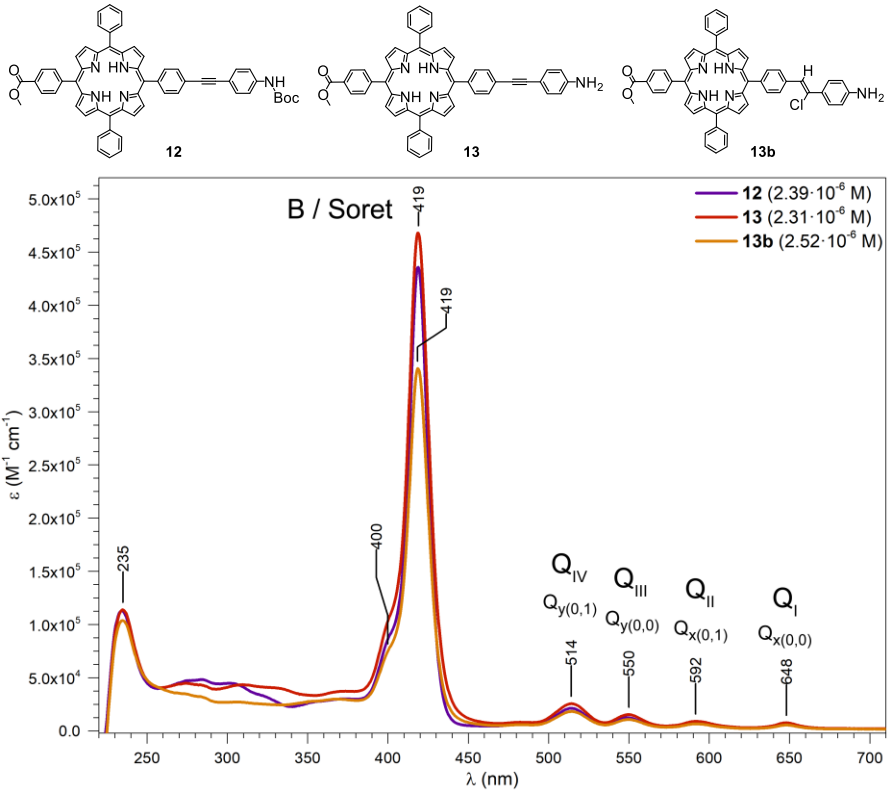

Figure 5.17. UV-Vis spectrum (in THF) of free-base porphyrin precursors **12**, **13** and **13b** with a Soret band at 419 nm and four Q bands at 500 to 650 nm.

The Four-Orbital model. According to the Four-Orbital model by GOUTERMAN, which concentrates on the two (coincidentally equal-energetic) highest occupied π orbitals (HOMO, a_{1u}, a_{2u}) and the two degenerate lowest unoccupied π* orbitals (LUMO, e_{gx}, e_{gy}), the existence of the observed Soret and Q absorptions can be explained as follows (Figure 5.18):[254-256]

The main absorption band (Soret band) arises from the excitation of electrons from the ground state to the second excited state ($S_0 \rightarrow S_2$, *i.e.*, HOMO→LUMO+1).[257] Both π–π* transitions from a_{2u} to e_{gx} and e_{gy} are symmetry allowed to occur simultaneously, which results in the very intense absorption.[258] Upon metallation, the porphyrin a_{2u} orbital is directly influenced by the metal p orbital and thus the Soret band intensifies and is shifted bathochromically to around 430 nm.[258]

The Q bands are attributed to the transition from the ground state to two distinct vibrational levels ($Q_{(0\text{-}0)}$ and $Q_{(0\text{-}1)}$) of the first excited state ($S_0 \rightarrow S_1$ *i.e.*, HOMO→LUMO).[256] The intensity of the Q bands is weaker, as the affected orbitals are degenerate and the simultaneous excitation from a_{1u} to e_{gx} and e_{gy} is symmetry forbidden.[258] The intensity of the Q bands decreases continuously (from Q_{IV} to Q_I) at increasing wavelength, which can be classified as *etio* type.[13,259] In metallated or protonated porphyrins, the porphyrin core possesses D_{4h} symmetry, thus usually just two distinct Q bands are observed.[257] In contrast, the symmetry of free-base porphyrins is lowered to C_{2v}. Hence, these two excitations are polarized in x and y direction, resulting in four detectable Q bands ($Q_{y(0\text{-}1)}$, $Q_{y(0\text{-}0)}$, $Q_{x(0\text{-}1)}$, $Q_{x(0\text{-}0)}$).[65,256-257,260]

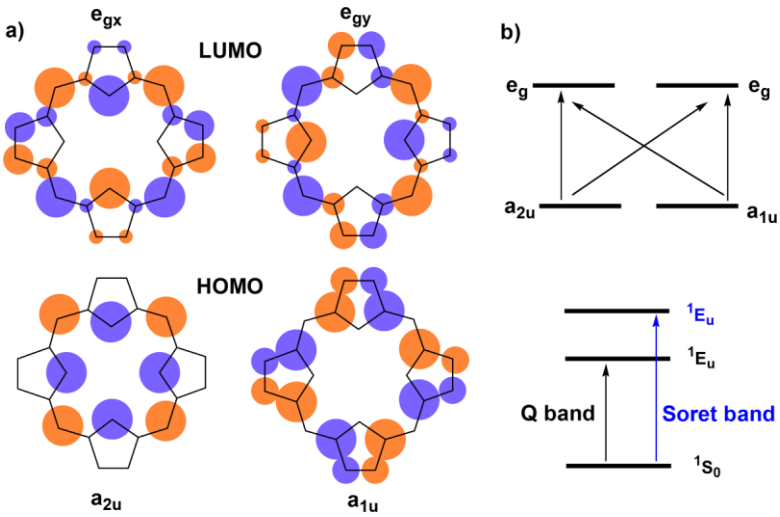

Figure 5.18. HOMOs and LUMOs of porphyrins. a) The four orbital model by Gouterman. b) Energy levels and the electronic transitions for a porphyrin (picture licensed under CreativeCommons, cc by-nc-sa 3.0).[4]

UV-Vis spectra of perylene precursors. Compared to the porphyrins, the spectra of the perylene precursors are considerably more diverse. The functionalization sequence from PTE_{10} **14** over $PABE_{10}$ **15** and PI_SBE_{10} **16** to PI_SA **17** directly influences the aromatic center which is the reason for the strong color of this class of molecules. Hence, the color changes notably depend on the functionalization (Figure 5.19). The observed ratio-of-fronts in the TLC experiment are caused by the polarity differences of lipophilic esters, anhydrides, and other functional groups. These polarity differences were also crucial for the separation strategy of different perylenes (*cf.* p. 53). In the following paragraphs, it shall be explained why there is a color transition from red (PTCDA) over yellow (PTE_{10}) and orange (PABE, PI_SBE_{10} and other perylene imide diesters) to once again red (PI_SA).

In the UV-Vis spectra measured in THF, PTE_{10} **14** displays three characteristic peaks and one shoulder at 392, 417, 442, and 470 nm, the intensity increasing with wavelength (Figure 5.20).[101] The distance between the peak maxima is relatively constant around 25 nm each. The observed peaks can be assigned to a π–π^* electronic excitation in two polarization directions: along the long molecular axis (350–550 nm) and along the short axis (200–300 nm, not displayed in this spectrum).[261] The multiple bands are attributed to a HOMO–LUMO ($S_0 \rightarrow S_1$) transition at ground state and higher vibrational states ($S_{(0+x)}$, x = 0–3).[86] Due to the symmetry and intensity distribution of these peaks, it is even possible to map the absorption spectra in very high quality using gauss curves.[262]

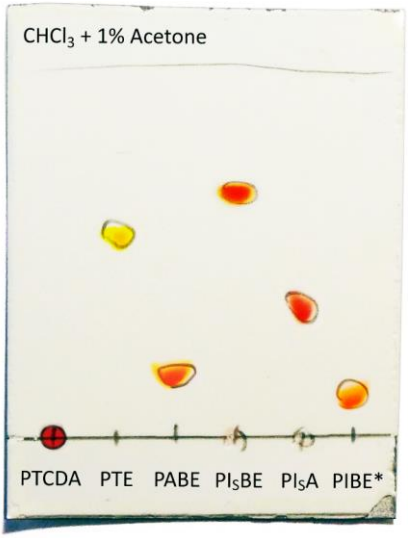

Figure 5.19. Silica gel TLC plate with different perylene compounds (PIBE* = Perylene (hexanoic acid)imide bisdecylester). This figure is a digitally enhanced collage which represents the ratio-of-fronts and colors of an ideal TLC experiment.

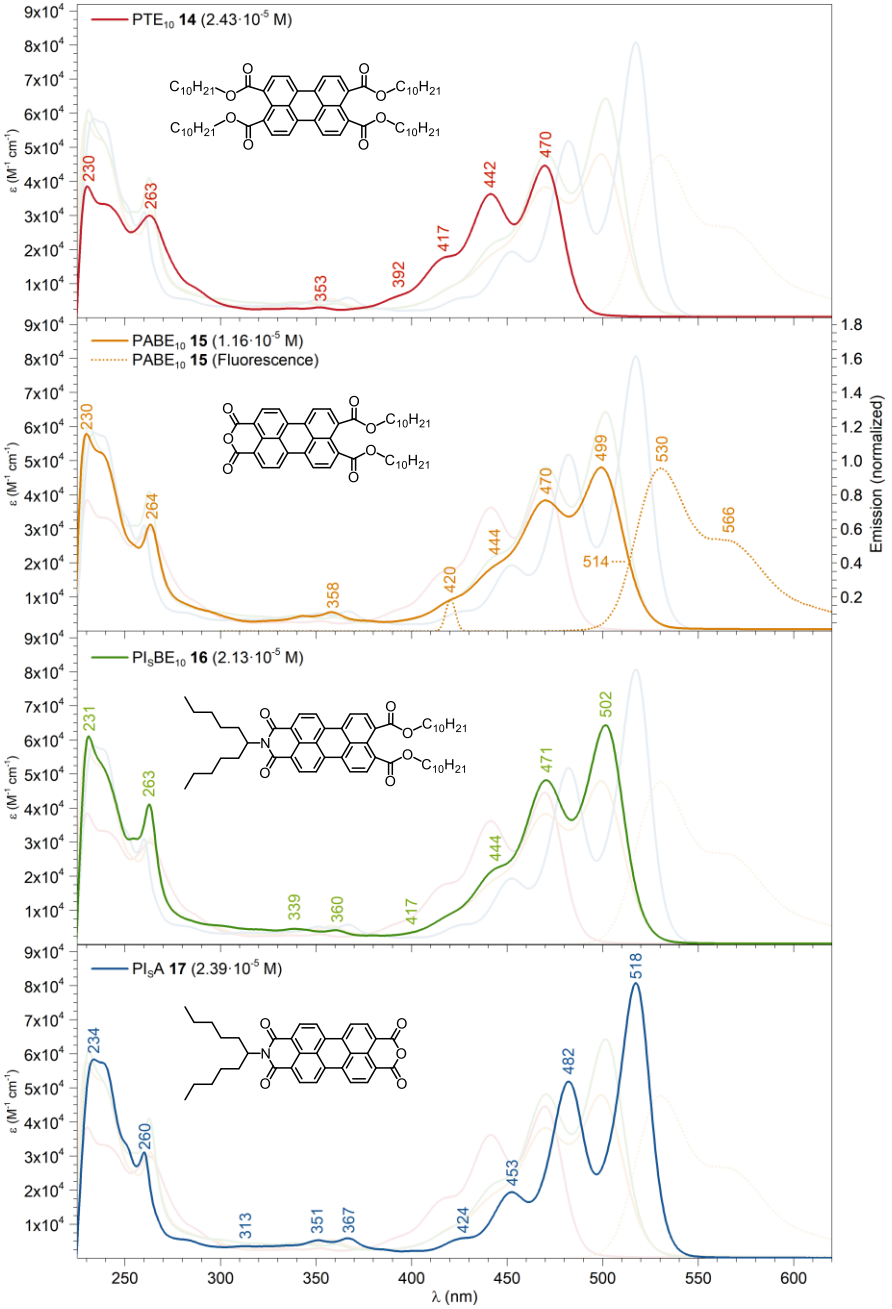

Figure 5.20. UV-Vis spectra of perylene precursors **14** to **17** in THF. Higher conjugation increases the redshift of the spectrum, higher polarization increases the absorption intensity. The emission spectrum of $PABE_{10}$ **15** is roughly a mirror image of the UV-Vis spectrum. The intersection of both graphs can be estimated as HOMO–LUMO gap energy $E_{g,\,514\,nm}$ = 2.58 eV.

Estimating the HOMO–LUMO gap. The HOMO–LUMO gap E_g for PTE_{10} **14** can be estimated from the spectra using the formula $E_{g,\,480\,nm} = h{\cdot}f = h{\cdot}c/\lambda = 2.58$ eV, with $h{\cdot}c \approx 1240$ eV·nm. The wavelength $\lambda = 480$ nm is the intersection point between normalized absorption and emission spectra (obtained from the literature, *cf.* also Figure 5.20, orange).[88,263] This is the case since the HOMO–LUMO gap has to be identical both for absorption and emission spectra.[264] Due to a multitude of vibronic states of S_0 and S_1 energetic levels, several electronic transitions can occur, leading to a broadening of the spectral peaks. There can even be found a certain percentage of emission energies higher than E_g (Figure 5.20, orange). Another possibility would be to measure the HOMO–LUMO gap by cyclic voltammetry (CV). In the literature, the $E_{g,CV}$ was determined at values between 1.93 and 2.2 eV. It is common that the spectroscopically determined HOMO–LUMO gap energies $E_{g,opt}$ are slightly larger than $E_{g,CV}$.[119,265]

The spectrum of $PABE_{10}$ **15** shows the same regular characteristics but is considerably shifted bathochromically (+29 nm) with peaks at 420, 444, 470, and 499 nm ($E_{g,\,514\,nm} = 2.41$ eV, Figure 5.20, orange).[88,266] PI_SBE_{10} **16** has nearly the same absorption maxima (417, 444, 471, 502 nm, $E_{g,\,518\,nm} = 2.39$ eV),[88] but possesses a notably higher molar absorptivity (increase by 25%, $1.6{\cdot}10^4$ $M^{-1}cm^{-1}$). Finally, PI_SA **17** is again redshifted (+16 nm) with peaks at 424, 453, 482, and 518 nm ($E_{g,\,525\,nm} = 2.36$ eV, $E_{g,CV} = 2.15$ eV).[119,267-268] The extinction coefficient is further increased by $1.6{\cdot}10^4$ $M^{-1}cm^{-1}$ to 81 000 $M^{-1}cm^{-1}$.

Elongation of the aromatic system. Both the bathochromic shift and the increase in absorption can be explained by the functional groups affecting the extended aromatic system, as stated before. In the case of PTE_{10} **14**, the aromaticity distributes over five fused rings, causing a strong yellow color. Both $PABE_{10}$ **15** and PI_SBE_{10} **16** possess a sixth cyclic system (the anhydride or the imide, respectively) which directly contributes to the extended aromatic ring structure, resulting in a change of color (orange) and a bathochromic shift. For PI_SA **17** (as well as perylene diimides (PDI) such as in dyads **18b** and **1c**), the further elongation of the perylene system to seven fused rings renders this molecule electronically similar to starting compound PTCDA. Likewise, the color now is an intense red. However, the long aliphatic swallowtail provides a considerably higher solubility compared to PTCDA.

Excursus: The homologue series of rylene imides. The same effect can be observed very impressively when regarding the homologue series of higher rylene imides (Figure 5.21). Upon elongation of the perylene core, the aromatic π system is extended and the HOMO level rises, leading both to a decrease of the maximum absorption energy (*i.e.*, a bathochromic shift to longer wavelengths) and an increase in molar absorptivity (*i.e.*, the molar extinction coefficient rises and the color intensifies).[81,243]

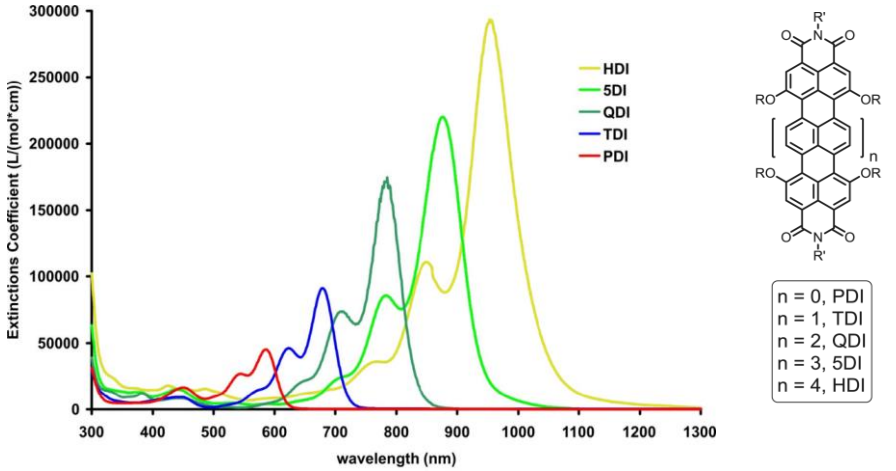

Figure 5.21. Homologue series of rylenes: Upon elongation of the aromatic system, the absorption shifts to lower energy and the extinction coefficient increases.[81,87,269]

Comparison of influences on the UV-Vis spectra of perylenes. In addition to the ring enlargement effect, several other effects can be discussed, such as the influence of (a) the functional groups (*e.g.*, imide, diester, anhydride), (b) the residues attached to the functional groups, (c) polarization of the perylene core, and (d) solubility/aggregation.

(a) It is obvious that the kind of the functional groups at the *peri* positions have an effect on both the HOMO and the LUMO – and hence directly on the color of the molecule. Imides are strong electron-withdrawing substituents which thereby improve the electron-accepting property of the perylene.[79,81,270] Compared to imides, anhydrides are less electron-withdrawing and have a slightly hypsochromically shifted absorption. This can be found by comparing the absorption maxima of three seven-ring systems: Perylene diimide (PDI, 526 nm),[78] perylene monoanhydride monoimide (PI_SA, 518 nm) and perylene dianhydride (PTCDA, *ca.* 494 nm). The literature-known spectrum of PTCDA was measured in H_2SO_4 conc. (574 nm) and corrected by 80 nm.[78,105] The slight bathochromic shift induced by electron-withdrawing substituents can also be confirmed when comparing the six-ring systems $PABE_{10}$ **15** (499 nm) and PI_SBE_{10} **16** (502 nm) in Figure 5.20 (p. 84).

While esters are moderately electron-withdrawing, this comes at the cost of one fused delocalized ring.[270-271] This is why both six-ring bis-decylesters PI_SBE_{10} **16** and $PABE_{10}$ **15** have absorption maxima at around 500 nm, compared to PTE_{10} **14** (five rings, 470 nm), and the seven-ring systems PTCDA (~494 nm) and PDI (526 nm).[78,105]

(b) Interestingly, the HOMO–LUMO levels of the perylene (and thus the interrelated absorption maxima) are completely unaffected by the additional functional groups attached to the imide or ester moiety. This can be explained regarding the molecular frontier orbitals (Figure 5.22). LANGHALS found that *"nodes or very small atomic coefficients are calculated for the orbital HOMO and LUMO at the N-atoms [...], even for the orbitals HOMO-1 and LUMO+1. [...] Thus, the N atoms are decoupled from the chromophore concerning optical excitation."*[80] In other words, the electronic interaction between the perylene core and the peripheral substituents is reduced to a minimum and the type of functional groups will not influence the UV-Vis spectra.[86,111,116]

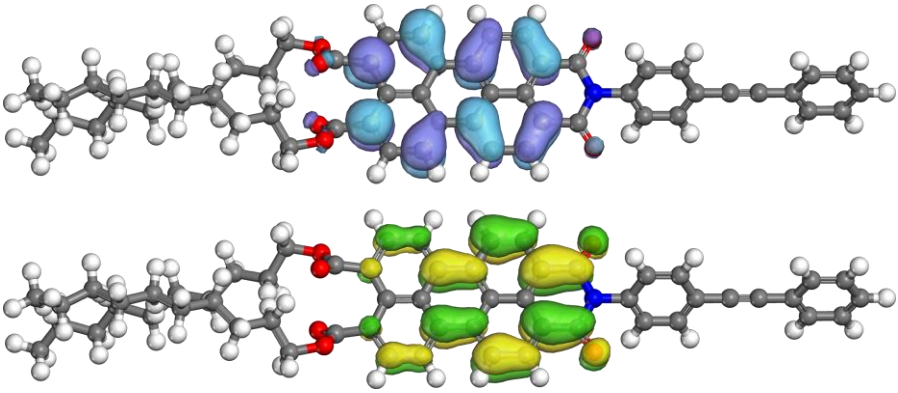

Figure 5.22. HOMO (top, blue) and LUMO (bottom, green) orbitals of $PIBE_{10}$ model compound. Note that both imide N and diester O are (almost) not contributing to these orbitals (semi-emp. GeomOpt NDDO PM6/UHF).[156]

(c) However, the type of molecules at the *peri* positions actually does influence the molecular orbitals in a certain way: Depending on the polarization of the long axis of the perylene core, the bathochromic shift differs notably.[79,81] This can clearly be observed in Figure 5.20: PTE_{10} **14** is a symmetrical and thus a weakly polarized molecule with an absorption maxima of 470 nm. Ring closure to $PABE_{10}$ **15** leads to an asymmetric polarized system, which has its maximum at 499 nm (+29 nm).[80] Transformation to PI_SBE_{10} **16** changes the shift only marginally (502 nm, +3 nm), as only a slight polarity difference between anhydride and the imide exists (*cf.* point a).

One would expect that the second ring closure to PI_SA **17** (518 nm) would lead to a similar considerable bathochromic shift. However, the polarity difference between imide and anhydride stays minor, so that the additional ring closure leads only to a comparatively small redshift (+16 nm) for a rather unpolarized molecule. Subsequently, the conversion to a PDI (522–526 nm) leads to a marginal change in absorption for the same reasons.[78,80]

As explained in point (b), it is more or less insignificant which groups are attached to the diimide, *i.e.,* if the PDI is symmetrical or unsymmetrical, as these groups have no effect on the polarization of the HOMO/LUMO orbitals.[111]

The same observation can be made by comparing the literature regarding the bathochromic shifts of pristine perylene (442 nm) with a perylene monoimide (polarized, +1 ring, 506 nm, +64 nm) and finally a perylene diimide (not polarized, +1 ring, 526 nm, +20 nm).[78-79,261] When using push–pull systems with functionalization in the bay region, even higher polarization of the perylene scaffold can be achieved.[89,117,266,269,272]

(d) The effects of solubility on spectroscopic measurements of perylene are well-investigated. At low concentrations between 10^{-4} and 10^{-6} M, there usually is no shift in wavelength.[77] However, the molar absorptivity (*i.e.*, the absorption strength and the color intensity) is directly dependent on the concentration, and the extinction coefficient decreases on increasing concentration.[86,110] The explanation lies in the aggregation effects: Perylenes tend to form aggregates or dimers even in dilute solutions due to their strong intermolecular π interactions. High aggregation behavior can also be tracked by the line-broadening of the peaks and the diminishment of the vibronic fine structure.[86] The higher the concentration, the more aggregation occurs which results in lower molar absorptivity.[77,88,273] This can be counteracted by introducing certain substituents such as aliphatic – ideally branched – chains (*cf.* swallowtail or dendron). These groups enhance the solubility (*e.g.,* by increasing the steric hindrance) and thus suppress the formation of aggregates.[77,86] In the spectroscopic measurements (Figure 5.20, p. 84), the concentrations were kept as constant as possible and the molar extinction coefficients should be comparable. $PABE_{10}$ **15** has a greater aggregation affinity than its precursor PTE_{10} **14**, thus a decrease of absorption is expected.[86] On the other hand, the π system is elongated by one fused aromatic ring, which should linearly increase the absorption.[81,243] In conclusion, both effects equalize each other, resulting in only a weak rise of molar absorptivity for $PABE_{10}$ **15**.

Comparing $PABE_{10}$ and PI_SBE_{10} **16**, this observation is even more compelling. While the perylene core stays unaltered both in ring size and polarization (*cf.* point c), the molar extinction coefficient increases by 25% (Figure 5.20, p. 84). This corresponds to the higher solubility and lower aggregation tendency of PI_SBE_{10} compared to $PABE_{10}$ (*cf.* the polarity differences in the TLC experiment, Figure 5.19, p. 83).

Comparison of UV-Vis spectra of porphyrin, perylene and dyad. When comparing the porphyrin/perylene precursor molecules **13** and **15** to the dyad **18c** and the G^1 dyad **1d**, it can be found that the spectrum of the dyad is approximately a combination of the precursor spectra

(Figure 5.23). The resemblance of spectrum **1d** to the sum spectrum (dotted green line) indicates that no ground-state interaction occurs in the dyad (*cf.* chapter 5.7.5, p. 94). Apart from the higher extinction coefficient of porphyrin **13** and a slight shift of the peak at 514 nm owing to an overlap with the perylene peaks, the porphyrinic features (Soret and Q bands) remain unchanged. The peaks for $PABE_{10}$ **15** at 470 and 499 nm are shifted bathochromically to 472 and 505 nm in dyads **18c** and **1d** as the perylene in the dyad is now a monoimide diester. This is analog to the observations for PI_SBE_{10} **16** (dashed red line, *cf.* Figure 5.20, p. 84). The small change in the molar absorptivity is attributed to deviations in experimental parameters and characteristic molecular features of the probe.

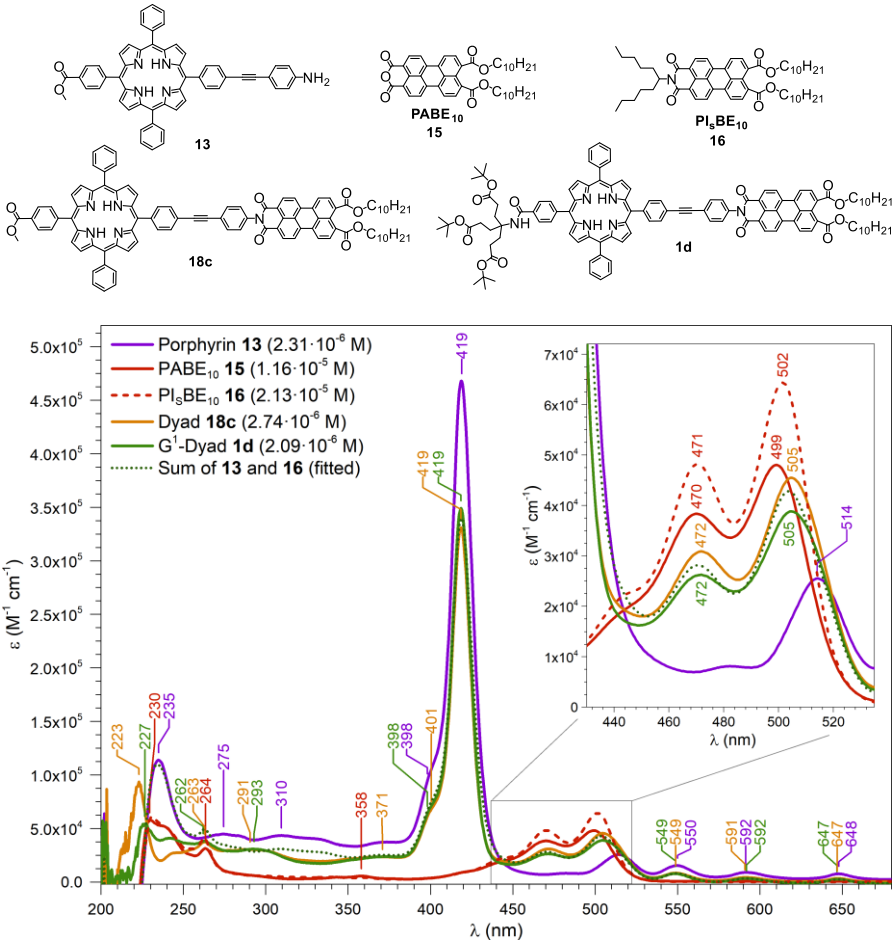

Figure 5.23. UV-Vis spectrum of porphyrin and perylene precursors and the non-metallated dyads **18c** and **1d** in THF.

In the high-energetic region between 200 and 300 nm, distinct differences can be found: A weak new peak at 291–293 nm appears in dyads **18c** and **1d**. The porphyrin signal of **13** at 235 nm vanishes completely. The vibrational structure along the short axis of the perylenes **15** and **16** (*cf.* p. 83) is considerably weakened. Instead, a new peak at 223–227 nm ($E_g \approx 5.5$ eV) appears. Unfortunately, both the limited spectroscopic window of the quartz glass cuvette (~ 200 nm) and the self-absorption of the solvent THF (~ 220 nm) do not allow a precise deduction and attribution of this peak (Figure 5.23).[274]

Quenching of perylene emission. In fluorescence spectroscopy, the normalized characteristic porphyrinic emissions at 652 and 715 nm of porphyrin **12**, dyad **18c** and G^1 dyad **1d** are completely superimposable (Figure 5.24). Typically, perylenes have a very high quantum yield of approximately 100%,[80,83-84] which is magnitudes higher than the porphyrin fluorescence quantum yield (usually 10 – 15%,[65,275] seldom < 5%).[15,276-277] Irradiation at 420 nm leads to direct excitation at the porphyrin S_2 level (Soret band), while the perylene is only excited indirectly, owing to its weak absorption at 420 nm (Figure 5.23). Nevertheless, a notable peryleneic excitation at 531 and 563 nm can be found (Figure 5.24).

The measured intensities of the peryleneic features of $PABE_{10}$ **15** (red curve) and dyad **18c** (yellow curve) are incommensurable in this normalized emission spectrum. Hence, an equimolar mixture of porphyrin **12** and perylene **15** was prepared in such a way that the mixture exhibited the exact same UV-Vis absorption pattern as the dyad **18c**. This porphyrin–perylene mixture (blue curve) can now be compared to the dyads **18c** and **1d** (yellow and green curves). It can be found that the peryleneic emission (relative to the porphyrin emission) is nearly completely quenched in the dyads **18c** and **1d**. This very interesting observation is a clear hint that intramolecular electronic interaction between porphyrin and perylene occurs. A detailed discussion will be performed in the following chapter 5.7.5 ("Investigation of Electron Transfer in the Dyad", p. 94).

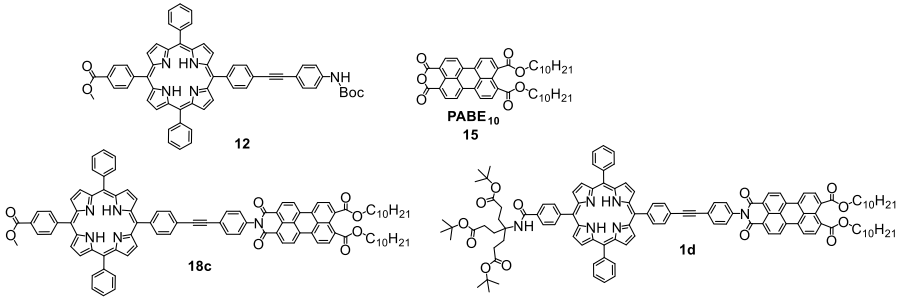

molecules depicted in Figure 5.24 (see right).

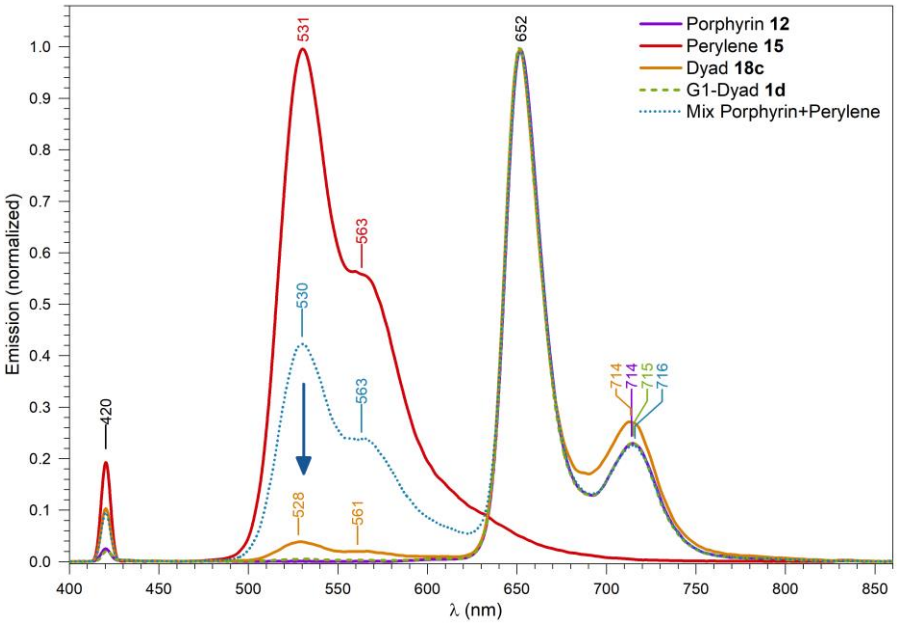

Figure 5.24. Normalized emission spectrum of porphyrin and perylene precursors and the non-metallated dyads **18c** and **1d** in THF. An equimolar mixture of porphyrin **12** and perylene **15** features a notably reduced perylene emission compared to the dyad **18c**.

UV-Vis and emission spectra of dyads 1a-d. As soon as the porphyrin is metallated, the position of the Soret band as well as the number of Q bands change (as explained before, p. 82). This can be seen impressively in Figure 5.25. For metalloporphyrins **1a-c**, the Soret band is shifted bathochromically by 6 nm to 425 nm. The symmetry is enhanced. Thus, the four Q_x and Q_y bands of the free-base dyad **1d** at 505 (superimposed by the perylene absorption), 549, 591, and 647 nm are reduced to two Q bands at 557 and 597 nm for the metallated dyads **1a-c**. The emission spectrum (Figure 5.26), normalized to 591/597 nm (absorption) and 605/649 nm (emission, dashed line) shows further differences: The Q bands of the metallated porphyrins possess a small STOKES shift of 8 nm (absorption: 597 nm, emission: 605 nm) and a derived energy gap $E_{g,\,600\,nm}$ of 2.07 eV. This intersection of the porphyrinic Q absorption and emission bands (as explained on p. 84) matches the optically determined HOMO–LUMO energy gap of pure Zn porphyrin (*e.g.*, Zn TPP).[15] The HOMO–LUMO transition of the dyads (from porphyrin to perylene) cannot be measured by UV-Vis. Instead, the energy transition between HOMO and LUMO+1 orbitals located at the porphyrin core is detected. The emission maxima for free-base porphyrin **1d** are shifted to 652 and 717 nm, the STOKES shift is 5 nm and the porphyrinic HOMO–LUMO+1 energy gap $E_{g,\,649\,nm}$ can be calculated as 1.91 eV.

Furthermore, the perylene moieties of **1a/b/d** are composed of $PIBE_{10}$ (six fused rings, *cf.* p. 84) whereas **1c** is the only dyad employing a PDI_5 (seven fused rings). The difference can be found regarding the perylene absorptions at 455, 487 and 522 nm, which clearly confirm the presence of a perylene diimide (Figure 5.25, green).[80] Comparing the perylene emission maxima (520 to 570 nm) to the porphyrin emission maxima (605, 653, 717 nm), it can again be found that the (normalized) emissions of the perylene group in the dyads are strongly quenched, indicating an electronic interaction between porphyrin and perylene (Figure 5.26).

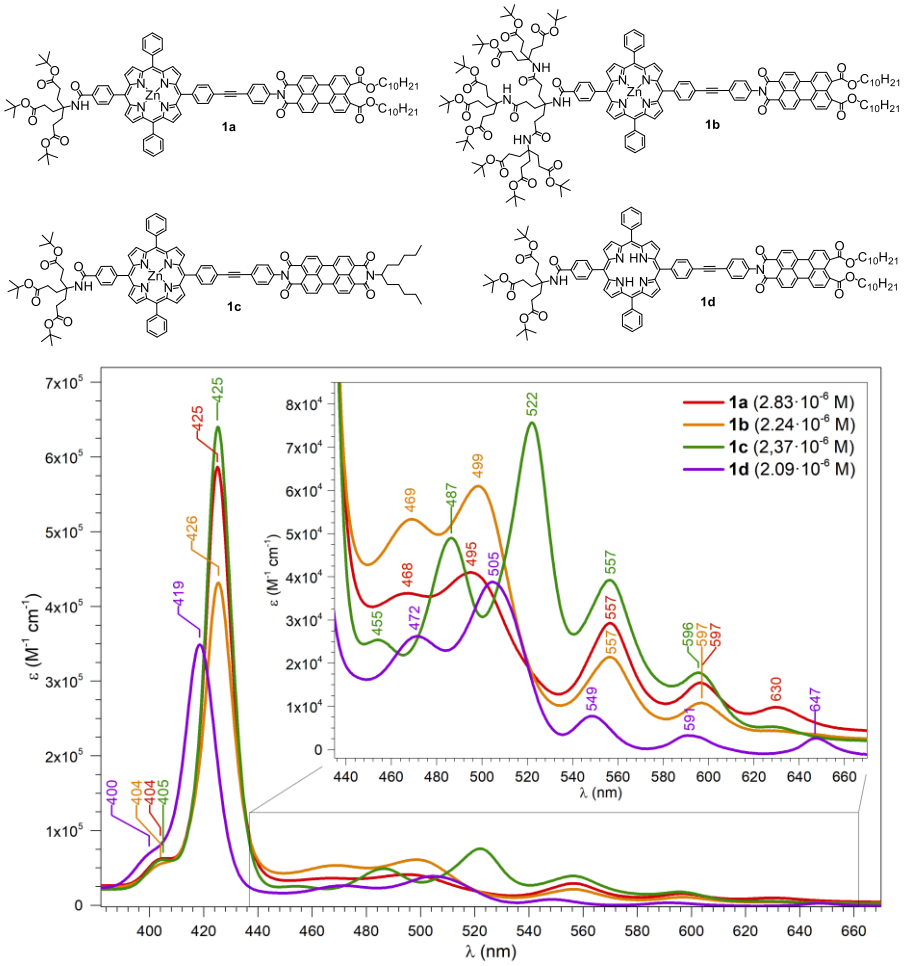

Figure 5.25. UV-Vis spectrum of porphyrin dyads **1a-d** in THF. Differences between the typical spectroscopic features can be found for non-metallated porphyrin **1d** (purple) and perylene diimide dyad **1c** (green).

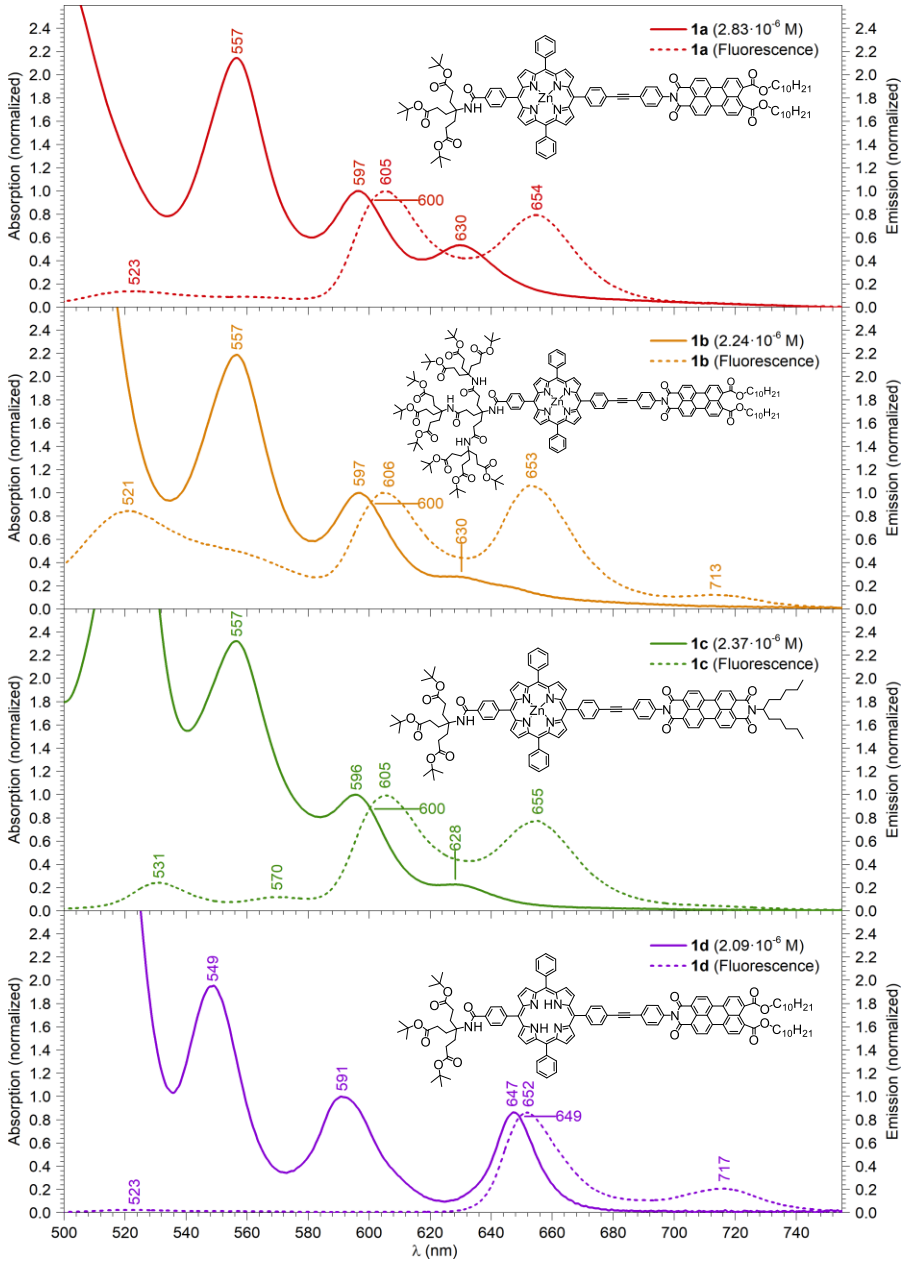

Figure 5.26. The normalized absorption/emission spectra after irradiation at 420 nm. Differences between the typical spectroscopic features of metallated (**1a-c**) and non-metallated (**1d**) porphyrins can be found. The intersection point of absorption and emission spectra lies at $E_{g,\,600\,nm}$ = 2.07 eV for dyads **1a-c** and $E_{g,\,649\,nm}$ = 1.91 eV for dyad **1d**.

5.7.5 Investigation of Electron Transfer in the Dyads

HOMO–LUMO energies. It was expected that in the porphyrin–perylene dyad, the HOMO level is located at the porphyrin whilst the LUMO level lies completely at the perylene. Hence, the porphyrin would act as electron donor,[278-279] and the perylene would be the electron acceptor in this system.[115,157,280] Semi-empirical calculations and simulations (GeomOpt NDDO PM6/UHF) substantiated this hypothesis (Figure 5.27).[156]

The HOMO energy in the gas phase was calculated to be -7.82 eV for the metallated dyad **2a** and -8.09 eV for the free-base dyad **2d**. These values closely resemble the HOMO values for the corresponding isolated porphyrins (-8.04 and -8.41 eV, respectively). Likewise, the LUMO energy of $PIBE_{10}$ in the gas phase was calculated to be -2.39 eV, which is in close concordance to the LUMO of the dyads (-2.58 and -2.57 eV for metallated and free-base dyad, respectively). Together with the observation that the absorption spectrum of the dyad is superimposable to the spectra of the single compounds (*cf.* p. 89), this is an indication of a relatively weak ground-state interaction between the porphyrin and perylene constituents of the dyad.[15]

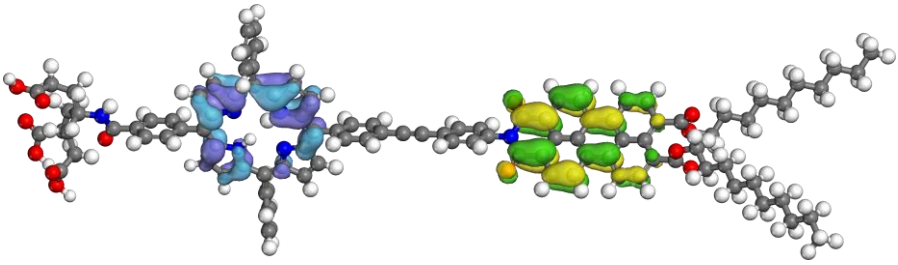

Figure 5.27. HOMO (blue) and LUMO (green) orbitals of G^1 porphyrin-PEP-$PIBE_{10}$ dyad **2d**. Note that the HOMO lies at the porphyrin and the LUMO is found at the perylene (semi-emp. GeomOpt NDDO PM6/UHF).[156]

Influence of the linker. The linear phenyl-ethynyl-phenyl (PEP) spacer between the porphyrin core and the perylene moiety of the dyad consists completely of sp^2 hybridized carbon atoms. The π electron system of the spacer is completely delocalized and thus suitable to transfer charges from the porphyrin to the perylene and *vice-versa*, over a distance of 12.58 Å.[156]

Although the porphyrin, the perylene and the PEP bridge each for themselves are aromatic systems, there is no direct electronic delocalization between these three parts. The PEP bridge is twisted due to steric repulsion between the β-pyrrole hydrogens of the porphyrin (as well as the peryleneic imide group) on the one hand and the phenylic hydrogens on the other hand. Semi-empirical calculations indicate torsion angles of 70–90° (PEP–porphyrin) and 50–52° (PEP–perylene) which can be seen impressively in Figure 5.27.[156] An important prerequisite of aromatic systems is planarity, which is clearly not satisfied by this system.

This, however, is not necessarily a disadvantage. It is possible that an electron or hole transfer is enabled by tunneling effects or *via* triplet states.[15] If that occurs, the charge separation lifetime is expected to be magnitudes higher than in directly electronically linked systems. This would be the case as the charge recombination is equally hindered, thus the chance of other relaxation pathways is increased.[157] Instead of electron transfer, an energy transfer from the perylene to the porphyrin across the PEP linker can be predicted, leading from the photoexcited Por-PEP-Per* to Por*-PEP-Per.

Prior investigations of electron/energy transfer in the dyad. Indeed, in 2001 the LINDSEY group performed a series of experiments using a porphyrin and a perylene diimide linked by a phenyl-ethynyl-phenyl bridge.[15,164-167] These preceding investigations were the reason why it was chosen to settle on the PEP bridge when the synthesis of other bisethynyl linkers failed during the development of this thesis.

To conclude this essential work, LINDSEY showed that *"the photoexcited perylene unit (PDI*) decays very rapidly (lifetimes of 2.5 (toluene) and 2.4 ps (acetonitrile)) by energy transfer to the porphyrin, forming PDI-pep-Zn* in high yield (80%, toluene; 70% acetonitrile), and hole transfer to the porphyrin, forming PDI^--pep-Zn^+ in lesser yield (20%, toluene; 30% acetonitrile). In both toluene and acetonitrile, the Zn* excited state subsequently decays with a lifetime of 0.4 ns primarily (80%) by electron transfer to the perylene (forming PDI^--pep-Zn^+). In the nonpolar solvent (toluene), the PDI^--pep-Zn^+ charge-transfer product has a lifetime of >10 ns and decays by charge recombination primarily to the ground state but also by thermal repopulation of the Zn* excited state."*[15] In other words: A high-yielding (80%) energy transfer of PDI* to Zn* (*i.e.*, ~1000-fold higher than remaining perylene fluorescence) was observed which concluded mainly (80%) in a charge separate PDI^--pep-Zn^+ [to temporarily maintain LINDSEY's naming scheme] state *via* electron transfer. The lifetime of PDI^--pep-Zn^+ prior to ground-state charge recombination was long-lived (>10 ns) in nonpolar solvents and short-lived (<0.5 ns) in polar solvents.

For free-base dyad PDI-pep-Fb, LINDSEY described in a following publication, that here as well the perylene emission was strongly quenched by energy transfer from PDI* to Fb* (85%).[165] In contrast to the metallated dyads, the yield and lifetime (50 – 500 ps) of charge-separated PDI^--pep-Fb^+ was notably lower in favor of charge recombination returning to Fb*. This was followed by typical porphyrin relaxation (*i.e.*, ~5% fluorescence, ~90% intersystem crossing to a triplet state).[277] In such a dyad, one could make use of the whole spectrum of light: Irradiation of porphyrin Soret and Q bands as well as irradiation of perylene eventually lead to the same PDI-pep-Fb* system. Again, the lifetime of charge-transfer product PDI^--pep-Fb^+ in polar media was drastically decreased.[165]

It can be legitimately expected that the presented target molecules **2a-d** possess similar charge-transfer and -recombination routes in THF. However, due to the basic molecular

architecture in LINDSEY's work, it has not been possible for them to investigate the electronical behavior in water and especially upon aggregation in lipid layers, where other close-range intermolecular interactions might play a role.

Observation of the energy transfer in the dyad 1d. The processes described above – especially the energy transfer from the excited perylene to the porphyrin – will be investigated and explained in this chapter. Excitation at 420 nm of the H_2Por-PEP-Per dyad **1d** in THF was already examined before (*cf.* Figure 5.24, p. 91). Using a three-dimensional fluorescence spectrum at different excitation wavelengths, a complete survey of optical excitation–emission features of **1d** can be performed (Figure 5.28). As shown before, the perylene fluorescence is very weak (expected quantum yield: $\Phi \sim 0.1\%$),[165] even when directly exciting at the perylene (*i.e.*, at 470 and 500 nm, green curve). Rather than fluorescence, an energy transfer to the porphyrin can be observed (Por-PEP-Per* → Por*-PEP-Per). The free-base porphyrin **1d** could form a charge-separated state Por^+-PEP-Per^- *via* electron transfer. However, in contrast to metalloporphyrins, this charge-separated state is not energetically favored. If electron transfer occurs, the free-base dyad is quickly reverted to the more stable Por*-PEP-Per state.[165] From here, typical decays of the excited porphyrin to the ground state occurs, including fluorescence at 652 and 715 nm.[277]

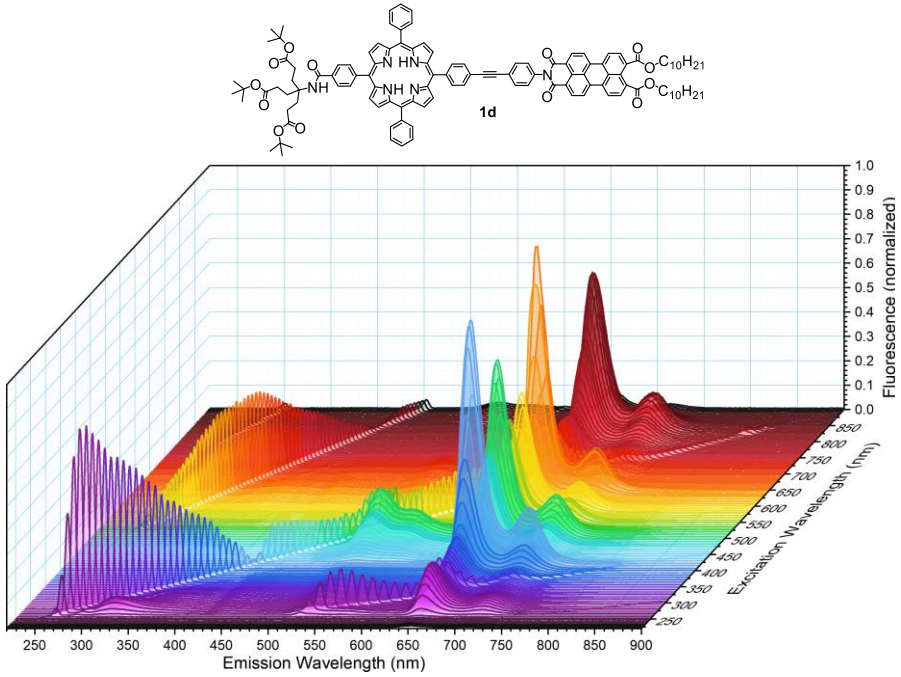

Figure 5.28. 3D excitation–emission spectrum of dyad **1d** in THF.

Excitation of the porphyrin at 280 (purple), 420 (blue), and 650 nm (orange) directly leads to porphyrin fluorescence with no energy transfer to the perylene. Excitation of the perylene in the range of 450 (blue) to 530 nm (green) leads to partial perylene fluorescence and increased porphyrin fluorescence. The porphyrinic emission at 650/715 nm observed for excitation at 800–850 nm is due to diffraction grating at the fluorometer, which by second-order diffraction also excites in the range of 400-425 nm (porphyrin Soret band).

The excitation spectra at particular emission wavelengths (530 nm for perylene, 650 nm for porphyrin) and variable excitation wavelengths (220 to 900 nm) are displayed in Figure 5.29. These spectra are an vertical intersection of the excitation-emission spectrum above (Figure 5.28) and are normalized to the porphyrin maximum at 512 nm. The UV-Vis spectra of porphyrin **13** and perylene **16** are displayed for comparison. The absorption spectrum of **13** (purple) was scaled to match the excitation spectrum (blue) at the peak maxima at 514 and 550 nm.

As explained before on page 89, the ground-state interactions between porphyrin and perylene in the dyad is negligible and the UV-Vis spectra of porphyrin **13** and PI_SBE_{10} **16** can be added up to give approximately the UV-Vis spectrum of the dyad **1d**. Using excitation spectra, the excited-state interactions in the dyad could be observed: In isolated molecules with distinct absorption–emission characteristics, the excitation spectrum would closely reflect the UV-Vis spectra, since emission would only occur after irradiation/excitation at the molecular absorption bands. Any deviation could be seen as interference of impurities – or, in this case, electronical interactions between the two chromophores. Due to instrumental limitations and light scattering, additional peaks are observed when the excitation wavelength equals the emission wavelength. These peaks are highlighted by colored vertical bars at 530 nm for the perylene spectrum (orange) and 615 nm for the porphyrin spectrum (blue).

As expected, emission at 530 nm (orange, perylene) is only triggered after perylene absorption at 450 to 530 nm, matching exactly the included absorption spectrum of PI_SBE_{10} **16** (red). At 420 nm excitation wavelength, no emission of the perylene is observed.

Excitation at the porphyrin's Soret and Q bands (420, 514, 550, 590 and 650 nm) exclusively leads to porphyrinic emission, which can be monitored by emission at 650 nm (blue). The excitation spectrum can thus be best correlated to absorption spectrum for free-base porphyrin **13** (purple). The maximum at 512 nm mainly stems from the excitation at the porphyrin Q_{IV} band (514 nm). However, it is also possible that excitation at the perylene (absorption maximum at 502 nm, red) is present but not detectable due to superposition of these peaks.

The peak at 479 nm might emerge from excitation at the perylene (*cf.* perylene excitation spectrum, orange) which then leads to energy transfer and porphyrin fluorescence at 650 nm. However, it is quite possible that the time-resolution of this spectrum is not suitable to clearly observe the energy transfer process from perylene to porphyrin with rate constants of *ca.* 3 ps.[15,165] In future research, additional time-resolved and differential fluorescence spectroscopy has to be performed to make a reliable estimation of the energy transfer between perylene and porphyrin.

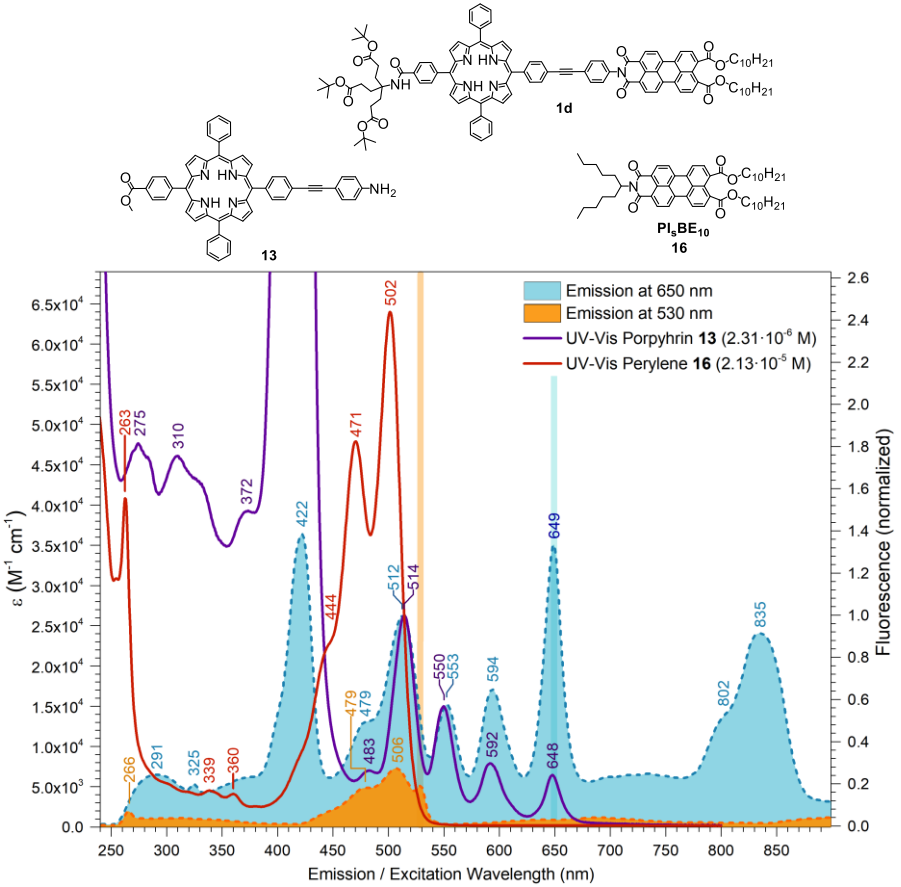

Figure 5.29. Normalized excitation spectrum of **1d** with fixed emission wavelengths at 650 (blue dashed, porphyrin moiety) and 530 nm (orange dashed, perylene moiety). The excitation wavelengths of 650 and 530 nm (distorting the fluorescence intensity observed at these wavelengths) are highlighted in the corresponding excitation spectra by vertical bars. Normalized UV-Vis spectra of porphyrin **13** (purple) and perylene **16** (red) are displayed for comparison.

Theoretical consideration of energy transfer processes. The energy transfer from the perylene excited state Por-PEP-Per* to the porphyrin excited state Por*-PEP-Per and subsequent ground-state relaxation with emission at 605 nm (ZnPor) or 650 nm (H_2Por) was already shown in this thesis both for non-metallated dyads (*vide supra* and p. 80) and ZnPor dyads (*cf.* p. 93), regardless of the structure of the perylene (PIBE$_{10}$ and PDI$_S$).

To shed light onto the underlying processes, the HOMO–LUMO orbital energies of the sub-molecules and the dyads shall be considered (Figure 5.30) and depicted in an energy diagram (Figure 5.31). These energies represent semiempirical calculations of molecules in the gas phase

(green) and thus can only be applied for a rough comparison.[156] Additionally, the spectroscopically determined HOMO–LUMO energies E_g for porphyrins and perylene are plotted (blue, *cf.* p. 93) and compared to the literature (purple).[15,165] It can be found that the calculated energy gaps (H_2Por > ZnPor) deviate from the analytically measured energy gaps (ZnPor > H_2Por). These observations are consistent with the literature. As there was not enough material and time left to measure the oxidation/reduction potentials by cyclic voltammetry (CV), one has to resort to literature values (red) in order to find reasonable energies for the HOMO–LUMO energy gap respectively the energy of the Por^+-PEP-Per^- charge-separated state.[15,165]

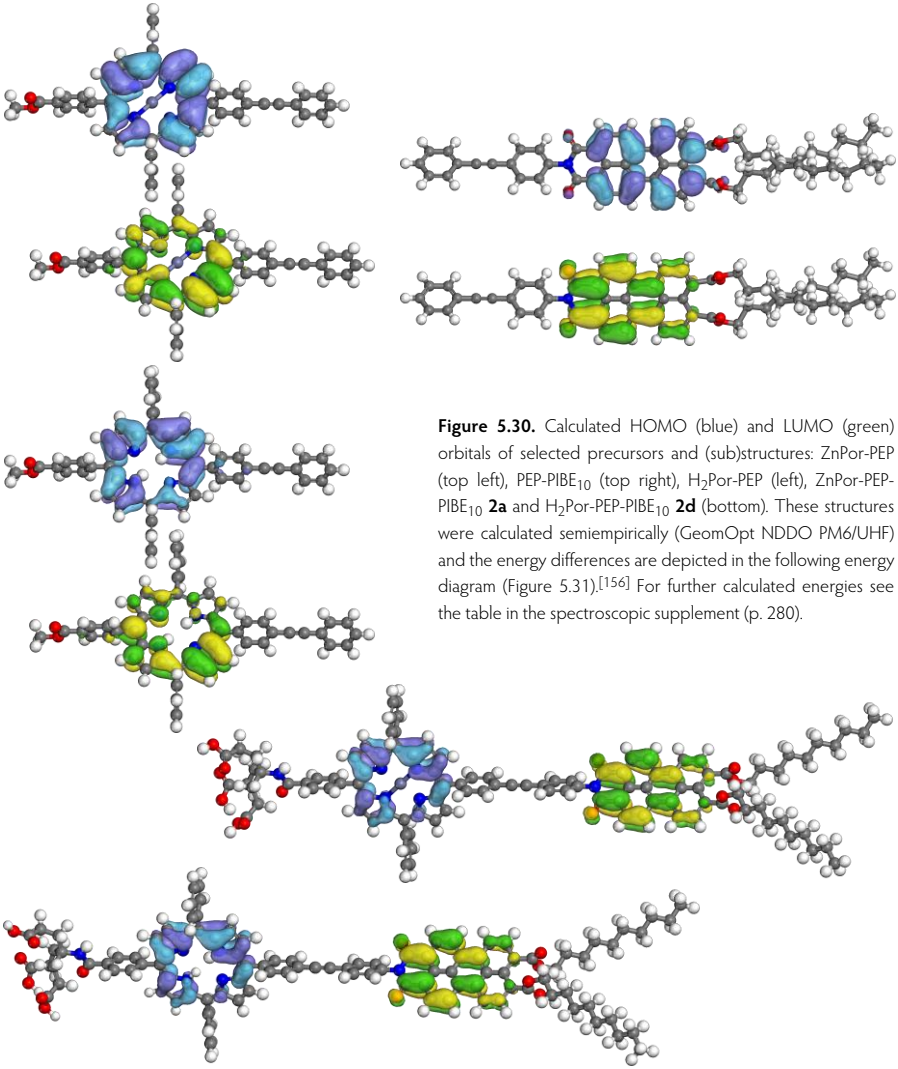

Figure 5.30. Calculated HOMO (blue) and LUMO (green) orbitals of selected precursors and (sub)structures: ZnPor-PEP (top left), PEP-$PIBE_{10}$ (top right), H_2Por-PEP (left), ZnPor-PEP-$PIBE_{10}$ **2a** and H_2Por-PEP-$PIBE_{10}$ **2d** (bottom). These structures were calculated semiempirically (GeomOpt NDDO PM6/UHF) and the energy differences are depicted in the following energy diagram (Figure 5.31).[156] For further calculated energies see the table in the spectroscopic supplement (p. 280).

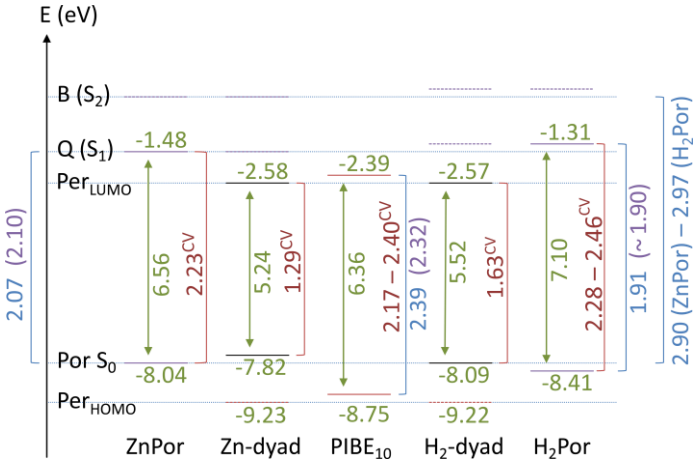

Figure 5.31. Energy diagram of porphyrin model compounds (ZnPor *vs.* H_2Por), perylene imide bisdecylester (middle) and the resulting dyads **2a/d**. The absolute energy levels (green) were calculated (semi-emp. GeomOpt NDDO PM6/UHF).[156] The HOMO–LUMO energy gaps (blue) were determined experimentally from the intersection point of the corresponding UV-Vis and emission spectra. Further literature-known $E_{g,\,opt.}$ (purple) and $E_{g,CV}$ (red) values for the dyads and its precursors were depicted for comparison.[15,119,165,265,267-268,275,281] See also the table in the spectroscopic supplement (p. 280).

It is again clearly visible that the HOMO energy of the dyad resembles the HOMO of the isolated porphyrins and the LUMO energy of the dyad resembles the LUMO of the isolated perylene. Naturally, the energy levels of the isolated monads are still populated and can be spectroscopically excited. Both the Q and Soret energy levels of the porphyrin and the vibronic structure of the perylene continue to coexist in the dyad. In a publication by ZHOU *et al.*, the HOMO–LUMO energy gap $E_{g,CV}$ of a dyad similar to free-base H_2Por-PEP-PDI was estimated at 1.63 eV by CV measurements.[281] The energy of the charge-separated Por^+-spacer-PDI^- state was estimated to be 1.45 eV relative to the ground state.

Jabłoński diagram. From the energy levels depicted in Figure 5.31, the observed energy and electron transfer processes in the dyad can be summarized using a JABŁOŃSKI diagram (Figure 5.32). Analog to the isolated porphyrin, no Soret band fluorescence is observed upon irradiation at 420 nm. Corresponding to KASHA's rule, a fast internal conversion (IC) from the Soret band to the Q band takes place, leading to fluorescence at 600 and 650 nm for metallated (**1a-c/2a-c**) and free-base dyad (**1d/2d**), respectively (Figure 5.32 (1), *cf.* Figure 5.26, p. 93).

Irradiation at 490 nm excites almost exclusively the perylene ($E_{g,\,514\,nm}$ = 2.39 eV). As shown before, the usually strong perylene fluorescence is considerably quenched (2). LINDSEY demonstrated two decay pathways:[15,165] First, by energy transfer from Per* excited state to Por*

excited state, forming Por*-PEP-Per. This was depicted in the JABŁOŃSKI diagram using a concerted relaxation–excitation pathway (3). As a second possibility, a ground-state electron/hole transfer from porphyrin HOMO to perylene SOMO can be found, leading to the charge-separated Por^{+}-PEP-Per^{-} state with a hole at the porphyrin S_0 SOMO (4).

From the porphyrin excited state Por*-PEP-Per – independent on the excitation pathway – several decay mechanisms can be found. Direct relaxation leads to fluorescence at 600 / 650 nm (see above). Intersystem crossing (ISC) to an excited triplet state is typical for porphyrins,[277] but will not be further regarded herein. Electron transfer from the porphyrin excited state to the perylene LUMO again forms the charge-separated state Por^{+}-PEP-Per^{-} (5). A hole remains at the porphyrin S_0 SOMO. This electron transfer probably proceeds over the (not fully conjugated) PEP linker. The lifetime of this charge-separated state is strongly dependent on the solvent (toluene: >10 ns, acetonitrile: <0.5 ns)[15] and the porphyrin: Using H_2Por, it is energetically favored to return to Por^{*}-PEP-Per (0.5 ns). Although in ZnPor and MgPor a thermal repopulation to Por^{*}-PEP-Per is unfavored but possible (due to the small energy difference), the lifetimes of Por^{+}-PEP-Per^{-} usually exceed 10 ns.[165] LINDSEY showed that in metallated dyads, the main pathway (>99%) proceeds over charge recombination to the ground state.[15,165] These observations from the literature, however, will have to be reproduced for the dyads at hand in future measurements.

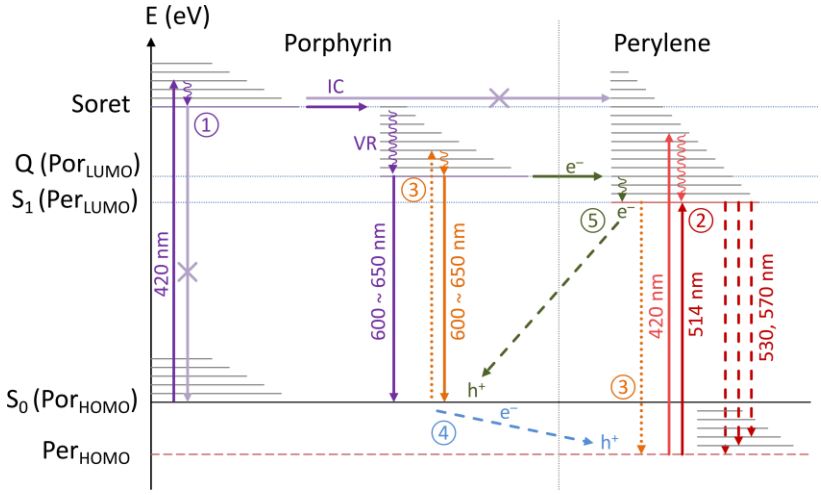

Figure 5.32. Jabłoński diagram of energetic processes (intersystem crossing to triplet states are left out for clarity): (1) irradiation on porphyrin Soret band does not lead to emission at 420 nm. Instead, internal conversion to Q bands and fluorescence at 600-650 nm is observed. No energy or electron transfer to perylene occurs. (2) Irradiation on perylene only partially (0.1%) leads to fluorescence at 530 and 570 nm. (3) Instead, energy transfer of 514 nm (2.4 eV) from Per* to Por* at the Q band energy is observed (80%), here displayed by a combined relaxation–excitation process. (4) To a small fraction (20%), an electron/hole transfer from Por HOMO to Per SOMO takes place, leading to a Por^{+}-PEP-Per^{-} charge separated state. (5) From Por* excited state of metalloporphyrins, electron transfer over the PEP bridge to Per* excited state can occur, also forming Por^{+}-PEP-Per^{-}. This charge separated state recombines to the ground state after several ns.[15,165]

Application fields of the dyad. The determination that the HOMO–LUMO energy gap lies between 1.45 and ~2.2 eV is an important prerequisite for a great field of application: Catalytic water-splitting is only possible if the free energy is larger than 1.23 eV.[282-283] Potentially, this class of molecules could be applied to self-assemble to lipid membranes in aqueous media. Intercalating water-splitting catalysts into this membrane could lead to an *in situ* generation of hydrogen and oxygen.[284] The presence of compartments which are separated by the lipid layers could then prevent catalyst poisoning.[283] Furthermore, the self-assembled membranes would be utilized both as light harvester,[17-18] and as molecular wire to transport the generated charges to the active catalysts.[16,122] Other application fields for the dyads **1a-d** and **2a-d** could be found as optoelectrical gates/switches (if a high percentage of Por^{+}-PEP-Per^{-} charge-separated states are generated and stable), or as light-input/transfer devices, for example in photovoltaics (if rapid and high-yielding energy transfer from Por-PEP-Per* over Por*-PEP-Per to an energy-acceptor-layer is favored).[15,155,157,160,162-166,281,285]

To gain further insights into these application fields, the self-aggregation behavior of the dyad in water and its influence on the absorption/emission properties will have to be investigated with larger amounts of dyads **2a-d**.

5.7.6 Solubility Studies of Dyads 2a-d in THF and Water

For the first time, water-soluble porphyrin–perylene dyads were prepared. The final dyads **2a-d** (see p. 69ff), carrying three or nine acid groups, were mostly soluble both in THF and in alkaline H_2O. As only too little amounts of products were available, no dilution series to obtain accurate concentrations could be performed for these dyads. Hence, the following spectra are presented without exact extinction coefficients. Instead, the spectra are normalized to provide a certain degree of comparability.

In THF, the UV-Vis spectra of **2a/b/d** show the typical features expected for porphyrins and perylenes (Figure 5.33). Surprisingly, dyad **2c** (carrying the swallowtail group) was virtually insoluble in (non-acidified) THF and no absorption spectrum could be measured. Prior to UV-Vis spectroscopy, the compounds were characterized by NMR spectroscopy in TFA-*d*, amongst others. Due to the lack of substance, the same samples had to be re-used for the subsequent optical characterization. Unfortunately, the zinc porphyrin **2a** was completely de-metallated after exposition to TFA in the NMR sample: The Soret band at 432 was shifted to 419 nm and the now four Q peaks resemble free-base dyad **2d** (Figure 5.33). Thus, in the following spectroscopic discussion, **2a** must be considered as de-metallated dyad equivalent to **2d**.

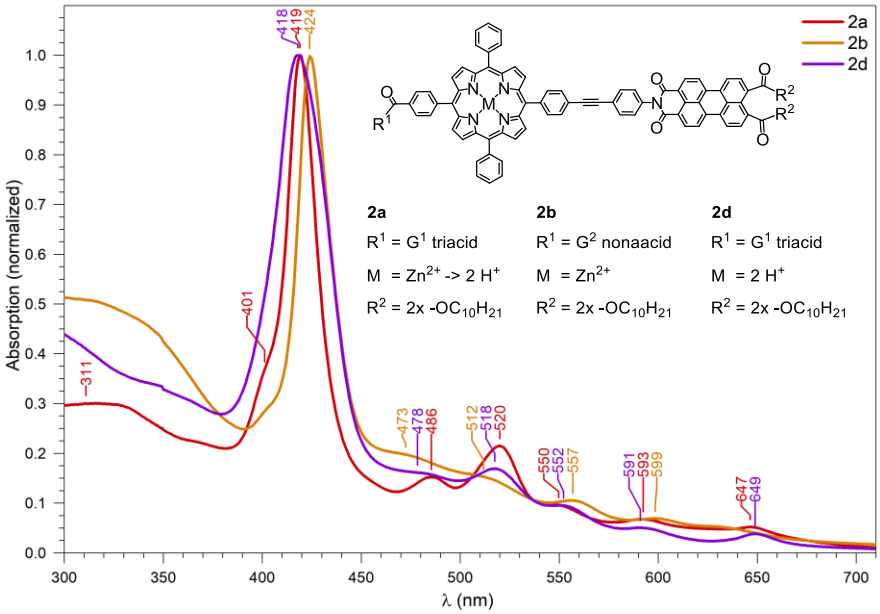

Figure 5.33. Normalized UV-Vis spectrum of porphyrin dyads **2a/b/d** in THF. It can be found that dyad **2a** was de-metallated after NMR measurements in TFA-*d*, the spectrum resembling free-base dyad **2d**. Dyad **2c** was insoluble in THF.

Compared to **1b** (Figure 5.25, p. 92), the UV-Vis spectrum of **2b** has notably less pronounced and therefore broadened perylene absorptions. This is an indication of the formation of peryleneic aggregates.[113,286] Here, the sterical hindrance of the NEWKOME G^2 dendron could play a role. Although a higher steric demand usually leads to de-aggregation, the dendrons could lead to an oppositional effect in this situation by promoting a new aggregation type: Possibly, the increased hydrophilicity of the polar end groups induces an (*e.g.*, columnar) aggregated structure in polar media where the hydrophobic perylenes are stacked in direct proximity to each other. The resulting π–π interactions would strongly quench the peryleneic absorbance and fluorescence. When changing the solvent from THF to water, this observation should be even more prominent.

Axial porphyrin complexes with pyridine. According to the literature, it is highly probable that the water-soluble amphiphilic dyads will form aggregates, micelles and lipid layers or even more complex supramolecular structures in polar solvents due to their extended hydrophobic groups.[139,181-182,189,287] To counteract and – more importantly – fine-tune this behavior, a LEWIS base can be added as a ligand which coordinates axially to the porphyrin.[162] Pyridine with its electron-donating nitrogen is a suitable and well-investigated molecule for this purpose.[288] By

variation of the axial ligand (*e.g.*, bipyridines and (di)amines), the porphyrin–porphyrin distance as well as the overall aggregation behavior could be adjusted extensively. Possibly, this could manipulate the intermolecular interactions and could enforce the self-assembly of different aggregate structures.

Prior to the aggregation experiments, the general coordination properties of pyridine and their influence on UV-Vis spectroscopy were examined. Pyridine was titrated to a solution of dyad **1c** (see p. 67) in THF (Figure 5.34). Both the Soret band and the Q bands where shifted bathochromically (4-6 nm). The intensity of the Soret band was first reduced, followed by an increase to approximately the original level. This is an indication that the pyridine interacts electronically with the porphyrin and donates electrons into the LUMO+1 orbital. The intensity of the Q bands decrease slightly, partially due to dilution effects. In contrast, the position and intensity of the perylene bands at 487 and 522 nm stay completely unaffected by addition of pyridine, as no interactions exist between perylene and pyridine. For unmetallated porphyrins, no axial ligand coordination is possible, thus the influence on the electronic structure is expected to be minimal.

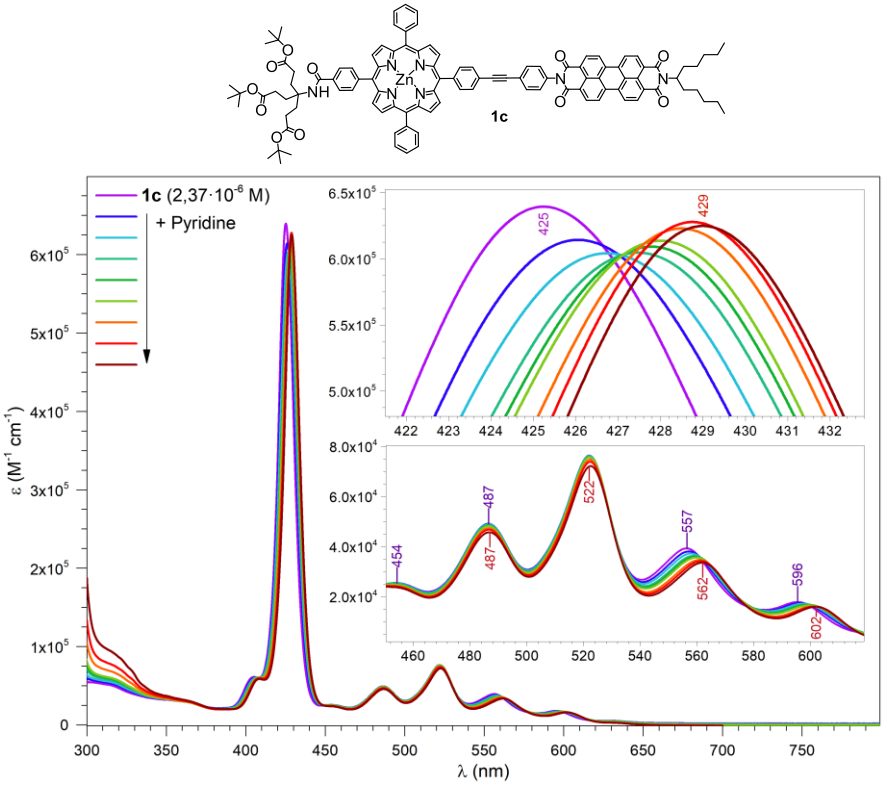

Figure 5.34. Addition of pyridine to a solution of **1c** in THF. Pyridine forms an axial complex with porphyrin, which influences the positions of Soret and B bands while leaving the perylene bands unchanged.[288]

Pyridine/THF titration to porphyrin in water. Indeed, when comparing the UV-Vis spectra of metallated dyad **2b** with unmetallated dyad **2d** in water, several interesting observations can be made upon titration of pyridine (Figure 5.35). In case of **2b** (Figure 5.35, left), the Soret band is shifted bathochromically from 426 nm to 423 nm (Δ 6 nm). The Q bands are shifted likewise from 557 and 600 nm to 563 and 606 nm (Δ 6 nm). This corroborates the expected coordination and electronical interaction between zinc porphyrin and pyridine. Again, the (weakly visible) perylene absorption features are not shifted. The overall absorption intensity increases slightly as the dyads are better soluble in pyridine compared to the initial H_2O/NaOH solvent mixture (this effect will be further investigated on p. 106).

Regarding free-base dyad **2d** (Figure 5.35, right), the absorptivity of the Soret band (421 nm) is increased and symmetrized (hence the seemingly shifted absorption maximum from 418 nm). This can be attributed to the solubility enhancement and de-aggregation upon addition of pyridine. No significant peak shift is observed. The perylene features (expected at 470 and 500 nm) are again only very weakly visible and partially superimposed by the Q_{IV} band at 516 nm.

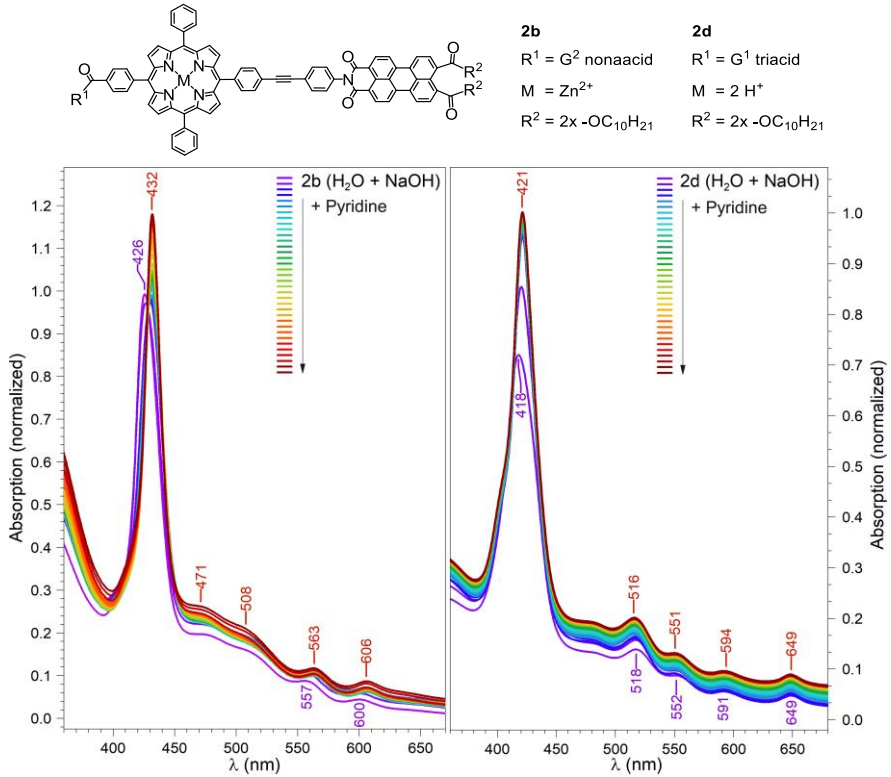

Figure 5.35. UV-Vis spectrum of **2b** (left) and **2d** (right) in H_2O + NaOH (pH 10). Upon titration of pyridine, the overall intensity increases due to solubility enhancement. The Soret band of **2b** changes slightly to longer wavelength due to electronical interactions or coordination of pyridine to the zinc porphyrin. In case of **2d** (right), no bathochromic shift can be detected.

Intramolecular self-aggregation behavior. As described for dyad **2b** in THF (Figure 5.33), the weak and broad perylene absorptions lead to the conclusion that these perylene substructures are strongly aggregated. For the porphyrin moiety, the degree of aggregation is decidedly lower. The absorption maximum of the Soret band matches the expected monomeric absorption. If porphyrin aggregation was present, this would usually result in a strongly shifted and often broader and weaker absorption of the Soret band.[181,188,288-290]

These observations lead to the conclusion that the perylene structures are aggregated while the porphyrins exist as monomers. Probably, the sterical demanding NEWKOME dendrons (which are directly attached to the porphyrin) do not allow the aggregation of the porphyrins. Thus, a possible aggregation pattern would be the formation of columnar helical structures with NEWKOME acid groups at the outside and strongly π stacking perylenes at the center. However, there will be additional experiments (*e.g.* DLS, DOSY NMR, zeta potential determinations, microscopy) necessary to reveal the exact nature and characteristics of the observed aggregates.

Solubility enhancement by addition of THF in water. The solubilization of dyad **2a** (which was de-metallated after NMR studies in TFA-*d*) can also be enhanced in H_2O + NaOH using THF instead of pyridine as co-solvent (Figure 5.36).

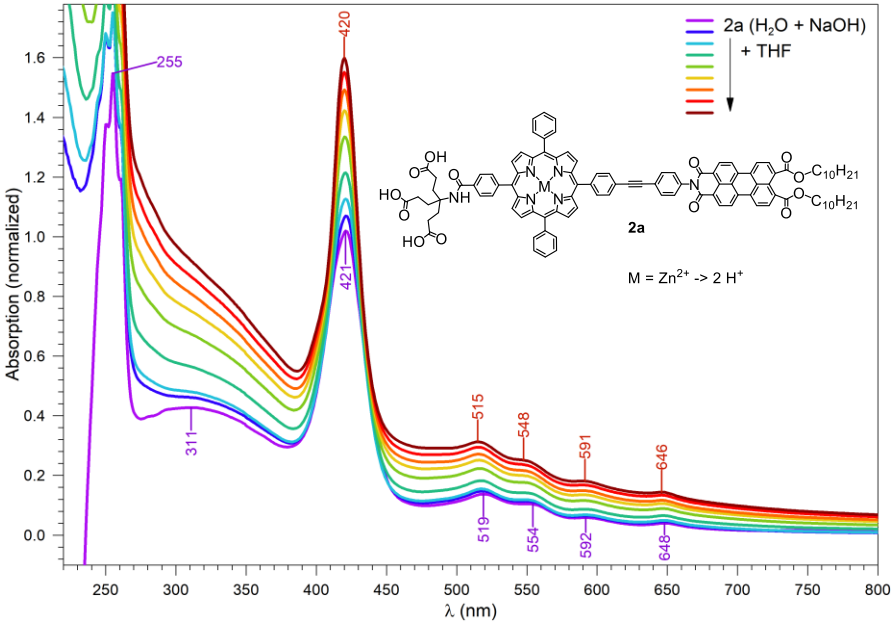

Figure 5.36. UV-Vis spectrum of (de-metallated) dyad **2a** in H_2O + NaOH. Upon titration of THF as co-solvent, the overall intensity increases due to solubility enhancement.

Upon titration of THF, the intensity of the Soret band drastically increases as the solubility of **2a** in the H_2O/NaOH/THF mixture improves. Again, the perylene absorptions are extremely weak and partially superimposed by the Q_{IV} band. In these observations, the UV-Vis spectrum of **2a** (+THF, Figure 5.36) completely resembles the one of **2d** (+pyridine, Figure 5.35, right).

Investigations of NaOH *vs.* pyridine as co-solvents. The NEWKOME dendron with its three (or nine) carboxylic acid groups only render the molecule soluble in protic media when the acid groups are deprotonated, *i.e.*, at pH > 8. NaOH or other suitable bases/buffers can be used for this purpose. However, due to the intermolecular π–π stacking forces of porphyrins and perylenes as well as the high percentage of hydrophobic groups in these dyads, solely tuning the pH sometimes does not suffice to solubilize the molecules **2a-d** in water. This could be shown impressively in Figure 5.37, where dyad **2c** (which already turned out to be insoluble in THF, *cf.* Figure 5.33, p. 103) was suspended in water at pH 7 without detectable dissolution. As expected, no porphyrin features could be found in the UV-Vis spectrum. Instead, large particles, a colorless suspension and a very weak and broad absorption at 334 nm were observed.

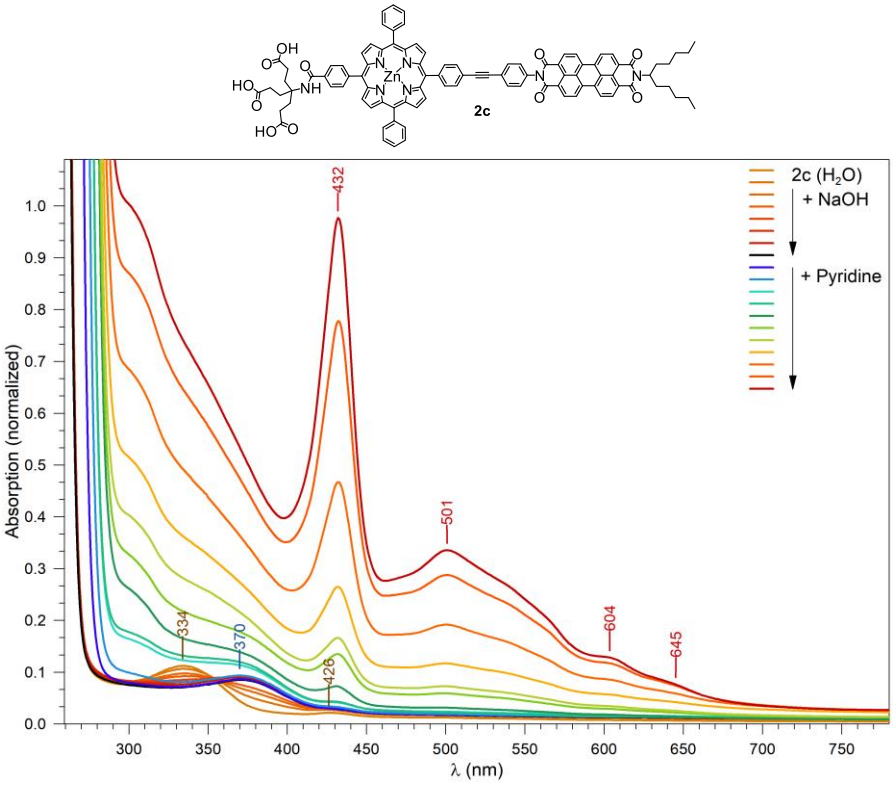

Figure 5.37. Solubility studies of **2c** in H_2O, upon successive addition of NaOH (up to pH 10), followed by addition of pyridine as co-solvent.

Upon addition of NaOH, the deprotonation of the dendritic acid groups should render the dyad soluble, as shown before for **2a** (Figure 5.36) and **2b/d** (Figure 5.35). In contrast, dyad **2c** did not dissolve in H_2O/NaOH (diverse ratios/pH values). The peak at 334 nm disappears while a new, faint peak at 370 nm arises. Both peaks do most certainly not represent porphyrin aggregates: While J-type aggregates appear at longer wavelengths, the hypsochromic shift for H-type aggregation can be estimated to be not less than ~400 nm.[290-291] Further addition of NaOH did not lead to dissolution of the particles and to the evolution of the characteristic Soret band.

When switching to pyridine as co-solvent, the particles dissolve gradually and the solution is slightly colored. In Figure 5.37, this observation can be followed by the growth of the Soret band at 432 nm as expected for metallated, monomeric porphyrins with axial ligand coordination (*cf.* Figure 5.35 left). The Q bands are considerably less intense and the newly originated broad peak at 501 nm is an indication of highly aggregated perylenes. This could be another hint to the formation of columnar aggregates with π stacked perylenes in the center and helically arranged porphyrins with sterically demanding dendrons at the periphery (Figure 5.38).

To complement this survey, the solubilization characteristics of dyad **2c** in H_2O upon addition of pyridine as first co-solvent and the subsequent addition of NaOH as second co-solvent are investigated (Figure 5.39). Starting from the already observed spectrum in pure water, the characteristic pyridine-ZnPor coordination band at 432 nm quickly arises. Both the porphyrin Q bands at 565 and 602 nm (weak) and the perylene (PDI_S) features at 498 and 533 nm (intense) can be clearly assigned. The particles dissolved completely and a homogeneous solution could be obtained. In comparison to Figure 5.37, it can be found that the pH value (which increased from pH 7 to 9 upon pyridine addition) has little or no effect on the solubilization of the dyad. The main effect is due to the good solubility of the dyad in the co-solvent (pyridine or THF). If axial coordination to the metalloporphyrin is possible, further solubility enhancement can be observed.

When successively adding NaOH, the solution turns turbid as the miscibility is reduced. At first, the intensity of the whole spectrum increases due to particle formation and refraction. This is followed by a decrease of the peak intensities owing to dilution. While the Soret band stays rather unaffected, the perylene absorption maxima at 498 and 533 nm decrease and quickly convert to the broad peak at 522 nm which was already observed for aggregated perylenes.[113,151,273]

In conclusion, the solubility in water for triacid G^1 ZnPor-PEP-PDI_S dyad **2c** is inferior to dyads **2a/b/c**. This has to be accounted to the branched swallowtail group: While increasing the solubility in organic solvents in the course of the synthesis, the solubility of the dyad in alkaline water and in THF (*cf.* chapter 5.7.6, p. 102) was drastically reduced compared to the bis-decylester end groups. Possibly, the sterically demanding swallowtail group attached to the perylene hinders an effective π stacking and thus impedes the (columnar) aggregation of the amphiphile. In all cases, the spectroscopic features of the perylene are broadened upon addition of NaOH, which indicates increased intramolecular interactions and π stacking between the perylene moieties.

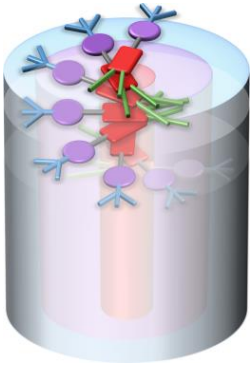

Figure 5.38. A proposed helical columnar stacking of the water-soluble porphyrin–perylene dyads **2a-d**: The perylene subparts show strong aggregation (at 522 nm) and intermolecular π interactions while the porphyrin compounds (at 432 nm) do not interact and can be interpreted as monomers. The sterical demanding Newkome dendrons are arranged at the outside to induce water-solubility.

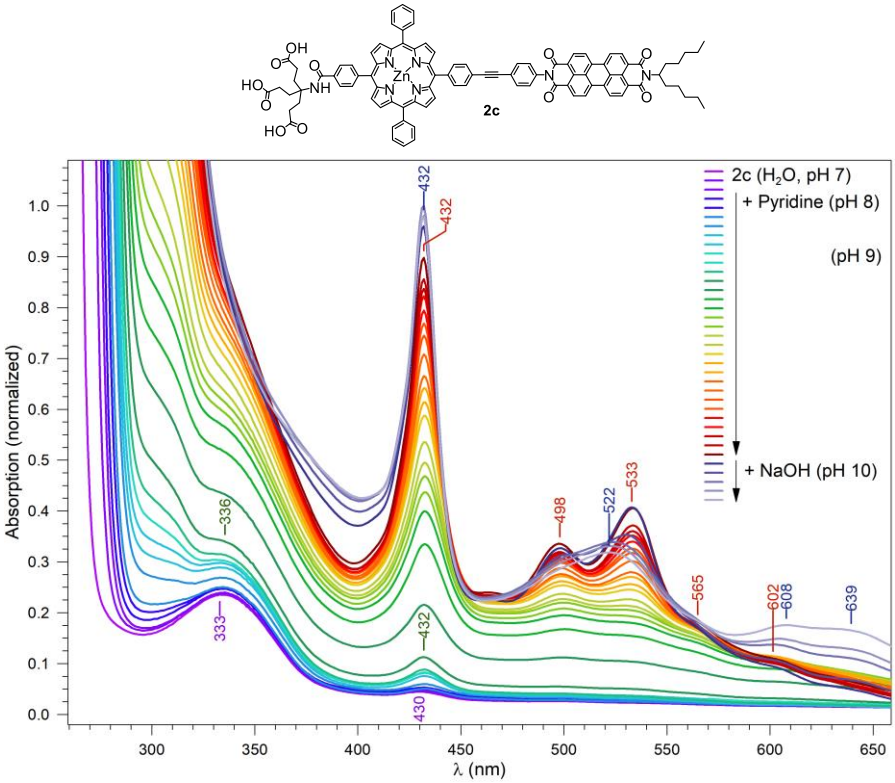

Figure 5.39. Solubility studies of **2c** in H_2O, upon successive addition of pyridine, followed by addition of NaOH as co-solvent. The absorption at 522 nm can be interpreted as perylene aggregation band.

Overview on the photophysical properties. The investigated molecules with the corresponding absorption/emission in the different solvents are listed in Table 5.12. As stated before, the absorption and emission maxima of the chromophores are generally independent of their molecular composition due to virtually nonexistent ground-state interaction. The isolated dyes show basically the same characteristics as the dyad (Figure 5.40, *cf.* entries 1/2 and 11/12).

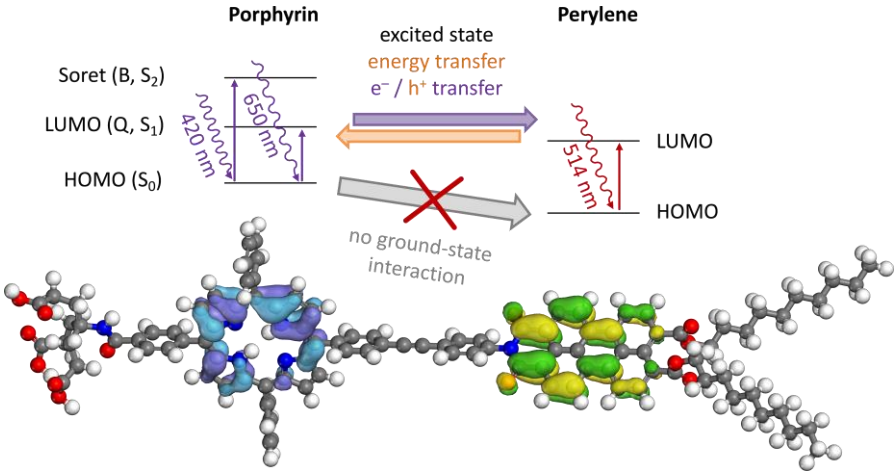

Figure 5.40. Schematic representation of energy transfer in dyad **2d**: No ground-state interaction between porphyrin and perylene occurs. Hence, the UV-Vis spectrum of dyad **2d** closely resembles the sum spectra of pristine porphyrin and perylene. Instead, energy/electron/hole transfers of the Por-PEP-Per* excited state take place (see Jabłoński diagram on p. 101), which can be detected by comparing the fluorescence excitation spectra.[156]

The free-base porphyrin shows weak solvatochromism especially at the Soret band (419 nm in THF, 421 nm in H_2O/NaOH/pyridine, entries 2 and 4). The emission wavelength is stronger influenced by the surrounding solvent (652 and 715 nm in THF, entry 2) and is shifted hypsochromically in water (647 and 701 nm, entry 4). In case of metalloporphyrin, a shift of the Soret band to 425 nm and reduction to two Q bands (557 and 596 nm) can be found (entry 5). The absorption wavelengths are nearly independent from the solvent (entries 5 and 7) whereas a strong shift can be found upon addition of pyridine, which coordinates axially to the zinc porphyrin (entries 5/6 and 7/8/9). Upon aggregation, the emission spectra change notably: In THF, peak maxima of 605 and 655 nm are observed for all metallated porphyrins (entry 5). Aggregation in water leads to strong reduction of fluorescence intensity at 605 nm while a new peak at 714 nm arises (entry 9). The emission spectra of H_2Por and ZnPor in H_2O/NaOH/pyridine exhibit a very similar peak structure (entries 4 and 9) but with remarkably different fluorescence intensities (as discussed later on p. 120).

Table 5.12. Absorption and emission peak maxima of compounds in THF and multiple solvent mixtures (H_2O/NaOH/pyridine).

entry	type / compound		solvent	absorption (nm)	emission (nm)	$E_{g,\,opt}$[a]
1	H_2Por	**13**	THF	419 (B), 514, 550, 592, 648 (Q)	652, 714	
2	H_2Por (dyad)	**1d**	THF	419 (B), 514,[d] 549, 592, 647 (Q)[f,i]	652, 715	1.91 eV
3	H_2Por (dyad)	**2d**	H_2O[b]	418 (B), 518, 552, 591, 649 (Q)	*not measured*	
4	H_2Por (dyad)	**2d**	H_2O[b,c]	421 (B), 516, 551, 594, 649 (Q)	(605), 647, 701	
5	ZnPor (dyad)	**1c**	THF	425 (B), 557, 596 (Q)	605, 655[e,g,h]	2.07 eV
6	ZnPor (dyad)	**1c**	THF[c]	429 (B), 562, 602 (Q)[g,h]	*not measured*	
7	ZnPor (dyad)	**2b**	H_2O[b]	426 (B), 557, 600 (Q)	*not measured*	
8	ZnPor (dyad)	**2c**	H_2O[c]	432 (B), 565, 602 (Q, weak)	*not measured*	
9	ZnPor (dyad)	**2c**	H_2O[b,c]	432 (B),[h] 608, 639 (Q, weak)	(610), 652, (716)[h]	
10	$PABE_{10}$	**15**	THF	(420), 444, 470, 499	531, 563	2.41 eV
11	PI_SBE_{10}	**16**	THF	(417), 444, 471, 502	525[88]	2.39 eV
12	$PIBE_{10}$ (dyad)	**1d**	THF	(444),[d] 472, 505[g]	528, 561[e,f]	
13	$PIBE_{10}$ (dyad)	**2d**	THF	(444),[d] 478, 518	531, 568[e,f,g,h]	
14	$PIBE_{10}$ (dyad)	**2d**	H_2O[b,c]	*too weak*[d]	550[h] – 610 (broad)[f]	
15	PDI_S (dyad)	**1c**	THF	(455), 487, 522	531, 570	
16	PDI_S (dyad)	**2c**	THF	*solubility too low*	530, 570	
17	PDI_S (dyad)	**2c**	H_2O[c]	498, 533	*not measured*	
18	PDI_S (dyad)	**2c**	H_2O[b,c]	522 (very broad)	585, 650	

[a] energy gap determined by the intersection point of absorption and emission spectra. [b] minor amounts of NaOH added to obtain alkaline pH. [c] minor amounts of pyridine added to enhance solubility. [d] peak not visible due to superposition. [e] values measured for **1a** are in the same range. [f] values measured for **2a** (de-metallated and thus equatable to **2d**) are in the same range. [g] values measured for **1b** are in the same range. [h] values measured for **2b** are in the same range. [i] values measured for **2d** are in the same range.

The perylene absorption spectra are strongly dependent on the type of molecule: PI_SBE_{10} **16** has peak maxima at 444 (superimposed in the dyads), 472 and 505 nm (entries 11 and 12). PDI_S in dyads **1c/2c** possesses an additional aromatic ring and has bathochromatically shifted peak maxima at 455, 487 and 522 nm (entry 15, *cf.* discussion on p. 86ff). Comparing dyads **1d** and **2d** (entries 12 and 13), the perylene absorption is strongly quenched in relation to the porphyrin absorption. Due to the perylene peak broadening and the contribution of the porphyrin Q_{IV} band, the peak seems to be shifted from 505 to 518 nm. In water, the perylene absorption is often very weak, which can be attributed to strong aggregation (entries 14 and 18, Figure 5.41). Regardless of the low peak intensity, a pronounced solvatochromism between THF (487 and 522 nm) and water/pyridine (498 and 533 nm) can be found for the intense perylene peaks of PDI_S (entries 15 and 17). Upon addition of NaOH, a broad aggregation peak at 522 nm was observed (entry 18, *cf.* Figure 5.39). The absorption and emission quenching of the perylene components of the dyads is a strong hint that peryleneic π stacking aggregation occurs in polar media. In contrast, the

porphyrin absorption and emission features stay rather unaffected, which leads to the conclusion that little or no porphyrinic intermolecular interaction occurs (Figure 5.41 bottom left). A typical aggregation pattern would be a columnar structure where the dyad self-assembles in a helical pattern (Figure 5.41 right). The hydrophilic dendrons at the exterior are exposed to the polar solvent whereas the hydrophobic perylenes are aggregated in the center of the column. Hence, the exposure of the hydrophobic parts of the dyad to water is minimized.

Interestingly, the emission maxima for $PIBE_{10}$ (in dyads **1a/b/d** and **2a/b/d**) and PDIs (in dyads **1c/2c**) are nearly identical in THF (~530 and ~570 nm, entries 12, 13, 15 and 16). For both molecules, the emission shifts to longer wavelength in water (~585 and 650 nm, entries 14 and 18). The observed emission maxima are occasionally superimposed by the porphyrin emission at 650 nm and are usually very broad and weak. In the following chapter, the emission spectra of the dyads will be investigated more closely in solvent titration experiments.

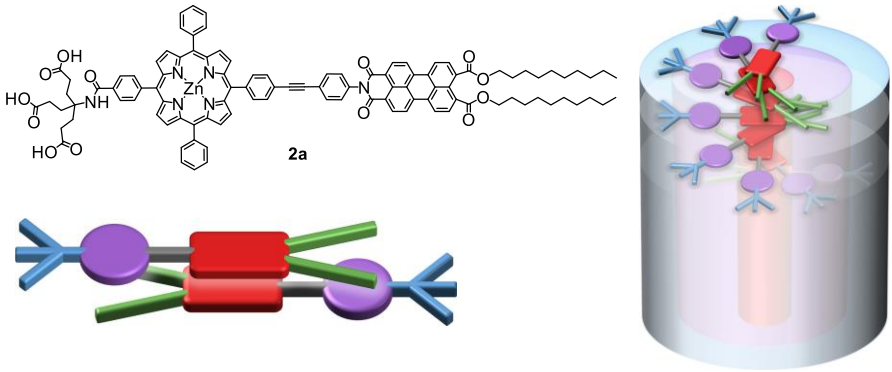

Figure 5.41. The absorption and emission spectra of the amphiphilic dyads lead to the conclusion that the perylene subcomponents are aggregated (and interacting intermolecularly) whereas the porphyrins remain monomeric (bottom left). A typical aggregation pattern could be a columnar helical self-assembly (right).

Solvent titration experiment. Dyad **2a** (~10^{-5} M, de-metallated after NMR studies in TFA-*d*) was dissolved in different THF/H_2O solvent ratios (Figure 5.42, from left: pure THF, to right: H_2O, with minor amounts of NaOH and pyridine). In the leftmost vial, THF without dyad **2a** is shown for comparison. While the visible colors of these vials differ only slightly, the fluorescence (at 366 nm excitation wavelength) varies strongly: In pure THF and up to a ~1:1 THF/H_2O solvent ratio, the dyad emits an intense yellow fluorescence. This emission can be attributed to the perylene and is quenched upon further addition of water. Instead, a weak red fluorescence can be observed (at 1:3 THF/H_2O ratio), which can be accounted either to perylene aggregates or to porphyrin fluorescence.

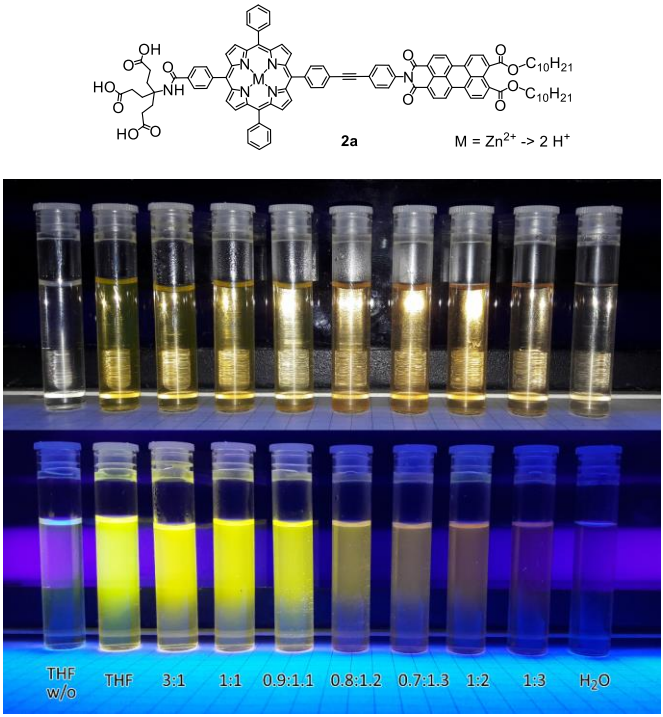

Figure 5.42. Color (top, visible light) and fluorescence (bottom, excitation wavelength: 366 nm) of dyad **2a** in different THF/H_2O solvent ratios. The fluorescence intensity decreases and a red shift can be observed. This is attributed to aggregation effects in water and the weaker porphyrin fluorescence.

This solvent quenching effect can also be observed by fluorescence spectroscopy. For this purpose, the emission of dyad **2c** was monitored for certain sets of excitation/emission wavelengths in a titration experiment from water to THF (Figure 5.43). Although the solubility of **2c** was too low to obtain a suitable UV-Vis spectrum in THF (*cf.* p. 102), it was no problem to measure fluorescence spectroscopy, as much lower concentrations were needed. Upon excitation at 480 and 520 nm (perylene), the emission intensities at 530 and 570 nm (perylene) and 650 nm (porphyrin) were monitored. Likewise, the porphyrin fluorescence was measured upon excitation at 420 nm and emission at 650 nm. Excitation at 265 nm with emission at 300 nm should track the influence of THF.

First, dyad **2c** was dissolved in approx. 3 mL water with few drops of NaOH/pyridine (*cf.* Figure 5.39). The emission intensity of the dyad was very low and the slit settings of the fluorospectrometer had to be adjusted accordingly. Upon dropwise addition of THF, the porphyrin emission (purple/blue) started to be magnitudes more intense than the perylene emission (red/orange and green). Due to the limitations of the fluorospectrometer, the slit settings

had to be narrowed gradually to reduce the sensitivity and to prevent overstraining the detector. As basically a linear relation between excitation/emission intensity can be presumed, the spectral data points were carefully fitted to give a continuous dataset. At 0.8 mL THF, the incline of the perylene emission intensity outpaced the porphyrin fluorescence and further increased to a maximum at 3 mL THF. As shown before in Figure 5.42, the perylene fluorescence – although far from $\Phi \approx 1$ quantum yield – was magnitudes higher than the porphyrin emission at this point. Despite the reduced sensitivity, a large variation for the measured values was observed which might be an indication of slow, competing processes (such as amphiphilic aggregation–deaggregation equilibria) in the solution. From 3 to 10 mL THF, the emission intensity of all peaks decreased drastically. Naturally, the titration progress caused a decline of the concentration of dyad **2c**. The dilution was estimated by linear regression curves (Figure 5.43). The excitation/emission at 265/300 nm continued to increase linearly upon addition of THF and is therefore a measure for the solvent emission.

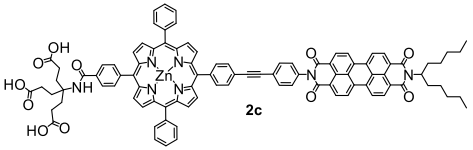

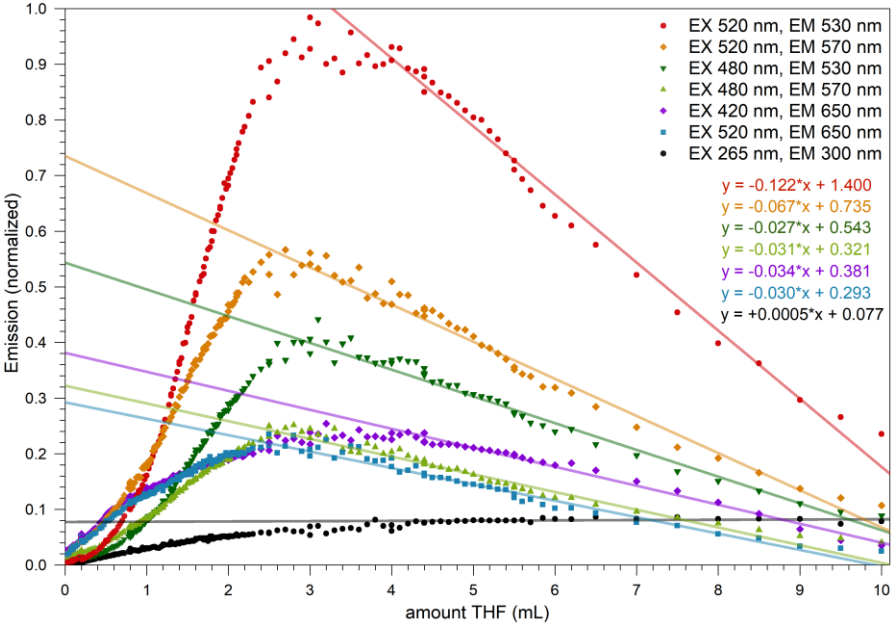

Figure 5.43. Solvent titration of **2c** from H_2O to THF at different excitation/emission wavelengths. A linear regression can be calculated to recompensate the dilution effects from 4 to 10 ml THF.

For selected H_2O/THF solvent ratios, full emission spectra were recorded at 420 nm excitation wavelength (porphyrin, Figure 5.44) and at 520 nm excitation wavelength (perylene, Figure 5.45). Here, the evolution and shift of the fluorescence can be monitored and compared. The emission intensity is normalized and scaled to fit the values presented in Figure 5.43. Using the aforementioned linear dilution regression, the emission intensities of dyad **2c** in pure THF can be extrapolated from the highly diluted 10 mL THF spectrum (red, dashed) and can therefore be displayed as an undiluted spectrum (red, dotted) at the correct intensity ratios. This spectrum can now be compared to pure, undiluted H_2O (purple, dashed).

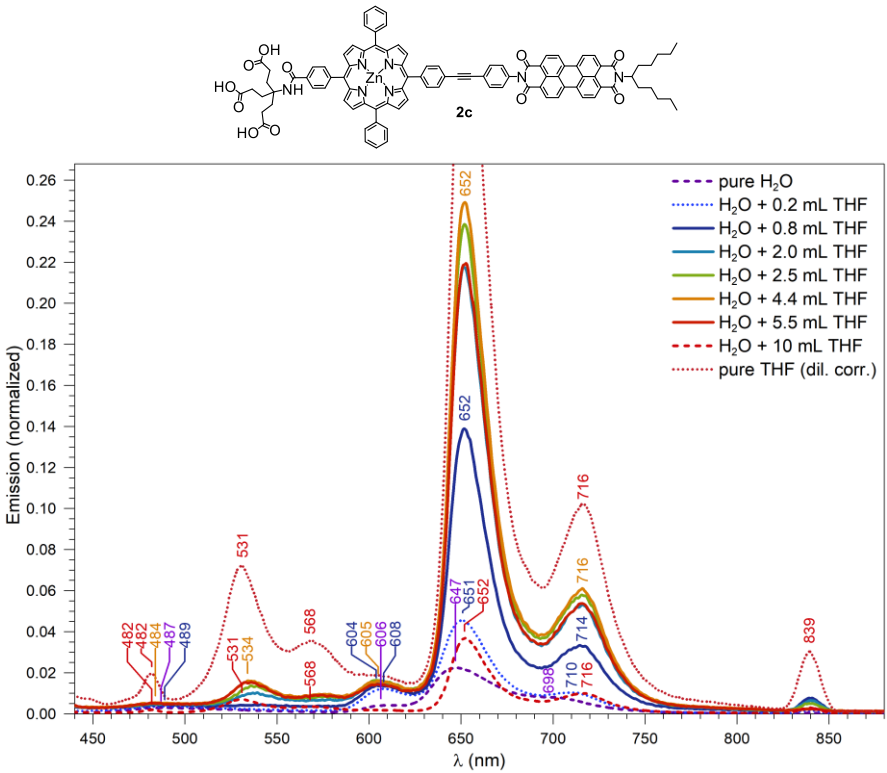

Figure 5.44. Selected emission spectra of dyad **2c** at different H_2O/THF solvent ratios at 420 nm excitation wavelength (porphyrin). The dashed purple line represents the spectrum in pure H_2O, the red dotted line is an extrapolation of the emission of **2c** in pure THF after factoring out the linear dilution regression. The emission intensities are scaled to fit the titration experiment in Figure 5.43.

At 420 nm excitation wavelength (porphyrin, Figure 5.44) in pure H_2O (*i.e.*, with a few drops of NaOH/pyridine), the perylene emission is not detectable and the porphyrin emission at 647 nm is extremely weak (purple, dashed). Upon addition of THF, the porphyrin Q band

fluorescence peaks start to grow (0.2 mL, blue, dotted) and shift slightly to longer wavelength (651 nm). Further addition of THF leads to the evolution of very weak perylene features at around 535 nm. As most of the spectra are not dilution corrected, a decrease in emission intensity can be found after addition of 4.4 mL THF (yellow). In contrast, a very intense porphyrin emission at 650 and 716 nm can be found (red, dotted) if the dilution effects for H_2O + 10 mL THF (red, dashed) are taken into account. Furthermore, the perylene emission at 531 and 568 nm is present but weak in comparison to the porphyrin fluorescence (Figure 5.44). This can be attributed to both the excitation exclusively at the porphyrin (420 nm) and the energy transfer from the perylene to the porphyrin, as explained before (chapter 5.7.5, p. 94ff).

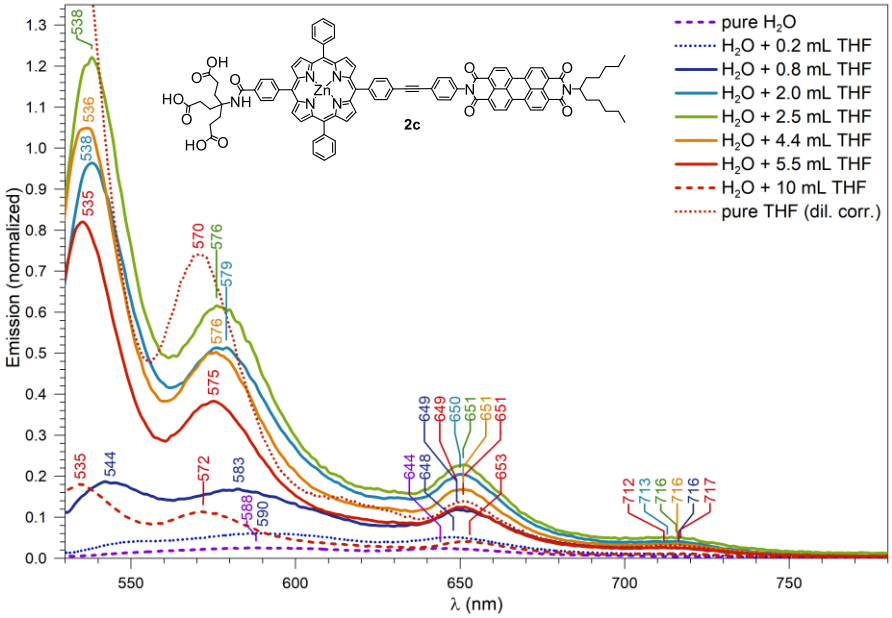

Figure 5.45. Selected emission spectra of dyad **2c** at different H_2O/THF solvent ratios at 520 nm excitation wavelength (perylene). The dashed purple line represents the spectrum in pure H_2O, the red dotted line is an extrapolation of the emission of **2c** in pure THF after factoring out the linear dilution regression. The emission intensities are scaled to fit the titration experiment in Figure 5.43.

Irradiation at 520 nm directly excites the perylene (Figure 5.45). In water, the dyad emission is completely quenched (purple, dashed). Addition of THF (blue) leads both to evolution of porphyrinic features (649 and 716 nm) and perylene fluorescence (544 and 583 nm).

Upon further addition of THF, the perylene emission increases strongly and shifts hypsochromatically (from 544/583 to 535/570 nm). The dilution for H_2O + 10 mL THF (red, dashed) was taken into account and again a dilution corrected spectrum in pure THF (red, dotted) was created. In comparison to porphyrin fluorescence (0.14 at 651 nm), the perylene features are tenfold more intense (1.4 at 535 nm). Naturally, the close-range excitation at 520 nm leads to increased perylene emission at 535 nm. Notwithstanding, the perylene fluorescence quantum yield in the dyad still is strongly quenched in comparison to isolated perylene ($\Phi \approx 1$). As exclusively the perylene was excited at this wavelength, the additional fluorescence of the porphyrin is a strong sign for energy transfer within the dyad. Moreover, it was shown for metalloporphyrin **2c** that the porphyrin excited state will only partially decay *via* fluorescence. The main decay pathway is the formation of a charge-separated $ZnPor^{+}$-PEP-Per^{-} state (*cf.* chapter 5.7.5, p. 94ff).

5.7.7 Stability and Equilibrium of Dyad 2a in Water

After longer measurements, it was found that the fluorescence intensity decreased. To investigate this phenomenon, a long-term experiment of dyad **2a** (de-metallated after NMR studies in TFA-*d*) in H_2O with a few drops of NaOH/pyridine was recorded. Over a period of 18 hours with alternating phases of steady irradiation at 420 nm and darkness, the porphyrin emission at 650 nm was monitored. After 18 h, the fluorescence at 650 nm was only 35% of the initial intensity. Interestingly, the absorption spectra (which had to be recorded at higher concentrations) did not show any change in intensity over several days.

The decrease in fluorescence intensity did not only occur upon irradiation, but also in darkness. Hence, this observed effect is clearly not due to photobleaching, and the dyad seems to be stable in solution. Another possibility would be a very slow equilibrium, *e.g.*, the movement of molecules and formation of larger particles in solution. The observed measurements could be fitted with a BOLTZMANN equation, which describes the statistical behavior of particles in a non-equilibrium system/fluid.

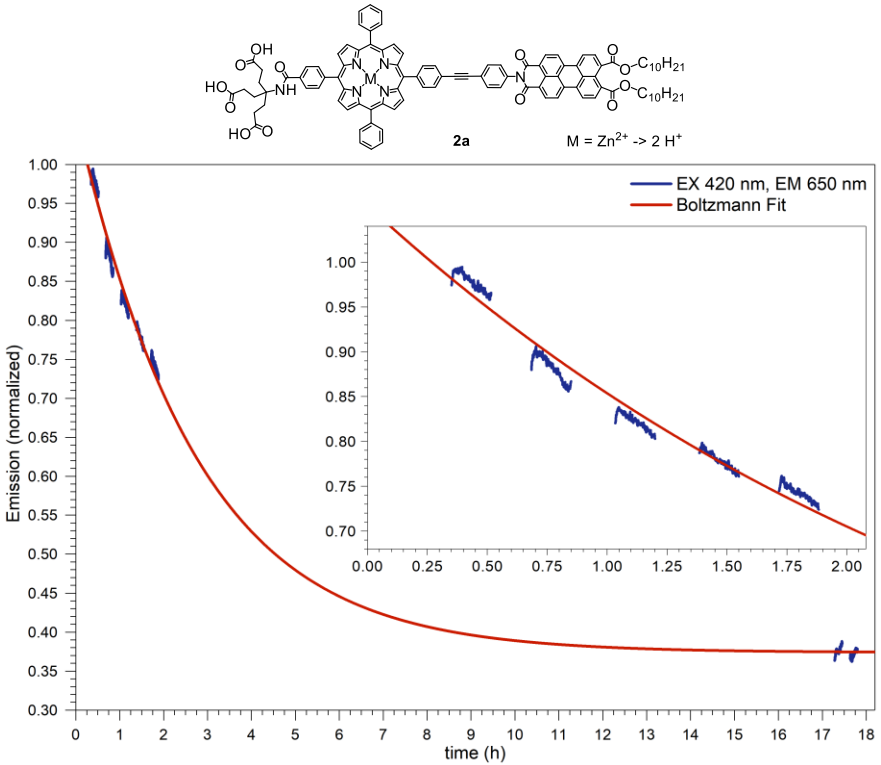

Figure 5.46. Long-term measurement of **2a** (de-metallated) at 420 nm excitation wavelength and 650 nm emission wavelength. The decrease in intensity occurs both upon irradiation and in the dark. The data can be fitted using a Boltzmann equation.

Probably, the amphiphilic dyad molecules aggregate dynamically. Diverse forms of lipid structures are imaginable, for example double layers, membranes, vesicles and micelles, and nanorods or nanotubular structures (see chapter "Self-Assembly of Water-Soluble Porphyrin-Perylene Systems", p. 21ff).[181-182,185,187-188,265] These supramolecular structures grow over time, which directly affects the fluorescence intensity. This hypothesis of self-aggregation over time has to be substantiated in further experiments – which are not part of this thesis – to determine additional data, such as particle size, hydrodynamic radii and charge distribution.

5.7.8 Three-Dimensional Excitation–Emission Spectra in Water

The excitation and emission characteristics for zinc porphyrin–PEP–PDI_S dyad **2c** and free-base porphyrin–PEP–$PIBE_{10}$ dyad **2d** were surveyed by 3D excitation–emission spectroscopy. The spectrum for dyad **2c** in H_2O/NaOH/pyridine is displayed in Figure 5.47, (*cf.* Figure 5.39, p. 109). The associated UV-Vis spectrum (blue) is inserted as an overlay. Significant emission spectra at excitation wavelengths of 420 (porphyrin, purple), 500 nm (perylene, orange) and 520 nm (perylene, red) are also depicted. Upon direct excitation at the perylene (500 and 520 nm), emission at 585 and 650 nm was detected. Although this emission is strong compared to the other emissions in this spectrum, it is weak compared to the usual fluorescence intensity for isolated and non-aggregated perylenes. Weak porphyrin emissions can be found at 610, 655 and 714 nm. For non-aggregated metalloporphyrins, emission at 614 and 658 is expected (*cf.* Table 5.12, p. 111). The emission at 655 nm with a weak additional emission at 714 nm is an indication of aggregated porphyrinic structures.[276,288] This should not be confused with the emission for non-metallated porphyrins, which are typically found at 652 and 715 nm in THF and at 601 (very weak), 647 and 701 nm in water (Figure 5.48).[290]

The observed fluorescence of the perylene moiety of dyad **2c** is extremely weak compared to the usual quantum yield of ~100% for the perylene. The fluorescence of the porphyrin sub-part is almost nonexistent. As explained before (p. 94ff), the excitation of the dyad **2c** does scarcely lead to immediate fluorescence. Instead, the energy is mostly transferred from the perylene to the porphyrin. Here, obviously a non-fluorescing energy quenching occurs, which proceeds either *via* the formation of a Por^+-PEP-Per^- charge-separated state or by intersystem crossing to a triplet state at the porphyrin.[15,277] Naturally, other quenching mechanisms with involvement of the polar solvent can be envisaged as well.

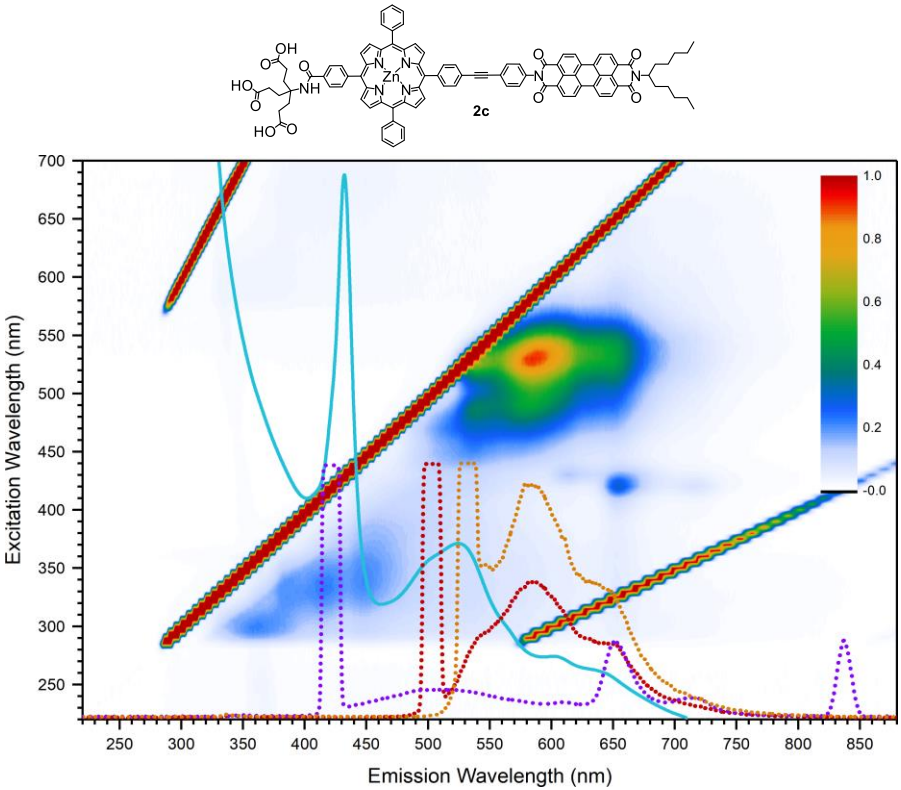

Figure 5.47. 3D excitation–emission spectrum of **2c** in H_2O+NaOH+pyridine. The overlays display the absorption spectrum (blue) as well as a selection of significant emission spectra at 420 nm (purple), 500 nm (red) and 530 nm (orange) excitation wavelength.

Comparing the findings for zinc-porphyrin dyad **2c** with the 3D excitation–emission spectrum of free-base dyad **2d** in H_2O (+NaOH/pyridine), the energy transfer from the excited perylene (500, 520 nm) to the porphyrin is even more pronounced (Figure 5.48). Upon excitation at the perylene (500 and 520 nm), the fluorescence is almost completely quenched and energy transfer to the porphyrin takes place in very high yield. As shown earlier, the free-base porphyrin in dyad **2d** is not capable of forming a stable H_2Por^+-PEP-Per^- charge-separated state (p. 95). It is energetically favored to revert to the H_2Por^*-PEP-Per excited state, which can decay to the ground state *via* typical routes expected for (isolated) porphyrins. Thus, excitation both at the porphyrin and the perylene leads to considerable porphyrin fluorescence at 647 and 701 nm (Figure 5.48).

Although the exhaustive investigation into the photophysical properties of the dyads **1a-d** and **2a-d** would exceed the limits of this synthesis-focused thesis, the results presented herein are strongly encouraging to further explore the properties and field of application for the synthesized amphiphilic, linear and water-soluble porphyrin–perylene dyads.

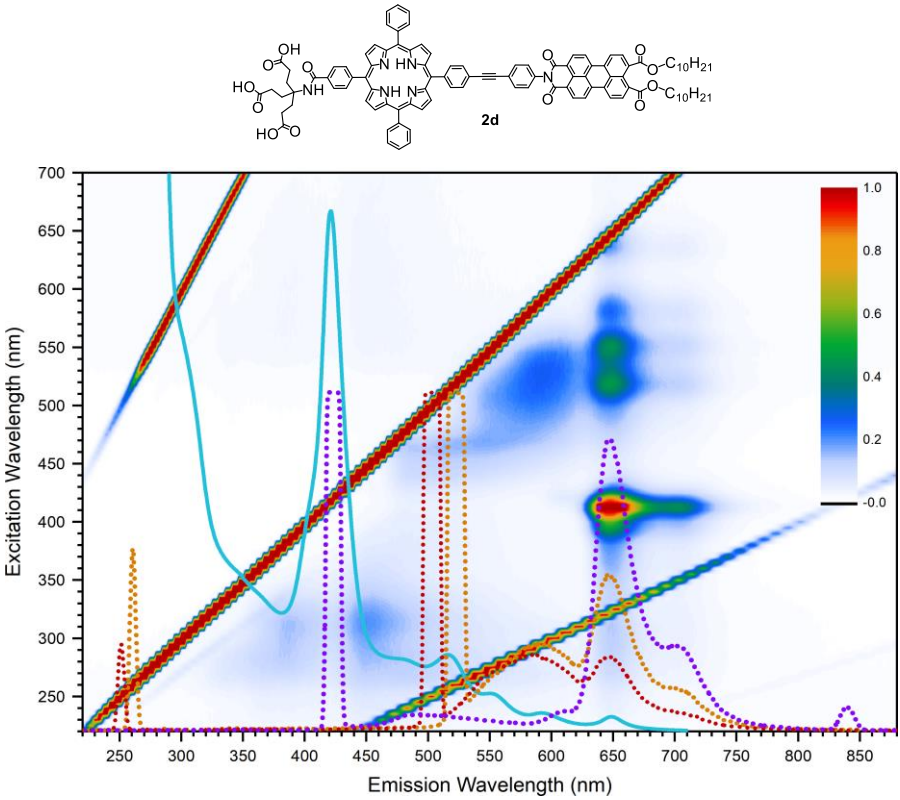

Figure 5.48. 3D excitation–emission spectrum of **2d** in H_2O+NaOH+pyridine. The overlays display the absorption spectrum (blue) as well as a selection of significant emission spectra at 420 nm (purple), 500 nm (red) and 520 nm (orange) excitation wavelength.

6 Conclusion and Outlook

Synthesis. In this dissertation, a synthesis procedure to a set of four water-soluble and amphiphilic dyads **2a-d** with two chromophores (porphyrin and perylene) was developed (Figure 6.1 top left). The proposed 18 – 21 step synthesis pathway was analyzed in terms of orthogonal protecting group strategies and under diligent consideration of the literature (p. 28f). The porphyrin precursors (**3-10**, p. 32ff) were synthesized and fully characterized.

Porphyrins **12/13** (p. 41ff) were obtained using the hardly literature-known multistep AB_2C porphyrin synthesis *via* a VILSMEIER-analogous reaction of a dipyrromethane **7** and a dicarbinol intermediate **11**. A deprotection reaction for the Boc protective group under solvent-free conditions without impairing other sensitive groups was tested and refined. By application of the reagent on silica gel and heating *in vacuo*, the Boc group of porphyrin **13** could be detached and the formation of undesired side products was prevented (p. 45ff).

Perylenes **14-17** were synthesized by optimizing a literature-known straightforward multistep reaction cascade. A novel purification strategy was developed to make complex perylene imides readily available. By utilizing suitable solvents and smart purification methods, a separation of the products can be achieved just by silica-gel filtration. Lyophilization renders the molecules manageable and prevents the formation of varnishes (p. 50ff).

The two chromophores were connected to porphyrin–perylene dyads **18-19** *via* a linear phenyl-ethynyl-phenyl spacer (p. 57ff). First and second generation NEWKOME dendrons **20-24** were synthesized (p. 63ff) and attached to dyads **19/b/c** by DCC coupling reactions (p. 66ff). Hydrolysis of the dyads **1a-d** resulted in water-soluble target molecules **2a-d** (p. 69ff).

Electronical properties and photophysical experiments. Until today, no water-soluble porphyrin–perylene dyads with a linear and rigid linker have been reported in literature. The synthesized dyads **1a-d** and **2a-d** were fully characterized by NMR, IR, UV-Vis and fluorescence spectroscopy (p. 74ff). It proved difficult to detect dyads carrying metallated porphyrins by MS (p. 77). The HOMO/LUMO energies of dyads **1a-d** were determined spectroscopically (p. 93f) and by calculation (p. 94ff). It was simulated that the HOMO orbitals (located at the porphyrin) and the LUMO orbitals (located at the perylene) of the dyads **2a-d** closely resemble the energies of the corresponding porphyrin/perylene precursors (Figure 6.1 bottom, p. 94ff). Additionally, the absorption spectra of the products **1a-d** matched the sum spectra of the porphyrin (**13**) and perylene (**15-17**) sub-components, which led to the conclusion that no ground-state interaction between the two chromophores takes place (p. 89). Instead, a strong fluorescence quenching of dyads **18c/1d** in comparison to pristine perylene **15** at 530 nm could be observed (p. 91). 3D excitation-emission spectroscopy of **1d** in THF (p. 94ff) and **2c/d** in water (p. 119ff) indicated an

excited-state energy transfer (Por-PEP-Per* → Por*-PEP-Per) and – in the case of metalloporphyrin dyads – the formation of a Por^{+}-PEP-Per^{-} charge-separated state. In the case of free-base porphyrin dyads **1d/2d**, the Por*-PEP-Per excited state returned to ground state by fluorescence at the porphyrin Q bands (p. 121). These observations were discussed in detail using energy calculations and a JABŁOŃSKI diagram (p. 99ff).

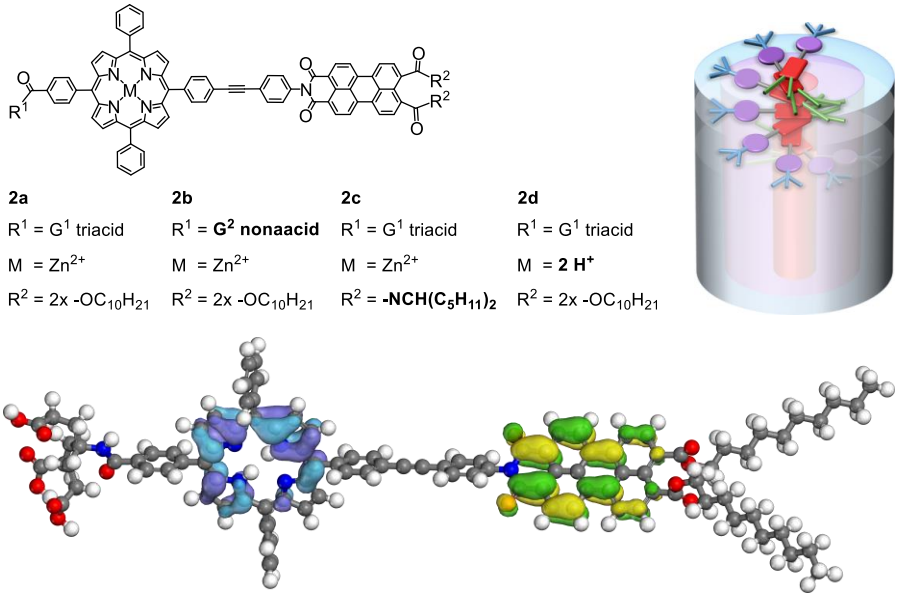

Figure 6.1. A set of water-soluble porphyrin–perylene dyads **2a-d** was synthesized and characterized (top left): The G^1 (**2a,c,d**) and G^2 (**2b**) Newkome dendrons render the dyads water-soluble at pH > 7. The zinc (**2a-c**) or free-base porphyrins (**2d**) exhibit distinct spectroscopic and chemical characteristics. Two linear decyl ester chains (**2a,b,d**) and a branched swallowtail chain (**2c**) were applied as hydrophobic tails. The absorption and fluorescence of the perylene chromophores are quenched in polar media while the characteristic porphyrin features are maintained. This could be a hint to helical columnar aggregation (right). The HOMO and LUMO orbitals and energies of porphyrin/perylene precursors and dyads **2a-d** were calculated and measured (bottom: semi-emp. GeomOpt NDDO PM6/UHF caclulated structure of dyad **2d** in gas phase).[156]

Solubility and aggregation studies. The dyads **1a-d** were well soluble in THF and marginally soluble in $CHCl_3$. The swallowtail alkyl chain of **1c/2c** slightly increased the solubility of the dyad in organic solvents. Upon hydrolysis of the NEWKOME dendrons, the dyads **2a-d** became water-soluble at alkaline pH (p. 102ff). For zinc porphyrin dyads **1c** and **2b** (in contrast to free-base porphyrin dyad **2d**), the addition of pyridine led to a bathochromic shift of the Soret band due to axial coordination of the amine ligand to the zinc center (p. 104f). UV-Vis and fluorescence spectra

of dyad **2c** showed peryleneic aggregation and quenching (p. 103ff), which could be an effect of a helical columnar aggregation pattern (Figure 6.1 top right). Titration experiments of dyad **2c** from water to THF showed the gradual increase of perylene and porphyrin fluorescence (p. 113ff). The dilution corrected comparison between perylene fluorescence in water and THF demonstrated the strong emission quenching due to solvation and aggregation effects in water (p. 115f). The time-dependent fluorescence quenching of **2a** over several hours suggested the steady growth of supramolecular assemblies (Figure 6.1 top right, p. 118ff).

Outlook. This synthesis-focused dissertation in organic chemistry did not allow for a deeper immersion into the field of physical chemistry. To understand the full capabilities of the dyads **1a-d** and **2a-d** synthesized herein, further experiments are necessary.

The stability issues of the imide bond of dyads **18/1d** have to be addressed and fixed (p. 60/67). The aggregation behavior and particle size should be investigated by dynamic light scattering and fluorescence correlation spectroscopy to provide insight into the structure of the supramolecular self-assemblies. A survey on amine ligands coordinating axially to the metalloporphyrin of the dyads will enable the fine-tuning of the self-assemblies and will help to broaden the scope and diversity of the aggregates. Using cyclic voltammetry, the results found in the literature for non-aggregated porphyrin–PEP–perylene dyads will be confirmed and unprecedented data for various aggregation forms in water will be collected.

The hypotheses in this dissertation concerning electron transfer and charge-separated states have to be substantiated by suitable measurements. Transient absorption spectroscopy as well as time-resolved fluorescence spectroscopy are essential to determine the fluorescence lifetimes in order to gain fundamental knowledge of the kinetic processes upon photoexcitation.

After these experiments, the next steps would be to explore the fields of application which these dyads provide. The use as an all-optical gating element or molecular switch is imaginable. Besides, it should be possible to incorporate suitable water-splitting catalysts into the self-aggregated lipid structure of the amphiphilic dyads. The dyads could prove great potential in photonics applications, where they could perform both as light-harvesting membranes and as molecular wire to combine charge-generation and -transport to power the catalyst.

Zusammenfassung und Ausblick

Synthese. Im Rahmen dieser Dissertation wurde eine Syntheseprozedur für vier wasserlösliche und amphiphile Dyaden **2a-d** mit zwei Chromophoren (Porphyrin und Perylen) entwickelt (Figure 6.2 oben links). Die 18 – 21 stufige Synthese unter Verwendung von orthogonalen Schutzgruppenstrategien wurde nach sorgfältiger Berücksichtigung der Literatur geplant und geprüft (S. 28f). Die Porphyrin-Vorstufen (**3-10**, S. 32ff) wurden synthetisiert und vollständig charakterisiert.

Die Porphyrine **12/13** (S. 41ff) wurden durch eine kaum literaturbekannte, mehrstufige AB_2C Porphyrinsynthese über eine VILSMEIER-analoge Reaktion aus einem Dipyrromethan **7** und einer Dicarbinol-Zwischenstufe **11** hergestellt. Eine Möglichkeit zur Abspaltung einer Boc-Schutzgruppe ohne Verwendung von Lösungsmitteln und ohne negative Auswirkungen auf weitere sensible Gruppen wurde getestet und verfeinert. Die Boc-Schutzgruppe des Porphyrins **13** konnte durch Auftragen auf Silikagel und Erhitzen im Vakuum abgespalten werden. Gleichzeitig wurde so die Bildung unerwünschter Nebenprodukte verhindert (S. 45ff).

Die Perylene **14-17** wurden durch die Optimierung einer literaturbekannten, mehrstufigen Reaktionskaskade synthetisiert. Eine neuartige Aufreinigungsstrategie wurde entwickelt, um komplexe Perylenimide leicht zugänglich zu machen. Durch die Verwendung von geeigneten Lösungsmitteln konnten die Reaktionsprodukte allein durch Filtrierung mit Silikagel aufgereinigt werden. Die Entstehung von schwer verarbeitbaren, lackartigen Perylen-Schichten konnte durch Gefriertrocknung verhindert werden (S. 50ff).

Die beiden Chromophore wurden zu den Porphyrin–Perylen-Dyaden **18-19** verbunden und über eine Phenyl-ethinyl-phenyl-Brücke linear verknüpft (S. 57ff). NEWKOME-Dendrone **20-24** der ersten und zweiten Generation wurden synthetisiert (S. 63ff) und durch DCC-Kopplungsreaktionen an die Dyaden **19/b/c** angefügt (S. 66ff). Durch Hydrolyse der Dyaden **1a-d** wurden die wasserlöslichen Zielmoleküle **2a-d** erhalten (S. 69ff).

Elektronische Eigenschaften und photophysikalische Experimente. Bis zu diesem Zeitpunkt gibt es keine Literaturhinweise auf wasserlösliche Porphyrin–Perylen-Dyaden, die durch eine lineare und starre Brücke verbunden sind. Die hier synthetisierten Dyaden **1a-d** und **2a-d** wurden mittels NMR, IR, UV-Vis und Fluoreszenzspektroskopie vollständig charakterisiert (S. 74ff). Es stellte sich heraus, dass Dyaden mit metallierten Porphyrinen schwer oder gar nicht durch MS detektierbar waren (S. 77). Die HOMO/LUMO-Energien der Dyaden **1a-d** wurden spektrophotometrisch bestimmt (S. 93f) und berechnet (S. 94ff). Simulationen zeigten, dass die HOMO-Orbitale (am Porphyrin) sowie die LUMO-Orbitale (am Perylen) der Dyaden **2a-d** den Orbitalenergien der jeweiligen Porphyrin/Perylen-Vorstufen stark ähnelten (Figure 6.2 unten,

S. 94ff). Die Absorptionsspektren der Produkte **1a-d** stimmten außerdem gut mit den Summenspektren der Porphyrin- (**13**) und Perylen-Untereinheiten überein (**15-17**). Dies führte zu der Schlussfolgerung, dass keine elektronische Interaktion der Chromophore im Grundzustand stattfindet (S. 89). Stattdessen konnte – im Vergleich zum reinen Perylen **15**– bei 530 nm eine starke Fluoreszenzauslöschung der Perylen-Untereinheiten in den Dyaden **18c/1d** beobachtet werden (S. 91). 3D-Anregungs/Emissions-Spektroskopie von **1d** in THF (S. 94ff) und **2c/d** in Wasser (S. 119ff) zeigte einen Energietransfer im angeregten Zustand (Por-PEP-Per* → Por*-PEP-Per) und – im Fall von Metalloporphyrin-Dyaden – die Bildung eines ladungsgetrennten Por^{+}-PEP-Per^{-} Zustands. Bei den unmetallierten Porphyrin-Dyaden **1d/2d** relaxierte der angeregte Por*-PEP-Per Zustand durch Fluoreszenz in den Q-Banden wieder in den Grundzustand (S. 121). Diese Beobachtungen wurden durch energetische Berechnungen gestützt und unter Verwendung eines JABŁOŃSKI-Diagramms ausführlich diskutiert (S. 99ff).

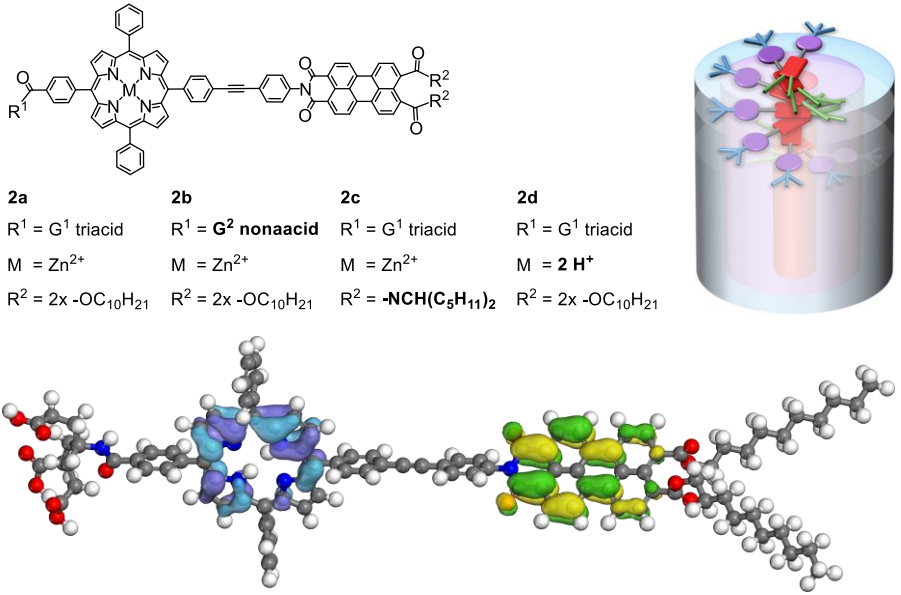

Figure 6.2. Eine Serie wasserlöslicher Porphyrin–Perylen-Dyaden **2a-d** wurde synthetisiert und charakterisiert (links oben): Durch die G^1 (**2a,c,d**) und G^2 (**2b**) Newkome-Dendronen werden die Dyaden wasserlöslich bei pH > 7. Die Zink- (**2a-c**) oder Freie-Base-Porphyrine (**2d**) besitzen spezifische spektroskopische und chemische Eingenschaften. Zwei lineare Decylester-Ketten (**2a,b,d**) bzw. eine verzweigte "Schwalbenschwanz"-Alkylkette (**2c**) wurden als hydrophobe Endgruppen eingesetzt. In polaren Lösungsmitteln werden Absorption und Fluoreszenz der Perylene-Farbstoffe gequencht während die charakteristischen Banden der Porphyrine größtenteils bestehen bleiben. Dies deutet z.B. auf helixartige säulenförmige Aggregate hin (rechts oben). Sowohl für die Porphyrin/Perylen-Vorstufen als auch für die Dyaden **2a-d** wurden die HOMO- und LUMO-Orbitale und -Energien berechnet und gemessen (unten: semi-empirisch mittels GeomOpt NDDO PM6/UHF berechnete Struktur der Dyade **2d** in der Gasphase).[156]

Studien zur Löslichkeit und Aggregation. Die Dyaden **1a-d** waren gut in THF und kaum in $CHCl_3$ löslich. Durch eine Schwalbenschwanz-Alkylkette in den Produkten **1c/2c** konnte die Löslichkeit in organischen Lösungsmitteln etwas verbessert werden. Nach Hydrolyse der NEWKOME-Dendrone wurden die Dyaden **2a-d** im basischen Milieu wasserlöslich (S. 102ff). Im Fall der Zink-Porphyrin-Dyaden **1c** und **2b** führte die Zugabe von Pyridin zu einer bathochromen Verschiebung der Soret-Bande durch axiale Koordinierung des Amin-Liganden an das Zink-Zentrum (S. 104f). Dies trat bei der Freie-Basen-Porphyrin-Dyade **2d** nicht auf. Die UV-Vis- und Fluoreszenzspektren der Dyade **2c** offenbarten Perylen-Aggregation und Fluoreszenzauslöschung (S. 103ff), was als Hinweis auf ein helikales, säulenförmiges Aggregationsmuster gewertet wurde (Figure 6.2 oben rechts). Titrationsexperimente mit der Dyade **2c** ausgehend von Wasser zu THF zeigten die schrittweise Zunahme der Fluoreszenz von Perylen und Porphyrin (S. 113ff). Durch den Vergleich von (verdünnungskorrigierten) Messungen in Wasser und THF konnte eine starke Emissionsauslöschung der Perylen-Chromophore in der Dyade **2c** festgestellt werden, welche durch Lösungs- und Aggregationseffekte in Wasser verursacht wurde (S. 115f). Das zeitaufgelöste Fluoreszenz-Quenching von Dyade **2a** über mehrere Stunden hinweg zeigte ein stetiges Wachstum von supramolekular angeordneten Partikeln (Figure 6.2 oben rechts, S. 118ff).

Ausblick. Diese Dissertation der organischen Chemie hat ihren Fokus auf der Synthese. Eine darüber hinausgehende tiefergreifende Untersuchung in dem Bereich der physikalischen Chemie hätte den Rahmen dieser Arbeit gesprengt. Um jedoch das volle Potential der hier synthetisierten Dyaden **1a-d** und **2a-d** zu verstehen sind weitere Experimente notwendig.

Die Stabilitätsprobleme der Imidbindung in den Dyaden **18/1d** müssen analysiert und behoben werden (S. 60/67). Das Aggregationsverhalten und die Partikelgröße sollten durch Dynamische Lichtstreuung und Fluoreszenz-Korrelations-Spektroskopie untersucht werden, um die Struktur der supramolekularen Aggregate aufzuklären. Eine Studie mit verschiedenen Aminliganden, welche axial an das Metalloporphyrin der Dyade koordinieren können, wird helfen die Selbstassemblierung in Wasser zu verstehen und zu beeinflussen. Dadurch wird die Herstellung einer großen und spezifischen Vielfalt von Aggregaten ermöglicht. Durch Cyclovoltammetrie können die literaturbekannten Ergebnisse für nicht-aggregierte Porphyrin-PEP-Perylen-Dyaden bestätigt werden. Darüber hinaus können bisher unbekannte Daten für unterschiedliche Aggregationsformen in Wasser gesammelt werden.

Die Hypothesen in dieser Dissertation bezüglich Elektronentransfer und ladungsgetrennte Zustände müssen durch geeignete zusätzliche Messungen weiter untermauert werden. Transiente-Absorptions-Spektroskopie und zeitaufgelöste Fluoreszenzspektroskopie sind essentiell wichtig um die Fluoreszenzlebensdauer und die Beschaffenheit der angeregten Zustände zu bestimmen. Dadurch können weitere fundamentale Einsichten über die kinetischen Prozesse bei Photoanregung in polaren Lösungsmitteln gewonnen werden.

Im Anschluss an diese Experimente können die Anwendungsmöglichkeiten dieser Dyaden erforscht werden. Die Verwendung als ein rein optisches elektronisches Gate oder als molekulare Schalter ist denkbar. Außerdem sollte es möglich sein, geeignete Katalysatoren zum Aufspalten von Wasser in die selbstaggregierten Lipidstrukturen der amphiphilen Dyaden einzubauen. Die Dyaden könnten ihr großes Potential in photonischen Anwendungen beweisen, wo sie gleichzeitig als lichtsammelnde Membran und als molekulare Leitung fungieren könnten. Dies würde sowohl die Erzeugung der Ladungen als auch den Ladungstransport zu den Katalysatoren in einer vielseitigen Molekülklasse vereinen.

7 Experimental Part

7.1 Chemicals and Instruments

Chemicals were purchased in reagent grade from Aldrich, Acros, Alfa Aesar or TCI Europe and used as received if not specified otherwise. Solvents such as dimethylformamide, tetrahydrofuran, toluene and $CHCl_3$ were acquired from VWR in HPLC grade. Other solvents were purified by distillation prior to use.

Thin Layer Chromatography. TLC analysis was performed on Silica gel 60 F_{254} TLC plates from Merck and visualized *via* UV light (254 nm / 365 nm) or standard coloring reagents.

Column Chromatography. Column chromatography was carried out using Silica Gel 60 (230-400 mesh, 0.04-0.063 mm) purchased from Merck or Macherey-Nagel. Flash Column Chromatography was performed with a Biotage Isolera One flash chromatograph. Gel permeation chromatography was carried out using Bio-Beads S-X1 from Bio-Rad with THF as solvent.

High Performance Liquid Chromatography. HPLC was conducted using following configuration: 2 pumps LC-8 A, Autoinjector SIL-10 A, BUS-Module CBM 10 A, UV-Detector SPD-10 A, fraction collector FRC-10A (Shimadzu Corporation, Analytical Instruments Division, Kyoto, Japan).

NMR Spectroscopy. ^{1}H NMR spectra and $^{13}C\{^{1}H\}$ NMR spectra were recorded at ambient temperature on JEOL JNM EX 400, JEOL JNM GX 400, BRUKER Avance 300 and BRUKER Avance 400 spectrometers. The chemical shifts are reported in parts per million (ppm) with reference to solvent residual peaks. Spectral splitting patterns are designated as singlet (s), doublet (d), triplet (t), quartet (q), quintet/pentet (p), multiplet (m) or as combinations thereof.

Infrared Spectroscopy. IR spectroscopy was performed on a Bruker FT-IR Tensor 27. The ATR unit was equipped with a diamond crystal plate. All absorptions are given in wave numbers (cm^{-1}).

UV-Vis Spectroscopy. UV-Vis absorption spectra were recorded with a Varian Cary 5000 UV-Vis-NIR Spectrometer in concentrations of 10^{-5} to 10^{-6} M with quartz cuvettes (path length: 1 cm) in the indicated solvents. The baseline was corrected before the measurements were taken. The absorption maxima λ_{max} are given in nm. Whenever possible, the molar exctinction coefficients ε in $L \cdot mol^{-1} \cdot cm^{-1}$ were determined by dilution series of a known concentration of compounds.

Fluorescence Spectroscopy. Fluorescence/emission and excitation spectra were measured using a RF-5301 PC Spectrofluorometer (Shimadzu Corporation, Analytical Instruments Division, Kyoto, Japan) with quartz cuvettes (path length: 1 cm) in the indicated solvent.

Mass Spectrometry. MALDI mass spectra were recorded with a Shimadzu AXIMA Confidence Spectrometer (nitrogen UV-laser, 50 Hz, 337 nm). EI spectroscopy was performed with a Finnigan MAT 95 XP. ESI mass spectrometry was carried out on a Bruker maXis 4G UHR TOF MS/MS-Spectrometer or a Bruker micrOTOF II focus TOF MS-Spectrometer. The used matrices are listed in the corresponding synthesis procedures.

Melting Point. MP were determined with an Electrothermal IA9100 melting point apparatus (Thermo Fisher Scientific).

7.2 Experimental Procedures

The bis(triphenylphosphine)palladium(II) dichloride (pre-)catalyst for SONOGASHIRA cross coupling reactions was ordered from Sigma-Aldrich or Acros in different qualities. However, the freshly self-prepared catalyst showed improved catalytic activity and yielded better results, which was confirmed not only in this thesis but also reproduced in different reactions in the bachelor's and master's laboratory course.

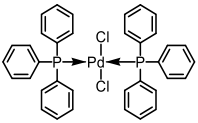

$Pd(PPh_3)_2Cl_2$ (CAS 13965-03-2).[292] To a solution of $PdCl_2$ (anhydrous, 5.07 g, 28.6 mmol) and LiCl (2.42 g, 57.1 mmol, 2 eq) in methanol (50 mL) was added PPh_3 (16.3 g, 62.1 mmol, 2.2 eq) and the mixture was heated to reflux for 18 h. After cooling, the yellow precipitate was filtered and washed with methanol (15 mL) to yield $Pd(PPh_3)_2Cl_2$ (19.28 g, 27.47 mmol, 96%) as yellow powder. The catalyst can be stored in air and at room temperature.

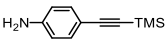

3

4-(TMS-ethynyl)aniline (3, CAS 75867-39-9).[204] In a 500 mL round bottom flask under Ar atmosphere was added 4-iodoaniline (40.00 g, 182.6 mmol), $Pd(PPh_3)_2Cl_2$ (1.00 g, 1.42 mmol, 0.77 mol-%), CuI (0.50 g, 2.6 mmol, 1.42 mol-%), NEt_3 (degassed, 200 mL), and THF (extra dry, 100 mL). TMS acetylene (30.0 g, 43.2 mL, 439 mmol, 2.40 eq) was added dropwise over 30 min. The black reaction mixture was stirred under Ar atmosphere for 21 h, passed through a plug of silica gel (eluent: ethyl acetate) and purified *via* Kugelrohr distillation at $1.2 \cdot 10^{-2}$ mbar and 280°C to yield 4-(TMS-ethynyl)aniline **3** (27.33 g, 144.4 mmol, 79%) as beige powder.

^{1}H NMR (300 MHz, $CDCl_3$): δ = 7.30 (d, *J* = 8.5 Hz, 2H, o_{amine}-Ph-*H*), 6.59 (d, *J* = 8.6 Hz, 2H, o_{amine}-Ph-*H*), 3.82 (s, 2H, amine-*H*), 0.25 (s, 9H, TMS-*H*) ppm; **^{13}C NMR** (101 MHz, $CDCl_3$): δ = 147.02 (i_{amino}-Ph-***C***), 133.56 (m_{amino}-Ph-***C***), 114.69 (o_{amino}-Ph-***C***), 112.59 (p_{amino}-Ph-***C***), 106.19 ($\boldsymbol{C}_{acetylene\text{-}phenyl}$), 91.52 ($\boldsymbol{C}_{acetylene\text{-}TMS}$), 0.17 (-***C***$H_3$) ppm; **FT-IR:** ṽ (int.) = 3464 (s), 3370 (s), 2959 (m), 2899 (w), 2146 (s), 1620 (s), 1601 (s), 1509 (s), 1409 (w), 1294 (s), 1250 (s), 1177 (m), 1129 (m), 828 (s) 756 (s), 700 (m), 632 (m) cm^{-1}; **MP**: 96.0 °C.

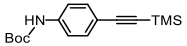

4

N*-(*tert*-Butoxycarbonyl)-4-(TMS-ethynyl)aniline (4, CAS 317842-68-5).** In a 250 mL round bottom flask was added 4-(TMS-ethynyl)aniline **3** (10.0 g, 52.8 mmol) in THF (50 mL) and Boc_2O (24.27 mL, 23.06 g, 105.6 mmol, 2 eq). The reaction mixture was stirred for 4 d at 50 °C. The solvents were removed *in vacuo* and the crude yellow product was recrystallized in ethyl acetate to yield N-Boc-4-(TMS-ethynyl)aniline **4** (13.03 g, 45.06 mmol, 85.3%) as yellow crystals. **^{1}H NMR** (400 MHz, $CDCl_3$): δ 7.94 – 7.86 (m, 2H, $o_{ethynyl}$-Ph-*H*), 7.83 (d, *J* = 8.6 Hz, 2H, o_{amide}-Ph-*H*), 2.04 (s, 1H, N-*H*), 2.02 (s, 9H, Boc-*H*), 0.76 (s, 9H, TMS-*H*) ppm; **^{13}C NMR** (101 MHz, $CDCl_3$): δ = 152.53 ($\boldsymbol{C}_{carbonyl}$), 138.78 ($i_{Boc}$-Ph-C***), 132.87 ($m_{Boc}$-Ph-***C***), 117.94 (br, o_{Boc}-Ph-***C***), 117.39 (p_{Boc}-Ph-***C***), 105.22 ($\boldsymbol{C}_{acetylene\text{-}(phenyl\text{-}Boc)}$), 93.16 ($\boldsymbol{C}_{acetylene\text{-}TMS}$), 80.88 ($\boldsymbol{C}_{Boc}$), 28.38 (*t*-butyl-$\boldsymbol{C}_{Boc}$), 0.11 (-TMS-***C***) ppm; **FT-IR:** ṽ (int.) = 3325 (m), 2981 (m), 2959 (m), 2935 (m), 2159 (m), 1695 (s), 1586 (m), 1519 (s), 1407 (m), 1369 (m), 1315 (s), 1238 (s), 1154 (s), 1115 (w),1058 (m), 869 (s), 836 (s), 757 (m), 739 (m), 695 (m), 636 (m) cm^{-1}; **MS (APPI)**: m/z for $C_{16}H_{23}NO_2Si$ $[M]^+$ calcd: 289.1498, found: 289.1497 (err: -1.4 ppm), 189.0974 (fragment 4-(TMS-ethynyl)aniline), 218.0636 (fragment [M – *t*-butyl]); **MP:** 160.4 °C.

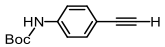

5

***N*-(*tert*-Butoxycarbonyl)-4-ethynylaniline (5, CAS 317842-48-1).**

From *N*-Boc-4-(TMS-ethynyl)aniline 4: In a 100 mL round bottom flask, N-Boc-4-(TMS-ethynyl)aniline **4** (1.00 g, 3.46 mmol) was dissolved in a THF/methanol mixture (30 mL, 2:1). K_2CO_3 (finely powdered, 10 g) and water (1.0 mL) were added and the reaction was stirred for 30 min. The solvents were removed and the crude brownish product was dissolved in water

(100 mL) and ethyl acetate (100 mL). The phases were separated, the organic phase was washed with water (2x 100 mL), dried over $MgSO_4$, passed through a plug of silica gel (eluent: ethyl acetate) and the solvent was removed *in vacuo*. The crude yellow oil was purified by column chromatography (eluent: hexanes/ethyl acetate 3:1) to yield N-Boc-4-ethynylaniline **5** (750 mg, 3.45 mmol, 99.8%) as beige powder.

Two-step one-pot reaction from 4-(TMS-ethynyl)aniline 3: In a 100 mL round bottom flask was added 4-(TMS-ethynyl)aniline **3** (5.00 g, 26.4 mmol) in PEG-400 (20 mL), THF (30 mL) and Boc_2O (8.25 mL, 7.84 g, 35.9 mmol, 1.36 eq). Additionally, K_2CO_3 (finely powdered, 10 g), water (10 mL), MeOH (10 mL) and TBAB (200 mg) were added and the reaction was stirred for 2.5 h. The solvents were removed *in vacuo*. The crude brownish viscous oil was suspended in water (300 mL), extracted with ethyl acetate (8x 50 mL) and purified by column chromatography (eluent: hexanes/ethyl acetate 3:1) to yield N-Boc-4-ethynylaniline **5** (4.00 g, 18.4 mmol, , 69.7%) as beige-colored powder.

^{1}H NMR (400 MHz, $CDCl_3$): δ = 8.04 – 7.95 (m, 2H, $o_{ethynyl}$-Ph-*H*), 7.96 – 7.88 (m, 2H, o_{amide}-Ph-*H*), 3.61 (s, 1H, acetylene-*H*), 2.10 (s, 9H, *t*-butyl-*H*) ppm; **^{13}C NMR** (101 MHz, $CDCl_3$): δ = 152.53 (***C***$_{carbonyl}$), 139.04 (i_{Boc}-Ph-***C***), 133.05 (m_{Boc}-Ph-***C***), 118.10 (br, o_{Boc}-Ph-***C***), 116.37 (p_{Boc}-Ph-***C***), 83.69 (***C***$_{acetylene-(phenyl-Boc)}$), 81.02 (***C***$_{Boc}$), 76.46 (***C***$_{acetylene-H}$), 28.40 (*t*-butyl-***C***$_{Boc}$) ppm; **FT-IR:** $\tilde{\nu}$ (int.) = 3384 (m), 3294 (m), 3010 (w), 2985 (m), 2938 (w), 2871 (w), 2106 (w), 1705 (s), 1609 (m), 1583 (s), 1518 (s), 1500 (s), 1459 (m), 1407 (s), 1390 (w), 1363 (m), 1315 (s), 1265 (w), 1229 (s) 1152 (s) 1113 (m), 1055 (s), 1019 (m), 902 (w) 834 (s), 773 (m), 761 (m), 704 (w), 636 (m) cm^{-1}; **MP:** 96.8 °C.

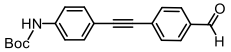

6

4-((4-(*N*-(*tert*-Butoxycarbonyl)amino)phenyl)ethynyl)benzaldehyde (6). In a 250 mL round bottom flask under argon atmosphere was added N-(*tert*-butoxycarbonyl)-4-(ethynyl)aniline **5** (3.80 g, 17.5 mmol), 4-bromobenzaldehyde (3.55 g, 19.2 mmol), $Pd(PPh_3)_2Cl_2$ (250 mg, 0.35 mmol, 2 mol-%), CuI (130 mg, 0.70 mmol, 4 mol-%), THF (extra dry, 75 mL), and NEt_3 (degassed, 25 mL). The reaction was stirred at 80 °C for 4 d. The reaction mixture was passed through a plug of silica gel (eluent: THF) and recrystallized in ethyl acetate. The residue was filtered and washed with hexanes to yield **6** (5.05 g, 15.70 mmol, 89.8%) as yellow crystals. **^{1}H NMR** (400 MHz, $CDCl_3$): δ = 10.01 (s, 1H, aldehyde-*H*), 7.92 – 7.82 (m, 2H, o_{amide}-

Ph-*H*), 7.70 – 7.61 (m, 2H, m_{amide}-Ph-*H*), 7.52 – 7.45 (m, 2H, $o_{aldehyde}$-Ph-*H*), 7.42 – 7.36 (m, 2H, $m_{aldehyde}$-Ph-*H*), 6.56 (s, 1H, N*H*), 1.53 (s, 9H, *t*-butyl-*H*) ppm; **^{13}C NMR** (101 MHz, $CDCl_3$): δ = 191.61 (***C***$_{aldehyde}$), 152.48 (***C***$_{ester}$), 139.29 (i_{Boc}-Ph-***C***), 135.33 ($i_{aldehyde}$-Ph-***C***), 132.86 ($m_{aldehyde}$-Ph-***C***), 132.08 (m_{Boc}-Ph-***C***), 130.03 ($p_{aldehyde}$-Ph-***C***), 129.73 ($o_{aldehyde}$-Ph-***C***), 118.21 (br, o_{Boc}-Ph-***C***), 116.76 (p_{Boc}-Ph-***C***), 93.79 (***C***$_{acetylene\text{-}(phenyl\text{-}Boc)}$), 88.06 (***C***$_{acetylene\text{-}(phenyl\text{-}aldehyde)}$), 81.19 (***C***$_{Boc}$), 28.44 ppm (*t*-butyl-***C***$_{Boc}$); **FT-IR:** $\tilde{\nu}$ (int.) = 3365 (m), 2992 (w), 2940 (w), 2863 (w), 2758 (w), 2211 (m), 1722 (s), 1685 (s), 1595 (s), 1579 (s), 1562 (m), 1520 (s), 1459 (w), 1407 (m), 1369 (m), 1312 (s), 1294 (m), 1261 (w), 1228 (s), 1206 (m), 1170 (m), 1150 (s), 1106 (w), 1053 (s), 1027 (m), 896 (m), 821 (s), 774 (m), 748 (w), 678 (m) cm^{-1}; **MS (APPI)**: m/z for $C_{20}H_{19}NO_3$ $[M]^+$ calcd: 321.1365, found: 321.1365, 221.0838 (fragment 4-((4-aminophenyl)ethynyl)-benzaldehyde); **MP:** 196.0 °C (decomp.).

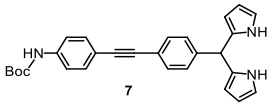

7

5-(4-((4-(*N*-(*tert*-Butoxycarbonyl)amino)phenyl)ethynyl)phenyl)dipyrromethane (7). In a 250 mL round bottom flask under N_2 atmosphere was added Boc-PEP-aldehyde **6** (7.95 g, 24.7 mmol), freshly distilled pyrrole (120 mL, 124 g, 1.85 mol, 75 eq) and THF (extra dry, 60 mL). The solution was degassed by a N_2 stream for 10 minutes under exclusion of light. $BF_3{\cdot}Et_2O$ (0.60 mL, 0.52 g, 3.68 mmol, 0.15 eq) was added and the reaction mixture was stirred for further 10 min under light exclusion while monitoring the reaction progress by TLC analysis (hexanes/ethanol 5:1, stain: $Br_{2(g)}$). After addition of NaOH (0.1 M, 200 mL) and ethyl acetate (200 mL), the organic phase was separated, the aqueous phase was washed with ethyl acetate (2x 200 mL), and the organic phases were combined and dried over $MgSO_4$. The solvent was removed *in vacuo* and the resulting yellow solid was passed through a plug of silica gel (eluent: hexanes/ethanol 5:1). Crystallization from ethanol yielded pure **7** (3.632 g, 8.301 mmol, 33.6%) as slightly yellowish solid. Further product (4.908 g, 11.22 mmol, 45.3%) was obtained by column chromatography (eluent: hexanes/ethanol 5:1). The product **7** (overall yield: 8.540 g, 19.52 mmol, 78.9%) can be stored at -10 °C under N_2 atmosphere and light exclusion.

^{1}H NMR (400 MHz, $CDCl_3$): δ = 7.96 (br-s, 2H, pyrrole-N*H*), 7.52 – 7.41 (m, 4H, $o_{ethynyl}$-Ph-*H*), 7.35 (d, *J*=8.7, 2H, o_{amide}-Ph-*H*), 7.18 (d, *J*=8.1, 2H, o_{DPM}-Ph-*H*), 6.74 – 6.66 (m, 2H, -NHC*H*-), 6.57 (s, 1H, amide-N*H*), 6.17 (ddd, *J*=2.9, 2.8, 2.8 Hz, 2H, -NHCHC*H*-), 5.95 – 5.88 (m, 2H, -NHCC*H*-), 5.47 (s, 1H, -C*H*-(pyrrole)$_2$), 1.54 (s, 9H, *t*-butyl-*H*) ppm; **^{13}C NMR** (101 MHz, $CDCl_3$): δ = 152.54 (***C***$_{carbonyl}$), 142.24 (i_{DPM}-Ph-***C***), 138.58 (i_{Boc}-Ph-***C***), 132.59 (m_{DPM}-Ph-***C***), 132.15 (pyrrole-NH-***C***$_{quart}$), 131.88 (m_{Boc}-Ph-***C***), 128.56 (o_{DPM}-Ph-***C***), 122.26 (p_{DPM}-

Ph-***C***), 118.21 (br, o_{Boc}-Ph-***C***), 117.65 (p_{Boc}-Ph-***C***), 117.53 (pyrrole-NH***C***H-), 108.64 (pyrrole-NHC***C***H-), 107.51 (pyrrole-NHCH***C***H-), 89.53 (***C***$_{acetylene\text{-}(phenyl\text{-}Boc)}$), 88.52 (***C***$_{acetylene\text{-}(phenyl\text{-}DPM)}$), 81.06 (***C***$_{Boc}$), 43.99 (-***C***H-(pyrrole)$_2$), 28.46 (*t*-butyl-***C***$_{Boc}$) ppm; **FT-IR:** $\tilde{\nu}$ (int.) = 3346 (br), 3100 (w), 2977 (m), 2932 (w), 2875 (w), 1700 (s), 1583 (m), 1520 (s), 1407 (m), 1367 (m), 1310 (m), 1227 (m), 1151 (s), 1093 (w), 1051 (s), 1027 (s), 971 (w), 899 (w), 885 (w), 835 (s), 767 (s), 714 (s) cm^{-1}; **MS (APPI)**: m/z for $C_{28}H_{27}N_3O_2$ $[M]^+$ calcd: 437.2098, found: 437.2101 (err: -0.8 ppm); **MP:** 193.9 °C (decomp.).

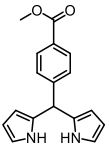

8

5-(4-Methoxycarbonylphenyl)dipyrromethane (8, CAS 167482-99-7).[39] In a 250 mL round bottom flask under N_2 atmosphere was added methyl 4-formylbenzoate (3.50 g, 21.3 mmol) and freshly distilled pyrrole (80.0 mL, 77.6 g, 1.16 mol, 55 eq). The solution was degassed by a N_2 stream for 10 minutes under exclusion of light. BF_3·Et_2O (0.50 mL, 0.56 g, 4.0 mmol, 0.2 eq) was added and the reaction mixture was stirred for further 10 min under light exclusion while monitoring the reaction progress by TLC analysis (CH_2Cl_2/ethyl acetate 19:1, stain: $Br_{2(g)}$). After addition of NaOH (0.1 M, 60 mL) and CH_2Cl_2 (60 mL), the organic phase was separated, the aqueous phase was washed with CH_2Cl_2 (2x 60 mL), and the organic phases were combined and dried over $MgSO_4$. The solvent was removed *in vacuo* and the resulting yellow solid was further purified by column chromatography (SiO_2, eluent: CH_2Cl_2/ethyl acetate 19:1 + 0.2% NEt_3) to yield **8** (5.27 g, 18.8 mmol, 88.3%) as a colorless solid which can be stored at -10 °C under N_2 atmosphere and light exclusion.

^{1}H NMR (300 MHz, $CDCl_3$): δ = 8.48 – 7.48 (m, 4H, -N*H*, $o_{carbonyl}$-Ph-*H*), 7.29 (d, *J* = 8.5 Hz, 2H, $m_{carbonyl}$-Ph-*H*), 6.72 (dd, *J* = 4.1, 2.6 Hz, 2H, -NHC*H*-), 6.17 (dd, *J* = 5.8, 2.8 Hz, 2H, -NHCHC*H*-), 5.89 (s, 2H, -NHCC*H*-), 5.53 (s, 1H, -C*H*-(pyrrole)$_2$), 3.91 (s, 3H, -CH_3) ppm; **^{13}C NMR** (75 MHz, $CDCl_3$, 25°C): δ = 167.06 (***C***$_{ester}$), 147.47 (p_{ester}-Ph-***C***), 131.74 (-NH-***C***$_{quart}$), 130.06 (o_{ester}-Ph-***C***), 128.99 (i_{ester}-Ph-***C***), 128.57 (m_{ester}-Ph-***C***), 117.71 (-NH***C***H-), 108.70 (-NHC***C***H-), 107.65 (-NHCH***C***H-), 52.26 (-***C***H_3), 44.09 (-***C***H-(pyrrole)$_2$) ppm; **FT-IR:** $\tilde{\nu}$ (int.) = 3333 (s), 3133 (w), 3099 (w), 3088 (w), 2952 (w), 1701 (s), 1605 (m), 1433 (s), 1418 (m), 1317 (m), 1290 (s), 1259 (m), 1196 (m), 1181 (m), 1114 (s), 1100 (s), 1030 (s), 960 (m), 866 (m), 819 (m), 801 (m), 783 (m) 727 (s), 703 (s) cm^{-1}; **MS** (ESI): m/z for $C_{17}H_{15}N_2O_2$ $[M\text{-}H]^-$ calcd: 279.11390, found: 279.11456 (err: -2.4 ppm); **MP:** 165.7 °C; **R$_f$** (CH_2Cl_2/ethyl acetate 19:1): 0.55.

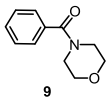

9

4-Benzoylmorpholine (9, CAS 1468-28-6).[217] In a 500 mL flask, benzoyl chloride (10.0 g, 71.1 mmol) in CH_2Cl_2 (50 mL) was placed. Morpholine (6.82 mL, 6.82 g, 78.3 mmol, 1.1 eq) in CH_2Cl_2 (50 mL) and NEt_3 (12 mL) under nitrogen atmosphere were added dropwise at 0 °C and stirred until formation of $HCl_{(g)}$ stopped. The reaction mixture was stirred at room temperature for 2 h and water (100 mL) was added. The organic phase was separated, washed with water (2x 100 mL), dried over $MgSO_4$ and filtered through a plug of silica gel (eluent: ethanol). The solvent was removed *in vacuo* and the resulting yellowish oil was dissolved in methanol (30 mL) and lyophilized to yield 4-benzoylmorpholine **9** (13.43 g, 70.20 mmol, 98.7%) as a fine white powder. The morpholine signals in ^{1}H and ^{13}C-NMR spectroscopy are diffuse, *i.e.,* very broad or not visible at all. **^{1}H NMR** (300 MHz, $CDCl_3$): δ = 7.44 – 7.36 (m, 5H, Ph-*H*), 3.90 – 3.33 (m, 8H, morpholine-*H*) ppm; **^{13}C NMR** (101 MHz, $CDCl_3$): δ = 170.54 (**C**$_{carbonyl}$), 135.46 (*i*-Ph-**C**), 129.98 (*p*-Ph-**C**), 128.68 (*m*-Ph-**C**), 127.20 (*o*-Ph-**C**), 67.02 (NC**C**O) ppm; **FT-IR:** $\tilde{\nu}$ (int.) = 3008 (w), 2978 (m), 2913 (m), 2985 (m), 2859 (s), 1624 (s), 1600 (m), 1577 (m), 1492 (w), 1450 (m), 1424 (s), 1361 (m), 1298 (m), 1271 (s), 1253 (s), 1148 (m), 1110 (s), 1064 (m), 1019 (s), 973 (w), 933 (m), 890 (w), 839 (m), 796 (s), 734 (s), 710 (s), 647 (m) cm^{-1}; **MS** (ESI+): m/z for $C_{11}H_{14}N_5O_2$ $[M+H]^+$ calcd: 192.1019, found: 192.1021 (err: -2.0 ppm); **MP**: 75.4 °C (Lit: 69-70 °C).[217]

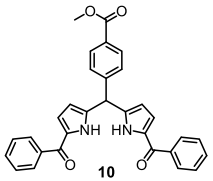

10

Bis(1,1'-benzoyl)-5-(4-methoxycarbonylphenyl)dipyrromethane (10). In a 500 mL flask under nitrogen atmosphere, 4-benzoylmorpholine **9** (6.73 g, 35.2 mmol, 4.3 eq) and $POCl_3$ (6.10 g, 39.8 mmol, 4.9 eq) were stirred at 65 °C for 3 h. 5-(4-Methoxycarbonylphenyl)dipyrromethane **8** (2.29 g, 8.17 mmol) in CH_2Cl_2 (dry, 50 mL) was added and the solution was stirred at 40 °C for 2 h. The reaction was quenched carefully with NaOAc (aq. satd., 100 mL) and stirred overnight at rt. Water (160 mL) and CH_2Cl_2 (160 mL) was added, the phases were separated. The aqueous phase was extracted with CH_2Cl_2 (2x 50 mL) and the combined organic phases were

washed with water (50 mL), brine (50 mL), dried over $MgSO_4$ and the solvent was removed *in vacuo*. The crude product was purified *via* column chromatographies (SiO_2, eluent: hexanes/ethyl acetate 1:1 + 1% NEt_3 and hexanes/ethyl acetate 3:1 + 1% NEt_3) and recrystallization from ethyl acetate. The product **10** was obtained either slightly impure as red viscous oil (fraction 1, 413 mg, 845 µmol, 10.3%) or pure as a light brown powder (2.72 g, 5.57 mmol, 68.1%, overall yield: 78.4%).

^{1}H NMR (400 MHz, $CDCl_3$): δ = 12.04 (s, 2H, -N*H*), 8.09 – 8.01 (m, 2H, o_{ester}-Ph-*H*), 7.77 – 7.71 (m, 4H, *o*-Ph-*H*), 7.71 – 7.63 (m, 2H, m_{ester}-Ph-*H*), 7.54 – 7.45 (m, 2H, *p*-Ph-*H*), 7.44 – 7.33 (m, 4H, *m*-Ph-*H*), 6.53 (dd, *J* = 3.9, 2.3 Hz, 2H, -NHC$_{\alpha\text{-carbonyl}}$C*H*-), 5.95 (dd, *J* = 3.9, 2.4 Hz, 2H, -NHC$_{\alpha\text{-carbonyl}}$CHC*H*-),), 5.81 (s, 1H, -C*H*-(pyrrole)$_2$), 3.93 (s, 3H, -CH_3) ppm; **^{13}C NMR** (75 MHz, $CDCl_3$): δ = 184.74 (***C***$_{ketone}$), 167.00 (***C***$_{ester}$), 145.68 (p_{ester}-Ph-***C***), 140.48 (-NH-***C***$_{quart\text{-}methylene}$), 138.13 ($i_{ketone}$-Ph-***C***), 131.85 ($p_{ketone}$-Ph-***C***), 131.25 (-NH-***C***$_{quart\text{-}ketone}$), 130.26 (o_{ester}-Ph-***C***), 129.79 (o_{ketone}-Ph-***C***), 129.38 (i_{ester}-Ph-***C***), 129.09 (m_{ester}-Ph-***C***), 128.11 (m_{ketone}-Ph-***C***), 121.10 (-NHC$_{quart\text{-}ketone}$***C***H-), 111.50 (-NHC$_{quart\text{-}methylene}$***C***H-), 52.27 (-***C***H$_3$), 45.11 (-***C***H-(pyrrole)$_2$) ppm; **FT-IR:** $\tilde{\nu}$ (int.) = 3229 (br), 3103 (w), 2949 (w), 1719 (s), 1597 (s), 1570 (s), 1474 (s), 1400 (s), 1337 (m), 1276 (s), 1253 (s), 1238 (s), 1218 (m), 1176 (m), 1108 (s), 1074 (w), 1049 (m), 1015 (m), 881 (s), 784 (m), 744 (m), 721 (s), 695 (s), 675 (s) cm^{-1}; **UV-Vis** (THF): λ_{max} (ε in L·mol^{-1}cm^{-1}) = 318 (43 000), 238 (34 000) nm; **MS** (APPI): m/z for $C_{31}H_{24}N_2O_4$ $[M]^+$ calcd: 488.173059, found: 488.173064 (err: -0.011 ppm); **MP:** 107.9 °C.

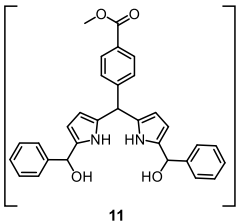

11

Bis(1,1'-(hydroxy(phenyl)methyl))-5-(4-methoxycarbonylphenyl)dipyrromethane (11). In a 250 mL flask, bis(1,1'-benzoyl)-5-(4-methoxycarbonylphenyl)dipyrromethane **10** (1.397 g, 2.860 mmol) was dissolved in a mixture of THF/methanol (10:1, dry, 30 mL). $NaBH_4$ (240 mg, 6.34 mmol, 2.2 eq) was added portion-wise and the solution was stirred for 2 h under light exclusion. The reaction was quenched by addition of NH_4Cl (aq. satd., 100 mL) and CH_2Cl_2 (100 mL). The phases were separated, the aqueous phase was washed with CH_2Cl_2 (2x 25 mL) and the combined organic phases were dried over $MgSO_4$ and the solvent was quickly removed *in vacuo*. The crude brown product **11** (1.5287 g, 3.1035 mmol, containing residual solvent) is unstable and was directly used in the next reaction without further purification or characterization.

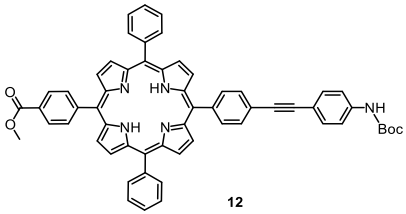

12

5-(4-Methoxycarbonylphenyl)-15-((4-(4-(*N*-(*tert*-butoxycarbonyl)amino)-phenyl)ethynyl)phenyl)-10,20-diphenylporphyrin (12). In a 1 L round-bottom flask under nitrogen atmosphere, acetonitrile (250 mL), DMF (1.5 mL) and TFA (1.5 mL) were placed at 0 °C. A mixture of crude dicarbinol **11** (theor. 1.409 g, 2.860 mmol) and N-Boc-PEP-dipyrromethane **7** (1.251 g, 2.860 mmol, 1.0 eq) was dissolved in acetonitrile (70 mL) and added dropwise over a duration of 15 min. The solution was stirred for another 15 min and DDQ (2.142 g, 9.436 mmol, 3.3 eq) was added to oxidize the intermediate porphyrinogen. After 30 min, the crude reaction mixture was passed through a plug of silica gel (eluent: ethyl acetate +5% NEt_3) to remove excess DDQ and the solution was quenched and washed with NaOH (aq., 0.1 M, 200 mL), brine (200 mL), and water (3x 200 mL). The solvent was removed *in vacuo* and the crude product was purified by short columns (SiO_2, eluent: CH_2Cl_2, 2x) and column chromatography (SiO_2, eluent: hexanes/ethyl acetate 3:2, then CH_2Cl_2 or CH_2Cl_2/hexanes 2:1) to yield porphyrin **12** (770.6 mg, 867.8 µmol, 30.3%) as violet powder.

^{1}H NMR (300 MHz, $CDCl_3$): δ = 8.94 – 8.77 (m, 8H, β-pyrrole-*H*), 8.50 – 8.42 (m, 2H, $m_{porphyrin}$-$o_{carboxyl}$-Ph-*H*), 8.37 – 8.29 (m, 2H, $o_{porphyrin}$-$m_{carboxyl}$-Ph-*H*), 8.28 – 8.15 (m, 6H, *o*-Ph-*H*, $o_{porphyrin}$-$m_{ethynyl}$-Ph-*H*), 7.97 – 7.88 (m, 2H, $m_{porphyrin}$-$o_{ethynyl}$-Ph-*H*), 7.85 – 7.70 (m, 6H, *m/p*-Ph-*H*), 7.66 – 7.57 (m, 2H, m_{Boc}-Ph-*H*), 7.49 – 7.39 (m, 2H, o_{Boc}-Ph-*H*), 6.60 (s, 1H, N*H*), 4.13 (s, 3H, -CH_3), 1.58 (s, 9H, *t*-butyl-*H*), -2.75 (s, 2H, Por-N*H*) ppm; **^{13}C NMR** (75 MHz, $CDCl_3$): δ = 167.47 (***C***$_{ester\text{-}carbonyl}$), 152.58 (***C***$_{Boc\text{-}carbonyl}$), 147.19 ($i_{porphyrin}$-p_{ester}-Ph-***C***), 144.34 (br, *α*-pyrrol-***C***), 142.17 ($i_{porphyrin}$-Ph-***C***), 142.09 (i_{Boc}-Ph-***C***), 140.88 ($i_{porphyrin}$-$p_{ethynyl}$-Ph-***C***), 134.72 ($o_{porphyrin}$-m_{ester}-Ph-***C***, $o_{porphyrin}$-$m_{ethynyl}$-Ph-***C***), 134.69 ($o_{porphyrin}$-Ph-***C***), 132.77 (m_{Boc}-Ph-***C***), 131.36 (br, *β*-pyrrol-***C***), 130.03 ($m_{porphyrin}$-$o_{ethynyl}$-Ph-***C***), 129.80 ($p_{porphyrin}$-i_{ester}-Ph-***C***), 128.07 ($m_{porphyrin}$-o_{ester}-Ph-***C***), 127.98 ($p_{porphyrin}$-Ph-***C***), 126.89 ($m_{porphyrin}$-Ph-***C***), 123.25 ($p_{porphyrin}$-$i_{ethynyl}$-Ph-***C***), 120.67 ($meso_{phenyl}$-***C***), 119.88 ($meso_{phenyl\text{-}ethynyl}$-***C***), 118.87 ($meso_{phenyl\text{-}ester}$-***C***), 118.36 ($o_{Boc}$-Ph-***C***), 117.72 ($p_{Boc}$-Ph-***C***), 90.80 (***C***$_{acetylene\text{-}(phenyl\text{-}Boc)}$), 81.13 (***C***$_{Boc}$), 52.54 (ester-***C***$H_3$), 28.52 (*t*-butyl-***C***$_{Boc}$) ppm; **FT-IR:** $\tilde{\nu}$ (int.) = 3441 (w), 3315 (w), 3032 (w), 2971 (w), 2949 (w), 2932 (w), 1720 (s), 1701 (s), 1605 (m), 1580 (m), 1559 (w), 1520 (s), 1495 (m), 1474 (m), 1405 (m), 1367 (m), 1276 (s), 1218 (s), 1156 (s), 1099 (s), 1052 (m), 964 (s), 795 (s), 722 (s), 703 (s) cm^{-1}; **UV-Vis** (THF): λ_{max} (ε in $L{\cdot}mol^{-1}cm^{-1}$) = 648 (6 000), 591 (7 000), 549.5 (12 000), 514 (21 000), 419 (436 000), 400.5 (88 000), 234.5 (113 000) nm; **MP:** 244.8 °C (decomp.).

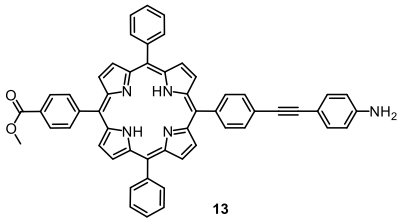

13

15-(4-((4-Aminophenyl)ethynyl)phenyl)-5-(4-methoxycarbonylphenyl)-10,20-diphenylporphyrin (13). Boc-protected porphyrin **12** (725 mg, 816 µmol) was dissolved in CH_2Cl_2 (30 mL +1% NEt_3), applied on silica gel (30 g), dried, and transferred into a 50 mL round bottom flask. The solid brownish powder was stirred at 120 °C and $2 \cdot 10^{-3}$ mbar for 4 h. To prevent possible side reactions, the reaction was stopped at this point, although TLC (hexanes/ethyl acetate 3:2) still showed the presence of starting compound. The solid was transferred into a plug, extracted with ethyl acetate and the solvent was removed *in vacuo*. Short flash column chromatography (SiO_2, eluent: hexanes/THF 2:1) yielded pure product **13** (294.3 mg, 373.5 µmol, 45.8%) and starting compound (388 mg, 437 µmol, 53.5%). The starting compound **12** was reacted accordingly a second time to yield **13** (291 mg, 369 µmol, 45.2%, overall yield: 585.3 mg, 742.8 µmol, 91.0%) and recovered starting compound (38 mg, 43 µmol, 5.2%). **^{1}H NMR** (400 MHz, $CDCl_3$): δ = 8.95 – 8.79 (m, 8H, β-pyrrole-*H*), 8.46 (d, *J* = 8.1 Hz, 2H, $m_{porphyrin}$-$o_{carboxyl}$-Ph-*H*), 8.33 (d, *J* = 8.0 Hz, 2H, $o_{porphyrin}$-$m_{carboxyl}$-Ph-*H*), 8.27 – 8.22 (m, 4H, *o*-Ph-*H*), 8.20 (d, *J* = 7.9 Hz, 2H, $o_{porphyrin}$-$m_{ethynyl}$-Ph-*H*), 7.91 (d, *J* = 8.0 Hz, 2H, $m_{porphyrin}$-$o_{ethynyl}$-Ph-*H*), 7.84 – 7.73(m, 6H, *m/p*-Ph-*H*), 7.53 – 7.44 (m, 2H, m_{amine}-Ph-*H*), 6.81 – 6.54 (m, 2H, o_{amine}-Ph-*H*), 4.13 (s, 3H, -CH_3), 3.83 (s, 2H, -NH_2), -2.73 (s, 2H, Por-N*H*) ppm; **^{13}C NMR** (101 MHz, $CDCl_3$): δ = 167.48 (***C***$_{ester\text{-}carbonyl}$), 147.17 ($i_{porphyrin}$-p_{ester}-Ph-***C***), 146.98 (i_{amine}-Ph-***C***), 144.90 (br, *α*-pyrrol-***C***), 142.15 ($i_{porphyrin}$-Ph-***C***), 141.61 ($i_{porphyrin}$-$p_{ethynyl}$-Ph-***C***), 134.72 ($o_{porphyrin}$-m_{ester}-Ph-***C***), 134.69 ($o_{porphyrin}$-Ph-***C***, $o_{porphyrin}$-$m_{ethynyl}$-Ph-***C***), 133.27 (m_{amine}-Ph-***C***), 131.46 (br, *β*-pyrrol-***C***), 129.87 ($m_{porphyrin}$-$o_{ethynyl}$-Ph-***C***), 129.73 ($p_{porphyrin}$-i_{ester}-Ph-***C***), 128.06 ($m_{porphyrin}$-o_{ester}-Ph-***C***), 127.96 ($p_{porphyrin}$-Ph-***C***), 126.89 ($m_{porphyrin}$-Ph-***C***), 123.67 ($p_{porphyrin}$-$i_{ethynyl}$-Ph-***C***), 120.63 ($meso_{phenyl}$-***C***), 120.04 ($meso_{phenyl\text{-}ethynyl}$-***C***), 118.81 ($meso_{phenyl\text{-}ester}$-***C***), 114.95 ($o_{amine}$-Ph-***C***), 112.72 ($p_{amine}$-Ph-***C***), 91.65 (***C***$_{acetylene\text{-}(phenyl\text{-}amine)}$), 87.44 (***C***$_{acetylene\text{-}(phenyl\text{-}porphyrin)}$), 52.56 (-***C***$H_3$) ppm; **FT-IR:** $\tilde{\nu}$ (int.) = 3445 (w), 3362 (m), 3316 (m), 3057 (w), 3031 (w), 2949 (m), 2914 (w), 2842 (w), 2707 (w), 1717 (s), 1597 (m), 1559 (w), 1516 (s), 1472 (m), 1430 (m), 1399 (m), 1348 (w), 1272 (s), 1176 (s), 1098 (s), 964 (s), 878 (w), 852 (m), 824 (m), 795 (s), 719 (s), 701 (s) cm^{-1}; **UV-Vis** (THF): λ_{max} (ε in $L \cdot mol^{-1}cm^{-1}$) = 648 (8 000), 591.5 (9 000), 549.5 (15 000), 514 (26 000), 419 (468 000), 400.5 (105 000) nm, 235 (114 000) nm; **MS** (MALDI): m/z for $C_{54}H_{37}N_5O_2$ $[M]^+$ calcd: 787.2947, found: 787.296.

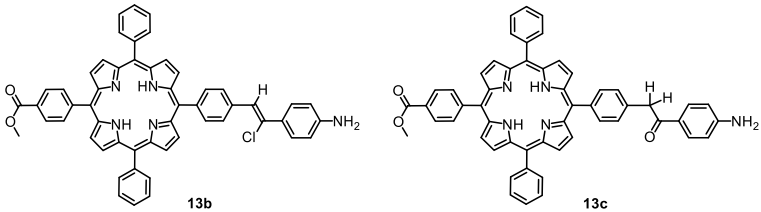

(Z)-15-(4-(2-(4-Aminophenyl)-2-chlorovinyl)phenyl)-5-(4-methoxycarbonylphenyl)-10,20-diphenylporphyrin (13b) and **15-(4-(2-(4-aminophenyl)acetyl)phenyl)-5-(4-methoxycarbonylphenyl)-10,20-diphenylporphyrin (13c).** In a 1 L flask, porphyrin **12** (630 mg, 709 µmol) was dissolved in THF (200 mL). HCl (3N in MeOH, 100 mL) was added and the green solution was stirred for 1.5 h. Since no progress was detected by TLC analysis (neutralization by addition of $NaHCO_{3(s)}$, eluent: hexanes/ethyl acetate 2:1), the temperature was raised to 80 °C for 1.5 h and the solvents were removed completely. A short column chromatography (SiO_2, eluent: CH_2Cl_2) yielded 16.8 mg (20.4 µmol, 2.9%) of side product **13b**. The recovered starting compound was dissolved in CH_2Cl_2 (15 mL) and TFA (15 mL) was added. The green solution was stirred for 2 h, the solvents were removed *in vacuo* and the residue dissolved in ethyl acetate (200 mL). $NaHCO_3$ (aq. satd., 200 mL) was added and the organic phase was washed with water (2x 200 mL), dried over $MgSO_4$ and purified by column chromatography (SiO_2, eluent: CH_2Cl_2 (**13**), then hexanes/ethyl acetate 1:1 (**13c**)). The expected product **13** (43.9 mg, 55.7 µmol, 7.9%) was produced only in minor amounts. Spectroscopic investigation revealed structure of **13b** (16.8 mg, 20.4 µmol, 2.9%) and **13c** (120.7 mg, 149.8 µmol, 21.1%) as side products from addition reactions to the triple bond.

13b: ^{1}H NMR (400 MHz, $CDCl_3$): δ = 8.96 – 8.74 (m, 8H, β-pyrrole-*H*), 8.46 (d, *J* = 8.2 Hz, 2H, $m_{porphyrin}$-o_{ester}-Ph-*H*), 8.32 (d, *J* = 8.2 Hz, 2H, $o_{porphyrin}$-m_{ester}-Ph-*H*), 8.26 – 8.18 (m, 4H, *o*-Ph-*H*), 8.03 (d, *J* = 8.1 Hz, 2H, $o_{porphyrin}$-m_{alkene}-Ph-*H*), 7.83 – 7.71 (m, 6H, *m/p*-Ph-*H*), 7.50 – 7.41 (m, 4H, $m_{porphyrin}$-o_{alkene}-Ph-*H*, m_{amine}-Ph-*H*), 7.15 (s, 1H, alkene-C*H*), 6.70 (d, *J* = 8.5 Hz, 2H, o_{amine}-Ph-*H*), 4.12 (s, 3H, -C*H*$_3$), 3.83 (s, *J* = 16.7 Hz, 2H, -N*H*$_2$), -2.75 (s, 2H, Por-N*H*) ppm; **^{13}C NMR** (101 MHz, $CDCl_3$): δ = 167.48 (***C***$_{ester\text{-}carbonyl}$), 147.44 (i_{amine}-Ph-***C***), 147.16 ($i_{porphyrin}$-p_{ester}-Ph-***C***), 142.17 ($i_{porphyrin}$-Ph-***C***), 140.88 ($i_{porphyrin}$-p_{alkene}-Ph-***C***), 135.64 ($p_{porphyrin}$-i_{alkene}-Ph-***C***), 134.93 (***C***$_{alkene}$-Cl), 134.71 ($o_{porphyrin}$-m_{ester}-Ph-***C***), 134.68 ($o_{porphyrin}$-m_{alkene}-Ph-***C***, $o_{porphyrin}$-Ph-***C***), 131.61 (br, β-pyrrol-***C***), 130.82 (m_{amine}-Ph-***C***), 129.71 ($p_{porphyrin}$-i_{ester}-Ph-***C***), 128.06 ($m_{porphyrin}$-o_{ester}-Ph-***C***), 127.94 ($p_{porphyrin}$-Ph-***C***), 127.69 (p_{amine}-Ph-***C***), 127.18 ($m_{porphyrin}$-o_{alkene}-Ph-***C***, ***C***$_{alkene}$-H), 126.86 ($m_{porphyrin}$-Ph-***C***), 120.54 ($meso_{phenyl}$-***C***), 120.30 ($meso_{phenyl\text{-}alkene}$-***C***), 118.72 ($meso_{phenyl\text{-}ester}$-***C***), 114.89 ($o_{amine}$-Ph-***C***), 52.56 (ester-***C***H$_3$) ppm; **FT-IR:** $\tilde{\nu}$ (int.) = 3941 (m), 3392 (s), 3321 (m), 3222 (w), 3059 (w), 3032 (w), 2946 (w), 2918 (w), 2849 (w), 2709 (w), 2615 (w), 2534 (w), 1711 (s), 1627 (w), 1603 (s), 1559 (m), 1516 (m), 1473 (m), 1437 (m), 1401 (m), 1349 (w), 1310 (w), 1276 (s), 1222 (w), 1177 (m), 1155 (w), 1113 (m), 1101 (m), 1072 (w), 1021 (w), 981 (w), 963 (s), 917 (w), 798 (s), 722 (s), 700 (s) cm^{-1}; **UV-Vis** (THF): λ_{max} (ε in

L·mol^{-1}cm^{-1}) = 648 (6 000), 592.5 (7 000), 550 (11 000), 514.5 (18 000), 418.5 (341 000), 399.5 (73 000) nm, 235 (104 000) nm; **MS** (APPI): m/z for $C_{54}H_{38}ClN_5O_2$ $[M]^+$ calcd: 823.270855, found: 823.273427 (err: -3.125 ppm).

13c:^{1}H NMR (400 MHz, $CDCl_3$): δ = 8.99 – 8.80 (m, 8H, β-pyrrole-*H*), 8.51 – 8.43 (m, 2H, $m_{porphyrin}$-o_{ester}-Ph-*H*), 8.34 (d, *J* = 8.1 Hz, 2H, $o_{porphyrin}$-m_{ester}-Ph-*H*), 8.29 – 8.21 (m, 4H, *o*-Ph-*H*), 8.21 – 8.15 (m, 2H, $o_{porphyrin}$-m_{ketone}-Ph-*H*), 8.06 – 7.97 (m, 2H, m_{amine}-Ph-*H*), 7.84 – 7.72 (m, 6H, *m*/*p*-Ph-*H*), 7.63 (d, *J* = 7.9 Hz, 2H, $m_{porphyrin}$-o_{ketone}-Ph-*H*), 6.69 – 6.60 (m, 2H, o_{amine}-Ph-*H*), 4.49 (s, 2H, -C*H*$_2$-), 4.13 (s, 3H, -C*H*$_3$), 4.06 (s, 2H, -N*H*$_2$), -2.70 (s, 2H, Por-N*H*) ppm; **^{13}C NMR** (101 MHz, $CDCl_3$): δ = 196.04 (***C***$_{ketone}$), 167.48 (***C***$_{ester\text{-}carbonyl}$), 151.44 (i_{amine}-Ph-***C***), 147.20 ($i_{porphyrin}$-p_{ester}-Ph-***C***), 142.18 ($i_{porphyrin}$-Ph-***C***), 140.43 ($i_{porphyrin}$-p_{ketone}-Ph-***C***), 135.21 ($p_{porphyrin}$-i_{ketone}-Ph-***C***), 134.89 ($o_{porphyrin}$-m_{ketone}-Ph-***C***), 134.72 ($o_{porphyrin}$-m_{ester}-Ph-***C***), 134.69 ($o_{porphyrin}$-Ph-***C***), 131.40 (br, β-pyrrol-***C***, m_{amine}-Ph-***C***), 129.67 ($p_{porphyrin}$-i_{ester}-Ph-***C***), 128.04 ($m_{porphyrin}$-o_{ester}-Ph-***C***), 127.98 ($p_{porphyrin}$-Ph-***C***), 127.91 ($m_{porphyrin}$-o_{ketone}-Ph-***C***), 127.29 (p_{amine}-Ph-***C***), 126.86 ($m_{porphyrin}$-Ph-***C***), 120.57 (*meso*$_{phenyl\text{-}ketone}$-***C***), 120.52 (*meso*$_{phenyl}$-***C***), 118.62 (*meso*$_{phenyl\text{-}ester}$-***C***), 113.97 (o_{amine}-Ph-***C***), 52.54 (ester-***C***H$_3$), 44.83 (-***C***H$_2$-)ppm; **MS** (MALDI): m/z for $C_{54}H_{39}N_5O_3$ $[M]^+$ calcd: 805.938, found: 805.337.

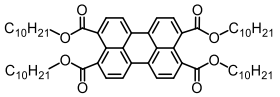

PTE$_{10}$

14

Perylenetetradecylester (PTE$_{10}$, 14) (CAS 288587-52-0, 3,4,9,10-tetra(decyloxycarbonyl)perylene).[100,236] In a 250 mL round bottom flask, perylenetetracarboxylic acid anhydride (PTCDA, 5.00 g, 12.7 mmol) was suspended in DMF (70 mL). Decanol (9.8 mL, 8.1 g, 51 mmol, 4.0 eq) and DBU (7.6 mL, 7.8 g, 51 mmol, 4.0 eq) were added and the suspension was stirred for 16 h until a homogeneous dark red, foaming solution was formed. Decyl bromide (7.9 mL, 8.4 g, 38 mmol, 3.0 eq) was added and the reaction was stirred for further 16 h while monitoring the reaction progress by TLC analysis (eluent: $CHCl_3$ + 1% acetone). The reaction mixture was poured on ice water (*ca.* 300 mL + 1 mL HCl_{conc}) and the resulting orange precipitate was filtered, washed with water (3x 100 mL) and dried *in vacuo*.

The solvents were removed *in vacuo* and the crude product was purified *via* a short plug of silica gel. Acetonitrile (1 L, recycled) eluted decyl bromide and decanol; $CHCl_3$ + 1% acetone (*ca.* 4 L, recycled) eluted pure product. The solvent was removed and the orange varnish was dissolved in THF and lyophilized with water to yield PTE$_{10}$ **14** (11.29 g, 11.33 mmol, 88.9%) as orange powder.

^{1}H NMR (300 MHz, $CDCl_3$): δ = 8.12 (d, *J* = 8.1 Hz, 4H, inner perylene-*H*), 7.95 (d, *J* = 7.9 Hz, 4H, outer perylene-*H*), 4.33 (t, *J* = 6.9 Hz, 8H, -OC*H*$_2$-), 1.80 (p, *J* = 7.0 Hz, 8H, -OCH$_2$C*H*$_2$-), 1.53 – 1.18 (m, 56H, -CH$_2$-), 0.95 – 0.81 (m, 12H, -CH$_3$) ppm; **^{13}C NMR** (101 MHz, $CDCl_3$): δ = 168.78, 133.17, 130.62, 130.59, 129.15, 128.95, 121.53, 65.78, 32.00, 29.67, 29.66, 29.45, 29.42, 28.70, 26.12, 22.76, 14.19 ppm;[238] **FT-IR:** $\tilde{\nu}$ (int.) = 2954 (m), 2917 (s), 2873 (m), 2849 (s), 1730 (s), 1718 (s), 1591 (m), 1516 (w), 1471 (m), 1411 (w), 1377 (w), 1333 (w), 1310 (m), 1277 (s), 1168 (s), 1141 (s), 1099 (m), 1051 (m), 1015 (m), 937 (w), 848 (m), 805 (s), 746 (s), 717 (m) cm^{-1}; **UV-Vis** (THF): λ_{max} (ε in L·mol^{-1}cm^{-1}) = 469.5 (45 000), 441.5 (36 000), 418 (18 000), 392.5 (6 000), 263 (30 000), 240 (33 000), 230 (39 000) nm; **MS** (APPI): m/z for $C_{64}H_{92}O_8$ $[M]^+$ calcd: 988.678671, found: 988.679097 (err: -0.431 ppm); **MP:** 92.6 °C; **R_f** ($CHCl_3$ + 1% acetone): 0.53.

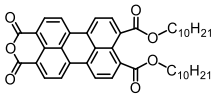

PABE$_{10}$

15

Perylene anhydride bisdecylester (PABE$_{10}$, 15) (CAS 1128107-64-1, 9,10-bis-(decyloxycarbonyl)-perylene-3,4-anhydride).[100,237] In a 50 mL round bottom flask, PTE$_{10}$ (10.24 g, 10.35 mmol) was placed and dodecane/toluene (5:1, 10.0 mL) was added. The mixture was melted at 75 °C and further heated to 95 °C. *p*-Toluenesulfonic acid (monohydrate, 2.20 g, 11.4 mmol, 1.1 eq) was added and stirred for 4 h at 95 °C. When the mass gets too viscous, the mixture is manually stirred with a spatula. The cooled-down mixture was dissolved in chloroform + 1% acetone (400 mL), applied on silica gel (250 g) and added on top of a short column (SiO_2). The mixture was washed with acetonitrile (6x 200 mL, recycled), ethyl acetate (7x 200 mL, recycled; elutes PTE$_{10}$ and negligible amounts of PABE$_{10}$, but tends to clog the column if the crude product is too concentrated) and extracted with chloroform + 1% acetone (15x 400 mL, recycled) when no PTE$_{10}$ was detectable by TLC analysis (chloroform + 1% acetone) anymore. Pure fractions of PABE$_{10}$ **15** were obtained. Crude fractions contaminated with residual PTE$_{10}$ were again applied on silica gel (200 g), washed with ethyl acetate (3x 200 mL) and extracted with chloroform + 1% acetone (10x 200 mL) to yield further pure product which was combined, dissolved in THF and lyophilized with water to give PABE$_{10}$ **15** (5.53 g, 8.00 mmol, 77.3%) as a voluminous red powder.

^{1}H NMR (400 MHz, $CDCl_3$): δ = 8.63 (d, *J* = 8.0 Hz, 2H, $o_{anhydride}$-Ph-*H*), 8.54 – 8.45 (m, 4H, inner perylene-*H*), 8.13 (d, *J* = 7.9 Hz, 2H, o_{ester}-Ph-*H*), 4.34 (t, *J* = 6.9 Hz, 4H, -OCH_2-), 1.81 (tt, *J* = 6.9 Hz, 6.9 Hz, 4H, -OCH$_2$CH_2-), 1.45 (m, 4H, -OCH$_2$CH$_2$CH_2-), 1.41 – 1.23 (m, 24H, -CH_2-), 0.92 – 0.83 (m, 6H, -CH_3) ppm; **^{13}C NMR** (101 MHz, $CDCl_3$): δ = 168.16, 160.37, 137.27, 133.65, 132.92, 131.89, 131.56, 130.48, 129.31, 126.42, 123.54, 122.18, 118.08, 66.18, 53.56, 42.84, 32.06, 31.07, 29.84, 29.72, 29.48, 28.72, 26.16, 22.83, 14.26 ppm;[238] **FT-IR:** $\tilde{\nu}$ (int.) = 3094 (w), 2954 (m), 2921 (s), 2852 (s), 2742 (w), 2670 (w), 1761 (s), 1728 (s), 1706 (s), 1592 (s), 1511 (m), 1467 (m), 1414 (w), 1340 (m), 1326 (m), 1283 (s), 1252 (s), 1204 (m), 1174 (m), 1149 (s), 1125 (s), 1106 (m), 1059 (m), 1009 (s), 984 (m), 857 (m), 840 (m), 806 (s), 751 (m), 736 (s), 721 (m), 691 (w) cm^{-1}; **UV-Vis** (THF): λ_{max} (ε in L·mol^{-1}cm^{-1}) = 499 (48 000), 470 (38 000), 442.5 (19 000), 420.5 (9 000), 358 (6 000), 263.5 (31 000), 237.5 (52 000), 229.5 (58 000) nm; **MS** (APPI): m/z for $C_{44}H_{50}O_7$ $[M]^+$ calcd: 690.355105, found: 690.354977 (err: 0.186 ppm); **MP:** 352.4 °C; **R_f** (chloroform + 1% acetone)**:** 0.87.

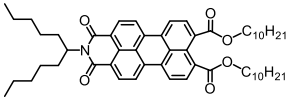

PI_sBE_{10}
16

Perylene(swallowtail)imide bisdecylester (PI_sBE_{10}, 16) (9,10-bis-(decyloxy-carbonyl)-*N*-(1-pentylhexyl)perylene-3,4-dicarboximide).[238] This compound was synthesized and provided by Corinna Weiß (team member of the HIRSCH group).

^{1}H NMR (300 MHz, $CDCl_3$): δ = 8.62 (br-s, 2H, o_{imide}-Per-*H*), 8.56 – 8.44 (m, 4H, m_{imide}-Per-*H*, m_{ester}-Per-*H*), 8.12 (d, *J* = 7.9 Hz, 2H, o_{ester}-Per-*H*), 5.32 – 5.07 (m, 1H, -NC*H*-), 4.33 (t, *J* = 6.9 Hz, 4H, -OCH_2), 2.24 (dt, *J* = 13.7, 9.0 Hz, 2H, -NCHCH_a-), 1.98 – 1.68 (m, 6H, -NCHCH_b-, -OCH$_2$CH_2-), 1.36 – 1.18 (m, 40H, -CH_2-), 0.96 – 0.74 (m, 12H, -CH$_3$) ppm; **^{13}C NMR** (101 MHz, $CDCl_3$): δ = 168.54, 165.07, 163.99, 135.31, 132.27, 131.95, 131.24, 131.21, 131.19, 131.16, 130.45, 129.49, 129.35, 129.22, 126.00, 122.59, 122.21, 121.94, 66.01, 54.64, 32.41, 31.99, 31.86, 29.66, 29.44, 29.41, 28.67, 26.74, 26.10, 22.76, 22.67, 14.19, 14.13 ppm;[238] **FT-IR:** $\tilde{\nu}$ (int.) = 3078 (w), 2954 (s), 2920 (s), 2852 (s), 1730 (m), 1715 (m), 1692 (s), 1656 (s), 1593 (s), 1579 (m), 1512 (w), 1466 (m), 1456 (m), 1416 (m), 1351 (s), 1293 (s), 1257 (s), 1202 (m), 1166 (s), 1103 (m), 1073 (m), 843 (w), 827 (w), 806 (s), 746 (s), 723 (m), 701 (w) cm^{-1}; **UV-Vis** (THF): λ_{max} (ε in L·mol^{-1}cm^{-1}) = 501.5 (64 000), 470.5 (48 000), 445 (23 000), 419.5 (9 000), 360 (4 000), 262.5 (41 000), 239(52 000), 231 (61 000) nm.

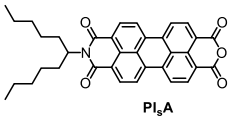

PI_SA

17

Perylene(swallowtail)imide anhydride (PI_SA, 17) (CAS 952581-96-3, *N*-(1-pentylhexyl)perylene-3,4-anhydride-9,10-dicarboximide). In a 50 mL flask, PI_SBE_{10} **16** (211.3 mg, 250.3 µmol) was placed.[238] A mixture of dodecane/toluene (5:1, 0.2 mL) was added and the mixture was heated to 95 °C. *p*-Toluenesulfonic acid (monohydrate, 52.4 mg, 275.5 µmol, 1.1 eq) was added and the reaction was stirred for 24 h at 95 °C. As the reaction was not completed, further *p*-toluenesulfonic acid (monohydrate, 20.0 mg, 105 µmol, 0.4 eq) was added and the red solution was stirred for 3 h at 95 °C. The cooled-down mixture was dissolved in THF (acidified by a few drops acetic acid), applied on silica gel (20 g) and added on top of a short column (SiO_2). The crude product was washed with hexanes (3x 100 mL), diethyl ether (3x 100 mL) and extracted with $CHCl_3$ + 1% acetone (10x 50 mL). In the first fraction, residual PI_SBE_{10} and minor amounts of PI_SA were eluted, the following fractions contained pure PI_SA **17** (112.1 mg, 205.4 µmol, 82.1%).

^{1}H NMR (400 MHz, $CDCl_3$): δ = 8.82 – 8.52 (m, 8H, Per-*H*), 5.18 (tt, *J* = 9.4, 5.8 Hz, 1H, -NC*H*-), 2.25 (m, 2H, -NCHCH_a-), 1.87 (m, 2H, -NCHCH_b-), 1.47 – 1.07 (m, 12H, -CH_2-), 1.00 – 0.72 (m, 6H, -CH_3) ppm; **^{13}C NMR** (101 MHz, $CDCl_3$): δ = 160.18, 136.59, 133.81, 133.75, 132.19, 132.15, 132.04, 131.49, 131.45, 131.40, 129.69, 126.97, 126.71, 124.12, 123.33, 119.17, 55.03, 32.36, 31.80, 26.69, 22.62, 14.09 ppm;[238] **FT-IR:** $\tilde{\nu}$ (int.) = 3097 (w), 2653 (s), 2927 (s), 2857 (s), 1764 (s), 1718 (m), 1700 (s), 1657 (s), 1592 (s), 1575 (m), 1505 (w), 1456 (w), 1427 (w), 1404 (m), 1355 (m), 1313 (s), 1266 (w), 1251 (m), 1200 (w), 1177 (w), 1140 (m), 1123 (m), 1104 (w), 1061 (w), 1107 (s), 863 (w), 809 (s), 793 (w), 777 (w), 753 (w), 737 (s), 635 (w) cm^{-1}; **UV-Vis** (THF): λ_{max} (ε in $L \cdot mol^{-1} cm^{-1}$) = 517.5 (81 000), 482 (52 000), 452.5 (19 000), 426 (6 000), 366.5 (6 000), 260 (31 000), 239.0 (57 000), 233.5 (58 000) nm; **MP:** 368.2 °C.

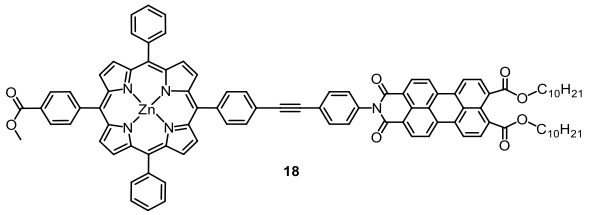

18

15-(4-((4-(9,10-Bis(decyloxycarbonyl)perylene-3,4-dicarboximid-1-yl)phenyl)-ethynyl)phenyl)-5-(4-methoxycarbonylphenyl)-10,20-diphenylporphyrinato-Zn(II) (16). In a 25 mL flask was added MeO-(Ph_2)Por-PEP-NH_2 **13** (400 mg, 508 µmol), $PABE_{10}$ **15** (414 mg, 599 µmol, 1.2 eq), $Zn(OAc)_2$ (115 mg, 627 µmol, 1.2 eq), NEt_3 (1 mL) and imidazole (4 g). The mixture was melted and stirred at 100 °C for 1 h. Under these reaction conditions, the free-base porphyrin was metallated. The cooled-down mixture was dissolved in chloroform (300 ml) and washed with water (3x 300 mL) to remove imidazole. The organic phase was dried over $MgSO_4$ and filtered through a plug of silica gel (eluent: $CHCl_3$ + 1% NEt_3) to yield pure MeO-(Ph_2)ZnPor-PEP-$PIBE_{10}$ **18** (716.7 mg, 470.2 µmol, 92.6%). Other impure fractions were eluted with $CHCl_3$ + 1% acetone and THF + 1% HAc.

^{1}H NMR (400 MHz, DMSO-d_6 + traces $CDCl_3$): δ = 8.92 – 8.74 (m, 12H, β-pyrrole-*H*, Per-*H*), 8.59 (d, *J* = 7.8 Hz, 2H, Per-*H*), 8.38 (d, *J* = 8.2 Hz, 2H, $m_{porphyrin}$-$o_{carboxyl}$-Ph-*H*), 8.33 (d, *J* = 8.2 Hz, 2H, $o_{porphyrin}$-$m_{carboxyl}$-Ph-*H*), 8.26 (d, *J* = 7.8 Hz, 2H, $o_{porphyrin}$-$m_{ethynyl}$-Ph-*H*), 8.19 (m, 4H, *o*-Ph-*H*), 8.12 (d, *J* = 7.7 Hz, 2H, Per-*H*), 8.03 (d, *J* = 7.8 Hz, 2H, $m_{porphyrin}$-$o_{ethynyl}$-Ph-*H*), 7.89 (d, *J* = 8.2 Hz, 2H, m_{imide}-Ph-*H*), 7.84 – 7.76 (m, 6H, *m/p*-Ph-*H*), 7.58 (d, *J* = 8.3 Hz, 2H, o_{imide}-Ph-*H*), 4.26 (t, *J* = 6.8 Hz, 4H, -OCH_2-), 4.05 (s, 3H, -OCH_3), 1.74 (q, *J* = 7.3 Hz, 4H, -OCH$_2$CH_2-), 1.42 (m, 4H, -OCH$_2$CH$_2$CH_2-), 1.36 – 1.12 (m, 24H, -CH_2-), 0.84 (t, *J* = 6.4 Hz, 6H, -CH_3) ppm; **COSY NMR** (400 MHz, DMSO-d_6 + traces $CDCl_3$, *aromatic region only*): δ = 8.85 – 8.72 (m, 8H, β-pyrrole-*H*), 8.70 (d, *J* = 8.1 Hz, 2H, m_{imide}-Per-*H*), 8.66 (d, *J* = 8.1 Hz, 2H, m_{ester}-Per-*H*), 8.58 (d, *J* = 7.8 Hz, 2H, o_{imide}-Per-*H*), 8.35 (d, *J* = 8.1 Hz, 2H, $m_{porphyrin}$-$o_{carboxyl}$-Ph-*H*), 8.25 (d, *J* = 8.1 Hz, 2H, $o_{porphyrin}$-$m_{carboxyl}$-Ph-*H*), 8.20 (d, *J* = 8.0 Hz, 2H, $o_{porphyrin}$-$m_{ethynyl}$-Ph-*H*), 8.14 (m, 4H, *o*-Ph-*H*), 8.08 (d, *J* = 7.6 Hz, 2H, o_{ester}-Per-*H*), 7.94 (d, *J* = 8.0 Hz, 2H, $m_{porphyrin}$-$o_{ethynyl}$-Ph-*H*), 7.82 (d, *J* = 8.1 Hz, 2H, m_{imide}-Ph-*H*), 7.77 – 7.68 (m, 6H, *m/p*-Ph-*H*), 7.48 (d, *J* = 8.0 Hz, 2H, o_{imide}-Ph-*H*) ppm; **^{13}C NMR** (DEPT-135, 101 MHz, $CDCl_3$): δ = 134.63, 134.57, 134.53, 132.70, 132.13, 131.79, 131.72, 131.36, 130.40, 129.88, 128.97, 127.65, 127.41, 126.49, 122.87, 121.89, 77.24, 67.53, 65.96, 56.99, 52.36, 46.00, 31.94, 29.73, 29.60, 29.37, 28.62, 26.05, 22.71, 14.13 ppm; **FT-IR:** $\tilde{\nu}$ (int.) = 3377 (w), 3055 (w), 3031 (w), 2951 (m), 2921 (s), 2850 (s), 1705 (s), 1665 (w), 1594 (m), 1559 (w), 1516 (m), 1485 (w), 1440 (m), 1415 (m), 1392 (m), 1360 (m), 1338 (m), 1265 (s), 1200 (m), 1173 (s), 1136 (w), 1101 (s), 1067 (s), 998 (s), 849 (w), 807 (m), 794 (s), 766 (m), 747 (m), 717 (s), 703 (s), 660 (w) cm^{-1}; **UV-Vis** (THF): λ_{max} (ε in L·mol^{-1}cm^{-1}) = 597 (8 000), 556.5 (19 000), 502 (45 000), 471 (36 000), 425.5 (451 000), 404 (42 000), 223 (113 000) nm; **MS** (ESI+): m/z for $C_{98}H_{84}N_5O_8Zn$ $[M+H]^+$ calcd: 1522.5606, found: 1522.5588

(err: 1.5 ppm); **MS** (MALDI): m/z for $C_{96}H_{58}N_8O_4Zn_2$ [ZnP-bisacetylene-ZnP homocoupling]$^+$ calcd: 1514.3164, found: 1514; **MP:** 339.2 °C (decomp.).

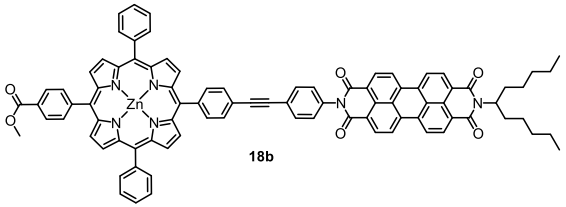

18b

5-(4-Methoxycarbonylphenyl)-15-(4-((4-(N-(1-pentylhexyl)perylene-3,4:9,10-bis-(dicarboximid)-1-yl)phenyl)ethynyl)phenyl)-10,20-diphenylporphyrinato-Zn(II) (18b).

In a 50 mL flask was added MeO-(Ph_2)Por-PEP-NH_2 **13** (164.8 mg, 209.2 µmol, 1.1 eq), PI_SA **17** (102.0 mg, 186.9 µmol), $Zn(OAc)_2$ (60.0 mg, 327 µmol, 1.7 eq), imidazole (1 g) and NEt_3 (0.5 mL). The mixture was melted and stirred at 100 °C for 3 h. The cooled-down mixture was dissolved in $CHCl_3$ (300 mL) and washed with water (300 mL), HCl (aq. 0.06 M, 300 mL), NaCl (aq, 15%, 300 mL) and water (300 mL) to remove imidazole. The organic phase was dried over $MgSO_4$ and the solvent was removed *in vacuo*. The solid was suspended in hexanes/ethyl acetate (3:2 + 1% acetone + 5% NEt_3) and filtered through a plug of silica gel (eluent: as above) to elute residual porphyrin. Crude product was eluted with $CHCl_3$ + 1% NEt_3 and $CHCl_3$ + 1% acetone and further purified by short column chromatography (SiO_2, eluent: chloroform → chloroform + 1% acetone) to yield MeO-(Ph_2)ZnPor-PEP-PDI_S **18b** (106.3 mg, 77.09 µmol, 41.2%).

^{1}H NMR (400 MHz, THF-d_8): δ = 8.99 – 8.71 (m, 8H, β-pyrrole-*H*), 8.65 (d, *J* = 7.8 Hz, 2H*, Per-*H*), 8.41 (dd, *J* = 8.2, 2.3 Hz, 2H, $m_{porphyrin}$-$o_{carboxyl}$-Ph-*H*), 8.34 – 8.26 (m, 2H, $o_{porphyrin}$-$m_{carboxyl}$-Ph-*H*), 8.25 (d, *J* = 8.1 Hz, 2H*, Per-*H*), 8.25 – 8.12 (m, 6H*, *o*-Ph-*H*, $o_{porphyrin}$-$m_{ethynyl}$-Ph-*H*), 8.01 – 7.96 (m, 2H*, Per-*H*), 7.87 – 7.79 (m, 2H, $m_{porphyrin}$-$o_{ethynyl}$-Ph-*H*), 7.78 – 7.69 (m, 6H, *m/p*-Ph-*H*), 7.52 – 7.45 (m, 2H*, Per-*H*), 7.37 – 7.30 (m, 2H*, m_{imide}-Ph-*H*), 6.65 – 6.57 (m, 2H*, o_{imide}-Ph-*H*), 4.92 (s, 1H, -NC*H*-), 4.04 (s, 3H, -OCH_3), 2.37 – 2.26 (m, 2H*, -NCHCH_a-), 1.88 (s, 2H*, -NCHCH_b-), 1.45 – 1.17 (m, 12H*, -CH_2-), 0.94 – 0.78 (m, 6H*, -CH_3) ppm (* the integrals of these peaks are significantly lower than expected); **^{13}C NMR** (DEPT-135, 101 MHz, $CDCl_3$): δ = 134.61, 131.96, 131.18, 128.94, 127.57, 127.29, 126.41, 67.47, 52.35, 51.42, 32.36, 31.82, 29.73, 29.39, 26.76, 25.25, 22.63, 14.13 ppm; **FT-IR:** $\tilde{\nu}$ (int.) = 3047 (w), 3032 (w), 2951 (m), 2921 (m), 2855 (m), 1694 (s), 1656 (s), 1593 (s), 1576 (m), 1514 (m), 1484 (w), 1434 (m), 1404 (m), 1338 (s), 1272 (s), 1253 (s), 1204 (w), 1174 (m), 1100 (m), 1069 (m), 993 (s), 962 (m), 856 (w), 822 (w), 809 (m), 794 (s), 746 (m), 717 (s), 700 (s), 660 (w) cm^{-1}; **UV-Vis** (THF): λ_{max} (ε in $L{\cdot}mol^{-1}cm^{-1}$) = 597 (10 000), 556.5 (24 000), 522 (60 000), 486.5 (38 000), 453.5 (19 000), 425.5 (550 000), 405 (50 000), 221.5 (101 000) nm.

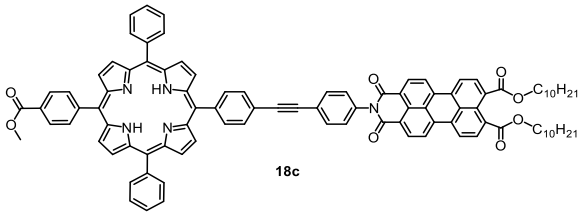

18c

15-(4-((4-(9,10-Bis(decyloxycarbonyl)perylene-3,4-dicarboximid-1-yl)phenyl)-ethynyl)phenyl)-5-(4-methoxycarbonylphenyl)-10,20-diphenylporphyrin (18c). In a 25 mL flask was added MeO-(Ph_2)Por-PEP-NH_2 **13** (150 mg, 190 µmol), $PABE_{10}$ **15** (140 mg, 203 µmol, 1.1 eq), imidazole (0.5 g) and a drop of THF. The mixture was melted and stirred at 120 °C for 16 h. The cooled-down mixture was dissolved in THF (100 ml) and filtered through a plug of silica gel (eluent: THF). The crude product was suspended in water and filtrated through celite and washed with water (3x 200 mL) to remove imidazole. The product was eluted with THF and purified *via* several GPCs (eluent: THF) to yield MeO-(Ph_2)Por-PEP-$PIBE_{10}$ **18c** (243.5 mg, 167 µmol, 87.6%).

^{1}H NMR (400 MHz, $CDCl_3$): δ = 8.94 – 8.76 (m, 8H, β-pyrrole-*H*), 8.59 (d, *J* = 7.9 Hz, 2H, Per-*H*), 8.49 – 8.41 (m, 2H, $m_{porphyrin}$-$o_{carboxyl}$-Ph-*H*), 8.35 (dd, *J* = 8.5, 1.7 Hz, 4H, Per-*H*), 8.33 – 8.28 (m, 2H, $o_{porphyrin}$-$m_{carboxyl}$-Ph-*H*), 8.27 – 8.19 (m, 6H, *o*-Ph-*H*, $o_{porphyrin}$-$m_{ethynyl}$-Ph-*H*), 8.10 (d, *J* = 7.8 Hz, 2H, Per-*H*), 8.02 – 7.96 (m, 2H, $m_{porphyrin}$-$o_{ethynyl}$-Ph-*H*), 7.92 – 7.87 (m, 2H, m_{imide}-Ph-*H*), 7.83 – 7.72 (m, 5H, *m/p*-Ph-*H*), 7.50 – 7.42 (m, 2H, o_{imide}-Ph-*H*), 4.37 (t, *J* = 6.9 Hz, 4H, -OCH_2-), 4.12 (s, 3H, -OCH_3), 1.84 (p, *J* = 7.1 Hz, 4H, -OCH$_2$CH_2-), 1.54 – 1.43 (m, 4H, -OCH$_2$CH$_2$CH_2-), 1.43 – 1.21 (m, 24H, -CH_2-), 1.04 – 0.80 (m, 6H, -CH_3), -2.78 (s, 2H, Por-N*H*); **^{13}C NMR** (101 MHz, $CDCl_3$): δ = 189.43, 168.33, 167.48, 163.69, 142.10, 134.71, 132.90, 130.29, 128.07, 126.91, 122.90, 121.91, 120.65, 108.09, 66.11, 45.91, 32.07, 29.74, 29.53, 29.49, 28.77, 26.19, 22.84, 14.27, 8.73, 1.18 ppm;**^{13}C NMR** (DEPT-135, 101 MHz, $CDCl_3$): δ = 134.72, 133.12, 132.89, 131.80, 130.40, 129.17, 128.08, 126.92, 123.35, 122.86, 121.89, 121.71, 66.20, 52.57, 32.07, 29.74, 29.50, 28.77, 26.20, 22.85, 14.27.ppm; **FT-IR:** $\tilde{\nu}$ (int.) = 3317 (w), 3051 (w), 2950 (m), 2922 (s), 2850 (s), 1704 (s), 1665 (m), 1593 (m), 1512 (w), 1415 (w), 1359 (m), 1262 (s), 1153 (m), 1099 (m), 1064 (m), 1020 (m), 1001 (w), 965 (s), 848 (w), 798 (s), 746 (m), 720 (m), 702 (m) cm^{-1}; **UV-Vis** (THF): λ_{max} (ε in $L{\cdot}mol^{-1}cm^{-1}$) = 647 (3 000), 591 (4 000), 549 (8 000), 504.5 (46 000), 471.5 (31 000), 418.5 (331 000), 400 (68 000), 223 (94 000) nm; **MS (MALDI)**: m/z for $C_{98}H_{86}N_5O_8$ $[M+H]^+$ calcd: 1460.6471, found: 1460.6169.

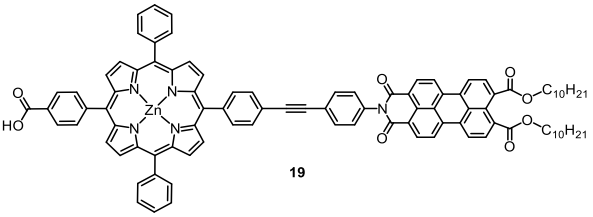

19

5-(4-Carboxyphenyl)-15-(4-((4-(9,10-bis(decyloxycarbonyl)perylene-3,4-dicarboximid-1-yl)phenyl)ethynyl)phenyl)-10,20-diphenylporphyrinato-Zn(II) (19). In a 100 mL flask MeO-(Ph_2)ZnPor-PEP-PIBE$_{10}$ **18** (648.2 mg, 452.3 µmol) was dissolved in THF (50 mL), MeOH (5 mL) and water (0.5 mL). LiOH (685 mg, 28.6 mmol, 63 eq) was added and the reaction was stirred at 80 °C for 2 h. The solvents were removed *in vacuo*, the crude product was dissolved in THF (+ one drop HAc to provide solubility), applied on silica gel and filtered through a plug of silica gel (eluent: chloroform + 1% acetone, then THF + 1% HAc). The solvent was removed *in vacuo* to yield acidPh-(Ph_2)ZnPor-PEP-PIBE$_{10}$ **19** (638.4 mg, 422.7 µmol, 93.5%).

^{1}H NMR (400 MHz, THF-d_8): δ = 10.83 (s, 1H, -COO*H*), 8.92 – 8.79 (m, 8H, β-pyrrole-*H*), 8.79 – 8.68 (m, 4H, Per-*H*), 8.63 (d, *J* = 7.9 Hz, 2H, Per-*H*), 8.42 (d, *J* = 8.1 Hz, 2H, $m_{porphyrin}$-$o_{carboxyl}$-Ph-*H*), 8.32 – 8.22 (m, 4H, $o_{porphyrin}$-$m_{carboxyl}$-Ph-*H*, $o_{porphyrin}$-$m_{ethynyl}$-Ph-*H*), 8.22 – 8.15 (m, 4H, *o*-Ph-*H*), 8.11 (d, *J* = 7.8 Hz, 2H, Per-*H*), 8.01 – 7.94 (m, 2H, $m_{porphyrin}$-$o_{ethynyl}$-Ph-*H*), 7.85 – 7.78 (m, 2H, m_{imide}-Ph-*H*), 7.78 – 7.70 (m, 6H, *m/p*-Ph-*H*), 7.51 – 7.44 (m, 2H, o_{imide}-Ph-*H*), 4.31 (t, *J* = 6.8 Hz, 4H, -OCH_2-), 1.97 – 1.76 (m, 4H, -OCH$_2$CH_2-), 1.54 – 1.20 (m, 28H, -CH_2-), 1.04 – 0.70 (m, 6H, -CH_3) ppm; **^{13}C NMR** (DEPT-135, 101 MHz, THF-d_8): δ = 135.03, 133.27, 132.20, 132.12, 132.12, 131.91, 131.60, 129.65, 128.24, 127.83, 126.88, 114.35, 108.07, 67.27, 32.46, 30.30, 29.62, 26.05, 24.54, 14.11 ppm; **FT-IR** (diluted, THF): $\tilde{\nu}$ (int.) = 2982 (s), 2966 (m), 2924 (m), 2855 (m), 1734 (m), 1718 (s), 1700 (s), 1684 (m), 1653 (m), 1595 (w), 1558 (m), 1507 (m), 1457 (w), 1420 (w), 1363 (m), 1339 (w), 1297 (w), 1267 (m), 1203 (w), 1168 (m), 1084 (s), 997 (m), 922 (w), 810 (w), 796 (w), 668 (s) cm^{-1}; **UV-Vis** (THF): λ_{max} (qualitative) = 596.5, 556.5, 502, 471, 425, 404.5 nm; **MS (MALDI)**: m/z for $C_{97}H_{81}N_5O_8Zn$ $[M]^+$ calcd: 1507.5377, found: 1507.5361.

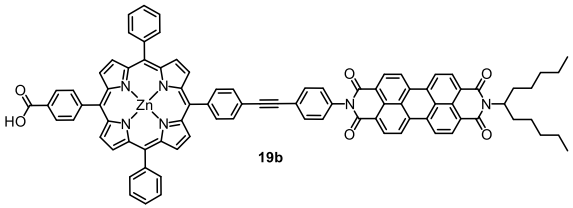

19b

5-(4-Carboxyphenyl)-15-(4-((4-(*N*-(1-pentylhexyl)perylene-3,4:9,10-bis-(dicarboximid)-1-yl)phenyl)ethynyl)phenyl)-10,20-diphenylporphyrinato-Zn(II) (19b).

In a 25 mL flask, MeO-(Ph_2)ZnPor-PEP-PDI$_S$ **18b** (67.3 mg, 48.8 µmol) was dissolved in THF (10 mL), MeOH (1 mL) and water (0.1 mL). LiOH (70 mg, 2.9 mmol, 60 eq) was added and the reaction was stirred at 80 °C for 2 h. The solvents were removed *in vacuo*, the crude product was dissolved in THF (+ one drop HAc to provide solubility), applied on silica gel and filtered through a plug of silica gel. Washing with CH_2Cl_2 eluted minor amounts of PI$_S$A **17** and the corresponding counterpart, acid-ZnPor-PEP-NH_2, which were partially cleaved under these reaction conditions. The product (inseparable mixture) was eluted using THF (+1% HAc). The solvent was removed *in vacuo* to yield AcidPh-(Ph_2)ZnPor-PEP-PDI$_S$ **19b** (41.1 mg, 30.1 µmol, 61.7%).

^{1}H NMR (400 MHz, THF-d_8): δ = 10.87 (s, 1H, -COO*H*), 8.94 – 8.77 (m, 8H, β-pyrrole-*H*), 8.52 (d, *J* = 8.0 Hz, 2H, Per-*H*), 8.43 (d, *J* = 7.8 Hz, 2H, $m_{porphyrin}$-$o_{carboxyl}$-Ph-*H*), 8.29 (d, *J* = 8.0 Hz, 2H, $o_{porphyrin}$-$m_{carboxyl}$-Ph-*H*), 8.24 (d, *J* = 3.6 Hz, 2H, Per-*H*), 8.23 – 8.13 (m, 6H, *o*-Ph-*H*, $o_{porphyrin}$-$m_{ethynyl}$-Ph-*H*), 7.99 (d, *J* = 7.0 Hz, 2H, Per-*H*), 7.83 (dd, *J* = 8.0, 5.7 Hz, 2H, $m_{porphyrin}$-$o_{ethynyl}$-Ph-*H*), 7.80 – 7.68 (m, 6H, *m/p*-Ph-*H*), 7.51 (d, *J* = 7.8 Hz, 2H, Per-*H*), 7.37 – 7.29 (m, 2H, m_{imide}-Ph-*H*), 6.66 – 6.57 (m, 2H, o_{imide}-Ph-*H*), 5.22 (td, *J* = 9.5, 4.8 Hz, 1H, -NC*H*-), 2.01 – 1.80 (m, 2H, -NCHCH_a-), 1.81 – 1.63 (m, 2H, -NCHCH_b-), 1.43 – 1.19 (m, 12H, -CH_2-), 0.99 – 0.79 (m, 6H, -CH_3) ppm; **FT-IR:** $\tilde{\nu}$ (int.) = 2982 (m), 2952 (m), 2924 (m), 2855 (m), 1769 (m), 1696 (s), 1653 (m), 1594 (s), 1517 (m), 1490 (w), 1405 (m), 1339 (s), 1317 (m), 1277 (m), 1253 (s), 1204 (m), 1176 (m), 1101 (w), 1066 (m), 993 (s), 808 (m), 796 (s), 737 (m), 719 (m), 702 (m) cm^{-1}; **UV-Vis** (THF): λ_{max} (qualitative) = 596.5, 556.5, 518, 483, 425.5, 404.5 nm; **MS (MALDI)**: m/z for $C_{53}H_{33}N_5O_2Zn$ [cleaved by-product Acid-ZnPor-PEP-NH_2]$^+$ calcd: 835.1926, found: 835.1853.

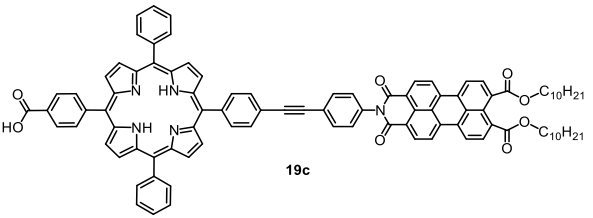

19c

5-(4-Carboxyphenyl)-15-(4-((4-(9,10-bis(decyloxycarbonyl)perylene-3,4-dicarboximid-1-yl)phenyl)ethynyl)phenyl)-10,20-diphenylporphyrin (19c). In a 100 mL flask, MeO-(Ph_2)Por-PEP-$PIBE_{10}$ **18c** (210 mg, 144 µmol) was dissolved in THF (50 mL), MeOH (10 mL) and water (1 mL). LiOH (50 mg, 2.1 mmol, 15 eq) was added and the reaction was stirred at 80 °C for 3 d. The crude product was filtered with silica gel (eluent: THF → THF + 1% HAc), applied on silica gel and passed through a plug of silica gel (eluent: CH_2Cl_2, hexanes/THF 1:1, then THF +1% HAc). The solvent was removed *in vacuo* to yield AcidPh-(Ph_2)Por-PEP-$PIBE_{10}$ **19c** (87.5 mg, 60.5 µmol, 42.1%).

^{1}H NMR (400 MHz, $CDCl_3$): δ = 8.93 – 8.77 (m, 8H, β-pyrrole-*H*), 8.65 (d, *J* = 7.8 Hz, 2H, Per-*H*), 8.52 (d, *J* = 7.7 Hz, 2H, $m_{porphyrin}$-$o_{carboxyl}$-Ph-*H*), 8.45 (dd, *J* = 8.4, 4.1 Hz, 4H, Per-*H*), 8.40 – 8.31 (m, 2H, $o_{porphyrin}$-$m_{carboxyl}$-Ph-*H*), 8.28 – 8.14 (m, 6H, $o_{porphyrin}$-$m_{ethynyl}$-Ph-*H, o*-Ph-*H*), 8.14 (d, *J* = 7.8 Hz, 2H, Per-*H*), 7.97 (d, *J* = 7.9 Hz, 2H, $m_{porphyrin}$-$o_{ethynyl}$-Ph-*H*), 7.89 (dd, *J* = 8.3, 3.5 Hz, 2H, m_{imide}-Ph-*H*), 7.84 – 7.72 (m, 6H, *m/p*-Ph-*H*), 7.54 – 7.46 (m, 2H, o_{imide}-Ph-*H*), 4.36 (td, *J* = 6.9, 4.0 Hz, 4H, -OCH_2-), 2.15 (s, *residual acetic acid*), 1.92 – 1.77 (m, 4H, -OCH_2CH_2-), 1.54 – 1.42 (m, 4H, -$OCH_2CH_2CH_2$-), 1.44 (s, -COOH/*residual acetic acid*), 1.42 – 1.22 (m, 24H, -CH_2-), 0.96 – 0.84 (m, 6H, CH_3), -2.76 (s, 2H, Por-N*H*) ppm; **FT-IR:** $\tilde{\nu}$ (int.) = 3344 (br), 2958 (m), 2921 (s), 2851 (s), 1705 (s), 1664 (s), 1594 (m), 1534 (w), 1513 (w), 1455 (m), 1392 (m), 1365 (s), 1313 (w), 1256 (s), 1150 (s), 1098 (m), 1066 (m), 1018 (m), 966 (m), 843 (m), 799 (s), 748 (w), 728 (m), 701 (m) cm^{-1}; **UV-Vis** (THF): λ_{max} (qualitative) = 647.5, 591.5, 548, 505, 472.5, 418, 400, 228 nm; **MS (MALDI)**: m/z for $C_{97}H_{83}N_5O_8$ $[M]^+$ calcd: 1445.7580, found: 1445.754; **MP:** 144.5 °C.

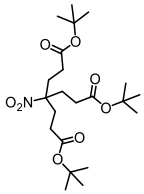

20

4-Nitro-4-[2-(*tert*-butoxycarbonyl)ethyl)]-heptanedioate (20, CAS 136587-00-3).[134] This compound is prepared as a standard compound in Bachelor laboratory course and is available in kilogram amounts.

^{1}H NMR (300 MHz, $CDCl_3$,): δ = 2.20 (s, 12H, -CH_2CH_2COO-), 1.43 (s, 27H, -$C(CH_3)_3$); **R_f** (hexanes/ethyl acetate 2:1): 0.85.

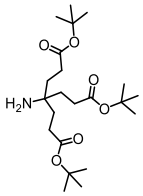

21

4-Amino-4-[2-(*tert*-butoxycarbonyl)ethyl)]-heptanedioate (21, CAS 136586-99-7).[134] Raney nickel (preactivated catalyst, Acros, 50% slurry in H_2O, 27.04 g) was carefully weighed and thoroughly washed with EtOH (3x 75 mL) and cyclohexane (3x 75 mL) in such a way that it was always covered with liquid. The suspension was transferred into a 1 L Schlenk flask. Then, 4-nitro-4-[2-(*tert*-butoxycarbonyl)ethyl)]-heptanedioate **20** (35.00 g, 78.55 mmol) in cyclohexane (500 mL) was added and the reaction mixture was hydrogenated for 27 h at rt and atmospheric pressure. The reaction progress was monitored by TLC analysis (hexanes/ethyl acetate 2:1, stain: SiO_2/iodine). The mixture was filtered through celite and washed with cyclohexane (300 mL) and ethanol (200 mL) without letting the catalyst run dry. The slightly yellowish filtrate was evaporated and the crude product was purified through flash column chromatography (SiO_2, eluent: ethyl acetate) to yield **21** (30.11 g, 72.46 mmol, 92.2%) as a white powder.

^{1}H NMR (300 MHz, $CDCl_3$): δ = 2.10 (dd, J = 9.3, 7.0 Hz, 6H, -CH_2COO-), 1.46 (dd, J = 9.3, 7.0 Hz, 6H, -CH_2CH_2COO-), 1.30 (s, 27H, -$C(CH_3)_3$), 0.87 (s, 2H, -NH_2) ppm; **FT-IR:** $\tilde{\nu}$ (int.) = 3377 (m), 3005 (m), 2977 (s), 2934 (s), 2878 (m), 1718 (s), 1447 (m), 1393 (m), 1366 (s), 1343 (m), 1315 (m), 1219 (m), 1259 (m), 1209 (m), 1145 (s), 1126 (s), 1113 (s), 994 (w), 944 (m), 973 (m), 847 (s), 785 (w), 757 (s) cm^{-1}; **MP:** 61.3 °C; **R_f** (hexanes/ethyl acetate 2:1): 0.00 – 0.49.

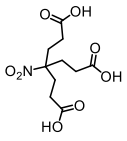

22

4-Nitro-4-[2-(carboxyethyl)]heptanediacid (22, CAS 59085-15-3).[134] To a 500 mL flask was added 4-nitro-4-[2-(*tert*-butoxycarbonyl)ethyl)]-heptanedioate **20** (10.00 g, 22.44 mmol) in formic acid (300 mL). The solution was stirred for 20 h at rt. The solvent was removed *in vacuo* and toluene (3x 100 mL) was added to remove the formic acid azeotropically. The white residue was dissolved in NaOH (0.5 M, 200 mL) and HCl (37%, 20 mL) was added until a white solid precipitated. The solid was filtered, washed with cold water (4x 20 mL), and dried *in vacuo* to yield **22** (6.12 g, 22.1 mmol, 98.4%) as a white solid.

^{1}H NMR (300 MHz, DMSO-d_6): δ = 12.31 (s, 3H, -COOH), 2.15 (m, 12H, -CH_2-); **R_f** (ethyl acetate): 0.00 – 0.36.

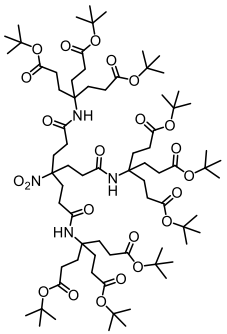

23

9-Cascade:nitromethane[3]:(2-aza-3-oxopentylidyne):propionicacid-*tert*-butyl-ester (23, CAS 220215-00-9).[134,196] To a 250 mL flask were added triacid **22** (1.00 g, 3.61 mmol), amine **21** (5.10 g, 12.3 mmol, 3.4 eq), HOBt·H_2O (2.00 g, 13.1 mmol, 3.6 eq), DMF (75 mL), and the mixture was cooled to 0 °C. DCC (2.70 g, 13.1 mmol, 3.6 eq) in DMF (25 mL) was added slowly at 0 °C and the reaction was stirred for 6 d at rt. The DCU was filtered off and washed with ethyl acetate (2x 20 mL), the filtrate was concentrated *in vacuo*. The crude yellow oil was passed through a plug of silica gel (eluent: ethyl acetate) and purified by column chromatography (SiO_2, eluent: hexanes/ethyl acetate 3:2, stain: SiO_2/iodine) to yield **23** (4.53 g, 3.08 mmol, 85.4%) as a colorless crystalline foam.

^{1}H NMR (300 MHz, $CDCl_3$): δ = 6.11 (s, 3H, -CON*H*-), 2.27 – 2.15 (m, 24H, -CH_2CO-), 2.12 (m, 6H, O_2NCCH_2-), 2.00 – 1.87 (m, 18H, -CH_2CH_2CO-), 1.43 (s, 81H, -CH_3) ppm; **FT-IR:** $\tilde{\nu}$ (int.) = 3349 (m), 2977 (s), 2934 (s), 1725 (s), 1681 (m), 1660 (m), 1537 (m), 1546 (w), 1392 (w), 1366 (s), 1313 (m), 1250 (m), 1216 (w), 1145 (s), 1100 (m), 1034 (w), 952 (m), 847 (s), 758 (m) cm^{-1}; **MP**: 178.2 °C; **R_f** (cyclohexane/ethyl acetate 3:2): 0.32.

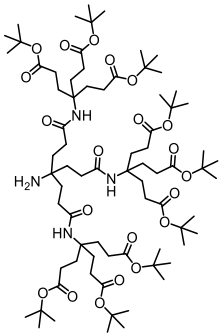

24

9-Cascade:aminomethane[3]:(2-aza-3-oxopentylidyne):propanoicacid-*tert*-butyl-ester (24, CAS 207444-65-3).[196] Raney nickel (preactivated catalyst, Acros, 50% slurry in H_2O, 5.6 g) was carefully weighed and thoroughly washed with EtOH (dry, 3 x 100 mL) under argon atmosphere in such a way that it was always covered with liquid. Then, **23** (4.10 g, 2.79 mmol) was added, the equipment was flushed with hydrogen and the reaction was stirred under hydrogen atmosphere for 24 h at room temperature and atmospheric pressure. The mixture was filtered through celite and thoroughly washed with EtOH (400 mL) without letting the catalyst run dry. The filtrate was evaporated and the pure product was dissolved in THF (20 mL) and lyophilized to yield **24** (4.00 g, 2.78 mmol, 99.6%) as a white powder.

^{1}H NMR (300 MHz, $CDCl_3$): δ = 6.05 (s, 3H, -CON*H*-), 2.20 (m, 24H, -CH_2CO-), 1.94 (m, 18H, -CH_2CH_2COO-), 1.70 – 1.56 (m, 6H, H_2NCCH_2-), 1.43 (s, 81H, -CH_3), 1.23 (br s, 2H, -NH_2) ppm; **MP:** 186.5 °C; **R_f** (cyclohexane/ethyl acetate 3:2): 0.00 – 0.11.

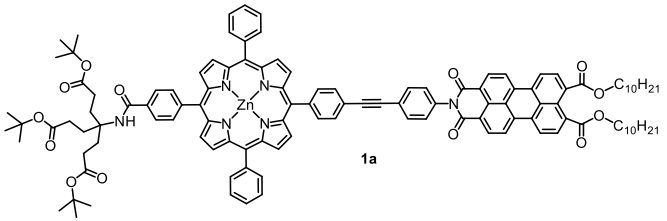

1a

15-(4-((4-(9,10-Bis(decyloxycarbonyl)perylene-3,4-dicarboximid-1-yl)phenyl)-ethynyl)phenyl)-5-(4-(G^1-(tri-*tert*-butylester)amido)phenyl)-10,20-diphenylporphyrinato-Zn(II) (1a). In a 50 mL flask, acid zinc porphyrin–perylene dyad **19** (209.5 mg, 109.8 µmol), amine G^1 triester **21** (86.5 mg, 208 µmol, 1.5 eq) and HOBt·H_2O (27.62 mg, 180.3 µmol, 1.3 eq) were dissolved in DMF (40 mL) and the mixture was cooled to 0 °C. DCC (37.21 mg, 180.3 µmol, 1.3 eq) in DMF (10 mL) was added slowly at 0 °C and the reaction was stirred for 11 d at rt. The DCU was filtered off and washed with THF (3x 30 mL, + 1% HAc); the filtrate was concentrated *in vacuo*. The crude product was purified by column chromatographies (eluents: $CHCl_3$ + 1% acetone, → hexanes/ethyl acetate 1:2, $CHCl_3$/ethyl acetate/acetone 100:10:1, $CHCl_3$/ethyl acetate 3:1). Excess amine G^1 triester **21** could be easily removed; however, it proved difficult to separate the product **1a** from residual **19**. Moreover, $PABE_{10}$ **15** had been partially cleaved under these conditions and had to be separated from the product. The overall yield of pure G^1 perylene porphyrin dyad **1a** was quite low (30.51 mg, 15.99 µmol, 11.5%).

^{1}H NMR (400 MHz, THF-d_8) δ = 8.99 – 8.78 (m, 8H, β-pyrrole-*H*), 8.65 – 8.50 (m, 2H, Per-*H*), 8.50 – 8.42 (m, 2H, Per-*H*), 8.32 – 8.16 (m, 10H, *o*-Ph-*H*, $m_{porphyrin}$-$o_{carboxyl}$-Ph-*H*, $o_{porphyrin}$-$m_{carboxyl}$-Ph-*H*, $o_{porphyrin}$-$m_{ethynyl}$-Ph-*H*), 8.16 – 8.06 (m, 2H, Per-*H*), 7.98 (d, *J* = 7.7 Hz, 2H, $m_{porphyrin}$-$o_{ethynyl}$-Ph-*H*), 7.94 – 7.86 (m, 2H, Per-*H*), 7.83 (d, *J* = 8.0 Hz, 2H, m_{imide}-Ph-*H*), 7.81 – 7.69 (m, 6H, *m/p*-Ph-*H*), 7.54 – 7.43 (m, 2H, o_{imide}-Ph-*H*), 7.33 (s, 1H, -CON*H*-), 4.44 – 4.23 (m, 4H, -Per-COOCH_2-), 2.45 – 2.35 (m, 6H, -CH_2COO-*t*-butyl), 2.29 – 2.17 (m, 6H, -CONHCCH_2-), 1.83 – 1.77 (m, 4H, -Per-COOCH$_2$CH_2-), 1.51 – 1.45 (m, 31H, *t*-butyl-*H*, -Per-COOCH$_2$CH$_2$CH_2-) , 1.45 – 1.22 (m, 24H, -CH_2-), 0.89 (t, *J* = 6.6 Hz, 6H, -CH_3) ppm; **^{13}C NMR** (101 MHz, THF-d_8) δ = 173.24, 167.16, 151.09, 150.75, 144.45, 135.33, 135.04, 132.79, 132.51, 132.07, 131.05, 130.57, 128.17, 127.21, 126.31, 121.73, 120.76, 80.34, 58.78, 32.88, 30.63, 30.44, 30.37, 30.32, 29.59, 28.36, 28.31, 27.02, 23.57, 14.44 ppm; **FT-IR** (diluted, THF): $\tilde{\nu}$ (int.) = 2959 (m), 2926 (m), 2857 (m), 1719 (s), 1701 (s), 1670 (m), 1653 (m), 1636 (w), 1595 (w), 1517 (m), 1507 (m), 1457 (w), 1364 (m), 1339 (w), 1246 (m), 1204 (w), 1151 (s), 1066 (w), 995 (s), 843 (w), 808 (m), 795 (s), 749 (m), 717 (m), 701 (m), 668 (s) cm^{-1}; **UV-Vis** (THF): λ_{max} (ε in L·mol^{-1}cm^{-1}) = 629.5 (10 000), 596.5 (15 000), 556.5 (29 000), 495 (41 000), 425 (587 000), 404 (62 000), 228 (129 000) nm; **MP:** 168.4 °C (decomp.).

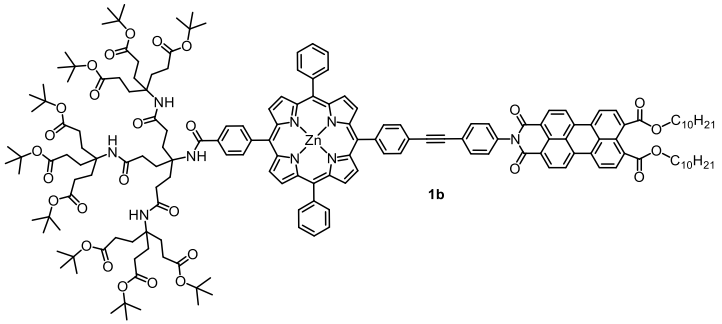

1b

15-(4-((4-(9,10-Bis(decyloxycarbonyl)perylene-3,4-dicarboximid-1-yl)phenyl)-ethynyl)phenyl)-5-(4-(G²-(nona-*tert*-butylester)amido)phenyl)-10,20-diphenylporphyrinato-Zn(II) (1b). In a 50 mL flask, acid zinc porphyrin–perylene dyad **19** (182.3 mg, 120.7 µmol), amine G² nonaester **24** (260.7 mg, 181.1 µmol, 1.5 eq) and HOBt·H_2O (24.03 mg, 156.9 µmol, 1.3 eq) were dissolved in DMF (50 mL) and the mixture was cooled to 0 °C. DCC (32.38 mg, 156.9 µmol, 1.3 eq) in DMF (10 mL) was added slowly at 0 °C and the reaction was stirred for 7 d at rt. The DCU was filtered off and washed with THF (3x 50 mL, + 1% HAc); the filtrate was concentrated *in vacuo*. By column chromatography (eluents: $CHCl_3$ to elute perylene, then ethyl acetate to elute crude product) a mixture of amine G² nonaester **24** and product **1b** was obtained. Further purification *via* GPC (eluent: THF) eluted G² perylene porphyrin dyad **1b** (51.3 mg, 17.5 µmol, 14.5%) and traces of $PABE_{10}$ **15**, which was cleaved during the reaction and in the chromatography steps.

^{1}H NMR (400 MHz, $CDCl_3$): δ = 9.00 – 8.81 (m, 8H, -pyrrole-*H*), 8.64 (d, *J* = 7.8 Hz, 2H, Per-*H*), 8.53 – 8.42 (m, 2H, $m_{porphyrin}$-o_{amide}-Ph-*H*), 8.43 – 8.34 (m, 2H, Per-*H*), 8.30 (s, 2H, $o_{porphyrin}$-m_{amide}-Ph-*H*), 8.27 – 8.17 (m, 6H, *o*-Ph-*H*, Per-*H*), 8.17 – 8.07 (m, 2H, $o_{porphyrin}$-$m_{ethynyl}$-Ph-*H*), 7.98 – 7.91 (m, 2H, $m_{porphyrin}$-$o_{ethynyl}$-Ph-*H*), 7.91 – 7.82 (m, 2H, Per-*H*), 7.82 – 7.69 (m, 6H, *m/p*-Ph-*H*), 7.66 – 7.55 (m, 2H, m_{imide}-Ph-*H*), 7.48 – 7.36 (m, 2H, o_{imide}-Ph-*H*), 6.24 (s, 1H, -N*H*COPh-), 4.35 (t, *J* = 6.7 Hz, 2H, -Per-COOCH_2-), 3.76 – 3.52 (m, 3H, -N*H*COCH_2-), 2.47 – 2.32 (m, 6H, -NHCOCH_2-), 2.34 – 2.12 (m, 18H, *t*-butyl-OCOCH_2-), 2.06 – 1.89 (m, 18H, *t*-butyl-OCOCH$_2$CH_2), 1.87 – 1.77 (m, 4H, -Per-COOCH$_2$CH_2-), 1.72 – 1.57 (m, 6H, -NHCO-CH$_2$CH_2-), 1.47 – 1.43 (m, 4H, -Per-COOCH$_2$CH$_2$CH_2-), 1.40 (s, 81H, *t*-butyl-*H*), 1.37 – 1.20 (m, 12H, -CH_2-), 0.98 – 0.79 (m, 12H, -CH_3) ppm; **^{13}C NMR** (DEPT-135, 101 MHz, $CDCl_3$): δ = 170.07, 128.63, 114.05, 92.89, 66.03, 49.12, 47.71, 34.72, 33.84, 31.90, 30.11, 29.82, 29.33, 29.32, 28.10, 28.05, 26.91, 26.44, 26.01, 25.59, 24.90, 23.41, 22.67, 14.10 ppm; **FT-IR:** $\tilde{\nu}$ (int.) = 3328 (br), 3005 (w), 2977 (m), 2931 (m), 2856 (w), 1728 (s), 1653 (m), 1596 (w), 1539 (m), 1456 (m), 1419 (w), 1392 (m), 1367 (s), 1314 (m), 1255 (m), 1215 (w), 1151 (s), 1103 (m), 1066 (w), 1037 (w), 996 (w), 954 (w), 848 (m), 810 (w), 796 (w), 758 (m), 721 (w) cm^{-1}; **UV-Vis** (THF): λ_{max} (ε in $L \cdot mol^{-1}cm^{-1}$) = 597 (11 000), 556.5 (21 000), 498.5 (61 000), 468.5 (53 000), 425.5 (432 000), 404 (55 000), 228 (113 000) nm.

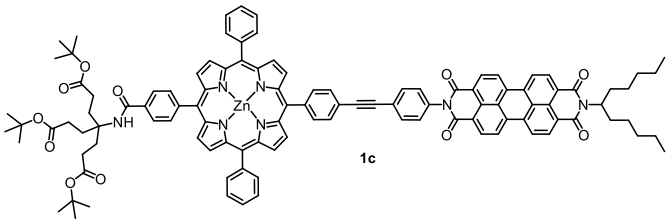

5-(4-(G^1-(tri-*tert*-butylester)amido)phenyl)-15-(4-((4-(*N*-(1-pentylhexyl)-perylene-3,4:9,10-bis(dicarboximid)-1-yl)phenyl)ethynyl)phenyl)-10,20-diphenylporphyrinato-Zn(II) (1c). In a 50 mL flask, acidPh-(Ph$_2$)ZnPor-PEP-PDI$_S$ **19b** (34.9 mg, 25.6 μmol), amine G^1 triester **21** (16.88 mg, 40.62 μmol, 1.6 eq) and HOBt·H$_2$O (5.10 mg, 33.3 μmol, 1.3 eq) were dissolved in DMF (10 mL) at 0 °C. DCC (6.94 mg, 33.6 μmol, 1.3 eq) in DMF (10 mL) was slowly added at 0 °C and the reaction was stirred for 7 d at rt. The mixture was filtered through a plug of silica gel (eluent: chloroform) and the solvents were evaporated *in vacuo*. The crude product was purified by flash column chromatography (SiO_2, eluent: hexanes / ethyl acetate 0 → 50%) to elute product and amine G^1 triester and further purified by a plug of silica gel (eluent: chloroform + 1% acetone) to yield G^1-Ph-(Ph$_2$)ZnPor-PEP-PDI$_S$ **1c** (17.1 mg, 9.70 μmol, 37.9%) as dark red-brown solid.

^{1}H NMR (400 MHz, $CDCl_3$): δ = 9.05 – 8.84 (m, 8H, β-pyrrole-*H*), 8.59 – 8.36 (m, 4H, $m_{porphyrin}$-o_{amide}-Ph-*H*, Per-*H*), 8.35 – 8.14 (m, 10H, *o*-Ph-*H*, $o_{porphyrin}$-m_{amide}-Ph-*H*, $o_{porphyrin}$-$m_{ethynyl}$-Ph-*H*), 8.14 – 8.03 (m, 4H, Per-*H*), 8.03 – 7.94 (m, 2H, $m_{porphyrin}$-$o_{ethynyl}$-Ph-*H*), 7.87 (dd, *J* = 8.4, 2.1 Hz, 2H, m_{imide}-Ph-*H*), 7.84 – 7.72 (m, 6H, *m/p*-Ph-*H*), 7.59 – 7.48 (m, 2H, Per-*H*), 7.39 (d, *J* = 8.0 Hz, 2H, o_{imide}-Ph-*H*), 7.20 (s, 1H, -N*H*-), 5.34 – 4.97 (m, 1H, -Per-NC*H*-), 2.38 (t, *J* = 7.4 Hz, 6H, *t*-butyl-OCOCH_2-), 2.33 – 2.24 (m, 2H, -Per-NCHCH_a-), 2.24 – 2.13 (m, 6H, *t*-butyl-OCOCHCH_2-), 1.88 (dd, *J* = 13.6, 6.5 Hz, 2H, -Per-NCHCH_b-), 1.48 (s, 27H, *t*-butyl-*H*), 1.39 – 1.18 (m, 12H, -CH_2-), 0.86 (t, *J* = 6.7 Hz, 6H, -CH_3) ppm; **^{13}C NMR** (101 MHz, {^{1}H}^{13}C and DEPT-135, $CDCl_3$): δ = 173.35 (C), 167.02 (C), 163.36 (C), 150.42 (C), 150.37 (C), 150.01 (C), 149.97 (C), 149.89 (C), 146.17 (C), 143.27 (C), 142.85 (C), 135.04 (C), 134.63 (CH), 134.28 (C), 133.85 (C), 133.02 (CH), 132.85 (CH), 132.39, 131.88 (br, CH), 131.62 (CH), 130.14 (CH), 129.06, 127.70 (CH), 126.75 (CH), 126.12, 125.45 (CH), 125.35 (CH), 124.26 (C), 123.10 (CH), 122.88, 122.73 (CH), 122.46, 122.07, 121.44, 120.37, 120.04, 107.87, 104.51, 90.70, 89.92, 81.04, 68.60, 58.19 (C), 54.95 (CH), 32.45 (CH_2) , 31.93 (CH_2) , 31.90 (CH_2) , 30.42 (CH_2) , 30.16 (CH_2) , 28.26 (CH_3) , 26.81 (CH_2) , 22.73 (CH_2) , 14.22 (CH_3) ppm; **FT-IR:** $\tilde{\nu}$ (int.) = 3370 (br), 3056 (w), 2976 (m), 2953 (s), 2926 (s), 2858 (m), 1723 (s), 1709 (s), 1695 (s), 1656 (s), 1593 (s), 1581 (m), 1516 (m), 1489 (m), 1460 (w), 1405 (w), 1367 (m), 1340 (s), 1313 (w), 1253 (s), 1205 (w), 1151 (s), 1104 (m), 1070 (m), 1037 (w), 995 (s), 963 (w), 844 (m), 825 (m), 810 (s), 796 (s), 756 (m), 747 (m), 718 (m), 703 (m), 668 (w) cm^{-1}; **UV-Vis** (THF): λ_{max} (ε in L·mol^{-1}cm^{-1}) = 595.5(18 000), 556.5 (39 000), 522 (76 000), 486.5 (49 000),

454.5 (25 000), 425 (640 000), 405 (61 000), 227 (82 000) nm; **MS (APPI)**: m/z for $C_{110}H_{101}N_7O_{11}Zn$ $[M]^+$ calcd: 1759.6851, found: 1759.6971.

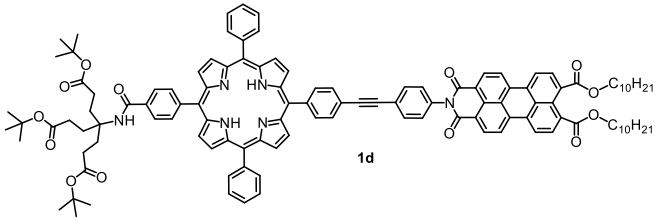

1d

15-(4-((4-(9,10-Bis(decyloxycarbonyl)perylene-3,4-dicarboximid-1-yl)phenyl)-ethynyl)phenyl)-5-(4-(G^1-(tri-*tert*-butylester)amido)phenyl)-10,20-diphenylporphyrin (1d). In a 50 mL flask, acid porphyrin–perylene dyad **19c** (64.9 mg, 44.9 µmol), amine G^1 triester **21** (22.37 mg, 53.82 µmol, 1.2 eq) and HOBt·H_2O (11.0 mg, 71.8 µmol, 1.6 eq) were dissolved in DMF (20 mL) at 0 °C. DCC (15.0 mg, 72.7 µmol, 1.6 eq) in DMF (10 mL) was slowly added at 0 °C and the reaction was stirred for 1 d at rt and 4 d at 80 °C. The solvent was evaporated *in vacuo* and the crude product was purified *via* short column chromatography (eluent: THF/hexanes 1:1) and GPC (eluent: THF). A fraction of pure product **1d** (30.2 mg, 16.4 µmol, 36.5%) and a second fraction of **1d** (29.7 mg, 16.1 µmol, 35.9%) with partially cleaved $PABE_{10}$ **17** were obtained (overall yield: 59.9 mg, 32.5 µmol, 72.4%).

^{1}H NMR (400 MHz, $CDCl_3$): δ = 8.92 – 8.78 (m, 8H, β-pyrrole-*H*), 8.70 (d, *J* = 8.0 Hz, 2H, Per-*H*), 8.59 – 8.48(m, 4H, Per-*H*), 8.30 – 8.18 (m, 10H, $m_{porphyrin}$-$o_{carboxyl}$-Ph-*H*, $o_{porphyrin}$-$m_{carboxyl}$-Ph-*H*, *o*-Ph-*H*, Per-*H*), 8.16 (d, *J* = 7.8 Hz, 2H, $o_{porphyrin}$-$m_{ethynyl}$-Ph-*H*), 7.98 (d, *J* = 8.1 Hz, 2H, $m_{porphyrin}$-$o_{ethynyl}$-Ph-*H*), 7.88 (dd, *J* = 8.4, 2.0 Hz, 2H, m_{imide}-Ph-*H*), 7.83 – 7.73 (m, 6H, *m/p*-Ph-*H*), 7.45 (d, *J* = 8.4 Hz, 2H, o_{imide}-Ph-*H*), 7.32 (s, 1H, -CON*H*-), 4.36 (t, *J* = 6.7 Hz, 4H, -Per-COOCH_2-), 2.47 (t, *J* = 7.6 Hz, 6H, -CH_2COO-*t*-butyl), 2.29 (t, *J* = 8.0 Hz, 6H, -CONHCCH_2-), 1.82 (t, *J* = 7.4 Hz, 4H, -Per-COOCH$_2$CH_2-), 1.50 (s, 27H, *t*-butyl-*H*), 1.41 – 1.21 (m, 28H, -CH_2-), 0.94 – 0.79 (m, 6H, -CH_3), -2.77 (s, 2H, Por-N*H*) ppm; **FT-IR:** $\tilde{\nu}$ (int.) = 3381 (w), 3313 (w), 3060 (w), 2957 (m), 2923 (s), 2852 (s), 1724 (s), 1704 (s), 1665 (s), 1593 (m), 1516 (m), 1498 (ws), 1456 (m), 1414 (w), 1392 (w), 1365 (m), 1296 (w), 1259 (s), 1150 (s), 1094 (s), 1062 (s), 1020 (s), 966 (m), 845 (m), 798 (s), 748 (w), 730 (m), 701 (m), 668 (w) cm^{-1}; **UV-Vis** (THF): λ_{max} (ε in $L{\cdot}mol^{-1}cm^{-1}$) = 647 (3 000), 591 (3 000), 549 (8 000), 504.5 (39 000), 471.5 (26 000), 418.5 (349 000), 400 (70 000), 226.5 (54 000) nm; **MS (MALDI)**: m/z for $C_{119}H_{122}N_6O_{13}$ $[M]^+$ calcd: 1842.9070, found: 1843.009; **MP:** 189.4 °C (decomp.).

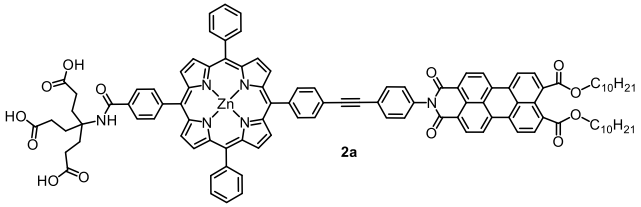

2a

5-(4-(G^1-(triacid)amido)phenyl)-15-(4-((4-(9,10-bis(decyloxycarbonyl)perylene-3,4-dicarboximid-1-yl)phenyl)ethynyl)phenyl)-10,20-diphenylporphyrinato-Zn(II) (2a). In a 50 mL flask, G^1-porphyrin-PEP-PIBE$_{10}$ **1a** (13.2 mg, 6.92 µmol) was dissolved in formic acid (10 mL). The reaction was stirred for 2 d and the solvent was removed *in vacuo* at 40 °C. Toluene (2x 100 mL) was added to remove the formic acid azeotropically. The crude product was filtered through a plug of celite and washed with water (500 mL), EtOH (200 mL), and CH_2Cl_2 (200 mL). Pure product **2a** (10.7 mg, 6.15 µmol, 88.9%) was eluted with THF (200 mL, +1% acetic acid).

^{1}H NMR (400 MHz, THF-d_8+TFA-d) δ = 9.68 (s, 3H, acid-H [+TFA-H]), 9.12 – 6.72 (m, 39H, aromatic H [porphyrin, phenyl, perylene] + NH), 4.29 (d, J = 27.5 Hz, 4H, -Per-COOCH_2-), 2.49 (d, J = 14.2 Hz, 6H, -CH_2COOH), 2.31 (s, 6H, -CH_2CH$_2$COOH), 2.18 (d, J = 6.5 Hz, 2H, -Per-COOCH_2-), 1.84 (d, J = 31.8 Hz, 4H, -Per-COOCH$_2$CH_2-), 1.62 – 1.10 (m, 24H, -CH$_2$-), 0.88 (t, J = 6.3 Hz, 6H, -CH$_3$) ppm; **^{13}C NMR** (DEPT-135, 101 MHz, THF-d_8+TFA-d): δ = 134.77, 134.71, 132.39, 132.26, 131.95, 131.54, 129.96, 129.73, 129.02, 128.36, 128.22, 127.20, 126.66, 125.77, 123.28, 122.39, 65.64, 57.41, 37.16, 34.60, 32.31, 30.17, 30.00, 29.80, 29.75, 29.03, 28.37, 27.44, 27.21, 26.45, 24.52, 24.33, 22.99, 19.71, 13.85 ppm; **^{13}C NMR** (101 MHz, THF-d_8+TFA-d): δ = 175.00, 159.38*, 158.99*, 158.58*, 158.18*, 151.00, 150.62, 149.79, 140.71, 135.22, 134.90, 133.15, 132.74, 132.68, 132.27, 132.01, 131.26, 130.50, 130.41, 130.19, 129.85, 129.74, 129.07, 128.43, 128.27, 128.06, 127.28, 127.10, 126.20, 120.25*, 117.40*, 114.55*, 111.70*, 103.82, 87.68, 67.79, 67.57, 67.34, 32.63, 30.39, 30.33, 30.13, 30.07, 29.33, 28.65, 27.74, 26.76, 25.58, 25.37, 25.17, 24.95, 24.75, 24.47, 23.31, 20.03, 14.16 ppm (* = signals of TFA); **FT-IR:** $\tilde{\nu}$ (int.) = 3333 (br), 2957 (w), 2925 (m), 2854 (m), 1668 (s), 1539 (m), 1436 (m), 1410 (m), 1366 (w), 1320 (m), 1281 (m), 1186 (s), 1135 (s), 1054 (m), 1015 (w), 930 (w), 878 (w), 841 (m), 799 (s), 722 (s) cm^{-1}; **UV-Vis** (THF): λ_{max} (qualitative) = 646.5, 592.5, 550, 520, 485.5, 419, 401, 311 nm.

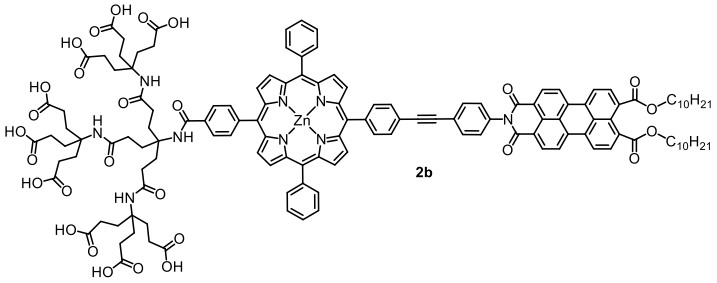

5-(4-(G²-(nonaacid)amido)phenyl)-15-(4-((4-(9,10-bis(decyloxycarbonyl)-perylene-3,4-dicarboximid-1-yl)phenyl)ethynyl)phenyl)-10,20-diphenylporphyrinato-Zn(II) (2b). In a 50 mL flask, G^2-porphyrin-PEP-$PIBE_{10}$ **1b** (33.2 mg, 4.94 μmol) was dissolved in formic acid (10 mL). The reaction was stirred for 2 d and the solvent was removed *in vacuo* at 40 °C. Toluene (2x 100 mL) was added to remove the formic acid azeotropically. The crude product was filtered through a plug of celite and washed with water (500 mL), EtOH (200 mL), and CH_2Cl_2 (200 mL). Pure product **2b** (12.0 mg, 4.94 μmol, 43.7%) was eluted with THF (200 mL, +1% acetic acid).

^{1}H NMR (400 MHz, THF-d_8+TFA-d): δ = 8.97 – 6.13 (m, 48H, acid-H [+TFA-H], aromatic H [porphyrin, phenyl, perylene] + -N*H*COPh-), 4.31 (m, 4H, -Per-COOC*H*$_2$-), 2.45 (m, 6H, -NHCOC*H*$_2$-), 2.24 (m, 18H, -C*H*$_2$COOH), 2.14 – 1.94 (m, 18H, -C*H*$_2$CH$_2$COOH), 1.92-1.84 (m, 6H, -NHCOCH$_2$C*H*$_2$-, overlapped by traces of acetic acid at 1.88 ppm), 1.67 – 1.01 (m, 28H, -C*H*$_2$-), 0.87 (d, J = 6.8 Hz, 6H, -CH$_3$) ppm [the residual three -N*H*COCH$_2$- are probably covered by the THF solvent signal at 3.58 ppm]; **FT-IR:** $\tilde{\nu}$ (int.) = 3268 (br), 2957 (w), 2925 (m), 2853 (m), 1663 (s), 1594 (s), 1543 (s), 1437 (m), 1414 (m), 1634 (w), 1274 (m), 1190 (s), 1137 (s), 1069 (w), 1012 (w), 984 (w), 879 (w), 844 (m), 796 (s), 723 (s), 700 (w) cm^{-1}; **UV-Vis** (THF): λ_{max} (qualitative) = 599, 557, 512, 472.5, 424 nm.

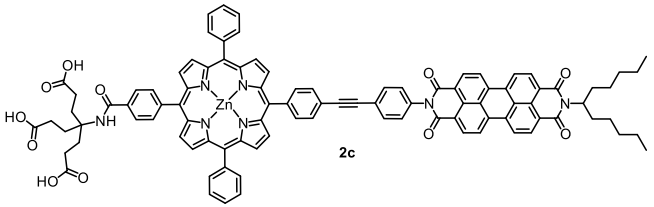

5-(4-(G^1-(triacid)amido)phenyl)-15-(4-((4-(*N*-(1-pentylhexyl)perylene-3,4:9,10-bis(dicarboximid)-1-yl)phenyl)ethynyl)phenyl)-10,20-diphenylporphyrinato-Zn(II) (2c). In a 50 mL flask, G^1-porphyrin-PEP-PDI$_S$ **1c** (14.9 mg, 8.45 µmol) was dissolved in formic acid (10 mL). The reaction was stirred for 5 d and the solvent was removed *in vacuo* at 40 °C. Toluene (2x 100 mL) was added to remove the formic acid azeotropically. The crude product was filtered through a plug of celite and washed with water (300 mL), EtOH (150 mL), and CH_2Cl_2 (150 mL). Pure product **2c** (11.5 mg, 7.21 µmol, 85.3%) was eluted with THF (250 mL, +1% acetic acid).

^{1}H NMR (400 MHz, THF-d_8): δ = 9.42 – 6.92 (m, 39H, aromatic H [porphyrin, phenyl, perylene] + -N*H*), 5.22 (s, 1H, -Per-NC*H*-), 4.15 (br s, 1H, acid-H [+TFA-H]), 2.56 – 2.42 (m, 6H, -C*H*$_2$COOH), 2.43 – 2.24 (m, 6H, -C*H*$_2$CH$_2$COOH,), 2.18 (dt, *J* = 18.8, 7.8 Hz, 2H, -Per-NCHC*H*$_a$-), 1.97 – 1.83 (m, 2H, -Per-NCHC*H*$_b$-), 1.52 – 1.16 (m, 12H, -CH$_2$-), 1.04 – 0.74 (m, 6H, -C*H*$_3$) ppm; **^{13}C NMR** (DEPT-135, 101 MHz, THF-d_8+TFA-*d*): δ = 138.65, 138.58, 138.53, 138.47, 137.11, 137.09, 136.98, 136.68, 133.00, 129.00, 128.75, 128.54, 127.82, 127.46, 127.20, 123.75, 123.71, 121.06, 49.58, 43.64, 33.62, 30.14, 28.35, 25.83, 25.21, 24.75, 19.68 ppm; **FT-IR:** $\tilde{\nu}$ (int.) = 3214 (br), 3052 (w), 2954 (m), 2923 (m), 2850 (m), 1696 (s), 1654 (s), 1592 (s), 1517 (w), 1491 (w), 1460 (w), 1404 (w), 1341 (m), 1314 (w), 1278 (m), 1258 (m), 1176 (s), 1137 (s), 1098 (s), 1012 (m), 879 (w), 796 (s), 746 (w), 719 (m), 699 (m) cm^{-1}; **UV-Vis** (THF): λ_{max} (qualitative) = 603, 564, 533, 498, 464.5, 432 nm.

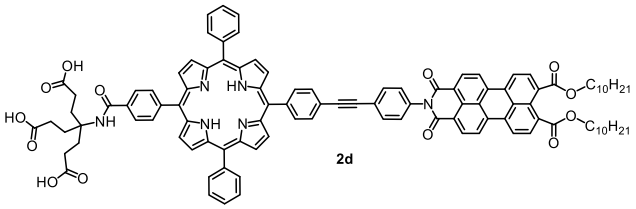

2d

5-(4-(G^1-(triacid)amido)phenyl)-15-(4-((4-(9,10-bis(decyloxycarbonyl)perylene-3,4-dicarboximid-1-yl)phenyl)ethynyl)phenyl)-10,20-diphenylporphyrin (2d). In a 50 mL flask was dissolved G^1-porphyrin-PEP-PIBE$_{10}$ **1d** (28.3 mg, 15.3 µmol) in formic acid (15 mL). The green solution was stirred for 3 d and the solvent was removed *in vacuo* at 40 °C. Toluene (3x 50 mL) was added to remove the formic acid azeotropically. The crude product was filtered through a plug of celite and washed with water (300 mL +1% acetic acid), EtOH (150 mL), and CH_2Cl_2 (150 mL). Reasonably pure product was eluted with THF (250 mL, +1% acetic acid). Precipitation by addition of hexanes led to **2d** (18.0 mg, 10.7 µmol, 70.0%) as dark brown/purple solid.

^{1}H NMR (400 MHz, THF-d_8+TFA-d): δ = 9.11 – 6.79 (m, 39H, aromatic H [porphyrin, phenyl, perylene] + -N*H*), 4.30 (dd, J = 20.2, 5.5 Hz, 4H, -Per-COOC*H*$_2$-), 2.63 (br s, 3H, acid-H [+TFA-H]), 2.51 – 2.41 (m, 6H, -C*H*$_2$COOH), 2.32 (dt, J = 16.6, 5.6 Hz, 6H, -C*H*$_2$CH$_2$COOH), 2.20 (t, J = 7.4 Hz, 4H, -Per-COOCH$_2$C*H*$_2$-), 1.66 – 1.00 (m, 24H*, -CH$_2$-), 1.00 – 0.74 (m, 6H*, -CH$_3$), -2.71 (s, 2H, Por-NH) ppm [*traces of hexanes are still present]; **FT-IR:** $\tilde{\nu}$ (int.) = 3295 (br), 3056 (w), 2954 (m), 2918 (s), 2850 (s), 1705 (s), 1663 (m), 1595 (m), 1540 (w), 1517 (w), 1457 (m), 1405 (m), 1363 (m), 1261 (s), 1171 (s), 1157 (s), 1098 (s), 1066 (s), 1021 (m), 966 (m), 879 (w), 853 (w), 799 (s), 748 (m), 720 (s), 699 (s) cm^{-1}; **UV-Vis** (THF): λ_{max} (qualitative) = 649, 591, 522, 517.5, 478.5, 418 nm; **MS (ESI+)**: m/z for $C_{107}H_{99}N_6O_{13}$ $[M+H]^+$ calcd: 1675.7238, found: 1675.7265 (err: 1.6 ppm).

8 List of Figures, Tables and Schemes

Figures

Tables

Schemes

9 References

1 S. J. Williams, *What Your Atheist Professor Doesn't Know (But Should)*, CreateSpace Independent Publishing Platform, **2013**.
2 R. Lemberg, *Porphyrins in Nature* in *Progress in the Chemistry of Organic Natural Products* (Ed.: L. Zechmeister), Springer, Vienna, **1954**, pp. 299-349.
3 J. Barona-Castaño, C. Carmona-Vargas, T. Brocksom, K. de Oliveira, *Molecules* **2016**, *21*, 310-336.
4 M. Senge, A. Ryan, K. Letchford, S. MacGowan, T. Mielke, *Symmetry* **2014**, *6*, 781-843, publication licensed under CreativeCommons (cc by-nc-sa 3.0).
5 D. Werck-Reichhart, R. Feyereisen, *Genome Biol.* **2000**, *1*, reviews3003, 1-6.
6 S. Lin, C. S. Diercks, Y.-B. Zhang, N. Kornienko, E. M. Nichols, Y. Zhao, A. R. Paris, D. Kim, P. Yang, O. M. Yaghi, C. J. Chang, *Science* **2015**, *349*, 1208-1213.
7 A. R. Battersby, E. McDonald, *Acc. Chem. Res.* **1979**, *12*, 14-22.
8 S. Shanmugathasan, C. Edwards, R. W. Boyle, *Tetrahedron* **2000**, *56*, 1025-1046.
9 H. Scheer, J. J. Katz, *Nuclear magnetic resonance spectroscopy of porphyrins and metalloporphyrins* in *Porphyrins and Metalloporphyrins* (Eds.: J. E. Falk, K. M. Smith), Elsevier, Amsterdam, **1975**, pp. 399-524.
10 A. Butler, Master Thesis, Talladega College (Athens, Georgia), **1999**.
11 P. Martin, M. Mueller, D. Flubacher, A. Boudier, H.-U. Blaser, D. Spielvogel, *Org. Process Res. Dev.* **2010**, *14*, 799-804.
12 R. Bonnett, *Chem. Soc. Rev.* **1995**, *24*, 19-33.
13 E. Fagadar-Cosma, V. Dana, M. I. Birdeanu, G. Fagadar-Cosma, *Arab. J. Chem.* **2014**, *36*, in press, https://doi.org/10.1016/j.arabjc.2014.10.011.
14 M. Jurow, A. E. Schuckman, J. D. Batteas, C. M. Drain, *Coord. Chem. Rev.* **2010**, *254*, 2297-2310.
15 S. Prathapan, S. I. Yang, J. Seth, M. A. Miller, D. F. Bocian, D. Holten, J. S. Lindsey, *J. Phys. Chem. B* **2001**, *105*, 8237-8248.
16 M. J. Crossley, P. L. Burn, *J. Chem. Soc., Chem. Commun.* **1991**, 1569-1571.
17 R. Takahashi, Y. Kobuke, *J. Am. Chem. Soc.* **2003**, *125*, 2372-2373.
18 M. Wolf, A. Herrmann, A. Hirsch, D. M. Guldi, *J. Am. Chem. Soc.* **2017**, *139*, 11779-11788.
19 A. Yella, H.-W. Lee, H. N. Tsao, C. Yi, A. K. Chandiran, M. K. Nazeeruddin, E. W.-G. Diau, C.-Y. Yeh, S. M. Zakeeruddin, M. Grätzel, *Science* **2011**, *334*, 629-634.
20 N.-n. Zhang, Y.-q. Feng, Y.-c. Li, X. Peng, C.-z. Gu, X.-d. Xue, J.-y. Yan, Q.-l. Chen, X.-g. Li, B. Zhang, *New J. Chem.* **2013**, *37*, 1134-1141.
21 A. R. Battersby, *Science* **1994**, *264*, 1551-1557.
22 O. zu Stolberg-Wernigerode, *Neue deutsche Biographie, Vol. 5 (Falck - Fyner)*, Berlin, **1961**.
23 P. Rothemund, *J. Am. Chem. Soc.* **1935**, *57*, 2010-2011.
24 A. D. Adler, F. R. Longo, J. D. Finarelli, J. Goldmacher, J. Assour, L. Korsakoff, *J. Org. Chem.* **1967**, *32*, 476.
25 G. R. Geier, J. S. Lindsey, *J. Chem. Soc., Perkin Trans. 2* **2001**, 677-686.
26 G. R. Geier, Y. Ciringh, F. Li, D. M. Haynes, J. S. Lindsey, *Org. Lett.* **2000**, *2*, 1745-1748.
27 B. J. Littler, Y. Ciringh, J. S. Lindsey, *J. Org. Chem.* **1999**, *64*, 2864-2872.
28 F. Li, Y. Kexin, J. S. Tyhonas, K. A. MacCrum, J. S. Lindsey, *Tetrahedron* **1997**, *53*, 12339-12360.
29 J. S. Lindsey, J. N. Woodford, *Inorg. Chem.* **1995**, *34*, 1063-1069.
30 J. S. Lindsey, K. A. MacCrum, J. S. Tyhonas, Y. Y. Chuang, *J. Org. Chem.* **1994**, *59*, 579-587.
31 R. W. Wagner, D. S. Lawrence, J. S. Lindsey, *Tetrahedron Lett.* **1987**, *28*, 3069-3070.
32 J. S. Lindsey, I. C. Schreiman, H. C. Hsu, P. C. Kearney, A. M. Marguerettaz, *J. Org. Chem.* **1987**, *52*, 827-836.
33 J. S. Lindsey, H. C. Hsu, I. C. Schreiman, *Tetrahedron Lett.* **1986**, *27*, 4969-4970.
34 T. D. Lash, *J. Porphyr. Phthalocyanines* **2016**, *20*, 855-888.

35 I. P. Beletskaya, V. S. Tyurin, A. Uglov, C. Stern, R. Guilard, *Survey of Synthetic Routes for Synthesis and Substitution in Porphyrins* in *Handbook of Porphyrin Science*, World Scientific Publishing Company, **2012**, p. 190ff.

36 G. P. Arsenault, E. Bullock, S. F. MacDonald, *J. Am. Chem. Soc.* **1960**, *82*, 4384-4389.

37 D. T. Gryko, M. Tasior, *Tetrahedron Lett.* **2003**, *44*, 3317-3321.

38 J. K. Laha, S. Dhanalekshmi, M. Taniguchi, A. Ambroise, J. S. Lindsey, *Org. Process Res. Dev.* **2003**, *7*, 799-812.

39 C. Brückner, Y. Zhang, S. J. Rettig, D. Dolphin, *Inorg. Chim. Acta* **1997**, *263*, 279-286.

40 P. D. Rao, S. Dhanalekshmi, B. J. Littler, J. S. Lindsey, *J. Org. Chem.* **2000**, *65*, 7323-7344.

41 C.-H. Lee, F. Li, K. Iwamoto, J. Dadok, A. A. Bothner-By, J. S. Lindsey, *Tetrahedron* **1995**, *51*, 11645-11672.

42 B. J. Littler, M. A. Miller, C.-H. Hung, R. W. Wagner, D. F. O'Shea, P. D. Boyle, J. S. Lindsey, *J. Org. Chem.* **1999**, *64*, 1391-1396.

43 R. de Paula, M. A. F. Faustino, D. C. G. A. Pinto, M. G. P. M. S. Neves, J. A. S. Cavaleiro, *J. Heterocycl. Chem.* **2008**, *45*, 453-459.

44 H. Furuta, T. Asano, T. Ogawa, *J. Am. Chem. Soc.* **1994**, *116*, 767-768.

45 S. Taniguchi, H. Hasegawa, M. Nishimura, M. Takahashi, *Synlett* **1999**, *1999*, 73-74.

46 J. S. Lindsey, *Acc. Chem. Res.* **2009**, *43*, 300-311.

47 C. B. Nielsen, F. C. Krebs, *Tetrahedron Lett.* **2005**, *46*, 5935-5939.

48 H. Sharghi, A. Hassani Nejad, *Tetrahedron* **2004**, *60*, 1863-1868.

49 J. S. Manka, D. S. Lawrence, *Tetrahedron Lett.* **1989**, *30*, 6989-6992.

50 C. D. Methfessel, Master Thesis, Friedrich-Alexander University Erlangen-Nürnberg (Erlangen), **2012**.

51 K. M. Kadish, K. M. Smith, R. Guilard, *The Porphyrin Handbook*, Academic Press, San Diego, **2000**.

52 M. Taniguchi, J. S. Lindsey, *Enumeration of Isomers of Substituted Tetrapyrrole Macrocycles: From Classical Problems in Biology to Modern Combinatorial Libraries* in *Handbook of Porphyrin Science, Vol. 23*, World Scientific Publishing Company, **2012**, pp. 1-80.

53 G. Pólya, *Acta Math.* **1937**, *68*, 145-254.

54 E. J. Tarlton, S. F. MacDonald, E. Baltazzi, *J. Am. Chem. Soc.* **1960**, *82*, 4389-4395.

55 A. M. d'A. Rocha Gonsalves, M. M. Pereira, *J. Heterocycl. Chem.* **1985**, *22*, 931-933.

56 A. N. Cammidge, O. Öztürk, *Tetrahedron Lett.* **2001**, *42*, 355-358.

57 D. K. Dogutan, M. Ptaszek, J. S. Lindsey, *J. Org. Chem.* **2008**, *73*, 6187-6201.

58 R. Lucas, J. Vergnaud, K. Teste, R. Zerrouki, V. Sol, P. Krausz, *Tetrahedron Lett.* **2008**, *49*, 5537-5539.

59 D. K. Dogutan, S. H. H. Zaidi, P. Thamyongkit, J. S. Lindsey, *J. Org. Chem.* **2007**, *72*, 7701-7714.

60 J. S. Lindsey, M. Taniguchi, A. Balakumar, D. Fan, *Methods and Intermediates for the Synthesis of Porphyrins*, Pat. No. US2007027312 (A1), **2007**.

61 I. Tabushi, K.-i. Sakai, K. Yamamura, *Tetrahedron Lett.* **1978**, *19*, 1821-1824.

62 D. K. Dogutan, M. Ptaszek, J. S. Lindsey, *J. Org. Chem.* **2007**, *72*, 5008-5011.

63 D. S. Sharada, A. Z. Muresan, K. Muthukumaran, J. S. Lindsey, *J. Org. Chem.* **2005**, *70*, 3500-3510.

64 S. I. Tamaru, L. Yu, W. J. Youngblood, K. Muthukumaran, M. Taniguchi, J. S. Lindsey, *J. Org. Chem.* **2004**, *69*, 765-777.

65 A. Reinhart, Dissertation, Ruprecht-Karls-Universität (Heidelberg), **2009**.

66 T. Laue, A. Plagens, *Namen-und Schlagwort-Reaktionen der Organischen Chemie*, 5th ed., Vieweg+Teubner, GWV Fachverlage, Wiesbaden, **2009**, pp. 330-332.

67 C. M. Drain, X. Gong, *Chem. Commun.* **1997**, 2117-2118.

68 B. Boëns, P.-A. Faugeras, J. Vergnaud, R. Lucas, K. Teste, R. Zerrouki, *Tetrahedron* **2010**, *66*, 1994-1996.

69 A. Bohnen, K. H. Koch, W. Lüttke, K. Müllen, *Angew. Chem.* **1990**, *102*, 548-550.

70 R. Scholl, C. Seer, R. Weitzenböck, *Ber. Dtsch. Chem. Ges.* **1910**, *43*, 2202-2209.

71 Z. Wang, *Comprehensive Organic Name Reactions and Reagents*, 1st ed., John Wiley & Sons, New Jersey, **2009**, pp. 2518-2521.

72 A. Mathey, W. van Roy, L. van Vaeck, G. Eckhardt, W. Steglich, *Rapid Commun. Mass Spectrom.* **1994**, *8*, 46-52.
73 J. W. Cook, C. L. Hewett, I. Hieger, *J. Chem. Soc.* **1933**, 395-405.
74 X.-J. Luo, S.-J. Chen, B.-X. Mai, Q.-S. Yang, G.-Y. Sheng, J.-M. Fu, *Environ. Pollut.* **2006**, *139*, 9-20.
75 P. Sotero, R. Arce, *J. Photochem. Photobiol., A* **2008**, *199*, 14-22.
76 J. C. Fetzer, J. R. Kershaw, *Fuel* **1995**, *74*, 1533-1536.
77 C. D. Schmidt, Master Thesis, Friedrich-Alexander University Erlangen-Nürnberg (Erlangen), **2006**.
78 H. Langhals, *Heterocycles* **1995**, *40*, 477-500.
79 H. Langhals, W. Lona, *Eur. J. Org. Chem.* **1998**, *1998*, 847-851.
80 H. Langhals, *Helv. Chim. Acta* **2005**, *88*, 1309-1343.
81 S. Berngruber, Dissertation, Friedrich-Alexander University Erlangen-Nürnberg (Erlangen), **2014**.
82 T. Weil, T. Vosch, J. Hofkens, K. Peneva, K. Müllen, *Angew. Chem. Int. Ed.* **2010**, *49*, 9068-9093.
83 F. Süßmeier, H. Langhals, *Eur. J. Org. Chem.* **2001**, *2001*, 607-610.
84 H. Langhals, *Chem. Ber.* **1985**, *118*, 4641-4645.
85 A. Rademacher, S. Märkle, H. Langhals, *Chem. Ber.* **1982**, *115*, 2927-2934.
86 F. Würthner, *Chem. Commun.* **2004**, 1564-1579.
87 K. Peneva, Dissertation, Johannes Gutenberg Universität (Mainz), **2008**.
88 R. Wang, Z. Shi, C. Zhang, A. Zhang, J. Chen, W. Guo, Z. Sun, *Dyes Pigm.* **2013**, *98*, 450-458.
89 C. Huang, S. Barlow, S. R. Marder, *J. Org. Chem.* **2011**, *76*, 2386-2407.
90 H. Zhao, Y.-y. Zhang, H. Xu, Z.-m. He, Z.-L. Zhang, H.-q. Zhang, *Tetrahedron* **2015**, *71*, 7752-7757.
91 S. K. Lee, Y. Zu, A. Herrmann, Y. Geerts, K. Müllen, A. J. Bard, *J. Am. Chem. Soc.* **1999**, *121*, 3513-3520.
92 Y. Nagao, T. Misono, *Bull. Chem. Soc. Jpn.* **1981**, *54*, 1191-1194.
93 H. Kaiser, J. Lindner, H. Langhals, *Chem. Ber.* **1991**, *124*, 529-535.
94 S. Berngruber, Diploma thesis, Friedrich-Alexander University Erlangen-Nürnberg (Erlangen), **2010**.
95 H. Tröster, *Dyes Pigm.* **1983**, *4*, 171-177.
96 Y. Nagao, T. Naito, Y. Abe, T. Misono, *Dyes Pigm.* **1996**, *32*, 71-83.
97 Y. Nagao, T. Misono, *Dyes Pigm.* **1984**, *5*, 171-188.
98 J. Kelber, H. Bock, O. Thiebaut, E. Grelet, H. Langhals, *Eur. J. Org. Chem.* **2011**, *2011*, 707-712.
99 X. Mo, H.-Z. Chen, M.-M. Shi, M. Wang, *Chem. Phys. Lett.* **2006**, *417*, 457-460.
100 C. Xue, R. Sun, R. Annab, D. Abadi, S. Jin, *Tetrahedron Lett.* **2009**, *50*, 853-856.
101 X. Mo, M.-M. Shi, J.-C. Huang, M. Wang, H.-Z. Chen, *Dyes Pigm.* **2008**, *76*, 236-242.
102 V. Kunz, V. Stepanenko, F. Würthner, *Chem. Commun.* **2015**, *51*, 290-293.
103 W. Herbst, K. Hunger, G. Wilker, *Industrial organic pigments: Production, properties, applications*, 3rd ed., Wiley-VCH, Weinheim, **2004**.
104 H. Zollinger, *Color chemistry: syntheses, properties, and applications of organic dyes and pigments*, John Wiley & Sons, New Jersey, **2003**.
105 H. Langhals, *Anal. Bioanal. Chem.* **2002**, *374*, 573-578.
106 M. Greene, *Perylene Pigments* in *High Performance Pigments*, 2nd ed. (Eds.: E. B. Faulkner, R. J. Schwartz), Wiley-VCH, Weinheim, **2009**.
107 the pictures were obtained from the following suppliers to present an overview on typical industrial applications of perylene pigments: https://kingsframingandartgallery.com, https://okchem.com, https://autoblog.com.
108 S. Demmig, H. Langhals, *Chem. Ber.* **1988**, *121*, 225-230.
109 G. Geissler, H. Remy (Farbwerke Hoechst A.-G.), *Verfahren zur Herstellung von Fluoreszenzfarbstoffen*, Pat. No. DE 1130099, **1962**.
110 P. M. Montes Navajas, Academic Thesis, Universitat Politècnica de València (València, Spain), **2017**.
111 H. Langhals, C. Dietl, A. Zimpel, P. Mayer, *J. Org. Chem.* **2012**, *77*, 5965-5970.
112 S. Ponader, K. Rosenlehner, E. Vairaktaris, C. Wilmowsky, K. A. Schlegel, F. W. Neukam, C. D. Schmidt, T. Schunk, A. Hirsch, E. Nkenke, *J. Mater. Sci.: Mater. Med.* **2009**, *20*, 2455-2463.

113 T. Heek, J. Nikolaus, R. Schwarzer, C. Fasting, P. Welker, K. Licha, A. Herrmann, R. Haag, *Bioconjug. Chem.* **2013**, *24*, 153-158.
114 M. K. Brennaman, M. R. Norris, M. K. Gish, E. M. Grumstrup, L. Alibabaei, D. L. Ashford, A. M. Lapides, J. M. Papanikolas, J. L. Templeton, T. J. Meyer, *J. Phys. Chem. Lett.* **2015**, *6*, 4736-4742.
115 D. Rolland, J. C. Brauer, L. Hartmann, L. Biniek, M. Brinkmann, N. Banerji, H. Frauenrath, *J. Mater. Chem. C* **2017**, *5*, 1383-1393.
116 C. Li, H. Wonneberger, *Adv. Mater.* **2012**, *24*, 613-636.
117 L. E. Shoer, S. W. Eaton, E. A. Margulies, M. R. Wasielewski, *J. Phys. Chem. B* **2015**, *119*, 7635-7643.
118 R. Kota, R. Samudrala, D. L. Mattern, *J. Org. Chem.* **2012**, *77*, 9641-9651.
119 Y. Jiang, L. Lu, M. Yang, C. Zhan, Z. Xie, F. Verpoort, S. Xiao, *Polym. Chem.* **2013**, *4*, 5612-5620.
120 H.-H. Chou, Y.-C. Liu, G. Fang, Q.-K. Cao, T.-C. Wei, C.-Y. Yeh, *ACS Appl. Mater. Interfaces* **2017**, *9*, 37786-37796.
121 L. Flamigni, B. Ventura, A. Barbieri, H. Langhals, F. Wetzel, K. Fuchs, A. Walter, *Chem. Eur. J.* **2010**, *16*, 13406-13416.
122 D. Chaudhuri, D. Li, Y. Che, E. Shafran, J. M. Gerton, L. Zang, J. M. Lupton, *Nano Lett.* **2011**, *11*, 488-492.
123 K. Petritsch, Dissertation, Technische Universität Graz (Graz, Austria), **2000**.
124 C. Backes, F. Hauke, C. D. Schmidt, A. Hirsch, *Chem. Commun.* **2009**, 2643-2645.
125 C. Backes, C. D. Schmidt, F. Hauke, A. Hirsch, *Chem. Asian J.* **2011**, *6*, 438-444.
126 C. Backes, U. Mundloch, C. D. Schmidt, J. N. Coleman, W. Wohlleben, F. Hauke, A. Hirsch, *Chem. Eur. J.* **2010**, *16*, 13185-13192.
127 C. Backes, C. D. Schmidt, K. Rosenlehner, F. Hauke, J. N. Coleman, A. Hirsch, *Adv. Mater.* **2010**, *22*, 788-802.
128 U. Hahn, S. Engmann, C. Oelsner, C. Ehli, D. M. Guldi, T. Torres, *J. Am. Chem. Soc.* **2010**, *132*, 6392-6401.
129 J. M. Englert, J. Röhrl, C. D. Schmidt, R. Graupner, M. Hundhausen, F. Hauke, A. Hirsch, *Adv. Mater.* **2009**, *21*, 4265-4269.
130 N. V. Kozhemyakina, J. M. Englert, G. Yang, E. Spiecker, C. D. Schmidt, F. Hauke, A. Hirsch, *Adv. Mater.* **2010**, *22*, 5483-5487.
131 F. Vögtle, G. Richardt, N. Werner, *Dendrimer chemistry: Concepts, syntheses, properties, applications*, 1st ed., Wiley-VCH, Weinheim, **2009**.
132 J. H. Friedhofen, Dissertation, Rheinische Friedrich-Wilhelms Universität (Bonn), **2006**.
133 printed with kind permission of the author (F. Vögtle, G. Richardt, N. Werner, in *Dendrimer chemistry: Concepts, syntheses, properties, applications*, Wiley-VCH, Weinheim, **2009**).
134 G. R. Newkome, R. K. Behera, C. N. Moorefield, G. R. Baker, *J. Org. Chem.* **1991**, *56*, 7162–7167.
135 E. Buhleier, W. Wehner, F. Vögtle, *Synthesis* **1978**, *1978*, 155–158.
136 G. Franc, A. K. Kakkar, *Chem. Eur. J.* **2009**, *15*, 5630–5639.
137 G. Franc, A. K. Kakkar, *Chem. Commun.* **2008**, 5267–5276.
138 K. Yoon, P. Goyal, M. Weck, *Org. Lett.* **2007**, *9*, 2051–2054.
139 U. Hahn, T. Torres, *J. Porphyr. Phthalocyanines* **2011**, *15*, 364–372.
140 K. L. Killops, L. M. Campos, C. J. Hawker, *J. Am. Chem. Soc.* **2008**, *130*, 5062–5064.
141 M. Kimura, K. Nakada, Y. Yamaguchi, K. H. Hirofusa Shirai, N. Kobayashi, *Chem. Commun.* **1997**, 1215–1216.
142 U. Hahn, M. Gorka, F. Vögtle, V. Vicinelli, P. Ceroni, M. Maestri, V. Balzani, *Angew. Chem. Int. Ed.* **2002**, *41*, 3595–3598.
143 C. Ornelas, J. Broichhagen, M. Weck, *J. Am. Chem. Soc.* **2010**, *132*, 3923–3931.
144 C. J. Hawker, J. M. J. Fréchet, *J. Am. Chem. Soc.* **1990**, *112*, 7638–7647.
145 T. Kawaguchi, K. L. Walker, C. L. Wilkins, J. S. Moore, *J. Am. Chem. Soc.* **1995**, *117*, 2159–2165.
146 E. Karabudak, C. Backes, F. Hauke, C. D. Schmidt, H. Cölfen, A. Hirsch, W. Wohlleben, *ChemPhysChem* **2010**, *11*, 3224-3227.

147 C. Backes, E. Karabudak , C. D. Schmidt, F. Hauke, A. Hirsch, W. Wohlleben, *Chem. Eur. J.* **2010**, *16*, 13176-13184.

148 C. Ehli, C. Oelsner, D. M. Guldi, A. Mateo-Alonso, M. Prato, C. Schmidt, C. Backes, F. Hauke, A. Hirsch, *Nat. Chem.* **2009**, *1*, 243-249.

149 C. Backes, C. D. Schmidt, F. Hauke, C. Böttcher, A. Hirsch, *J. Am. Chem. Soc.* **2009**, *131*, 2172-2184.

150 C. D. Schmidt, Dissertation, Friedrich-Alexander University Erlangen-Nürnberg (Erlangen), **2011**.

151 C. D. Schmidt, C. Böttcher, A. Hirsch, *Eur. J. Org. Chem.* **2009**, *2009*, 5337-5349.

152 C. D. Schmidt, C. Böttcher, A. Hirsch, *Eur. J. Org. Chem.* **2007**, *2007*, 5497-5505.

153 G. R. Newkome, G. R. Baker, J. K. Young, J. G. Traynham, *J. Polym. Sci., Part A: Polym. Chem.* **1993**, *31*, 641–651.

154 J. H. Friedhofen, F. Vögtle, *New J. Chem.* **2006**, *30*, 32–43.

155 X. Huang, Q. Shi, W.-Q. Chen, C. Zhu, W. Zhou, Z. Zhao, X.-M. Duan, X. Zhan, *Macromolecules* **2010**, *43*, 9620-9626.

156 these energetic values and/or geometrically optimized structures were calculated by the author of this PhD thesis using semiempirical methods (Geom.Opt. NDDO PM6/UHF) for single molecules in the gas phase. A complete survey of HOMO/LUMO energies and the calculated or spectroscopically determined Eg energies for products and selected sub-components can be found in the spectroscopic supplement at the end of this thesis.

157 M. P. O'Neil, M. P. Niemczyk, W. A. Svec, D. Gosztola, G. L. Gaines, M. R. Wasielewski, *Science* **1992**, *257*, 63-65.

158 R. F. Kelley, W. S. Shin, B. Rybtchinski, L. E. Sinks, M. R. Wasielewski, *J. Am. Chem. Soc.* **2007**, *129*, 3173-3181.

159 S. A. Odom, R. F. Kelley, S. Ohira, T. R. Ensley, C. Huang, L. A. Padilha, S. Webster, V. Coropceanu, S. Barlow, D. J. Hagan, E. W. Van Stryland, J.-L. Brédas, H. L. Anderson, M. R. Wasielewski, S. R. Marder, *J. Phys. Chem. A* **2009**, *113*, 10826-10832.

160 C.-C. You, F. Würthner, *Org. Lett.* **2004**, *6*, 2401-2404.

161 M. Ghirotti, C. Chiorboli, C.-C. You, F. Würthner, F. Scandola, *J. Phys. Chem. A* **2008**, *112*, 3376-3385.

162 M. T. Indelli, C. Chiorboli, F. Scandola, E. Iengo, P. Osswald, F. Würthner, *J. Phys. Chem. B* **2010**, *114*, 14495-14504.

163 M. A. Miller, R. K. Lammi, S. Prathapan, D. Holten, J. S. Lindsey, *J. Org. Chem.* **2000**, *65*, 6634-6649.

164 S. I. Yang, R. K. Lammi, S. Prathapan, M. A. Miller, J. Seth, J. R. Diers, D. F. Bocian, J. S. Lindsey, D. Holten, *J. Mater. Chem.* **2001**, *11*, 2420-2430.

165 S. I. Yang, S. Prathapan, M. A. Miller, J. Seth, D. F. Bocian, J. S. Lindsey, D. Holten, *J. Phys. Chem. B* **2001**, *105*, 8249-8258.

166 C. Kirmaier, S. I. Yang, S. Prathapan, M. A. Miller, J. R. Diers, D. F. Bocian, J. S. Lindsey, D. Holten, *Res. Chem. Intermed.* **2002**, *28*, 719-740.

167 C. Kirmaier, H.-e. Song, E. Yang, J. K. Schwartz, E. Hindin, J. R. Diers, R. S. Loewe, K.-y. Tomizaki, F. Chevalier, L. Ramos, R. R. Birge, J. S. Lindsey, D. F. Bocian, D. Holten, *J. Phys. Chem. B* **2010**, *114*, 14249-14264.

168 A. K. Mandal, J. R. Diers, D. M. Niedzwiedzki, G. Hu, R. Liu, E. J. Alexy, J. S. Lindsey, D. F. Bocian, D. Holten, *J. Am. Chem. Soc.* **2017**, *139*, 17547-17564.

169 J. Luo, M. Xu, R. Li, K.-W. Huang, C. Jiang, Q. Qi, W. Zeng, J. Zhang, C. Chi, P. Wang, J. Wu, *J. Am. Chem. Soc.* **2014**, *136*, 265-272.

170 G. M. Hasselman, D. F. Watson, J. R. Stromberg, D. F. Bocian, D. Holten, J. S. Lindsey, G. J. Meyer, *J. Phys. Chem. B* **2006**, *110*, 25430-25440.

171 J. S. High, K. A. Virgil, E. Jakubikova, *J. Phys. Chem. A* **2015**, *119*, 9879-9888.

172 K. Paredes-Gil, F. Mendizabal, D. Páez-Hernández, R. Arratia-Pérez, *Comput. Mater. Sci.* **2017**, *126*, 514-527.

173 A. Zhang, C. Li, F. Yang, J. Zhang, Z. Wang, Z. Wei, W. Li, *Angew. Chem. Int. Ed.* **2017**, *56*, 2694-2698.

174 C.-W. Lee, H.-P. Lu, N. M. Reddy, H.-W. Lee, E. W.-G. Diau, C.-Y. Yeh, *Dyes Pigm.* **2011**, *91*, 317-323.
175 D. K. Panda, F. S. Goodson, S. Ray, R. Lowell, S. Saha, *Chem. Commun.* **2012**, *48*, 8775-8777.
176 K. Y. Tomizaki, R. S. Loewe, C. Kirmaier, J. K. Schwartz, J. L. Retsek, D. F. Bocian, D. Holten, J. S. Lindsey, *J. Org. Chem.* **2002**, *67*, 6519-6534.
177 R. S. Loewe, K.-y. Tomizaki, W. J. Youngblood, Z. Bo, J. S. Lindsey, *J. Mater. Chem.* **2002**, *12*, 3438-3451.
178 J. Amanpour, G. Hu, E. J. Alexy, A. K. Mandal, H. S. Kang, J. M. Yuen, J. R. Diers, D. F. Bocian, J. S. Lindsey, D. Holten, *J. Phys. Chem. A* **2016**, *120*, 7434-7450.
179 E. Yang, J. Wang, J. R. Diers, D. M. Niedzwiedzki, C. Kirmaier, D. F. Bocian, J. S. Lindsey, D. Holten, *J. Phys. Chem. B* **2014**, *118*, 1630-1647.
180 E. J. Alexy, J. M. Yuen, V. Chandrashaker, J. R. Diers, C. Kirmaier, D. F. Bocian, D. Holten, J. S. Lindsey, *Chem. Commun.* **2014**, *50*, 14512-14515.
181 S. Tu, S. H. Kim, J. Joseph, D. A. Modarelli, J. R. Parquette, *J. Am. Chem. Soc.* **2011**, *133*, 19125-19130.
182 S. Tu, S. H. Kim, J. Joseph, D. A. Modarelli, J. R. Parquette, *ChemPhysChem* **2013**, *14*, 1609-1617.
183 H. Shao, J. R. Parquette, *Angew. Chem. Int. Ed.* **2009**, *48*, 2525-2528.
184 S. Yagai, M. Yamauchi, A. Kobayashi, T. Karatsu, A. Kitamura, T. Ohba, Y. Kikkawa, *J. Am. Chem. Soc.* **2012**, *134*, 18205-18208.
185 L. Zang, Y. Che, J. S. Moore, *Acc. Chem. Res.* **2008**, *41*, 1596-1608.
186 H. Shao, J. Seifert, N. C. Romano, M. Gao, J. J. Helmus, C. P. Jaroniec, D. A. Modarelli, J. R. Parquette, *Angew. Chem. Int. Ed.* **2010**, *49*, 7688-7691.
187 Y. Yamamoto, *Sci. Technol. Adv. Mater.* **2012**, *13*, 033001-033016.
188 S. S. Babu, D. Bonifazi, *ChemPlusChem* **2014**, *79*, 895-906.
189 H. Chung, P. M. Barron, R. W. Novotny, H.-T. Son, C. Hu, W. Choe, *Cryst. Growth Des.* **2009**, *9*, 3327-3332.
190 J. A. A. W. Elemans, R. van Hameren, R. J. M. Nolte, A. E. Rowan, *Adv. Mater.* **2006**, *18*, 1251-1266.
191 P. W. Bohn, *Annu. Rev. Phys. Chem.* **1993**, *44*, 37-60.
192 K.-R. Wang, D.-S. Guo, B.-P. Jiang, Y. Liu, *Chem. Commun.* **2012**, *48*, 3644-3646.
193 printed with kind permission of the author (S. Tu, S. H. Kim, J. Joseph, D. A. Modarelli, J. R. Parquette, in *Self-assembly of a donor-acceptor nanotube. A strategy to create bicontinuous arrays*, **2011**).
194 E. J. Corey, *Chem. Soc. Rev.* **1988**, *17*, 111-133.
195 M. A. Sierra, M. C. de la Torre, *Angew. Chem. Int. Ed.* **2000**, *39*, 1538-1559.
196 M. Brettreich, A. Hirsch, *Synlett* **1998**, *1998*, 1396–1398.
197 G. B. Bachman, L. V. Heisey, *J. Am. Chem. Soc.* **1946**, *68*, 2496-2499.
198 R. S. Alexander, A. R. Butler, *J. Chem. Soc., Perkin Trans. 2* **1976**, *0*, 696-701.
199 P. G. M. Wuts, T. W. Greene, *Protection for the Carboxyl Group* in *Greene's Protective Groups in Organic Synthesis*, 4th ed., John Wiley & Sons, New Jersey, **2006**, pp. 533-646.
200 P. G. M. Wuts, T. W. Greene, *Protection for the Alkyne -CH* in *Greene's Protective Groups in Organic Synthesis*, 4th ed., John Wiley & Sons, New Jersey, **2006**, pp. 927-933.
201 P. G. M. Wuts, T. W. Greene, *Protection for the Amino Group* in *Greene's Protective Groups in Organic Synthesis*, 4th ed., John Wiley & Sons, New Jersey, **2006**, pp. 696-926.
202 T. Apelqvist, D. Wensbo, *Tetrahedron Lett.* **1996**, *37*, 1471-1472.
203 V. H. Rawal, M. P. Cava, *Tetrahedron Lett.* **1985**, *26*, 6141-6142.
204 S. Takahashi, Y. Kuroyama, K. Sonogashira, N. Hagihara, *Synthesis* **1980**, *1980*, 627-630.
205 A. Jutand, *Pure Appl. Chem.* **2009**, *76*, 565-576.
206 F. Maya, S. H. Chanteau, L. Cheng, M. P. Stewart, J. M. Tour, *Chem. Mater.* **2005**, *17*, 1331-1345.
207 B. Gharib, A. Hirsch, *Eur. J. Org. Chem.* **2014**, *2014*, 4123-4136.
208 L. Grehn, U. Ragnarsson, *Angew. Chem., Int. Ed. Engl.* **1984**, *23*, 296-301.
209 H. Zeng, Y. Li, H. Shao, *Synth. Commun.* **2012**, *42*, 25-32.
210 H. Doucet, J.-C. Hierso, *Angew. Chem. Int. Ed.* **2007**, *46*, 834-871.
211 C.-H. Lee, J. S. Lindsey, *Tetrahedron* **1994**, *50*, 11427-11440.

212 J. White, G. McGillivray, *J. Org. Chem.* **1977**, *42*, 4248-4251.
213 M. Hesse, H. Meier, B. Zeeh, *Spektroskopische Methoden in der organischen Chemie*, 7th ed., Georg Thieme Verlag, Stuttgart, New York, **2005**.
214 A. W. Overhauser, *Phys. Rev.* **1953**, *92*, 411-415.
215 G. Binsch, *The Study of Intramolecular Rate Processes by Dynamic Nuclear Magnetic Resonance* in *Topics in Stereochemistry*, John Wiley & Sons, New Jersey, **2007**, pp. 97-192.
216 J. A. Hirsch, R. L. Augustine, G. Koletar, H. G. Wolf, *J. Org. Chem.* **1975**, *40*, 3547-3550.
217 B. M. Pinto, D. M. Vyas, W. A. Szarek, *Can. J. Chem.* **1977**, *55*, 937-948.
218 J. E. Taylor, M. D. Jones, J. M. J. Williams, S. D. Bull, *Org. Lett.* **2010**, *12*, 5740-5743.
219 R. A. Decréau, J. P. Collman, *Tetrahedron Lett.* **2003**, *44*, 3323-3327.
220 Y. Terazono, E. J. North, A. L. Moore, T. A. Moore, D. Gust, *Org. Lett.* **2012**, *14*, 1776-1779.
221 D. Lahaye, K. Muthukumaran, C.-H. Hung, D. Gryko, J. S. Rebouças, I. Spasojević, I. Batinić-Haberle, J. S. Lindsey, *Bioorg. Med. Chem.* **2007**, *15*, 7066-7086.
222 D. M. Shendage, R. Fröhlich, G. Haufe, *Org. Lett.* **2004**, *6*, 3675-3678.
223 S. Albrecht, A. Defoin, C. Tarnus, *Synthesis* **2006**, *2006*, 1635-1638.
224 E. A. Englund, H. N. Gopi, D. H. Appella, *Org. Lett.* **2004**, *6*, 213-215.
225 U. Jacquemard, V. Bénéteau, M. Lefoix, S. Routier, J.-Y. Mérour, G. Coudert, *Tetrahedron* **2004**, *60*, 10039-10047.
226 S. Routier, L. Saugé, N. Ayerbe, G. Coudert, J.-Y. Mérour, *Tetrahedron Lett.* **2002**, *43*, 589-591.
227 R. K. Dieter, N. Chen, V. K. Gore, *J. Org. Chem.* **2006**, *71*, 8755-8760.
228 S. El Kazzouli, J. Koubachi, S. Berteina-Raboin, A. Mouaddib, G. Guillaumet, *Tetrahedron Lett.* **2006**, *47*, 8575-8577.
229 O. R. Suárez-Castillo, L. A. Montiel-Ortega, M. Meléndez-Rodríguez, M. Sánchez-Zavala, *Tetrahedron Lett.* **2007**, *48*, 17-20.
230 V. A. Montes, R. Pohl, J. Shinar, P. Anzenbacher, *Chem. Eur. J.* **2006**, *12*, 4523-4535.
231 D. Bhavsar, S. Thakrar, S. Parekh, J. Lunagariya, A. Bavishi, H. Vala, A. Radadiya, D. Detroja, A. Shah, *Chem. Biol. Interf.* **2011**, *1*, 251-262.
232 A. Thaqi, A. McCluskey, J. L. Scott, *Tetrahedron Lett.* **2008**, *49*, 6962-6964.
233 S. A. May, M. D. Johnson, T. M. Braden, J. R. Calvin, B. D. Haeberle, A. R. Jines, R. D. Miller, E. F. Plocharczyk, G. A. Rener, R. N. Richey, C. R. Schmid, R. K. Vaid, H. Yu, *Org. Process Res. Dev.* **2012**, *16*, 982-1002.
234 A. R. Bogdan, M. Charaschanya, A. W. Dombrowski, Y. Wang, S. W. Djuric, *Org. Lett.* **2016**, *18*, 1732-1735.
235 E. Merck, *Anfärbereagentien für Dünnschicht- und Papierchromatographie*, E. Merck AG, Darmstadt, **1970**.
236 author, 0.74 g -> 1.55 g (82.9%); author, 0.50 g -> 1.11 g (88.0%); M. Muth, 5.00 g -> 11.47 g (87.9%); C. Zehe, 5.00 g -> 11.29 g (88.9%); the reaction performed by C. Zehe was described in the exp. part.
237 author, 5.00 g -> 1.51 g (43.2%, low yield due to 21 h heating time); author, 10.00 g -> 5.05 g (72.3%); author, 3.00 g -> 1.59 g (75.8%); M. Muth, 10.24 g -> 5.53 g (77.3%); the reaction performed by M. Muth was described in the exp. part.
238 C. Weiß, Master Thesis, Friedrich-Alexander University Erlangen-Nürnberg (Erlangen), **2016**.
239 A. Wicklein, A. Lang, M. Muth, M. Thelakkat, *J. Am. Chem. Soc.* **2009**, *131*, 14442-14453.
240 A. Williams, I. T. Ibrahim, *Chem. Rev.* **1981**, *81*, 589-636.
241 C. A. G. N. Montalbetti, V. Falque, *Tetrahedron* **2005**, *61*, 10827-10852.
242 D. H. Rich, J. Singh, *The Carbodiimide Method* in *Major Methods of Peptide Bond Formation, Vol. 1* (Eds.: E. Gross, J. Meienhofer), Academic Press, Elsevier, **1979**, pp. 241-261.
243 Y. Avlasevich, C. Li, K. Mullen, *J. Mater. Chem.* **2010**, *20*, 3814-3826.
244 A. I. Donskikh, G. M. Tseitlin, O. I. Tomina, Z. F. Saikina, J. E. Doroshenko, *Periodica Polytech., Chem. Eng.* **1989**, *33*, 61-67.

245 C. J. Medforth, *NMR Spectroscopy of Diamagnetic Porphyrins* in *The Porphyrin Handbook, Vol. 5* (Eds.: K. M. Kadish, K. M. Smith, R. Guilard), Academic Press, **2000**.
246 K. M. Merz, C. H. Reynolds, *J. Chem. Soc., Chem. Commun.* **1988**, 90-92.
247 T. D. W. Claridge, *Separating Shifts and Couplings: J-Resolved and Pure Shift Spectroscopy* in *High-Resolution NMR Techniques in Organic Chemistry*, 3rd ed., Elsevier, Boston, **2016**, pp. 295-313.
248 G. R. Fulmer, A. J. M. Miller, N. H. Sherden, H. E. Gottlieb, A. Nudelman, B. M. Stoltz, J. E. Bercaw, K. I. Goldberg, *Organometallics* **2010**, *29*, 2176-2179.
249 Spectral Database for Organic Compounds (SDBS), http://sdbs.db.aist.go.jp
250 J. F. Hitzenberger, C. Dammann, N. Lang, D. Lungerich, M. Garcia-Iglesias, G. Bottari, T. Torres, N. Jux, T. Drewello, *Analyst* **2016**, *141*, 1347-1355.
251 J. Hitzenberger, Dissertation, Friedrich-Alexander University Erlangen-Nürnberg (Erlangen), **2017**.
252 J. O. Alben, S. S. Choi, A. D. Adler, W. S. Caughey, *Ann. N. Y. Acad. Sci.* **1973**, *206*, 278-295.
253 R. É. Garibov, E. M. Danilenko, A. K. Sokolov, G. B. Maravin, G. V. Ponomarev, *Theor. Exper. Chem.* **1991**, *27*, 103-107.
254 M. Gouterman, G. H. Wagnière, L. C. Snyder, *J. Mol. Spectrosc.* **1963**, *11*, 108-127.
255 M. Gouterman, *J. Mol. Spectrosc.* **1961**, *6*, 138-163.
256 P. J. Spellane, M. Gouterman, A. Antipas, S. Kim, Y. C. Liu, *Inorg. Chem.* **1980**, *19*, 386-391.
257 R. Giovannetti, *The Use of Spectrophotometry UV-Vis for the Study of Porphyrins* in *Macro to Nano Spectroscopy* (Ed.: J. Uddin), InTech, **2012**.
258 J. Mößler, Dissertation, Freie Universität Berlin (Berlin), **1999**.
259 J. Mack, N. Kobayashi, Z. Shen, *The Effect of Structural Modifications on the Properties of Porphyrinoids* in *Handbook of Porphyrin Science, Vol. 23* (Eds.: K. M. Kadish, K. M. Smith, R. Guilard), World Scientific Pub. Co., Singapore, **2012**, pp. 281-371.
260 F. Wessendorf, Dissertation, Friedrich-Alexander University Erlangen-Nürnberg (Erlangen), **2010**.
261 Y. Tanizaki, T. Yoshinaga, H. Hiratsuka, *Spectrochim. Acta, Part A* **1978**, *34*, 205-210.
262 H. Langhals, *Spectrochim. Acta, Part A* **2000**, *56*, 2207-2210.
263 J. P. Wojciechowski, A. D. Martin, M. Bhadbhade, J. E. A. Webb, P. Thordarson, *CrystEngComm* **2016**, *18*, 4513-4517.
264 B. Valeur, M. N. Berberan-Santos, *Characteristics of Fluorescence Emission* in *Molecular Fluorescence*, Wiley-VCH, Weinheim, **2012**, pp. 53-74.
265 R. K. Gupta, S. K. Pathak, B. Pradhan, D. S. Shankar Rao, S. Krishna Prasad, A. S. Achalkumar, *Soft Matter* **2015**, *11*, 3629-3636.
266 D. Inan, R. K. Dubey, N. Westerveld, J. Bleeker, W. F. Jager, F. C. Grozema, *J. Phys. Chem. A* **2017**, *121*, 4633-4644.
267 D. Sriramulu, S. Valiyaveettil, *Dyes Pigm.* **2016**, *134*, 306-314.
268 W. E. Ford, P. V. Kamat, *J. Phys. Chem.* **1987**, *91*, 6373-6380.
269 M. Lelle, Diploma Thesis, Max-Planck-Institut für Polymerforschung (Mainz), **2009**.
270 L. Yang, M. Shi, M. Wang, H. Chen, *Tetrahedron* **2008**, *64*, 5404-5409.
271 T. Heek, Dissertation, Freie Universität Berlin (Berlin), **2013**.
272 R. K. Dubey, D. Inan, S. Sengupta, E. J. R. Sudholter, F. C. Grozema, W. F. Jager, *Chem. Sci.* **2016**, *7*, 3517-3532.
273 G. Echue, I. Hamley, G. C. Lloyd Jones, C. F. J. Faul, *Langmuir* **2016**, *32*, 9023-9032.
274 L. W. Pickett, N. J. Hoeflich, T.-C. Liu, *J. Am. Chem. Soc.* **1951**, *73*, 4865-4869.
275 P. G. Seybold, M. Gouterman, *J. Mol. Spectrosc.* **1969**, *31*, 1-13.
276 S. Akimoto, T. Yamazaki, I. Yamazaki, A. Osuka, *Chem. Phys. Lett.* **1999**, *309*, 177-182.
277 S. Perun, J. Tatchen, C. M. Marian, *ChemPhysChem* **2008**, *9*, 282-292.
278 M. Huber, M. Fuhs, *Ber. Bunsen-Ges. Phys. Chem.* **1996**, *100*, 2057-2064.
279 C. Fierro, A. B. Anderson, D. A. Scherson, *J. Phys. Chem.* **1988**, *92*, 6902-6907.
280 M. C. Ruiz Delgado, E.-G. Kim, D. A. da Silva Filho, J.-L. Bredas, *J. Am. Chem. Soc.* **2010**, *132*, 3375-3387.

281 X. Zhou, D. Liu, T. Wang, X. Hu, J. Guo, K. C. Weerasinghe, L. Wang, W. Li, *J. Photochem. Photobiol., A* **2014**, *274*, 57-63.
282 J. Wirth, R. Neumann, M. Antonietti, P. Saalfrank, *Phys. Chem. Chem. Phys.* **2014**, *16*, 15917-15926.
283 M. G. Walter, E. L. Warren, J. R. McKone, S. W. Boettcher, Q. Mi, E. A. Santori, N. S. Lewis, *Chem. Rev.* **2010**, *110*, 6446-6473.
284 H. Zhou, F. Yu, J. Sun, R. He, S. Chen, C.-W. Chu, Z. Ren, *Proc. Natl. Acad. Sci.* **2017**, *114*, 5607-5611.
285 R. S. Loewe, K.-y. Tomizaki, F. Chevalier, J. S. Lindsey, *J. Porphyr. Phthalocyanines* **2002**, *06*, 626-642.
286 M. J. Farooqi, M. A. Penick, J. Burch, G. R. Negrete, L. Brancaleon, *Spectrochim. Acta, Part A* **2016**, *153*, 124-131.
287 H. Shao, J. R. Parquette, *Chem. Commun.* **2010**, *46*, 4285-4287.
288 M. Morisue, T. Morita, Y. Kuroda, *Org. Biomol. Chem.* **2010**, *8*, 3457-3463.
289 R. Charvet, Y. Yamamoto, T. Sasaki, J. Kim, K. Kato, M. Takata, A. Saeki, S. Seki, T. Aida, *J. Am. Chem. Soc.* **2012**, *134*, 2524-2527.
290 N. C. Maiti, S. Mazumdar, N. Periasamy, *J. Phys. Chem. B* **1998**, *102*, 1528-1538.
291 R. F. Khairutdinov, N. Serpone, *J. Phys. Chem. B* **1999**, *103*, 761-769.
292 D. R. Coulson, L. C. Satek, S. O. Grim, *Tetrakis(triphenylphosphine)palladium(0)* in *Inorg. Synth., Vol. XIII* (Ed.: F. A. Cotton), McGraw-Hill, Inc., **1972**, p. 121.
293 J. P. Stambuli, R. Kuwano, J. F. Hartwig, *Angew. Chem. Int. Ed.* **2002**, *41*, 4746-4748.
294 D. W. Old, J. P. Wolfe, S. L. Buchwald, *J. Am. Chem. Soc.* **1998**, *120*, 9722-9723.
295 A. S. Guram, R. A. Rennels, S. L. Buchwald, *Angew. Chem., Int. Ed. Engl.* **1995**, *34*, 1348-1350.
296 F. Paul, J. Patt, J. F. Hartwig, *J. Am. Chem. Soc.* **1994**, *116*, 5969-5970.
297 R. W. Wagner, T. E. Johnson, F. Li, J. S. Lindsey, *J. Org. Chem.* **1995**, *60*, 5266-5273.
298 F. E. J. Fischer, Laboratory Course Thesis, Friedrich-Alexander University Erlangen-Nürnberg (Erlangen), **2015**.
299 B. Wenninger, Bachelor Thesis, Friedrich-Alexander University Erlangen-Nürnberg (Erlangen), **2015**.
300 V. Lloret, Laboratory Course Thesis, Friedrich-Alexander University Erlangen-Nürnberg (Erlangen), **2015**.
301 I. Papadopoulous, M. Wagner, Laboratory Course Thesis, Friedrich-Alexander University Erlangen-Nürnberg (Erlangen), **2014**.
302 M. Hönle, P. Haines, Laboratory Course Thesis, Friedrich-Alexander University Erlangen-Nürnberg (Erlangen), **2014**.
303 J. Krausmann, M. Volland, Laboratory Course Thesis, Friedrich-Alexander University Erlangen-Nürnberg (Erlangen), **2013**.

10 Acknowledgements

This thesis was written from October 2012 until September 2019 at the Department of Chemistry and Pharmacy at the Friedrich-Alexander University Erlangen-Nürnberg under guidance of Prof. Andreas Hirsch.

First of all, I would like to express my sincere thankfulness to my supervisor Prof. Andreas Hirsch for the exciting and very colorful topic. At any deadlock or unexpected results, you were always ready to support me with advice and suggestions.

I would like to thank all my colleagues who helped me with chemicals, advice, and – most importantly – a warm and welcoming atmosphere. I especially thank Prof. Max von Delius, Dr. Michael Brettreich, Prof. Norbert Jux and Dr. Marcus Speck for their advice during the progress of this thesis. Your aggregated chemical knowledge and experience is unmatched.

All of my students deserve my special thanks as they taught me how to be a good teacher and supervisor. Namely I would like to address my thanks to Florian Fischer, Sarah Seefried, Vicent Lloret, Alexander Miller and Brian Wenniger for their great synthetic work during their laboratory practical courses or Bachelor theses.

My dearest thanks are of course reserved for my loving wife Lisa, as the major part of the thesis was not conquered in the Lab. You are always at my side with advice, understanding and patience.

Thank you.

Herewith, I affirm that this PhD Thesis at hand was written autonomously and only with help of the listed auxiliaries. External sources were cited correctly and comprehensively, derived synthetic work from my students or colleagues is accounted accordingly.

Erlangen,

Christian Methfessel

11 Spectroscopic Supplement

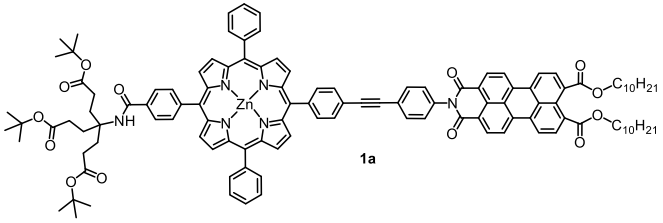

1a

$C_{119}H_{120}N_6O_{13}Zn$

ex. M. 1904.8205

MW 1907.6780

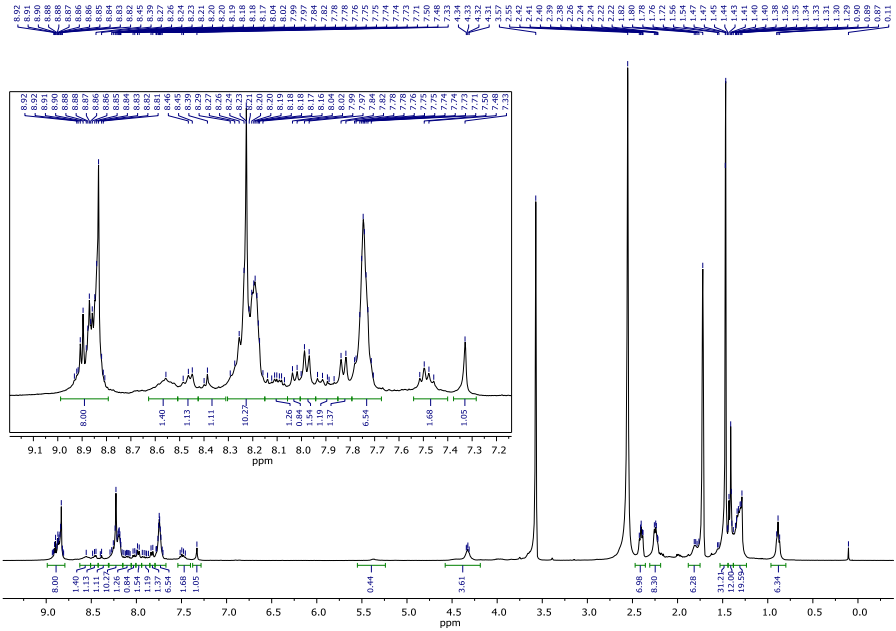

^{1}H NMR spectrum of **1a** in THF-d_8.

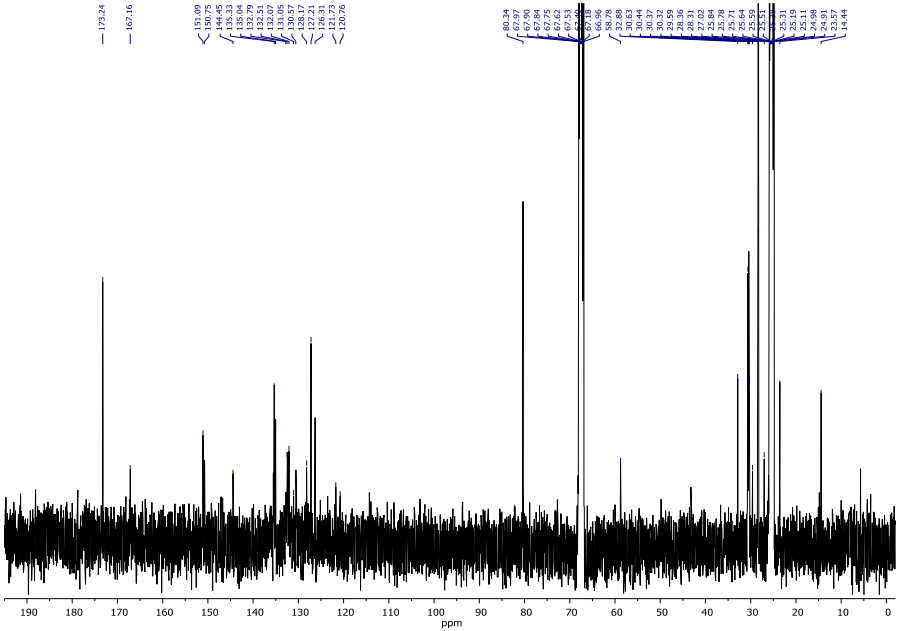

^{13}C NMR spectrum of **1a** in THF-d_8.

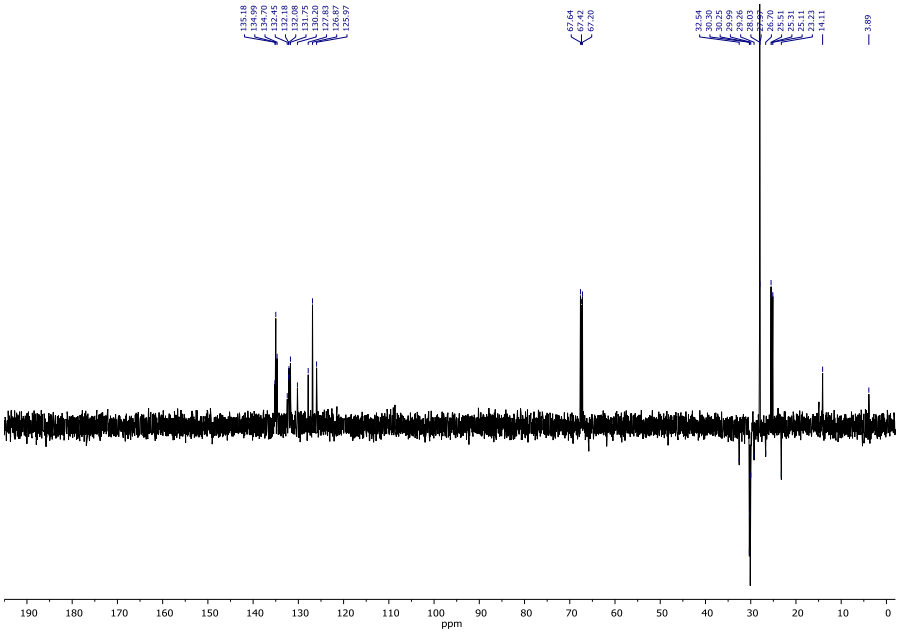

DEPT-135 NMR spectrum of **1a** in THF-d_8 (CH/CH_3 positive, CH_2 negative, C not visible).

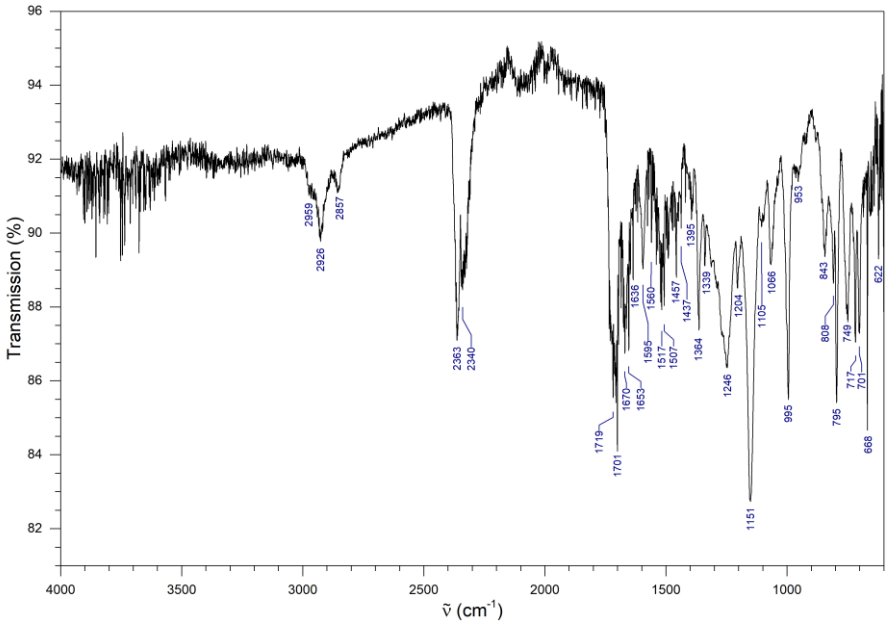

FT-IR spectrum of **1a**. The compound was dissolved in THF and applied.

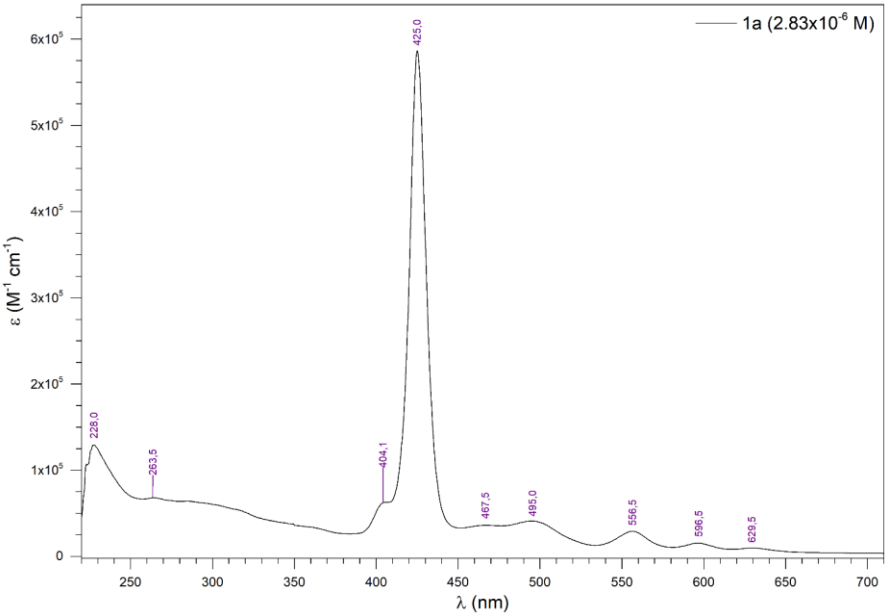

UV-Vis spectrum of **1a** in THF.

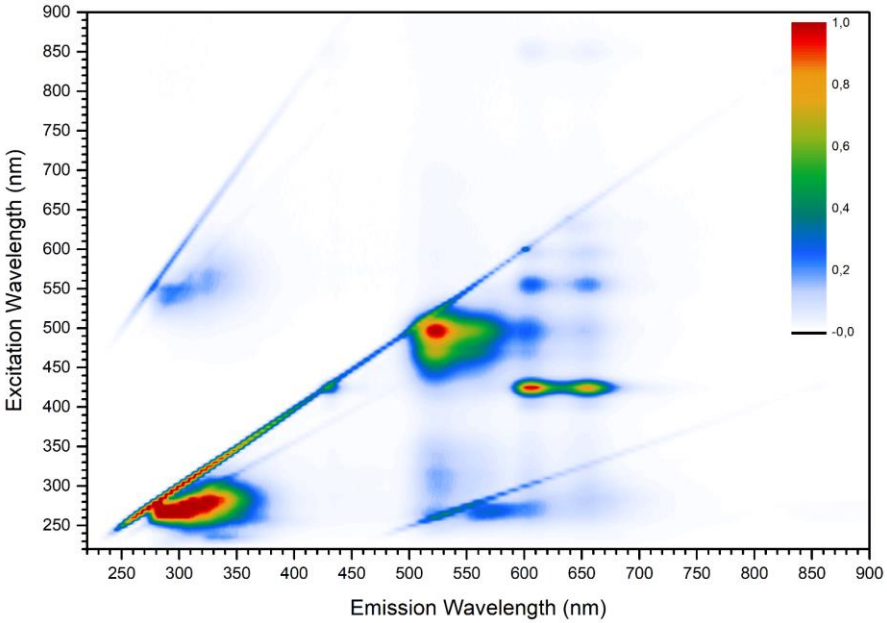

3D excitation-emission spectrum of **1a** in THF.

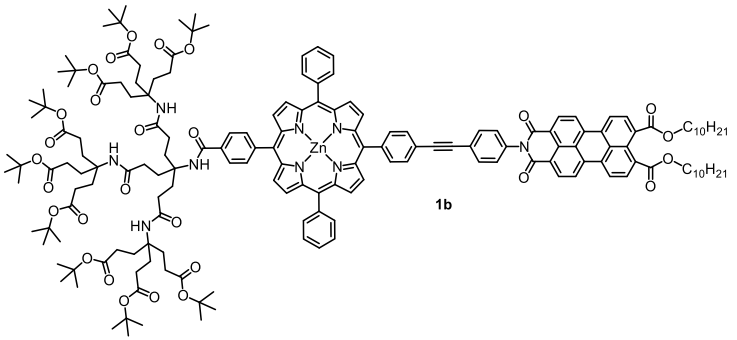

1b

$C_{173}H_{213}N_9O_{28}Zn$

ex .M. 2928.4812

MW 2932.0220

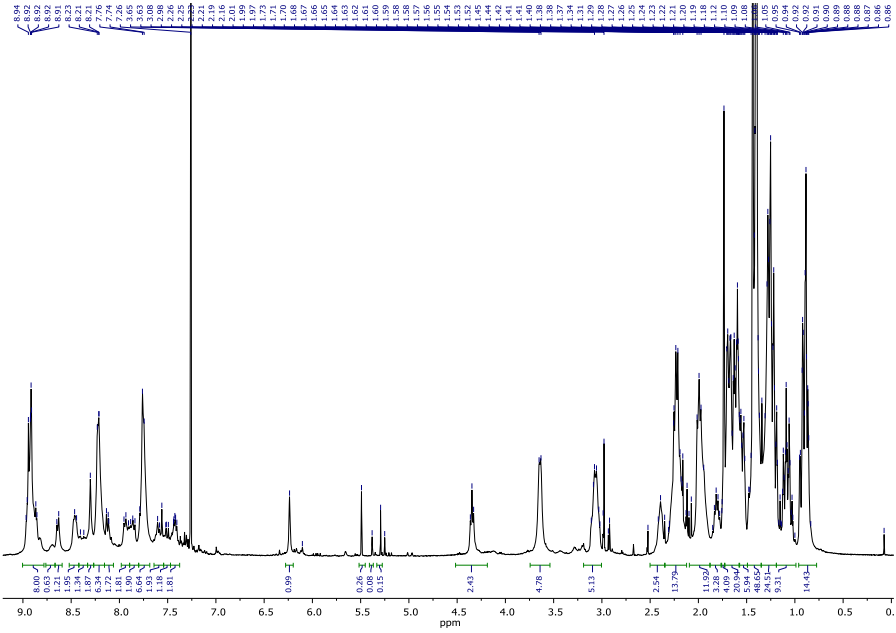

^{1}H NMR spectrum of **1b** in $CDCl_3$. The dyad was partially cleaved during the reaction and in the chromatography steps.

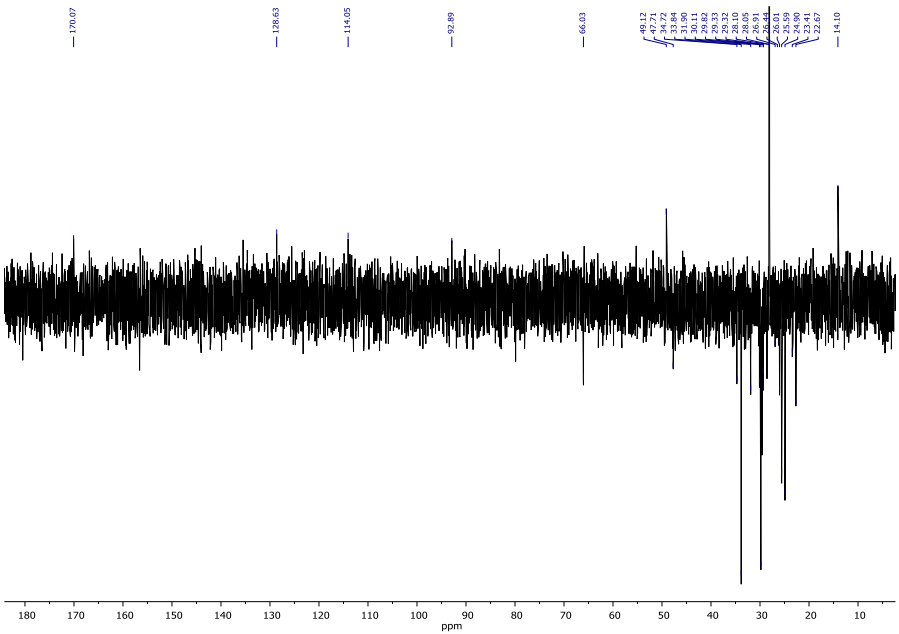

DEPT-135 NMR spectrum of **1b** in $CDCl_3$ (CH/CH_3 positive, CH_2 negative, C not visible).

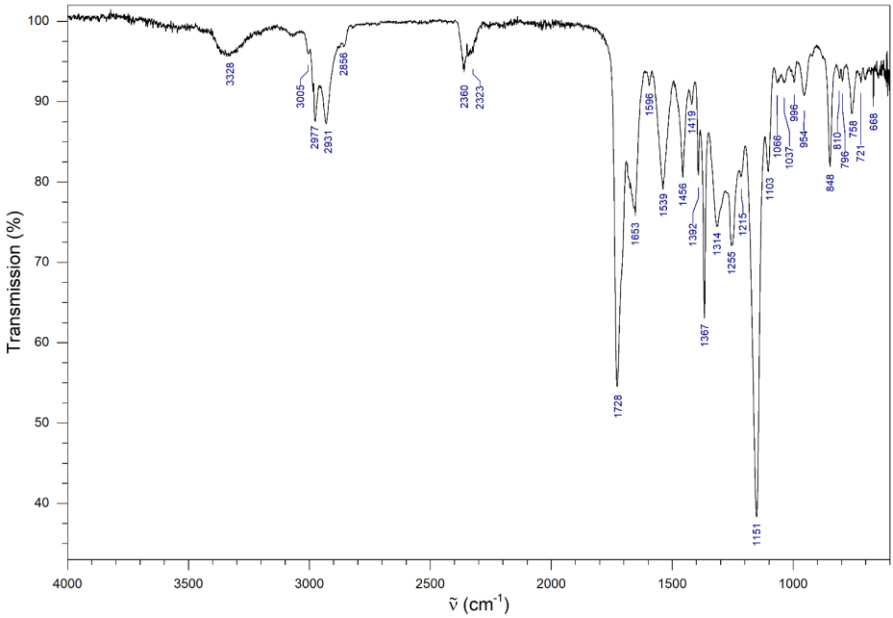

FT-IR spectrum of **1b**.

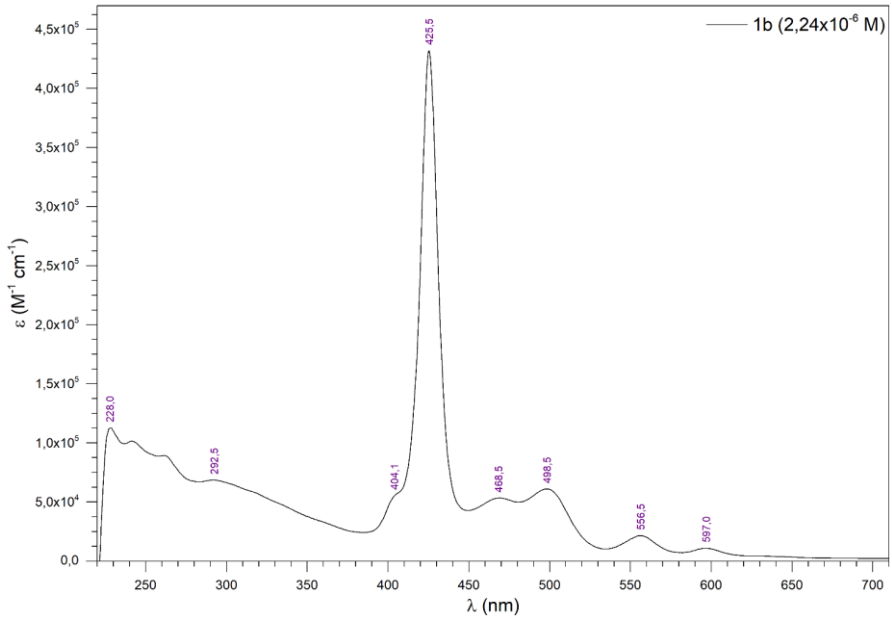

UV-Vis spectrum of **1b** in THF.

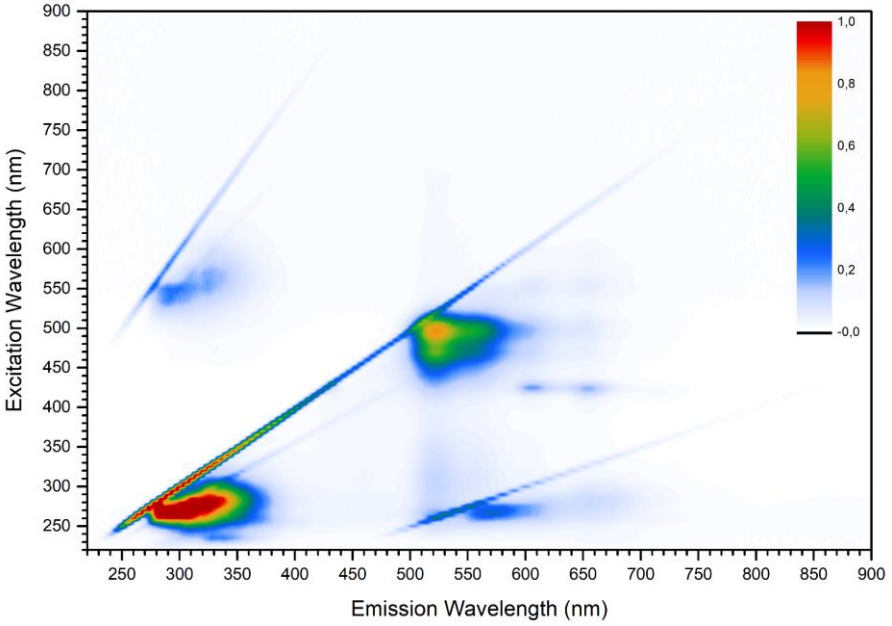

3D excitation-emission spectrum of **1b** in THF.

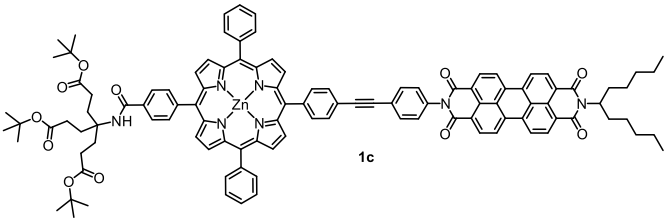

1c

$C_{110}H_{101}N_7O_{11}Zn$

ex. M. 1759.6851

MW 1762.4360

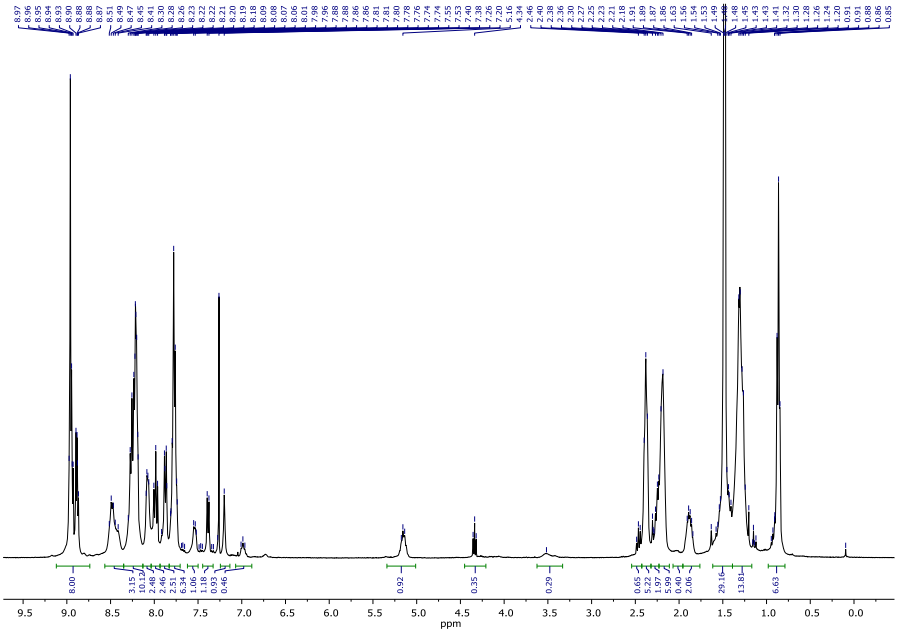

^{1}H NMR spectrum of **1c** in $CDCl_3$.

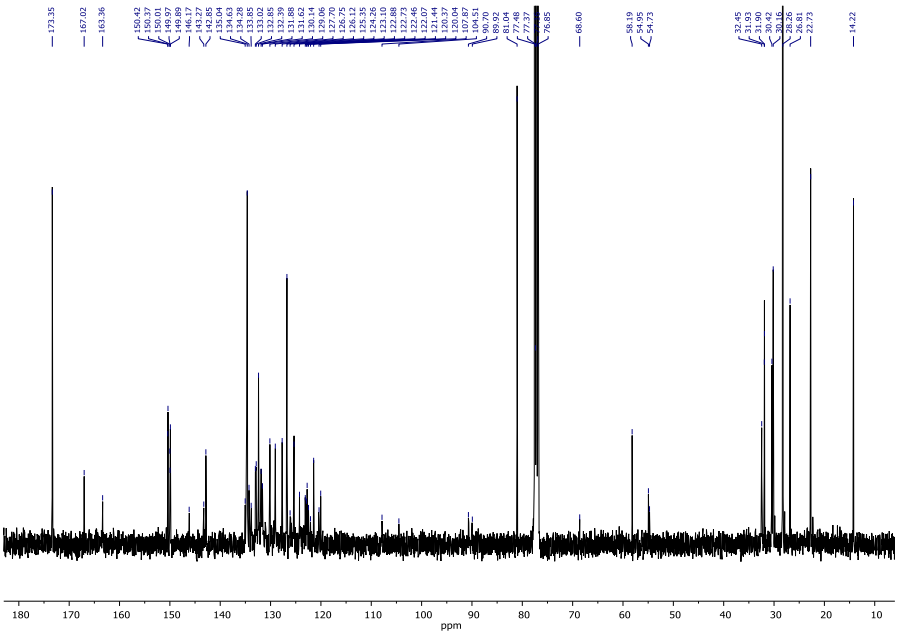

^{13}C NMR spectrum of **1c** in $CDCl_3$.

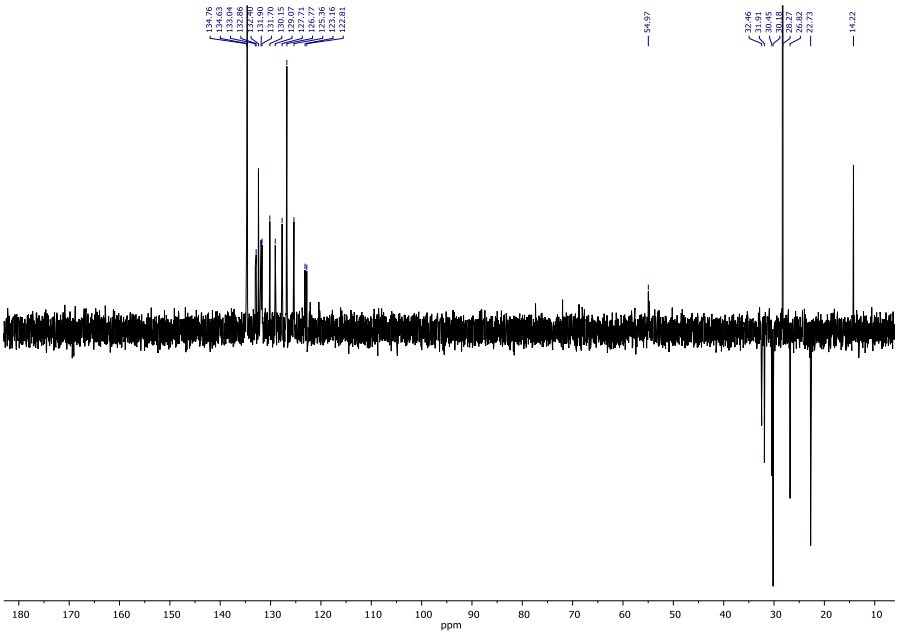

DEPT-135 NMR spectrum of **1c** in $CDCl_3$ (CH/CH_3 positive, CH_2 negative, C not visible).

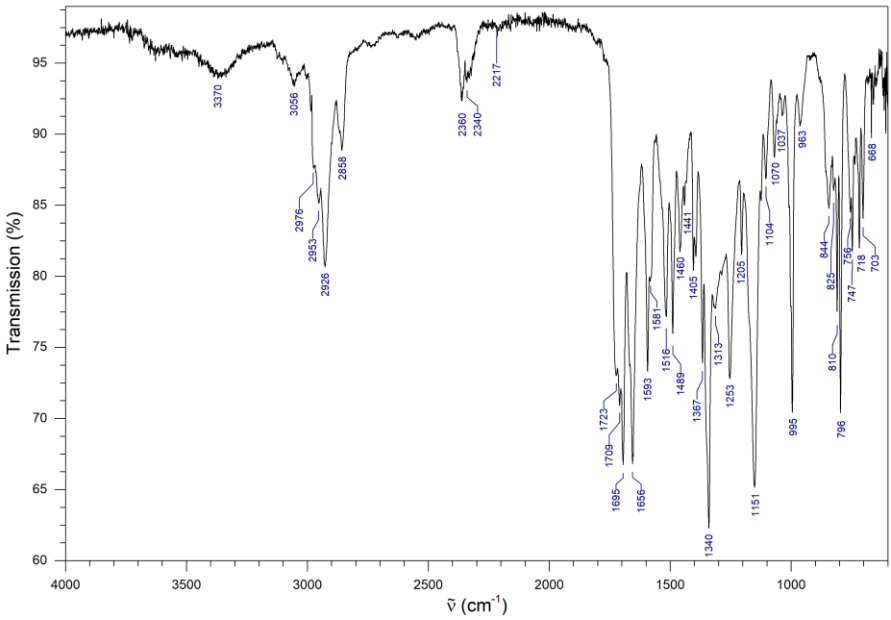

FT-IR spectrum of **1c**.

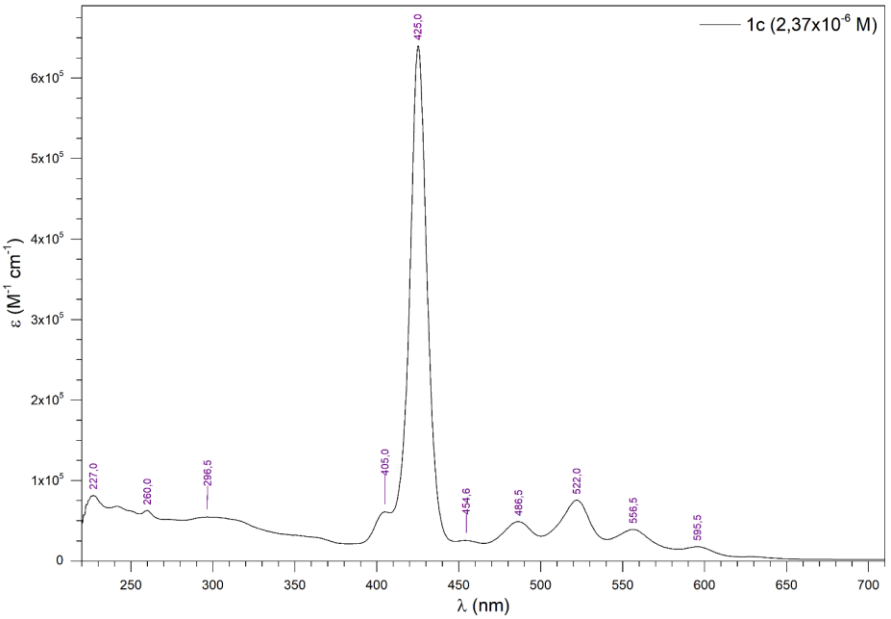

UV-Vis spectrum of **1c** in THF.

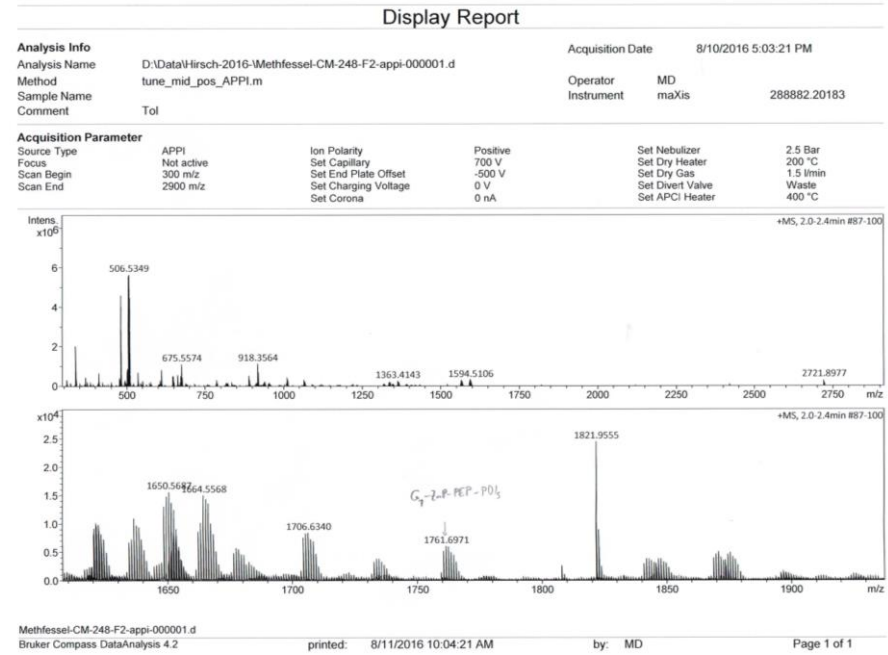

MS (APPI+) of **1c**.

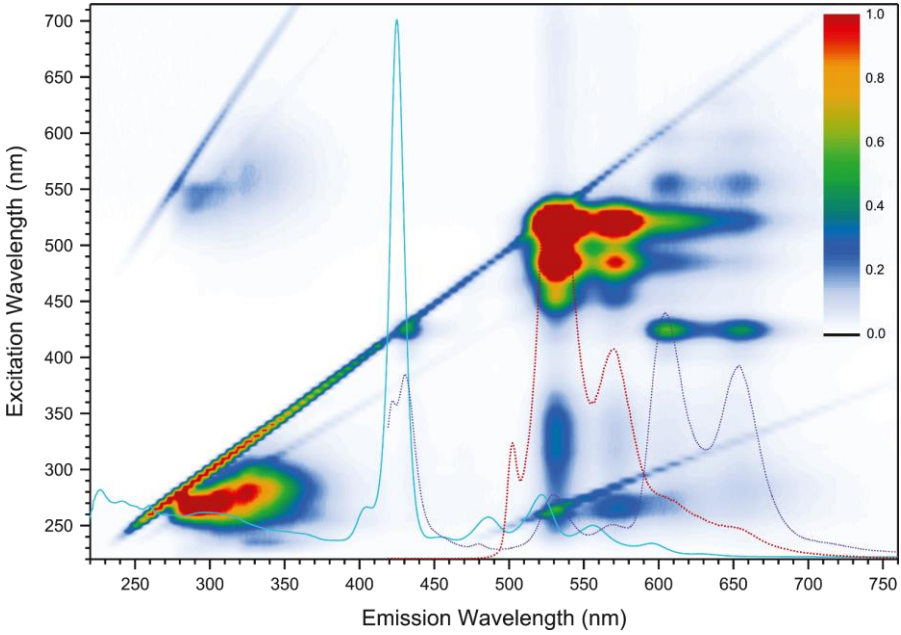

3D excitation-emission spectrum of **1c** in THF.

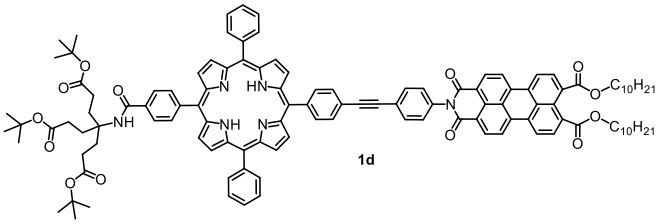

1d

$C_{119}H_{122}N_6O_{13}$

ex. M.1842.9070

MW 1844.3140

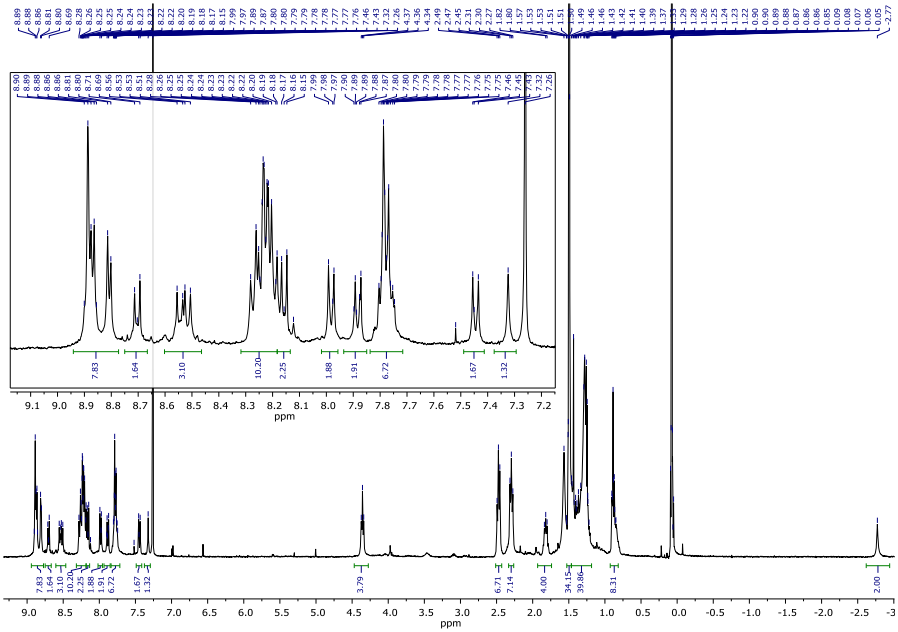

^{1}H NMR spectrum of **1d** in $CDCl_3$.

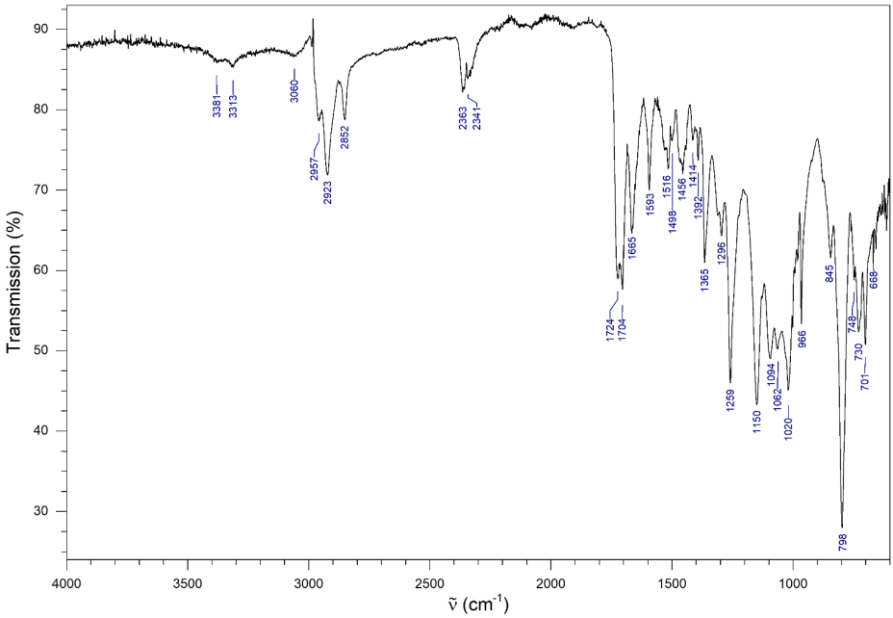

FT-IR spectrum of **1d**.

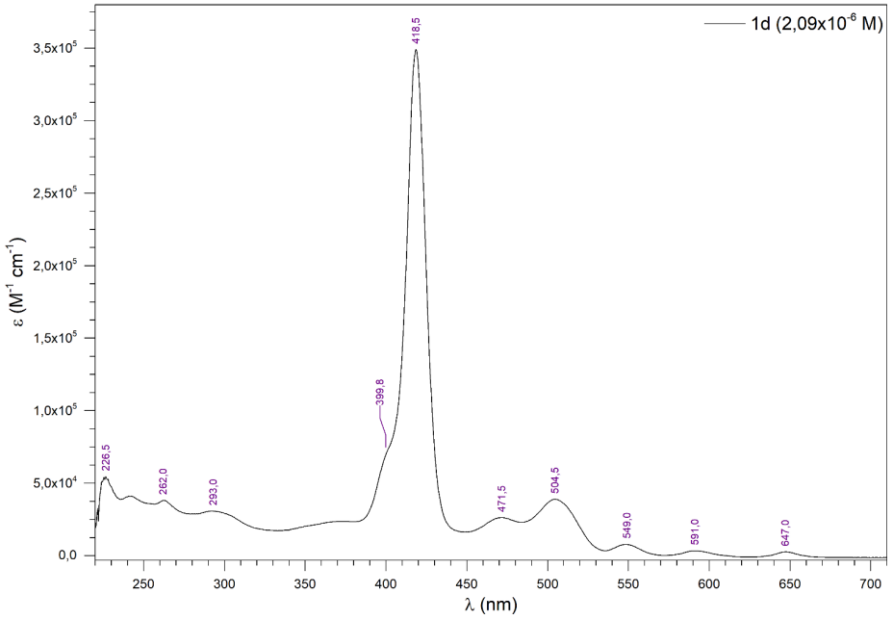

UV-Vis spectrum of **1d** in THF.

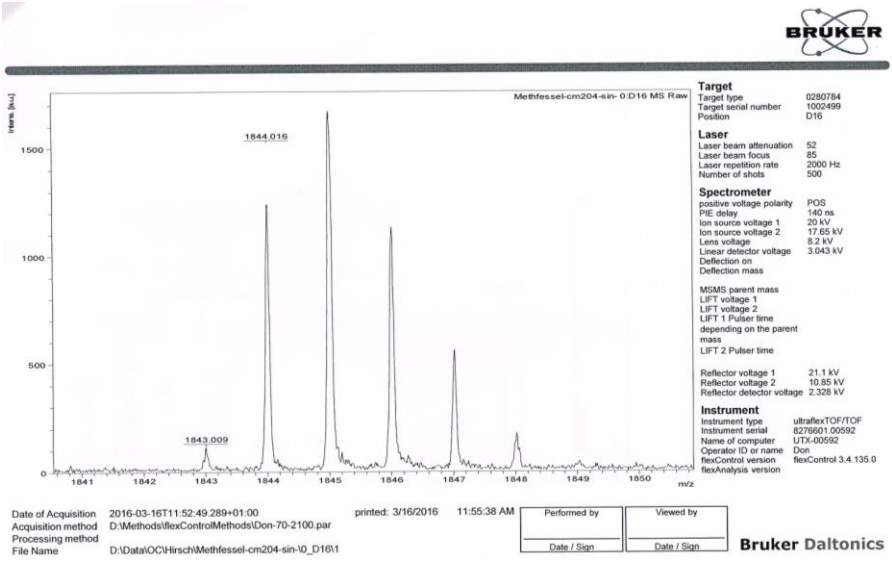

MS (MALDI) of **1d**.

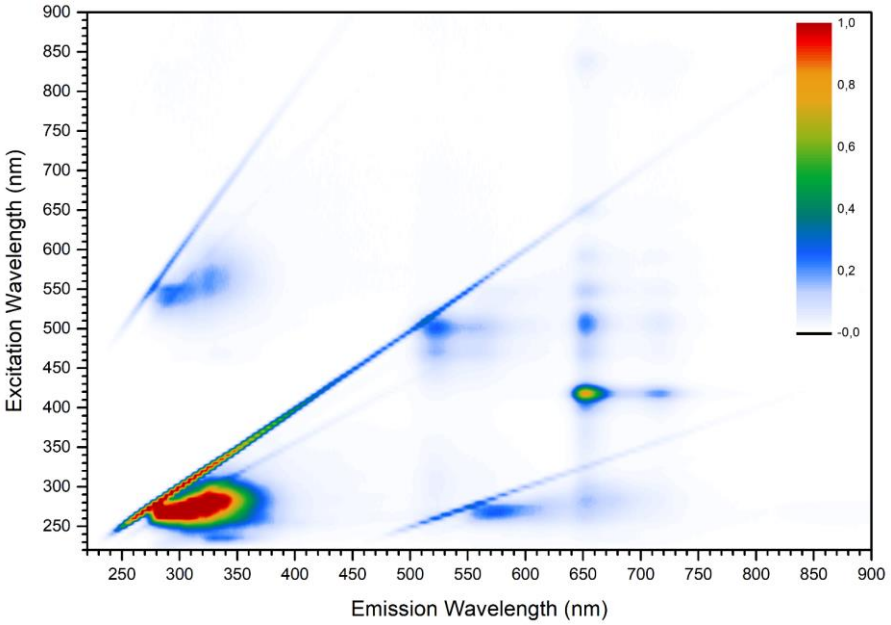

3D excitation-emission spectrum of **1d** in THF.

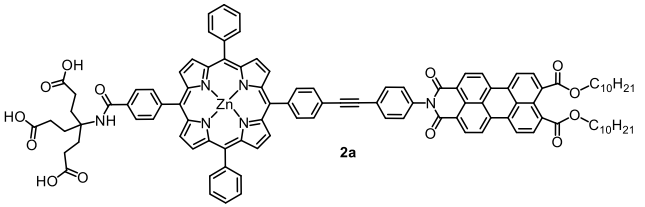

2a

$C_{107}H_{96}N_6O_{13}Zn$

ex. M. 1736.6327

MW 1739.3540

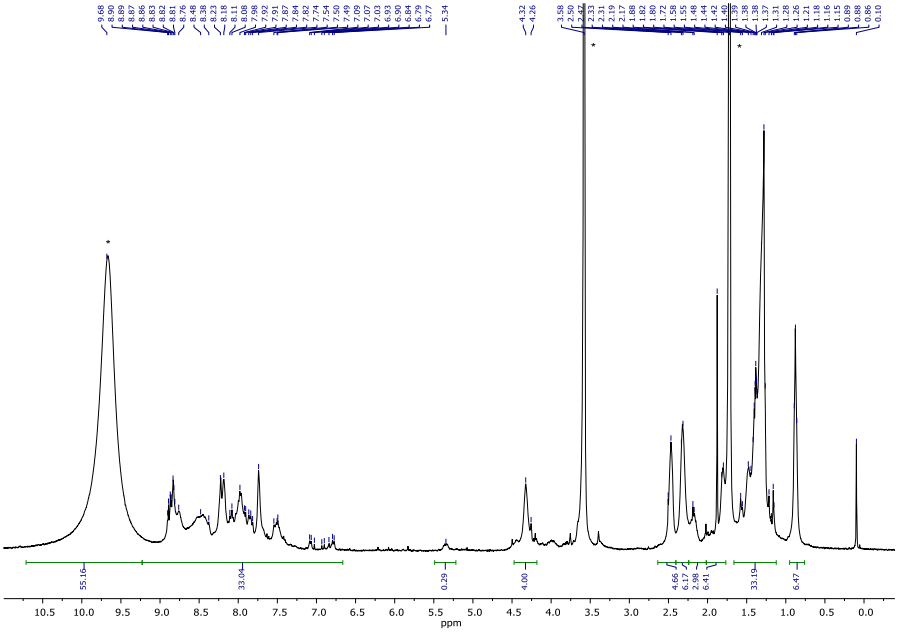

^{1}H NMR spectrum of **2a** in THF-d_8 with TFA-*d* (*).

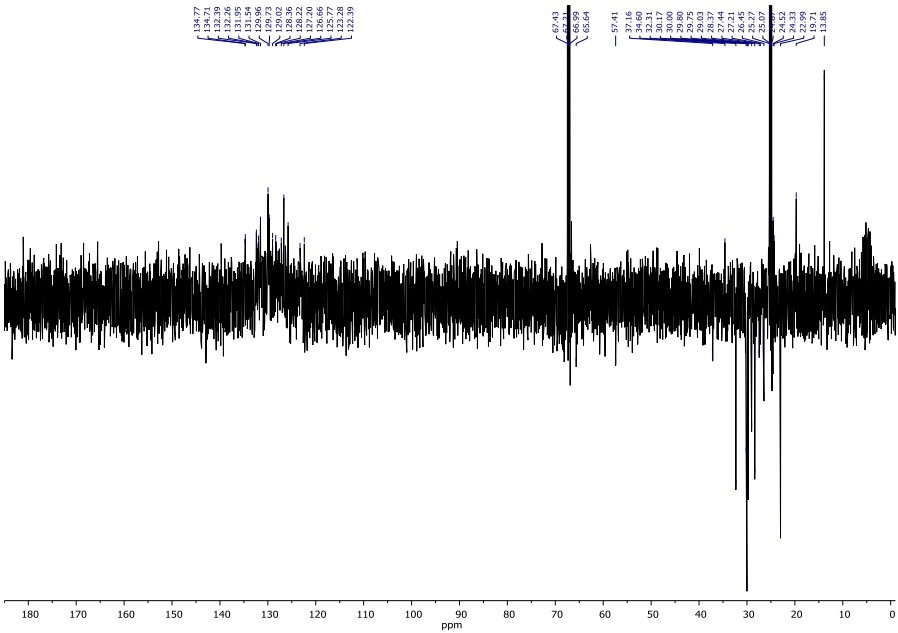

DEPT-135 NMR spectrum of **2a** in THF-d_8/TFA-d (CH/CH_3 positive, CH_2 negative).

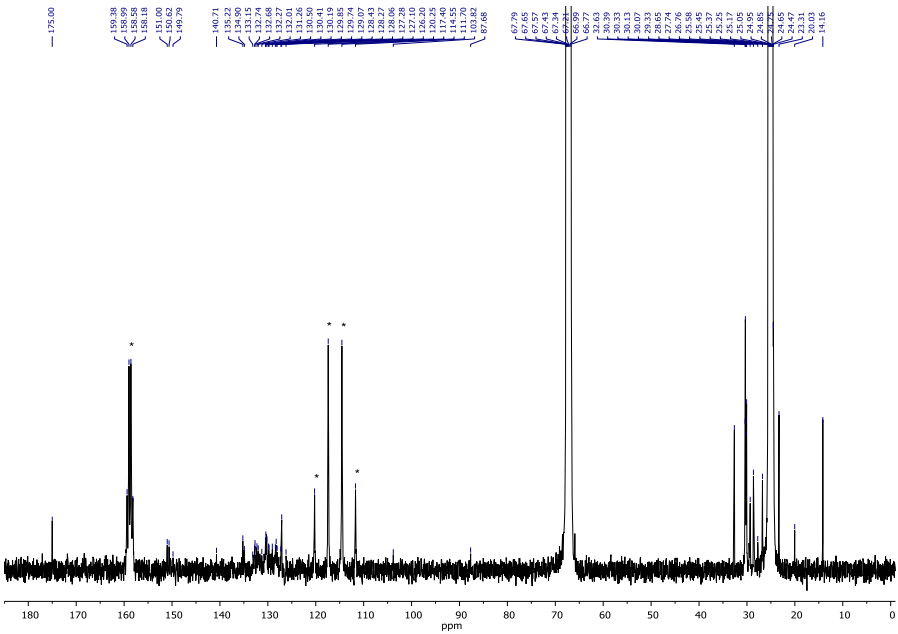

^{13}C NMR spectrum of **2a** in THF-d_8 with TFA-d (*).

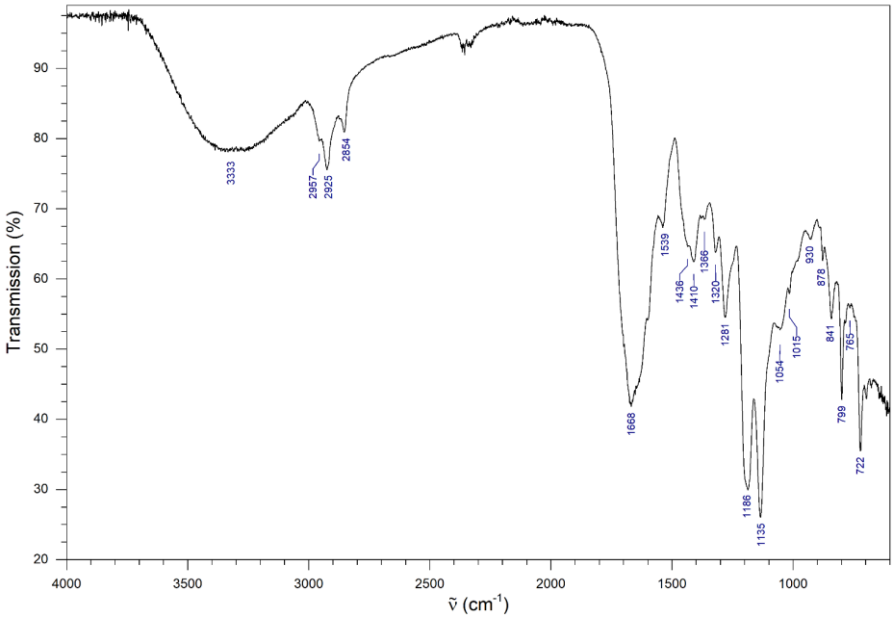

FT-IR spectrum of **2a**.

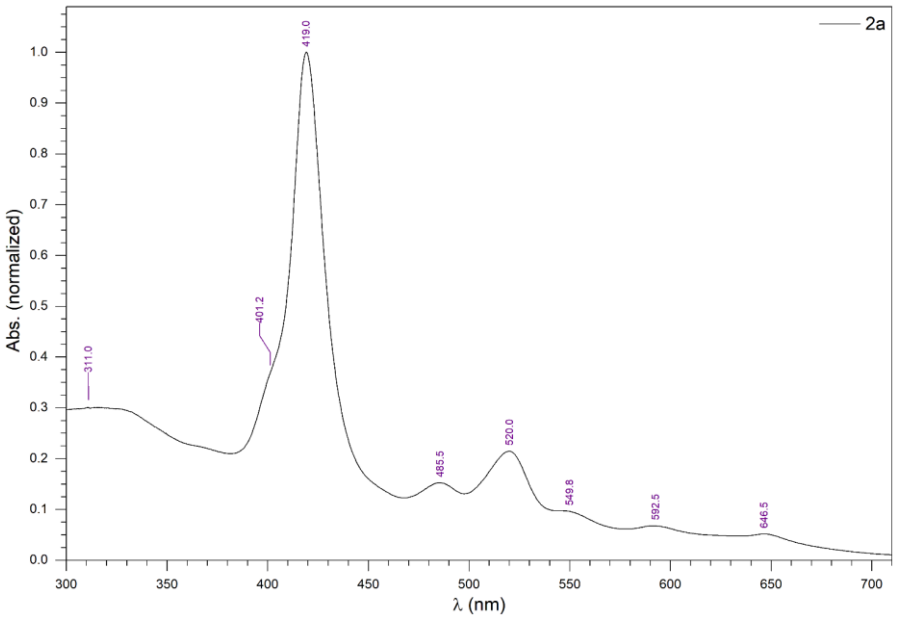

UV-Vis spectrum of **2a** (de-metallated) in THF.

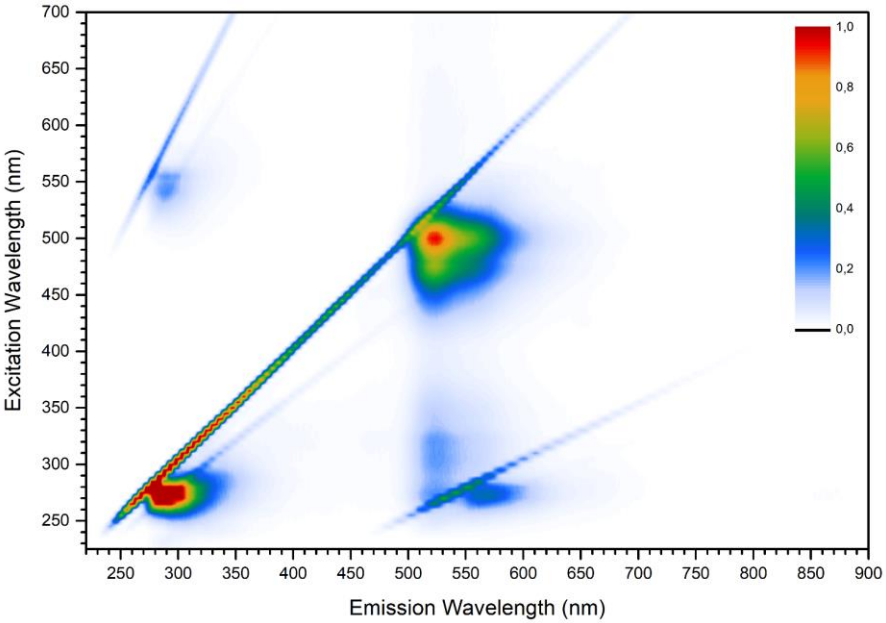

3D excitation-emission spectrum of **2a** (de-metallated) in THF.

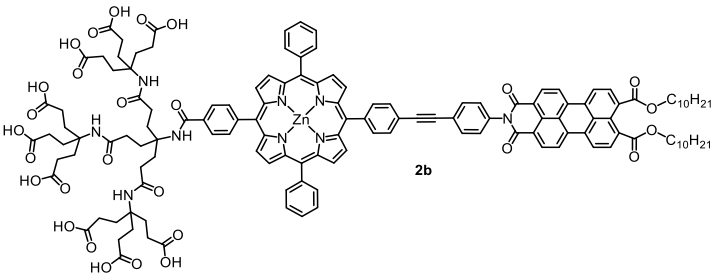

2b

$C_{137}H_{141}N_9O_{28}Zn$

ex. M. 2423.9178

MW 2427.0500

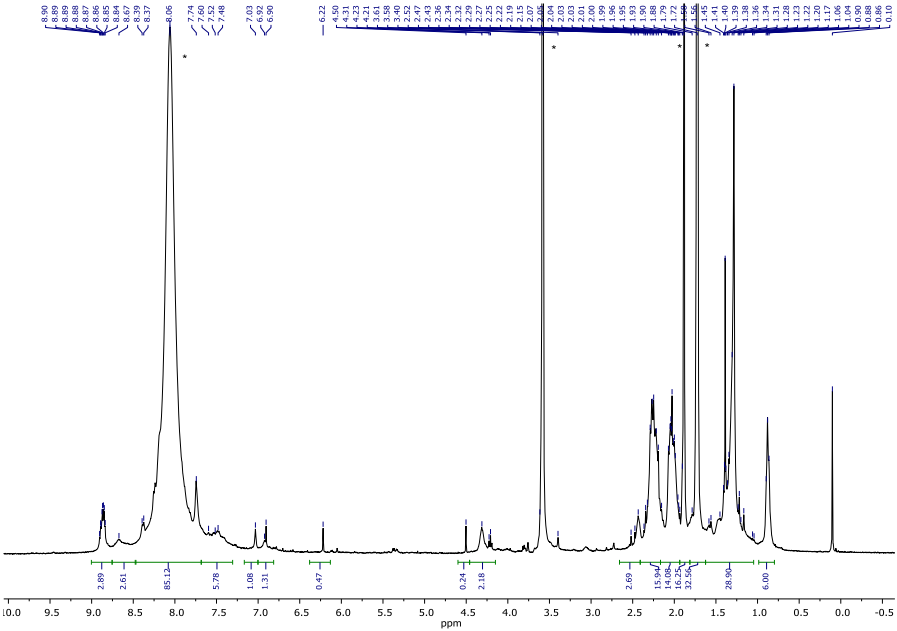

^{1}H NMR spectrum of **2b** in THF-d_8 with TFA-d (*).

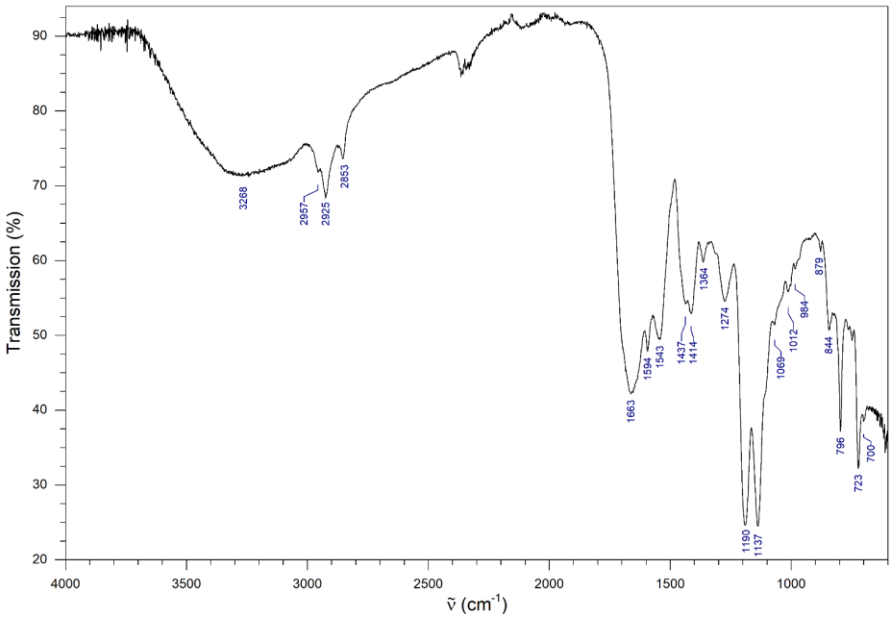

FT-IR spectrum of **2b**.

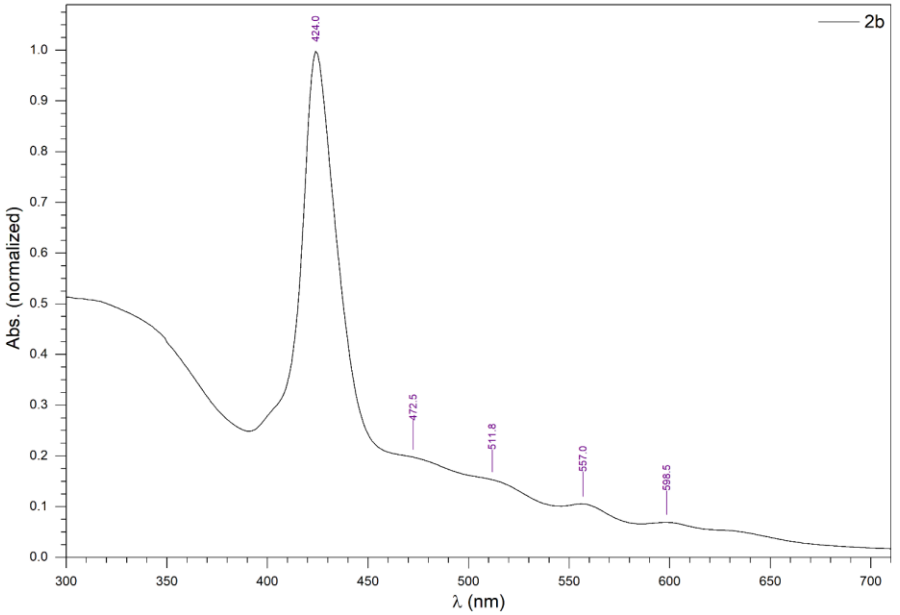

UV-Vis spectrum of **2b** in THF.

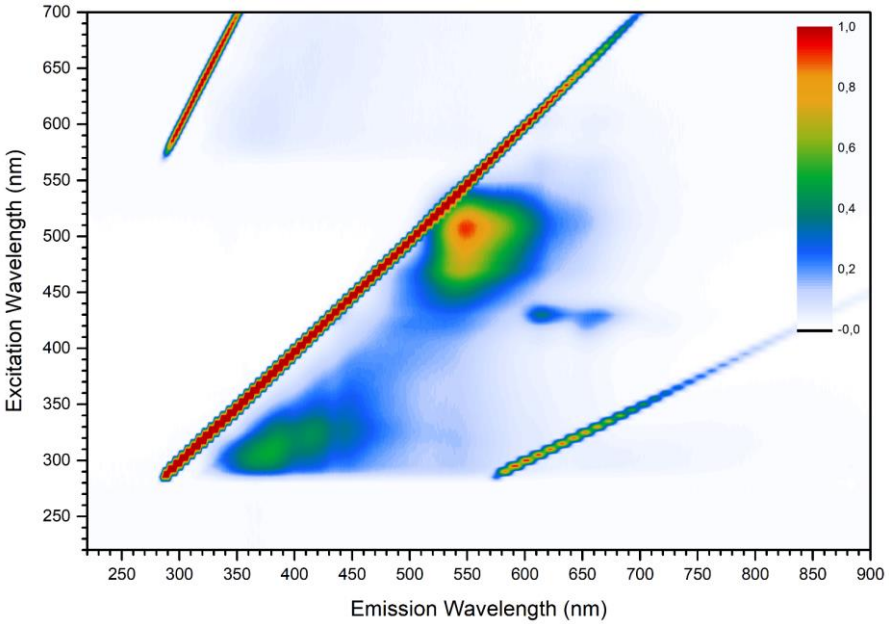

3D excitation-emission spectrum of **2b** in H_2O/NaOH/pyridine.

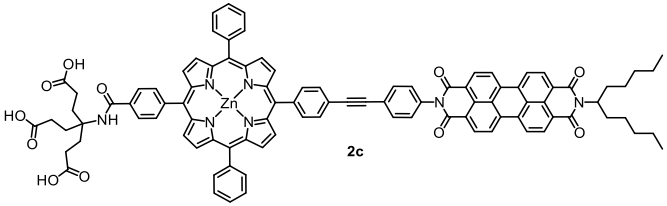

2c

$C_{98}H_{77}N_7O_{11}Zn$

ex. M. 1591.4973

MW 1594.1120

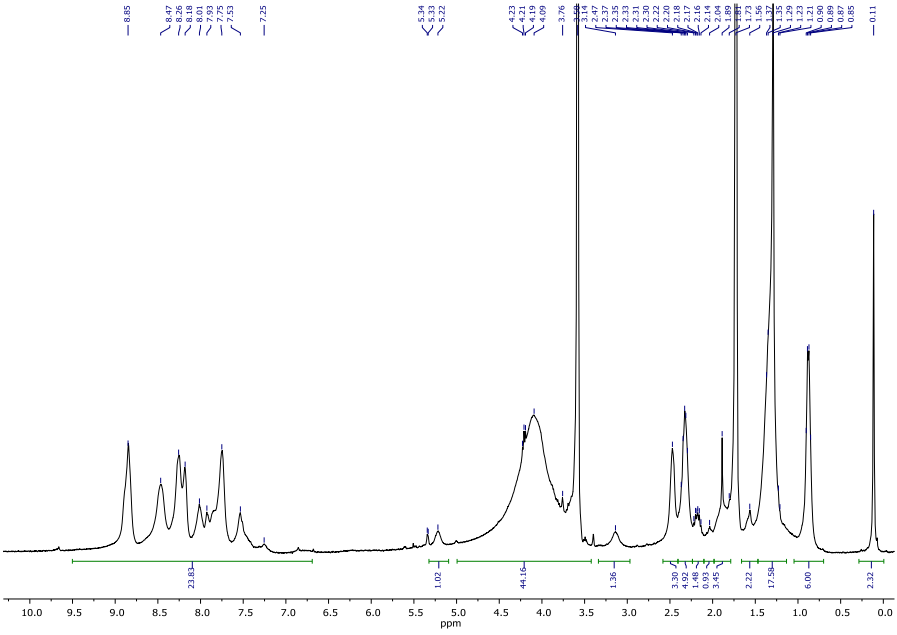

^{1}H NMR spectrum of **2c** in THF-d_8.

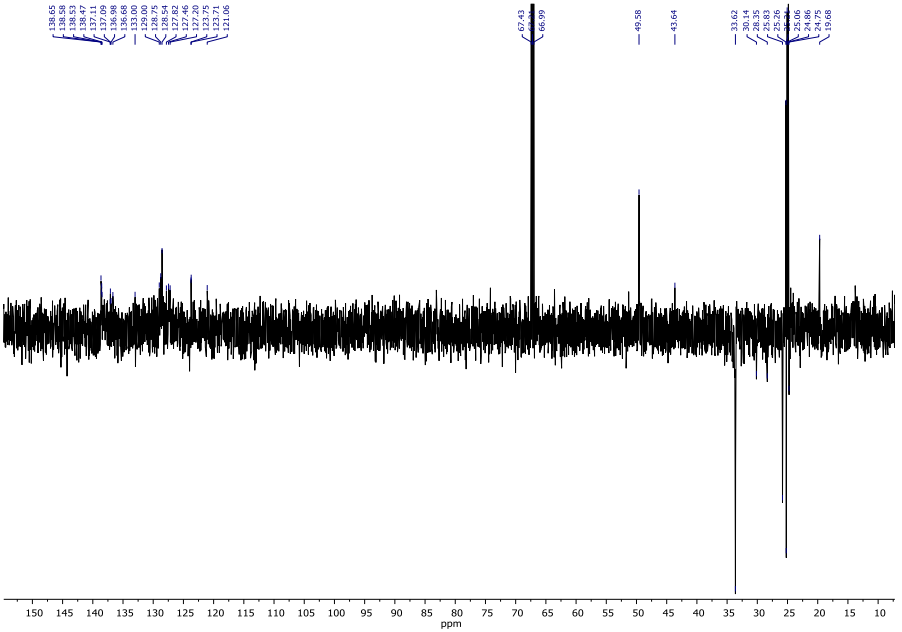

DEPT-135 NMR spectrum of **2c** in THF-d_8 (CH/CH_3 positive, CH_2 negative, C not visible).

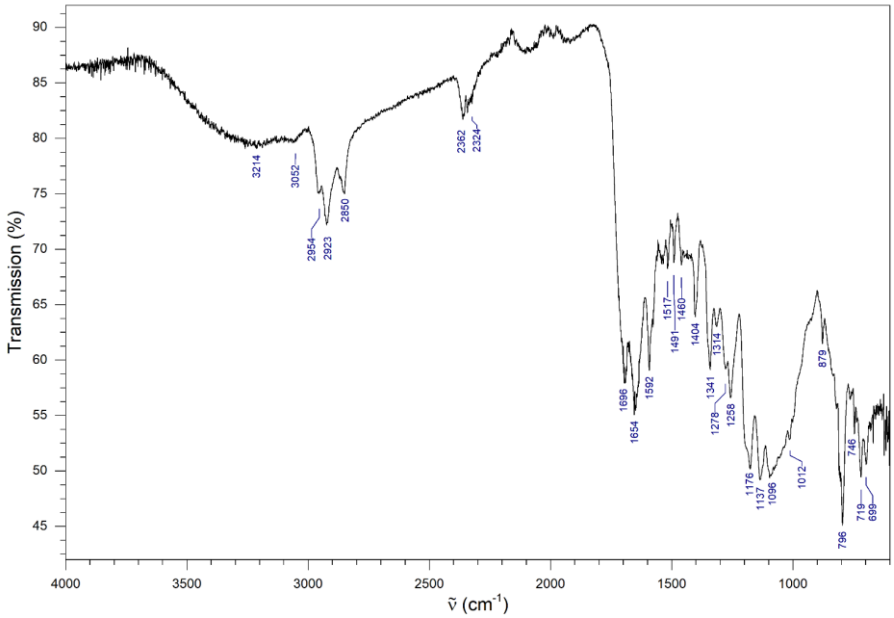

FT-IR spectrum of **2c**.

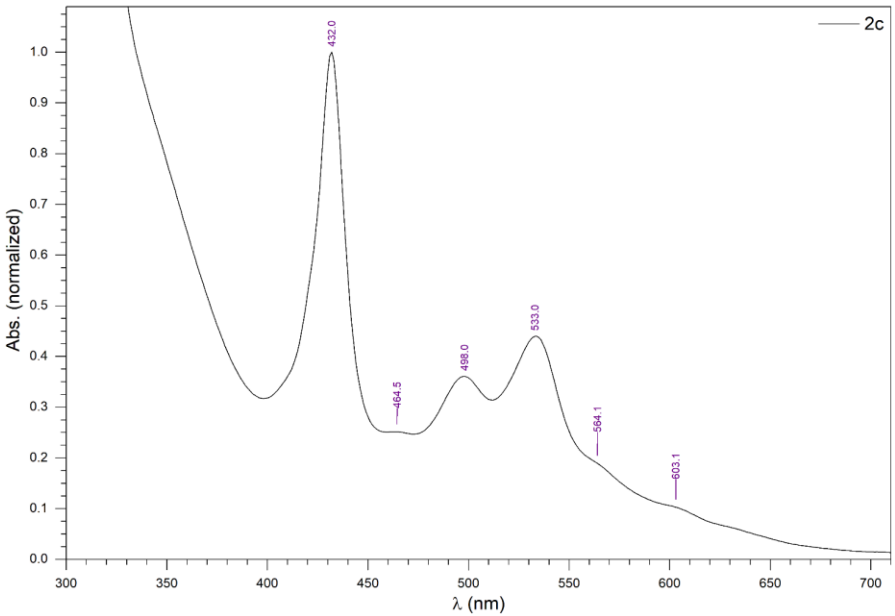

UV-Vis spectrum of **2c** in H_2O + pyridine (without NaOH).

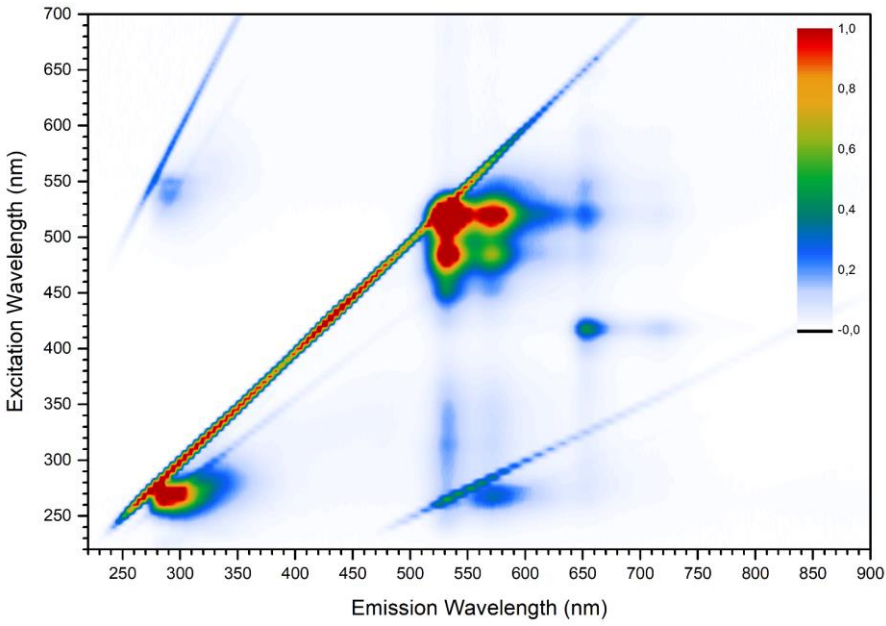

3D excitation-emission spectrum of **2c** in THF.

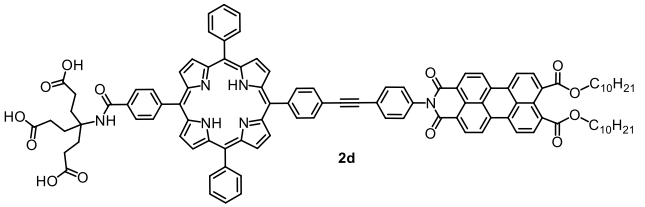

2d

$C_{107}H_{98}N_6O_{13}$

ex. M. 1674.7192

MW 1675.9900

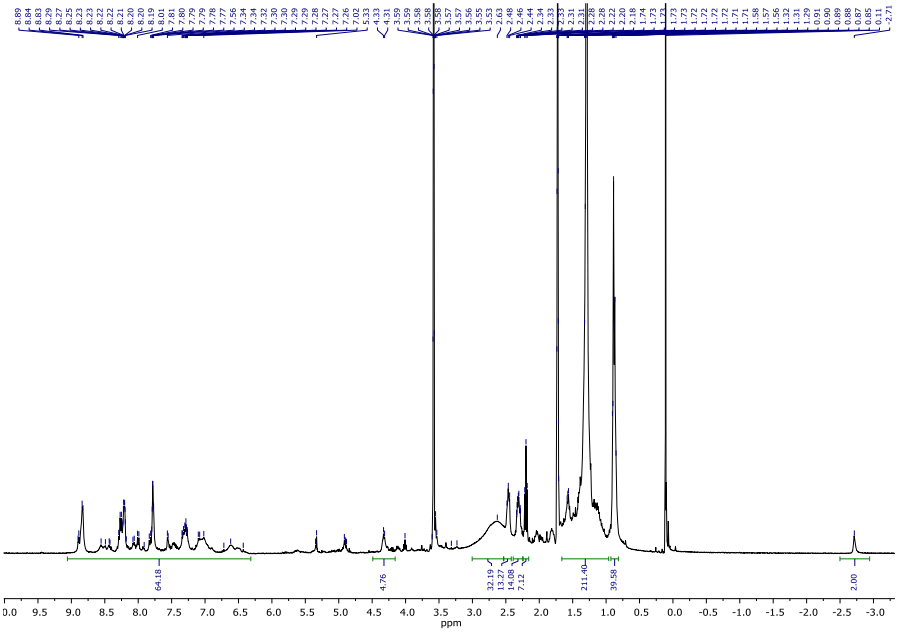

^{1}H NMR spectrum of **2d** in THF-d_8.

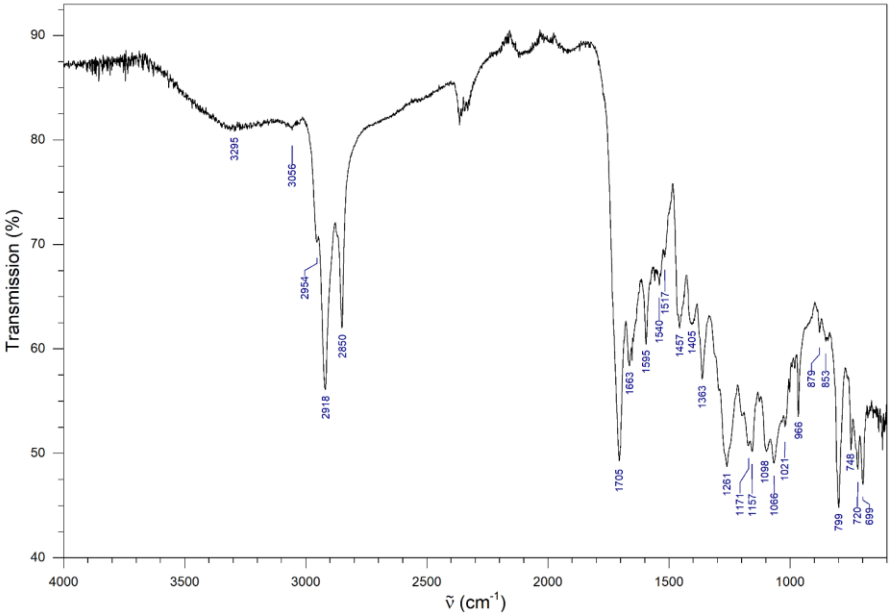

FT-IR spectrum of **2d**.

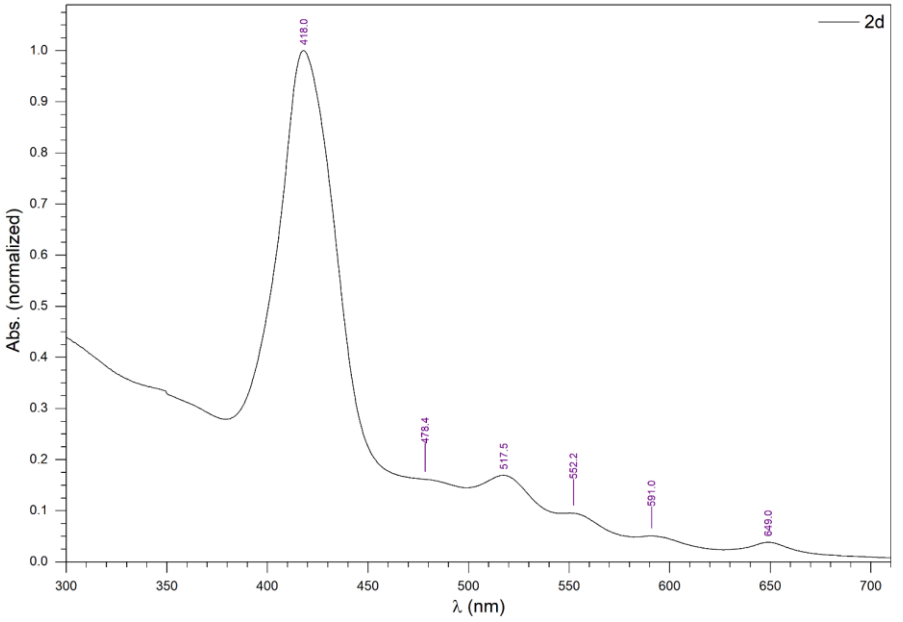

UV-Vis spectrum of **2d** in THF.

Display Report

Analysis Info

Analysis Name	D:\Data\Hirsch-2016-\Methfessel-CM-243--2-000001.d	Acquisition Date	8/4/2016 3:00:46 PM
Method	tune_pos_wide.m	Operator	MD
Sample Name		Instrument / Ser#	micrOTOF 213750.10364
Comment	CH2CL2		

Acquisition Parameter

Source Type	ESI	Ion Polarity	Positive	Set Nebulizer	0.3 Bar
Focus	Not active			Set Dry Heater	180 °C
Scan Begin	50 m/z	Set Capillary	4500 V	Set Dry Gas	4.0 l/min
Scan End	3000 m/z	Set End Plate Offset	-500 V	Set Divert Valve	Waste

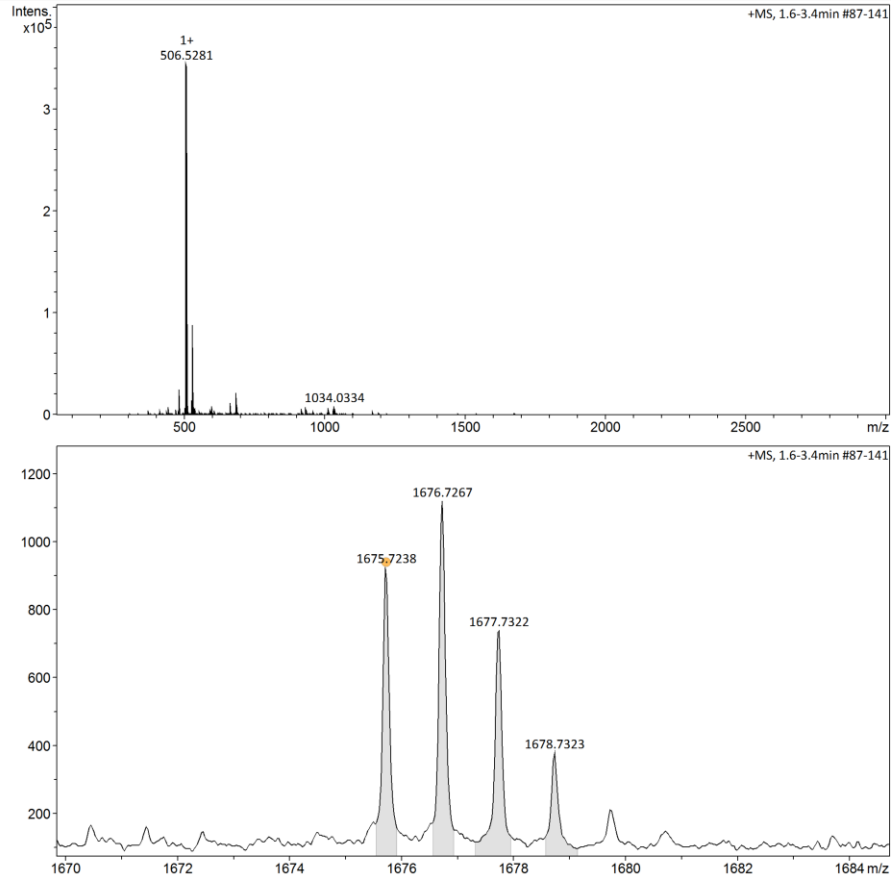

Bruker Compass DataAnalysis 4.2 printed: 8/4/2016 4:01:35 PM Page 1 of 1

MS (ESI+) of **2d**. For comparison of simulated data, see p. 77.

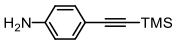

3

$C_{11}H_{15}NSi$

ex. M. 189.0974

MW 189.3330

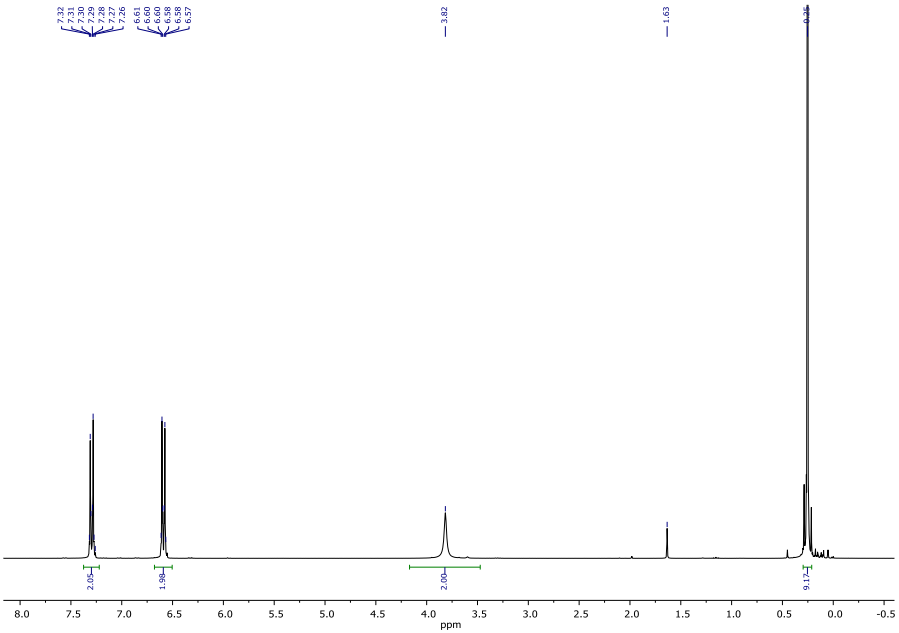

^{1}H NMR spectrum of **3** in $CDCl_3$.

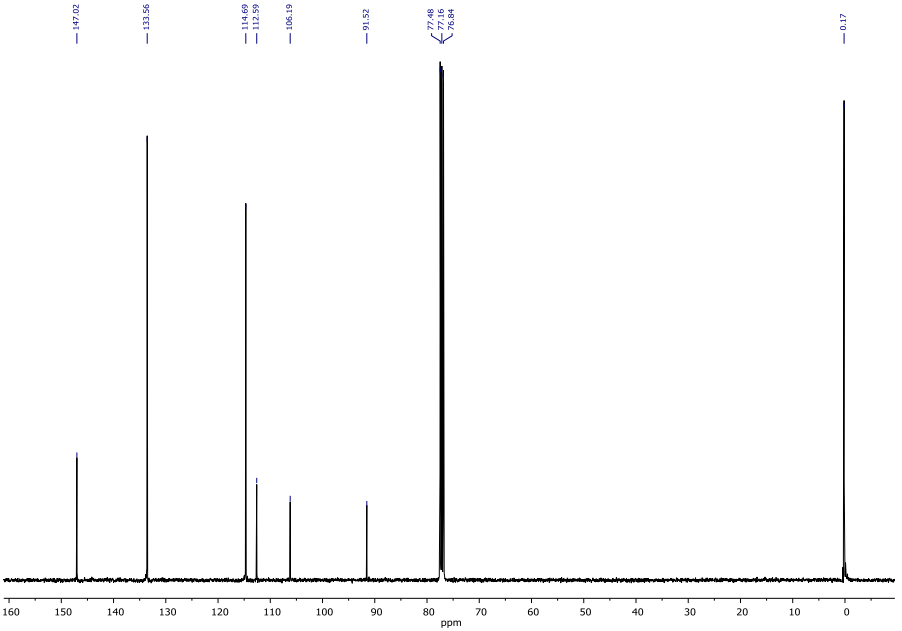

^{13}C NMR spectrum of **3** in $CDCl_3$.

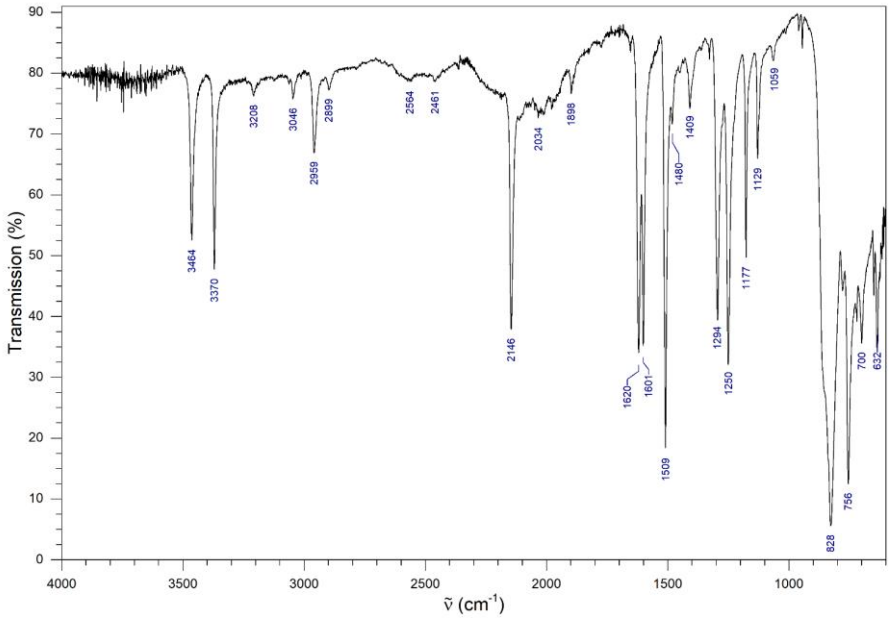

FT-IR spectrum of **3**.

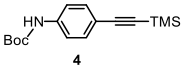

4

$C_{16}H_{23}NO_2Si$

ex. M. 289.1498

MW 289.4500

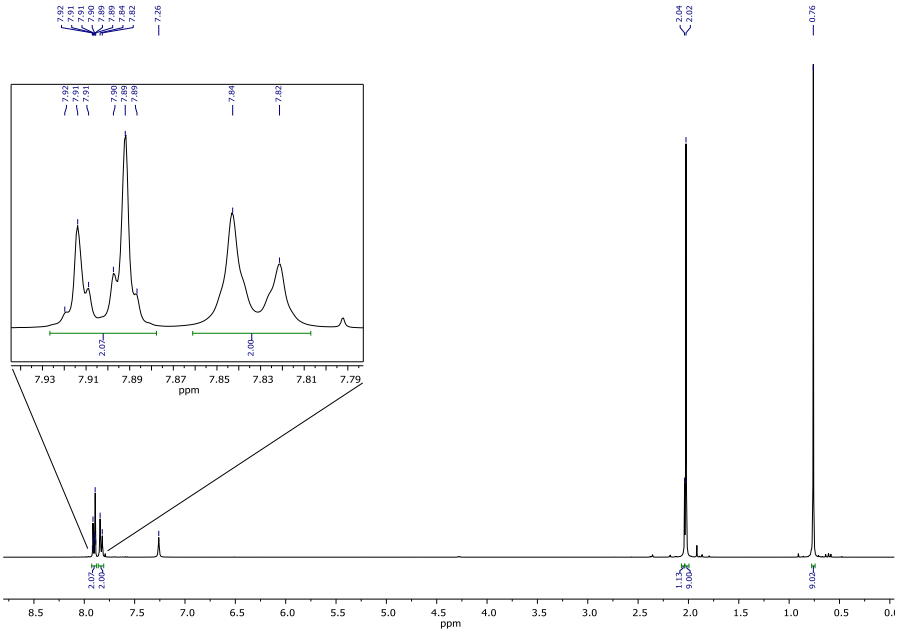

^{1}H NMR spectrum of **4** in $CDCl_3$.

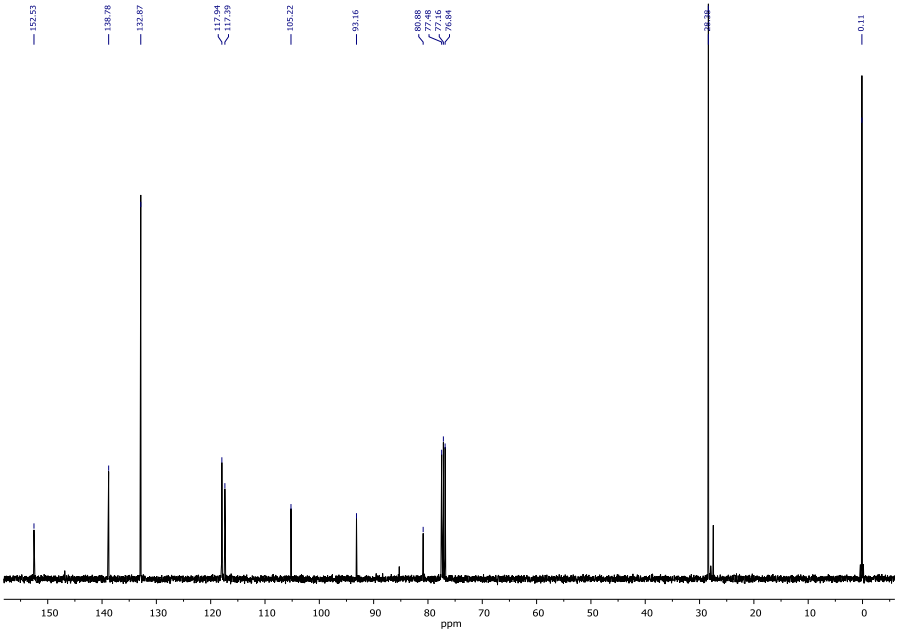

^{13}C NMR spectrum of **4** in $CDCl_3$.

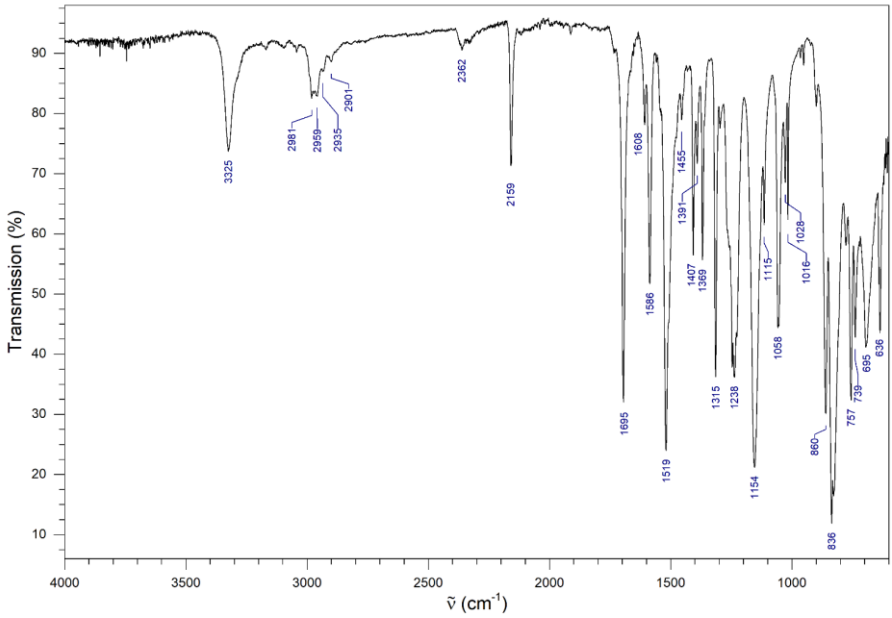

FT-IR spectrum of **4**.

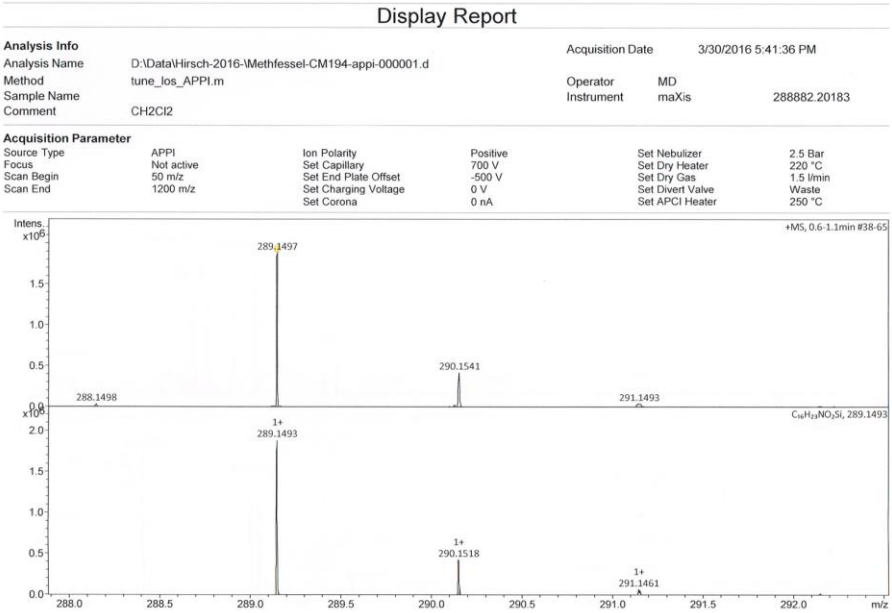

MS (APPI+) of **4** (detail): Recorded (top) and calculated (bottom) mass spectra.

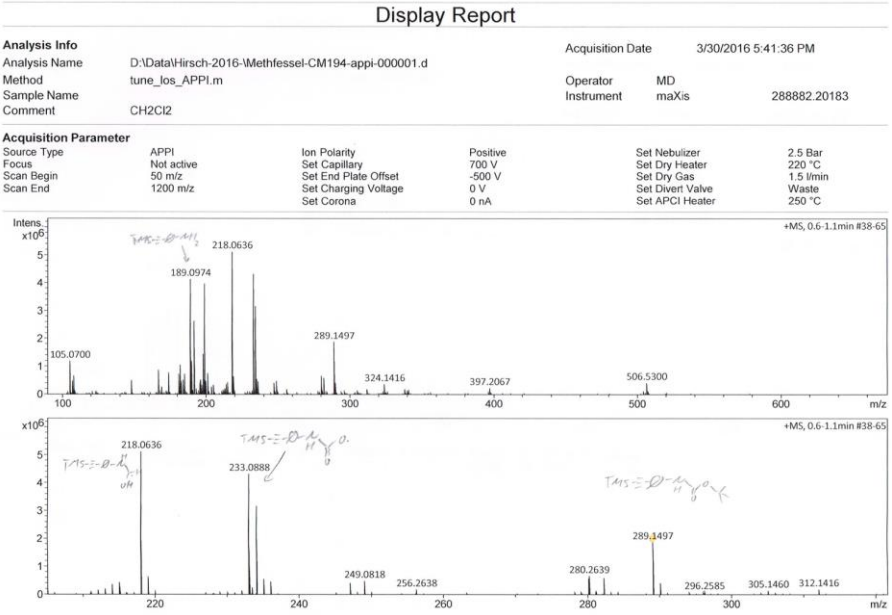

MS (APPI+) of **4** (overview).

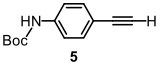

5

$C_{13}H_{15}NO_2$

ex. M.217.1103

MW 217.2680

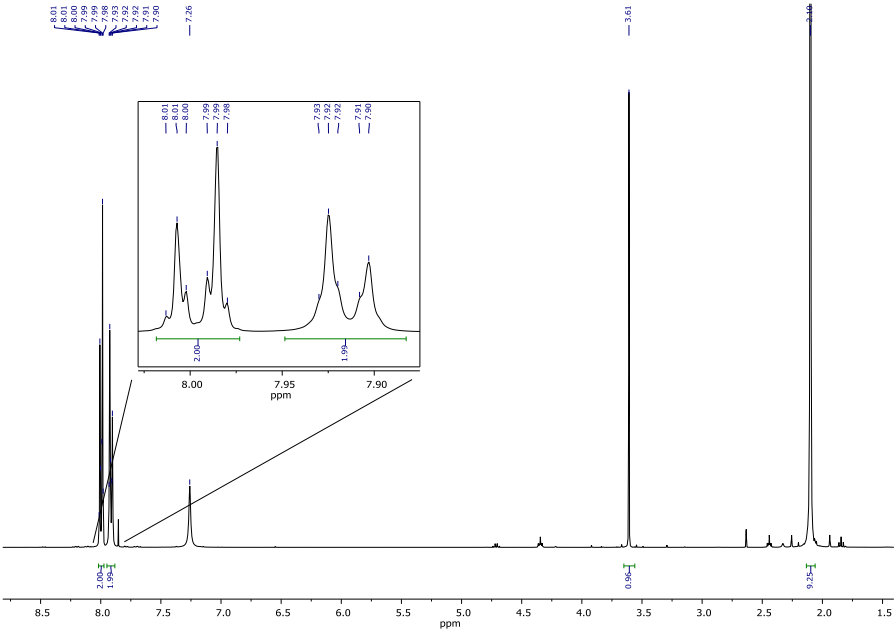

^{1}H NMR spectrum of **5** in $CDCl_3$.

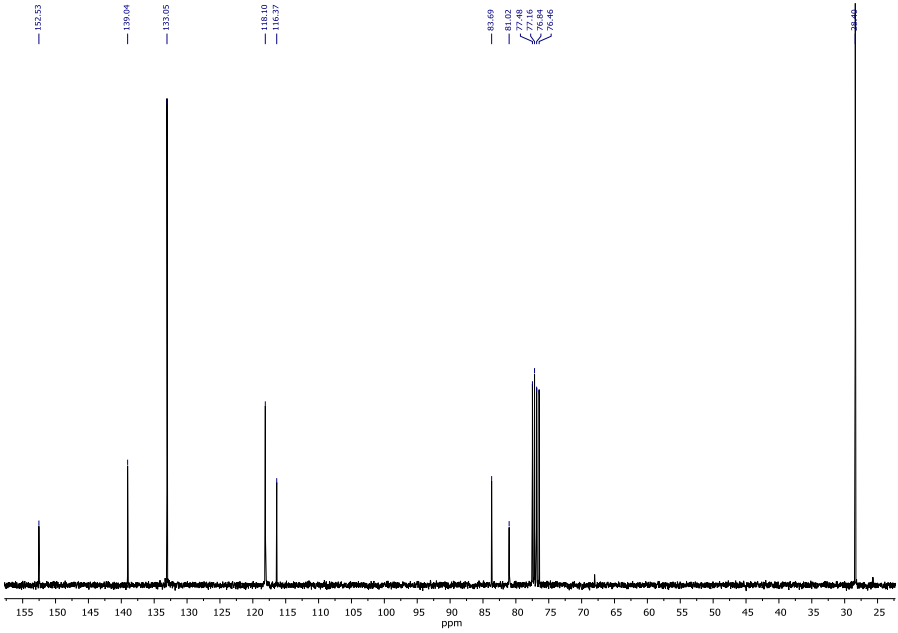

^{13}C NMR spectrum of **5** in $CDCl_3$.

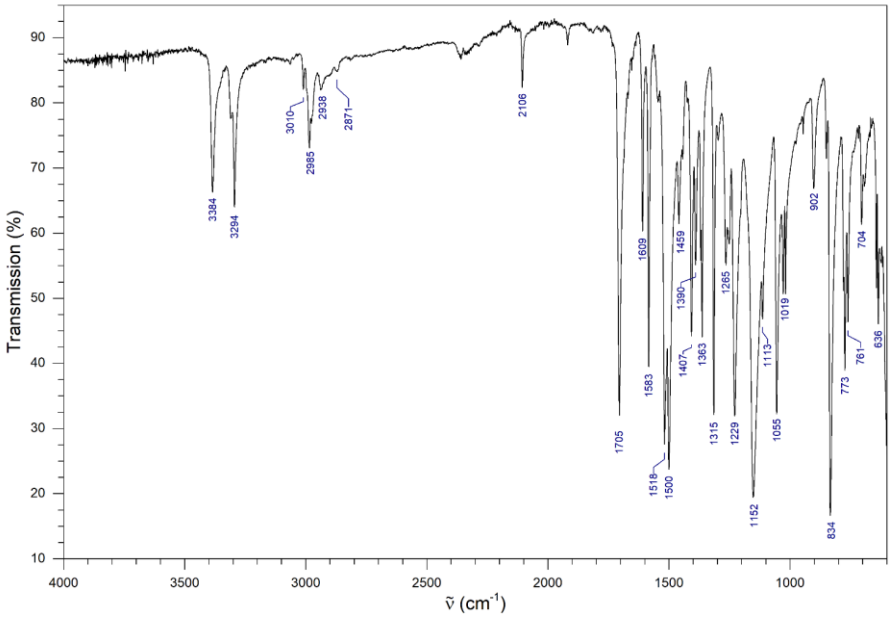

FT-IR spectrum of **5**.

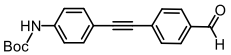

6

$C_{20}H_{19}NO_3$

ex. M. 321.1365

MW 321.3760

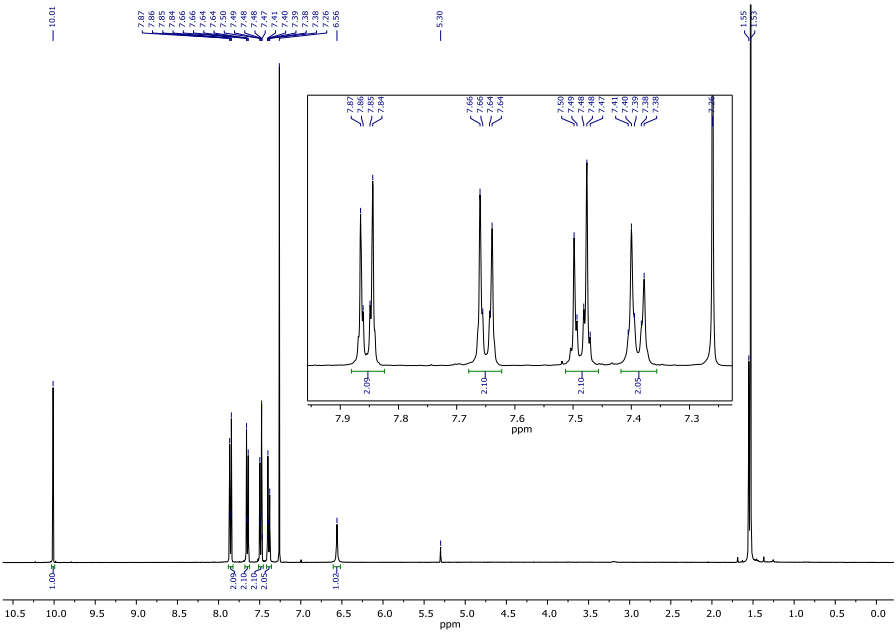

^{1}H NMR spectrum of ***6*** in $CDCl_3$.

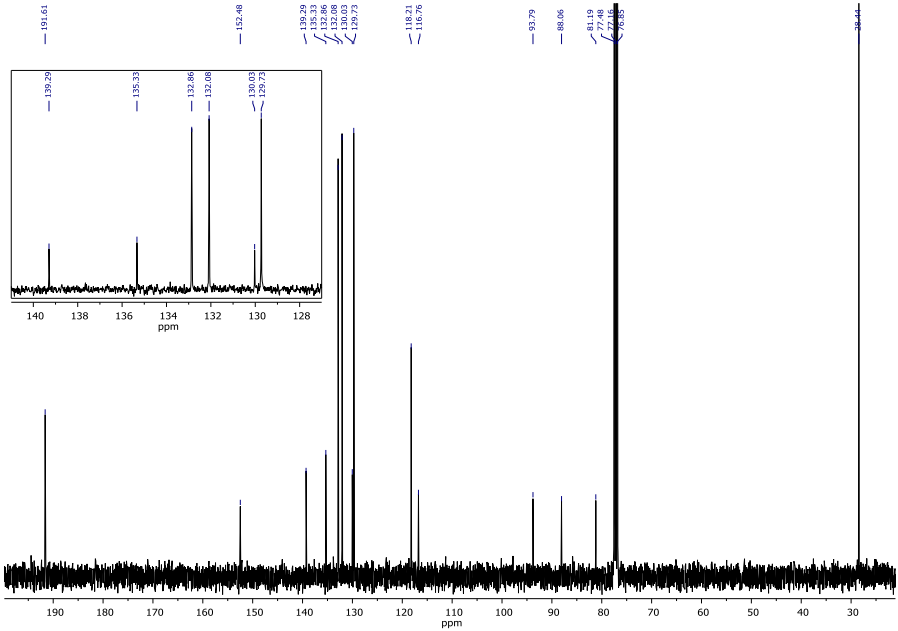

^{13}C NMR spectrum of ***6*** in $CDCl_3$.

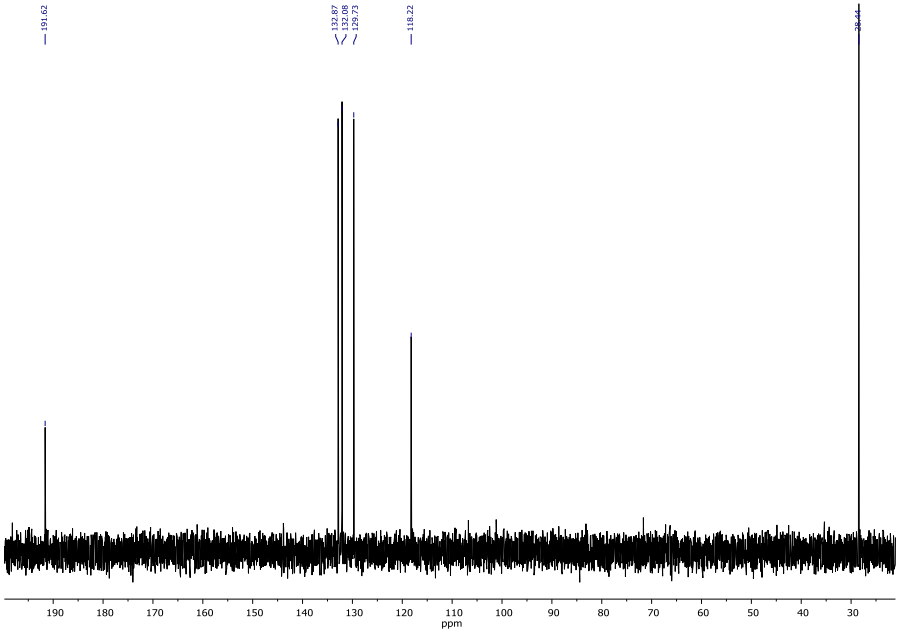

DEPT-135 NMR spectrum of ***6*** in $CDCl_3$ (CH/CH_3 positive, CH_2 negative, C not visible).

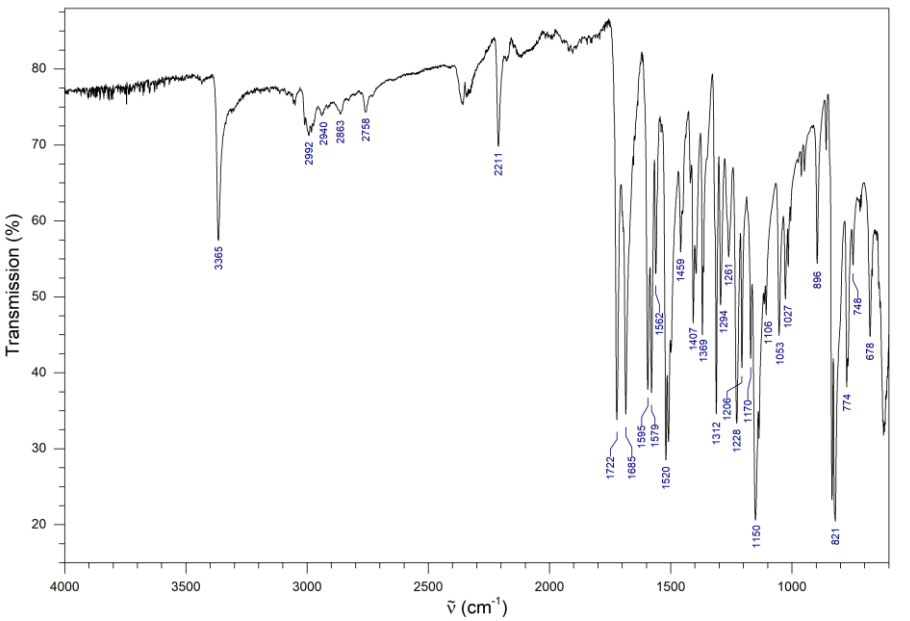

FT-IR spectrum of **6**.

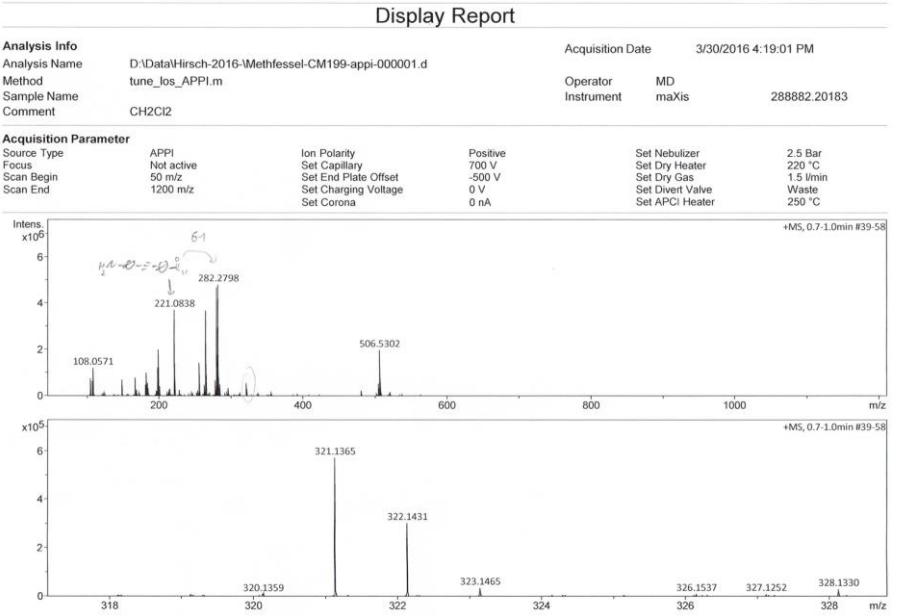

MS (APPI+) of **6**.

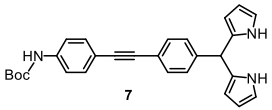

7

$C_{28}H_{27}N_3O_2$

ex. M. 437.2103

MW 437.5430

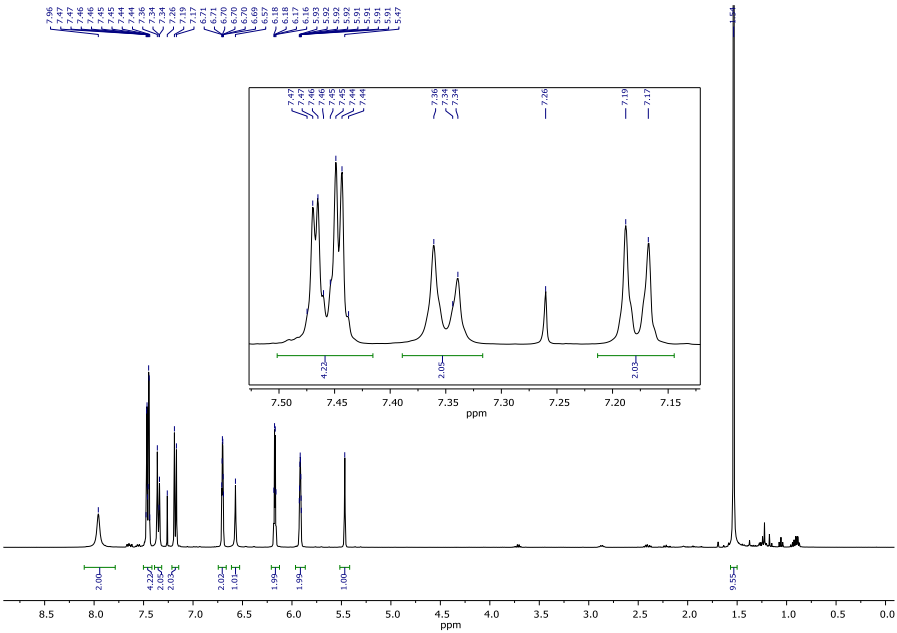

^{1}H NMR spectrum of **7** in $CDCl_3$.

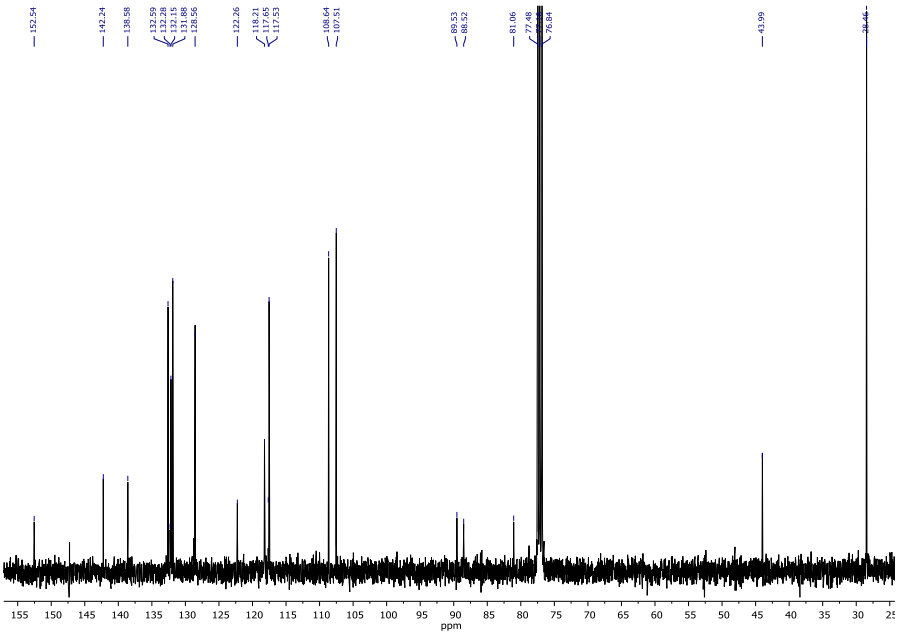

^{13}C NMR spectrum of **7** in $CDCl_3$.

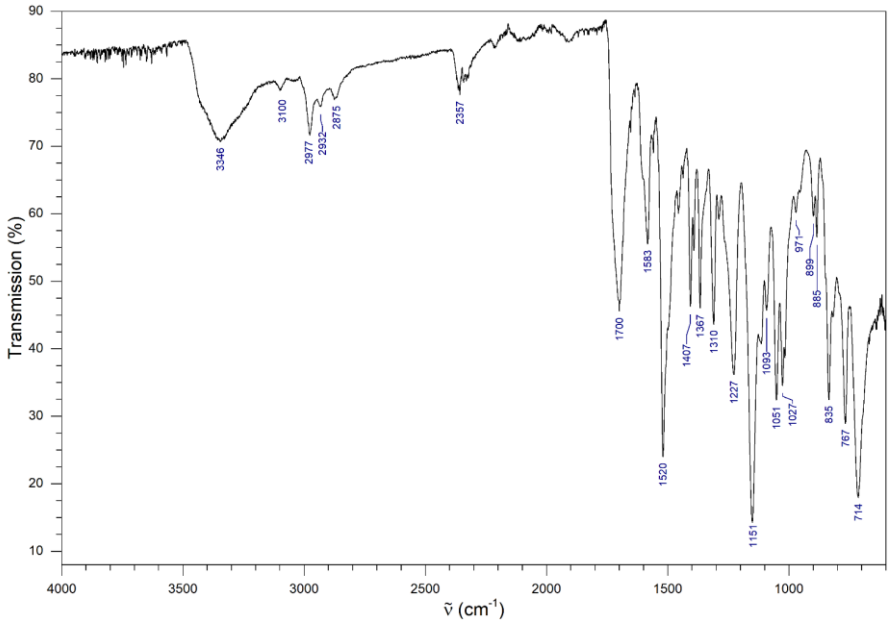

FT-IR spectrum of **7**.

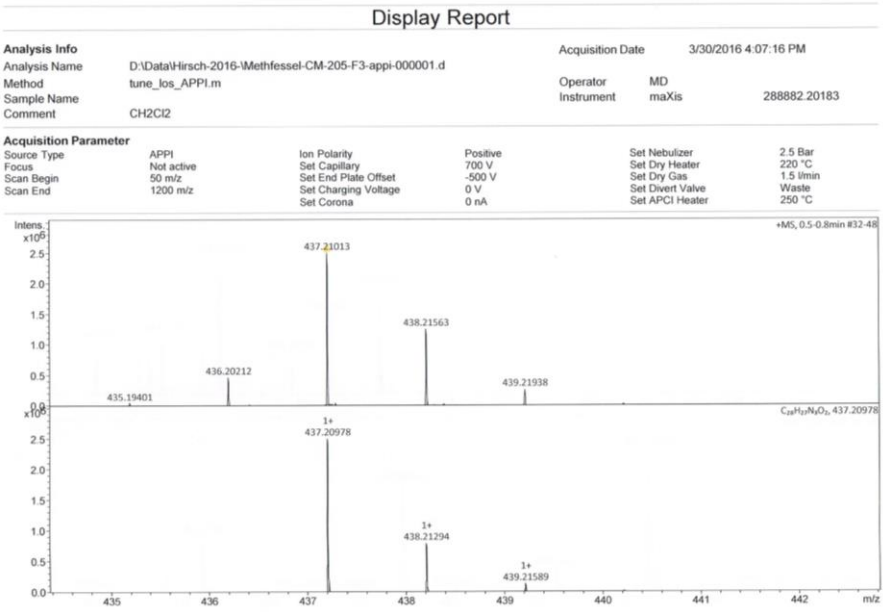

MS (APPI+) spectrum of **4**. Recorded (top) and calculated (bottom) mass spectra. The $[M\text{-}H]^+$ peak is common for DPMs in APPI measurements.

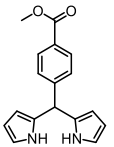

8

$C_{17}H_{16}N_2O_2$

ex. M. 280.1212

MW 280.3270

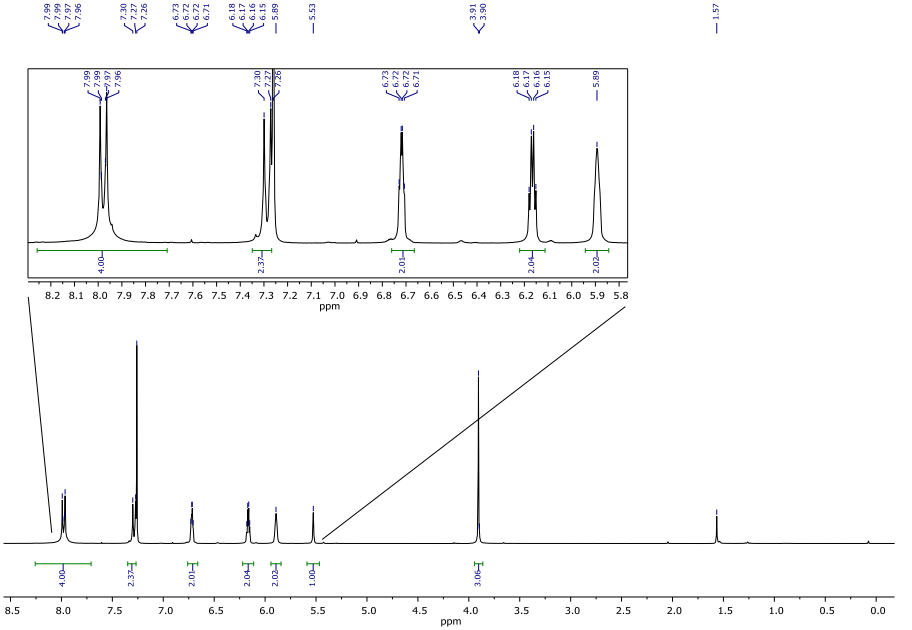

^{1}H NMR spectrum of **8** in $CDCl_3$.

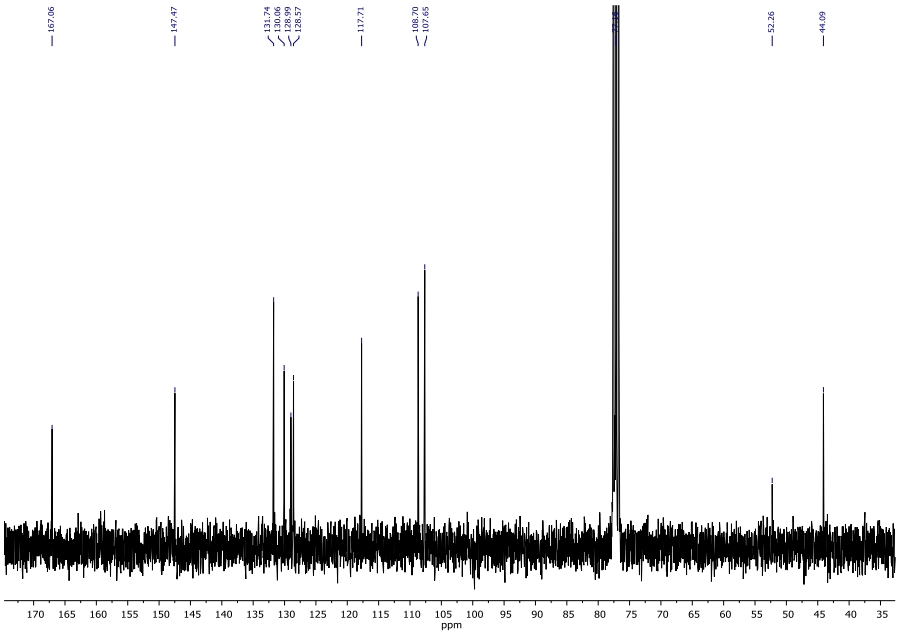

^{13}C NMR spectrum of **8** in $CDCl_3$.

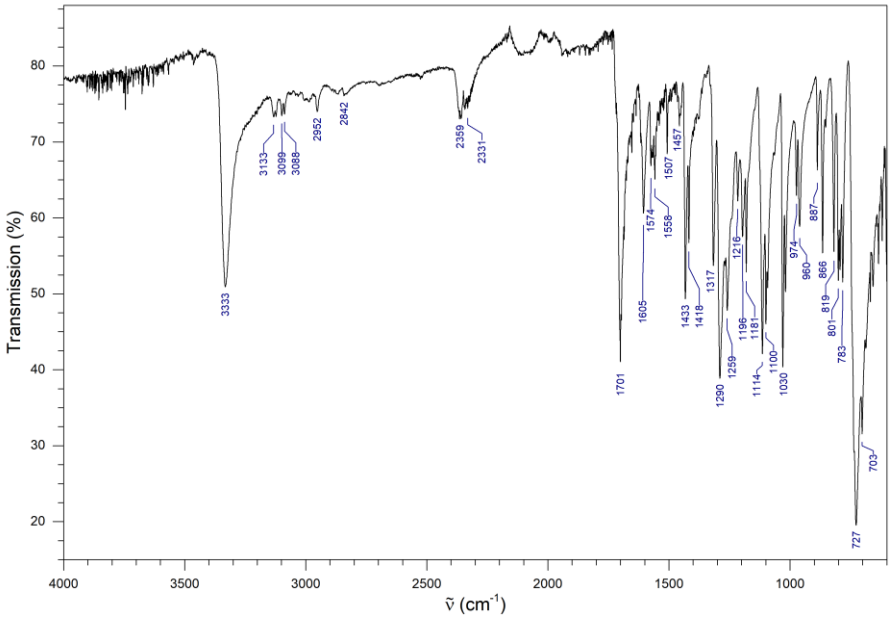

FT-IR spectrum of **8**.

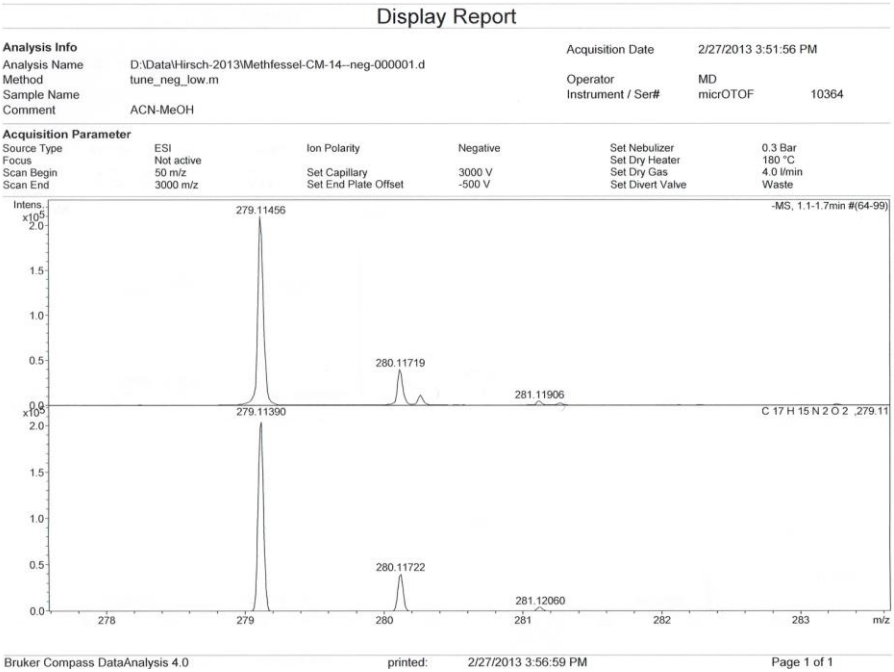

MS (ESI-) spectrum of **8**. Recorded (top) and calculated (bottom) mass spectra.

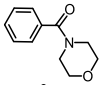

9

$C_{11}H_{13}NO_2$

ex. M. 191.0946

MW 191.2300

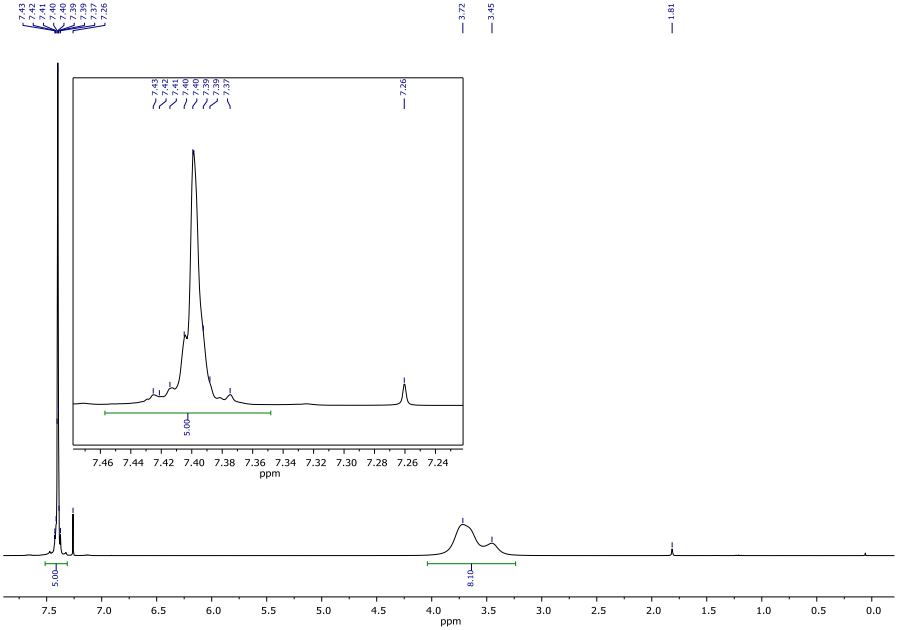

^{1}H NMR spectrum of **9** in $CDCl_3$.

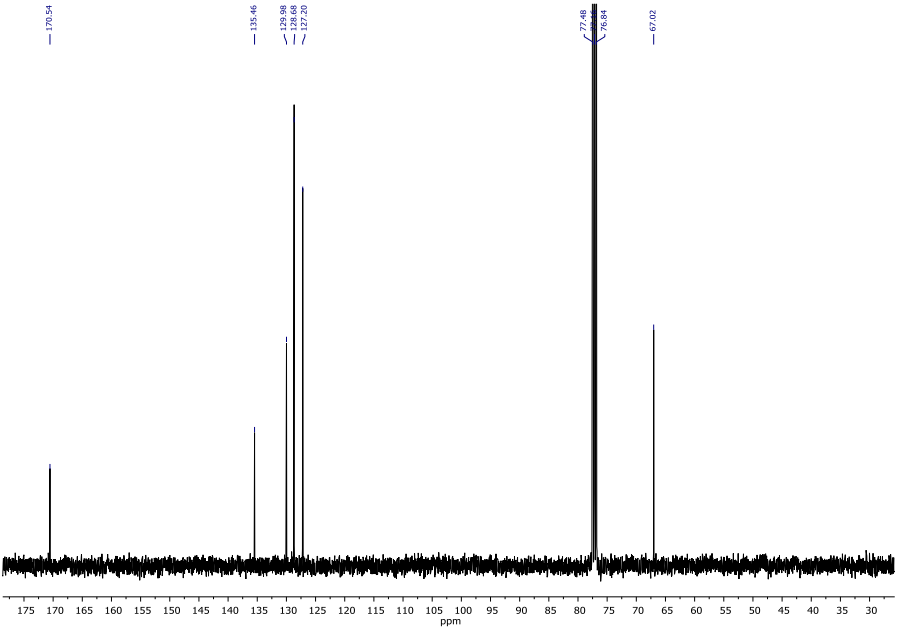

^{13}C NMR spectrum of **9** in $CDCl_3$.

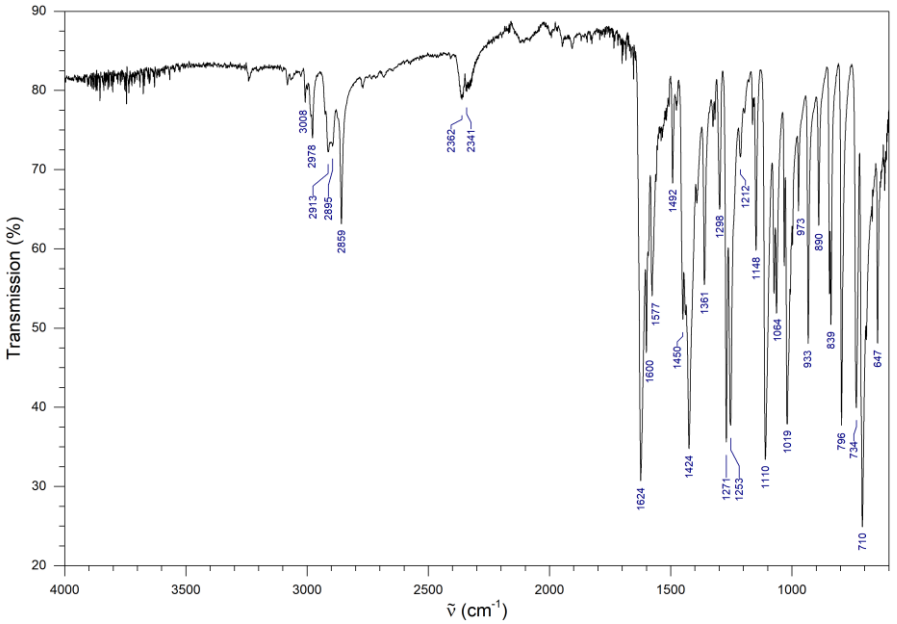

FT-IR spectrum of **9**.

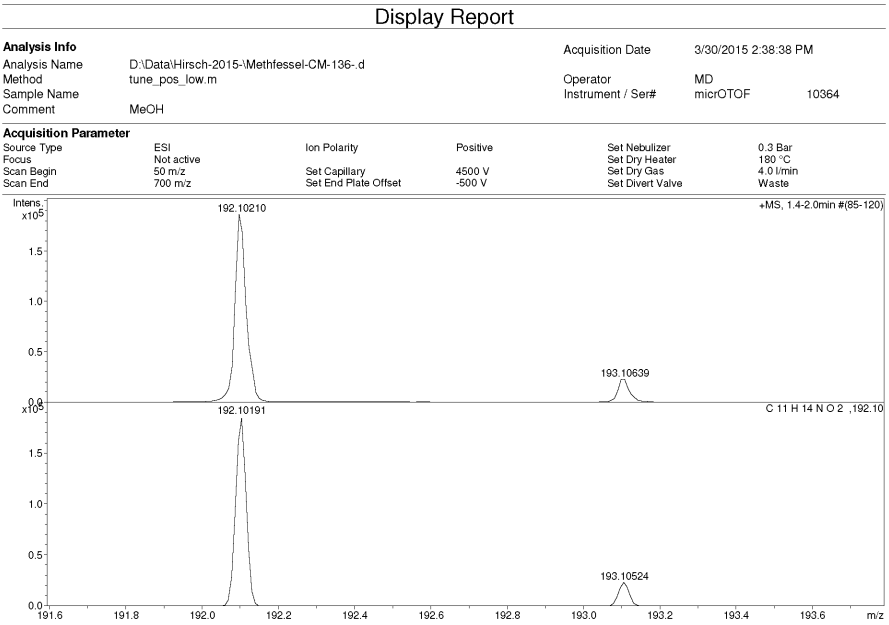

MS (ESI+) spectrum of **9**. Recorded (top) and calculated (bottom) mass spectra.

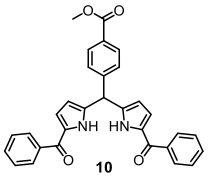

10

$C_{31}H_{24}N_2O_4$

ex. M. 488.1736

MW 488.5430

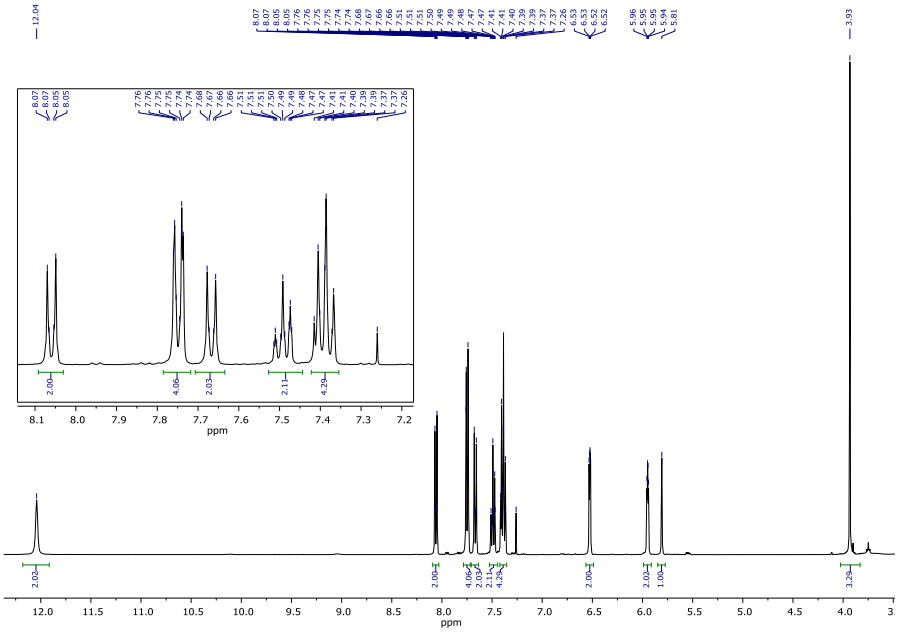

^{1}H NMR spectrum of **10** in $CDCl_3$.

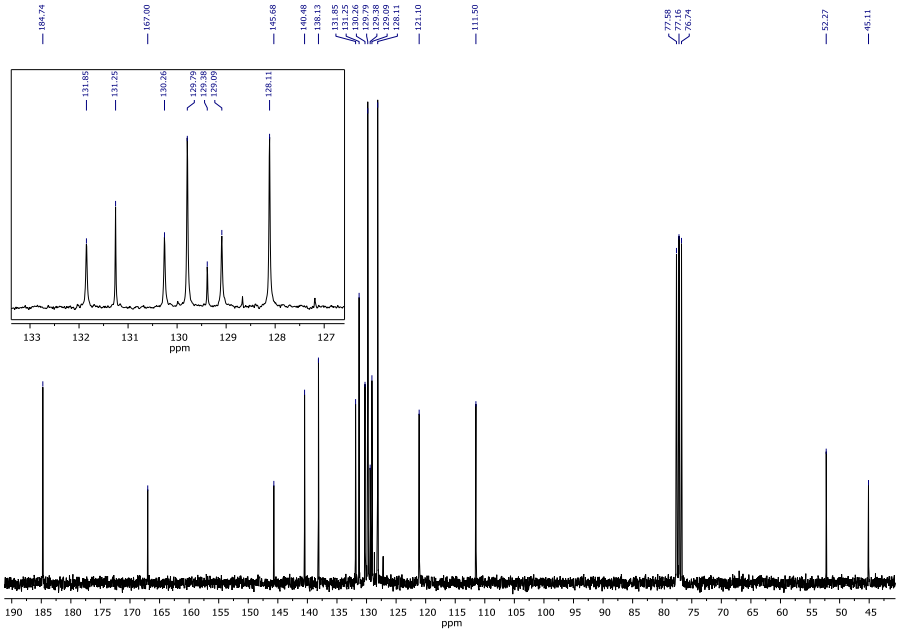

^{13}C NMR spectrum of **10** in $CDCl_3$.

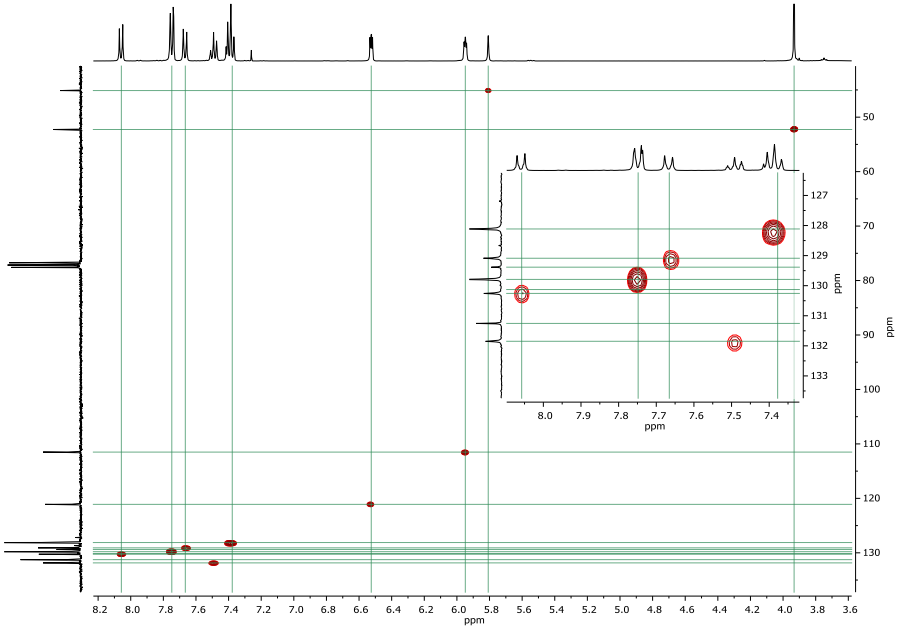

HSQC NMR spectrum of **10** in $CDCl_3$.

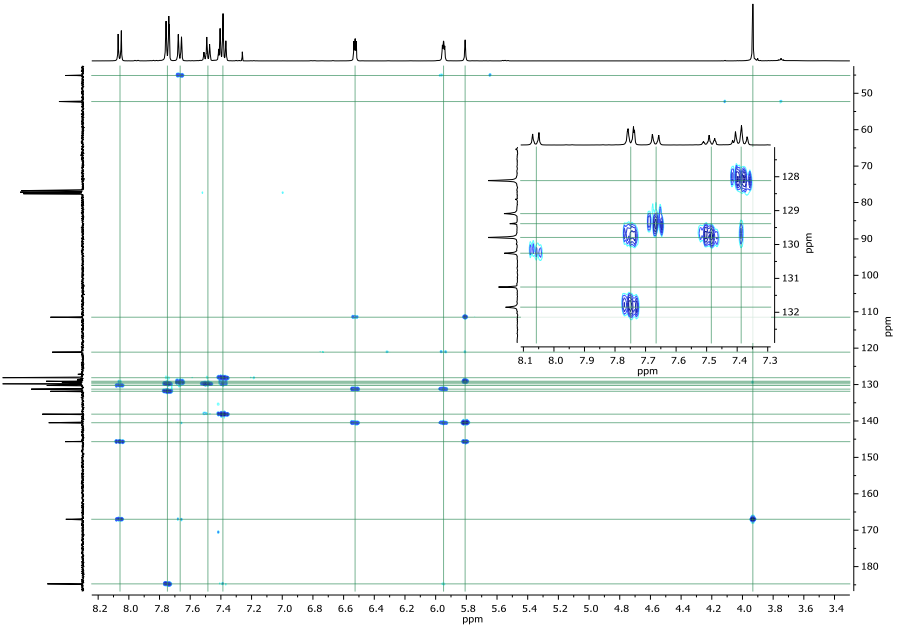

HMBC NMR spectrum of **10** in $CDCl_3$.

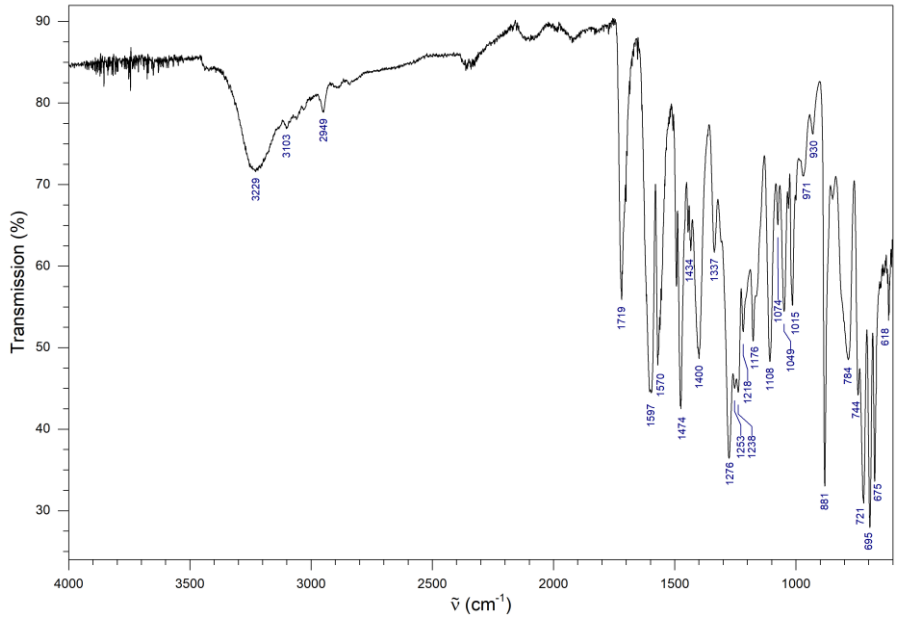

FT-IR spectrum of **10**.

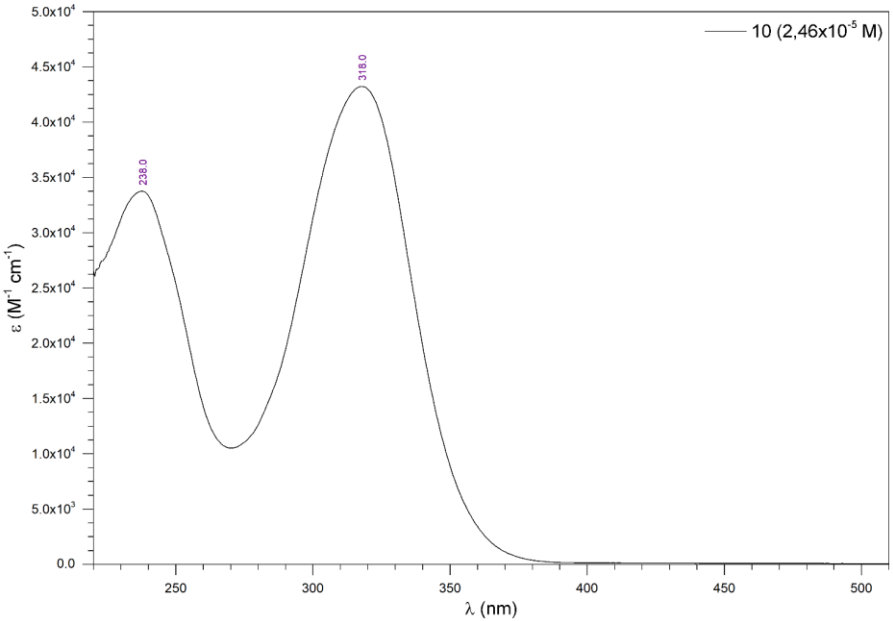

UV-Vis spectrum of **10** in THF.

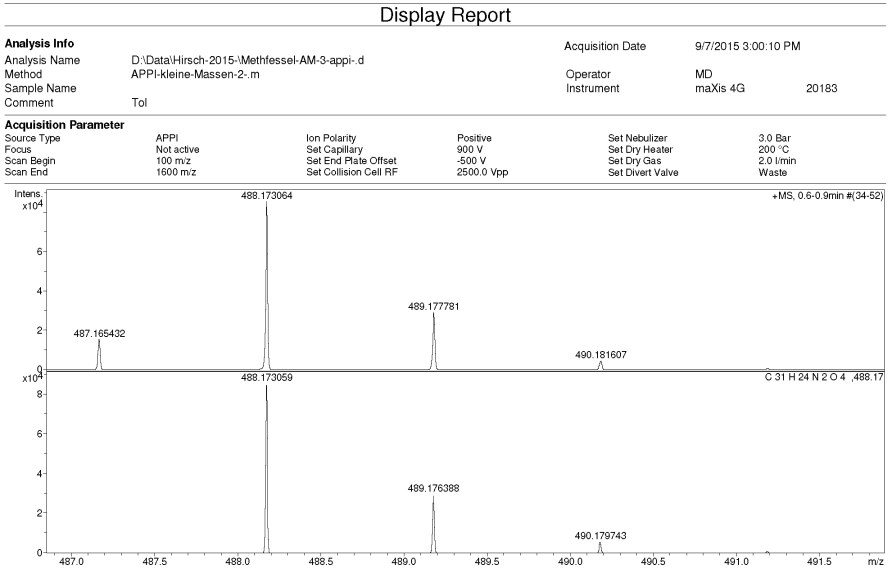

MS (APPI+) spectrum of **10**. Recorded (top) and calculated (bottom) mass spectra. The $[M\text{-}H]^+$ peak is common for DPMs in APPI measurements.

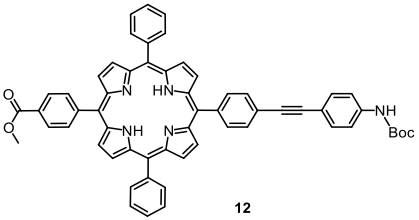

12

$C_{59}H_{45}N_5O_4$

ex. M. 887.3472

MW 888.0400

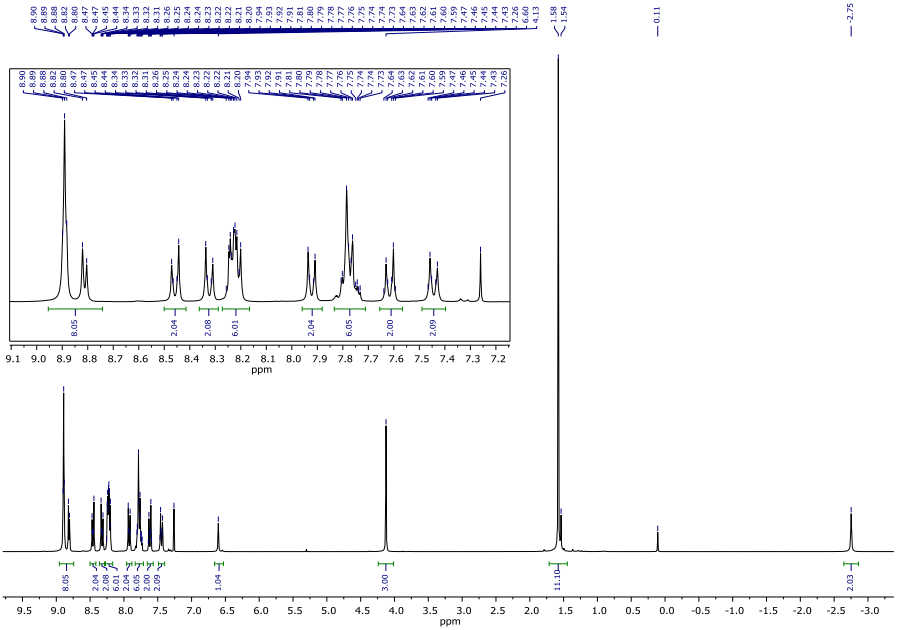

^{1}H NMR spectrum of **12** in $CDCl_3$.

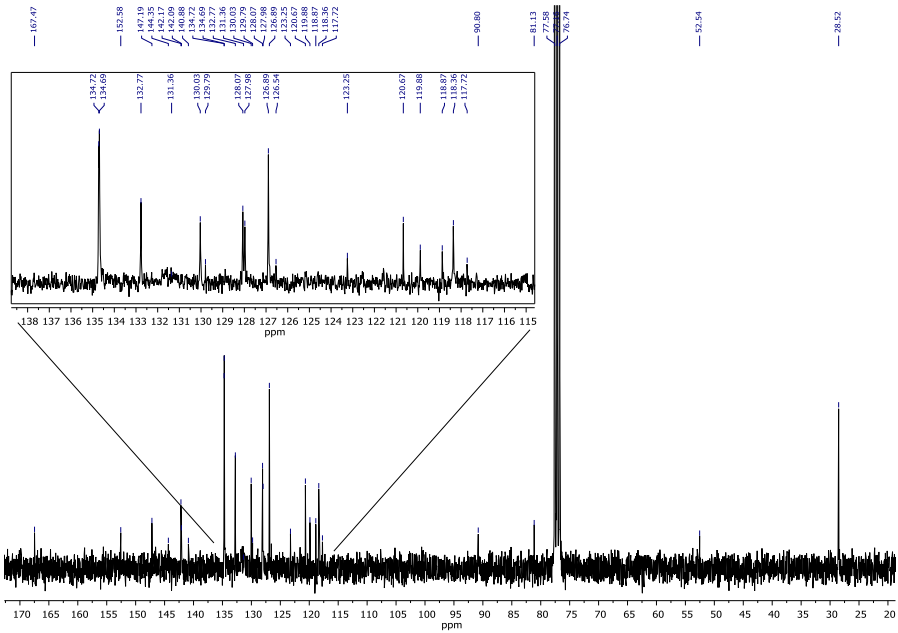

^{13}C NMR spectrum of **12** in $CDCl_3$.

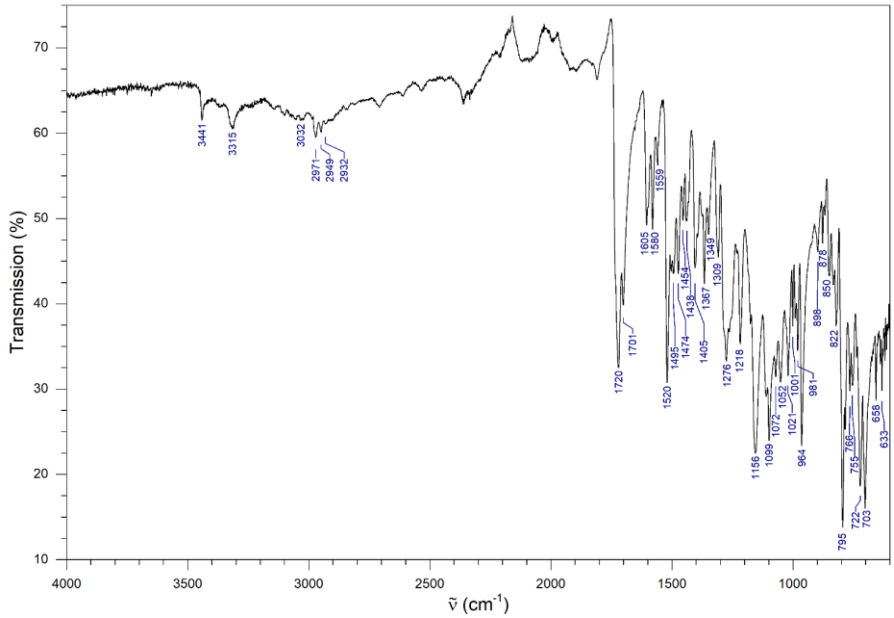

FT-IR spectrum of **12**.

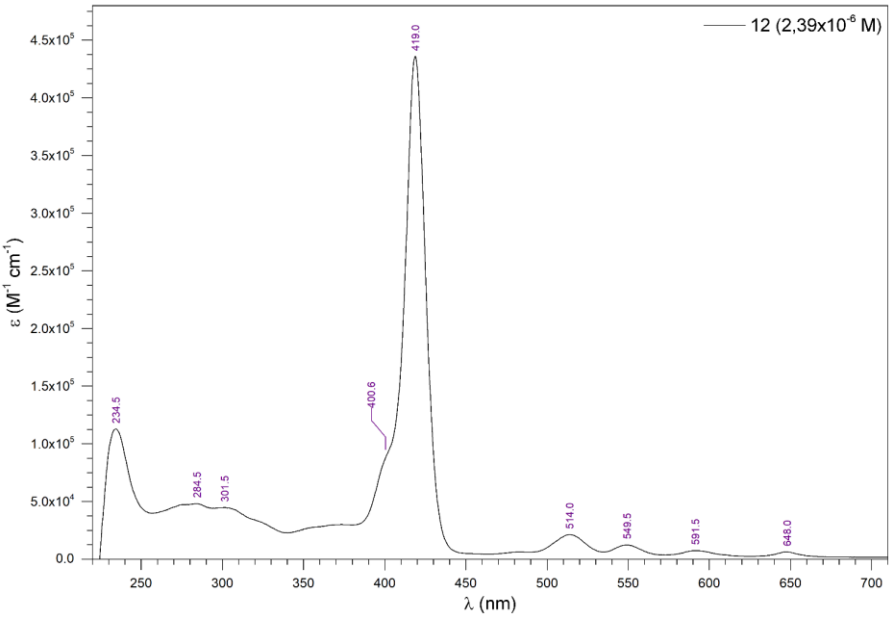

UV-Vis spectrum of **12** in THF.

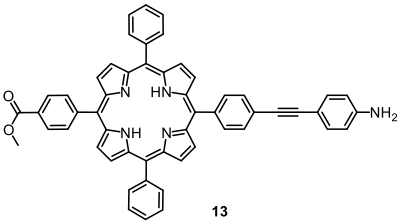

13

$C_{54}H_{37}N_5O_2$

ex. M. 787.2947

MW 787.9230

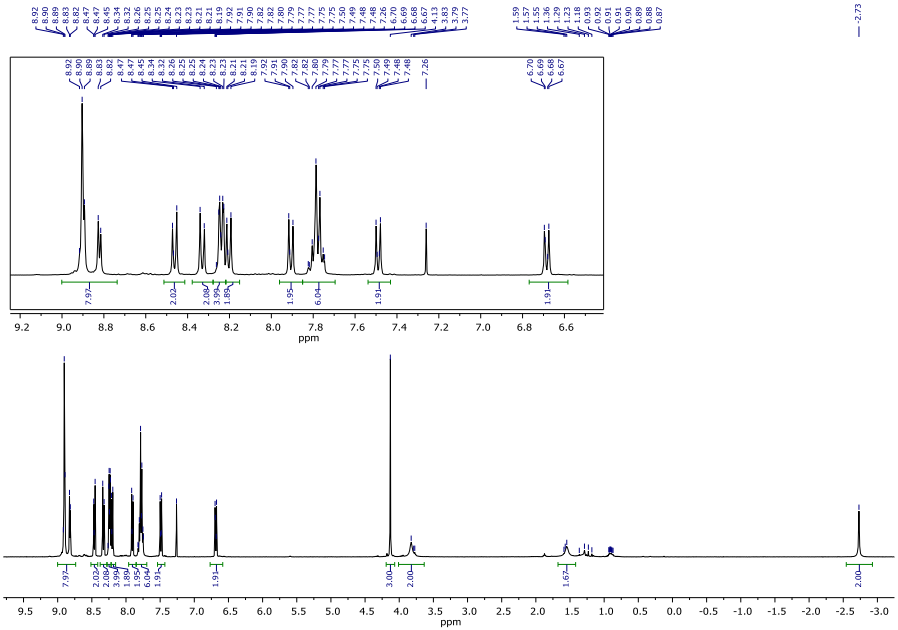

^{1}H NMR spectrum of **13** in $CDCl_3$.

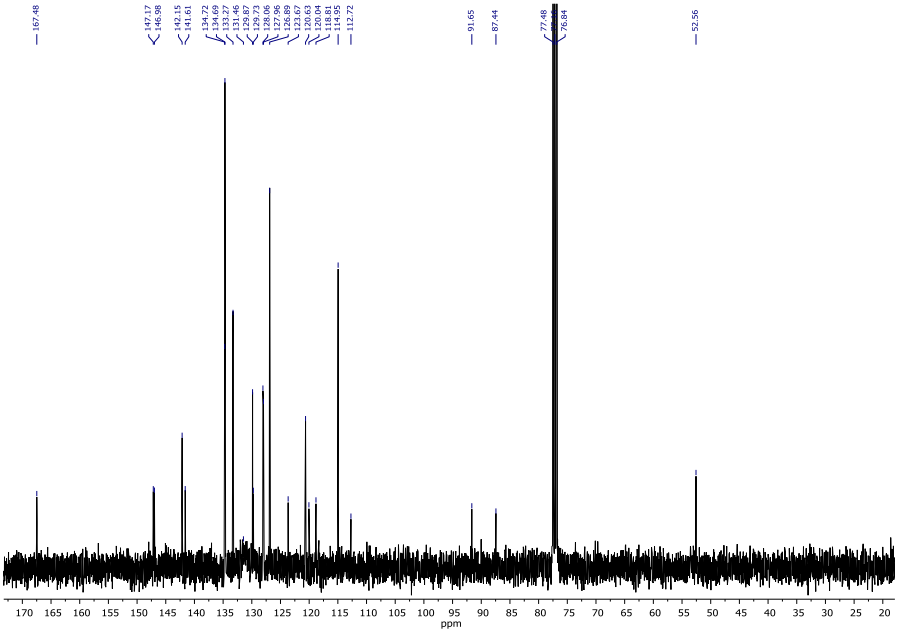

^{13}C NMR spectrum of **13** in $CDCl_3$.

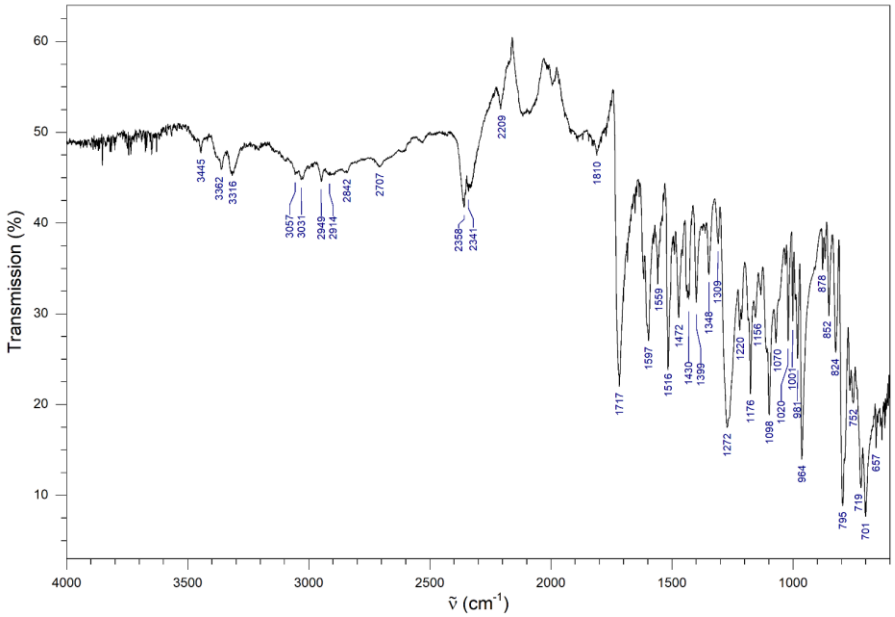

FT-IR spectrum of **13**.

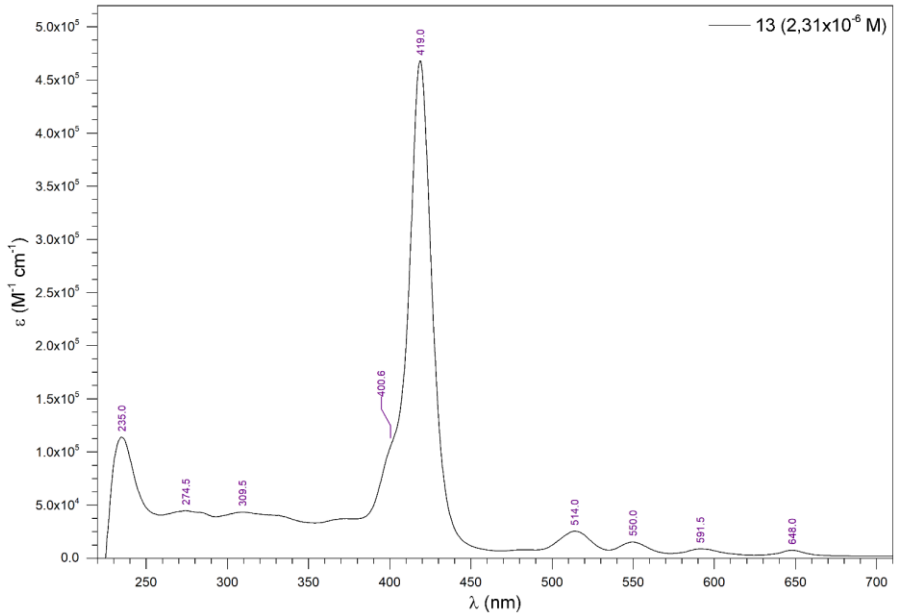

UV-Vis spectrum of **13** in THF.

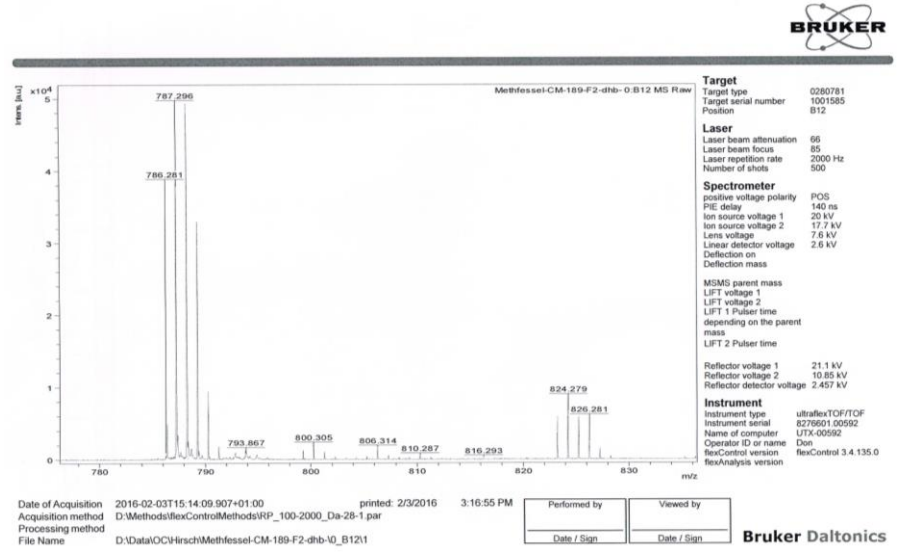

MS (MALDI) spectrum of **13**.

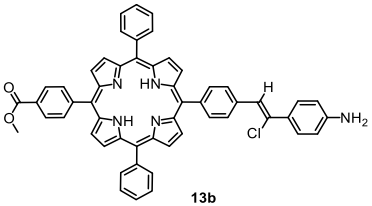

13b

$C_{54}H_{38}ClN_5O_2$

ex. M. 823.2714

MW 824.3810

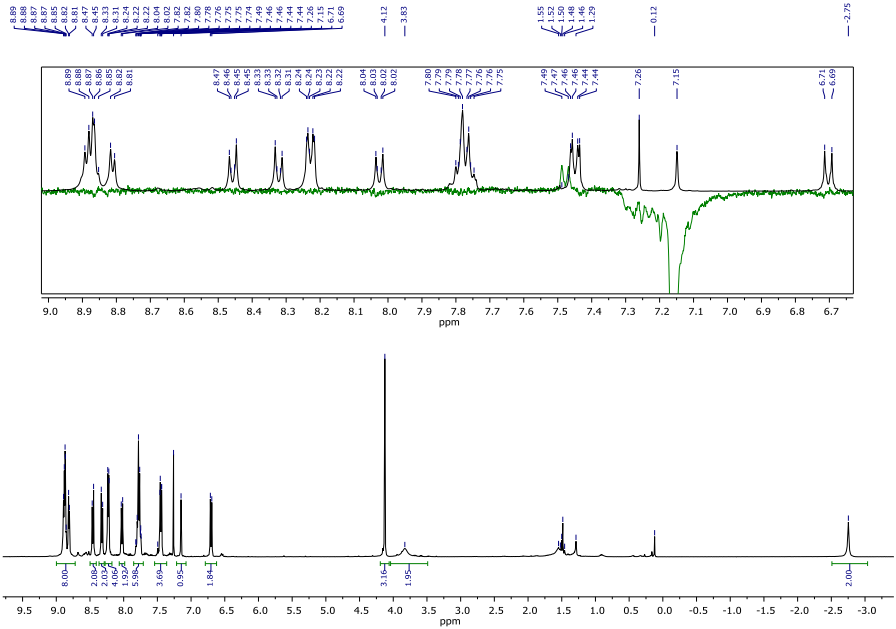

[1]H NMR spectrum of **13b** in $CDCl_3$. Detail: Selective 1D NOESY spectrum in CD_2Cl_2 (green).

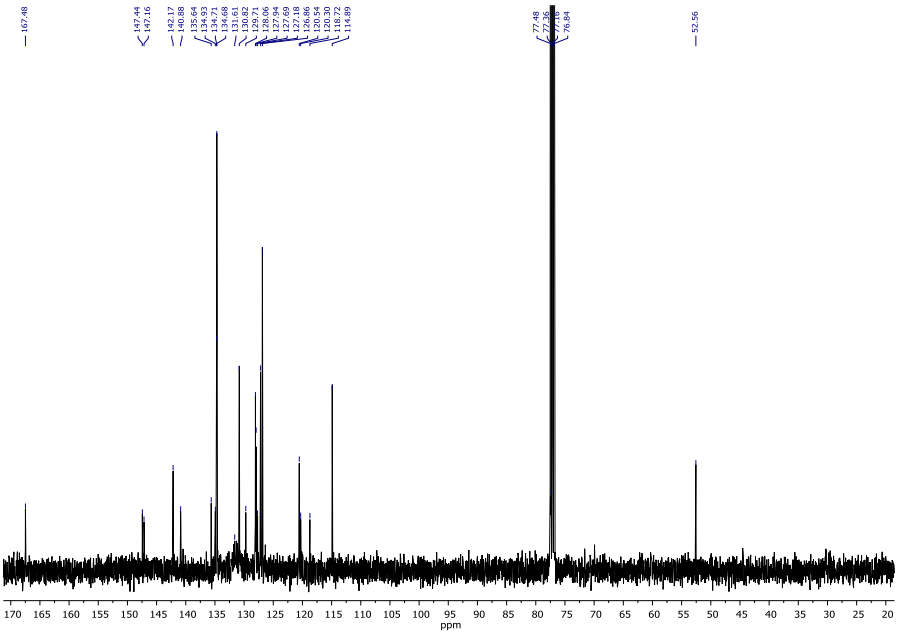

^{13}C NMR spectrum of **13b** in $CDCl_3$.

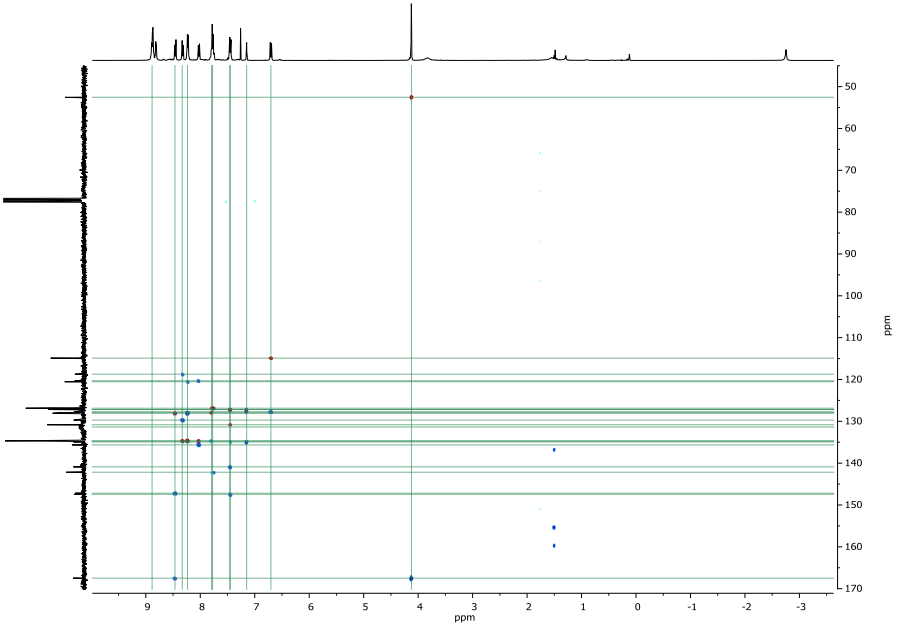

Combined HSQC (red) / HMBC (blue) NMR spectrum of **13b** in $CDCl_3$ (overview).

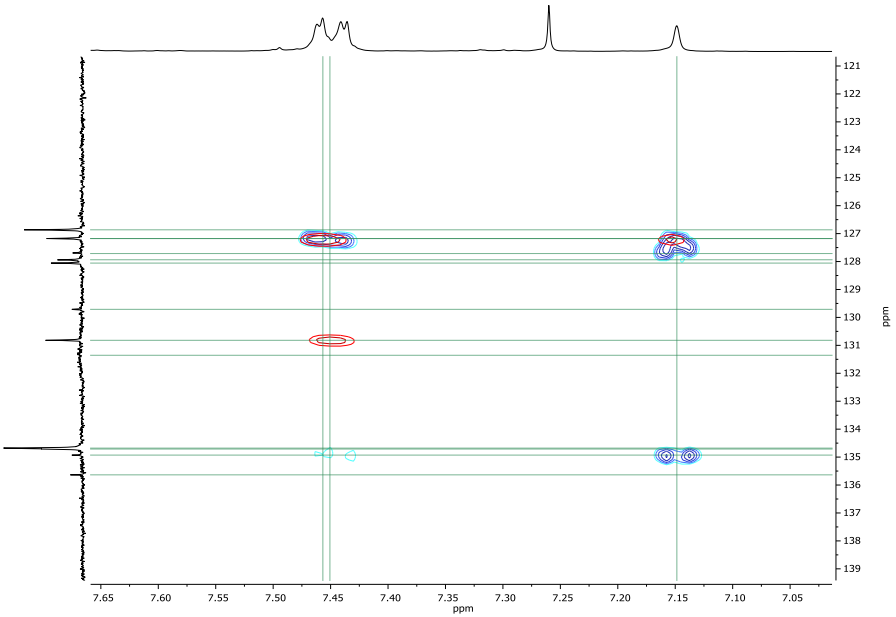

Combined HSQC (red) / HMBC (blue) NMR spectrum of **13b** in $CDCl_3$ (detail).

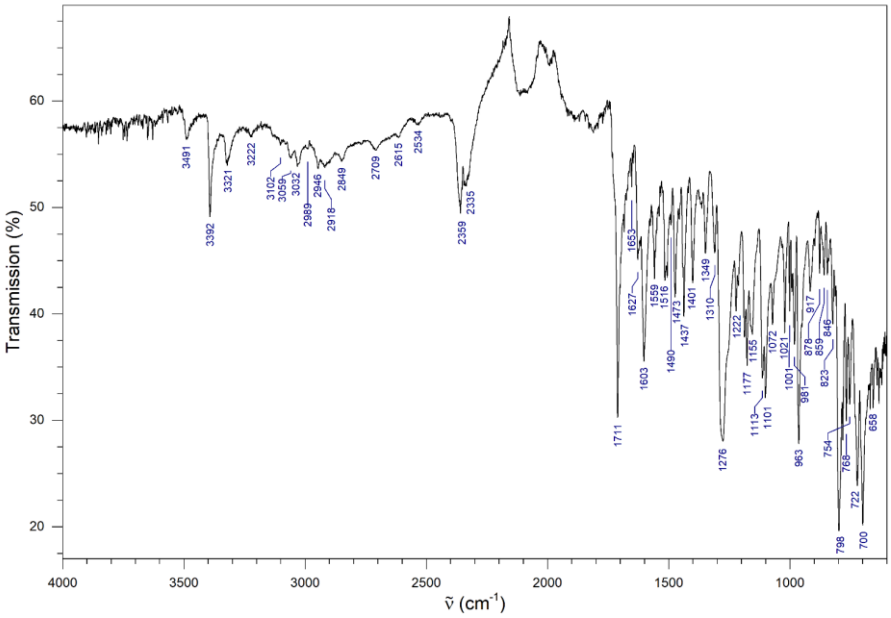

FT-IR spectrum of **13b**.

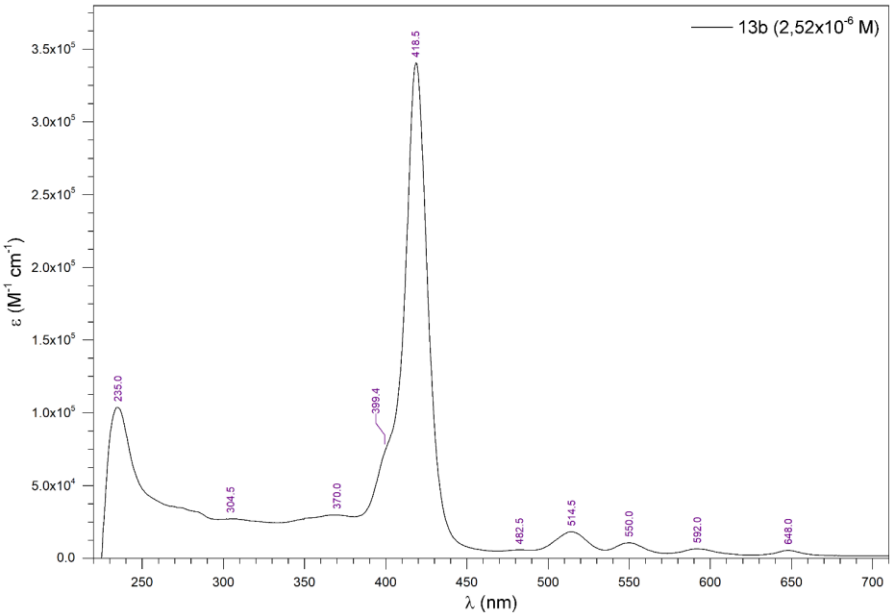

UV-Vis spectrum of **13b** in THF.

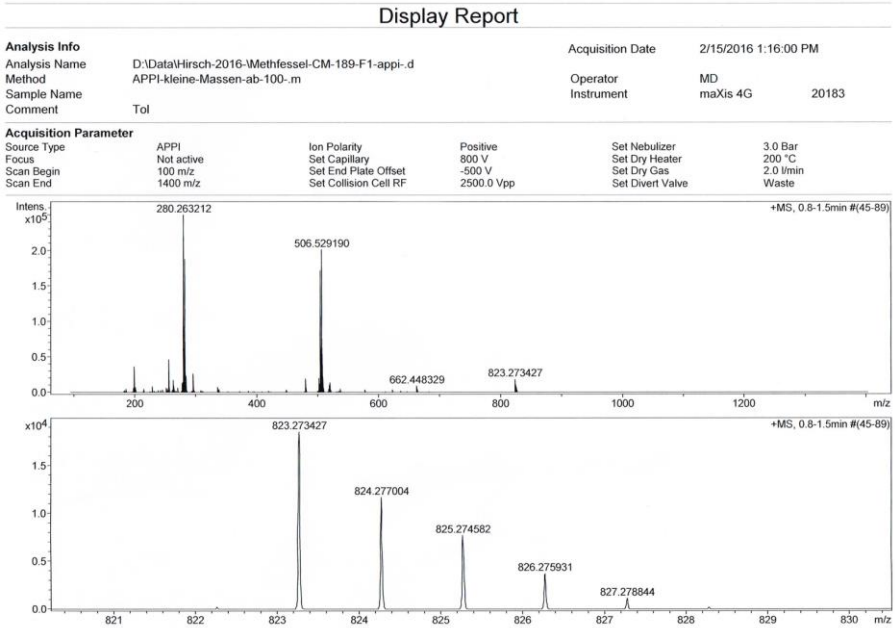

MS (APPI+) spectrum of **13b**.

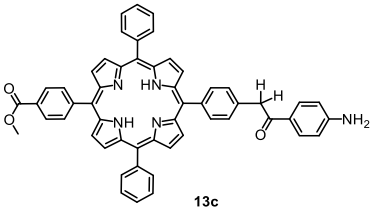

13c

$C_{54}H_{39}N_5O_3$

ex. M. 805.3053

MW 805.9380

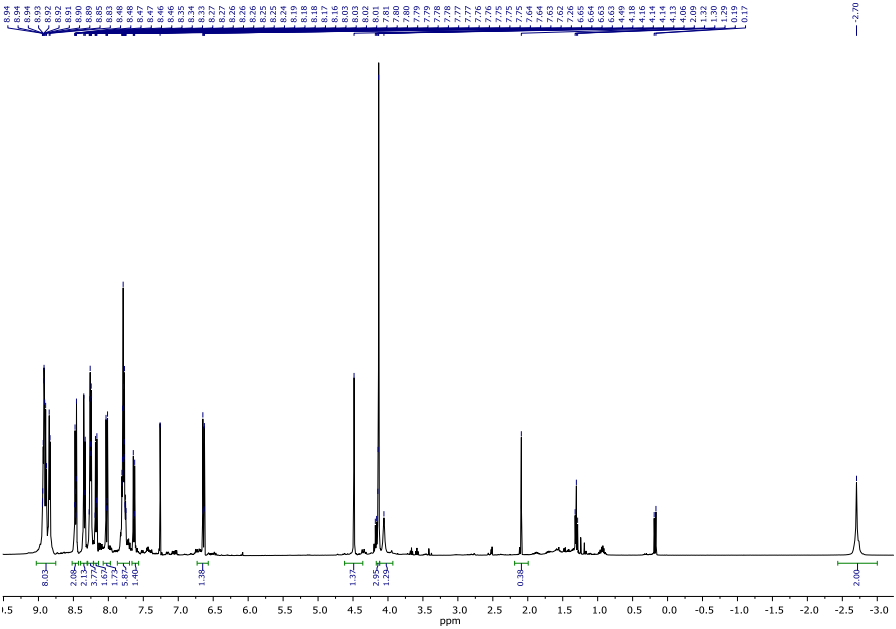

^{1}H NMR spectrum of **13c** in $CDCl_3$.

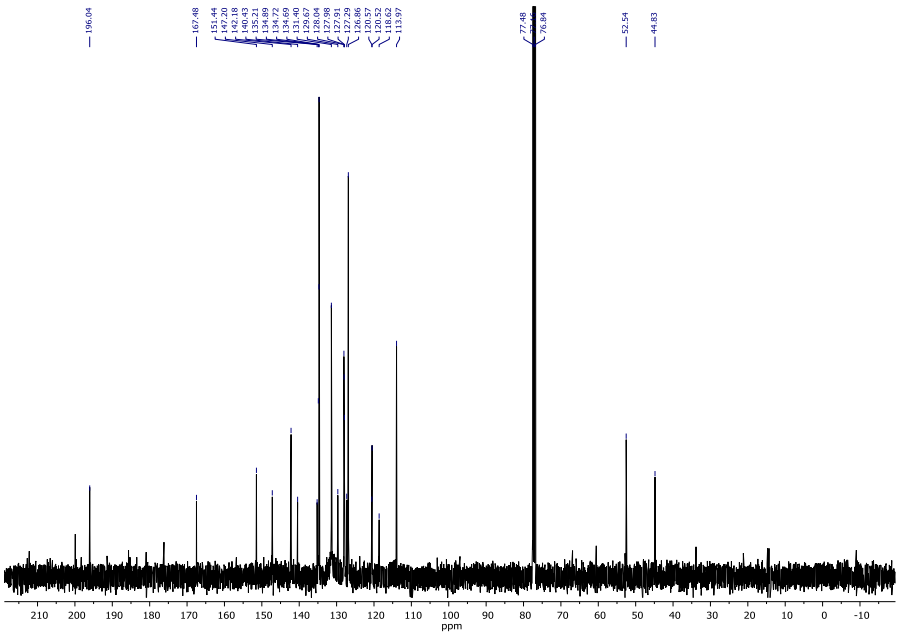

^{13}C NMR spectrum of **13c** in $CDCl_3$.

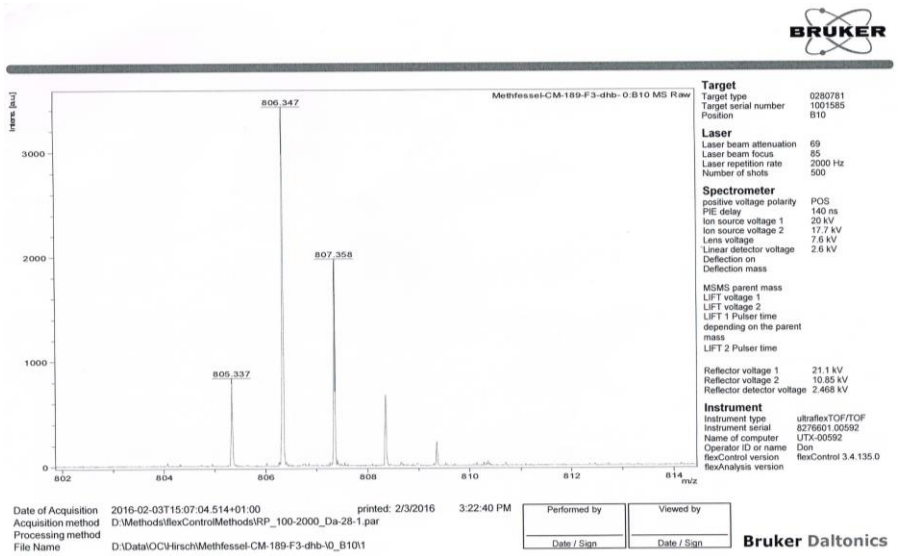

MS (MALDI) spectrum of **13c**.

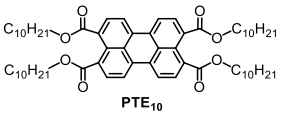

PTE$_{10}$

14

$C_{64}H_{92}O_8$

ex. M. 988.6792

MW 989.4320

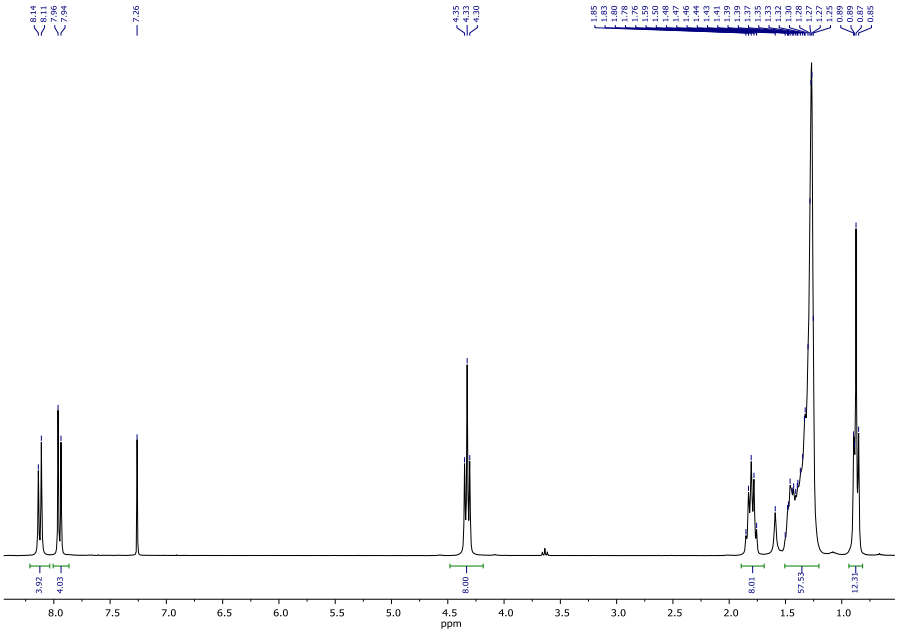

^{1}H NMR spectrum of **14** in $CDCl_3$.

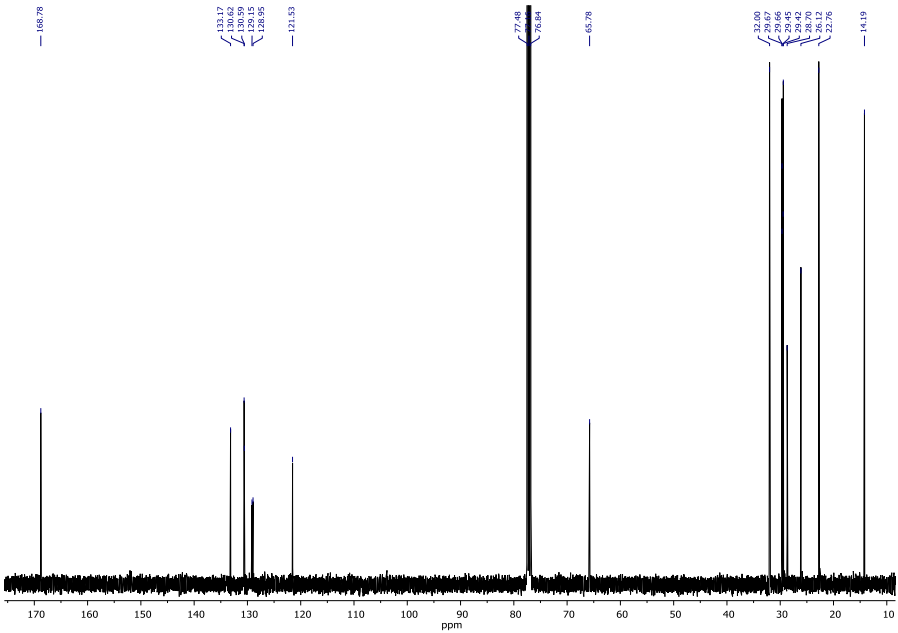

^{13}C NMR spectrum of **14** in $CDCl_3$, spectrum printed with kind permission.[238]

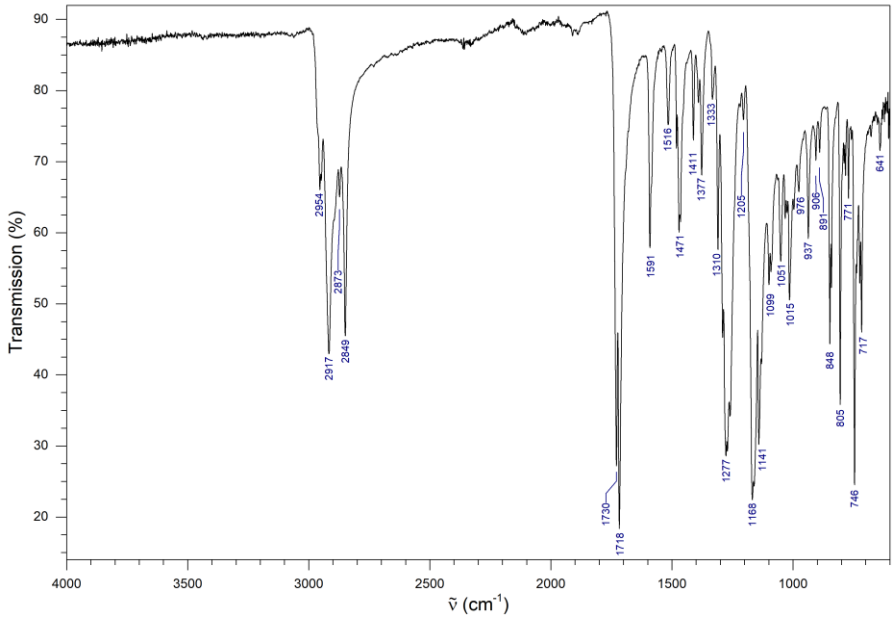

FT-IR spectrum of **14**.

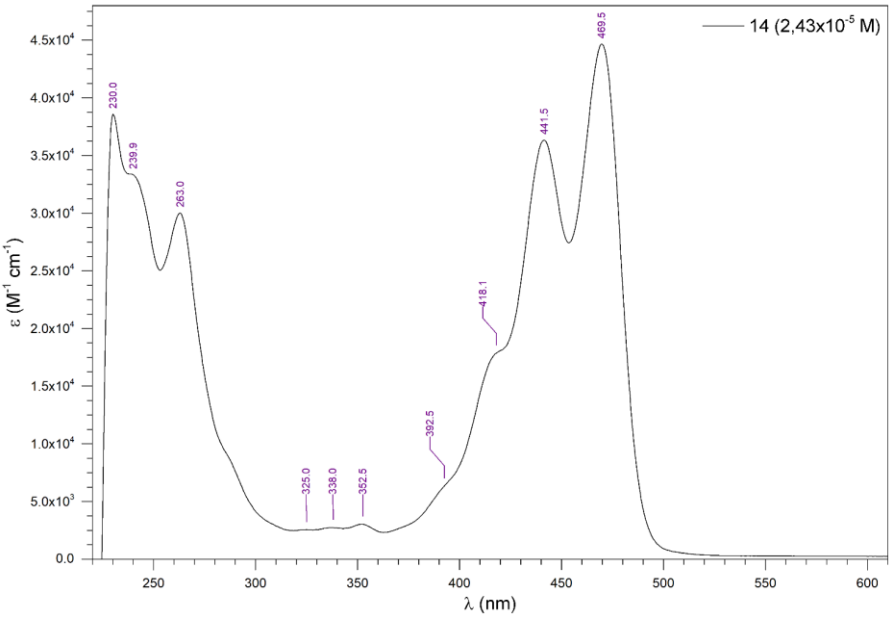

UV-Vis spectrum of **14** in THF.

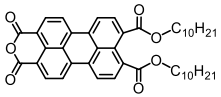

PABE$_{10}$

15

$C_{44}H_{50}O_7$

ex. M. 690.3557

MW 690.8770

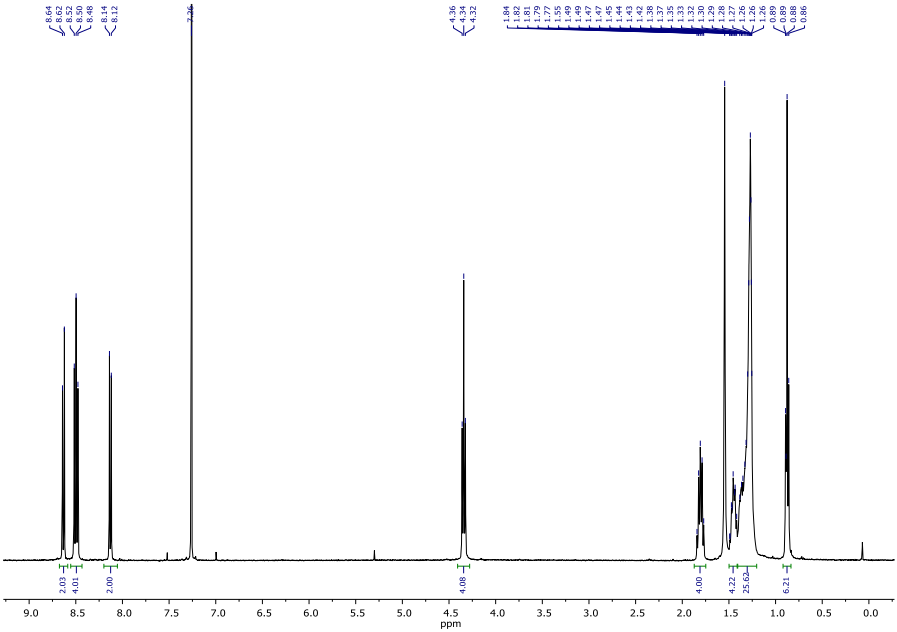

^{1}H NMR spectrum of **15** in $CDCl_3$.

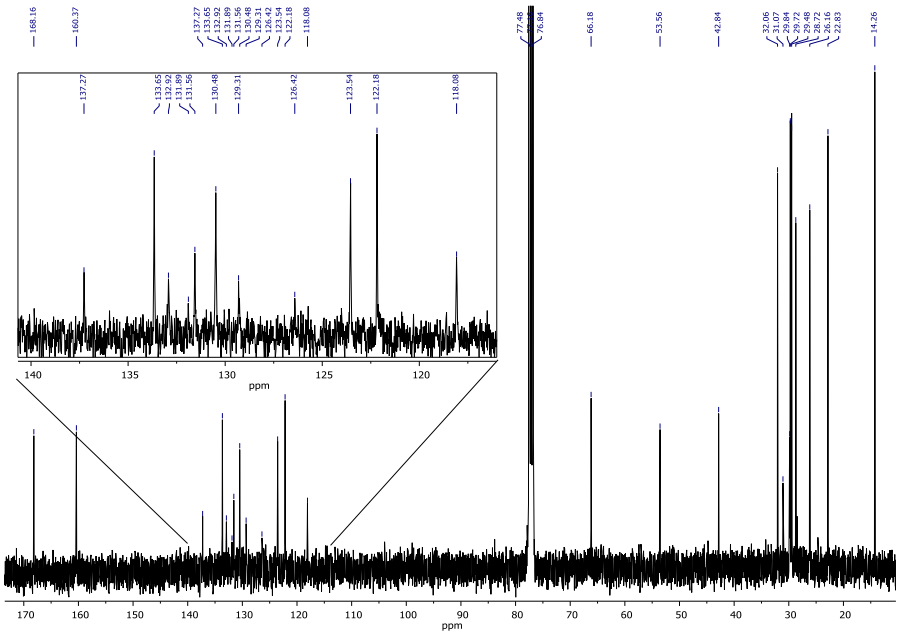

^{13}C NMR spectrum of **15** in $CDCl_3$, spectrum printed with kind permission.[238]

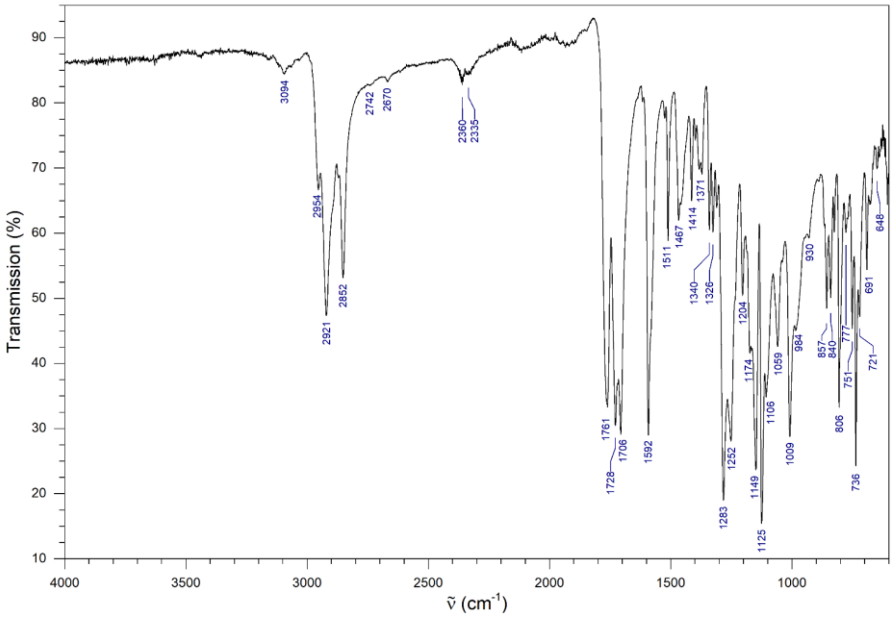

FT-IR spectrum of **15**.

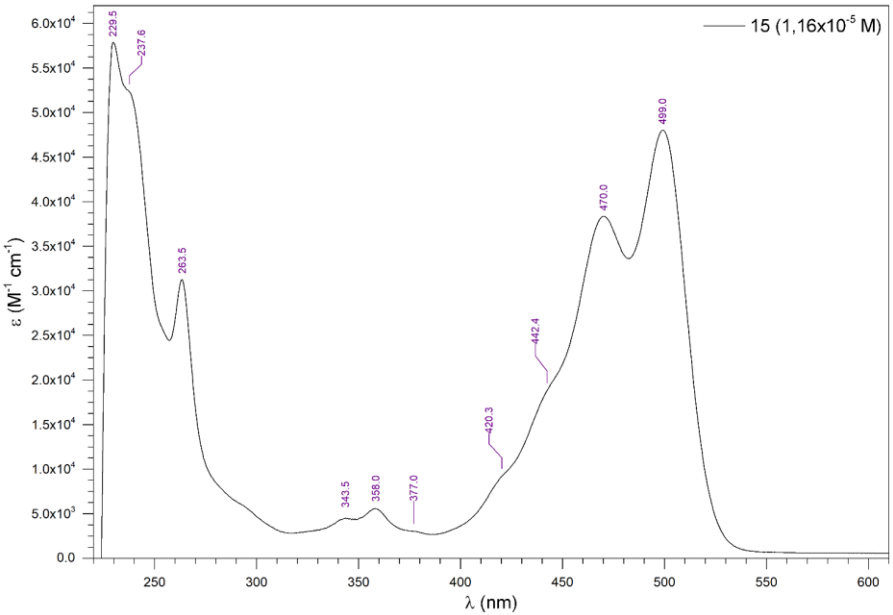

UV-Vis spectrum of **15** in THF.

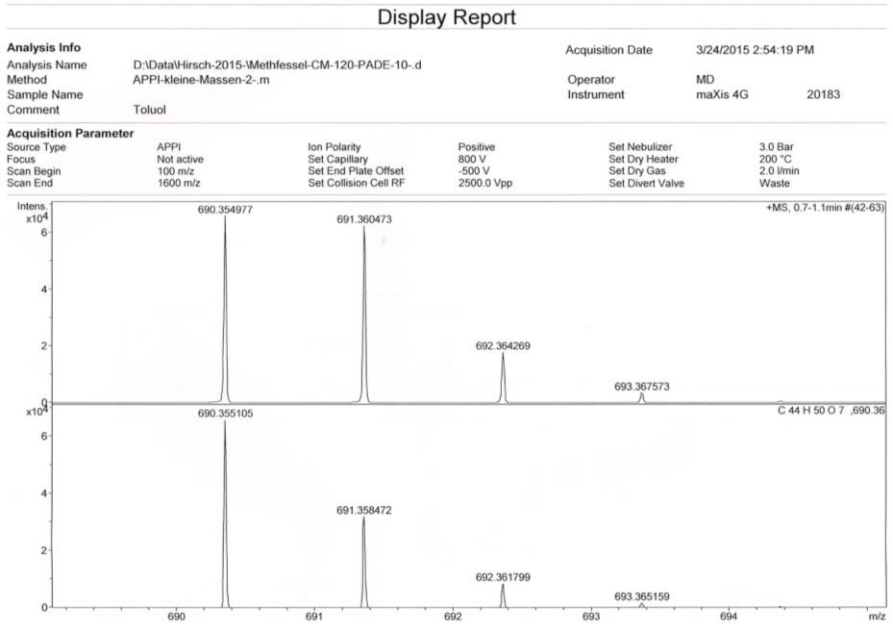

MS (APPI+) spectrum of **15**. Recorded (top) and calculated (bottom) mass spectra.

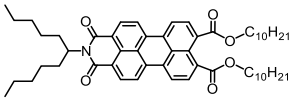

PI_sBE_{10}

16

$C_{55}H_{73}NO_6$

ex. M. 843.5438

MW 844.1900

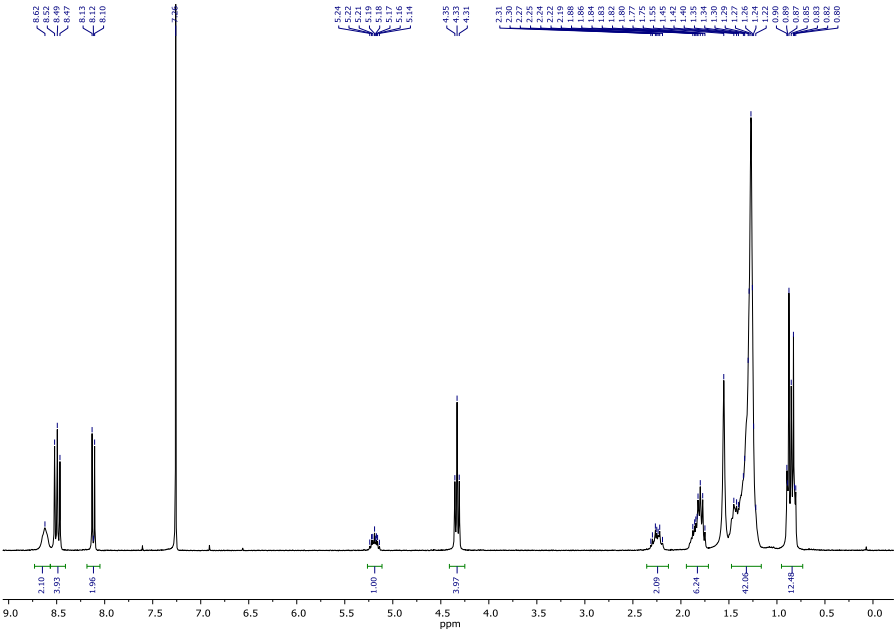

^{1}H NMR spectrum of **16** in $CDCl_3$.

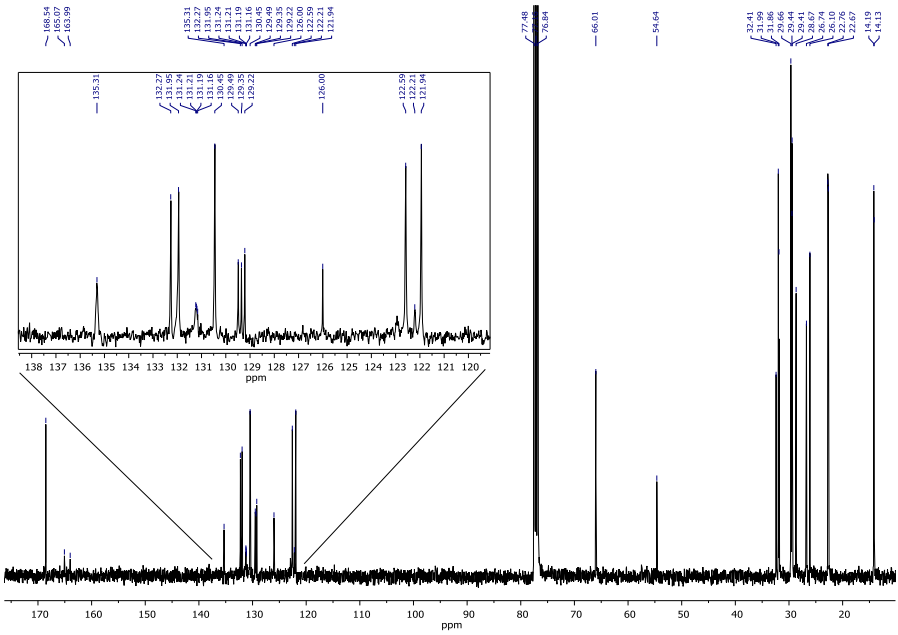

^{13}C NMR spectrum of **16** in $CDCl_3$, spectrum printed with kind permission.[238]

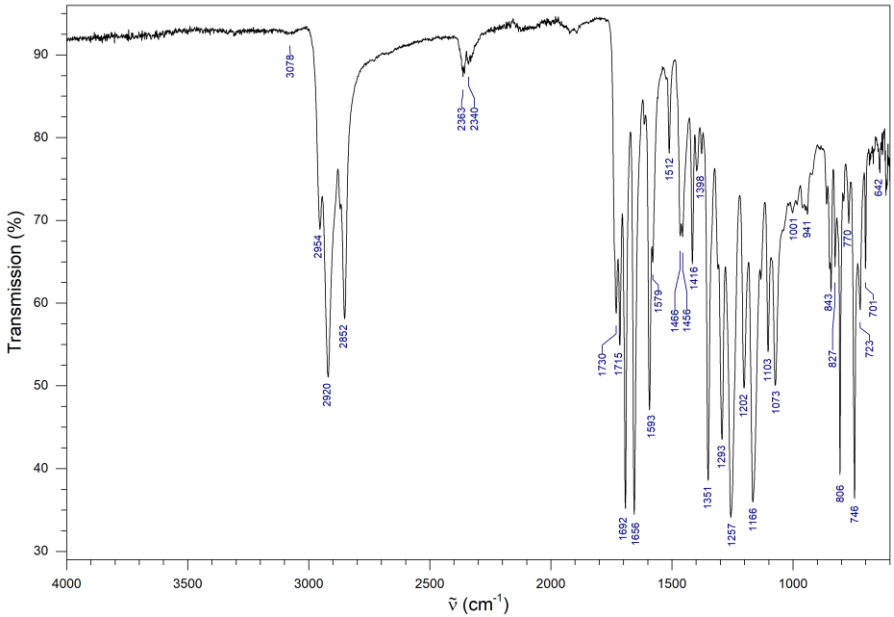

FT-IR spectrum of **16**.

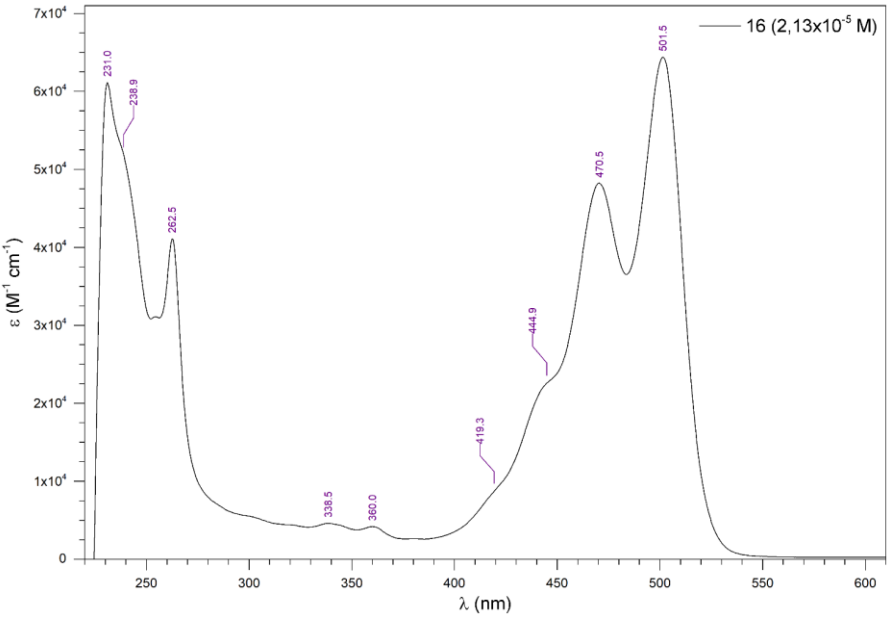

UV-Vis spectrum of **16** in THF.

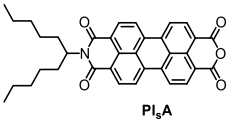

PI_sA

17

$C_{35}H_{31}NO_5$

ex. M. 545.2202

MW 545.6350

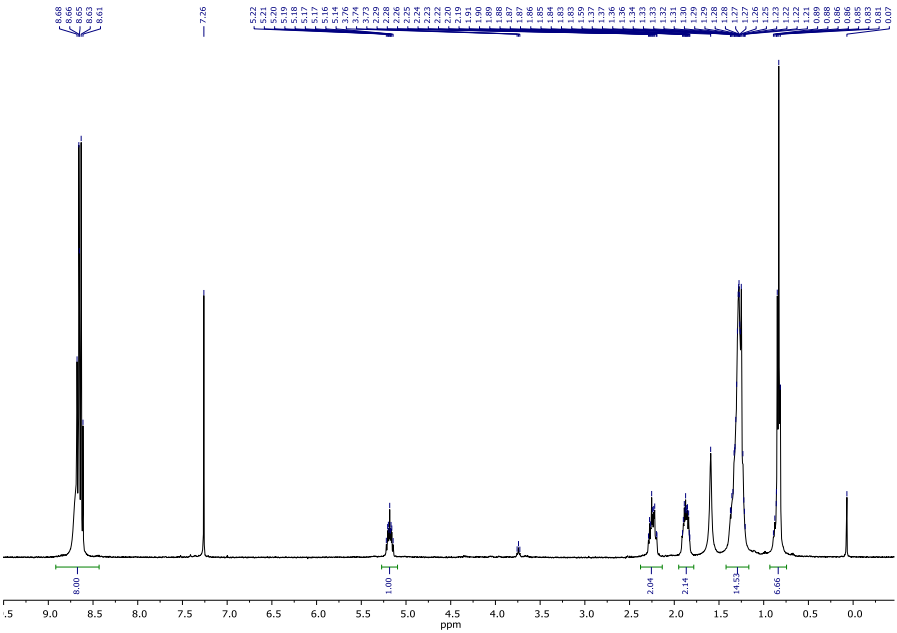

^{1}H NMR spectrum of **17** in $CDCl_3$.

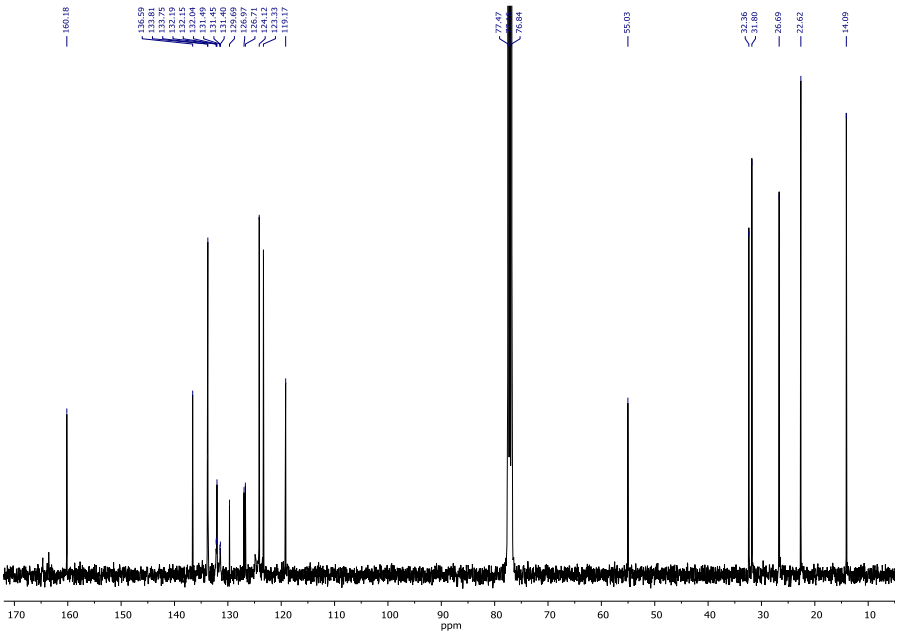

^{13}C NMR spectrum of **17** in $CDCl_3$.

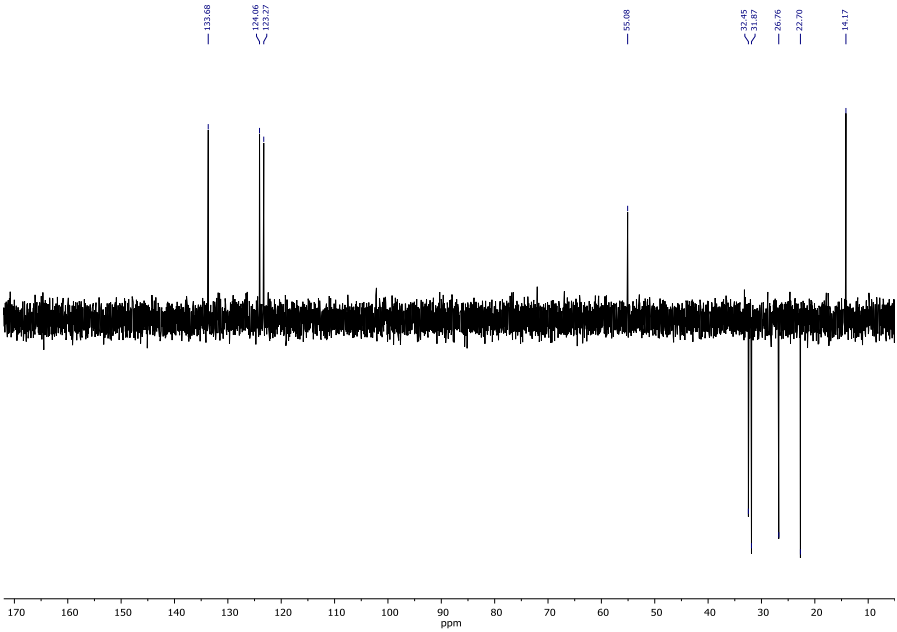

DEPT-135 NMR spectrum of **17** in $CDCl_3$ (CH/CH_3 positive, CH_2 negative, C not visible).

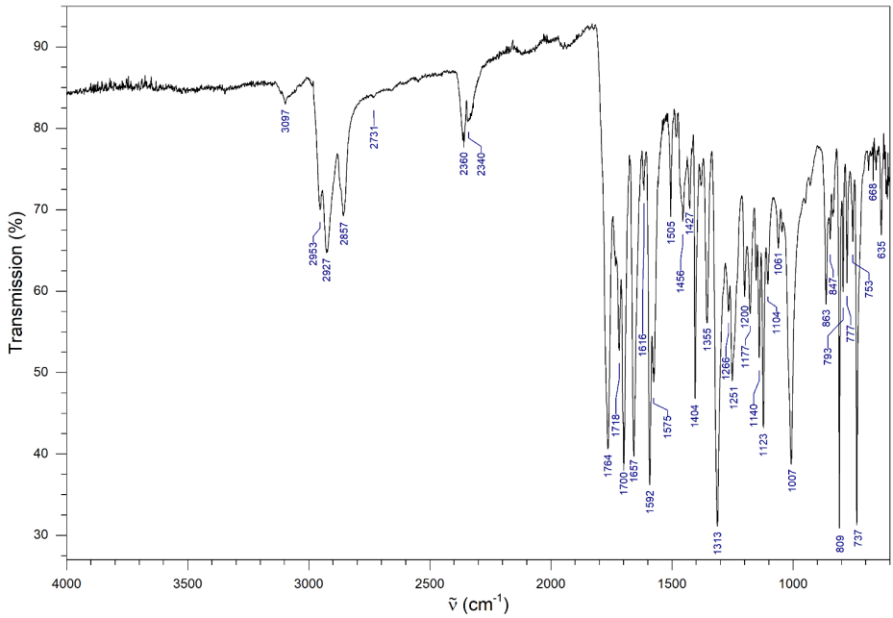

FT-IR spectrum of **17**.

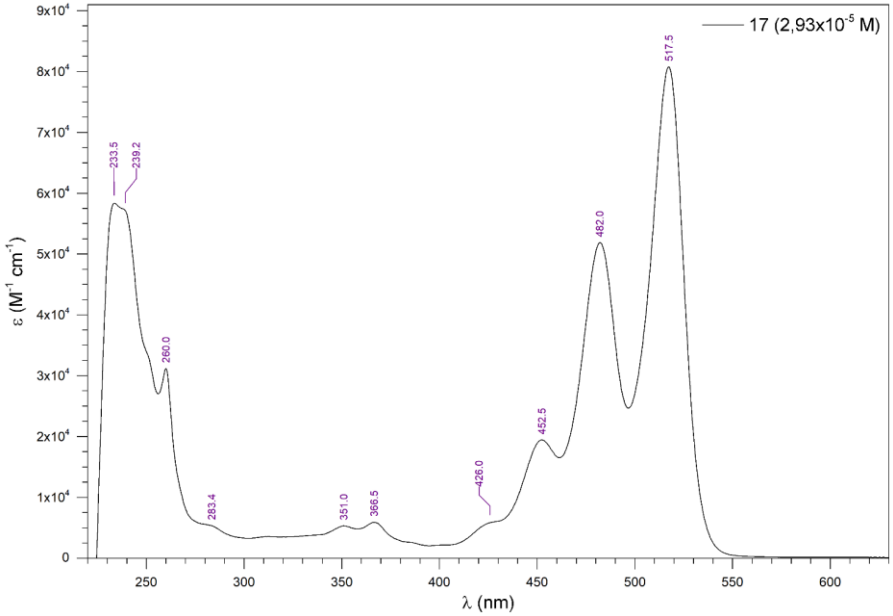

UV-Vis spectrum of **17** in THF.

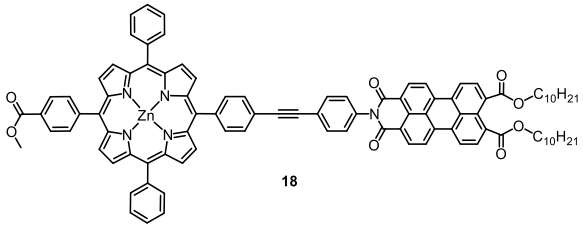

18

$C_{98}H_{83}N_5O_8Zn$

ex. M. 1521.5533

MW 1524.1490

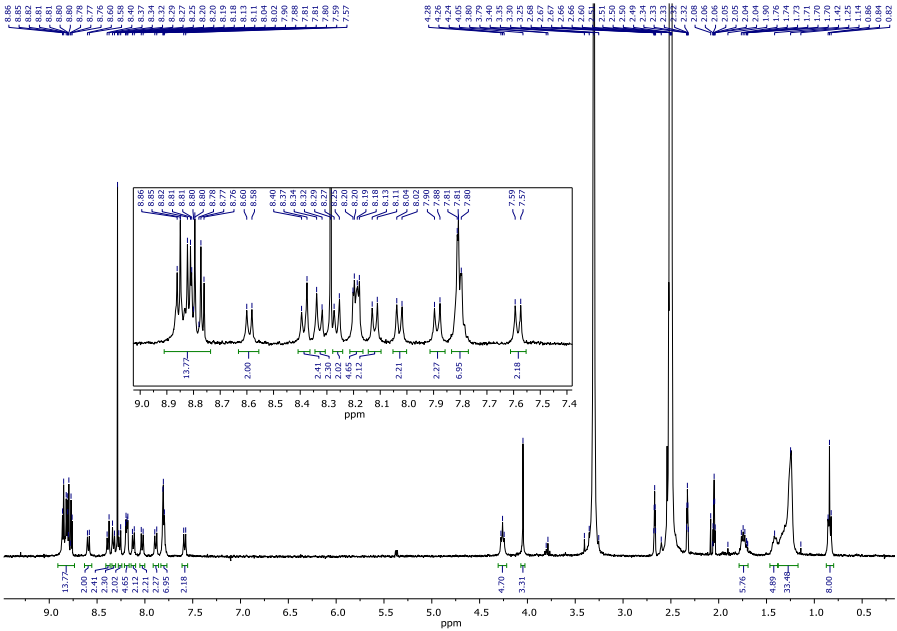

^{1}H NMR spectrum of **18** in DMSO-d_6 with traces of $CDCl_3$ (8.29 ppm) for increased resolution.

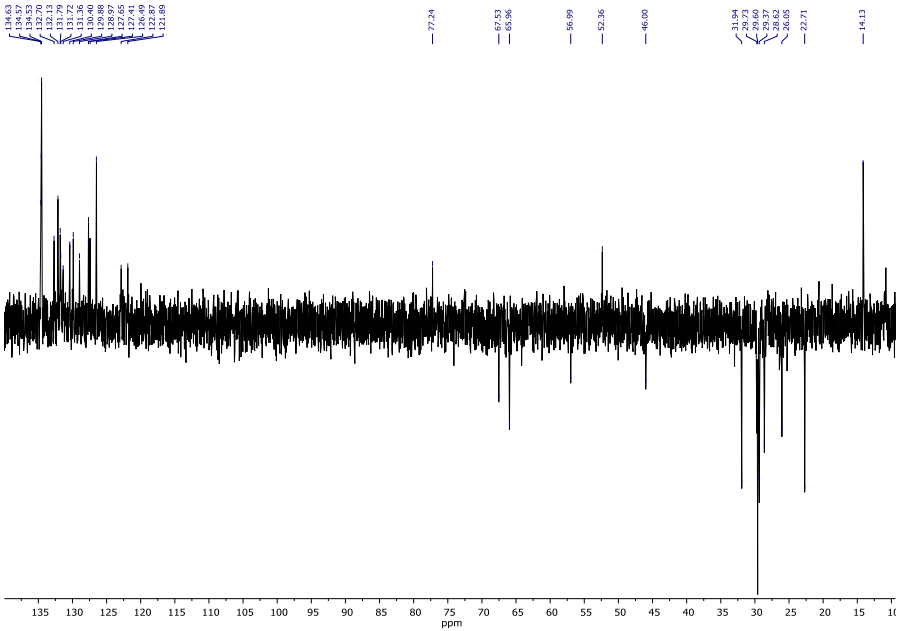

DEPT-135 NMR spectrum of **18** in $CDCl_3$ (CH/CH_3 positive, CH_2 negative, C not visible).

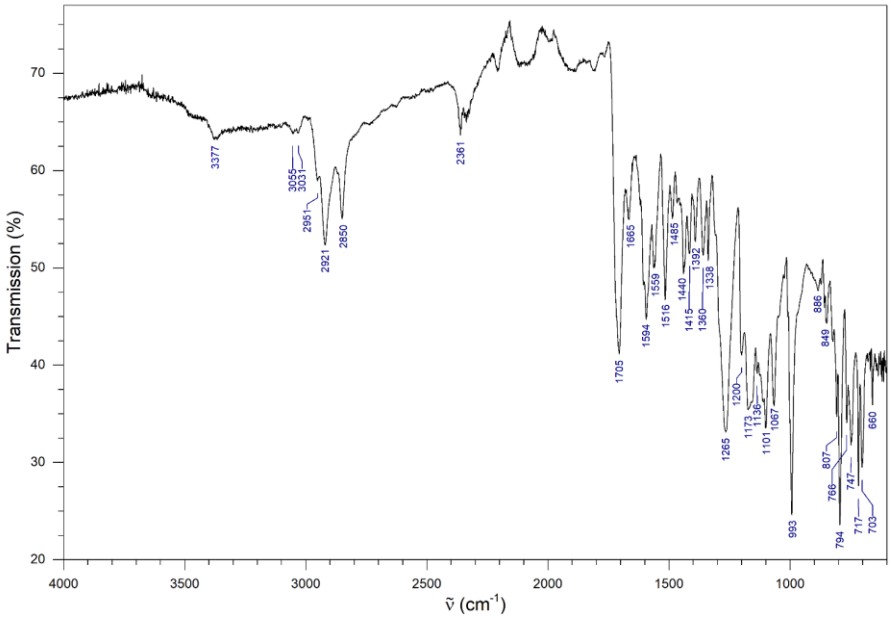

FT-IR spectrum of **18**.

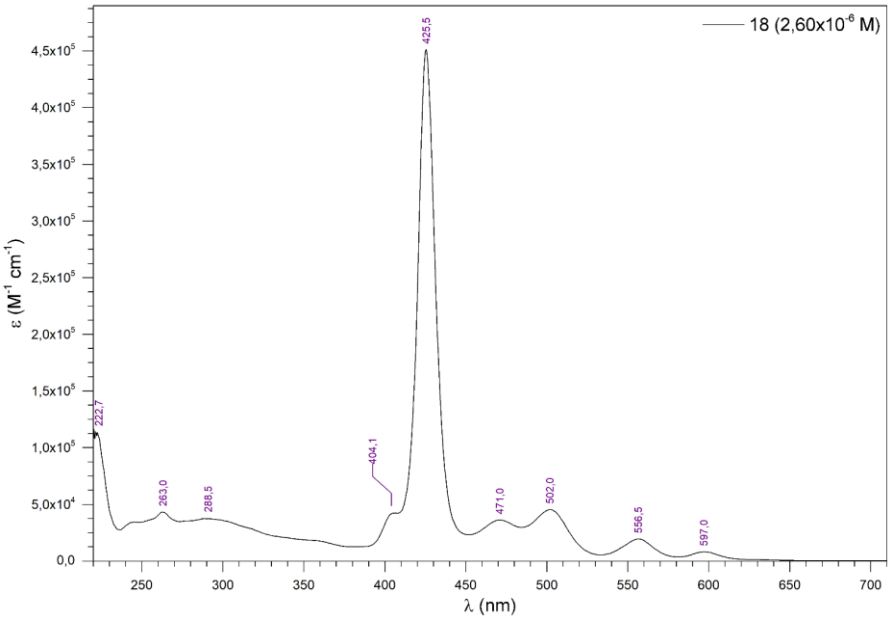

UV-Vis spectrum of **18** in THF.

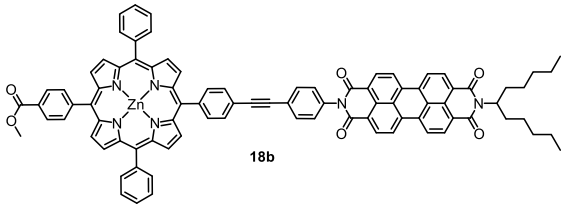

18b

$C_{89}H_{64}N_6O_6Zn$

ex. M. 1376.4179

MW 1378.9070

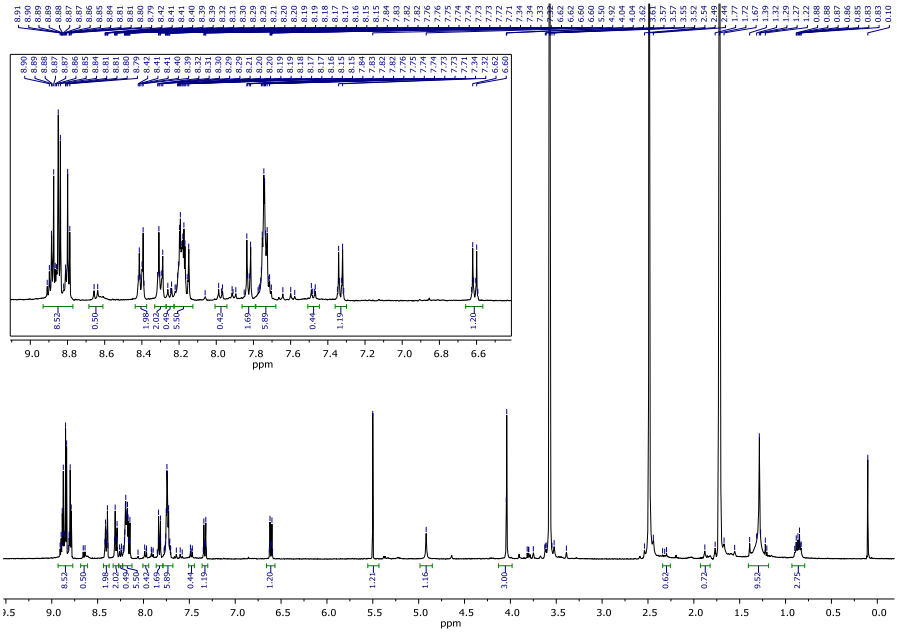

^{1}H NMR spectrum of **18b** in THF-d_8.

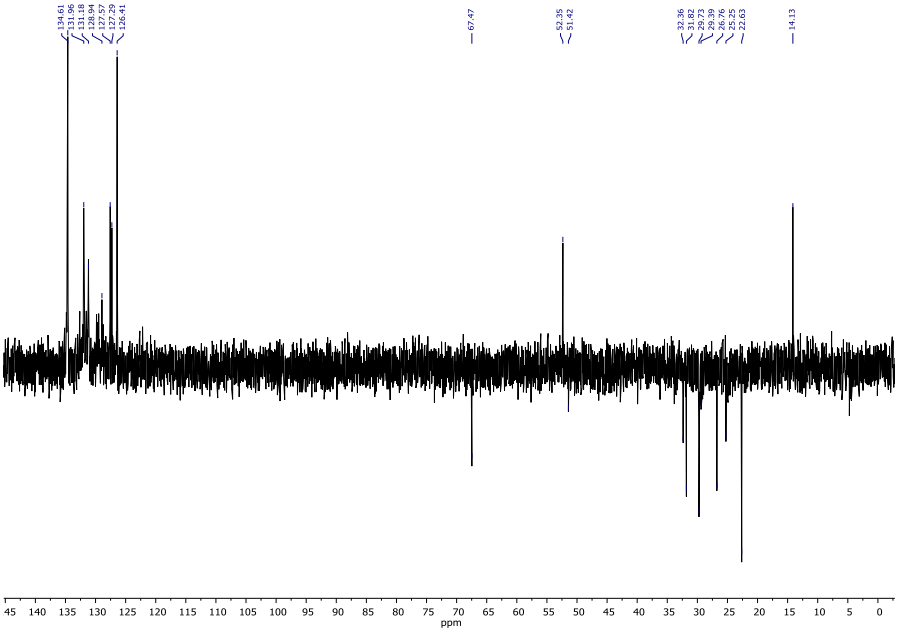

DEPT-135 NMR spectrum of **18b** in THF-d_8 (CH/CH_3 positive, CH_2 negative, C not visible).

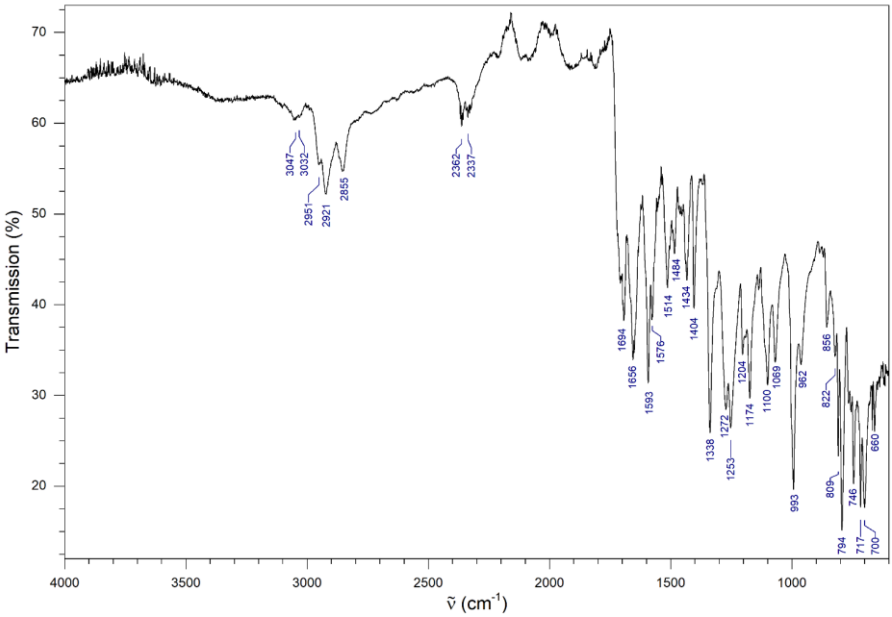

FT-IR spectrum of **18b**.

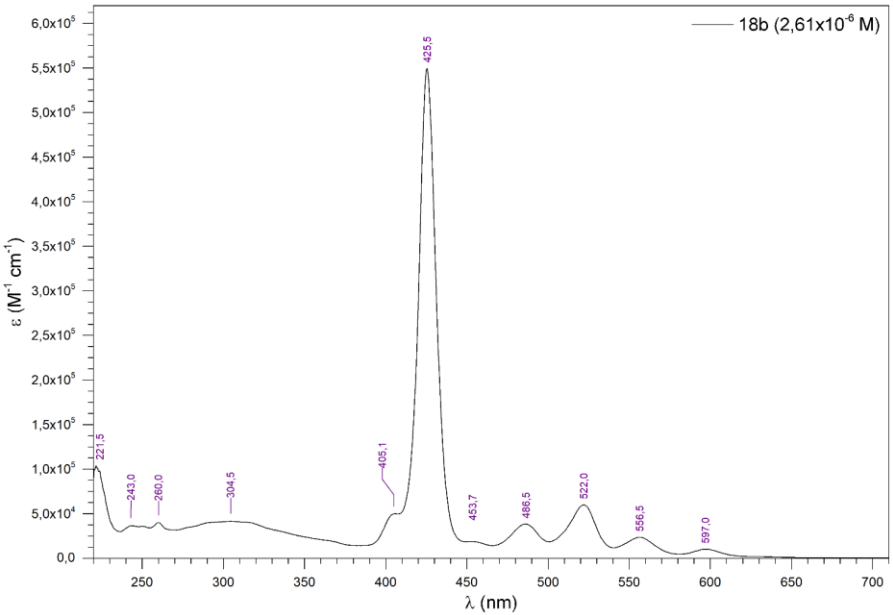

UV-Vis spectrum of **18b** in THF.

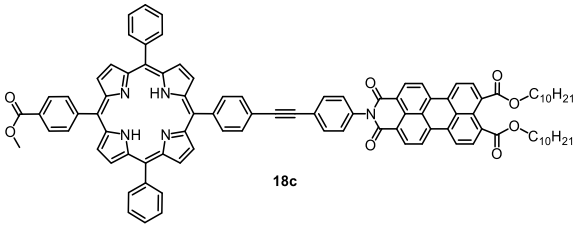

18c

$C_{98}H_{85}N_5O_8$

ex. M. 1459.6398

MW 1460.7850

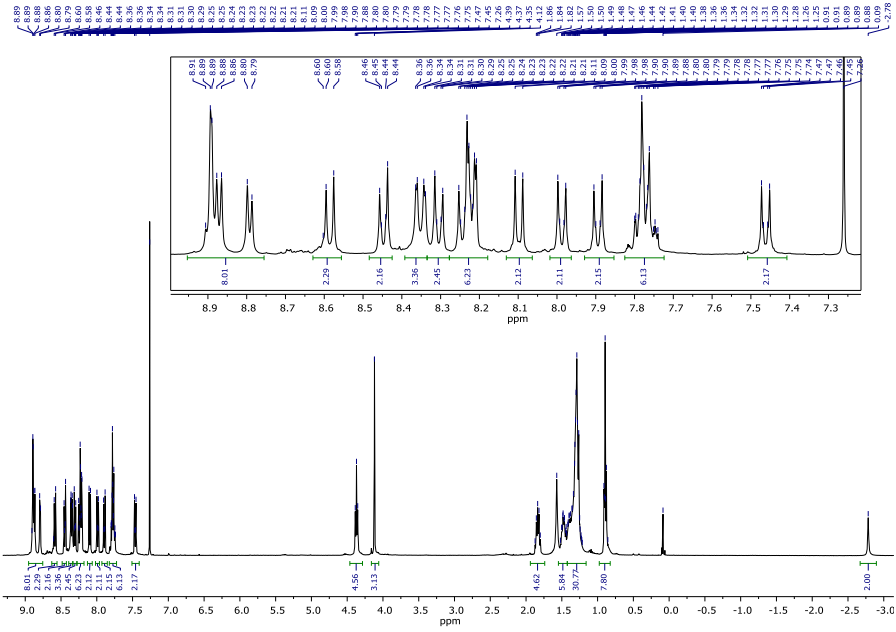

^{1}H NMR spectrum of **18c** in $CDCl_3$.

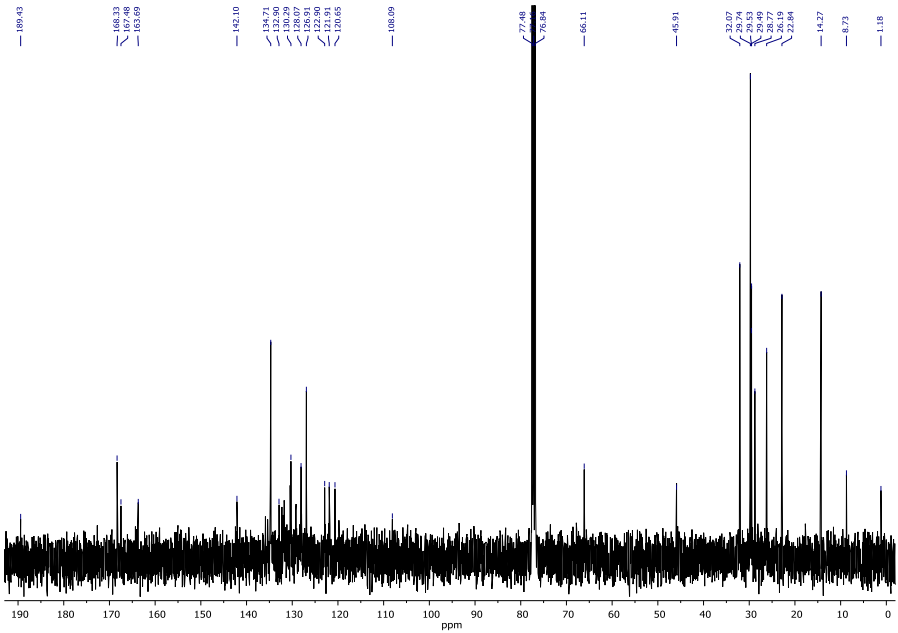

^{13}C NMR spectrum of **18c** in $CDCl_3$.

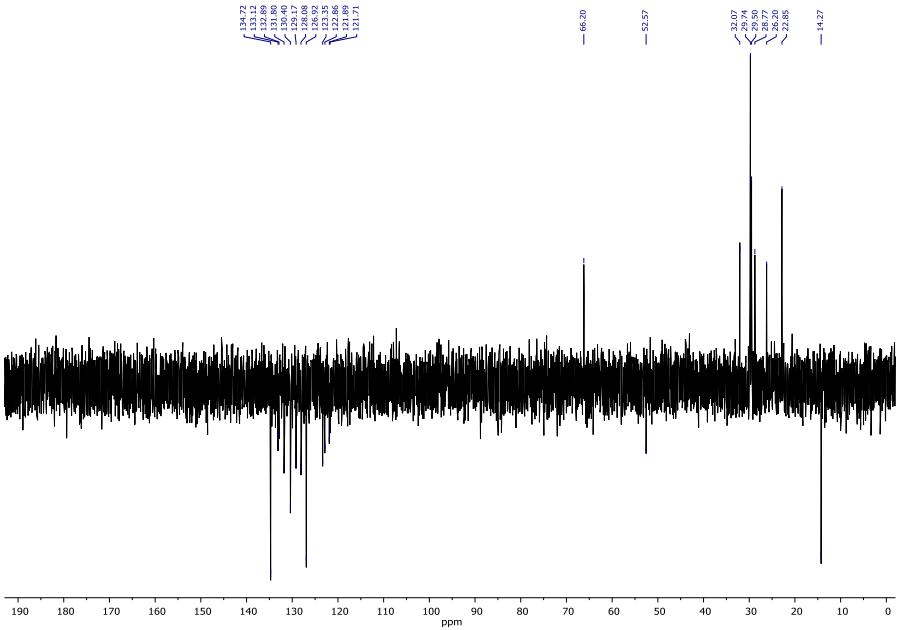

DEPT-135 NMR spectrum of **18c** in $CDCl_3$ (CH/CH_3 positive, CH_2 negative, C not visible).

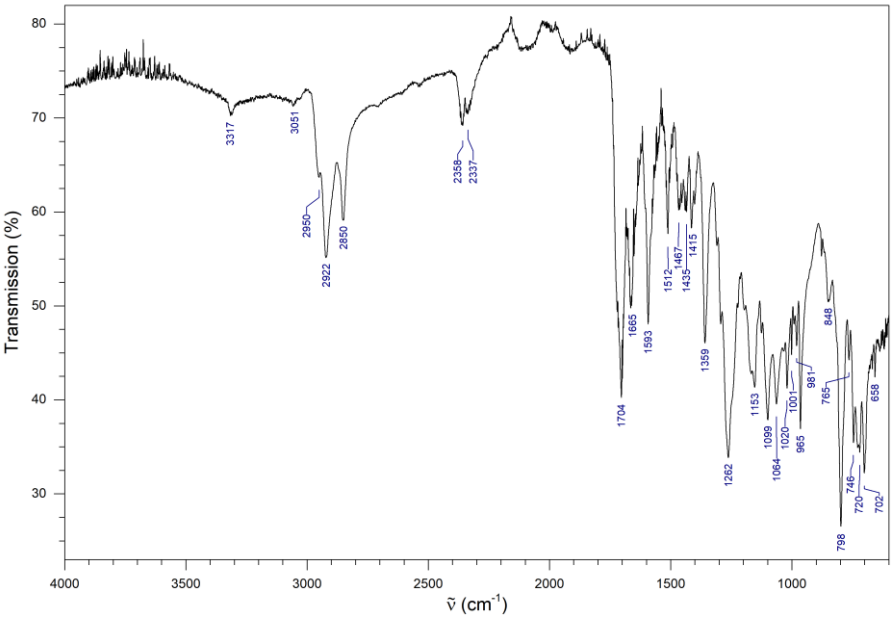

FT-IR spectrum of **18c**.

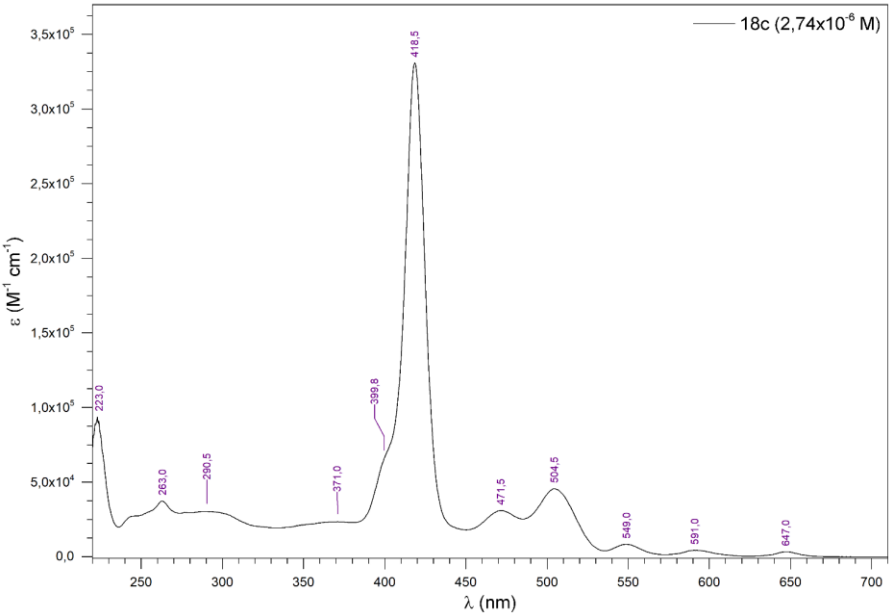

UV-Vis spectrum of **18c** in THF.

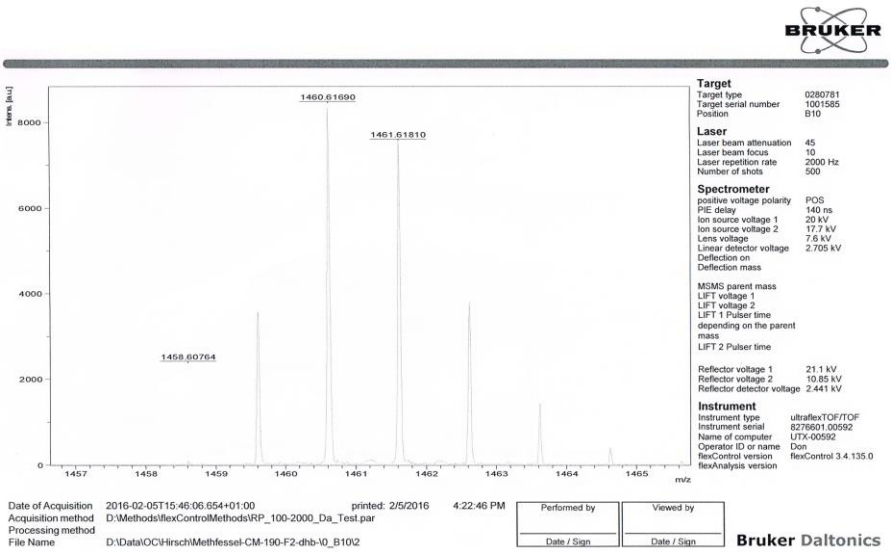

MS (MALDI) of **18c**.

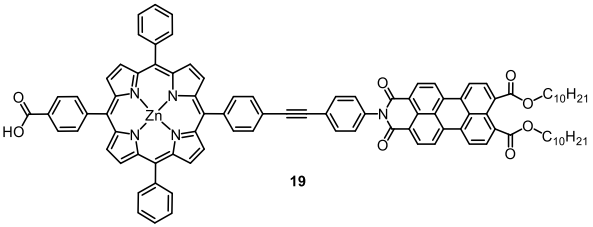

19

$C_{97}H_{81}N_5O_8Zn$

ex. M. 1507.5377

MW 1510.1220

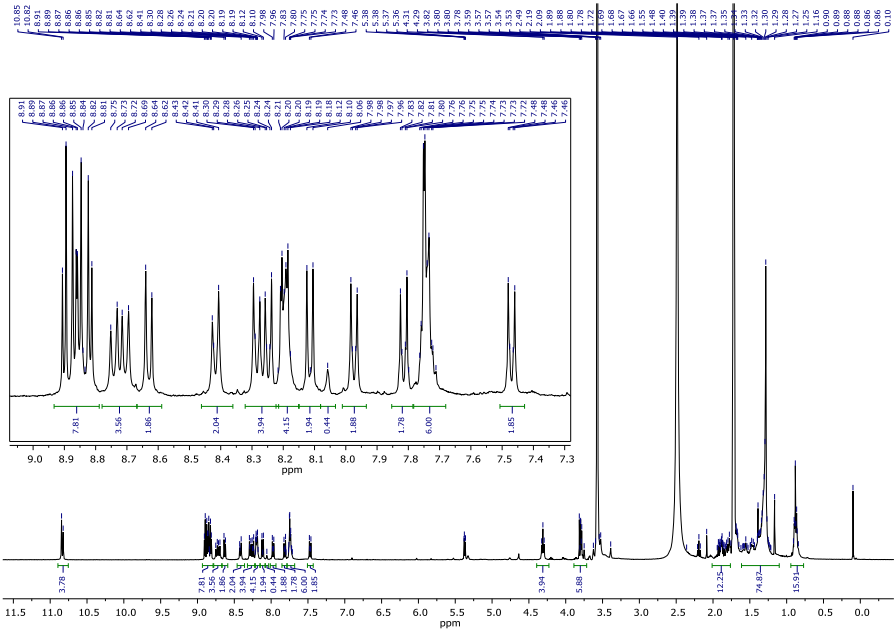

^{1}H NMR spectrum of **19** in THF-d_8.

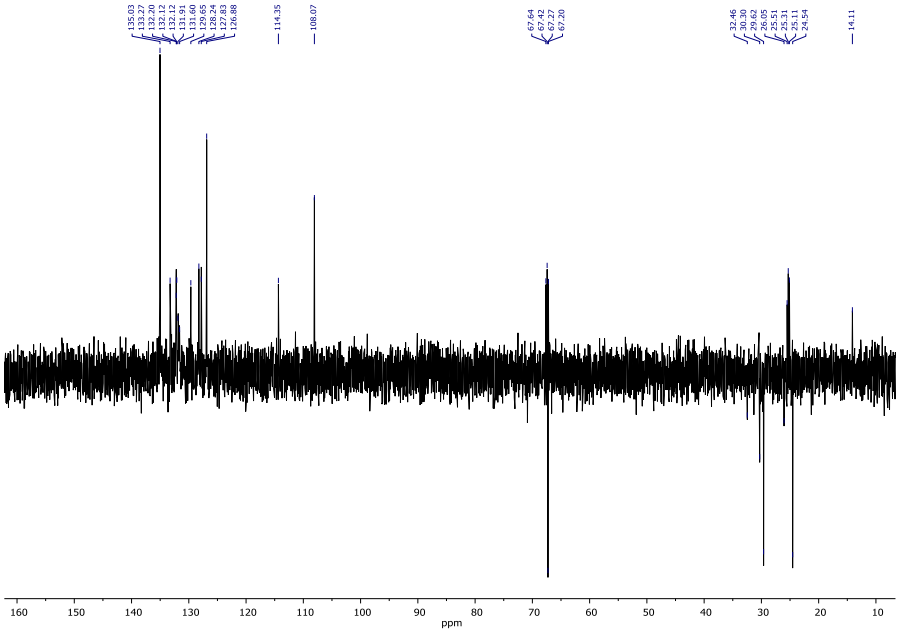

DEPT-135 NMR spectrum of **19** in THF-d_8 (CH/CH_3 positive, CH_2 negative, C not visible).

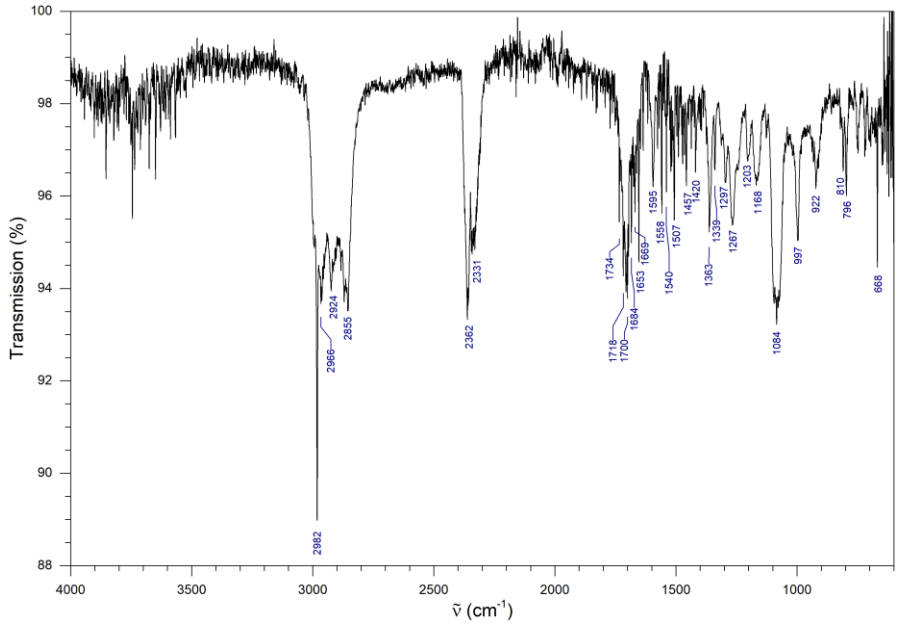

FT-IR spectrum of **19**. The compound was dissolved in THF and applied.

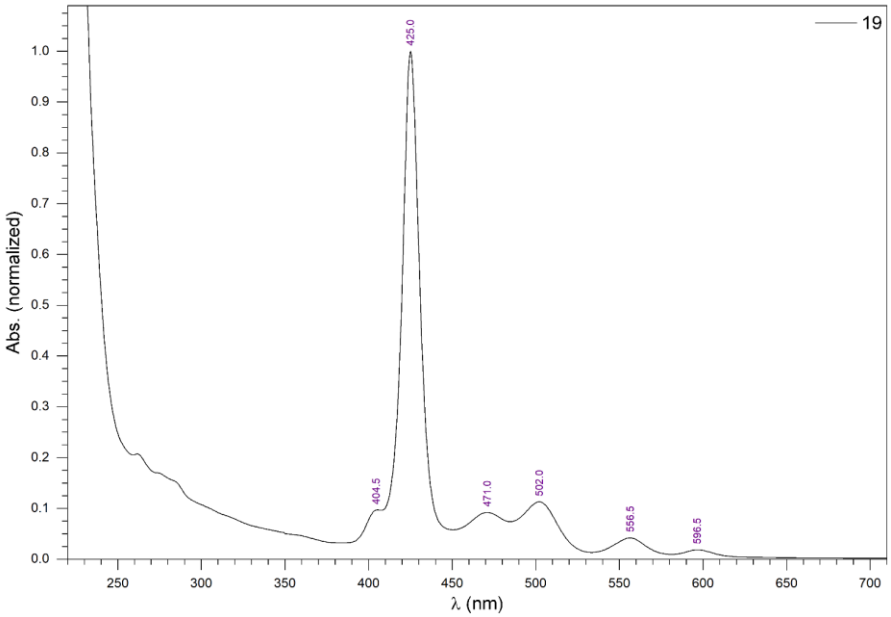

UV-Vis spectrum of **19** in THF (qualitative, normalized).

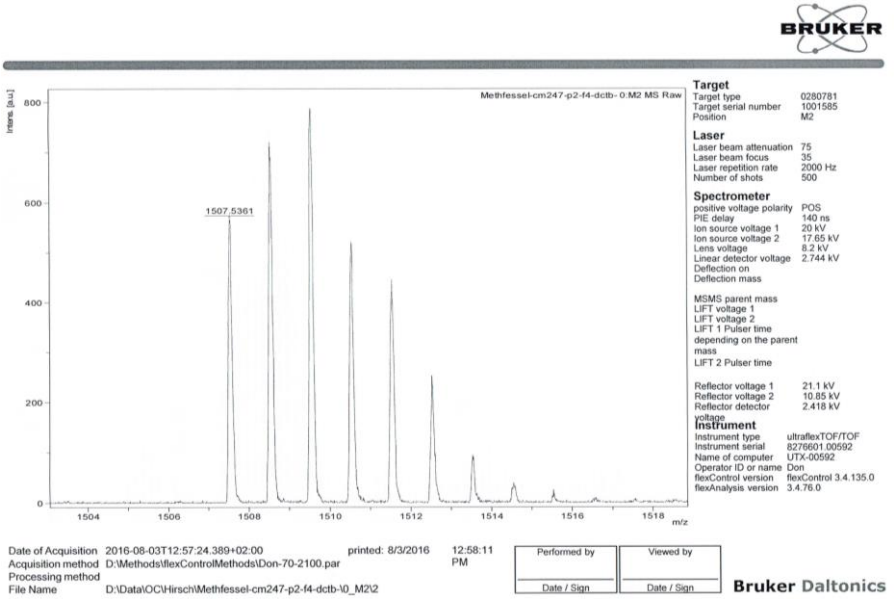

MS (MALDI) of **19**.

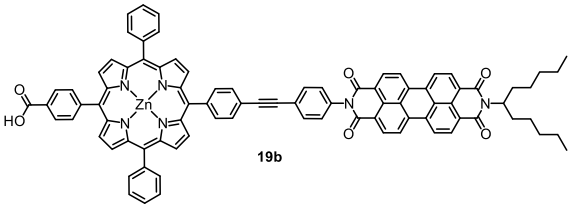

19b

$C_{88}H_{62}N_6O_6Zn$

ex. M. 1362.4022

MW 1364.8800

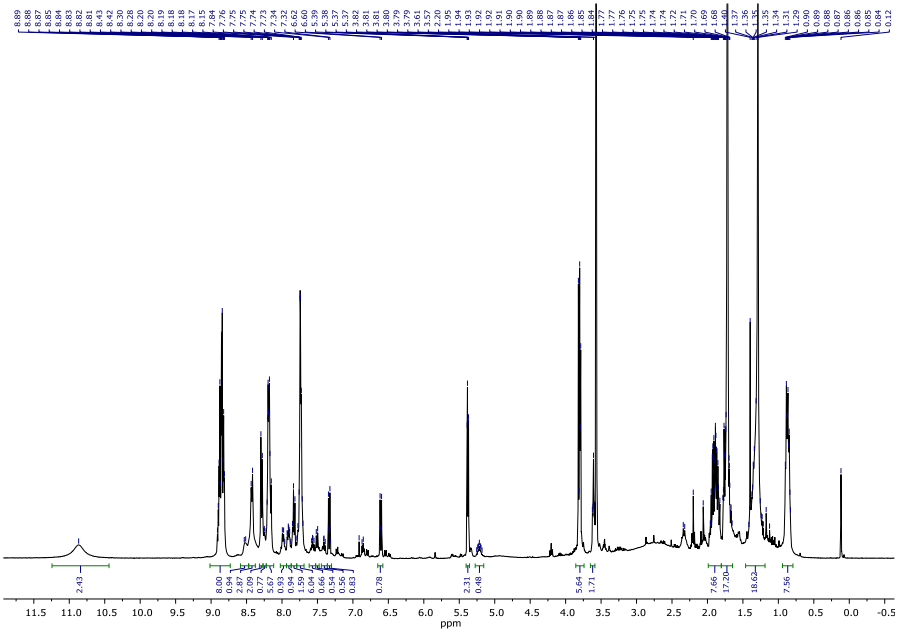

^{1}H NMR spectrum of **19b** in THF-d_8.

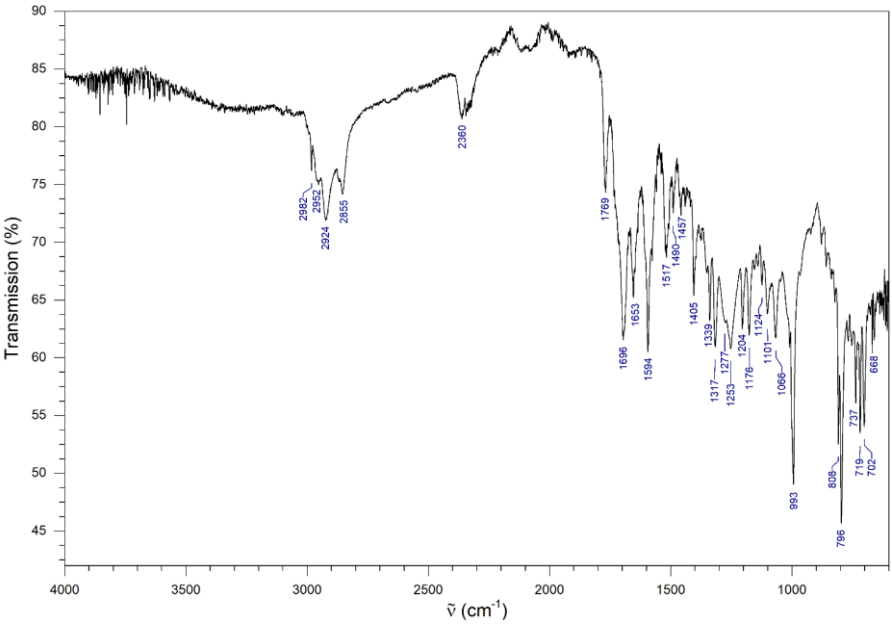

FT-IR spectrum of **19b**.

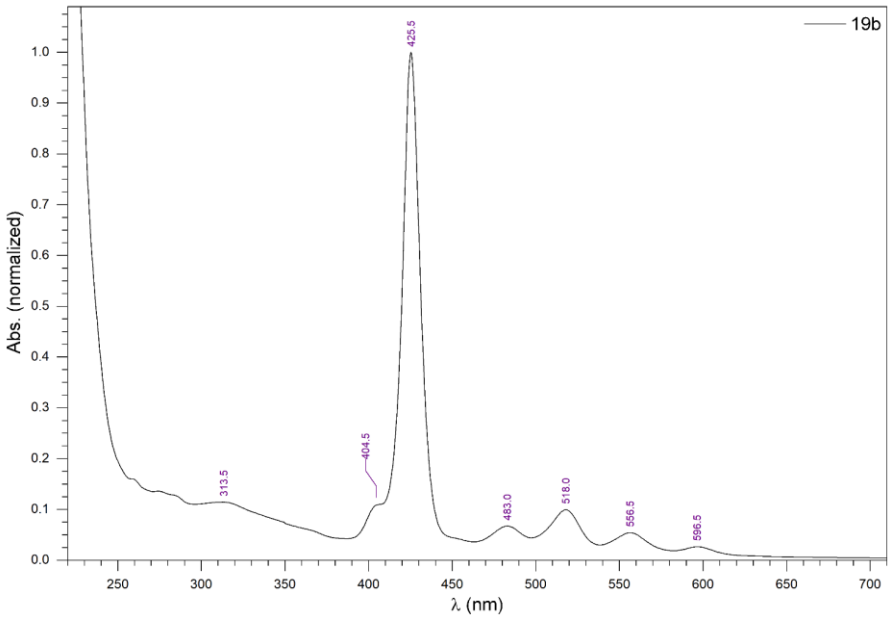

UV-Vis spectrum of **19b** in THF (qualitative, normalized).

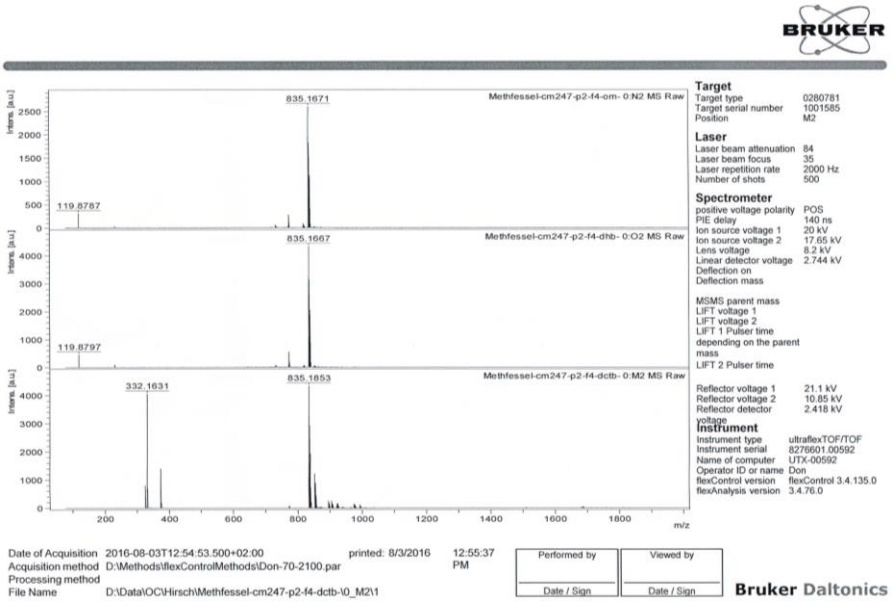

MS (MALDI) of by-product (acid-Zn-porphyrin-PEP-amine) of **19b**.

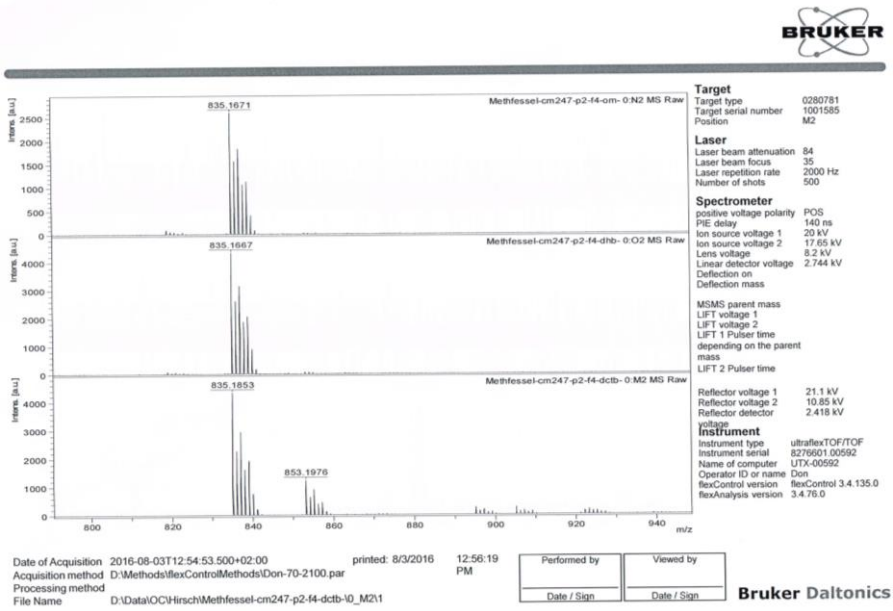

MS (MALDI) of by-product (acid-Zn-porphyrin-PEP-amine, M = 835.1926) of **19b** (detail).

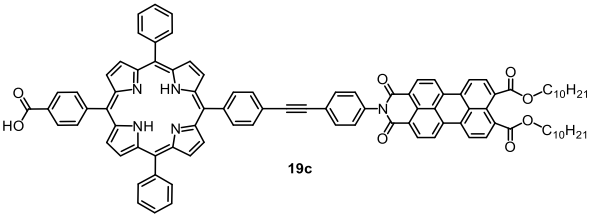

19c

$C_{97}H_{83}N_5O_8$

ex. M. 1445.6242

MW 1446.7580

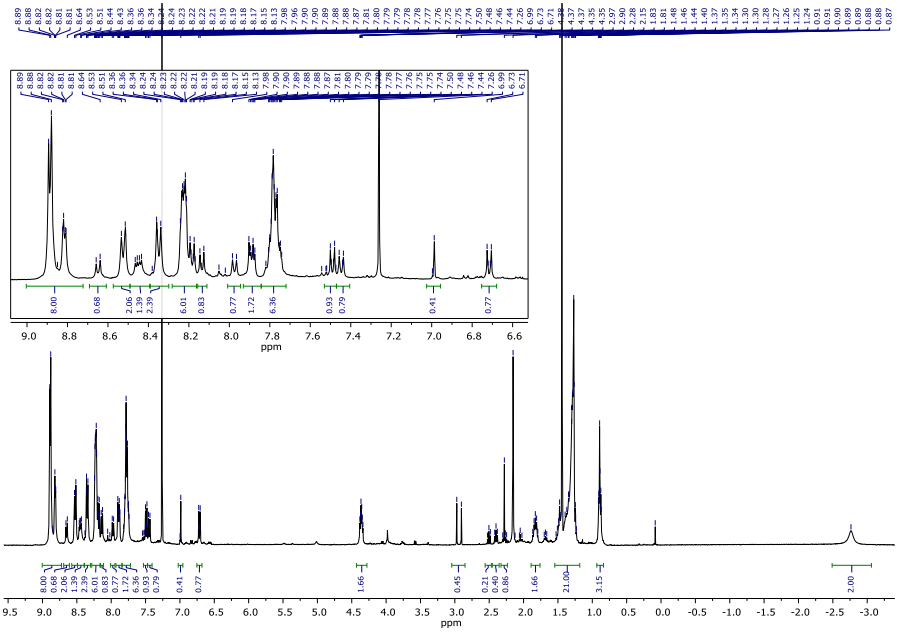

^{1}H NMR spectrum of **19c** in $CDCl_3$.

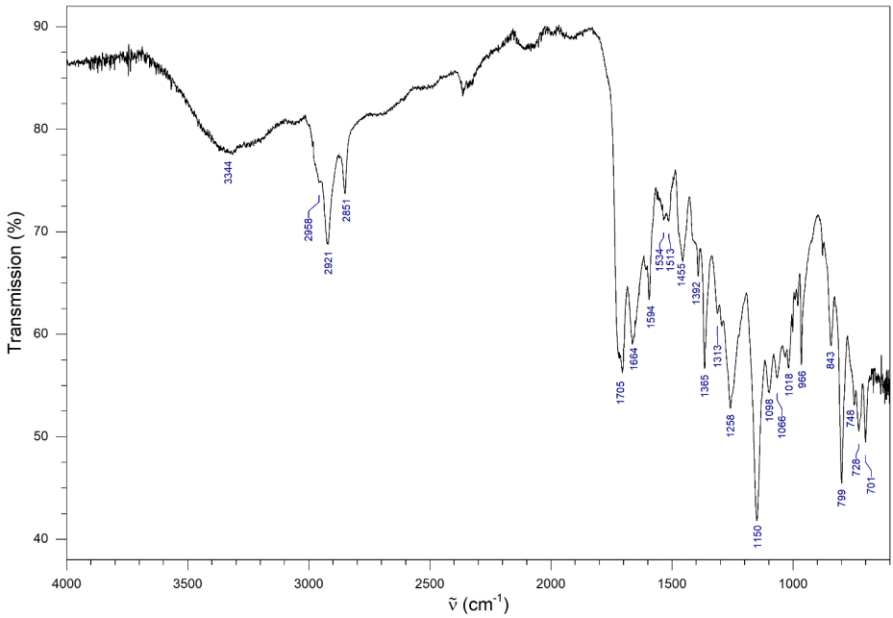

FT-IR spectrum of **19c**.

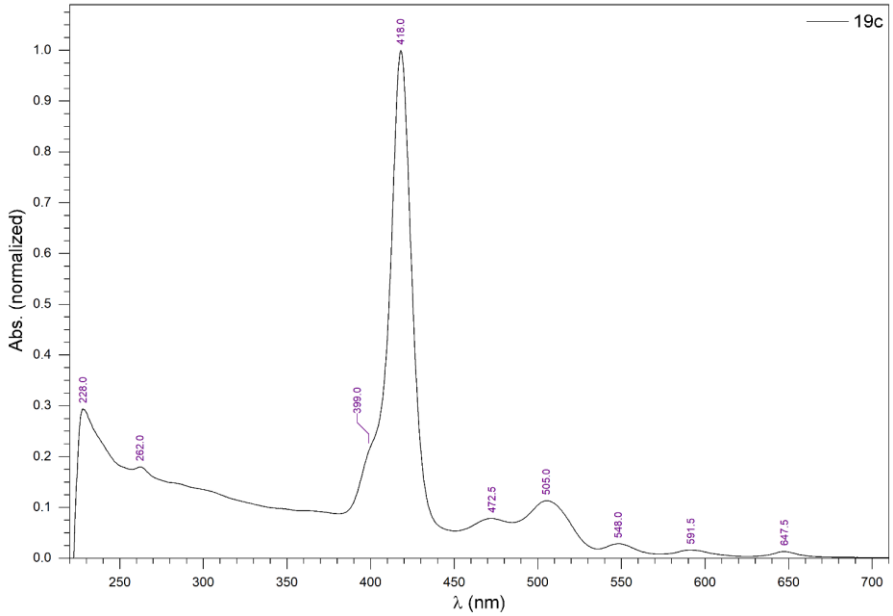

UV-Vis spectrum of **19c** in THF (qualitative, normalized).

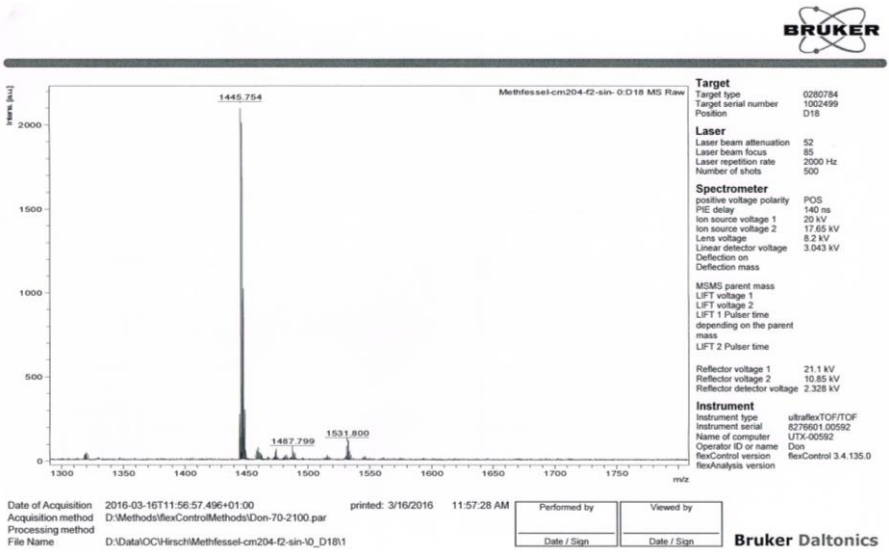

MS (MALDI) of **19c**.

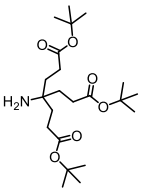

21

$C_{22}H_{41}NO_6$

ex. M. 415.2934

MW 415.5710

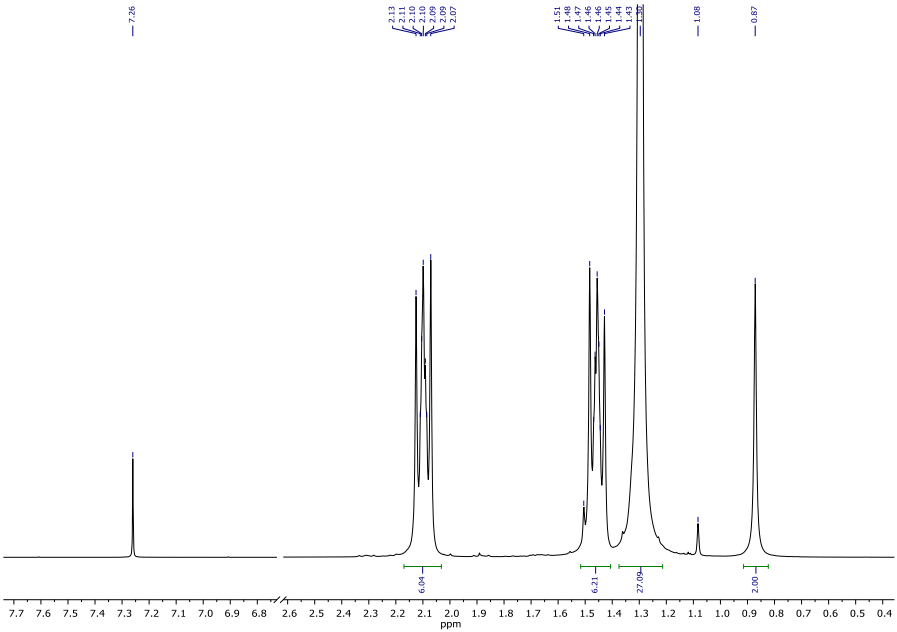

^{1}H NMR spectrum of **21** in $CDCl_3$.

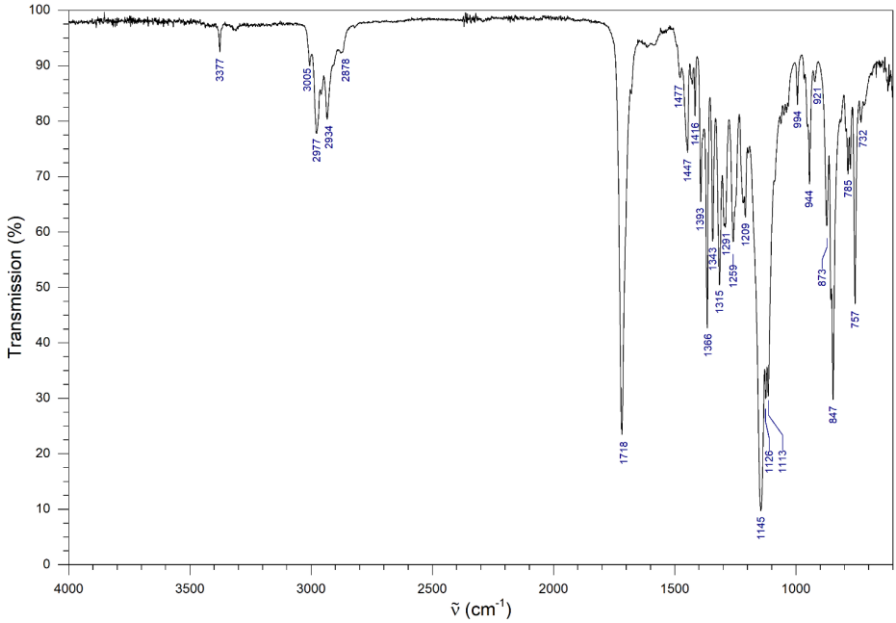

FT-IR spectrum of **21**.

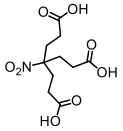

22

$C_{10}H_{15}NO_8$

ex. M. 277.0798

MW 277.2290

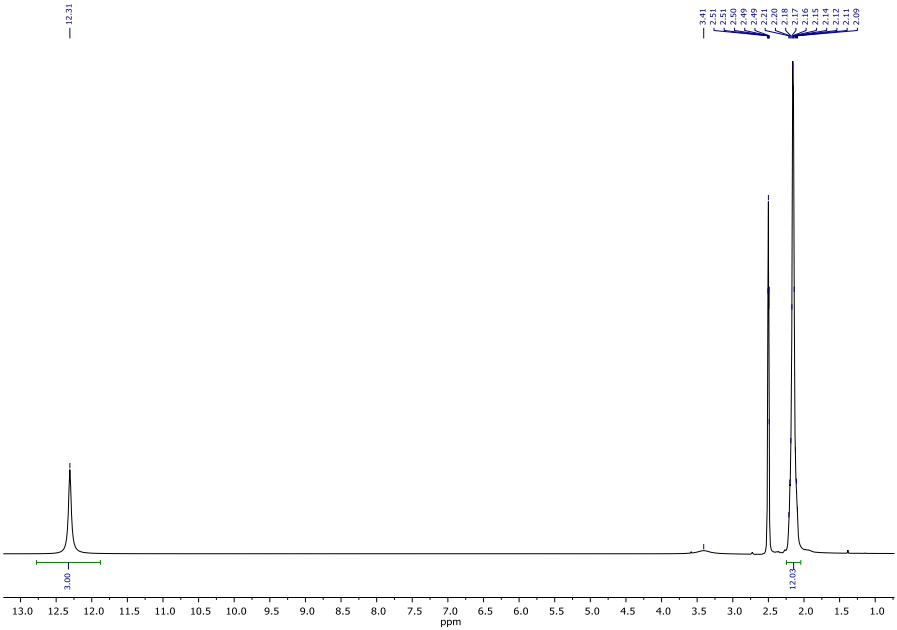

^{1}H NMR spectrum of **22** in $CDCl_3$.

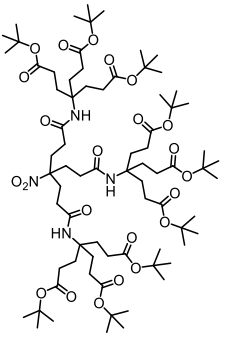

23

$C_{76}H_{132}N_4O_{23}$

ex. M. 1468.9282

MW 1469.8970

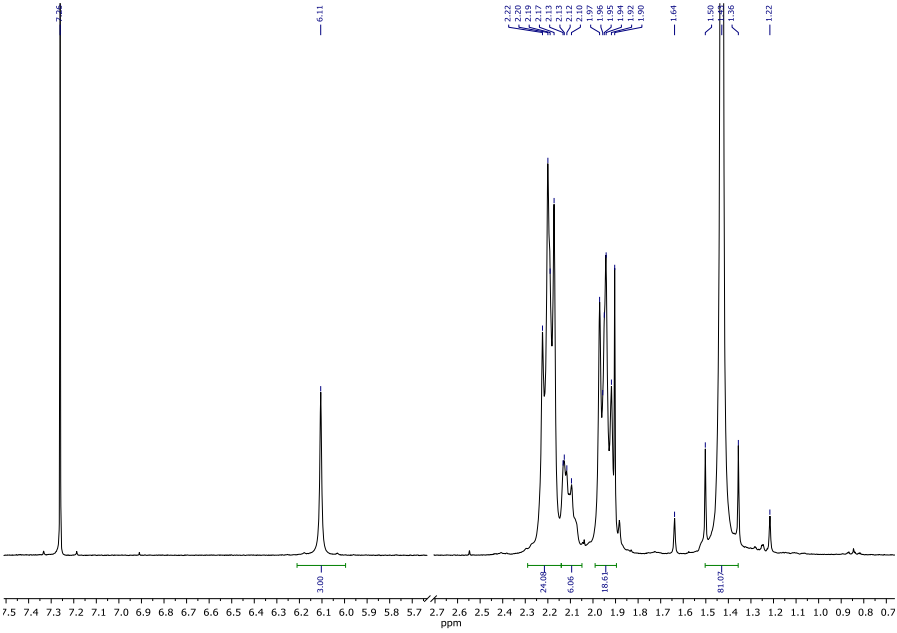

^{1}H NMR spectrum of **23** in $CDCl_3$.

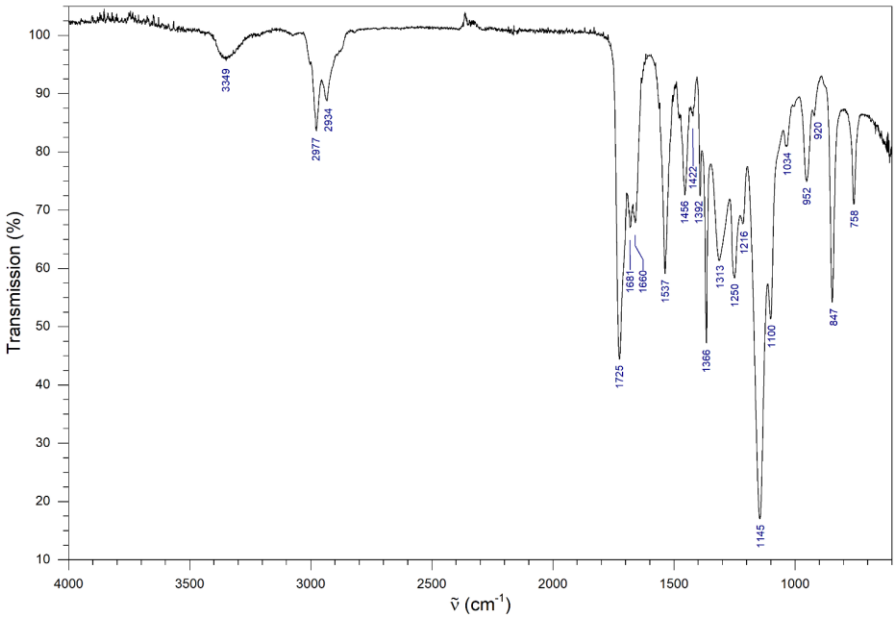

FT-IR spectrum of **23**.

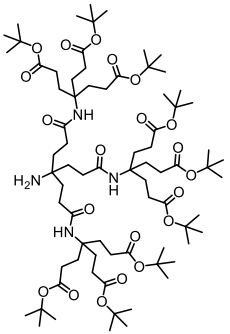

24

$C_{76}H_{134}N_4O_{21}$

ex. M. 1438.9541

MW 1439.9150

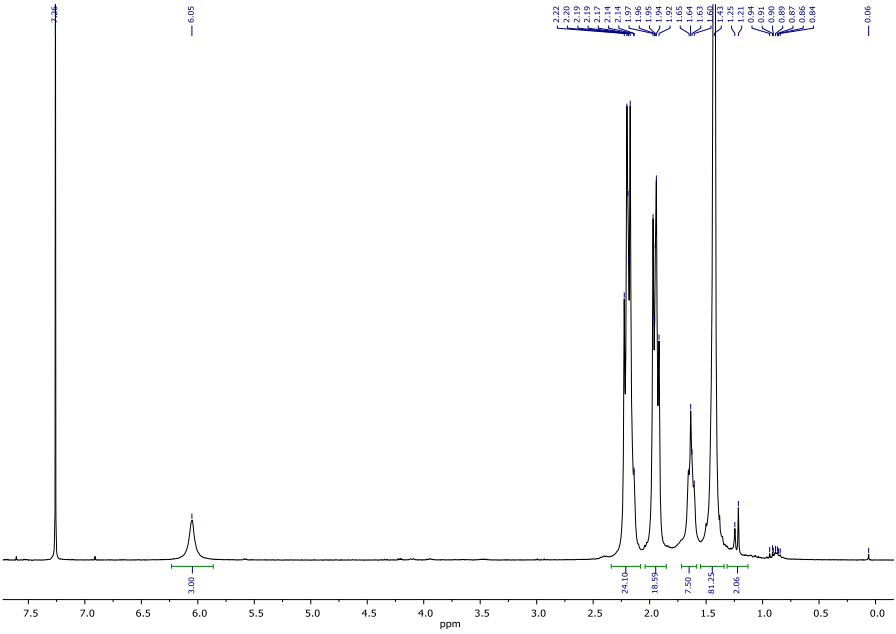

^{1}H NMR spectrum of **24** in $CDCl_3$.

Table. Calculated energies (Materials Studio, semiempirical calculation method: VAMP Geometry Optimization NDDO PM6/UHF) for products and sub-components. Comparison to spectroscopically determined HOMO–LUMO values (in nm and UV-Vis) and E_g values found in the literature.

compound	no.	HOMO calcd.	LUMO calcd.	Eg (gas phase) eV (calcd.)	Eg (gas phase) nm (calcd.)	IP	EA	EA (rel. to ZnTPP)	Eg (measured) nm (opt.)	Eg (measured) eV (opt.)	eV (opt, lit.)	eV (CV, lit.)
TPP		-8.41	-1.31	7.11	174.5	8.41	1.31	-0.18	649.0[a]	**1.91**	**1.89-2.01**[15,165,275]	**2.28**[281]
Zn-TPP		-8.04	-1.48	6.56	189.1	8.04	1.48	–	600.0[a]	**2.07**	**2.10**[15]	
Perylene		-8.44	-0.88	7.57	163.8	8.44	0.88	-0.60				
PTCDA		-10.03	-2.93	7.10	174.6	10.03	2.93	1.45				
PTE_{10}	14								480.0	2.58	2.46[265]	1.93-2.20[119,265]
$PABE_{10}$	15	-9.14	-2.49	6.66	186.3	9.14	2.49	1.01	514.0	2.41		
PI_2A	17								525.0	2.36		2.15[119]
$PEP\text{-}PIBE_{10}$	~16	**-8.75**	**-2.39**	**6.36**	194.9	8.75	2.39	0.91	518.0	2.39	**2.32**[119,267-268]	***2.17-2.40***[b][15,281]
MeO-P-PEP (H_2Por)	~12	**-8.41**	**-1.31**	**7.11**	174.5	8.41	1.31	-0.18			**1.89-2.01**[15,165,275]	**2.46**[281]
MeO-Zn-PEP (ZnPor)		**-8.04**	**-1.48**	**6.56**	189.0	8.04	1.48	-0.01			**2.10**[15]	**2.23**[15]
MeO-P-PEP-PIA		-8.06	-3.05	5.01	247.5	8.06	3.05	1.57				
MeO-ZnP-PEP-PIA		-7.78	-3.06	4.73	262.4	7.78	3.06	1.58				
$MeO\text{-}P\text{-}PEP\text{-}PIBE_{10}$	18c	-8.01	-2.59	5.41	229.0	8.01	2.59	1.11				
$MeO\text{-}ZnP\text{-}PEP\text{-}PIBE_{10}$	18	-7.73	-2.55	5.18	239.5	7.73	2.55	1.07				
$G^1\text{-}P\text{-}PEP\text{-}PIBE_{10}$	1d	-8.38	-2.41	5.96	207.9	8.39	2.41	0.93	649.0[a]			
$G^1\text{-}ZnP\text{-}PEP\text{-}PIBE_{10}$	1a	-7.73	-2.55	5.19	239.1	7.73	2.55	1.07	600.0[a]			
Acid-G^1-P-PEP-$PIBE_{10}$	**2d**	**-8.09**	**-2.57**	**5.52**	224.4	8.09	2.57	1.09				**1.63**[281]
Acid-G^1-ZnP-PEP-$PIBE_{10}$	**2a**	**-7.82**	**-2.58**	**5.24**	236.5	7.82	2.58	1.10				**1.29**[15]

[a] The spectroscopically determined HOMO–LUMO gap (*cf.* p. 84f) for free-base and Zn porphyrins is found at 649 and 600 nm, respectively (*cf.* p. 91). [b] The $E_{g,CV}$ was determined for a PDI instead of a PIBE.[15,281]

Bold values are also displayed in the energy diagram in Figure 5.31 on p. 100.

IP = Ionization potential = $-E_{HOMO}$, EA = Electron affinity = $-E_{LUMO}$

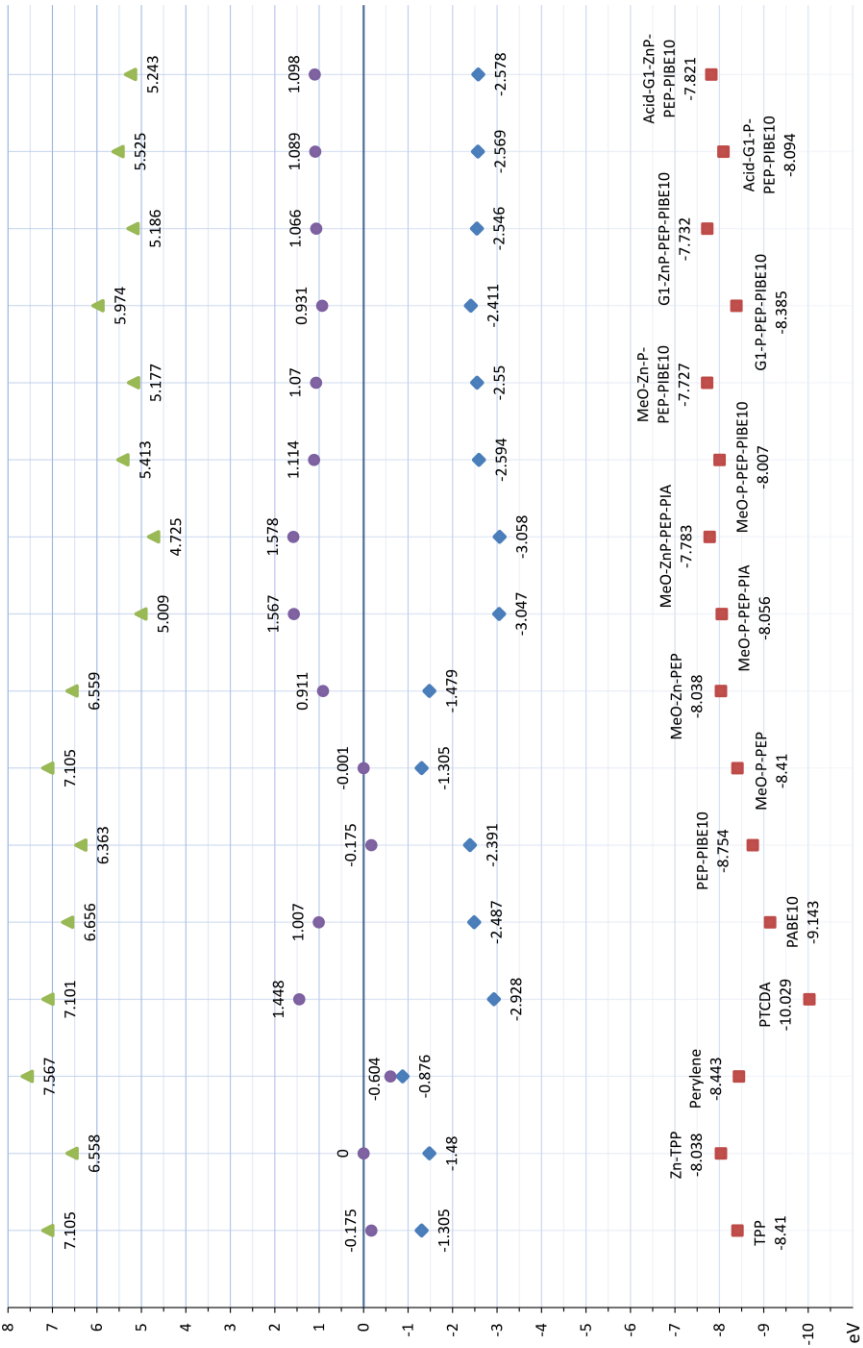

Correlation diagram of calculated energies (HOMO, LUMO, E_g, EA) for selected molecules.

12 Addendum: Additional Discoveries

To provide additional benefits for the scientific community, some discoveries which did not contribute to the final synthesis pathway are presented in this chapter. Although these discarded syntheses are no longer part of the synthesis strategy of this thesis, it is the strong belief of the author that the gathered knowledge should not be lost.[195] Hence, some alternative syntheses as well as interesting (but low-yielding or failing) approaches are identified and briefly discussed.

Linking porphyrin and perylene. To join distinct groups at each side of the acetylene linker, two separate SONOGASHIRA coupling reactions had to be performed. Initially, it was planned to link the two chromophores with the acetylene linker as a last step *via* a SONOGASHIRA reaction. This would have allowed to generate a larger library of both porphyrin and perylene compounds and to combine them freely, leading to a grand portfolio of different dyads.

Unfortunately, the final SONOGASHIRA reaction was extremely delicate. It usually resulted in extremely low yields (max. 2%) or – more commonly – in complete failures. Several trials and pathways were performed with different catalysts, solvents and reaction conditions. The halogen (iodine or bromine) was placed at the porphyrin and the acetylene at the perylene (which should be electronically more favorable) or *vice versa* to no avail. It is known that amines can coordinate to palladium. This would promote other undesirable reactions (*e.g.,* BUCHWALD-HARTWIG amination),[293-296] or coordinate/deactivate the catalyst. Furthermore, the success of the reaction is often limited when handling larger molecules. Usually, it is essential to find and test very special reaction conditions to obtain high yields and reliability.[15,297]

As a workaround, the concept was changed and it was decided to set both SONOGASHIRA reactions for the acetylene linker as early as possible with molecules as small as possible. But even then, yields did not meet the expectations. Only after protecting the free aniline and using freshly self-prepared catalyst, the second reaction step could be performed successfully in high yields (90%, see p. 34). The difunctionalized acetylene was further converted into a dipyrromethane, a porphyrin and finally reacted with the perylene to give the dyad.

Porphyrin synthesis under LINDSEY conditions. The statistical synthesis of the unsymmetric trans-AB_2C porphyrin using standard LINDSEY conditions led to a broad product distribution and tedious chromatographical workup. Under these conditions, a high degree of scrambling (*i.e.*, recombination of the porphyrinic composition) was observed, which increased the number of different products drastically and reduced the amount of the target product. From the overall porphyrin yield of 20 – 40%, only 0.2% of desired product could be isolated after multiple HPLC purification steps due to massive scrambling. It was decided that this reaction strategy is definitely inapplicable for the synthesis of larger amounts of complex AB_2C porphyrins.

Novel scrambling-free porphyrin condensation reaction. To suppress the scrambling (which mainly takes place under acidic conditions) and to be able to synthesize this unsymmetric AB_2C porphyrin in higher yields, a novel, scrambling-free porphyrin synthesis under alkaline conditions was developed. Up to date, only very few and highly specialized porphyrin syntheses under neutral,[58,68] or alkaline conditions are known in the literature.[57,62-63,220]

For this purpose, the standard reaction conditions for phthalocyanine synthesis were applied, tested and optimized: $Zn(OAc)_2$ as a templating metal, DBU as a strong base, a high-boiling alcohol (n-pentanol) as solvent and the required components (two types of dipyrromethane plus benzaldehyde) to give the unsymmetric AB_2C zinc porphyrin. The reaction could be performed at notably higher concentrations (10–100 x) compared to standard LINDSEY conditions. After the reaction, DDQ was added to oxidize the intermediate porphyrinogen to the final zinc porphyrin. This is the only reaction in literature which relies on basic conditions to obtain scrambling-free porphyrins. Using this strategy, especially acid-sensitive compounds could be condensed into novel porphyrin with no scrambling.

After 20 h refluxing at 138 °C, it was shown that scrambling could be suppressed completely. The three statistical products (carrying 0–2 methyl ester groups) were easily separated by column chromatography and yields of up to 7.4% were obtained. The same reaction was also successfully performed in 6.5% yield when using $Cu(OAc)_2$ to give an unsymmetric AB_2C copper porphyrin. Under supervision, Florian Fischer, MSc., conducted small-scale microwave-assisted syntheses at 180 °C which reduced the reaction time to 1.5 h yielding up to 11.2% with only minor scrambling.[298]

However, one large drawback in the given synthesis strategy is the reactivity of the solvent n-pentanol: Under these conditions, a trans-esterification of the porphyrinic methyl ester to a pentyl ester takes place. The cleavage of this ester is considerably more elaborate and the presence of several long-chained esters would render the orthogonal protecting group strategy (p. 28ff) virtually impossible. To counteract this issue, a class of high-boiling ether compounds (methyl–pentyl ether and ethyl–pentyl ether) was synthesized. In small-scale test reactions with spectroscopic yields of 15.5% and 26.1%, respectively, it could be shown that no trans-esterification occurred under these conditions.

Further investigations of this novel alkaline porphyrin synthesis method were discontinued, after the stepwise porphyrin synthesis *via* a VILSMEIER-analogous reaction and the *in situ* generation of a dicarbinol turned out to be more promising for the way towards the final target molecule.[65] Indeed, the multistep reaction led to a consecutive yield of 23% with high purity and without any scrambling (*cf.* chapter 5.1.3, p. 37).

Hence, the alkaline scrambling-free statistical porphyrin synthesis is not part of this thesis. If deeper insight into this synthetic method is desired, please contact the author or refer to the accompanied theses of my students.[298-303]